A UNITED STATES DEPARTMENT OF COMMERCE PUBLICATION

SECTION A

JOURNAL OF RESEARCH

of the NATIONAL BUREAU OF STANDARDS

JNBAAR 77A (1) 1–177 Jan.-Feb. 1973

Physics and Chemistry

U.S. DEPARTMENT OF COMMERCE
National Bureau of Standards

Journal of Research

of the

National Bureau of Standards

A. Physics and Chemistry

Jan.–Feb. • 1973

VOLUME • 77A

NUMBER • 1

Editor: C. W. Beckett

Associate Editor: D. D. Wagman

Publication dates:
Feb. 1, Apr. 1, June 1, Aug. 1, Oct. 1, Dec. 1, 1973

J. Res. Nat. Bur. Stand. (U.S.), A

JOURNAL OF RESEARCH

The National Bureau of Standards Journal of Research reports research and development in the fields of activity shown at right. Also included from time to time are survey articles on topics closely related to the Bureau's scientific and technical program.

The Journal is published in two separate sections as follows:

A. Physics and Chemistry

Contains papers of interest primarily to scientists working in these fields. Issued six times a year. Annual subscription: domestic, $17.00; foreign, $21.25. Single copy, varies.

B. Mathematical Sciences

Presents studies and compilations designed mainly for the mathematician and the theoretical physicist. Issued quarterly. Annual subscription: domestic, $9.00; foreign, $11.25. Single copy, $2.25.

The National Bureau of Standards[1] was established by an act of Congress March 3, 1901. The Bureau's overall goal is to strengthen and advance the Nation's science and technology and facilitate their effective application for public benefit. To this end, the Bureau conducts research and provides: (1) a basis for the Nation's physical measurement system, (2) scientific and technological services for industry and government, (3) a technical basis for equity in trade, and (4) technical services to promote public safety. The Bureau consists of the Institute for Basic Standards, the Institute for Materials Research, the Institute for Applied Technology, the Center for Computer Sciences and Technology, and the Office for Information Programs.

THE INSTITUTE FOR BASIC STANDARDS provides the central basis within the United States of a complete and consistent system of physical measurement; coordinates that system with measurement systems of other nations; and furnishes essential services leading to accurate and uniform physical measurements throughout the Nation's scientific community, industry, and commerce. The Institute consists of a Center for Radiation Research, an Office of Measurement Services and the following divisions:

Applied Mathematics — Electricity — Mechanics — Heat — Optical Physics — Linac Radiation[2] — Nuclear Radiation[2] — Applied Radiation[2] — Quantum Electronics[3] — Electromagnetics[3] — Time and Frequency[3] — Laboratory Astrophysics[3] — Cryogenics[3].

THE INSTITUTE FOR MATERIALS RESEARCH conducts materials research leading to improved methods of measurement, standards, and data on the properties of well-characterized materials needed by industry, commerce, educational institutions, and Government; provides advisory and research services to other Government agencies; and develops, produces, and distributes standard reference materials. The Institute consists of the Office of Standard Reference Materials and the following divisions:

Analytical Chemistry—Polymers—Metallurgy—Inorganic Materials—Reactor Radiation—Physical Chemistry.

THE INSTITUTE FOR APPLIED TECHNOLOGY provides technical services to promote the use of available technology and to facilitate technological innovation in industry and Government; cooperates with public and private organizations leading to the development of technological standards (including mandatory safety standards), codes and methods of test; and provides technical advice and services to Government agencies upon request. The Institute also monitors NBS engineering standards activities and provides liaison between NBS and national and international engineering standards bodies. The Institute consists of a Center for Building Technology and the following divisions and offices:

Engineering and Product Standards—Weights and Measures—Invention and Innovation—Product Evaluation Technology—Electronic Technology—Technical Analysis—Measurement Engineering—Building Standards and Code Services[4]—Housing Technology[4]—Federal Building Technology[4]—Structures, Materials and Life Safety[4]—Building Environment[4]—Technical Evaluation and Application[4]—Fire Technology.

THE INSTITUTE FOR COMPUTER SCIENCES AND TECHNOLOGY conducts research and provides technical services designed to aid Government agencies in improving cost effectiveness in the conduct of their programs through the selection, acquisition, and effective utilization of automatic data processing equipment; and serves as the principal focus within the executive branch for the development of Federal standards for automatic data processing equipment, techniques, and computer languages. The Center consists of the following offices and divisions:

Information Processing Standards—Computer Information—Computer Services—Systems Development—Information Processing Technology.

THE OFFICE FOR INFORMATION PROGRAMS promotes optimum dissemination and accessibility of scientific information generated within NBS and other agencies of the Federal Government; promotes the development of the National Standard Reference Data System and a system of information analysis centers dealing with the broader aspects of the National Measurement System; provides appropriate services to ensure that the NBS staff has optimum accessibility to the scientific information of the world, and directs the public information activities of the Bureau. The Office consists of the following organizational units:

Office of Standard Reference Data—Office of Technical Information and Publications—Library—Office of International Relations.

[1] Headquarters and Laboratories at Gaithersburg, Maryland, unless otherwise noted; mailing address Washington, D.C. 20234.
[2] Part of the Center for Radiation Research.
[3] Located at Boulder, Colorado 80302.
[4] Part of the Center for Building Technology.

U.S. DEPARTMENT OF COMMERCE
Frederick B. Dent, Secretary

NATIONAL BUREAU OF STANDARDS
Richard W. Roberts, Director

Order all publications from the Superintendent of Documents
U.S. Government Printing Office, Washington, D.C. 20402

The Secretary of Commerce has determined that the publication of this periodical is necessary in the transaction of the public business required by law of this Department. Use of funds for printing this periodical has been approved by the Director of the Office of Management and Budget through June 30, 1976.

JOURNAL OF RESEARCH of the National Bureau of Standards—A. Physics and Chemistry
Vol. 77A, No. 1, January–February 1973

Spectrum and Energy Levels of Neutral Thulium

J. Sugar and W. F. Meggers*

Institute for Basic Standards, National Bureau of Standards, Washington, D.C. 20234

and

P. Camus

Laboratoire Aimé Cotton, Centre National de la Recherche Scientifique, 91-Orsay, France

(July 11, 1972)

A new set of measurements of the spectrum of neutral thulium covering the range of 2513 Å to 11750 Å is given. The light source utilized for the observations was a microwave-excited thulium-iodide lamp. Second spectrum lines were recognized by comparing the output of this lamp with that of a 6A sliding spark. The results of Zeeman effect studies of these lines are included. Analysis of these new data led to the discovery of 348 new energy levels and provided revised values for the 142 already published. Measured Landé g factors are given for most of the levels.

Key words: Energy levels; spectrum; thulium; wavelengths.

1. Introduction

The fundamental energy interval in neutral thulium of 8771 cm^{-1} was discovered by Meggers in 1942 [1].[1] He identified it as the ^2F interval of the $4f^{13}6s^2$ normal electronic configuration. Sixteen pairs of lines were found with this wave number difference, giving as many upper levels. The line list was obtained by comparing spectra of Tm, Yb, and Lu oxides, each containing the other two as considerable impurities. Although the availability of the pure metal by the middle 1950's allowed spectroscopic studies to be made much more easily and completely, it was not until 1963 that the first new results were obtained [2, 3] by Blaise and co-workers at Laboratoire Aimé Cotton. They studied the *hfs* of 70 strong lines utilizing a cooled hollow cathode light source and a Fabry-Perot spectrometer. Their investigation confirmed the 16 levels of even parity found by Meggers, assigned J values to them, and extended the analysis to include ten high-lying levels of odd parity (including the discovery of the $4f^{13}6s7s$ configuration), as well as 12 new even levels.

At about this time the work of making a completely new description of the spectra of thulium was initiated at the National Bureau of Standards in Washington, D.C. The program was to make as complete as practical a set of wavelengths of the first and second spectra in the range of 2000 Å to 12000 Å. This was to be done with the microwave-excited metal-halide lamp and the low current sliding spark, the distinction between first and second spectra being provided by their relative enhancement in these two light sources. The work, which occupied a span of three years, resulted in the measurement of a set of 4378 lines of Tm I and 12842 lines of Tm II with an accuracy of about 0.03 cm^{-1}. In addition, there appeared in the spark 848 lines of higher ionization which were identified as such by comparison with the spectrum of a higher current spark. Of these, 454 have been classified in a level scheme of doubly ionized thulium [4].

Two new sets of observations acquired by Laboratoire Aimé Cotton led to the next breakthrough in the analysis of Tm I: spectrograms of the Zeeman effect taken at the Argonne National Laboratory and a line list extending from 0.9 μm to 2.4 μm obtained from observations made with the S.I.S.A.M. spectrometer [5]. These data enabled the assignment of J values and g values to nearly every known level and led to the discovery of 42 new even levels and 62 new odd levels [5–7].

The information on Tm I and Tm II was now sufficient to permit all the low-lying configurations to be interpreted through parametric calculations of the energy levels, eigenvectors, and g values. These calculations were carried out by Camus [8] for the mixed configurations $4f^{12}5d6s^2$ and $4f^{13}6s6p$ of even parity, and for $4f^{12}6s^26p$ and $4f^{13}5d6s$ of odd parity [9]. The

*Deceased.

[1]Figures in brackets indicate the literature references at the end of this paper.

simple configurations $4f^{13}6s7s$ and $4f^{13}6s8s$ had already been interpreted and utilized in a determination of the ionization energy in reference [7].

With the completion of the measurements of Tm I and Tm II at the National Bureau of Standards, a collaboration was established with Laboratoire Aimé Cotton to pool resources and to search for the higher-lying energy levels of Tm. Part of the fruits of this labor are presented here. The new results in Tm I consist mainly of the discovery and interpretation of the levels belonging to the $4f^{13}5d6p$, $4f^{12}5d6s6p$, $4f^{13}6s6d$, and $4f^{13}6p^2$ configurations as well as of additional levels belonging to the known configurations mentioned above. The known even levels were augmented by 138 additions, and the odd levels by 210 with the position of all the energy levels based on the new wavelength measurements.

We present here all the previously published energy levels of Tm I as well as those new ones found with the NBS line list and the Zeeman data, their measured g values, and their designations obtained from the parametric calculations [23]. The line list of Tm I measured at NBS is given in its entirety, with classifications and Zeeman data given where known. The results of the calculations of the newly identified configurations will be given in a later publication.

2. Observations and Measurements

The microwave-excited metal-halide lamp was used as the light source for the first spectrum of thulium, both for the wavelength measurements at the National Bureau of Standards and for the Zeeman effect measurements at the Argonne National Laboratories. A description of the method of preparation and the desirable features of these lamps has been given in detail [10, 11]. Because this light source produces a considerable excitation of singly ionized thulium, a clear distinction between the spectra of the neutral and singly ionized species must be made. This was accomplished unambiguously for practically all lines by comparing the lamp spectrum with that obtained by means of a low-current, low-voltage sliding spark. The versatility of this spark (described in detail in ref. [12]) in separating various ionic spectra by variations of the peak discharge current was previously demonstrated in studies of the third spectra of praseodymium [12] and cerium [13]. For the Pr III work it was operated at 50A and 1000A to produce relatively enhanced third or fourth spectrum. The lines of Pr II were distinguished by comparison with an arc spectrum of Pr. In the cerium work the spark was found to operate well at 6A peak current and to produce a second spectrum which was comparable to the arc spectrum in relative enhancement but much sharper. A line width of ~ 0.1 cm^{-1} is obtained with the sliding spark at 6A peak current. For our analysis the spectrum obtained in this operating condition was compared with that of the metal-halide lamp to pick out second spectrum lines and to provide the line list of Tm II.

A variety of spectrographs was used to obtain the wavelength coverage for our observations. From 2000 to 2600 Å a Wadsworth mounting of a 6.4 m grating with 1200 grooves/mm was used in the third order giving a plate factor of 0.6 Å/mm and in second order from 2600 to 4400 Å. The data from 4400 to 6850 Å was obtained with an Eagle mounting of a 10.7 m grating having 600 grooves/mm utilized in the second order. Averaged in with the data from the Eagle spectrograph are some measurements in first order of the 6.4 m Wadsworth. Two more Wadsworth mountings were used to carry the observations to 12000 Å: one containing a 6.4 m grating with 600 grooves/mm and blazed at 9500 Å, and the second with a grating of the same radius of curvature but with 300 grooves/mm and a blaze at 12000 Å. This same spectral range is now covered at NBS by two Eagle mountings, one in vacuum and one in air, with 10.7 m gratings.

The observations of the Zeeman effect were made using the Paschen-Runge mounting of a 9.15 m grating at the Argonne National Laboratory and using a magnetic field of $\sim$ 24000 Oe. The construction and operation of this excellent facility is described in two papers [14, 15] by Tomkins and Fred, who generously provided the thulium exposures for us.

Maximum exposure times for the Tm lamp varied from 1 h in the ultraviolet below 3000 Å to 10 min in the visible and to 3 h in the extreme photographic infrared. Shorter exposures were, of course, used to obtain the stronger lines with good images. Exposure times for the 6A spark followed a similar pattern with maxima of 3 to 5 h in the extreme wavelength regions to 5 min in the visible. A spark repetition rate of about 20/s was used with a rotating external spark gap placed in the series discharge circuit. The 50A spark operating at one-third of the exposure time of the 6A spark produced weaker second spectrum and stronger third or higher spectra, thus giving the desired separation.

Calibration standards in the region of 2000 to 3000 Å were obtained from a copper hollow-cathode discharge containing a few grams of germanium supplemented by an iron-iodide lamp which provided Fe I and Fe II in this region. The copper standard wavelengths used were the interferometric measurements of Reader, Meissner, and Andrew [16]; the germanium measurements in this region are those of Van Veld and Meissner [17]. Since these lines are fairly sparsely distributed in the region of 2000 to 2600 Å, the calibration was augmented by Fe II lines measured by Meggers and Humphreys [18]. No shift was detectable among these spectra. From 2600 to 3300 Å interferometrically measured lines of Fe I were used [19]. The longer wavelength regions were well covered in first or second order by the thorium measurements of Meggers and Stanley [20] which were available prior to publication.

A pulsed high-current arc in He at 1 atm was used as a source to aid in the recognition of resonance and other low-excitation lines of Tm I and Tm II [21]. It produced self-reversal of 120 first spectrum lines and 126 of the second spectrum. The self-reversals are two types: one for which there appears only a gap in the continuum with little trace of a line left (designated

"a" in the line list under "intensity"), and a second type for which most of the wings of the lines still remain (designated "r"). Eleven such lines remain unclassified. The classified ones arise mainly from the ground ^{2}F term, but some have the low level as high as 19466 cm^{-1}. All such low levels for these lines were found to be metastable because of their J values.

Each spectral line included in the list has been measured on at least two separate plates, and on as many as ten for some of the stronger lines. We found that 95 percent of the classified lines fit the energy level scheme to within ± 0.05 cm^{-1}. A measure of the wave number precision was made by finding the rms deviation in repeating wave number differences determining the low-lying level intervals. For the 27 pairs determining the lowest interval of 8771.243 cm^{-1}, the rms deviation is 0.02 cm^{-1}. Intervals between the level pairs of even parity 13119.610 − 15587.811 cm^{-1} and 15587.811 − 17454.818 cm^{-1} having 59 and 51 line pairs, respectively, are determined with rms deviations of 0.03 cm^{-1} each. Therefore, the rms error in the individual wave number measurements is estimated to be $0.03/1.4 = 0.02$ cm^{-1}.

A total of 2734 lines are classified, and, of these, 47 are classified twice. These are mostly weak lines with no observed Zeeman effect. The complete line list is given in the appendix which includes the measured wavelengths, visually estimated relative intensities from 1 to 50,000, vacuum wave numbers, classifications of the lines, and measured Zeeman effect. The intensity numbers are sometimes followed by letters indicating the following characteristics of the lines:

h = hazy
d = a double line
w = wide
r = reversed in pulsed arc
a = nearly completely absorbed in pulsed arc.

The classifications contain the values of the energy levels responsible for the transition, their J values given as subscripts, and a superscript degree symbol to indicate odd parity. The column headed "Zeeman Effect" generally contains the three following pieces of information:

1. The type of Zeeman pattern observed which is indicated by the symbols:
   - $\Delta J = 0$ where the p-components are shaded toward the center,
   - *SI* where the n-components are shaded toward the center,
   - *SO* where the n-components are shaded away from the center,
   - *SOO* where n-components are shaded away from center and are overlapping,
   - *T* where only a triplet was observed.
2. Half the interval between the two corresponding strong n-components in Lorentz units, denoted by "f".
3. Half the interval between the two outer p-components in Lorentz units, denoted by "Je" where "e" is the interval between components ($e = \Delta g$).

When the pattern is completely resolved. the two derived g factors are given in the columns "f" and "Je" with star (*) in the "Je" column to indicate such cases. The limit of resolution for "e" was 0.05, and the uncertainty in the g factors is estimated to be ± 0.01.

3. Energy Levels

Neutral thulium is one of the simpler rare earths at low energy because of its nearly closed $4f$ shell. The ground configuration, $4f^{13}6s^2$, consists of two levels with a separation of 8771 cm^{-1}. Above 13119 cm^{-1} the level structure begins to exhibit a complex character resulting from excitation of an electron from the $4f$ into the $5d$ shell, and at somewhat higher energy, the excitation of a $6s$ electron into the $6p$ shell. The resulting overlapping configurations of even parity, $4f^{12}5d6s^2$ and $4f^{13}6s6p$, are heavily mixed and form a dense complex of levels. There is a corresponding low energy complex of levels of odd parity beginning at 20406 cm^{-1} formed by one-electron excitations out of the ground configuration. They arise from the configurations $4f^{13}5d6s$ and $4f^{12}6s^26p$. Because these two low-lying complex groups of levels of opposite parity can combine by one-electron transitions, they produce a strong spectrum in the infrared.

A diagram showing the start of each of the known configurations is given in figure 1. Transitions in the infrared are indicated by heavy lines while those in the visible and shorter wavelength regions are indicated by the fine lines. The arrows show the order of discovery of the various configurations as the analysis progressed. Strong configuration interaction in the two low groups accounts for the observation of "forbidden" transitions $4f^{12}6s^26p - 4f^{13}6s6p$ and $4f^{12}5d6s^2 - 4f^{13}5d6s$.

The next stage of complexity begins at the threshold for 2-electron excitations out of the ground configuration. The observed odd configuration of this type, $4f^{12}5d6s6p$, accounts for the bulk of the known levels of this parity. Levels of this configuration begin at 29308 cm^{-1} and extend far beyond the ionization energy. Within their bounds were found four much simpler configurations: $4f^{13}6s7s$, $4f^{13}6s8s$, $4f^{13}6s6d$, and $4f^{13}6p^2$.

No even configuration of comparable complexity has been found, but Brewer [22] predicted the presence of $4f^{12}5d^26s$ at about 27600 cm^{-1}. In this parity there are many known high-lying levels without interpretation. It is likely that they belong to this configuration, but they cannot be understood as such until the low structure of this configuration is discovered. The limitation here is that $4f^{12}5d^26s$ lies so close to $4f^{12}5d6s6p$ that the strong transitions are in the far infrared. The simpler higher-lying even configuration $4f^{13}5d6p$ has been identified at 38318 cm^{-1}.

Many higher-lying energy levels of even parity based on single lines seen in photoabsorption have been

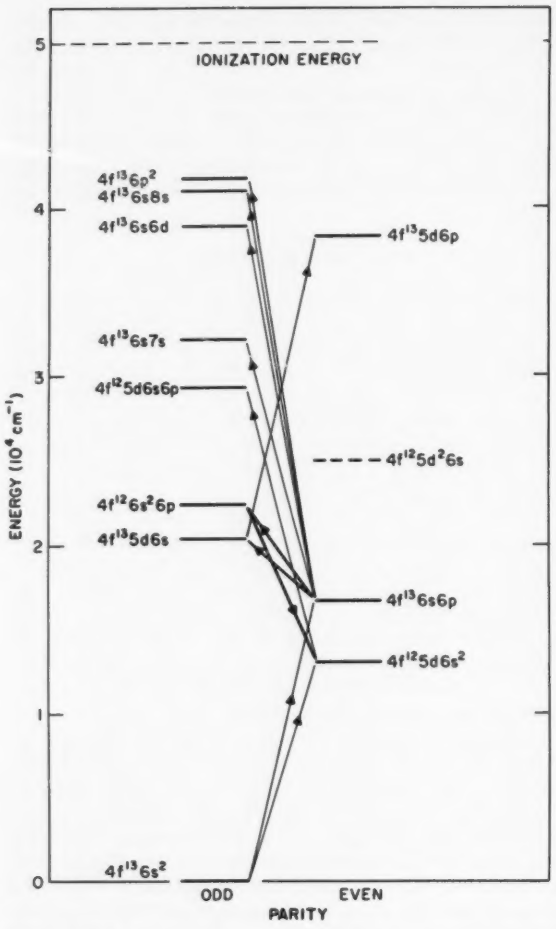

FIGURE 1. *Relative positions of known configurations of neutral thulium, with each configuration represented by lowest level.*

Dashed line gives predicted position for $4f^{12}5d^26s$. Arrows show the order of discovery of the configurations. Heavy arrows indicate where infrared lines were used.

reported by Camus [23]. He was able to follow the $4f^{13}6snp$ series from $n=17$ to $n=48$. Many of the levels reported here are supported by the absorption data, but we include no levels which are not in evidence in emission.

Table I contains all levels of Tm I of even parity which are deduced from the present line list. Nearly all of those below 35000 cm^{-1} have been reported before. Their source is indicated by a number in the last column denoting the reference appearing in section 5. The levels of the three configurations identified are grouped into J_1J_2 coupling terms. For $4f^{12}5d6s^2$ and $4f^{13}6s6p$ the designations are taken from reference [8]. The designations of $4f^{13}5d6p$ are from calculations which we will soon publish.

Table 2 contains all the known levels of odd parity. The configurations $4f^{12}6s^26p$, $4f^{12}5d6s6p$, $4f^{13}6s7s$, $4f^{13}6s8s$, and $4f^{13}6p^2$, are designated in J_1J_2 coupling as indicated by the parametric treatment [9, 23]. The coupling scheme applied to the configurations $4f^{13}5d6s$ and $4f^{13}6s6d$ is J_1L_2 coupling. The J_1 vector refers to the $4f^{13}$ angular momentum, and L_2 denotes the orbital angular momentum of the ds system. The resultant angular momentum K is enclosed in a square bracket with a superscript on the left of the bracket denoting the spin of the ds system. Those few odd levels which have not been assigned to a configuration appear in numerical order in the total list. Many levels of $4f^{12}5d6s6p$ have only a configuration assignment because of technical limitations in the theoretical treatment of this extremely large configuration. These limitations will be discussed in a later paper on the theoretical treatment of the high configurations, including the $4f^{13}6s6d$ and $4f^{13}6p^2$ and $4f^{13}5d6p$. Designations for levels of the configurations $4f^{12}6s^26p$ and $4f^{13}5d6s$ are taken from references [5] and [9]. The sources for levels previously published are denoted as in table 1.

The level values for both parities were adjusted by least squares fitting to the measured lines with a computer code written by Radziemski, Fisher, Steinhaus, and Goldman for this purpose [24]. For levels given to three decimal places the standard deviation varies from 0.004 to 0.010 cm^{-1}. For those given to two it varies from 0.010 to 0.02 cm^{-1}. The rms deviation of the measured lines from the spectrum calculated with the adjusted level values is 0.02 cm^{-1}.

TABLE 1. *Energy levels of neutral thulium, even parity, in units of cm^{-1}. Ref. is given for levels previously published*

Configuration	Designation	J	Energy	g-Factor	Ref.
$4f^{12}(^3H_6)5d_{3/2}\ 6s^2$	$(6,1^1/_2)$	$4^1/_2$	13119.610	1.305	6
		$7^1/_2$	15271.002	1.08	5
		$5^1/_2$	15587.811	1.255	7
		$6^1/_2$	17454.818	1.15	7
$4f^{12}(^3H_6)5d_{5/2}\ 6s^2$	$(6,2^1/_2)$	$8^1/_2$	16456.913	1.175	5
		$3^1/_2$	16957.006	1.169	2
		$7^1/_2$	18693.074	1.18	5
		$4^1/_2$	18837.385	1.13	2
		$5^1/_2$	18853.823	1.15	6
		$6^1/_2$	19466.663	1.15	7
$4f^{13}(^2F_{7/2})6s6p(^3P_0)$	$(3^1/_2,0)$	$3^1/_2$	16742.237	1.325	2
$4f^{13}(^2F_{7/2})6s6p(^3P_1)$	$(3^1/_2,1)$	$3^1/_2$	17343.374	1.022	2
		$4^1/_2$	17613.659	1.188	2
		$2^1/_2$	17752.634	1.186	2
$4f^{13}(^2F_{7/2})6s6p(^3P_2)$	$(3^1/_2,2)$	$5^1/_2$	18990.406	1.215	6
		$1^1/_2$	19132.245	0.88	6
		$2^1/_2$	19548.834	0.983	2
		$4^1/_2$	19748.543	1.29	6
		$3^1/_2$	19753.830	1.18	2
$4f^{12}(^3F_4)5d_{5/2}\ 6s^2$	$(4,1^1/_2)$	$3^1/_2$	21120.836	1.175	2
		$2^1/_2$	21161.401	1.14	1
		$4^1/_2$	21737.685	1.13	2
		$5^1/_2$	21997.473	1.06	5
$4f^{12}(^3H_5)5d_{3/2}\ 6s^2$	$(5,1^1/_2)$	$3^1/_2$	22791.176	1.14	1
		$6^1/_2$	23374.681	0.98	
		$4^1/_2$	24348.692	1.12	2
		$5^1/_2$	25488.545		
$4f^{12}(^3F_4)5d_{5/2}\ 6s^2$	$(4,2^1/_2)$	$2^1/_2$	22929.717	1.152	1
		$5^1/_2$	23309.979	1.11	5
		$4^1/_2$	23781.698	1.14	2
		$3^1/_2$	23873.207	1.135	2
		$1^1/_2$	23882.41		
		$6^1/_2$	24137.196	1.128	5
$4f^{13}(^2F_{7/2})6s6p(^1P_1)$	$(3^1/_2,1)$	$2^1/_2$	24418.018	1.06	2
		$3^1/_2$	26701.325	1.076	3
		$4^1/_2$	26889.125	1.11	3
$4f^{12}(^3H_5)5d_{5/2}\ 6s^2$	$(5,2^1/_2)$	$7^1/_2$	25130.453	1.10	
		$3^1/_2$	25717.197	1.02	1
		$2^1/_2$	25745.117	1.09	6
		$4^1/_2$	26646.214	0.961	3
		$6^1/_2$	27377.13	1.12	
		$5^1/_2$	27491.31		
$4f^{13}(^2F_{5/2})6s6p(^3P_0)$	$(2^1/_2,0)$	$2^1/_2$	25656.019	0.724	1
$4f^{13}(^2F_{5/2})6s6p(^3P_1)$	$(2^1/_2,1)$	$2^1/_2$	26126.907	1.10	1
		$3^1/_2$	26439.491	1.000	1
		$1^1/_2$	26488.70	0.85	6
$4f^{13}(^2F_{5/2})6s6p(^3P_2)$	$(2^1/_2,2)$	$0^1/_2$	27314.56	−0.015	6
		$4^1/_2$	28024.01	1.15	6
		$1^1/_2$	28143.67	0.66	6
		$2^1/_2$	28448.585	1.000	6
		$3^1/_2$	28555.799	1.157	6
$4f^{12}(^3H_4)5d_{5/2}\ 6s^2$	$(4,1^1/_2)$	$2^1/_2$	28051.37	0.96	1
		$4^1/_2$	29316.690	0.978	6
		$3^1/_2$	31510.24	1.11	1
$4f^{12}(^3F_3)5d_{3/2}\ 6s^2$	$(3,1^1/_2)$	$3^1/_2$	29260.59	0.928	6
		$2^1/_2$	31431.88	1.07	1
		$4^1/_2$	31440.54	1.13	7
		$1^1/_2$	31520.98	0.79	6
$4f^{12}(^3F_2)5d_{3/2}\ 6s^2$	$(2,1^1/_2)$	$2^1/_2$	30082.18	0.81	6
		$1^1/_2$	30585.65	1.085	7
		$3^1/_2$	32446.26	0.89	1
$4f^{12}(^3H_4)5d_{3/2}\ 6s^2$	$(4,2^1/_2)$	$3^1/_2$	30124.02	0.955	6
		$6^1/_2$	30125.61		
		$2^1/_2$	30302.42	0.91	1
		$4^1/_2$	30915.02	0.99	6
		$5^1/_2$	30972.46		
$4f^{12}(^3F_3)5d_{5/2}\ 6s^2$	$(3,2^1/_2)$	$2^1/_2$	32174.49	1.16	1
		$4^1/_2$	32407.78		
		$3^1/_2$	32811.02	1.04	1
		$1^1/_2$	32928.76	0.935	6
$4f^{12}(^3F_2)5d_{5/2}\ 6s^2$	$(2,2^1/_2)$	$1^1/_2$	33489.36	1.468	6
		$3^1/_2$	33623.78	0.92	6
		$2^1/_2$	35026.22	1.022	6
$4f^{13}(^2F_{5/2})6s6p(^1P_1)$	$(2^1/_2,1)$	$2^1/_2$	34085.20	0.95	1
		$3^1/_2$	34297.17	0.915	1
		$1^1/_2$	35089.67	0.85	6
		$2^1/_2$	35261.762	1.346	
		$2^1/_2$	37064.18	1.42	
		$1^1/_2$	37138.57	1.56	
		$4^1/_2$	37576.866	1.19	
		$4^1/_2$	37711.074	1.14	
		$2^1/_2$	37724.84		
		$4^1/_2$	37946.39		
$4f^{12}(^1G_4)5d_{5/2}\ 6s^2$	$(4,2^1/_2)$	$2^1/_2$	38014.37	1.11	
		$3^1/_2$	38342.57	1.108	
		$1^1/_2$	39514.74	0.80	
		$4^1/_2$	39768.79		
$4f^{12}(^1G_4)5d_{3/2}\ 6s^2$	$(4,1^1/_2)$	$4^1/_2$	38120.71		
		$3^1/_2$	39560.41	0.895	7
		$2^1/_2$	40787.24	0.91	6
		$3^1/_2$	38123.02	1.14	
		$2^1/_2$	38128.37	1.05	
		$1^1/_2$	38237.89	1.04	

TABLE 1. *Energy levels of neutral thulium, even parity, in units of cm^{-1}. Ref. is given for levels previously published*—Continued

Configuration	Designation	J	Energy	g-Factor	Ref
$4f^{13}(^2F_{7/2})5d6p(^3F_2)$	$(3^1/_2,2)$	$1^1/_2$	38318.62	1.195	
		$2^1/_2$	39547.31	1.285	
		$5^1/_2$	40128.384	1.10	
		$3^1/_2$	40802.56	1.185	
		$4^1/_2$	41074.45	1.07	
		$2^1/_2$	38433.92		
		$4^1/_2$	38502.00	1.10	6
		$2^1/_2$	38696.79		
		$5^1/_2$	38844.072	1.08	
		$4^1/_2$	39123.17		
		$2^1/_2$	39161.45		
		$4^1/_2$	39206.84		
		$2^1/_2$	39259.92	1.20	
		$1^1/_2$	39635.56	1.34	
		$4^1/_2$	39698.70		
		$3^1/_2$	39847.04	1.285	
		$5^1/_2$	39942.571	1.191	
		$3^1/_2$	39996.221		
		$2^1/_2$	40066.70	1.36	
		$1^1/_2$	40091.58	1.13	
		$4^1/_2$	40101.72		
		$3^1/_2$	40360.37		
		$5^1/_2$	40503.326	1.105	
		$4^1/_2$	40516.66		
		$4^1/_2$	40563.90		
		$2^1/_2$	40584.52		
		$6^1/_2$	40586.40	1.175	
		$3^1/_2$	40649.441		
$4f^{13}(^2F_{7/2})5d6p(^3F_3)$	$(3^1/_2,3)$	$1^1/_2$	40693.63	1.31	
		$0^1/_2$	41089.05	1.50	
		$6^1/_2$	41469.44	1.15	
		$5^1/_2$	42429.385	1.19	
		$2^1/_2$	42596.49		
		$4^1/_2$	42764.664		
		$3^1/_2$	42783.46		
		$6^1/_2$	40855.53	1.17	
		$3^1/_2$	41144.66		
		$4^1/_2$	41151.10		
		$6^1/_2$	41193.16	1.17	
		$5^1/_2$	41352.806	1.07	
		$4^1/_2$	41391.10	1.17	
		$5^1/_2$	41430.237		
$4f^{13}(^2F_{7/2})5d6p(^1D_2)$	$(3^1/_2,2)$	$2^1/_2$	41493.034	1.29	
		$5^1/_2$	42080.152	1.12	
		$1^1/_2$	42357.42	1.18	
		$4^1/_2$	42667.745	1.10	
		$3^1/_2$	43098.19		
$4f^{13}(^2F_{7/2})5d6p(^3D_1)$	$(3^1/_2,1)$	$2^1/_2$	41544.59	1.25	
		$4^1/_2$	42139.01	1.06	
		$3^1/_2$	42543.119	1.12	
$4f^{13}(^2F_{7/2})5d6p(^3P_1)$	$(3^1/_2,1)$	$3^1/_2$	41617.243	1.29	
		$5^1/_2$	41700.222	1.13	
		$4^1/_2$	41728.003	1.06	
		$2^1/_2$	41751.03	1.08	
		$2^1/_2$	41836.02		
		$2^1/_2$	42198.77	1.25	
		$3^1/_2$	42325.81		
		$6^1/_2$	42456.47	1.20	
		$6^1/_2$	42545.150		
		$4^1/_2$	42576.01		
		$5^1/_2$	42595.791	1.20	
		$4^1/_2$	42718.44	1.12	
$4f^{13}(^2F_{7/2})5d6p(^3F_4)$	$(3^1/_2,4)$	$7^1/_2$	42733.10	1.19	
		$1^1/_2$	43800.88	1.21	
		$2^1/_2$	43958.23	1.11	
		$3^1/_2$	44265.285	1.10	
		$5^1/_2$	44417.48	1.17	
		$4^1/_2$	44582.64	1.07	
		$5^1/_2$	42868.255		
		$6^1/_2$	42869.748		
		$2^1/_2$	42876.38		
		$4^1/_2$	42902.55		
		$3^1/_2$	42952.02	1.14	
		$5^1/_2$	42957.138		
		$2^1/_2$	42957.52		
		$2^1/_2$	43056.22		
		$4^1/_2$	43115.42		
		$1^1/_2$	43160.53		
$4f^{13}(^2F_{7/2})5d6p(^3D_2)$	$(3^1/_2,2)$	$5^1/_2$	43196.848		
		$1^1/_2$	43221.84	1.20	
		$2^1/_2$	43481.28		
		$4^1/_2$	43755.64	1.08	
		$3^1/_2$	43981.104		
		$2^1/_2$	43243.00		
		$4^1/_2$	43292.24		
		$3^1/_2$	43303.151		
		$2^1/_{62}$	43318.02		
		$4^1/_2$	43354.65		
		$4^1/_2$	43464.15		
		$3^1/_2$	43514.41		
		$2^1/_2$	43571.61		
		$3^1/_2$	43590.42		
		$5^1/_2$	43715.572		

TABLE 1. *Energy levels of neutral thulium, even parity, in units of cm^{-1}. Ref. is given for levels previously published*—Continued

Configuration	Designation	J	Energy	g-Factor	Ref.
$4f^{13}(^2F_{7/2})5d6p(^3D_3)$	(3½,3)	5½	43788.44	1.17	
		6½	43836.666	1.18	
		4½	44380.90	1.15	
		2½	44518.91	1.205	
		1½	44545.90	1.10	
		3½	44750.078	1.16	
		2½	43859.06	1.11	
		3½	44206.39	1.04	
		4½	44238.85		
		2½	44243.40		
		5½	44276.41	1.16	
		3½	44323.00	1.09	
		6½	44515.01	1.125	
		3½	44529.428	0.95	
		4½	44689.913		
		3½	44891.22		
		4½	44919.302	1.19	
		3½	45018.23		
		4½	45091.022	1.04	
$4f^{13}(^2F_{7/2})5d6p(^3P_0)$	(3½,0)	3½	45131.67		
		3½	45149.63		
		5½	45714.11		
$4f^{13}(^2F_{7/2})5d6p(^3P_2)$	(3½,2)	5½	46262.14	1.15	
		4½	48547.98		

TABLE 2. *Energy levels of neutral thulium, odd parity, in units of cm^{-1}. Ref. is given for levels previously published*

Configuration	Designation	J	Energy	g-Factor	Ref.
$4f^{13}\,6s^2$	^{2}F°	3½	0.000	1.143	1
		2½	8771.243	0.855	1
$4f^{13}(^2F_{7/2})5d6s(^3D)$	$^3[1^1/_2]°$	2½	20406.840	1.58	5
		1½	21799.380	1.45	5
		0½	24160.63	1.010	5
	$^3[5^1/_2]°$	4½	22419.764	0.934	6
		5½	22559.502	1.15	7
		6½	22742.777	1.198	5
$4f^{12}(^3H_6)6s^2\ 6p_{1/2}$	$(6,^1/_2)°$	5½	22468.046	1.21	7
		6½	22902.127	1.138	5
$4f^{13}(^2F_{7/2})5d6s(^3D)$	$^3[2^1/_2]°$	3½	23335.111	1.362	6
		2½	23431.844	1.22	6
		1½	23574.415	0.83	5
	$^3[3^1/_2]°$	4½	23941.071	1.29	6
		2½	24611.303	0.92	6
		3½	24708.041	1.08	5
	$^3[4^1/_2]°$	3½	24246.425	1.02	6
		4½	24701.058	1.145	6
		5½	24957.469	1.235	5
$4f^{13}(^2F_{7/2})5d6s(^1D)$	$^1[1^1/_2]°$	1½	25207.732	1.365	5
	$^1[5^1/_2]°$	5½	25520.987	1.10	6
$4f^{12}(^3H_6)6s^2\ 6p_{3/2}$	$(6,1^1/_2)°$	7½	25536.116	1.20	5
		4½	25699.714	1.12	6
		6½	26357.736	1.188	7
		5½	26368.412	1.125	6
$4f^{13}(^2F_{7/2})5d6s(^1D)$	$^1[2^1/_2]°$	2½	26448.274	1.14	5
	$^1[3^1/_2]°$	3½	27037.468	1.11	5
	$^1[4^1/_2]°$	4½	27440.858		6
$4f^{12}(^3F_4)6s^2\ 6p_{1/2}$	$(4,^1/_2)°$	3½	28340.29		5
		4½	28514.423	1.085	5
$4f^{12}(^3H_6)5d6s6p(^4F_{3/2})$	$(6,1^1/_2)°$	4½	29308.69	1.49	7
		5½	31080.846	1.37	
		7½	32112.98	0.98	
		6½	32950.10	1.31	
$4f^{13}(^2F_{5/2})5d6s(^3D)$	$^3[4^1/_2]°$	3½	30921.58	0.69	5
		4½	31388.303	0.98	5
		5½	32107.268	1.115	5
$4f^{12}(^3H_5)6s^2\ 6p_{1/2}$	$(5,^1/_2)°$	4½	30947.175		5
		5½	31007.60	1.00	5
$4f^{12}(^3H_6)5d6s6p(^4F_{5/2})$	$(6,2^1/_2)°$	3½	31367.728	1.33	
		4½	32441.714	1.25	
		8½	32761.54	1.11	
		5½	33793.154	1.24	
		7½	34046.54	1.18	
		6½	34449.774	1.18	
$4f^{12}(^3F_4)6s^2\ 6p_{3/2}$	$(4,1^1/_2)°$	4½	31454.298		5
		5½	31519.495		5
		2½	31593.70		5
		3½	31694.749	1.17	5
$4f^{13}(^2F_{5/2})5d6s(^3D)$	$^3[1^1/_2]°$	1½	31499.06	1.33	6
	$^3[1^1/_2]°$	2½	31773.78	1.23	5
		1½	32780.04	1.05	5
	$^3[2^1/_2]°$	1½	32181.49	0.725	6
		2½	32856.613	1.051	5
		3½	33240.362	1.17	5
$4f^{13}(^2F_{7/2})6s7s(^3S_1)$	$(3^1/_2,1)°$	4½	32217.195	1.333	2
		3½	32359.372	1.195	2
		2½	32479.326	0.89	2
$4f^{13}(^2F_{5/2})5d6s(^3D)$	$^3[3^1/_2]°$	2½	33292.78	0.624	5
		3½	33395.984		
		4½	33726.70	1.14	
$4f^{12}(^3H_6)5d6s6p(^4D_{1/2})$	$(6,^1/_2)°$	5½	33638.74	1.42	
		6½	33812.149	1.15	
$4f^{12}(^3H_6)5d6s6p(^4F_{7/2})$	$(6,3^1/_2)°$	9½	33644.74	1.18	
		2½	34194.09	1.24	
		7½	36273.94	1.13	
$4f^{12}(^3H_5)6s^2\ 6p_{3/2}$	$(5,1^1/_2)°$	3½	33778.36		
		6½	33943.282	1.13	5
		4½	34310.330	0.995	5
		5½	34532.898	1.126	5
$4f^{13}(^2F_{7/2})6s7s(^1S_0)$	$(3^1/_2,0)°$	3½	33961.044	1.15	6
$4f^{13}(^2F_{5/2})5d6s(^1D)$	$^1[^1/_2]°$	0½	34069.26	0.666	6
	$^1[4^1/_2]°$	4½	34587.982	1.00	5
	$^1[1^1/_2]°$	1½	34999.008	0.897	5
	$^1[2^1/_2]°$	2½	35673.62		
	$^1[3^1/_2]°$	3½	36435.78		
$4f^{12}(^3H_6)5d6s6p(^4D_{5/2})$	$(6,2^1/_2)°$	3½	34365.624	1.205	
		4½	35054.681	1.28	
		6½	35958.880	1.134	
		7½	36179.60	1.155	
		5½	36329.786	1.035	
$4f^{12}(^3H_6)5d6s6p(^4D_{3/2})$	$(6,1^1/_2)°$	4½	34457.853	1.185	
		5½	34691.802	1.16	
		7½	35557.70	1.255	
$4f^{12}(^3H_4)6s^2\ 6p_{1/2}$	$(4,^1/_2)°$	4½	35363.77	0.91	
		3½	35389.94	0.965	
$4f^{12}(^3H_6)5d6s6p(^2D_{5/2})$	$(6,2^1/_2)°$	8½	35633.01	1.18	
		7½	37159.51	1.225	

TABLE 2. *Energy levels of neutral thulium, odd parity, in units of cm^{-1}. Ref. is given for levels previously published*—Continued

Configuration	Designation	J	Energy	g-Factor	Ref.
$4f^{12}\ 5d6s6p$		$3^1/_2$	35682.251	1.222	
		$6^1/_2$	36223.628	1.12	
		$4^1/_2$	36377.733	1.21	
$4f^{12}(^3H_6)5d6s6p(^2D_{3/2})$	$(6,1^1/_2)°$	$7^1/_2$	36653.924	1.13	
$4f^{12}\ 5d6s6p$		$5^1/_2$	36656.724	1.16	
		$3^1/_2$	36934.216	1.285	
		$4^1/_2$	37010.534	1.11	
$4f^{12}(^3F_3)6s^2\ 6p_{1/2}$	$(3,^1/_2)°$	$3^1/_2$	37221.455		
$4f^{12}(^3H_6)5d6s6p(^4D_{7/2})$	$(6,3^1/_2)°$	$8^1/_2$	37252.03	1.20	
		$7^1/_2$	37858.62	1.20	
$4f^{12}\ 5d6s6p$		$5^1/_2$	37276.778	1.25	
		$6^1/_2$	37365.13	1.20	
		$3^1/_2$	37519.484	1.09	
		$6^1/_2$	37646.186	1.175	
		$5^1/_2$	37657.928	1.01	
		$4^1/_2$	37768.662	1.215	
		$6^1/_2$	38012.795	1.09	
		$5^1/_2$	38161.255	1.125	
		$3^1/_2$	38211.625	1.175	
$4f^{12}(^3H_4)6s^2\ 6p_{3/2}$	$(4,1^1/_2)°$	$5^1/_2$	38347.875	1.07	
		$3^1/_2$	38664.184	1.042	
		$4^1/_2$	38685.555	1.043	
$4f^{12}\ 5d6s6p$		$4^1/_2$	38384.926	1.134	
		$3^1/_2$	38482.584	1.25	
$4f^{12}(^3H_6)5d6s6p(^4F_{9/2})$	$(6,4^1/_2)°$	$7^1/_2$	38485.85	1.145	
$4f^{12}\ 5d6s6p$		$4^1/_2$	38499.016	1.064	
		$5^1/_2$	38529.686	1.17	
		$6^1/_2$	38588.46	1.212	
		$2^1/_2$	38751.812	1.215	
$4f^{13}(^2F_{7/2})6s6d(^3D)$	$^3[1^1/_2]°$	$2^1/_2$	38861.937	1.565	7
		$1^1/_2$	39602.902	1.30	7
		$0^1/_2$	39737.58	0.81	
$4f^{12}\ 5d6s6p$		$5^1/_2$	38877.211	1.065	
		$6^1/_2$	38915.90	1.22	
$4f^{13}(^2F_{7/2})6s6d(^1D)$	$^1[1^1/_2]°$	$1^1/_2$	39061.819	1.34	
	$^1[5^1/_2]°$	$5^1/_2$	39362.651	1.13	2
	$^1[2^1/_2]°$	$2^1/_2$	39470.489	1.04	
	$^1[3^1/_2]°$	$3^1/_2$	39542.165	1.06	
	$^1[4^1/_2]°$	$4^1/_2$	39741.913	1.112	2
$4f^{13}(^2F_{7/2})6s6d(^3D)$	$^3[5^1/_2]°$	$5^1/_2$	39089.533	1.09	2
		$6^1/_2$	39157.57	1.24	6
		$4^1/_2$	39220.035	1.12	2
	$^3[2^1/_2]°$	$3^1/_2$	39187.473	1.336	
		$2^1/_2$	39277.087	1.184	2
		$1^1/_2$	39419.90	0.916	7
$4f^{12}\ 5d6s6p$		$4^1/_2$	39244.584	1.05	2
$4f^{13}(^2F_{7/2})6s6d(^3D)$	$^3[3^1/_2]°$	$4^1/_2$	39322.014	1.153	
		$3^1/_2$	39462.782	1.12	
		$2^1/_2$	39658.852	0.96	
$4f^{12}\ 5d6s6p$		$2^1/_2$	39386.959	0.982	
		$3^1/_2$	39413.672	1.165	
		$6^1/_2$	39434.151	1.15	
$4f^{13}(^2F_{7/2})6s6d(^3D)$	$^3[4^1/_2]°$	$4^1/_2$	39444.295	1.13	
		$5^1/_2$	39479.873	1.21	
		$3^1/_2$	39627.996	1.04	
$4f^{12}\ 5d6s6p$		$3^1/_2$	39480.272	1.17	
		$4^1/_2$	39488.236	1.095	
		$5^1/_2$	39563.003	1.11	
		$5^1/_2$	39709.038	1.17	
$4f^{12}(^3F_3)6s^2\ 6p_{3/2}$	$(3,1^1/_2)°$	$3^1/_2$	40061.324	1.13	
		$4^1/_2$	40208.499	1.18	
$4f^{12}\ 5d6s6p$		$6^1/_2$	40113.75		
		$4^1/_2$	40322.536	1.115	
		$2^1/_2$	40347.267	1.14	
		$6^1/_2$	40376.20		
		$4^1/_2$	40517.661	1.153	
		$3^1/_2$	40533.825	1.24	
		$3^1/_2$	40596.302	1.305	
		$5^1/_2$	40663.129		
		$3^1/_2$	40763.892	1.178	2
		$6^1/_2$	40780.904	1.22	
		$4^1/_2$	40855.580	1.08	
		$2^1/_2$	40938.61	1.20	
$4f^{13}(^2F_{5/2})6s7s(^3S_1)$	$(2^1/_2,1)°$	$1^1/_2$	40989.73	0.40	6
		$2^1/_2$	41074.399	0.99	6
		$3^1/_2$	41189.162	1.19	7
$4f^{12}\ 5d6s6p$		$3^1/_2$	41012.387	1.15	
		$5^1/_2$	41081.384	1.295	
$4f^{13}(^2F_{7/2})6s8s(^3S_1)$	$(3^1/_2,1)°$	$4^1/_2$	41078.537	1.32	7
		$3^1/_2$	41211.943	1.18	6
		$2^1/_2$	41325.87	0.90	7

TABLE 2. *Energy levels of neutral thulium, odd parity, in units of cm⁻¹. Ref. is given for levels previously published*—Continued

Configuration	Designation	J	Energy	g-Factor	Ref.
$4f^{12}(^3F_2)6s^2\ 6p_{3/2}$	$(2,1^1/_2)°$	$3^1/_2$	41085.039	1.005	
$4f^{12}\ 5d6s6p$		$4^1/_2$	41109.364	1.19	
		$4^1/_2$	41124.334	1.244	
$4f^{12}\ 5d6s6p$		$6^1/_2$	41274.90	1.12	
		$8^1/_2$	41299.37	1.08	
$4f^{12}\ 5d6s6p$		$3^1/_2$	41425.474	1.10	
		$3^1/_2$	41525.20	1.105	
		$2^1/_2$	41533.564	1.025	
		$5^1/_2$	41569.114	1.205	
		$4^1/_2$	41576.146	1.249	
$4f^{13}(^2F_{7/2})6s8s(^1S_0)$	$(3^1/_2,0)°$	$3^1/_2$	41646.129	1.16	
$4f^{12}\ 5d6s6p$		$5^1/_2$	41687.404	1.145	
		$1^1/_2$	41743.39	0.913	
		$4^1/_2$	41786.249	1.25	
$4f^{13}(^2F_{7/2})6p^2(^3P_0)$	$(3^1/_2,0)°$	$3^1/_2$	41841.602	1.21	
$4f^{12}\ 5d6s6p$		$5^1/_2$	41874.369	1.16	
$4f^{12}(^3F_4)5d6s6p(^4F_{7/2})$	$(4,3^1/_2)°$	$7^1/_2$	41880.13		
$4f^{12}\ 5d6s6p$		$4^1/_2$	41881.739	1.18	
		$6^1/_2$	41917.235	1.15	
		$5^1/_2$	42119.080	1.10	
		$3^1/_2$	42133.263	1.17	
		$2^1/_2$	42179.886	1.05	
		$2^1/_2$	42367.610	1.20	
		$3^1/_2$	42370.718	1.043	
		$6^1/_2$	42406.656	1.125	
		$5^1/_2$	42541.367	1.10	
		$4^1/_2$	42561.536	1.06	
		$5^1/_2$	42581.974	1.135	
		$4^1/_2$	42594.049	1.09	
		$2^1/_2$	42705.880	1.095	
$4f^{13}(^2F_{5/2})6s7s(^1S_0)$	$(2^1/_2,0)°$	$2^1/_2$	42735.208		
$4f^{12}\ 5d6s6p$		$3^1/_2$	42742.008	1.19	
		$4^1/_2$	42770.792	1.215	
		$4^1/_2$	42839.493	1.086	
$4f^{12}(^3F_4)5d6s6p(^4F_{9/2})$	$(4,4^1/_2)°$	$7^1/_2$	42855.44	1.124	
		$2^1/_2$	42902.504	1.04	
$4f^{12}\ 5d6s6p$		$6^1/_2$	42910.043	1.20	
		$5^1/_2$	42961.884	1.205	
		$4^1/_2$	43030.299	1.143	
		$3^1/_2$	43034.166	1.15	
$4f^{12}(^3H_6)5d6s6p(^2F_{5/2})$	$(6,2^1/_2)°$	$7^1/_2$	43051.55	1.19	
$4f^{13}(^2F_{7/2})6p^2(^3P_1)$	$(3^1/_2,1)°$	$3^1/_2$	43052.541	1.055	
		$4^1/_2$	43429.363	1.20	
		$2^1/_2$	43430.758	1.09	
$4f^{12}\ 5d6s6p$		$2^1/_2$	43113.646	1.114	
		$5^1/_2$	43186.335	1.196	
		$1^1/_2$	43230.70	0.99	
		$6^1/_2$	43288.722	1.175	
		$5^1/_2$	43408.960	1.20	
		$3^1/_2$	43428.780	1.155	
		$6^1/_2$	43438.251	1.23	
		$5^1/_2$	43447.878	1.105	
		$4^1/_2$	43544.574		
		$3^1/_2$	43588.180	1.248	
$4f^{12}(^3H_5)5d6s6p(^4F_{7/2})$	$(5,3^1/_2)°$	$7^1/_2$	43614.261	1.12	
$4f^{12}\ 5d6s6p$		$4^1/_2$	43675.258	1.04	
		$5^1/_2$	43974.645	1.14	
		$6^1/_2$	43979.308		
$4f^{12}(^1G_4)6s^2\ 6p_{1/2}$	$(4,^1/_2)°$	$4^1/_2$	44001.272	1.04	
		$3^1/_2$	44142.395	1.02	
$4f^{12}\ 5d6s6p$		$6^1/_2$	44072.61		
$4f^{13}(^2F_{7/2})6p^2(^3P_2)$	$(3^1/_2,2)°$	$5^1/_2$	44180.935	1.17	
		$4^1/_2$	44316.715	1.15	
		$3^1/_2$	44456.230		
		$1^1/_2$	44483.351	1.005	
		$2^1/_2$	44855.240	1.045	
$4f^{12}\ 5d6s6p$		$2^1/_2$	44182.324	1.17	
$4f^{12}(^3H_5)5d6s6p(^2D_{5/2})$	$(5,2^1/_2)°$	$7^1/_2$	44210.42	1.15	
$4f^{12}\ 5d6s6p$		$3^1/_2$	44263.974	0.905	
		$2^1/_2$	44300.233	1.09	
		$6^1/_2$	44307.188	1.13	
$4f^{12}(^3H_5)5d6s6p(^4F_{9/2})$	$(5,4^1/_2)°$	$9^1/_2$	44334.66	1.18	
$4f^{12}\ 5d6s6p$		$5^1/_2$	44383.637		
		$3^1/_2$	44418.396		
		$6^1/_2$	44418.695	1.13	
$4f^{12}(^3H_6)5d6s6p(^2D_{3/2})$	$(6,1^1/_2)°$	$7^1/_2$	44565.85	1.135	
$4f^{12}(^3H_6)5d6s6p(^2F_{7/2})$	$(6,3^1/_2)$	$8^1/_2$	44571.82	1.18	
$4f^{12}\ 5d6s6p$		$6^1/_2$	44591.133	1.04	
		$5^1/_2$	44747.009	1.17	
		$4^1/_2$	44774.242		
		$6^1/_2$	44803.868	1.105	
		$4^1/_2$	44868.173	1.10	
		$5^1/_2$	45058.379	1.055	

TABLE 2. *Energy levels of neutral thulium, odd parity, in units of cm^{-1}. Ref. is given for levels previously published*—Continued

Configuration	Designation	J	Energy	g-Factor	Ref.
		$4^1/_2$	45070.577		
		$4^1/_2$	45147.300		
		$5^1/_2$	45289.01	1.155	
		$6^1/_2$	45389.06		
		$3^1/_2$	45408.656	1.105	
		$4^1/_2$	45467.723		
		$5^1/_2$	45485.87		
$4f^{12}(^3H_6)5d6s6p(^2F_{5/2})$	$(6,2^1/_2)°$	$7^1/_2$	45557.72	1.164	
$4f^{12}(^3H_5)5d6s6p(^4D_{5/2})$	$(5,2^1/_2)°$	$7^1/_2$	45608.78	1.15	
$4f^{12}$ $5d6s6p$		$5^1/_2$	45635.737	1.14	
		$6^1/_2$	45660.65	1.19	
		$5^1/_2$	45810.508	1.225	
$4f^{12}(^3H_5)5d6s6p(^4D_{7/2})$	$(5,3^1/_2)°$	$7^1/_2$	45934.52	1.165	
$4f^{12}$ $5d6s6p$		$5^1/_2$	46163.587		
		$5^1/_2$	46221.416		
$4f^{12}(^3H_6)5d6s6p(^2F_{7/2})$	$(6,3^1/_2)°$	$7^1/_2$	46461.06	1.18	
		$8^1/_2$	46767.71	1.17	
$4f^{12}$ $5d6s6p$		$6^1/_2$	46597.694	1.18	
		$6^1/_2$	46694.096	1.16	
		$5^1/_2$	46850.44	1.145	
		$6^1/_2$	47027.45	1.17	
		$6^1/_2$	47214.313	1.135	
		$5^1/_2$	47484.84	1.115	
$4f^{12}(^3H_5)5d6s6p(^2F_{5/2})$	$(5,2^1/_2)°$	$7^1/_2$	47630.53	1.162	
$4f^{12}$ $5d6s6p$		$6^1/_2$	47644.931	1.175	
		$6^1/_2$	47759.379	1.16	
$4f^{12}(^3H_4)5d6s6p(^4F_{7/2})$	$(4,3^1/_2)°$	$7^1/_2$	47886.05	1.15	
$4f^{12}$ $5d6s6p$		$6^1/_2$	48115.671	1.17	
		$7^1/_2$	50563.91	1.18	
		$6^1/_2$	51298.366		
		$6^1/_2$	51466.730		
		$5^1/_2$	51756.675		

4. Ionization Energy

An accurate value for the ionization energy of neutral thulium was derived by Camus [23] from his observations of the $4f^{13}(^2F_{7/2})6snp$ series in absorption for $17 \leq n \leq 48$. He obtained the value 49879.5 ± 0.5 cm^{-1}. This supports the value obtained from the $4f^{13}(^2F_{7/2})6sns$ series $(7 \leq n \leq 8)$. From the data reported in table 2 we have:

$$\text{center of gravity } 4f^{13}(^2F_{7/2})6s7s = 32737.9 \text{ cm}^{-1}$$

$$6s8s = 41300.2 \text{ cm}^{-1}.$$

Assuming a change in quantum defect of 1.031 ± 0.005 deduced from the corresponding configurations of Ba I, [25] we obtain a series limit of 49994.4 ± 20 cm^{-1}. Since the limit occurs at 103.7 cm^{-1} above the ground state of Tm II, the ionization energy equals 49891 ± 20 cm^{-1}. We note that this result confirms the predicted value by Reader and Sugar [26] of 49900 ± 160 cm^{-1}, based on interpolation of the $6sns$ series for all the rare earths.

We wish to thank L. J. Radziemski for processing our line list with his computer program (see ref. [24]) to determine the best values for the energy levels.

5. References

[1] Meggers, W. F., Rev. Mod. Phys. **14**, 96 (1942).
[2] Blaise, J., and Vetter, R., Compt. Rend. **256**, 630 (1963).
[3] Bordarier, Y., Vetter, R., and Blaise, J., Jour. de Physique **24**, 1107 (1963).
[4] Sugar, J., J. Opt. Soc. Am. **60**, 454 (1970).
[5] Camus, P., Guelachvilli, G., and Verges, J., Spectr. Act. **24B**, 373 (1969).
[6] Blaise, J., and Camus, P., Compt. Rend. **260**, 4693 (1965).
[7] Camus, P., and Blaise, J., Compt. Rend. **261**, 4359 (1965).
[8] Camus, P., Jour. de Phys. **27**, 717 (1966).
[9] Camus, P., Jour. de Phys. **33**, 203 (1972).
[10] Corliss, C. H., Bozman, W. R., and Westfall, F. O., J. Opt. Soc. Am. **43**, 398 (1953).
[11] Tomkins, F. S., and Fred, M., J. Opt. Soc. Am. **47**, 1087 (1957).
[12] Sugar, J., J. Opt. Soc. Am. **53**, 831 (1963).
[13] Sugar, J., J. Opt. Soc. Am. **55**, 33 (1965).
[14] Tomkins, F. S., and Fred, M., Spectrochim. Acta **6**, 139 (1954).
[15] Tomkins, F. S., and Fred, M., Appl. Opt. **2**, 715 (1963).
[16] Reader. J., Meissner, K. W., and Andrew, K. L., J. Opt. Soc. Am. **50**, 221 (1960).
[17] Van Veld, R. D., and Meissner, K. W., J. Opt. Soc. Am. **46**, 598 (1956).
[18] Meggers, W. F., and Humphreys, C. J., J. Res. Nat. Bur. Stand. (U.S.), **18**, 543 (1937) RP992.
[19] Crosswhite, H. M., Johns Hopkins Spectroscopic Rept. **13** (1958).
[20] Meggers, W. F., and Stanley, R. W., J. Res. Nat. Bur. Stand. (U.S.), **69A** (Phys. and Chem.), No. 2, 109–118 (Mar.–Apr. (1965)).
[21] Sugar, J., J. Res. Nat. Bur. Stand. (U.S.), **66A** (Phys. and Chem.), No. 4, 321–324 (July–Aug. 1962).
[22] Brewer, L., J. Opt. Soc. Am. **61**, 1101 (1971).
[23] Camus, P., Thesis, Orsay (1971).
[24] Radziemski, L. J., Fisher, K. J., Steinhaus, D. W., and Goldman, A. S., Comp. Phys. Comm. **3**, 9 (1972).
[25] Russell H. N., and Moore, C. E., J. Res. Nat. Bur. Stand. (U.S.), **55**, 299 (1955) RP2633.
[26] Reader, J., and Sugar, J., J. Opt. Soc. Am. **56**, 1189 (1966).

(Paper 77A1–752)

Wavelength in air Å	Intensity	Wavenumber cm⁻¹	Classification	Zeeman effect type	f	Je
11749.50	5	8508.67				
11662.00	5*h*	8572.51				
11650.30	4	8581.12				
11649.00	5*h*	8582.08	$33961^{\circ}_{7/2} - 42543_{7/2}$			
11544.00	5	8660.14				
11540.00	5	8663.14	$22791_{7/2} - 31454^{\circ}_{9/2}$			
11538.90	3	8663.97	$22929_{9/2} - 31593^{\circ}_{9/2}$			
11522.70	1	8676.15				
11515.30	50	8681.72	$25130_{13/2} - 33812^{\circ}_{13/2}$			
11496.90	10	8695.62	$17752_{5/2} - 26448^{\circ}_{5/2}$			
11452.30	1	8729.48				
11434.90	200	8742.76	$16957_{7/2} - 25699^{\circ}_{9/2}$			
11423.20	1	8751.72				
11419.20	10	8754.78	$17613_{9/2} - 26368^{\circ}_{11/2}$			
11405.90	7	8764.99	$22929_{9/2} - 31694^{\circ}_{7/2}$			
11397.80	1	8771.22				
11395.80	1	8772.76	$28448_{9/2} - 37221^{\circ}_{7/2}$			
11387.40	4	8779.23				
11357.30	3	8802.50	$22791_{7/2} - 31593^{\circ}_{9/2}$			
"			$27377_{13/2} - 36179^{\circ}_{13/2}$			
11344.00	30	8812.82	$25130_{13/2} - 33943^{\circ}_{13/2}$			
"			$24137_{13/2} - 32950^{\circ}_{13/2}$			
11332.50	5	8821.76	$25488_{11/2} - 34310^{\circ}_{9/2}$			
11285.80	3	8858.27				
11284.10	4	8859.60				
11269.90	6	8870.76	$25717_{7/2} - 34587^{\circ}_{9/2}$			
11268.20	8	8872.10	$26126_{9/2} - 34999^{\circ}_{9/2}$			
11261.40	2	8877.46	$25207^{\circ}_{9/2} - 34085_{9/2}$			
11229.20	100	8902.92	$17454_{13/2} - 26357^{\circ}_{13/2}$			
11228.40	10	8903.55	$22791_{7/2} - 31694^{\circ}_{7/2}$			
11215.70	200	8913.63	$17454_{13/2} - 26368^{\circ}_{11/2}$			
11207.00	2	8920.55	$35261_{9/2} - 44182^{\circ}_{9/2}$			
11202.40	2	8924.22	$26439_{7/2} - 35363^{\circ}_{9/2}$			
11175.30	1	8945.86				
11172.50	2	8948.10				
11165.00	70	8954.11				
11164.30	20	8954.67	$31694^{\circ}_{7/2} - 40649_{7/2}$			
11160.80	5	8957.48	$16742_{7/2} - 25699^{\circ}_{9/2}$			
11154.30	1	8962.70				
11153.30	1	8963.50				
11144.40	2	8970.66				
11135.30	40	8977.99	$24418_{9/2} - 33396^{\circ}_{7/2}$			
11131.10	2	8981.38	$8771^{\circ}_{9/2} - 17752_{5/2}$			
11128.55	3*h*	8983.44	$23873_{7/2} - 32856^{\circ}_{9/2}$			
11104.25	2	9003.10				
11100.90	2	9005.81	$39542^{\circ}_{7/2} - 48547_{9/2}$			
11095.60	20	9010.11	$21997_{13/2} - 31007^{\circ}_{11/2}$			
11071.28	2	9029.91				
11069.71	2	9031.19	$29316_{9/2} - 38347^{\circ}_{11/2}$			
11053.60	20	9044.35	$25488_{11/2} - 34583^{\circ}_{11/2}$			
11039.95	20	9055.53				
11029.96	5	9063.73				
11011.15	2000	9079.22	$16456_{17/2} - 25536^{\circ}_{15/2}$			
11006.11	2	9083.37	$21997_{13/2} - 31080^{\circ}_{11/2}$			
10986.66	10	9099.46	$25488_{11/2} - 34587^{\circ}_{9/2}$			
10980.10	100	9104.89	$17343_{7/2} - 26448^{\circ}_{9/2}$			
10972.35	15	9111.32	$30302_{9/2} - 39413^{\circ}_{7/2}$			
10963.91	3	9118.34				
10953.48	10	9127.02				
10917.44	1	9157.15				
10907.07	3	9165.85	$29316_{9/2} - 38482^{\circ}_{7/2}$			
10889.90	4	9180.31				
10869.60	30	9197.45				
10862.75	4	9203.25	$25488_{11/2} - 34691^{\circ}_{11/2}$			
10852.52	10	9211.93				
10851.34	40	9212.93	$28555_{7/2} - 37768^{\circ}_{9/2}$			
10849.05	15	9214.87				
10840.50	2*h*	9222.14				
10838.90	1	9223.50				
10837.30	2*h*	9224.86				
10827.20	30	9233.47				
10812.73	5*h*	9245.83	$33489_{9/2} - 42735^{\circ}_{9/2}$			
10803.30	1	9253.90	$25745_{9/2} - 34999^{\circ}_{9/2}$			
10797.36	3	9258.99				
10786.90	2	9267.97				
10785.90	1	9268.82				
10784.67	4	9269.88	$21737_{9/2} - 31007^{\circ}_{11/2}$			
10767.31	80	9284.83	$17752_{5/2} - 27037^{\circ}_{7/2}$			
10763.70	3	9287.94				
10757.30	2	9293.47	$30915_{9/2} - 40208^{\circ}_{9/2}$			
10749.44	5	9300.26	$13119_{9/2} - 22419^{\circ}_{9/2}$			
10745.85	4	9303.37	$39244^{\circ}_{9/2} - 48547_{9/2}$			
10738.30	1	9309.91				
10727.00	5	9319.72				
10701.75	1	9341.71				
10700.30	8	9342.97	$25656_{9/2} - 34999^{\circ}_{9/2}$			
10694.03	2000	9348.45	$13119_{9/2} - 22468^{\circ}_{11/2}$			
10680.43	40	9360.35	$24418_{9/2} - 33778^{\circ}_{7/2}$			
10673.60	1	9366.34				
10672.70	6	9367.13	$23873_{7/2} - 33240^{\circ}_{7/2}$			
10670.80	1	9368.80				
10669.80	2	9369.68	$15587_{11/2} - 24957^{\circ}_{13/2}$			
10661.10	4	9377.33	$24246^{\circ}_{7/2} - 33623_{7/2}$			
10653.90	1	9383.66				
10631.55	20*d*	9403.39				
10613.80	2	9419.12				
10606.10	8	9425.95	$22791_{7/2} - 32217^{\circ}_{9/2}$			
10603.50	1	9428.27				
10602.00	7	9429.60	$22929_{9/2} - 32359^{\circ}_{7/2}$			
10590.45	2000	9439.88	$13119_{9/2} - 22559^{\circ}_{11/2}$			
10585.30	6	9444.48	$24348_{9/2} - 33793^{\circ}_{11/2}$			
10569.68	2	9458.43	$39089^{\circ}_{11/2} - 48547_{9/2}$			
10565.00	10	9462.62				
10539.95	20	9485.11				
10533.14	6	9491.24	$16957_{7/2} - 26448^{\circ}_{9/2}$			
10531.20	3	9492.99				
10530.25	3	9493.85				
10520.27	20	9502.86	$18837_{9/2} - 28340^{\circ}_{7/2}$			
10499.11	200	9522.01	$21997_{11/2} - 31519^{\circ}_{11/2}$			
10496.90	7	9524.01	$18990_{11/2} - 28514^{\circ}_{9/2}$			
10476.05	2000	9542.97	$24418_{9/2} - 33961^{\circ}_{7/2}$			
10471.96	5	9546.70	$26126_{9/2} - 35673^{\circ}_{9/2}$			
"			$26889_{9/2} - 36435^{\circ}_{7/2}$			
10454.60	10	9562.55				
10448.46	2	9568.17	$22791_{7/2} - 32359^{\circ}_{7/2}$			
10441.30	1	9574.73				
10400.48	2000	9612.31	$24348_{9/2} - 33961^{\circ}_{7/2}$			
10381.35	10	9630.02	$21737_{9/2} - 31367^{\circ}_{7/2}$			
10365.44	10	9644.80	$25745_{9/2} - 35389^{\circ}_{7/2}$			
10359.19	4	9650.62	$21737_{9/2} - 31388^{\circ}_{9/2}$			
10353.10	1	9656.30				
10348.50	40	9660.59	$18853_{11/2} - 28514^{\circ}_{9/2}$			
10343.88	200	9664.90				
10341.75	1	9666.89				
10334.53	2	9673.65	$31519^{\circ}_{11/2} - 41193_{13/2}$			
10319.12	6	9688.09	$22791_{7/2} - 32479^{\circ}_{9/2}$			
10316.32	4	9690.72	$30972_{11/2} - 40663^{\circ}_{11/2}$			
10312.75	200	9694.08	$17343_{7/2} - 27037^{\circ}_{7/2}$			
10300.07	3	9706.01	$16742_{7/2} - 26448^{\circ}_{9/2}$			
10288.86	80	9716.59	$21737_{9/2} - 31454^{\circ}_{9/2}$			
10282.10	1	9722.98				
10269.68	2	9734.73				
10229.61	20*h*	9772.87	$29316_{9/2} - 39089^{\circ}_{11/2}$			
10225.17	3*h*	9777.11	$32928_{9/2} - 42705^{\circ}_{9/2}$			
10220.30	100	9781.77	$21737_{9/2} - 31519^{\circ}_{11/2}$			
10216.05	1	9785.84				
10197.54	2	9803.60				
10194.60	30	9806.43	$32928_{9/2} - 42735^{\circ}_{9/2}$			
10182.06	20	9818.50	$25207^{\circ}_{9/2} - 35026_{9/2}$			
10173.95	4	9826.33	$21120_{7/2} - 30947^{\circ}_{9/2}$			

Wavelength in air Å	Intensity	Wavenumber cm⁻¹	Classification	Zeeman effect type	f	Je
10173.04	200	9827.21	$17613_{9/2} - 27440^{\circ}_{9/2}$			
10162.57	9	9837.33				
10155.20	2	9844.47				
10149.19	2	9850.30	$22929_{5/2} - 32780^{\circ}_{3/2}$			
10134.00	2 *h*	9865.07				
10088.78	6 *h*	9909.29	$24137_{13/2} - 34046^{\circ}_{13/2}$			
10067.80	1	9929.93				
10064.53	70	9933.16	$15587_{11/2} - 25520^{\circ}_{11/2}$			
10058.00	2	9939.61				
10051.04	2	9946.49				
10049.93	8	9947.59	$24418_{9/2} - 34365^{\circ}_{7/2}$			
10047.57	9	9949.93	$31519^{\circ}_{11/2} - 41469_{13/2}$			
10041.83	2	9955.62				
10040.37	30	9957.06	$21737_{9/2} - 31694^{\circ}_{7/2}$			
10035.76	10	9961.64	$24348_{9/2} - 34310^{\circ}_{9/2}$			
10032.31	2 *h*	9965.06	$25717_{7/2} - 35682^{\circ}_{7/2}$			
10011.38	5	9985.90				
10009.37	2 *h*	9987.90				
9971.06	2 *h*	10026.28	$25656_{9/2} - 35682^{\circ}_{7/2}$			
9951.47	20	10046.01	$29316_{9/2} - 39362^{\circ}_{11/2}$			
9943.55	1	10054.01	$25207^{\circ}_{9/2} - 35261_{9/2}$			
9928.65	1	10069.10				
9920.11	50	10077.77				
9917.45	10	10080.47	$16957_{7/2} - 27037^{\circ}_{7/2}$			
9910.20	1000	10087.85	$23873_{7/2} - 33961^{\circ}_{7/2}$			
9905.33	4	10092.81				
9900.72	80	10097.51	$17343_{7/2} - 27440^{\circ}_{9/2}$			
9886.58	30	10111.95	$15587_{11/2} - 25699^{\circ}_{9/2}$			
9879.16	6	10119.54				
9871.16	2	10127.74				
9863.14	2	10135.98	$27440^{\circ}_{9/2} - 37576_{9/2}$			
9857.30	1	10141.99				
9851.10	10	10148.37				
9850.14	2	10149.36				
9849.39	2	10150.13				
9833.43	5	10166.60	$27491_{11/2} - 37657^{\circ}_{11/2}$			
9826.44	3	10173.84				
9821.14	800	10179.33	$23781_{9/2} - 33961^{\circ}_{7/2}$			
9816.46	20	10184.18	$24348_{9/2} - 34532^{\circ}_{11/2}$			
9787.65	2	10214.16				
9786.37	40	10215.49	$13119_{9/2} - 23335^{\circ}_{7/2}$			
9746.48	3	10257.30				
9739.04	500	10265.14	$15271_{13/2} - 25536^{\circ}_{13/2}$			
9736.87	3	10267.43	$21120_{7/2} - 31388^{\circ}_{9/2}$			
9728.48	100	10276.28				
9717.87	9	10287.50				
9716.50	6	10288.95	$32446_{7/2} - 42735^{\circ}_{9/2}$			
9705.80	3000	10300.29				
9705.62	7	10300.48				
9697.70	2 *h*	10308.90	$26126_{9/2} - 36435^{\circ}_{7/2}$			
9675.50	10	10332.55				
9674.68	30	10333.43	$21120_{7/2} - 31454^{\circ}_{9/2}$			
9665.64	6	10343.09	$24348_{9/2} - 34691^{\circ}_{11/2}$			
9648.92	3	10361.01	$8771^{\circ}_{9/2} - 19132_{9/2}$			
9638.22	3	10372.52				
9616.73	5 *h*	10395.69	$24137_{13/2} - 34532^{\circ}_{11/2}$			
9601.10	20	10412.62				
9589.51	4 *h*	10425.20	$29316_{9/2} - 39741^{\circ}_{9/2}$			
9582.98	150	10432.31	$21161_{9/2} - 31593^{\circ}_{9/2}$			
9578.56	10	10437.12	$23873_{7/2} - 34310^{\circ}_{9/2}$			
9578.21	10	10437.50	$23374_{13/2} - 33812^{\circ}_{13/2}$			
9551.90	20	10466.25	$22929_{9/2} - 33396^{\circ}_{7/2}$			
9545.86	40	10472.87	$21120_{7/2} - 31593^{\circ}_{9/2}$			
9538.05	2 *h*	10481.45	$27377_{13/2} - 37858^{\circ}_{13/2}$			
9532.30	8	10487.77				
9497.14	2	10526.60				
9495.00	10 *w*	10528.97				
9474.82	1	10551.40				
9471.89	6	10554.66	$24137_{13/2} - 34691^{\circ}_{11/2}$			
9466.50	5 *h*	10560.67	$32174_{9/2} - 42735^{\circ}_{9/2}$			
"			$31519^{\circ}_{11/2} - 42080_{11/2}$			
9459.36	6	10568.64	$23374_{13/2} - 33943^{\circ}_{13/2}$			
9437.80	50	10592.78				
9420.61	7 *h*	10612.11				
9409.72	5 *h*	10624.39				
9358.82	5 *h*	10682.18	$27440^{\circ}_{9/2} - 38123_{7/2}$			
9357.20	2 *h*	10684.03				
9344.41	10	10698.65	$16742_{7/2} - 27440^{\circ}_{9/2}$			
9340.00	6 *h*	10703.70				
9330.79	5	10714.27				
9298.73	3 *h*	10751.21	$23781_{9/2} - 34532^{\circ}_{11/2}$			
9295.16	2 *h*	10755.34	$32112^{\circ}_{13/2} - 42868_{11/2}$			
9289.23	2	10762.20				
9288.01	5 *h*	10763.62				
9282.57	800	10769.92	$15587_{11/2} - 26357^{\circ}_{13/2}$			
9275.67	5 *d*	10777.94				
9273.38	200	10780.60	$15587_{11/2} - 26368^{\circ}_{11/2}$			
9238.37	6	10821.45	$13119_{9/2} - 23941^{\circ}_{9/2}$			
9231.58	10	10829.41				
9139.02	6	10939.09				
9063.52	10	11030.21	$33292^{\circ}_{9/2} - 44323_{7/2}$			
9062.62	10	11031.31	$22929_{9/2} - 33961^{\circ}_{7/2}$			
9018.24	3000	11085.60	$27037^{\circ}_{7/2} - 38123_{7/2}$			
9017.33	30	11086.71	$15271_{13/2} - 26357^{\circ}_{13/2}$			
"			$29260_{7/2} - 40347^{\circ}_{9/2}$			
9016.10	10	11088.23				
9015.14	3	11089.41				
8959.48	4	11158.30				
8950.12	9	11169.97	$22791_{7/2} - 33961^{\circ}_{7/2}$			
8895.48	8	11238.58	$21120_{7/2} - 32359^{\circ}_{7/2}$			
8833.13	10	11317.91	$21161_{9/2} - 32479^{\circ}_{9/2}$			
8801.57	10	11358.49	$21120_{7/2} - 32479^{\circ}_{9/2}$			
8800.57	2	11359.78				
8790.54	2	11372.74	$19548_{9/2} - 30921^{\circ}_{7/2}$			
8782.41	20	11383.27	$16957_{7/2} - 28340^{\circ}_{7/2}$			
8680.64	2	11516.73	$23873_{7/2} - 35389^{\circ}_{7/2}$			
8678.80	9	11519.17	$22791_{7/2} - 34310^{\circ}_{9/2}$			
8675.59	4 *h*	11523.43	$25130_{13/2} - 36653^{\circ}_{13/2}$			
"			$33623_{7/2} - 45147^{\circ}_{9/2}$			
8666.23	2	11535.87				
8662.44	10	11540.92	$19466_{13/2} - 31007^{\circ}_{11/2}$			
8650.10	20	11557.39	$16957_{7/2} - 28514^{\circ}_{9/2}$			
8643.60	2	11566.08	$26448^{\circ}_{9/2} - 38014_{9/2}$			
8636.17	3	11576.03				
8635.63	2 *h*	11576.75				
8632.13	50	11581.45	$13119_{9/2} - 24701^{\circ}_{9/2}$			
8626.98	1	11588.36	$13119_{9/2} - 24708^{\circ}_{7/2}$			
8623.97	20	11592.40				
8621.48	2	11595.75				
8619.77	2 *h*	11598.05	$16742_{7/2} - 28340^{\circ}_{7/2}$			
8607.79	30	11614.19	$19466_{13/2} - 31080^{\circ}_{11/2}$			
8604.50	1	11618.63	$21161_{9/2} - 32780^{\circ}_{9/2}$			
8604.10	70	11619.17	$19748_{9/2} - 31367^{\circ}_{7/2}$			
8599.18	5	11625.82				
8592.78	80	11634.48	$19753_{7/2} - 31388^{\circ}_{9/2}$			
8588.88	20	11639.76	$19748_{9/2} - 31388^{\circ}_{9/2}$			
8588.45	1	11640.35				
8563.19	10 *h*	11674.68	$26448^{\circ}_{9/2} - 38123_{7/2}$			
8556.48	2	11683.84	$31080^{\circ}_{11/2} - 42764_{9/2}$			
8555.41	2 *h*	11685.30				
8553.90	2 *h*	11687.36	$23574^{\circ}_{9/2} - 35261_{9/2}$			
8548.18	1	11695.18	$21161_{9/2} - 32856^{\circ}_{9/2}$			
8543.45	2	11701.66	$26646_{9/2} - 38347^{\circ}_{13/2}$			
8529.67	30 *h*	11720.56	$30947^{\circ}_{9/2} - 42667_{9/2}$			
8509.66	20	11748.12				
8500.50	1 *h*	11760.78				
8496.73	5 *h*	11766.00				
8493.16	2 *h*	11770.95	$19748_{9/2} - 31519^{\circ}_{11/2}$			
8479.52	2 *h*	11789.88				
8464.67	1	11810.56				

Wavelength in air Å	Intensity	Wavenumber cm^{-1}	Classification	Zeeman effect type	f	Je	
8461.77	3	11814.61					
8460.53	1	11816.34					
8445.15	20	11837.86	$13119_{9/2} - 24957^{\circ}_{11/2}$				
8435.00	100	11852.11					
8426.92	4 h	11863.47	$25656_{9/2} - 37519^{\circ}_{7/2}$				
8412.43	10	11883.91					
8405.17	10 h	11894.17					
8400.31	2 h	11901.05	$21737_{9/2} - 33638^{\circ}_{11/2}$				
8396.90	1	11905.89	$32359^{\circ}_{7/2} - 44265_{7/2}$				
8379.33	3	11930.85	$25207^{\circ}_{9/2} - 37138_{9/2}$				
8371.09	4 h	11942.59					
8368.83	2	11945.82	$21997_{11/2} - 33943^{\circ}_{13/2}$				
8368.55	3 h	11946.22	$19748_{9/2} - 31694^{\circ}_{7/2}$				
8365.75	200	11950.22	$19548_{9/2} - 31499^{\circ}_{9/2}$				
8351.86	10	11970.09					
8341.12	100 h	11985.50	$27377_{13/2} - 39362^{\circ}_{11/2}$	T	1.13		
8339.33	3 h	11988.08	$26889_{9/2} - 38877^{\circ}_{11/2}$				
8323.19	30 h	12011.32	$25699^{\circ}_{9/2} - 37711_{9/2}$				
8318.79	6	12017.68	$24418_{9/2} - 36435^{\circ}_{7/2}$				
8317.21	4	12019.96	$19753_{7/2} - 31773^{\circ}_{9/2}$				
8313.44	8	12025.41					
8311.32	4	12028.48					
8305.10	1	12037.49					
8303.97	1	12039.12					
8301.70	10	12042.42	$24137_{13/2} - 36179^{\circ}_{13/2}$				
8294.52	200	12052.84	$19466_{13/2} - 31519^{\circ}_{11/2}$				
8292.46	7 h	12055.83	$25520^{\circ}_{11/2} - 37576_{9/2}$				
"			$30124_{7/2} - 42179^{\circ}_{9/2}$				
8277.48	2 h	12077.65					
8267.94	5	12091.59					
8266.72	2 h	12093.37	$18853_{11/2} - 30947^{\circ}_{9/2}$				
8265.35	2	12095.38					
8264.84	6	12096.12					
8258.05	10	12106.07					
8255.50	15	12109.81	$18837_{9/2} - 30947^{\circ}_{9/2}$				
8248.86	4 h	12119.56	$27440^{\circ}_{9/2} - 39560_{7/2}$				
"			$21120_{7/2} - 33240^{\circ}_{7/2}$				
8245.89	40 h	12123.92					
8230.94	2	12145.94	$19548_{9/2} - 31694^{\circ}_{7/2}$				
8225.62	7	12153.80	$18853_{11/2} - 31007^{\circ}_{11/2}$				
8223.29	20	12157.24					
8215.07	2	12169.41	$25488_{11/2} - 37657^{\circ}_{11/2}$				
8214.48	6	12170.28	$36377^{\circ}_{9/2} - 48547_{9/2}$				
8202.10	7	12188.65					
8201.73	1	12189.20	$31007^{\circ}_{11/2} - 43196_{11/2}$				
8201.15	80 h	12190.06	$25520^{\circ}_{11/2} - 37711_{9/2}$				
8194.19	1000	12200.42	$26889_{9/2} - 39089^{\circ}_{11/2}$				
8182.48	8	12217.87					
8179.41	10	12222.46	$27037^{\circ}_{7/2} - 39259_{9/2}$				
8178.84	20 h	12223.31	$21737_{9/2} - 33961^{\circ}_{7/2}$				
8177.74	15 h	12224.96	$19548_{9/2} - 31773^{\circ}_{9/2}$				
8176.34	2 h	12227.05	$18853_{11/2} - 31080^{\circ}_{11/2}$				
8171.58	5	12234.17					
8171.30	1	12234.59	$21161_{9/2} - 33396^{\circ}_{7/2}$				
8167.60	2 h	12240.13					
8165.39	2 h	12243.45	$18837_{9/2} - 31080^{\circ}_{11/2}$				
8163.12	2 h	12246.85					
8162.34	6	12248.02					
8162.05	3 h	12248.46	$26448^{\circ}_{9/2} - 38696_{9/2}$				
8156.43	1	12256.90					
8140.40	50	12281.03	$30125_{13/2} - 42406^{\circ}_{13/2}$				
8119.35	9	12312.87	$21997_{11/2} - 34310^{\circ}_{9/2}$				
8116.52	4	12317.16	$31519^{\circ}_{11/2} - 43836_{13/2}$				
8109.39	2 h	12327.99	$32446_{7/2} - 44774^{\circ}_{9/2}$				
8107.02	8	12331.60					
8102.81	1	12338.01					
8095.19	9	12349.62	$8771^{\circ}_{9/2} - 21120_{7/2}$				
8093.82	1 h	12351.71	$16957_{7/2} - 29308^{\circ}_{9/2}$				
8089.20	40	12358.76	$19748_{9/2} - 32107^{\circ}_{11/2}$				
8083.92	100	12366.84	$19132_{9/2} - 31499^{\circ}_{9/2}$	ΔJ=0	0.88	1.33	*
8075.40	150	12379.88		SI	1.60	0.50	
8074.23	6	12381.68					
8073.43	3 h	12382.90					
8068.70	150	12390.16	$8771^{\circ}_{9/2} - 21161_{9/2}$	ΔJ=0	0.85	1.13	*
8063.67	1	12397.89	$18990_{11/2} - 31388^{\circ}_{9/2}$				
8061.40	100	12401.38	$13119_{9/2} - 25520^{\circ}_{11/2}$	S0	1.309	1.10	*
8056.45	1	12409.00	$32446^{\circ}_{7/2} - 44855^{\circ}_{9/2}$				
8045.82	10	12425.40	$25520^{\circ}_{11/2} - 37946_{9/2}$				
8040.09	1 h	12434.25					
8038.66	1	12436.46	$30972_{11/2} - 43408^{\circ}_{11/2}$				
8034.23	40 h	12443.32	$26646_{9/2} - 39089^{\circ}_{11/2}$	SI	?	0.37	
8028.44	1	12452.30	$21997_{11/2} - 34449^{\circ}_{13/2}$				
8021.33	200 h	12463.33	$19753^{\circ}_{7/2} - 32217^{\circ}_{9/2}$	SI	1.182	1.33	*
8017.90	20000	12468.66	$19748_{9/2} - 32217^{\circ}_{9/2}$	ΔJ=0	1.32	0.20	
8014.77	2000	12473.53	$26889_{9/2} - 39362^{\circ}_{11/2}$	T	1.20	0.08	
8006.55	1	12486.34	$26357^{\circ}_{13/2} - 38844_{11/2}$				
8004.15	1	12490.08	$28448_{9/2} - 40938^{\circ}_{9/2}$				
7994.89	2	12504.55	$23873^{\circ}_{7/2} - 36377^{\circ}_{9/2}$				
7991.47	100 h	12509.90	$27037^{\circ}_{7/2} - 39547_{9/2}$	S0	1.09	1.26	*
7985.93	300 h	12518.58	$28555_{7/2} - 41074^{\circ}_{9/2}$	SI	1.16	0.985	*
7983.14	2 h	12522.96	$27037^{\circ}_{7/2} - 39560_{7/2}$				
7981.43	2 h	12525.64	$29260_{7/2} - 41786^{\circ}_{9/2}$				
7979.22	7	12529.11	$18990_{11/2} - 31519^{\circ}_{11/2}$				
7978.44	50	12530.33	$18837_{9/2} - 31367^{\circ}_{7/2}$	S0	1.145	1.325	*
7975.79	2	12534.50	$18853_{11/2} - 31388^{\circ}_{9/2}$				
7975.19	4	12535.44	$21997_{11/2} - 34532^{\circ}_{11/2}$				
7971.56	200 h	12541.15	$28448_{9/2} - 40989^{\circ}_{9/2}$	SI	1.01	0.40	*
7970.23	6 h	12543.24	$26701_{7/2} - 39244^{\circ}_{9/2}$				
7967.13	1 h	12548.12	$23781_{9/2} - 36329^{\circ}_{11/2}$				
7962.63	60 h	12555.21	$26889_{9/2} - 39444^{\circ}_{9/2}$	ΔJ=0	1.13	0.12	
7951.60	4	12572.63	$21737_{9/2} - 34310^{\circ}_{9/2}$				
"			$22791_{7/2} - 35363^{\circ}_{9/2}$				
7949.63	40 h	12575.74	$26701^{\circ}_{7/2} - 39277^{\circ}_{9/2}$				
7946.88	30	12580.09	$13119_{9/2} - 25699^{\circ}_{9/2}$				
7940.14	70 h	12590.77	$26889_{9/2} - 39479^{\circ}_{11/2}$				
7934.84	100 h	12599.18	$26889_{9/2} - 39488^{\circ}_{9/2}$	T	1.09		
7934.00	4	12600.52	$18853_{11/2} - 31454^{\circ}_{9/2}$				
7930.84	30000	12605.54	$19753^{\circ}_{7/2} - 32359^{\circ}_{7/2}$	T	1.18		
7927.51	20000	12610.83	$19748_{9/2} - 32359^{\circ}_{7/2}$	SI	1.29	1.195	*
7923.65	6	12616.98					
7922.14	15 h	12619.38	$24957^{\circ}_{11/2} - 37576_{9/2}$				
7918.10	600	12625.82	$28448_{9/2} - 41074^{\circ}_{9/2}$	ΔJ=0	1.00	0.06	
7916.76	2 h	12627.96	$21737_{9/2} - 34365^{\circ}_{7/2}$				
7913.80	100	12632.68	$19548_{9/2} - 32181^{\circ}_{9/2}$	SI	0.98	0.70	*
7913.43	100 h	12633.27	$28555_{7/2} - 41189^{\circ}_{7/2}$	ΔJ=0	1.18	0.09	
7908.86	2	12640.57	$19466_{13/2} - 32107^{\circ}_{11/2}$				
7905.25	20	12646.34	$19466_{13/2} - 32112^{\circ}_{13/2}$				
7901.10	60 h	12652.99	$26889_{9/2} - 39542^{\circ}_{7/2}$	T	1.15		
7899.17	400 h	12656.08	$28555^{\circ}_{7/2} - 41211^{\circ}_{7/2}$	T	1.17		
7898.26	2	12657.53	$21120_{7/2} - 33778^{\circ}_{7/2}$				
7893.18	8	12665.68	$18853_{11/2} - 31519^{\circ}_{11/2}$				
7888.08	9 h	12673.87	$26889_{9/2} - 39563^{\circ}_{11/2}$				
7880.77	30 h	12685.63	$26701^{\circ}_{7/2} - 39386^{\circ}_{9/2}$				
7879.58	9	12687.54	$27440^{\circ}_{9/2} - 40128_{11/2}$				
7879.35	2	12687.91	$19753^{\circ}_{7/2} - 32441^{\circ}_{9/2}$				
7876.07	100	12693.20	$19748_{9/2} - 32441^{\circ}_{9/2}$	ΔJ=0	1.25	0.15	
7875.43	2 h	12694.23					
7869.99	2	12703.00					
7863.69	3 h	12713.18	$26448^{\circ}_{9/2} - 39161_{9/2}$				
7861.94	40	12716.01					
7861.67	50 h	12716.45	$26646_{9/2} - 39362^{\circ}_{11/2}$				
7856.08	5000	12725.49	$19753^{\circ}_{7/2} - 32479^{\circ}_{9/2}$	SI	1.18	0.89	*
7845.31	100 h	12742.96	$26701^{\circ}_{7/2} - 39444^{\circ}_{9/2}$	SI	1.24	0.12	
7839.42	3	12752.54	$22929_{9/2} - 35682^{\circ}_{7/2}$				
7838.78	20	12753.58	$24957^{\circ}_{11/2} - 37711_{9/2}$				
7838.05	5	12754.77	$26368^{\circ}_{11/2} - 39123_{9/2}$				
7833.94	50 h	12761.46	$26701^{\circ}_{7/2} - 39462^{\circ}_{7/2}$	ΔJ=0	1.08	0.08	
7831.53	1	12765.39	$25717^{\circ}_{7/2} - 38482^{\circ}_{7/2}$				
7829.22	100 h	12769.15	$26701^{\circ}_{7/2} - 39470^{\circ}_{9/2}$	T	1.13		
7823.22	7	12778.94	$26701^{\circ}_{7/2} - 39480^{\circ}_{7/2}$				

APPENDIX—*Spectral Lines of Neutral Thulium*—Continued

Wavelength in air Å	Intensity	Wavenumber cm⁻¹	Classification	Zeeman effect type	f	Je	
7818.35	70 *h*	12786.90	$26701_{7/2} - 39488^{\circ}_{9/2}$	T	1.05		
7813.27	2 *h*	12795.22	$21737_{9/2} - 34532^{\circ}_{11/2}$				
7811.52	7 *h*	12798.08	$26646_{9/2} - 39444^{\circ}_{9/2}$				
7810.60	5 *h*	12799.59	$21161_{3/2} - 33961^{\circ}_{7/2}$				
7808.24	2 *h*	12803.46	$24418_{5/2} - 37221^{\circ}_{7/2}$				
7807.34	2 *h*	12804.94	$23374_{13/2} - 36179^{\circ}_{13/2}$				
7803.93	1000	12810.53	$19548_{9/2} - 32359^{\circ}_{7/2}$	SI	0.97	1.19	*
7791.23	2	12831.41					
7785.90	150 *h*	12840.20	$21120_{7/2} - 33961^{\circ}_{7/2}$	ΔJ=0	1.15	0.09	
7785.51	200 *h*	12840.84	$26701_{7/2} - 39542^{\circ}_{7/2}$	ΔJ=0	1.07	0.11	
7782.35	500	12846.05	$28143_{5/2} - 40989^{\circ}_{5/2}$	ΔJ=0	0.66	0.40	*
7778.27	300 *h*	12852.79	$26889_{9/2} - 39741^{\circ}_{9/2}$	T	1.11		
7775.49	40	12857.39	$18837_{9/2} - 31694^{\circ}_{7/2}$	S0	0.98	0.15	
7764.37	40 *h*	12875.80	$24701^{\circ}_{9/2} - 37576_{9/2}$	ΔJ=0	1.15	0.15	
7754.67	1	12891.91					
7750.26	1	12899.24	$23374_{13/2} - 36273^{\circ}_{13/2}$				
7740.31	2	12915.83	$28514^{\circ}_{9/2} - 41430_{11/2}$				
7733.80	30 *h*	12926.70	$26701_{7/2} - 39628^{\circ}_{7/2}$	ΔJ=0	1.08	0.12	
7731.53	10000	12930.49	$19548_{9/2} - 32479^{\circ}_{9/2}$	ΔJ=0	0.983	0.89	*
7726.85	5 *h*	12938.32	$28051_{5/2} - 40989^{\circ}_{5/2}$				
7725.40	30	12940.75					
7721.73	8	12946.90					
7720.40	1	12949.13					
7717.43	5	12954.12	$21737_{9/2} - 34691^{\circ}_{11/2}$				
7715.38	5 *h*	12957.56	$26701_{7/2} - 39658^{\circ}_{5/2}$				
7714.67	5	12958.75	$27037^{\circ}_{7/2} - 39996_{7/2}$				
7702.71	50	12978.87		ΔJ=0	1.15	0.09	
7701.46	400 *h*	12980.98	$25520^{\circ}_{11/2} - 38502_{9/2}$	T	1.09		
7700.30	1 *h*	12982.93					
7696.81	100 *h*	12988.82		ΔJ=0	1.24	0.16	
7684.00	1	13010.47	$25488_{11/2} - 38499^{\circ}_{9/2}$				
7683.48	5	13011.35					
7682.31	2	13013.34					
7677.91	7	13022.32	$24137_{13/2} - 37159^{\circ}_{13/2}$				
7676.61	70 *h*	13023.00	$28051_{5/2} - 41074^{\circ}_{9/2}$	T	0.93		
7676.04	3	13023.97					
7673.66	5 *h*	13028.01					
7666.24	500 *h*	13040.62	$26701_{7/2} - 39741^{\circ}_{9/2}$	T	1.14		
7661.16	50	13049.26	$19132_{3/2} - 32181^{\circ}_{3/2}$	ΔJ=0	0.88	0.73	*
7660.32	150	13050.69	$28340^{\circ}_{7/2} - 41391_{9/2}$	S0	0.96	0.20	
7655.00	30	13059.76					
7652.41	9	13064.18	$27037^{\circ}_{7/2} - 40101_{9/2}$				
7645.60	1	13075.82	$27440^{\circ}_{9/2} - 40516_{9/2}$				
7633.98	15 *h*	13095.72	$26646_{9/2} - 39741^{\circ}_{9/2}$				
"			$25656_{9/2} - 38751^{\circ}_{9/2}$				
7631.41	3	13100.13	$30972_{11/2} - 44072^{\circ}_{13/2}$				
7630.44	10	13101.80					
7629.85	150	13102.81	$19753_{7/2} - 32856^{\circ}_{9/2}$	SI	1.19	1.06	*
7625.18	3 *h*	13110.84	$25207^{\circ}_{3/2} - 38318_{3/2}$				
7623.67	10 *h*	13113.43		ΔJ=0	?	0.68	
7621.67	80	13116.87	$18990_{11/2} - 32107^{\circ}_{11/2}$	ΔJ=0	1.215	1.115	*
7620.06	4	13119.64	$0^{\circ}_{7/2} - 13119_{9/2}$				
7612.17	1	13133.24					
7605.70	8	13144.42					
7600.99	9	13152.56	$23781_{9/2} - 36934^{\circ}_{7/2}$				
7594.90	100 *h*	13163.11	$30125_{13/2} - 43288^{\circ}_{13/2}$	T	1.11		
7593.74	400 *h*	13165.12	$28024_{9/2} - 41189^{\circ}_{7/2}$	S0	0.98	0.13	
7591.50	10	13169.00					
7590.51	4 *h*	13170.72					
7581.80	6	13185.85					
7580.61	400 *h*	13187.92	$28024_{9/2} - 41211^{\circ}_{7/2}$	S0	0.99	0.15	
7568.74	1	13208.60	$27440^{\circ}_{9/2} - 40649_{7/2}$				
7567.64	5 *h*	13210.52					
7558.33	20000	13226.79	$18990_{11/2} - 32217^{\circ}_{9/2}$	S0	1.215	1.335	*
7555.80	15	13231.22	$19548_{9/2} - 32780^{\circ}_{3/2}$				
7555.54	4	13231.68					
7548.06	5	13244.79	$21120_{7/2} - 34365^{\circ}_{7/2}$				
7545.78	300	13248.79	$13119_{9/2} - 26368^{\circ}_{11/2}$	S0	1.305	1.125	*
7543.13	20	13253.45	$18853_{11/2} - 32107^{\circ}_{11/2}$	ΔJ=0	?	0.20	
7539.36	2 *h*	13260.07	$26126_{9/2} - 39386^{\circ}_{9/2}$				
7532.99	3 *h*	13271.29					
7528.49	2	13279.22	$23374_{13/2} - 36653^{\circ}_{13/2}$				
7526.89	20	13282.04	$23374_{13/2} - 36656^{\circ}_{11/2}$				
7526.14	10	13283.37	$30125_{13/2} - 43408^{\circ}_{11/2}$				
7512.33	60	13307.79	$19548_{9/2} - 32856^{\circ}_{9/2}$	ΔJ=0	1.00	0.17	
7507.28	200 *h*	13316.74	$25745_{9/2} - 39061^{\circ}_{9/2}$	S0	1.09	1.34	*
7503.71	30	13323.07	$25520^{\circ}_{11/2} - 38844_{11/2}$	ΔJ=0	1.08	0.12	
7497.83	2	13333.52	$17613_{9/2} - 30947^{\circ}_{9/2}$				
7495.86	8	13337.02	$21120_{7/2} - 34457^{\circ}_{9/2}$				
7490.20	8000	13347.10	$19132_{3/2} - 32479^{\circ}_{9/2}$	T	0.91		
7481.08	10000	13363.37	$18853_{11/2} - 32217^{\circ}_{9/2}$	S0	1.15	1.338	*
7477.33	4 *h*	13370.08					
7474.67	30	13374.83		T	1.30		
7466.63	3 *h*	13389.24					
7461.31	2	13398.78	$26448^{\circ}_{9/2} - 39847_{7/2}$				
7452.35	20 *h*	13414.89	$24708^{\circ}_{7/2} - 38123_{7/2}$	ΔJ=0	1.11	0.25	
7449.80	4 *h*	13419.48					
7449.55	4	13419.93	$18693_{13/2} - 32112^{\circ}_{13/2}$				
"			$24348_{9/2} - 37768^{\circ}_{9/2}$				
7449.35	2	13420.29	$24708^{\circ}_{7/2} - 38128_{9/2}$				
7448.45	100 *h*	13421.92	$24701^{\circ}_{9/2} - 38123_{7/2}$	T	1.12		
7447.60	2	13423.45	$25699^{\circ}_{9/2} - 39123_{9/2}$				
7438.76	2	13439.40					
7435.43	5	13445.42					
7432.18	200	13451.30	$18990_{11/2} - 32441^{\circ}_{9/2}$	S0	1.09	0.12	
7426.07	2	13462.37	$21799^{\circ}_{3/2} - 35261_{9/2}$				
7417.28	20 *h*	13478.32					
7416.14	60	13480.39					
7411.36	5 *h*	13489.09	$25207^{\circ}_{3/2} - 38696_{9/2}$				
7409.86	70	13491.82	$19748_{9/2} - 33240^{\circ}_{7/2}$				
7408.83	6	13493.69					
7400.45	3	13508.97	$24137_{13/2} - 37646^{\circ}_{13/2}$				
7396.03	10	13517.04	$24611^{\circ}_{5/2} - 38128_{9/2}$				
7393.36	30	13521.93	$18837_{9/2} - 32359^{\circ}_{7/2}$	S0	0.90	0.23	
7390.26	100 *h*	13527.60		T	1.09		
7387.85	100 *h*	13532.01	$25745_{9/2} - 39277^{\circ}_{9/2}$	ΔJ=0	1.13	0.25	
7385.95	100 *h*	13535.49		ΔJ=0	0.92	0.17	
7384.06	4	13538.96	$19753_{7/2} - 33292^{\circ}_{9/2}$				
7381.13	10 *h*	13544.33					
7379.16	8	13547.95	$26448^{\circ}_{9/2} - 39996_{7/2}$				
7372.64	8 *h*	13559.93	$25717_{7/2} - 39277^{\circ}_{9/2}$				
7370.35	1 *h*	13564.14	$23574^{\circ}_{9/2} - 37138_{9/2}$				
7369.90	1 *h*	13564.97					
7369.50	2	13565.70	$28514^{\circ}_{9/2} - 42080_{11/2}$				
7368.39	8	13567.75					
7364.92	3	13574.14	$26368^{\circ}_{11/2} - 39942_{11/2}$				
7362.71	50	13578.22	$17343^{\circ}_{7/2} - 30921^{\circ}_{7/2}$	ΔJ=0	1.022	0.692	*
7360.42	1 *h*	13582.44					
7359.13	2	13584.82	$26357^{\circ}_{13/2} - 39942_{11/2}$				
7357.48	2	13587.87	$18853_{11/2} - 32441^{\circ}_{9/2}$				
7356.62	5 *h*	13589.46					
7348.87	1	13603.79	$17343^{\circ}_{7/2} - 30947^{\circ}_{9/2}$				
7344.45	2 *h*	13611.97	$27037^{\circ}_{7/2} - 40649_{7/2}$				
7342.76	4	13615.11	$17752_{9/2} - 31367^{\circ}_{9/2}$				
7342.22	50 *h*	13616.11		T	1.26		
7337.74	20 *h*	13624.42		ΔJ=0	0.90	0.36	
7336.86	70	13626.06	$17454_{13/2} - 31080^{\circ}_{11/2}$	S0	?	1.18	
7332.80	7	13633 60	$27440^{\circ}_{9/2} - 41074_{9/2}$				
7332.40	7 *h*	13634.34					
7331.65	40 *h*	13635.74	$23941^{\circ}_{9/2} - 37576_{9/2}$	ΔJ=0	1.24	0.43	
7328.40	10	13641.79					
7328.20	8	13642.16	$19753_{7/2} - 33396^{\circ}_{7/2}$				
7327.59	5	13643.29	$26448^{\circ}_{9/2} - 40091_{9/2}$	T	1.14		
7325.16	30	13647.82	$19132_{3/2} - 32780^{\circ}_{3/2}$	ΔJ=0	0.97	0.26	
7313.80	2 *h*	13669.02	$25488_{11/2} - 39157^{\circ}_{13/2}$				
7313.40	8 *h*	13669.76	$25717_{7/2} - 39386^{\circ}_{9/2}$				
7310.51	300	13675.17	$27314_{1/2} - 40989^{\circ}_{3/2}$	SI	0.605	0.205	
7303.27	5	13688.73					
7301.77	20	13691.54	$19548_{9/2} - 33240^{\circ}_{7/2}$				
7299.49	1 *h*	13695.81					

Wavelength in air Å	Intensity	Wavenumber cm⁻¹	Classification	Zeeman effect type	f	Je	
7293.67	6	13706.74	$23431^{\circ}_{9/2} - 37138_{9/2}$				
"			$31440_{9/2} - 45147^{\circ}_{9/2}$				
7293.43	5h	13707.19	$26889_{9/2} - 40596^{\circ}_{7/2}$				
7291.81	4	13710.24	$27440^{\circ}_{9/2} - 41151_{9/2}$				
7287.86	8h	13717.67	$25745_{9/2} - 39462^{\circ}_{7/2}$				
7286.16	200	13720.87	$15587_{11/2} - 29308^{\circ}_{9/2}$	S0	0.175	1.08	
7284.30	100	13724.37	$19132_{9/2} - 32856^{\circ}_{9/2}$	SI	0.86	1.06	*
7283.78	60h	13725.35	$25745_{9/2} - 39470^{\circ}_{9/2}$				
7282.85	10h	13727.11	$25717_{7/2} - 39444^{\circ}_{9/2}$				
7281.82	20	13729.05	$23335^{\circ}_{7/2} - 37064_{9/2}$	S0	1.30	0.07	
7280.34	3	13731.84					
7279.56	4h	13733.31	$26368^{\circ}_{11/2} - 40101_{9/2}$				
7279.02	3	13734.33					
7277.20	3	13737.76	$23781_{9/2} - 37519^{\circ}_{7/2}$				
7277.00	2	13738.14					
7276.15	7	13739.75					
7273.92	30	13743.96	$19548_{9/2} - 33292^{\circ}_{9/2}$	ΔJ=0	0.99	0.624	*
7272.62	500	13746.42	$17752_{9/2} - 31499^{\circ}_{9/2}$	S0	0.97	0.22	
7269.00	4h	13753.26	$25717_{7/2} - 39470^{\circ}_{9/2}$	T	0.98		
7265.46	2	13759.96	$26368^{\circ}_{11/2} - 40128_{11/2}$				
7263.81	1h	13763.09	$25717_{7/2} - 39480^{\circ}_{7/2}$				
7260.20	6	13769.93					
7259.63	20	13771.01	$25717_{7/2} - 39488^{\circ}_{9/2}$				
7257.72	50	13774.64	$17613_{9/2} - 31388^{\circ}_{9/2}$	ΔJ=0	?	0.85	
7249.43	3	13790.39					
7249.03	10	13791.15					
7245.97	40h	13796.97	$25745_{9/2} - 39542^{\circ}_{7/2}$	T	1.065		
7243.47	2	13801.73	$30972_{11/2} - 44774^{\circ}_{9/2}$				
7237.44	2h	13813.23					
7231.33	50h	13824.91	$25717_{7/2} - 39542^{\circ}_{7/2}$	ΔJ=0	1.03	0.15	
7230.36	5h	13826.76					
7214.17	100h	13857.79	$25745_{9/2} - 39602^{\circ}_{9/2}$	S0	0.79	0.30	
7212.63	4h	13860.75	$25699^{\circ}_{9/2} - 39560_{7/2}$				
7211.50	1h	13862.92	$24348_{9/2} - 38211^{\circ}_{7/2}$				
7211.15	2h	13863.59					
7209.58	6	13866.61					
7208.74	9	13868.23					
7205.35	7	13874.75	$26889_{9/2} - 40763^{\circ}_{7/2}$				
7202.19	30	13880.84					
7201.12	20h	13882.90	$25745_{9/2} - 39628^{\circ}_{7/2}$				
7199.20	4	13886.61	$24957^{\circ}_{11/2} - 38844_{11/2}$				
7198.47	30	13888.01		ΔJ=0	?	0.31	
7186.89	40	13910.39		ΔJ=0	?	0.22	
7186.09	2h	13911.94	$27440^{\circ}_{9/2} - 41352_{11/2}$				
7185.17	20h	13913.72	$25745_{9/2} - 39658^{\circ}_{9/2}$	ΔJ=0	?	0.34	
7174.78	3h	13933.87	$21120_{7/2} - 35054^{\circ}_{9/2}$				
7172.48	2	13938.34					
7169.27	20	13944.58	$21737_{9/2} - 35682^{\circ}_{7/2}$	T	1.10		
7161.52	2h	13959.67	$18990_{11/2} - 32950^{\circ}_{13/2}$				
7160.63	1	13961.40	$21997_{11/2} - 35958^{\circ}_{13/2}$				
7159.01	5	13964.56	$16957_{7/2} - 30921^{\circ}_{7/2}$				
7152.04	20	13978.17	$19748_{9/2} - 33726^{\circ}_{9/2}$	ΔJ=0	?	0.68	
7147.55	2	13986.95	$23781_{9/2} - 37768^{\circ}_{9/2}$				
7146.32	3h	13989.36	$27440^{\circ}_{9/2} - 41430_{11/2}$				
7145.92	10	13990.14	$16957_{7/2} - 30947^{\circ}_{9/2}$				
7139.95	60	14001.84		ΔJ=0	1.18	0.10	
7138.58	2h	14004.53	$22929_{9/2} - 36934^{\circ}_{7/2}$				
7138.21	5h	14005.25					
7134.25	3h	14013.03					
7132.62	2h	14016.23					
7130.73	50	14019.94	$8771^{\circ}_{9/2} - 22791_{7/2}$	SI	0.85	1.13	*
7130.13	1h	14021.12	$17752_{9/2} - 31773^{\circ}_{9/2}$				
7128.46	100h	14024.41	$17343_{7/2} - 31367^{\circ}_{7/2}$	ΔJ=0	?	1.09	
7128.32	40h	14024.69	$25717_{7/2} - 39741^{\circ}_{9/2}$	SI	1.44	0.33	
7123.95	2	14033.29					
7122.09	20	14036.95	$27037^{\circ}_{7/2} - 41074_{9/2}$				
7115.41	15	14050.13					
7109.63	2h	14061.55	$28514^{\circ}_{9/2} - 42576_{9/2}$				
7108.06	3h	14064.66	$17454_{13/2} - 31519^{\circ}_{13/2}$				
7106.14	150	14068.46	$18693_{13/2} - 32761^{\circ}_{17/2}$	S0	0.56	0.52	
7099.63	10h	14081.36	$28514^{\circ}_{9/2} - 42595_{11/2}$				
7095.21	50	14090.13	$34457^{\circ}_{9/2} - 48547_{9/2}$	ΔJ=0	1.085	0.21	
7092.06	5	14096.39	$18853_{11/2} - 32950^{\circ}_{13/2}$				
7083.40	5h	14113.62	$27037^{\circ}_{7/2} - 41151_{9/2}$				
7082.23	8h	14115.95	$30302_{9/2} - 44418^{\circ}_{7/2}$				
7077.57	5h	14125.25					
7072.74	1	14134.90	$26368^{\circ}_{11/2} - 40503_{11/2}$				
7066.52	2h	14147.34	$25699^{\circ}_{9/2} - 39847_{7/2}$				
7065.04	4h	14150.30	$24348_{9/2} - 38499^{\circ}_{9/2}$				
7061.27	3h	14157.85					
7060.97	100	14158.46	$8771^{\circ}_{9/2} - 22929_{9/2}$	ΔJ=0	0.85	1.142	*
7059.94	15	14160.52	$19132_{9/2} - 33292^{\circ}_{9/2}$				
7055.29	7	14169.85					
7054.30	7	14171.84					
7052.05	4	14176.37	$27440^{\circ}_{9/2} - 41617_{7/2}$				
7051.38	1	14177.71	$25520^{\circ}_{11/2} - 39698_{9/2}$				
7050.54	30h	14179.40	$28555_{7/2} - 42735^{\circ}_{9/2}$				
7039.74	3	14201.15	$26448^{\circ}_{9/2} - 40649_{7/2}$				
7034.34	150	14212.06		ΔJ=0	1.11	0.10	
7034.12	8	14212.50	$19748_{9/2} - 33961^{\circ}_{7/2}$				
7031.41	1	14217.98	$26368^{\circ}_{11/2} - 40586_{13/2}$				
7029.40	80h	14222.04		ΔJ=0	1.33	0.17	
7027.38	1	14226.13	$21997_{11/2} - 36223^{\circ}_{13/2}$				
7026.14	4	14228.64	$26357^{\circ}_{13/2} - 40586_{13/2}$				
7022.44	10	14236.14					
7021.74	3	14237.56					
7019.73	10h	14241.63					
7017.90	150	14245.35	$26448^{\circ}_{9/2} - 40693_{9/2}$	S0	1.14	1.32	*
7012.18	50	14256.97	$18693_{13/2} - 32950^{\circ}_{13/2}$				
7011.00	4	14259.37	$27440^{\circ}_{9/2} - 41700_{11/2}$				
7010.79	70	14259.80	$31454^{\circ}_{9/2} - 45714_{11/2}$	SI	1.36	0.10	
6997.38	40	14287.12	$27440^{\circ}_{9/2} - 41728_{9/2}$	ΔJ=0	1.08	0.18	
6994.59	30h	14292.82					
6992.80	8	14296.48	$25699^{\circ}_{9/2} - 39996_{7/2}$				
6989.13	40	14303.99		T	1.15		
6980.04	3h	14322.62					
6975.33	3h	14332.29	$21997_{11/2} - 36329^{\circ}_{11/2}$				
6971.78	10h	14339.58	$25207^{\circ}_{9/2} - 39547_{9/2}$	S0	1.20	0.09	
6969.74	7	14343.78					
6954.13	4	14375.98	$23335^{\circ}_{7/2} - 37711_{9/2}$				
6949.54	30	14385.47					
6946.15	2	14392.49	$24137_{13/2} - 38529^{\circ}_{11/2}$				
6941.79	3h	14401.53	$23941^{\circ}_{9/2} - 38342_{7/2}$				
6941.55	2	14402.03	$25699^{\circ}_{9/2} - 40101_{9/2}$				
6937.37	80	14410.71	$16957_{7/2} - 31367^{\circ}_{7/2}$	ΔJ=0	1.25	0.57	
6933.32	9	14419.13		T	1.15		
6932.13	4	14421.60	$25520^{\circ}_{11/2} - 39942_{11/2}$				
6928.66	30	14428.83	$17752_{9/2} - 32181^{\circ}_{9/2}$	SI	1.186	0.723	*
6927.90	6	14430.41	$17343_{7/2} - 31773^{\circ}_{9/2}$				
6927.46	3	14431.32	$16957_{7/2} - 31388^{\circ}_{9/2}$				
6923.16	10	14440.29	$19753_{7/2} - 34194^{\circ}_{9/2}$				
"			$30125_{13/2} - 44565^{\circ}_{13/2}$				
6915.86	40	14455.53	$27037^{\circ}_{7/2} - 41493_{9/2}$	S0	0.67	0.43	
6914.35	2h	14458.69	$23309_{11/2} - 37768^{\circ}_{9/2}$				
6898.56	80	14491.78		ΔJ=0	1.07	0.33	
6897.70	20	14493.59	$17613_{9/2} - 32107^{\circ}_{11/2}$				
6895.95	4	14497.27	$16957_{7/2} - 31454^{\circ}_{9/2}$				
6894.18	5h	14500.99	$26488_{9/2} - 40989^{\circ}_{9/2}$				
6891.27	7	14507.11	$27037^{\circ}_{7/2} - 41544_{9/2}$				
6888.71	9	14512.50					
6884.75	10	14520.85	$21161_{9/2} - 35682^{\circ}_{7/2}$				
6881.11	5	14528.53	$24348_{9/2} - 38877^{\circ}_{11/2}$				
6871.47	2	14548.91					
6869.69	3h	14552.68					
6865.58	10	14561.39	$21120_{7/2} - 35682^{\circ}_{7/2}$				
6861.95	2h	14569.10					
6856.863	50	14579.91	$19466_{13/2} - 34046^{\circ}_{13/2}$	T	1.22		
6854.115	200	14585.75	$26488_{9/2} - 41074^{\circ}_{9/2}$	SI	1.20	0.21	
6853.56	3	14586.93					
6852.89	2	14588.36					

Wavelength in air Å	Intensity	Wavenumber cm⁻¹	Classification	Zeeman effect type	f	Je	
6852.23	7	14589.76	$22929_{9/2} - 37519^{\circ}_{7/2}$				
6851.12	4	14592.13	$21737_{9/2} - 36329^{\circ}_{11/2}$				
6845.755	1000	14603.56	$17613_{9/2} - 32217^{\circ}_{9/2}$	ΔJ=0	1.19	1.33	*
6844.262	2000	14606.75	$17752_{9/2} - 32359^{\circ}_{7/2}$	T	1.23		
6835.494	100	14625.49	$16742_{7/2} - 31367^{\circ}_{7/2}$	T	1.335		
6831.092	300	14634.91	$26439_{7/2} - 41074^{\circ}_{9/2}$	T	1.01		
6826.954	200	14643.78	$24418_{9/2} - 39061^{\circ}_{9/2}$	S0	1.06	1.34	*
6820.266	200	14658.14	$17454_{13/2} - 32112^{\circ}_{13/2}$				
6805.234	20	14690.52	$27037^{\circ}_{7/2} - 41728_{9/2}$				
6794.576	20	14713.56	$27037^{\circ}_{7/2} - 41751_{9/2}$	T	1.16	0.5	
6788.516	300	14726.70	$17752_{9/2} - 32479^{\circ}_{9/2}$	ΔJ=0	1.185	0.90	*
6783.436	10	14737.72	$16957_{7/2} - 31694^{\circ}_{7/2}$	T	1.15		
6781.998	300	14740.85	$24348_{9/2} - 39089^{\circ}_{11/2}$	T	1.10		
6779.767	2000	14745.70	$17613_{9/2} - 32359^{\circ}_{7/2}$	T	1.19		
6777.927	100	14749.70	$26439_{7/2} - 41189^{\circ}_{7/2}$	ΔJ=0	?	0.7	
6767.477	100	14772.48	$26439_{7/2} - 41211^{\circ}_{7/2}$	ΔJ=0	1.00	1.18	*
6761.466	10	14785.61	$23335^{\circ}_{7/2} - 38120_{9/2}$				
6754.274	10	14801.35	$18837_{9/2} - 33638^{\circ}_{11/2}$				
6744.991	4	14821.73	$18990_{11/2} - 33812^{\circ}_{13/2}$				
6742.114	30	14828.05	$17613_{9/2} - 32441^{\circ}_{9/2}$				
6740.853	3	14830.82					
6739.222	50	14834.41		SI	1.13	0.27	
6726.338	100	14862.83	$26126_{9/2} - 40989^{\circ}_{9/2}$	SI	1.09	0.41	*
6723.371	3	14869.39	$23882_{9/2} - 38751^{\circ}_{9/2}$				
6721.365	1000	14873.82	$17343_{7/2} - 32217^{\circ}_{9/2}$	SI	1.022	1.333	*
6692.931	200	14937.01	$19132_{9/2} - 34069^{\circ}_{7/2}$	SI	1.02	0.125	
6688.241	10	14947.49	$26126_{9/2} - 41074^{\circ}_{9/2}$				
6685.990	4	14952.52	$16742_{7/2} - 31694^{\circ}_{7/2}$				
6684.533	30	14955.78	$18837_{9/2} - 33793^{\circ}_{11/2}$				
6678.652	10	14968.95	$24418_{9/2} - 39386^{\circ}_{9/2}$				
6678.431	3	14969.44					
6672.681	30	14982.34	$25520^{\circ}_{11/2} - 40503_{11/2}$	ΔJ=0	1.10	0.05	
6672.337	50	14983.12	$19466_{13/2} - 34449^{\circ}_{13/2}$	ΔJ=0	1.16	0.14	
6671.768	3	14984.39	$26368^{\circ}_{11/2} - 41352_{11/2}$				
6659.025	7	15013.07	$21997_{11/2} - 37010^{\circ}_{9/2}$				
6658.639	500	15013.94	$24348_{9/2} - 39362^{\circ}_{11/2}$	T	1.12		
6657.720	2000	15016.01	$17343_{7/2} - 32359^{\circ}_{7/2}$	ΔJ=0	1.02	1.19	*
6657.095	40	15017.42	$22559^{\circ}_{11/2} - 37576_{9/2}$				
6656.502	2	15018.76	$25745_{9/2} - 40763^{\circ}_{7/2}$				
6654.745	1	15022.72	$26368^{\circ}_{11/2} - 41391_{9/2}$				
6653.692	10	15025.10					
6652.675	30	15027.40	$17752_{9/2} - 32780^{\circ}_{9/2}$				
6650.852	100	15031.52	$16742_{7/2} - 31773^{\circ}_{9/2}$				
6645.212	40	15044.27					
6644.996	30	15044.76	$26448^{\circ}_{9/2} - 41493_{9/2}$				
"			$24418_{9/2} - 39467^{\circ}_{7/2}$				
6643.026	5	15049.23					
6642.556	7	15050.29	$25536^{\circ}_{13/2} - 40586_{13/2}$				
6641.592	30	15052.47	$24418_{9/2} - 39470^{\circ}_{9/2}$	T	1.08		
6637.463	3	15061.84	$26368^{\circ}_{11/2} - 41430_{11/2}$				
6637.273	100	15062.27	$26126_{9/2} - 41189^{\circ}_{7/2}$	SI	1.39	0.20	
6636.080	3	15064.98	$24348_{9/2} - 39413^{\circ}_{7/2}$				
6635.528	30	15066.23	$19466_{13/2} - 34532^{\circ}_{11/2}$	T	1.25		
6632.770	2	15072.50	$26357^{\circ}_{13/2} - 41430_{11/2}$				
6630.445	2	15077.78					
6627.248	100	15085.05	$26126_{9/2} - 41211^{\circ}_{7/2}$	SI	1.40	0.22	
6625.313	5	15089.46	$18853_{11/2} - 33943^{\circ}_{13/2}$				
6624.609	1	15091.06					
6622.619	20	15095.60	$24348_{9/2} - 39444^{\circ}_{9/2}$				
6621.420	30	15098.33	$17343_{7/2} - 32441^{\circ}_{9/2}$	ΔJ=1	?	0.80	
6620.230	2	15101.05	$26368^{\circ}_{11/2} - 41469_{13/2}$				
6619.814	10	15101.99	$8771^{\circ}_{9/2} - 23873_{7/2}$				
6619.698	5	15102.26	$27440^{\circ}_{9/2} - 42543_{7/2}$				
6619.433	1	15102.86	$25699^{\circ}_{9/2} - 40802_{7/2}$				
6618.946	2	15103.97	$17752_{9/2} - 32856^{\circ}_{9/2}$				
6616.797	40	15108.88	$22468^{\circ}_{11/2} - 37576_{9/2}$				
6615.563	10	15111.70	$26357^{\circ}_{13/2} - 41469_{13/2}$				
6613.516	2	15116.38					
6612.340	4	15119.06	$18693_{13/2} - 33812^{\circ}_{13/2}$				
6610.318	40	15123.69	$18837_{9/2} - 33961^{\circ}_{7/2}$	T	1.12		
6610.112	10h	15124.16	$24418_{9/2} - 39542^{\circ}_{7/2}$	T	1.03		
6607.045	3	15131.18	$24348_{9/2} - 39479^{\circ}_{11/2}$				
6604.955	2000	15135.97	$17343_{7/2} - 32479^{\circ}_{9/2}$	SI	1.02	0.89	*
6603.397	3	15139.54	$24348_{9/2} - 39488^{\circ}_{9/2}$				
6602.211	1	15142.26					
6600.516	5	15146.15					
6598.134	20	15151.62	$22559^{\circ}_{11/2} - 37711_{9/2}$	T	1.13		
6591.239	4	15167.47					
6590.585	1	15168.97	$26448^{\circ}_{9/2} - 41617_{7/2}$				
6589.744	5	15170.91	$24957^{\circ}_{11/2} - 40128_{11/2}$				
6583.684	20	15184.87	$24418_{9/2} - 39602^{\circ}_{9/2}$				
6581.884	1	15189.02	$23309_{11/2} - 38499^{\circ}_{9/2}$				
6580.963	5	15191.15	$30972_{11/2} - 46163^{\circ}_{11/2}$				
6580.057	1	15193.24					
6579.961	2	15193.46	$25745_{9/2} - 40938^{\circ}_{9/2}$				
"			$24348_{9/2} - 39542^{\circ}_{7/2}$				
6578.644	7	15196.50	$21737_{9/2} - 36934^{\circ}_{7/2}$				
6577.161	1	15199.93					
6575.542	100	15203.67		S0	0.66	0.31	
6573.521	2	15208.35					
6572.828	4	15209.95	$24418_{9/2} - 39628^{\circ}_{7/2}$				
6570.961	2	15214.27	$24348_{9/2} - 39563^{\circ}_{11/2}$				
6568.632	1	15219.67	$23309_{11/2} - 38529^{\circ}_{11/2}$				
6566.287	100	15225.10	$19466_{13/2} - 34691^{\circ}_{11/2}$	T	1.17		
6565.525	10	15226.87	$27440^{\circ}_{9/2} - 42667_{9/2}$				
6557.386	2	15245.77	$25130_{13/2} - 40376^{\circ}_{13/2}$				
6555.488	20	15250.18	$18693_{13/2} - 33943^{\circ}_{13/2}$				
6555.395	2	15250.40					
6552.617	2	15256.86	$21120_{7/2} - 36377^{\circ}_{9/2}$				
6551.623	5	15259.18					
6551.185	100	15260.20	$16957_{7/2} - 32217^{\circ}_{9/2}$				
6547.015	1	15269.92					
6543.725	5h	15277.60	$27440^{\circ}_{9/2} - 42718_{9/2}$				
6541.883	3	15281.90	$22929_{9/2} - 38211^{\circ}_{7/2}$				
6539.825	40	15286.71					
6539.134	1	15288.32	$24708^{\circ}_{7/2} - 39996_{7/2}$				
6535.449	20	15296.94	$24137_{13/2} - 39434^{\circ}_{13/2}$				
6534.406	100	15299.38		T	1.17	0.07	
6534.215	10	15299.83					
6533.784	1	15300.84	$19753_{7/2} - 35054^{\circ}_{9/2}$				
6531.528	2	15306.12	$19748_{9/2} - 35054^{\circ}_{9/2}$				
6530.807	50	15307.81	$23781_{9/2} - 39089^{\circ}_{11/2}$	S0	0.82	0.25	
6525.863	2	15319.41	$25536^{\circ}_{13/2} - 40855_{13/2}$				
6525.648	5	15319.92	$18990_{11/2} - 34310^{\circ}_{9/2}$				
6523.994	20h	15323.80	$27440^{\circ}_{9/2} - 42764_{9/2}$				
6519.778	200	15333.71	$25656_{9/2} - 40989^{\circ}_{9/2}$	SI	0.72	0.40	*
6519.421	1	15334.55	$25520^{\circ}_{11/2} - 40855_{13/2}$				
6517.443	5	15339.20	$21799^{\circ}_{9/2} - 37138_{9/2}$				
6515.094	3	15344.73					
6514.208	2	15346.82	$23873_{9/2} - 39220^{\circ}_{9/2}$				
6513.678	1	15348.07					
6513.640	1	15348.16					
6511.384	40	15353.48	$18693_{13/2} - 34046^{\circ}_{13/2}$	T	1.16		
6507.663	300	15362.26		S0	0.73	0.11	
6507.302	20	15363.11					
6503.803	2	15371.37	$23873_{7/2} - 39244^{\circ}_{9/2}$				
6498.085	1	15384.90	$24611^{\circ}_{9/2} - 39996_{7/2}$				
6496.873	3	15387.77	$26448^{\circ}_{9/2} - 41836_{9/2}$				
6494.573	40	15393.22	$24348_{9/2} - 39741^{\circ}_{9/2}$	T	1.10		
6493.905	3	15394.80	$13119_{9/2} - 28514^{\circ}_{9/2}$				
6490.703	200	15402.40	$16957_{7/2} - 32359^{\circ}_{7/2}$	ΔJ=0	1.18	0.10	
6489.080	20h	15406.25					
6485.678	1	15414.33					
6483.978	40	15418.37	$25656_{9/2} - 41074^{\circ}_{9/2}$				
6480.185	40	15427.40	$27440^{\circ}_{9/2} - 42868_{11/2}$				
6478.173	1	15432.19					
6476.494	20	15436.19					
6473.192	3	15444.06	$25745_{9/2} - 41189^{\circ}_{7/2}$				
6472.815	1	15444.96	$25699^{\circ}_{9/2} - 41144_{7/2}$				
6470.630	5	15450.18	$19548_{9/2} - 34999^{\circ}_{9/2}$				

487-412 OL - 73 - 2

Wavelength in air Å	Intensity	Wavenumber cm^{-1}	Classification	Zeeman effect type	f	Je	
6470.203	3	15451.20					
6467.980	7	15456.51	$18853_{11/2} - 34310^{\circ}_{9/2}$				
6467.389	1	15457.92					
6466.788	20	15459.36	$18990_{11/2} - 34449^{\circ}_{13/2}$				
6465.814	10	15461.68	$27440^{\circ}_{9/2} - 42902_{9/2}$				
6463.405	30	15467.45	$18990_{11/2} - 34457^{\circ}_{9/2}$	SI	1.30	0.09	
6462.940	1 *h*	15468.56					
6461.146	1	15472.85	$26646_{9/2} - 42119^{\circ}_{11/2}$				
6460.261	5000	15474.97	$16742_{7/2} - 32217^{\circ}_{9/2}$	T	1.35		
6458.850	2 *h*	15478.36					
6458.032	1	15480.32	$24611^{\circ}_{9/2} - 40091_{9/2}$				
6456.201	30	15484.71	$16957_{7/2} - 32441^{\circ}_{9/2}$	SI	1.53	0.27	
6455.985	2	15485.22					
6454.936	20	15487.74	$17752_{9/2} - 33240^{\circ}_{7/2}$	T	1.14		
6452.737	30	15493.02	$15587_{11/2} - 31080^{\circ}_{11/2}$				
6451.587	1	15495.78					
6444.334	30	15513.22	$17343_{7/2} - 32856^{\circ}_{9/2}$	T	0.98		
6444.117	20	15513.74	$23873_{7/2} - 39386^{\circ}_{9/2}$				
6443.060	2	15516.29	$27440^{\circ}_{9/2} - 42957_{11/2}$				
6442.656	2	15517.26					
6440.829	1	15521.66					
6440.540	100	15522.36	$16957_{7/2} - 32479^{\circ}_{9/2}$	SI	1.17	0.90	*
6438.105	200	15528.23	$18837_{9/2} - 34365^{\circ}_{7/2}$	S0	0.88	0.25	
6437.887	2	15528.76					
6436.070	30 *h*	15533.14	$25656_{9/2} - 41189^{\circ}_{7/2}$				
6433.173	5	15540.13	$17752_{9/2} - 33292^{\circ}_{9/2}$				
6432.197	1	15542.49	$18990_{11/2} - 34532^{\circ}_{11/2}$				
6427.655	4	15553.47	$25520^{\circ}_{11/2} - 41074_{9/2}$				
6426.638	20	15555.94	$25656_{9/2} - 41211^{\circ}_{7/2}$				
6425.366	4	15559.02					
6424.452	6 *h*	15561.23	$22559^{\circ}_{11/2} - 38120_{9/2}$				
6421.975	1	15567.23	$23309_{11/2} - 38877^{\circ}_{13/2}$				
6420.390	5	15571.07	$23873_{7/2} - 39444^{\circ}_{9/2}$				
6416.319	60	15580.95	$23781_{9/2} - 39362^{\circ}_{11/2}$	S0	1.05	0.08	
6412.770	10	15589.58	$23873_{7/2} - 39462^{\circ}_{7/2}$				
6410.978	3	15593.93					
6410.150	30	15595.95	$18853_{11/2} - 34449^{\circ}_{13/2}$				
6409.603	10	15597.28	$23873_{7/2} - 39470^{\circ}_{9/2}$				
6409.479	10	15597.58	$18990_{11/2} - 34587^{\circ}_{9/2}$				
6408.274	2 *h*	15600.51	$24246^{\circ}_{7/2} - 39847_{7/2}$				
6406.823	50	15604.05	$18853_{11/2} - 34457^{\circ}_{9/2}$	S0	0.99	0.16	
6405.582	3	15607.07	$23873_{7/2} - 39480^{\circ}_{7/2}$				
6403.209	20	15612.85					
6402.320	40	15615.02	$23873_{7/2} - 39488^{\circ}_{9/2}$	T	1.09		
6401.439	200	15617.17	$16742_{7/2} - 32359^{\circ}_{7/2}$	ΔJ=0	1.32	1.19	*
6398.121	5	15625.27	$30972_{11/2} - 46597^{\circ}_{13/2}$				
6397.533	10	15626.71	$17613_{9/2} - 33240^{\circ}_{7/2}$	T	1.21		
6396.134	2	15630.12	$25520^{\circ}_{11/2} - 41151_{9/2}$				
6396.065	20	15630.29	$27037^{\circ}_{7/2} - 42667_{9/2}$	T	1.08		
6389.319	10	15646.80	$8771^{\circ}_{9/2} - 24418_{9/2}$				
6388.534	5	15648.72	$21997_{11/2} - 37646^{\circ}_{13/2}$				
6386.912	6 *w*	15652.69	$22468^{\circ}_{11/2} - 38120_{9/2}$				
6386.744	4	15653.10	$25699^{\circ}_{9/2} - 41352_{11/2}$				
6385.527	4	15656.09	$16456_{7/2} - 32112^{\circ}_{9/2}$				
6385.130	6	15657.06	$25536^{\circ}_{13/2} - 41193_{13/2}$				
6384.951	1	15657.50					
6383.744	2	15660.46	$21997_{11/2} - 37657^{\circ}_{11/2}$				
6380.270	200	15668.99	$23873_{7/2} - 39542^{\circ}_{7/2}$	ΔJ=0	1.10	0.15	
6376.166	7	15679.07	$18853_{11/2} - 34532^{\circ}_{11/2}$				
6375.383	40	15681.00	$23781_{9/2} - 39462^{\circ}_{7/2}$	T	1.08		
6371.152	1	15691.41	$22791_{7/2} - 38482^{\circ}_{7/2}$				
6369.489	10	15695.51	$18837_{9/2} - 34532^{\circ}_{11/2}$				
6368.412	6	15698.16	$23781_{9/2} - 39479^{\circ}_{11/2}$				
6367.880	100	15699.47	$16742_{7/2} - 32441^{\circ}_{9/2}$	S0	0.99	0.25	
6365.022	8	15706.52	$23781_{9/2} - 39488^{\circ}_{9/2}$				
6364.489	1	15707.84	$22791_{7/2} - 38499^{\circ}_{9/2}$				
6364.323	1	15708.25	$28555_{7/2} - 44263^{\circ}_{7/2}$				
6362.908	10	15711.74	$26368^{\circ}_{11/2} - 42080_{11/2}$				
6359.156	3	15721.01					
6358.588	4	15722.42	$26357^{\circ}_{13/2} - 42080_{11/2}$				
6355.308	1	15730.53	$25699^{\circ}_{9/2} - 41430_{11/2}$				
6353.842	6	15734.16	$18853_{11/2} - 34587^{\circ}_{9/2}$				
6353.722	1	15734.46	$22929_{9/2} - 38664^{\circ}_{7/2}$				
6353.470	3	15735.08					
6352.660	300	15737.09	$16742_{7/2} - 32479^{\circ}_{9/2}$	SI	1.324	0.89	*
6349.066	30	15745.99	$27037^{\circ}_{7/2} - 42783_{7/2}$				
6347.203	1	15750.62	$18837_{9/2} - 34587^{\circ}_{9/2}$				
6345.885	1	15753.89	$29316_{9/2} - 45070^{\circ}_{9/2}$				
6345.528	20	15754.77	$23873_{7/2} - 39628^{\circ}_{7/2}$				
6344.748	100	15756.71	$18693_{13/2} - 34449^{\circ}_{13/2}$	T	1.17		
6344.373	1	15757.64	$23941^{\circ}_{9/2} - 39698_{9/2}$				
6338.916	2	15771.21	$21997_{11/2} - 37768^{\circ}_{9/2}$				
6338.520	10	15772.19		T	1.14	0.03	
6338.270	3	15772.81	$21161_{7/2} - 36934^{\circ}_{7/2}$				
6334.658	1	15781.81	$21737_{9/2} - 37519^{\circ}_{7/2}$				
6334.454	1	15782.32	$17613_{9/2} - 33396^{\circ}_{7/2}$				
6332.154	1	15788.05	$23335^{\circ}_{7/2} - 39123_{9/2}$				
6330.596	1	15791.93					
6325.911	1	15803.63					
6323.217	1	15810.36					
6322.015	1	15813.37	$21120_{7/2} - 36934^{\circ}_{7/2}$				
6318.529	3	15822.09	$22929_{9/2} - 38751^{\circ}_{9/2}$	ΔJ=0	1.18	0.215	
6314.649	7	15831.82	$25520^{\circ}_{11/2} - 41352_{11/2}$	ΔJ=0	1.09	0.19	
6312.195	20	15837.97	$18853_{11/2} - 34691^{\circ}_{11/2}$	T	1.153		
6310.012	1	15843.45					
6306.266	1	15852.86	$26889_{9/2} - 42742^{\circ}_{7/2}$				
6305.650	50	15854.41	$18837_{9/2} - 34691^{\circ}_{11/2}$	SI	1.205	0.045	
6302.513	10	15862.30	$27440^{\circ}_{9/2} - 43303_{7/2}$				
6300.742	1	15866.76	$19132_{9/2} - 34999^{\circ}_{9/2}$				
6299.975	100 *h*	15868.69	$23873_{7/2} - 39741^{\circ}_{9/2}$	S0	1.03	0.095	
6298.751	1	15871.77	$23335^{\circ}_{7/2} - 39206_{9/2}$				
6298.268	1	15872.99	$22791_{7/2} - 38664^{\circ}_{7/2}$				
6297.030	1	15876.11					
6296.465	2	15877.54	$25656_{9/2} - 41533^{\circ}_{9/2}$				
6295.570	1	15879.79					
6294.959	3	15881.34	$25207^{\circ}_{9/2} - 41089_{11/2}$				
6294.475	30	15882.56		S0	1.16	0.095	
6291.647	5	15889.70	$21120_{7/2} - 37010^{\circ}_{9/2}$	S0	0.84	0.27	
6288.756	3	15897.00	$17343_{7/2} - 33240^{\circ}_{7/2}$				
6288.335	2	15898.06	$24957^{\circ}_{11/2} - 40855_{13/2}$				
6286.746	1	15902.08					
6285.873	1	15904.29					
6285.205	2	15905.98	$23941^{\circ}_{9/2} - 39847_{7/2}$				
6283.915	7	15909.25	$25520^{\circ}_{11/2} - 41430_{11/2}$				
6279.574	2	15920.24	$21737_{9/2} - 37657^{\circ}_{11/2}$				
6278.563	1	15922.81	$22419^{\circ}_{9/2} - 38342_{7/2}$				
6277.767	5 *h*	15924.83	$23335^{\circ}_{7/2} - 39259_{9/2}$				
6277.515	50	15925.47	$21799^{\circ}_{9/2} - 37724_{9/2}$				
6276.349	6	15928.42	$19753_{7/2} - 35682^{\circ}_{7/2}$	ΔJ=0	1.14	0.23	
6276.191	1	15928.83					
6275.622	7	15930.27		ΔJ=0	1.00	0.44	
6274.882	6 *h*	15932.15	$22929_{9/2} - 38861^{\circ}_{9/2}$				
6274.417	10	15933.33	$25536^{\circ}_{13/2} - 41469_{13/2}$	T	1.20		
6271.029	1	15941.94	$22902^{\circ}_{13/2} - 38844_{11/2}$				
6269.050	1	15946.97	$27491_{11/2} - 43438^{\circ}_{13/2}$				
6263.850	20 *h*	15960.21	$23781_{9/2} - 39741^{\circ}_{9/2}$	ΔJ=0	1.12	0.13	
6257.635	2	15976.06					
6257.439	2	15976.56	$24137_{13/2} - 40113^{\circ}_{13/2}$				
6248.071	1	16000.51	$25699^{\circ}_{9/2} - 41700_{11/2}$				
6247.687	3	16001.50	$23941^{\circ}_{9/2} - 39942_{11/2}$				
6243.947	1	16011.08					
6242.292	2	16015.33	$21997_{11/2} - 38012^{\circ}_{13/2}$				
6241.869	1	16016.41					
6237.245	1	16028.29	$25699^{\circ}_{9/2} - 41728_{9/2}$				
6225.129	1	16059.48	$23374_{13/2} - 39434^{\circ}_{13/2}$				
6224.548	8	16060.98	$26368^{\circ}_{11/2} - 42429_{11/2}$	ΔJ=0	1.14	0.33	
6223.272	5	16064.27	$18990_{11/2} - 35054^{\circ}_{9/2}$	S0	0.90	0.30	
6220.419	1	16071.64	$26357^{\circ}_{13/2} - 42429_{11/2}$				
6216.288	3	16082.32	$24611^{\circ}_{9/2} - 40693_{9/2}$				
			$22419^{\circ}_{9/2} - 38502_{9/2}$				

Wavelength in air Å	Intensity	Wavenumber cm^{-1}	Classification	Zeeman effect type	f	Je	
6214.069	3	16088.06	$26368^{\circ}_{11/2}-42456_{13/2}$				
6211.445	40	16094.86	$26448^{\circ}_{9/2}-42543_{7/2}$	T	1.06		
6210.814	1	16096.50	$25745_{9/2}-41841^{\circ}_{7/2}$				
6209.952	10	16098.73	$26357^{\circ}_{13/2}-42456_{13/2}$	ΔJ=0	1.20	0.08	
6209.215	7	16100.64	$21120_{7/2}-37221^{\circ}_{7/2}$				
6204.446	5	16113.02	$17613_{9/2}-33726^{\circ}_{9/2}$				
6204.082	1	16113.96					
6203.927	20	16114.36	$16742_{7/2}-32856^{\circ}_{9/2}$	SI	1.33	1.06	*
6200.154	1	16124.17	$23309_{11/2}-39434^{\circ}_{13/2}$				
6199.916	1	16124.79	$19548_{9/2}-35673^{\circ}_{9/2}$				
6197.110	10	16132.09	$22929_{9/2}-39061^{\circ}_{9/2}$				
6196.602	4	16133.41	$19548_{9/2}-35682^{\circ}_{7/2}$				
6190.922	4	16148.22	$26448^{\circ}_{9/2}-42596_{9/2}$				
6184.958	2	16163.79	$21997_{11/2}-38161^{\circ}_{11/2}$				
6180.164	10	16176.32					
6180.011	1	16176.73	$26368^{\circ}_{13/2}-42545_{13/2}$				
6179.429	1	16178.25	$23309_{11/2}-39488^{\circ}_{9/2}$				
"			$24418_{9/2}-40596^{\circ}_{7/2}$				
6179.047	10	16179.25	$25520^{\circ}_{11/2}-41700_{11/2}$	ΔJ=0	1.14	0.16	
6178.956	1	16179.49	$17613_{9/2}-33793^{\circ}_{11/2}$				
6177.259	30	16183.93	$17454_{13/2}-33638^{\circ}_{11/2}$	S00	1.15	1.42	*
6175.947	1 ħ	16187.37	$26357^{\circ}_{13/2}-42545_{13/2}$				
6175.294	400	16189.08	$13119_{9/2}-29308^{\circ}_{9/2}$	ΔJ=0	1.40	0.80	
6170.806	8	16200.86	$18853_{13/2}-35054^{\circ}_{9/2}$	S0	0.55	0.60	
6169.821	1	16203.44					
6168.458	10	16207.02	$25520^{\circ}_{11/2}-41728_{9/2}$	SI	1.32	0.20	
6167.917	40	16208.44	$17752_{9/2}-33961^{\circ}_{7/2}$				
6166.500	20	16212.17	$23335^{\circ}_{7/2}-39547_{9/2}$	SI	1.55	0.19	
6164.550	2	16217.30	$18837_{9/2}-35054^{\circ}_{9/2}$				
6160.720	40	16227.38	$26368^{\circ}_{11/2}-42595_{11/2}$				
6156.671	10	16238.05	$26357^{\circ}_{13/2}-42595_{11/2}$				
6153.396	1	16246.69					
6151.992	1	16250.40					
6151.000	5	16253.02	$23309_{11/2}-39563^{\circ}_{13/2}$				
6146.215	2	16265.67	$27037^{\circ}_{7/2}-43303_{7/2}$				
6144.742	3	16269.57					
6142.800	5	16274.72	$27440^{\circ}_{9/2}-43715_{11/2}$				
6139.548	1	16283.34	$16957_{7/2}-33240^{\circ}_{7/2}$				
6139.086	1	16284.56	$22559^{\circ}_{11/2}-38844_{11/2}$				
6138.795	10	16285.34	$25207^{\circ}_{9/2}-41493_{9/2}$				
6131.532	200	16304.63	$16456_{17/2}-32761^{\circ}_{17/2}$	ΔJ=0	1.14	0.54	
6129.673	1	16309.57					
6119.445	2	16336.83	$25207^{\circ}_{9/2}-41544_{9/2}$				
6118.883	150	16338.33	$17454_{13/2}-33793^{\circ}_{11/2}$	S0	0.65	0.50	
6117.028	2	16343.28					
6115.490	5 ħ	16347.39	$17613_{9/2}-33961^{\circ}_{7/2}$				
6114.360	1	16350.42	$21997_{11/2}-38347^{\circ}_{11/2}$				
6111.778	5	16357.32	$17454_{13/2}-33812^{\circ}_{13/2}$				
6109.439	1	16363.59	$23335^{\circ}_{7/2}-39698_{9/2}$				
6104.797	2	16376.03	$22468^{\circ}_{11/2}-38844_{11/2}$				
6103.150	5	16380.45	$25699^{\circ}_{9/2}-42080_{11/2}$				
6101.149	1	16385.82	$25488_{11/2}-41874^{\circ}_{11/2}$				
6100.538	3	16387.46	$21997_{11/2}-38384^{\circ}_{9/2}$				
6096.377	1	16398.65	$21120_{7/2}-37519^{\circ}_{7/2}$				
6093.856	1	16405.43	$29308^{\circ}_{9/2}-45714_{11/2}$				
6092.771	1	16408.35					
6091.873	1	16410.77					
6090.220	2	16415.22	$24348_{9/2}-40763^{\circ}_{7/2}$				
"			$23431^{\circ}_{9/2}-39847_{7/2}$				
6088.713	1	16419.29					
6086.848	8	16424.32	$22419^{\circ}_{9/2}-38844_{11/2}$				
6085.977	2	16426.67	$27037^{\circ}_{7/2}-43464_{9/2}$				
6085.445	1	16428.10	$26448^{\circ}_{9/2}-42876_{9/2}$				
6084.574	1	16430.46					
6082.898	1	16434.98	$17343_{7/2}-33778^{\circ}_{7/2}$				
6081.586	1	16438.53	$21799^{\circ}_{7/2}-38237_{7/2}$				
6080.782	1	16440.70	$32107^{\circ}_{11/2}-48547_{9/2}$				
6080.504	10	16441.45	$17752_{9/2}-34194^{\circ}_{9/2}$				
6078.362	2	16447.25					
6075.555	4	16454.85					
6075.211	1	16455.78					
6074.670	1	16457.24	$22929_{9/2}-39386^{\circ}_{9/2}$				
6072.656	2	16462.70	$25717_{7/2}-42179^{\circ}_{9/2}$				
6068.945	1	16472.77	$24957^{\circ}_{11/2}-41430_{11/2}$				
6068.508	1	16473.95	$21737_{9/2}-38211^{\circ}_{7/2}$				
6067.411	10	16476.93	$27037^{\circ}_{7/2}-43514_{7/2}$				
6064.827	1	16483.95	$22929_{9/2}-39413^{\circ}_{7/2}$				
6063.169	20	16488.46	$17454_{13/2}-33943^{\circ}_{13/2}$				
6062.533	1	16490.19	$22929_{9/2}-39419^{\circ}_{9/2}$				
6059.091	2	16499.56					
6058.988	5	16499.84	$26368^{\circ}_{13/2}-42868_{13/2}$				
6057.992	1	16502.55					
6057.553	2	16503.75	$26448^{\circ}_{9/2}-42952_{7/2}$				
6055.655	2	16508.92					
6055.268	1	16509.97	$18853_{13/2}-35363^{\circ}_{9/2}$				
6055.072	2	16510.51	$26357^{\circ}_{13/2}-42868_{13/2}$				
6054.541	20	16511.96	$23335^{\circ}_{7/2}-39847_{7/2}$				
"			$24957^{\circ}_{11/2}-41469_{13/2}$				
6052.810	1	16516.68					
6049.419	1	16525.94	$24137_{13/2}-40663^{\circ}_{13/2}$				
6047.127	2	16532.20	$21997_{11/2}-38529^{\circ}_{13/2}$				
6046.804	1	16533.08	$22929_{9/2}-39462^{\circ}_{7/2}$				
6044.181	10	16540.26	$27440^{\circ}_{9/2}-43981_{7/2}$				
"			$26889_{9/2}-43429^{\circ}_{9/2}$				
6043.989	2	16540.78	$22929_{9/2}-39470^{\circ}_{9/2}$				
"			$24246^{\circ}_{7/2}-40787_{9/2}$				
6043.767	2	16541.39	$19132_{9/2}-35673^{\circ}_{9/2}$				
6043.068	10	16543.31	$25207^{\circ}_{9/2}-41751_{9/2}$	S0	1.06	1.36	
6040.260	1	16551.00	$28340^{\circ}_{7/2}-44891_{7/2}$				
6039.780	40	16552.31					
6038.380	2	16556.15	$24246^{\circ}_{7/2}-40802_{7/2}$				
6037.696	1	16558.02					
6037.279	15	16559.17	$25520^{\circ}_{11/2}-42080_{11/2}$				
6036.983	10	16559.98					
6035.639	1	16563.67	$22559^{\circ}_{11/2}-39123_{9/2}$				
6035.389	3	16564.35	$23431^{\circ}_{9/2}-39996_{7/2}$				
6034.254	1	16567.47					
6031.303	3	16575.58	$23941^{\circ}_{9/2}-40516_{9/2}$				
6026.521	1 ħ	16588.73	$26368^{\circ}_{13/2}-42957_{13/2}$				
6025.437	200	16591.71	$17454_{13/2}-34046^{\circ}_{13/2}$	SI	1.45	0.30	
6024.192	1	16595.14					
6021.645	2	16602.16	$27377_{13/2}-43979^{\circ}_{13/2}$				
6020.036	2	16606.60					
6019.165	1	16609.00					
6018.978	1	16609.52					
6018.732	1	16610.20	$21737_{9/2}-38347^{\circ}_{13/2}$				
6017.905	2	16612.48	$22929_{9/2}-39542^{\circ}_{7/2}$				
6017.724	2	16612.98	$17752_{9/2}-34365^{\circ}_{7/2}$				
6017.195	1	16614.44					
6016.016	7	16617.69	$17343_{7/2}-33961^{\circ}_{7/2}$				
6015.899	5	16618.02	$25520^{\circ}_{11/2}-42139_{9/2}$				
6014.283	1	16622.48	$22791_{7/2}-39413^{\circ}_{7/2}$				
6013.767	1	16623.91	$19753_{7/2}-36377^{\circ}_{9/2}$				
6013.417	1	16624.88	$26488_{7/2}-43113^{\circ}_{9/2}$				
6011.856	3	16629.19	$19748_{9/2}-36377^{\circ}_{9/2}$				
6011.777	8	16629.41	$15587_{13/2}-32217^{\circ}_{9/2}$				
6011.373	1	16630.53	$25488_{11/2}-42119^{\circ}_{11/2}$				
6010.058	3	16634.17					
6009.920	15	16634.55	$21799^{\circ}_{9/2}-38433_{9/2}$				
6009.812	2	16634.85	$23431^{\circ}_{9/2}-40066_{9/2}$				
6009.693	1	16635.18					
6009.191	1	16636.57					
6008.262	5	16639.14					
6006.610	1	16643.72	$24137_{13/2}-40780^{\circ}_{13/2}$				
6005.338	3	16647.24	$21737_{9/2}-38384^{\circ}_{9/2}$				
6005.315	1	16647.31	$22559^{\circ}_{11/2}-39206_{9/2}$				
6004.191	1	16650.42	$25717_{7/2}-42367^{\circ}_{9/2}$				
6003.711	3	16651.75	$24701^{\circ}_{9/2}-41352_{11/2}$				
6003.222	1	16653.11	$22791_{7/2}-39444^{\circ}_{9/2}$				
6002.998	1	16653.73	$16742_{7/2}-33396^{\circ}_{7/2}$				

Wavelength in air Å	Intensity	Wavenumber cm^{-1}	Classification	Zeeman effect type	f	Je	
6002.497	3	16655.12	$22468^{\circ}_{11/2}-39123_{9/2}$				
6001.692	30	16657.35	$20406^{\circ}_{9/2}-37064_{9/2}$	ΔJ=0	1.577	1.42	*
6000.840	3	16659.72	$23431^{\circ}_{9/2}-40091_{9/2}$				
5996.556	1	16671.62	$22791_{7/2}-39462^{\circ}_{7/2}$				
5995.988	3	16673.20	$22929_{9/2}-39602^{\circ}_{9/2}$				
5995.357	1	16674.96					
5992.659	1	16682.46					
5990.930	2	16687.28	$19748_{9/2}-36435^{\circ}_{7/2}$				
5990.275	1	16689.10	$22791_{7/2}-39480^{\circ}_{7/2}$				
5989.927	1	16690.07	$24701^{\circ}_{9/2}-41391_{9/2}$				
5989.377	1	16691.60					
5987.560	1	16696.67	$17613_{9/2}-34310^{\circ}_{9/2}$				
5984.867	40	16704.18		T	1.18		
5984.315	1	16705.72					
5981.978	2	16712.25	$26448^{\circ}_{9/2}-43160_{9/2}$				
5981.735	30	16712.93	$19466_{13/2}-36179^{\circ}_{13/2}$	T	1.16		
5978.100	1	16723.09	$23873_{7/2}-40596^{\circ}_{7/2}$				
5975.747	2	16729.68	$25699^{\circ}_{9/2}-42429_{11/2}$				
5975.070	3	16731.60	$23335^{\circ}_{7/2}-40066_{9/2}$	T	1.36		
5975.015	100	16731.73	$20406^{\circ}_{9/2}-37138_{9/2}$	T	1.56		
5974.670	3	16732.69	$24348_{9/2}-41081^{\circ}_{11/2}$				
5973.744	1	16735.29					
5972.514	1	16738.73					
5972.392	20	16739.07	$23374_{13/2}-40113^{\circ}_{13/2}$				
5971.264	2000 r	16742.24	$0^{\circ}_{7/2}-16742_{7/2}$	ΔJ=0	1.14	1.32	*
5970.310	3	16744.91	$21737_{9/2}-38482^{\circ}_{7/2}$				
5969.141	1	16748.19					
5968.784	1	16749.19					
5968.609	1	16749.68	$25130_{13/2}-41880^{\circ}_{13/2}$				
5968.135	3	16751.01	$22791_{7/2}-39542^{\circ}_{7/2}$				
5967.800	7	16751.95	$17613_{9/2}-34365^{\circ}_{7/2}$	T	1.15		
5967.734	2	16752.14	$23781_{9/2}-40533^{\circ}_{7/2}$				
5966.011	30	16756.98	$19466_{13/2}-36223^{\circ}_{13/2}$	ΔJ=0	1.10	0.22	
5961.186	1	16770.54	$24957^{\circ}_{11/2}-41728_{9/2}$				
5960.113	4	16773.56	$26448^{\circ}_{9/2}-43221_{9/2}$				
5958.162	1	16779.05					
5956.057	1	16784.98	$24708^{\circ}_{7/2}-41493_{9/2}$				
5954.390	1	16789.68					
5954.294	3	16789.95					
5953.565	10	16792.01	$21737_{9/2}-38529^{\circ}_{11/2}$				
5953.189	4	16793.07					
5952.534	1	16794.92					
5951.444	2	16797.99	$27440^{\circ}_{9/2}-44238_{9/2}$				
5949.396	1	16803.77	$23309_{11/2}-40113^{\circ}_{13/2}$				
5948.369	1	16806.67					
5948.156	15	16807.28	$19466_{13/2}-36273^{\circ}_{13/2}$				
5946.640	1	16811.56					
5944.945	10	16816.35					
5944.862	2	16816.59					
5943.090	1	16821.60	$27037^{\circ}_{7/2}-43859_{9/2}$				
5942.666	1	16822.80					
5940.820	6	16828.03	$24246^{\circ}_{7/2}-41074_{9/2}$				
5939.880	2	16830.69					
5939.804	10	16830.91					
5939.735	20	16831.11					
5939.674	3	16831.28					
5938.842	5	16833.64					
5937.714	1	16836.83	$22791_{7/2}-39628^{\circ}_{7/2}$				
5935.895	300	16841.99	$15271_{15/2}-32112^{\circ}_{13/2}$	ΔJ=0	1.08	0.973	*
5935.067	1	16844.34	$25717_{7/2}-42561^{\circ}_{9/2}$				
5934.889	30	16844.85	$18837_{9/2}-35682^{\circ}_{7/2}$	T	1.125		
5934.257	1	16846.64					
5932.826	1	16850.71	$17343_{7/2}-34194^{\circ}_{9/2}$				
5931.703	100	16853.90	$15587_{11/2}-32441^{\circ}_{9/2}$	T	1.25		
5931.355	10	16854.88	$26448^{\circ}_{9/2}-43303_{7/2}$				
5929.813	1	16859.27					
5928.457	20	16863.12	$19466_{13/2}-36329^{\circ}_{11/2}$				
5928.335	1	16863.47					
5927.921	5	16864.65	$18693_{15/2}-35557^{\circ}_{13/2}$				
5922.622	4	16879.74	$21997_{13/2}-38877^{\circ}_{13/2}$				
5921.988	2	16881.54					
5920.846	40	16884.80	$8771^{\circ}_{9/2}-25656_{9/2}$	ΔJ=0	0.82	0.34	
5918.914	10	16890.31					
5918.852	2	16890.49					
5916.891	30	16896.09	$25699^{\circ}_{9/2}-42595_{11/2}$				
5916.500	10	16897.20					
5916.020	10	16898.57	$23309_{11/2}-40208^{\circ}_{9/2}$				
5914.386	1	16903.24					
5913.874	4	16904.71	$29316^{\circ}_{9/2}-46221_{11/2}$				
"			$24246^{\circ}_{7/2}-41151_{9/2}$				
5912.582	50	16908.40	$25520^{\circ}_{11/2}-42429_{11/2}$	ΔJ=0	1.14	0.49	
5910.104	1	16915.49					
5909.185	5	16918.12	$25488_{11/2}-42406^{\circ}_{13/2}$				
5909.073	1	16918.44	$21997_{11/2}-38915^{\circ}_{13/2}$				
5908.792	1	16919.24	$17613_{9/2}-34532^{\circ}_{11/2}$				
5908.405	20	16920.35	$25536^{\circ}_{13/2}-42456_{13/2}$	T	1.18		
5907.008	1	16924.35					
5906.260	1	16926.50	$21737_{9/2}-38664^{\circ}_{7/2}$				
5905.976	1	16927.31					
5901.572	300	16939.94	$18693_{15/2}-35633^{\circ}_{17/2}$	T	1.10	0.05	
5900.864	1	16941.98	$26646_{9/2}-43588^{\circ}_{7/2}$				
5900.282	1	16943.65	$27037^{\circ}_{7/2}-43981_{7/2}$				
5900.091	1	16944.20	$24137_{13/2}-41081^{\circ}_{11/2}$				
5899.473	400	16945.97	$8771^{\circ}_{9/2}-25717_{7/2}$	SI	1.4		
5878.670	1	17005.94	$24611^{\circ}_{9/2}-41617_{7/2}$				
5878.139	1	17007.47	$24418_{9/2}-41425^{\circ}_{7/2}$				
5877.597	5	17009.04	$25536^{\circ}_{13/2}-42545_{13/2}$				
5876.918	20	17011.01					
5873.827	2	17019.96	$24708^{\circ}_{7/2}-41728_{9/2}$				
5873.037	1	17022.25	$17343_{7/2}-34365^{\circ}_{7/2}$				
5872.372	1	17024.18	$25520^{\circ}_{11/2}-42545_{13/2}$				
5872.147	1	17024.83	$25717_{7/2}-42742^{\circ}_{7/2}$				
5871.996	10	17025.27	$23335^{\circ}_{7/2}-40360_{7/2}$				
5871.584	1	17026.46					
5871.416	2	17026.95	$24701^{\circ}_{9/2}-41728_{9/2}$				
5866.753	1	17040.48	$22902^{\circ}_{13/2}-39942_{11/2}$				
5863.392	1	17050.25	$21161_{9/2}-38211^{\circ}_{7/2}$				
5862.921	1	17051.62					
5862.488	1	17052.88	$25488_{11/2}-42541^{\circ}_{11/2}$				
5861.748	4	17055.03	$25520^{\circ}_{11/2}-42576_{9/2}$				
5861.353	1	17056.18	$23882_{9/2}-40938^{\circ}_{9/2}$				
5858.018	2	17065.89					
5857.910	1	17066.20	$23309_{11/2}-40376^{\circ}_{13/2}$				
5855.580	1	17073.00	$25488_{11/2}-42561^{\circ}_{9/2}$				
5853.828	4	17078.11	$17454_{13/2}-34532^{\circ}_{11/2}$				
"			$17613_{9/2}-34691^{\circ}_{11/2}$				
5850.238	1	17088.59	$27440^{\circ}_{9/2}-44529_{7/2}$				
5848.579	1	17093.43	$25488_{11/2}-42581^{\circ}_{11/2}$				
5844.602	2	17105.06	$18853_{11/2}-35958^{\circ}_{13/2}$				
5844.056	10	17106.66					
5843.936	10	17107.01					
5843.802	8	17107.41	$23882_{9/2}-40989^{\circ}_{9/2}$				
5842.825	1	17110.27					
5841.385	4	17114.48	$17343_{7/2}-34457^{\circ}_{9/2}$				
5841.020	1	17115.55	$24418_{9/2}-41533^{\circ}_{9/2}$				
5839.362	1	17120.41					
5836.590	5	17122.68	$24957^{\circ}_{11/2}-42080_{11/2}$	ΔJ=0	1.18	0.62	
5835.837	1	17130.75					
5835.524	1	17131.67	$22929_{9/2}-40061^{\circ}_{7/2}$				
5834.939	20	17133.39	$23941^{\circ}_{9/2}-41074_{9/2}$	ΔJ=0	1.10	1.00	
5833.468	30	17137.71	$24137_{13/2}-41274^{\circ}_{13/2}$	T	1.14		
5832.966	10	17139.19	$23873_{7/2}-41012^{\circ}_{7/2}$				
5832.851	2	17139.52	$21737_{9/2}-38877^{\circ}_{11/2}$				
5831.910	1	17142.29					
5831.087	4	17144.71	$24246^{\circ}_{7/2}-41391_{9/2}$				
5830.387	10	17146.77	$25520^{\circ}_{11/2}-42667_{9/2}$	T	1.08		
5830.125	1	17147.54					
5829.527	3	17149.30					
5829.394	1	17149.69	$25207^{\circ}_{9/2}-42357_{9/2}$				
5829.136	40	17150.45					
5828.381	3	17152.67	$23431^{\circ}_{9/2}-40584_{9/2}$				
5822.995	5	17168.53	$25699^{\circ}_{9/2}-42868_{11/2}$				
5821.310	4	17173.50					

APPENDIX—*Spectral Lines of Neutral Thulium*—Continued

Wavelength in air Å	Intensity	Wavenumber cm⁻¹	Classification	Zeeman effect type	f	Je	
5818.337	1	17182.28					
5816.648	7	17187.27	$19466_{13/2} - 36653^{\circ}_{13/2}$				
5816.458	100	17187.83	$16456_{11/2} - 33644^{\circ}_{13/2}$	T	1.10	0.05	
5815.702	1	17190.06	$19466_{13/2} - 36656^{\circ}_{11/2}$				
5815.264	1	17191.36					
5812.909	2	17198.32					
5811.875	3	17201.38	$27037^{\circ}_{7/2} - 44238_{9/2}$				
5810.721	1	17204.80					
5810.589	3	17205.19					
5809.749	1	17207.68	$23309_{11/2} - 40517^{\circ}_{9/2}$				
5806.394	1	17217.62	$23431^{\circ}_{9/2} - 40649_{7/2}$				
5806.230	1	17218.11					
5805.838	7	17219.27					
5803.485	1	17226.25	$22902^{\circ}_{13/2} - 40128_{11/2}$				
5802.219	3	17230.01					
5801.998	2	17230.66	$23781_{9/2} - 41012^{\circ}_{7/2}$				
5801.134	6	17233.23	$18990_{11/2} - 36223^{\circ}_{13/2}$				
5799.862	100	17237.01	$17454_{13/2} - 34691^{\circ}_{11/2}$				
5797.617	5	17243.68	$25520^{\circ}_{11/2} - 42764_{9/2}$				
5797.308	2	17244.60	$17343_{7/2} - 34587^{\circ}_{9/2}$				
5796.790	1	17246.14					
5796.710	20	17246.38	$17752_{9/2} - 34999^{\circ}_{9/2}$	SI	1.187	0.898	*
5796.636	2	17246.60	$24246^{\circ}_{7/2} - 41493_{9/2}$				
5796.265	10	17247.71					
5793.244	7	17256.70	$19753_{7/2} - 37010^{\circ}_{9/2}$				
5793.008	2	17257.40	$25699^{\circ}_{9/2} - 42957_{11/2}$				
5791.532	8	17261.80	$23431^{\circ}_{9/2} - 40693_{9/2}$				
5791.470	1	17261.99	$19748_{9/2} - 37010^{\circ}_{9/2}$				
5790.765	10	17264.09	$21120_{7/2} - 38384^{\circ}_{9/2}$				
5790.187	2	17265.81	$18693_{13/2} - 35958^{\circ}_{13/2}$				
5788.139	1	17271.92					
5786.701	3	17276.21	$25130_{13/2} - 42406^{\circ}_{13/2}$				
5783.574	1	17285.55	$27037^{\circ}_{7/2} - 44323_{7/2}$				
5783.318	3	17286.32					
5781.484	1	17291.80	$26889_{9/2} - 44180^{\circ}_{11/2}$				
5776.268	1	17307.42	$25745_{9/2} - 43052^{\circ}_{7/2}$				
5775.664	2	17309.23	$27440^{\circ}_{9/2} - 44750_{7/2}$				
5774.317	1	17313.26					
5773.586	1	17315.46					
5773.116	1	17316.87					
5772.882	1	17317.57					
5772.733	9	17318.02	$20406^{\circ}_{9/2} - 37724_{9/2}$				
5772.211	1	17319.58					
5771.982	2	17320.27					
5771.672	2	17321.20	$21161_{9/2} - 38482^{\circ}_{7/2}$				
5771.552	6	17321.56					
5769.319	1	17328.26					
5767.531	10	17333.63	$25536^{\circ}_{15/2} - 42869_{13/2}$				
5765.570	8	17339.53					
5764.287	3000 r	17343.39	$0^{\circ}_{7/2} - 17343_{7/2}$	ΔJ=0	1.08	0.42	
5763.003	30	17347.25	$25520^{\circ}_{11/2} - 42868_{11/2}$				
5762.498	5	17348.77	$25520^{\circ}_{11/2} - 42869_{13/2}$				
5761.436	2	17351.97					
5761.215	5	17352.64	$26448^{\circ}_{9/2} - 43800_{7/2}$				
5761.041	2	17353.16	$23309_{11/2} - 40663^{\circ}_{11/2}$				
5760.982	1	17353.34	$16957_{7/2} - 34310^{\circ}_{9/2}$				
5760.545	3	17354.66					
5760.202	500 r	17355.69	$8771^{\circ}_{9/2} - 26126_{9/2}$	ΔJ=0	0.855	1.10	*
5758.186	1	17361.77	$21120_{7/2} - 38482^{\circ}_{7/2}$				
5758.020	300	17362.27	$15587_{11/2} - 32950^{\circ}_{13/2}$	SI	1.62	0.29	
5755.516	20	17369.82	$27377_{13/2} - 44747^{\circ}_{13/2}$				
5753.856	3	17374.83	$26889_{9/2} - 44263^{\circ}_{7/2}$				
5752.741	1	17378.20	$21120_{7/2} - 38499^{\circ}_{9/2}$				
5752.644	1	17378.49					
5752.441	4	17379.10	$24701^{\circ}_{9/2} - 42080_{11/2}$				
5751.626	1	17381.57	$25520^{\circ}_{11/2} - 42902_{9/2}$				
5751.127	4	17383.08	$22559^{\circ}_{11/2} - 39942_{11/2}$				
5750.285	4	17385.62	$22742^{\circ}_{13/2} - 40128_{11/2}$				
5749.774	1	17387.17					
5749.720	8	17387.33	$18990_{11/2} - 36377^{\circ}_{9/2}$				
5744.827	20	17402.14					
5743.860	1	17405.07					
5743.520	1	17406.10					
5742.692	30	17408.61	$16957_{7/2} - 34365^{\circ}_{7/2}$	ΔJ=0	1.18	0.12	
5741.659	1	17411.74	$23941^{\circ}_{9/2} - 41352_{11/2}$				
5739.817	1	17417.33	$22791_{7/2} - 40208^{\circ}_{9/2}$				
5738.446	1	17421.49	$25488_{11/2} - 42910^{\circ}_{13/2}$				
5737.914	1	17423.10					
5735.838	7	17429.41					
5735.394	2	17430.76	$26357^{\circ}_{13/2} - 43788_{13/2}$				
5733.616	20	17436.16	$25520^{\circ}_{11/2} - 42957_{11/2}$				
5733.446	20	17436.68	$21997_{11/2} - 39434^{\circ}_{13/2}$				
5732.969	1	17438.13					
5730.114	1	17446.82	$21997_{11/2} - 39444^{\circ}_{9/2}$				
5729.053	1	17450.05	$23941^{\circ}_{9/2} - 41391_{9/2}$				
5728.471	7	17451.82	$16742_{7/2} - 34194^{\circ}_{9/2}$				
5725.827	1	17459.88					
5725.539	20	17460.76	$21799^{\circ}_{7/2} - 39259_{9/2}$	S0	1.45	1.20	*
5724.404	1	17464.22					
5723.350	2	17467.44	$23335^{\circ}_{7/2} - 40802_{7/2}$				
5723.285	1	17467.64	$19753_{7/2} - 37221^{\circ}_{7/2}$				
5723.079	4	17468.27	$26368^{\circ}_{11/2} - 43836_{11/2}$				
5722.761	3	17469.24					
5720.571	5	17475.92	$18853_{11/2} - 36329^{\circ}_{13/2}$				
5722.206	1	17470.93	$23309_{11/2} - 40780^{\circ}_{13/2}$				
5721.887	5	17471.91	$24957^{\circ}_{11/2} - 42429_{11/2}$				
5721.031	1	17474.52	$22468^{\circ}_{11/2} - 39942_{11/2}$				
5720.180	1	17477.12					
5719.587	20	17478.93	$26357^{\circ}_{13/2} - 43836_{13/2}$	T	1.17		
5719.029	1	17480.64					
5718.718	30	17481.59	$24246^{\circ}_{7/2} - 41728_{9/2}$	T	1.06		
5718.462	1	17482.37	$21737_{9/2} - 39220^{\circ}_{9/2}$				
"			$21997_{13/2} - 39479^{\circ}_{13/2}$				
5718.365	1	17482.67					
5717.104	70	17486.52	$18693_{13/2} - 36179^{\circ}_{15/2}$	ΔJ=0	1.17	0.20	
5716.238	1	17489.17	$23941^{\circ}_{9/2} - 41430_{11/2}$				
5715.788	200	17490.55	$15271_{15/2} - 32761^{\circ}_{17/2}$	SI	1.30	0.20	
5715.181	40	17492.41	$18837_{9/2} - 36329^{\circ}_{11/2}$	S0	0.56	0.47	
5715.010	5	17492.93	$24348_{9/2} - 41841^{\circ}_{7/2}$				
5714.503	1	17494.48	$26889_{9/2} - 44383^{\circ}_{11/2}$				
5713.633	2	17497.15	$25699^{\circ}_{9/2} - 43196_{11/2}$				
5713.030	1	17498.99	$24957^{\circ}_{11/2} - 42456_{11/2}$				
5712.422	40	17500.85	$16957_{7/2} - 34457^{\circ}_{9/2}$	T	1.21		
5711.924	9	17502.38					
5711.793	1	17502.78	$21161_{9/2} - 38664^{\circ}_{7/2}$				
5709.750	100	17509.04		T	1.21		
5708.877	1	17511.72					
5707.929	1	17514.63	$23574^{\circ}_{9/2} - 41089_{7/2}$				
5706.715	1	17518.36					
5706.048	2	17520.40					
5705.900	4	17520.86					
5705.275	10	17522.78	$22419^{\circ}_{9/2} - 39942_{11/2}$	SI	0.93	1.19	*
5704.903	8	17523.92	$18853_{11/2} - 36377^{\circ}_{9/2}$				
5704.328	3	17525.69	$24348_{9/2} - 41874^{\circ}_{11/2}$				
5703.499	10	17528.23	$19748_{9/2} - 37276^{\circ}_{11/2}$				
5702.740	10	17530.57	$18693_{13/2} - 36223^{\circ}_{13/2}$				
5702.479	1	17531.37	$22791_{7/2} - 40322^{\circ}_{9/2}$				
5702.000	20	17532.84	$26448^{\circ}_{9/2} - 43981_{7/2}$				
5701.012	7	17535.88					
5698.581	1	17543.36	$21120_{7/2} - 38664^{\circ}_{7/2}$				
5697.987	1	17545.19	$27037^{\circ}_{7/2} - 44582_{9/2}$				
5696.987	2	17548.27					
5696.522	2	17549.70					
5696.186	1	17550.74					
5695.931	2	17551.52					
5694.449	1	17556.09	$22791_{7/2} - 40347^{\circ}_{9/2}$				
5694.262	1	17556.67					
5692.938	2	17560.75					
5692.323	2	17562.65	$26701_{7/2} - 44263^{\circ}_{7/2}$				
5691.650	1	17564.72	$21120_{7/2} - 38685^{\circ}_{9/2}$				

Wavelength in air Å	Intensity	Wavenumber cm⁻¹	Classification	Zeeman effect type	f	Je	
5691.387	3	17565.54	$21997_{11/2}-39563^{\circ}_{11/2}$				
5690.879	1	17567.10	$26889_{9/2}-44456^{\circ}_{7/2}$				
5690.559	2	17568.09	$16742_{7/2}-34310^{\circ}_{9/2}$				
5690.305	20	17568.88	$22559^{\circ}_{11/2}-40128_{11/2}$				
5687.555	1	17577.37	$27440^{\circ}_{9/2}-45018_{7/2}$				
5685.386	2	17584.08					
5684.222	1	17587.68	$24957^{\circ}_{11/2}-42545_{13/2}$				
5683.592	200	17589.63	$16456_{17/2}-34046^{\circ}_{15/2}$	T	1.16		
5683.335	3	17590.42	$21161_{9/2}-38751^{\circ}_{9/2}$	ΔJ=0	?	0.20	
5682.036	3	17594.44	$25520^{\circ}_{11/2}-43115_{9/2}$				
5680.591	2	17598.92	$26701_{7/2}-44300^{\circ}_{9/2}$				
5680.247	1	17599.98					
5679.856	1	17601.20	$22902^{\circ}_{13/2}-40503_{11/2}$				
5679.264	1	17603.03					
5679.130	1	17603.45	$25699^{\circ}_{9/2}-43303_{7/2}$				
5677.744	1	17607.74					
5675.835	5000 *r*	17613.67	$0^{\circ}_{7/2}-17613_{9/2}$	SI	1.34	0.14	
5673.484	2	17620.96					
5670.261	2	17630.98	$16957_{7/2}-34587^{\circ}_{9/2}$				
5669.950	10	17631.95					
5669.389	1	17633.69	$22468^{\circ}_{11/2}-40101_{9/2}$				
5667.897	1	17638.33	$24957^{\circ}_{11/2}-42595_{11/2}$				
5667.711	1	17638.91					
5666.257	1	17643.44					
5664.091	2	17650.19	$27440^{\circ}_{9/2}-45091_{9/2}$				
5663.975	1	17650.55					
5663.783	2	17651.15	$23882_{9/2}-41533^{\circ}_{9/2}$				
5662.920	4	17653.84					
5660.834	20	17660.34	$22468^{\circ}_{11/2}-40128_{11/2}$	ΔJ=0	1.13	0.53	
5658.918	7	17666.32	$18990_{11/2}-36656^{\circ}_{11/2}$				
5658.298	600	17668.26	$8771^{\circ}_{9/2}-26439_{7/2}$	SI	1.37	0.37	
5657.047	3	17672.16					
5656.896	4	17672.63	$19548_{9/2}-37221^{\circ}_{7/2}$				
5655.858	5*h*	17675.88	$25520^{\circ}_{11/2}-43196_{11/2}$				
5655.765	4	17676.17	$23941^{\circ}_{9/2}-41617_{7/2}$	T	1.30		
5655.135	1	17678.14					
5654.839	20	17679.06	$15271_{13/2}-32950^{\circ}_{13/2}$	S00	1.07	1.31	*
5653.910	1	17681.97	$22419^{\circ}_{9/2}-40101_{9/2}$				
5653.610	5	17682.91					
5652.610	8	17686.03		SI	1.32	0.23	
5650.879	1	17691.45					
5650.434	50	17692.85	$19466_{13/2}-37159^{\circ}_{15/2}$	SI	1.75	0.465	
5648.457	1	17699.04					
5647.213	1	17702.94	$23873_{7/2}-41576^{\circ}_{9/2}$				
"			$26439_{7/2}-44142^{\circ}_{7/2}$				
5645.400	200	17708.62	$22419^{\circ}_{9/2}-40128_{11/2}$	SI	0.95	1.12	*
5644.686	1	17710.86					
5644.546	1	17711.30	$17343_{7/2}-35054^{\circ}_{9/2}$				
5644.462	3	17711.56	$21997_{11/2}-39709^{\circ}_{11/2}$				
"			$25717_{7/2}-43428^{\circ}_{7/2}$				
5644.062	5	17712.82	$23431^{\circ}_{9/2}-41144_{7/2}$				
5643.525	1	17714.51	$24611^{\circ}_{9/2}-42325_{7/2}$				
5643.284	1	17715.26	$24418_{9/2}-42133^{\circ}_{7/2}$				
5642.960	1	17716.28	$20406^{\circ}_{9/2}-38123_{7/2}$				
5640.179	40	17725.01	$25130_{13/2}-42855^{\circ}_{15/2}$				
5639.714	1	17726.48	$22791_{7/2}-40517^{\circ}_{9/2}$				
5639.443	1	17727.33					
5639.127	2	17728.32	$24701^{\circ}_{9/2}-42429_{11/2}$				
5638.207	1	17731.21					
5636.309	3	17737.18	$24137_{13/2}-41874^{\circ}_{11/2}$				
5635.709	7	17739.07					
5635.623	5	17739.34	$23335^{\circ}_{7/2}-41074_{9/2}$				
5634.718	2	17742.19	$21737_{9/2}-39479^{\circ}_{11/2}$				
5634.481	2	17742.94	$24137_{13/2}-41880^{\circ}_{15/2}$				
5633.729	2	17745.31					
5632.902	60	17747.91	$21799^{\circ}_{9/2}-39547_{9/2}$	S0	1.03	0.25	
5632.061	2	17750.56	$21737_{9/2}-39488^{\circ}_{9/2}$				
5631.406	3000 *r*	17752.63	$0^{\circ}_{7/2}-17752_{9/2}$	S0	1.015	0.13	
5629.335	2	17759.16	$23941^{\circ}_{9/2}-41700_{11/2}$				
5629.063	2	17760.02					
5628.894	3	17760.55	$22742^{\circ}_{13/2}-40503_{11/2}$				
5628.474	1	17761.87	$24418_{9/2}-42179^{\circ}_{9/2}$				
5626.309	3	17768.71					
5625.457	5	17771.40	$23309_{11/2}-41081^{\circ}_{11/2}$	ΔJ=0	1.28	0.45	
5624.968	2	17772.95	$23873_{7/2}-41646^{\circ}_{7/2}$				
5623.525	1	17777.51					
5622.864	1	17779.60	$25130_{13/2}-42910^{\circ}_{13/2}$				
5622.723	50	17780.04	$24137_{13/2}-41917^{\circ}_{13/2}$	ΔJ=0	1.14	0.13	
5622.049	1	17782.17					
5621.288	2	17784.58	$24348_{9/2}-42133^{\circ}_{7/2}$				
5620.542	7	17786.94	$23941^{\circ}_{9/2}-41728_{9/2}$				
5620.391	2	17787.42	$23781_{9/2}-41569^{\circ}_{11/2}$				
5618.171	5	17794.45	$23781_{9/2}-41576^{\circ}_{9/2}$	ΔJ=0	1.20	0.485	
5617.799	2	17795.63					
5617.725	1	17795.86					
5617.578	2	17796.33					
5615.500	2	17802.91	$18853_{11/2}-36656^{\circ}_{11/2}$				
5615.318	1	17803.49					
5614.714	2	17805.40					
5614.148	2	17807.20	$24957^{\circ}_{11/2}-42764_{9/2}$				
5614.004	2	17807.66					
5613.694	40	17808.64					
5613.410	6	17809.54	$23335^{\circ}_{7/2}-41144_{7/2}$				
5613.230	70	17810.11	$19466_{13/2}-37276^{\circ}_{11/2}$	S0	0.62	0.50	
5611.893	2	17814.35	$23309_{11/2}-41124^{\circ}_{9/2}$				
5611.380	2	17815.98	$23335^{\circ}_{7/2}-41151_{9/2}$				
5609.947	2	17820.53					
5608.440	5	17825.32	$21737_{9/2}-39563^{\circ}_{11/2}$				
5606.643	50	17831.03	$20406^{\circ}_{9/2}-38237_{9/2}$	SI	1.58	1.04	*
5606.333	1	17832.02					
5605.652	1	17834.19	$22929_{9/2}-40763^{\circ}_{9/2}$				
5605.300	2	17835.31					
5604.640	20	17837.41		SI	1.30	0.16	
5603.184	5	17842.04	$24701^{\circ}_{9/2}-42543_{7/2}$				
5602.686	20	17843.63	$22742^{\circ}_{13/2}-40586_{13/2}$	ΔJ=0	1.19	0.11	
5599.508	4	17853.76	$27037^{\circ}_{7/2}-44891_{7/2}$				
5598.206	20	17857.91	$26889_{9/2}-44747^{\circ}_{11/2}$				
5597.957	1	17858.70					
5597.592	3	17859.87					
5596.928	2	17861.99					
5596.156	2	17864.45	$23781_{9/2}-41646^{\circ}_{7/2}$				
5595.869	3	17865.37					
5595.056	2	17867.96	$24708^{\circ}_{7/2}-42576_{9/2}$				
5594.945	1	17868.32					
5594.281	2	17870.44	$26368^{\circ}_{11/2}-44238_{9/2}$				
5586.252	1	17896.12					
5583.247	40	17905.75	$23781_{9/2}-41687^{\circ}_{11/2}$	T	1.145		
5581.369	200	17911.78	$20406^{\circ}_{9/2}-38318_{9/2}$	SI	1.58	1.20	*
5581.342	40	17911.86	$27377_{13/2}-45288^{\circ}_{13/2}$				
5581.215	40	17912.27	$24957^{\circ}_{11/2}-42869_{13/2}$				
5578.497	4	17921.00	$17752_{9/2}-35673^{\circ}_{9/2}$				
5577.407	2	17924.50					
5575.815	10	17929.62	$17752_{9/2}-35682^{\circ}_{7/2}$				
5575.135	20	17931.81	$24611^{\circ}_{9/2}-42543_{7/2}$				
5574.471	3	17933.94					
5571.608	10*h*	17943.16	$25520^{\circ}_{11/2}-43464_{9/2}$				
5571.402	20	17943.82	$22559^{\circ}_{11/2}-40503_{11/2}$	ΔJ=0	1.14	0.385	
5568.720	5	17952.46					
5568.630	5	17952.75	$24418_{9/2}-42370^{\circ}_{7/2}$				
"			$25207^{\circ}_{9/2}-43160_{9/2}$				
5568.427	5	17953.41	$22902^{\circ}_{13/2}-40855_{13/2}$				
5567.267	2	17957.15	$22559^{\circ}_{11/2}-40516_{9/2}$				
5566.479	1	17959.69	$24708^{\circ}_{7/2}-42667_{9/2}$				
5566.119	50	17960.85	$18693_{15/2}-36653^{\circ}_{15/2}$				
5566.005	300	17961.22	$13119_{9/2}-31080^{\circ}_{11/2}$	SI	1.64	0.29	
5564.862	2	17964.91	$23309_{11/2}-41274^{\circ}_{13/2}$				
5563.085	20	17970.65	$19548_{9/2}-37519^{\circ}_{7/2}$	SI	1.36	0.25	
5562.870	4	17971.34	$21737_{9/2}-39709^{\circ}_{11/2}$				
5562.447	2	17972.71	$22791_{7/2}-40763^{\circ}_{9/2}$				
5559.606	3	17981.89	$24137_{13/2}-42119^{\circ}_{11/2}$				

Wavelength in air Å	Intensity	Wavenumber cm^{-1}	Classification	Zeeman effect type	f	Je	
5556.248	3	17992.76					
5554.115	20	17999.67	$24957^{\circ}_{11/2} - 42957^{\circ}_{11/2}$				
5551.642	5	18007.69					
5551.385	1	18008.52	$23873^{\circ}_{7/2} - 41881^{\circ}_{9/2}$				
5550.802	3	18010.41	$24708^{\circ}_{7/2} - 42718^{\circ}_{9/2}$				
5549.665	20	18014.10	$25207^{\circ}_{3/2} - 43221^{\circ}_{3/2}$				
5549.442	10	18014.83	$19753^{\circ}_{7/2} - 37768^{\circ}_{9/2}$				
5549.121	6	18015.87	$25699^{\circ}_{9/2} - 43715^{\circ}_{11/2}$				
5548.787	3	18016.95					
5548.650	4	18017.40	$24701^{\circ}_{9/2} - 42718^{\circ}_{9/2}$				
5547.813	10	18020.12	$18990^{\circ}_{11/2} - 37010^{\circ}_{9/2}$				
"			$19748^{\circ}_{9/2} - 37768^{\circ}_{9/2}$				
5547.230	1	18022.01	$24348^{\circ}_{9/2} - 42370^{\circ}_{7/2}$				
5545.666	20	18027.09	$20406^{\circ}_{5/2} - 38433^{\circ}_{5/2}$				
5545.312	5	18028.24					
5544.968	8	18029.36					
5544.613	1	18030.52					
5543.148	4	18035.28	$22468^{\circ}_{11/2} - 40503^{\circ}_{11/2}$				
5541.949	15	18039.18					
5539.907	1	18045.83					
5539.260	1	18047.94					
5538.341	30	18050.94	$15587^{\circ}_{11/2} - 33638^{\circ}_{11/2}$	ΔJ=0	1.30	0.80	
5537.535	3	18053.56	$27037^{\circ}_{7/2} - 45091^{\circ}_{9/2}$				
5536.785	10	18056.01	$25488^{\circ}_{11/2} - 43544^{\circ}_{9/2}$				
"			$23335^{\circ}_{7/2} - 41391^{\circ}_{9/2}$				
5535.507	3	18060.18					
5535.195	30	18061.19	$23431^{\circ}_{9/2} - 41493^{\circ}_{9/2}$				
5532.301	2	18070.64	$26448^{\circ}_{9/2} - 44518^{\circ}_{9/2}$				
5531.600	3	18072.93	$26701^{\circ}_{7/2} - 44774^{\circ}_{9/2}$				
5529.083	2	18081.16	$26448^{\circ}_{9/2} - 44529^{\circ}_{7/2}$				
5528.702	2	18082.41	$24701^{\circ}_{9/2} - 42783^{\circ}_{7/2}$				
5528.343	200	18083.58	$22419^{\circ}_{9/2} - 40503^{\circ}_{11/2}$	SI	0.935	1.105	*
5526.614	2	18089.24					
5525.560	10	18092.69	$23781^{\circ}_{9/2} - 41874^{\circ}_{11/2}$				
5524.271	4	18096.91					
5524.034	3	18097.69	$16957^{\circ}_{7/2} - 35054^{\circ}_{9/2}$				
"			$26448^{\circ}_{9/2} - 44545^{\circ}_{9/2}$				
5522.451	1	18102.87	$17454^{\circ}_{13/2} - 35557^{\circ}_{13/2}$				
5520.169	1	18110.36					
5519.440	1	18112.75	$23431^{\circ}_{9/2} - 41544^{\circ}_{9/2}$				
"			$22742^{\circ}_{13/2} - 40855^{\circ}_{13/2}$				
5518.545	4	18115.69	$21161^{\circ}_{9/2} - 39277^{\circ}_{9/2}$				
5517.729	10	18118.37	$22468^{\circ}_{11/2} - 40586^{\circ}_{13/2}$				
5517.711	2	18118.42					
5517.115	2	18120.38					
5514.784	1	18128.04	$26646^{\circ}_{9/2} - 44774^{\circ}_{9/2}$				
5513.649	1	18131.77					
5513.566	1	18132.05					
5512.105	3	18136.85					
5511.425	3	18139.09	$23941^{\circ}_{9/2} - 42080^{\circ}_{11/2}$				
5509.890	1	18144.14	$22419^{\circ}_{9/2} - 40563^{\circ}_{9/2}$				
5507.311	10	18152.64		ΔJ=0	1.14	0.20	
5506.495	2	18155.33	$22929^{\circ}_{5/2} - 41085^{\circ}_{7/2}$				
5506.075	40	18156.71	$18853^{\circ}_{11/2} - 37010^{\circ}_{9/2}$	SI	1.36	0.20	
5505.999	1	18156.96					
5505.901	10	18157.29	$26357^{\circ}_{13/2} - 44515^{\circ}_{13/2}$				
5503.466	2	18165.32					
5501.340	20	18172.34					
5501.093	60	18173.16	$18837^{\circ}_{9/2} - 37010^{\circ}_{9/2}$	ΔJ=0	1.12	0.10	
5497.391	3	18185.39	$23431^{\circ}_{9/2} - 41617^{\circ}_{7/2}$				
5495.616	30	18191.27	$19466^{\circ}_{13/2} - 37657^{\circ}_{11/2}$	SI	1.95	0.77	
5495.189	1	18192.68	$24348^{\circ}_{9/2} - 42541^{\circ}_{11/2}$				
5494.617	50	18194.58	$25520^{\circ}_{11/2} - 43715^{\circ}_{11/2}$				
5493.950	4	18196.78	$24160^{\circ}_{3/2} - 42357^{\circ}_{5/2}$				
5491.365	10	18205.35	$15587^{\circ}_{11/2} - 33793^{\circ}_{11/2}$	T	1.26		
5490.046	3	18209.72					
5489.104	3	18212.85	$24348^{\circ}_{9/2} - 42561^{\circ}_{9/2}$				
5485.645	200	18224.33	$15587^{\circ}_{11/2} - 33812^{\circ}_{13/2}$	S0	0.56	0.58	
5483.420	3	18231.73	$27377^{\circ}_{13/2} - 45608^{\circ}_{15/2}$				
5483.200	2	18232.46					
5482.945	5	18233.31	$24348^{\circ}_{9/2} - 42581^{\circ}_{11/2}$	SI	1.26	0.11	
5482.533	2	18234.68	$25520^{\circ}_{11/2} - 43755^{\circ}_{9/2}$				
5481.113	3	18239.40	$24957^{\circ}_{11/2} - 43196^{\circ}_{11/2}$				
5481.054	10	18239.60					
5479.724	3	18244.03	$24708^{\circ}_{7/2} - 42952^{\circ}_{7/2}$				
5478.498	80	18248.11	$13119^{\circ}_{9/2} - 31367^{\circ}_{7/2}$	T	1.25	0.06	
5476.100	20	18256.10	$24701^{\circ}_{9/2} - 42957^{\circ}_{11/2}$				
5474.455	20	18261.58	$23574^{\circ}_{5/2} - 41836^{\circ}_{9/2}$				
5473.079	20	18266.18	$23309^{\circ}_{11/2} - 41576^{\circ}_{9/2}$				
5472.710	40	18267.41	$25520^{\circ}_{11/2} - 43788^{\circ}_{11/2}$				
5472.363	4	18268.57					
5470.913	10	18273.41					
5468.303	10	18282.13	$23335^{\circ}_{7/2} - 41617^{\circ}_{7/2}$				
5466.596	2	18287.84	$24418^{\circ}_{9/2} - 42705^{\circ}_{9/2}$				
5465.641	3	18291.03	$22902^{\circ}_{13/2} - 41193^{\circ}_{13/2}$				
5465.362	3	18291.97					
5465.299	10	18292.18	$21799^{\circ}_{3/2} - 40091^{\circ}_{3/2}$	ΔJ=0	1.47	1.15	*
5465.103	4	18292.83	$21120^{\circ}_{7/2} - 39413^{\circ}_{7/2}$				
5464.727	2	18294.09					
5464.621	1	18294.45					
5464.145	60	18296.04	$22559^{\circ}_{11/2} - 40855^{\circ}_{13/2}$	T	1.11	0.05	
5463.723	1	18297.45	$23882^{\circ}_{9/2} - 42179^{\circ}_{9/2}$				
5462.796	20	18300.56	$25536^{\circ}_{15/2} - 43836^{\circ}_{13/2}$	T	1.23		
5462.428	5	18301.79	$26448^{\circ}_{9/2} - 44750^{\circ}_{7/2}$				
5460.245	2	18309.11	$21161^{\circ}_{9/2} - 39470^{\circ}_{9/2}$				
5455.813	1	18323.98	$24418^{\circ}_{9/2} - 42742^{\circ}_{7/2}$				
5451.825	3	18337.39	$23781^{\circ}_{9/2} - 42119^{\circ}_{11/2}$				
5451.388	3	18338.86	$17343^{\circ}_{7/2} - 35682^{\circ}_{7/2}$				
5449.480	2	18345.28					
5642.596	300	17717.42	$8771^{\circ}_{9/2} - 26488^{\circ}_{9/2}$	T	0.85		
5641.273	15	17721.58	$20406^{\circ}_{5/2} - 38128^{\circ}_{5/2}$	ΔJ=0	1.58	1.05	*
5448.178	2	18349.66	$21120^{\circ}_{7/2} - 39470^{\circ}_{9/2}$				
5446.453	60	18355.47	$15587^{\circ}_{11/2} - 33943^{\circ}_{13/2}$	S0	0.45	0.67	
5440.751	6	18374.71	$18990^{\circ}_{11/2} - 37365^{\circ}_{13/2}$				
5440.438	1	18375.77					
5439.559	3	18378.74	$21997^{\circ}_{11/2} - 40376^{\circ}_{13/2}$				
5436.972	50	18387.48	$22468^{\circ}_{11/2} - 40855^{\circ}_{13/2}$	S0	0.94	0.22	
5435.645	20	18391.97	$19466^{\circ}_{13/2} - 37858^{\circ}_{13/2}$	SI	1.48	0.27	
5434.171	6	18396.96					
5433.334	5	18399.79					
5431.098	3	18407.37	$24708^{\circ}_{7/2} - 43115^{\circ}_{9/2}$				
5426.505	10	18422.95	$18853^{\circ}_{11/2} - 37276^{\circ}_{11/2}$	ΔJ=0	1.19	0.61	
5422.301	2	18437.23	$25745^{\circ}_{9/2} - 44182^{\circ}_{9/2}$				
5421.661	3	18439.41	$18837^{\circ}_{9/2} - 37276^{\circ}_{11/2}$				
5420.037	2	18444.93	$24611^{\circ}_{9/2} - 43056^{\circ}_{9/2}$				
5419.733	1	18445.97	$26701^{\circ}_{7/2} - 45147^{\circ}_{9/2}$				
5418.438	30	18450.37	$22742^{\circ}_{13/2} - 41193^{\circ}_{13/2}$	ΔJ=0	1.19	0.16	
5416.260	3	18457.79	$19753^{\circ}_{7/2} - 38211^{\circ}_{7/2}$				
5414.093	4	18465.18	$25717^{\circ}_{7/2} - 44182^{\circ}_{9/2}$				
5413.727	100	18466.43	$18693^{\circ}_{13/2} - 37159^{\circ}_{13/2}$	ΔJ=0	1.20	0.38	
5413.570	5	18466.97					
5413.476	10	18467.29		T	1.13	0.06	
5408.639	20	18483.80	$25130^{\circ}_{15/2} - 43614^{\circ}_{15/2}$				
5407.320	1	18488.31	$23941^{\circ}_{9/2} - 42429^{\circ}_{11/2}$				
5404.640	2	18497.48	$21161^{\circ}_{9/2} - 39658^{\circ}_{9/2}$				
"			$23873^{\circ}_{7/2} - 42370^{\circ}_{7/2}$				
5403.990	1	18499.70	$23374^{\circ}_{13/2} - 41874^{\circ}_{11/2}$				
5403.628	2	18500.94					
5402.716	40	18504.06	$17454^{\circ}_{13/2} - 35958^{\circ}_{13/2}$	ΔJ=0	1.14	0.15	
5402.231	200	18505.73		ΔJ=0	1.22	0.73	
5400.600	10	18511.31	$18853^{\circ}_{11/2} - 37365^{\circ}_{13/2}$	SI	1.39	0.20	
5391.912	50	18541.14	$15271^{\circ}_{13/2} - 33812^{\circ}_{13/2}$				
5391.500	3	18542.56	$23374^{\circ}_{13/2} - 41917^{\circ}_{13/2}$				
5391.172	1	18543.69					
5390.460	15	18546.14	$19466^{\circ}_{13/2} - 38012^{\circ}_{13/2}$				
5389.814	5	18548.36					
5386.736	10	18558.96	$18693^{\circ}_{13/2} - 37252^{\circ}_{17/2}$	SI	1.46	0.245	
5382.044	15	18575.14	$13119^{\circ}_{9/2} - 31694^{\circ}_{7/2}$	SI	1.77	0.45	
5377.280	4	18591.59	$22559^{\circ}_{11/2} - 41151^{\circ}_{9/2}$				
5376.834	3	18593.14	$25207^{\circ}_{5/2} - 43800^{\circ}_{9/2}$				

Wavelength in air Å	Intensity	Wavenumber cm⁻¹	Classification	Zeeman effect type	f	Je	
5374.984	1	18599.53	$25717_{9/2} - 44316^{*}_{9/2}$				
5374.242	1	18602.10	$24701^{*}_{9/2} - 43303_{7/2}$				
5372.754	4	18607.25	$23309_{11/2} - 41917^{*}_{13/2}$				
5371.810	2	18610.52	$24611^{*}_{9/2} - 43221_{9/2}$				
5368.756	5	18621.11	$21120_{7/2} - 39741^{*}_{9/2}$				
5365.141	2?	18633.66	$22559^{*}_{11/2} - 41193_{13/2}$	T	1.18		
5364.358	5	18636.38	$19748_{9/2} - 38384^{*}_{9/2}$				
5361.015	4	18648.00					
5358.782	5	18655.77	$18990_{11/2} - 37646^{*}_{13/2}$				
5355.945	2	18665.65	$21997_{11/2} - 40663^{*}_{11/2}$				
5355.547	2	18667.04					
5354.045	100	18672.27	$15271_{13/2} - 33943^{*}_{13/2}$	S0	0.77	0.29	
5350.089	2	18686.08					
5348.440	3	18691.84	$24611^{*}_{9/2} - 43303_{7/2}$				
5347.650	5	18694.60	$19466_{13/2} - 38161^{*}_{11/2}$				
5340.158	2	18720.83	$23873_{7/2} - 42594^{*}_{9/2}$				
5339.388	50	18723.53		SI	1.56	0.30	
5339.031	100	18724.78	$17454_{13/2} - 36179^{*}_{15/2}$	SI	1.25	0.08	
5338.940	20	18725.10	$22468^{*}_{11/2} - 41193_{13/2}$				
5338.900	50	18725.24	$16957_{7/2} - 35682^{*}_{7/2}$	ΔJ=0	1.15	0.17	
5338.495	4	18726.66	$22742^{*}_{13/2} - 41469_{13/2}$				
"			$23941^{*}_{9/2} - 42667_{9/2}$				
5335.193	2	18738.25	$25745_{9/2} - 44483^{*}_{9/2}$				
5333.442	3	18744.40	$23374_{13/2} - 42119^{*}_{11/2}$				
5333.222	2	18745.18	$19753_{7/2} - 38499^{*}_{9/2}$				
5331.710	4	18750.49	$19748_{9/2} - 38499^{*}_{9/2}$				
5330.105	2	18756.14	$24708^{*}_{7/2} - 43464_{9/2}$				
5329.547	2	18758.10	$24957^{*}_{11/2} - 43715_{11/2}$				
5327.848	4	18764.08	$17613_{9/2} - 36377^{*}_{9/2}$				
5326.503	2	18768.82	$17454_{13/2} - 36223^{*}_{13/2}$				
5325.363	2	18772.84	$24137_{13/2} - 42910^{*}_{13/2}$				
5324.595	50	18775.55	$15271_{13/2} - 34046^{*}_{13/2}$	ΔJ=0	1.13	0.75	
5323.828	40	18778.25	$18990_{11/2} - 37768^{*}_{9/2}$	T	1.20		
5321.885	7	18785.11	$21799^{*}_{9/2} - 40584_{9/2}$				
5318.190	2	18798.16	$24957^{*}_{11/2} - 43755_{9/2}$				
5317.590	1	18800.28	$23781_{9/2} - 42581^{*}_{11/2}$	T	1.13		
5315.093	3	18809.11	$23309_{11/2} - 42119^{*}_{11/2}$	ΔJ=0	1.10	0.15	
5314.177	2	18812.36	$23781_{9/2} - 42594^{*}_{9/2}$				
5312.267	100	18819.12	$17454_{13/2} - 36273^{*}_{13/2}$	S0	1.05	0.10	
5311.864	4	18820.55	$18837_{9/2} - 37657^{*}_{11/2}$				
5308.741	2	18831.62	$22559^{*}_{11/2} - 41391_{9/2}$	T	1.20		
5307.116	3000 r	18837.39	$0^{*}_{7/2} - 18837_{9/2}$	T	1.11	0.02	
5304.912	3	18845.21					
5303.054	5	18851.81					
5302.694	100	18853.09	$20406^{*}_{9/2} - 39259_{9/2}$	ΔJ=0	1.59	1.21	*
5300.205	300	18861.95	$15587_{11/2} - 34449^{*}_{13/2}$	S0	0.78	0.36	
5298.218	5	18869.02	$24246^{*}_{7/2} - 43115_{9/2}$				
5297.934	5	18870.03	$15587_{11/2} - 34457^{*}_{9/2}$	SI	1.44	0.25	
5296.550	5	18874.96	$17454_{13/2} - 36329^{*}_{11/2}$	SI	1.79	0.65	
5295.358	20	18879.21	$24957^{*}_{11/2} - 43836_{13/2}$	S0	0.86	0.31	
5294.324	100	18882.90	$25699^{*}_{9/2} - 44582_{9/2}$	T	1.20		
5291.143	100	18894.25	$21799^{*}_{9/2} - 40693_{9/2}$	ΔJ=0	1.45	1.30	*
5288.305	3	18904.39					
5286.756	20	18909.93	$22559^{*}_{11/2} - 41469_{13/2}$	SI	1.30	0.12	
5286.620	4	18910.42	$19753_{7/2} - 38664^{*}_{7/2}$				
5285.386	3	18914.83	$18853_{11/2} - 37768^{*}_{9/2}$				
5282.425	3	18925.43	$21737_{9/2} - 40663^{*}_{11/2}$				
5282.385	5	18925.58	$23431^{*}_{9/2} - 42357_{9/2}$	T	1.24	0.05	
5280.304	4	18933.04	$22419^{*}_{9/2} - 41352_{11/2}$				
5279.199	3	18937.00	$19748_{9/2} - 38685^{*}_{9/2}$				
5276.948	40	18945.08	$15587_{11/2} - 34532^{*}_{11/2}$	ΔJ=0	?	0.715	
5274.714	50	18953.10	$18693_{15/2} - 37646^{*}_{13/2}$	T	1.16		
5272.710	3	18960.30	$23781_{9/2} - 42742^{*}_{7/2}$				
5272.386	2	18961.47	$23941^{*}_{9/2} - 42902_{9/2}$				
5272.190	1	18962.17	$22468^{*}_{11/2} - 41430_{11/2}$				
5270.358	1	18968.76					
5267.543	10	18978.90	$25536^{*}_{15/2} - 44515_{13/2}$	SI	1.65	0.45	
5258.796	5	19010.47	$22419^{*}_{9/2} - 41430_{11/2}$				
5258.668	3	19010.93	$23941^{*}_{9/2} - 42952_{7/2}$				
5257.680	4	19014.50	$24701^{*}_{9/2} - 43715_{11/2}$				
5255.503	20	19022.38	$18990_{11/2} - 38012^{*}_{13/2}$	S0	0.36	0.70	
5253.593	2	19029.30	$23873_{7/2} - 42902^{*}_{9/2}$				
5252.284	4	19034.04					
5249.016	3	19045.89					
5248.550	7	19047.58	$24708^{*}_{7/2} - 43756_{9/2}$				
5244.798	5	19061.21	$24160^{*}_{7/2} - 43221_{9/2}$				
5241.942	5	19071.59	$24246^{*}_{7/2} - 43318_{9/2}$				
5239.640	20	19079.97	$25130_{13/2} - 44210^{*}_{13/2}$	ΔJ=0	1.12	0.38	
5234.800	7	19097.61	$13119_{9/2} - 32217^{*}_{9/2}$	T	1.30		
5234.555	10	19098.50					
5233.928	20	19100.79	$16456_{17/2} - 35557^{*}_{15/2}$	S0	0.58	0.60	
5233.440	5	19102.57	$25488_{11/2} - 44591^{*}_{13/2}$				
5233.053	30	19103.99	$15587_{11/2} - 34691^{*}_{11/2}$	ΔJ=0	?	0.56	
5232.397	3	19106.38	$27491_{11/2} - 46597^{*}_{13/2}$				
5231.916	20	19108.14	$19753_{7/2} - 38861^{*}_{9/2}$				
5231.055	2	19111.28	$23431^{*}_{9/2} - 42543_{7/2}$				
5230.535	2	19113.18					
5226.304	20	19128.66	$19748_{9/2} - 38877^{*}_{11/2}$				
5224.130	5	19136.62					
5223.082	30	19140.46	$20406^{*}_{9/2} - 39547_{9/2}$	ΔJ=0	1.58	1.29	*
5223.014	2	19140.70	$22559^{*}_{11/2} - 41700_{11/2}$				
5218.035	50	19158.97	$18853_{11/2} - 38012^{*}_{13/2}$	S0	0.73	0.32	
5216.243	3	19165.55	$18693_{15/2} - 37858^{*}_{15/2}$				
5215.445	20	19168.48	$22559^{*}_{11/2} - 41728_{9/2}$	SI	1.70	0.53	
5214.805	3	19170.84	$18990_{11/2} - 38161^{*}_{11/2}$				
5213.376	600	19176.09	$16456_{17/2} - 35633^{*}_{17/2}$	ΔJ=0	1.18	0.07	
5212.853	3	19178.01	$22902^{*}_{13/2} - 42080_{11/2}$				
5212.650	50	19178.76	$15271_{13/2} - 34449^{*}_{13/2}$	S0	0.41	0.65	
5207.125	30	19199.11	$17454_{13/2} - 36653^{*}_{15/2}$	T	1.11		
5206.366	15	19201.91	$17454_{13/2} - 36656^{*}_{11/2}$				
5205.916	1	19203.57	$22929_{9/2} - 42133^{*}_{7/2}$				
5204.128	30	19210.17					
5202.080	5	19217.73	$24246^{*}_{7/2} - 43464_{9/2}$				
5200.411	2	19223.90					
5199.726	1	19226.43	$21120_{7/2} - 40347^{*}_{9/2}$				
5199.107	70	19228.72	$20406^{*}_{9/2} - 39635_{9/2}$	SI	1.58	1.33	*
5198.436	1	19231.20	$23882_{9/2} - 43113^{*}_{9/2}$				
5198.176	1	19232.16	$22468^{*}_{11/2} - 41700_{11/2}$				
5193.960	20	19247.77	$24611^{*}_{9/2} - 43859_{9/2}$				
5193.312	2	19250.17	$22929_{9/2} - 42179^{*}_{9/2}$				
5191.796	20	19255.80	$23941^{*}_{9/2} - 43196_{11/2}$				
5190.673	7	19259.96	$22468^{*}_{11/2} - 41728_{9/2}$				
5190.655	30	19260.03	$22468^{*}_{11/2} - 41728_{9/2}$				
5190.622	10	19260.15					
5187.742	1	19270.84	$23781_{9/2} - 43052^{*}_{7/2}$				
5187.433	3	19271.99	$23309_{11/2} - 42581^{*}_{11/2}$				
5185.969	5	19277.43	$21997_{11/2} - 41274^{*}_{13/2}$				
5185.249	300	19280.11	$8771^{*}_{9/2} - 28051_{9/2}$	ΔJ=0	0.92	0.29	
5185.154	10	19280.46	$22419^{*}_{9/2} - 41700_{11/2}$				
5184.182	3	19284.08	$23309_{11/2} - 42594^{*}_{9/2}$				
5182.680	70	19289.66	$21799^{*}_{9/2} - 41089_{7/2}$	T	1.42	0.03	
5179.624	2	19301.05	$24137_{13/2} - 43438^{*}_{13/2}$				
5177.911	2	19307.43	$18853_{11/2} - 38161^{*}_{11/2}$				
5177.688	50	19308.26	$22419^{*}_{9/2} - 41728_{9/2}$	ΔJ=0	0.98	0.52	
5176.397	1	19313.08	$19548_{9/2} - 38861^{*}_{9/2}$				
5175.745	4	19315.51					
5174.823	3	19318.95	$24957^{*}_{11/2} - 44276_{11/2}$				
5174.612	6	19319.74	$18693_{15/2} - 38012^{*}_{13/2}$				
5174.584	30	19319.84					
5174.567	10	19319.91					
5174.393	10	19320.56	$17613_{9/2} - 36934^{*}_{7/2}$				
5171.832	5	19330.12					
5171.308	10	19332.08					
5171.162	3	19332.63	$23335^{*}_{7/2} - 42667_{9/2}$				
5169.679	10	19338.17	$25207^{*}_{9/2} - 44545_{7/2}$	ΔJ=0	1.20	0.40	
5168.927	40	19340.99	$19748_{9/2} - 39089^{*}_{13/2}$				
5168.198	3	19343.72	$21737_{9/2} - 41081^{*}_{13/2}$				
5168.124	2	19343.99	$24246^{*}_{7/2} - 43590_{7/2}$				
5166.397	3	19350.46					
5163.886	4	19359.87					

Wavelength in air Å	Intensity	Wavenumber cm⁻¹	Classification	Zeeman effect type	f	Je	
5163.290	1	19362.10	$23941^{\circ}_{9/2} - 43303_{7/2}$				
5160.543	200	19372.41	$8771^{\circ}_{9/2} - 28143_{7/2}$	SI	0.85	0.65	*
5160.053	20	19374.25	$18837_{9/2} - 38211^{\circ}_{7/2}$				
5156.207	2	19388.70	$22791_{7/2} - 42179^{\circ}_{9/2}$				
5154.482	3	19395.19					
5154.034	10	19396.87	$21120_{7/2} - 40517^{\circ}_{9/2}$				
5153.555	2	19398.68					
5150.405	5	19410.54	$19466_{13/2} - 38877^{\circ}_{11/2}$				
5149.600	10	19413.58	$23941^{\circ}_{9/2} - 43354_{9/2}$				
5147.705	50	19420.72	$16957_{7/2} - 36377^{\circ}_{9/2}$	SI	1.33	0.12	
5147.172	4	19422.73					
5145.367	5	19429.55	$23335^{\circ}_{7/2} - 42764_{9/2}$				
5142.886	300	19438.92	$19748_{9/2} - 39187^{\circ}_{7/2}$	S0	1.09	0.18	
5142.545	100	19440.21	$20406^{\circ}_{9/2} - 39847_{7/2}$	S0	0.54	0.73	
5141.405	4	19444.52	$23431^{\circ}_{9/2} - 42876_{9/2}$				
5140.392	4	19448.35	$23335^{\circ}_{7/2} - 42783_{7/2}$				
5137.310	3	19460.02	$24957^{\circ}_{11/2} - 44417_{11/2}$				
5137.102	2	19460.81	$23309_{11/2} - 42770^{\circ}_{9/2}$				
5135.682	10	19466.19	$19753_{7/2} - 39220^{\circ}_{9/2}$				
5135.503	15	19466.87	$15587_{11/2} - 35054^{\circ}_{9/2}$	S0	1.11	0.14	
5134.282	20	19471.50	$19748_{9/2} - 39220^{\circ}_{9/2}$				
5131.564	4	19481.81	$23574^{\circ}_{7/2} - 43056_{9/2}$				
5129.526	4	19489.55					
5129.210	3	19490.75	$19753_{7/2} - 39244^{\circ}_{9/2}$				
5129.127	15	19491.06		S0	0.83	0.23	
5127.819	20	19496.04	$19748_{9/2} - 39244^{\circ}_{9/2}$				
5127.215	2	19498.33	$24708^{\circ}_{7/2} - 44206_{7/2}$				
5125.593	2	19504.50					
5124.516	7	19508.60	$18990_{11/2} - 38499^{\circ}_{9/2}$				
5123.370	30	19512.97	$19548_{9/2} - 39061^{\circ}_{7/2}$				
5121.353	3	19520.65	$22559^{\circ}_{11/2} - 42080_{11/2}$				
5120.671	150	19523.25	$19753_{7/2} - 39277^{\circ}_{9/2}$	T	1.18		
5118.610	4	19531.11	$18853_{11/2} - 38384^{\circ}_{9/2}$				
5115.953	5 Å	19541.26	$23335^{\circ}_{7/2} - 42876_{9/2}$				
5113.970	500 *r*	19548.83	$0^{\circ}_{7/2} - 19548_{9/2}$	SI	1.53	0.39	
5113.890	10	19549.14					
5112.482	20	19554.52					
5112.065	2	19556.12	$23873_{7/2} - 43429^{\circ}_{9/2}$				
5111.776	7	19557.22	$24708^{\circ}_{7/2} - 44265_{7/2}$				
5111.691	30	19557.55	$24957^{\circ}_{11/2} - 44515_{13/2}$	S0	0.56	0.56	
5109.476	1	19566.03					
5109.103	2	19567.45	$23335^{\circ}_{7/2} - 42902_{9/2}$				
5108.426	1	19570.05	$25520^{\circ}_{13/2} - 45091_{9/2}$				
5107.533	400	19573.47	$19748_{9/2} - 39322^{\circ}_{9/2}$	ΔJ=0	1.22	0.64	
5106.760	2	19576.43	$22791^{\circ}_{7/2} - 42367_{9/2}$				
5106.174	2	19578.68	$21997_{11/2} - 41576^{\circ}_{9/2}$				
5105.526	2	19581.16					
5104.237	2	19586.11	$23574^{\circ}_{9/2} - 43160_{9/2}$				
5103.387	20	19589.37	$20406^{\circ}_{9/2} - 39996_{7/2}$				
5103.006	1	19590.83	$17343_{7/2} - 36934^{\circ}_{7/2}$				
5101.896	10	19595.10	$24611^{\circ}_{9/2} - 44206_{7/2}$	SI	1.35	0.29	
5101.821	2	19595.38					
5101.129	40	19598.04	$18990_{11/2} - 38588^{\circ}_{13/2}$	T	1.22		
5097.469	2	19612.11	$22468^{\circ}_{11/2} - 42080_{11/2}$				
5096.222	2	19616.91	$23335^{\circ}_{7/2} - 42952_{7/2}$				
5095.530	2	19619.58	$19132_{9/2} - 38751^{\circ}_{9/2}$				
5094.641	2	19623.00					
5094.277	30	19624.40	$23431^{\circ}_{9/2} - 43056_{9/2}$				
5092.277	2	19632.11	$24611^{\circ}_{9/2} - 44243_{9/2}$				
5092.009	4	19633.14	$19753_{7/2} - 39386^{\circ}_{9/2}$				
5091.391	2	19635.53	$16742_{7/2} - 36377^{\circ}_{9/2}$				
5090.162	7	19640.27	$24160^{\circ}_{7/2} - 43800_{9/2}$				
5089.437	2	19643.06	$22902^{\circ}_{13/2} - 42545_{13/2}$				
"			$21120_{7/2} - 40763^{\circ}_{7/2}$				
5088.881	40	19645.21	$18853_{11/2} - 38499^{\circ}_{9/2}$				
"			$18837_{9/2} - 38482^{\circ}_{7/2}$				
5088.302	15	19647.45	$23574^{\circ}_{9/2} - 43221_{9/2}$				
5087.323	10	19651.23					
5086.607	7	19653.99	$24611^{\circ}_{9/2} - 44265_{7/2}$				
5085.086	200	19659.87	$20406^{\circ}_{9/2} - 40066_{9/2}$	ΔJ=0	1.58	1.36	*
5084.950	20	19660.40	$22419^{\circ}_{9/2} - 42080_{11/2}$				
5084.624	6	19661.66	$18837_{9/2} - 38499^{\circ}_{9/2}$				
5084.244	4	19663.13	$17613_{9/2} - 37276^{\circ}_{11/2}$				
5083.914	5	19664.40					
5083.402	10	19666.38					
5083.197	5	19667.18	$17343_{7/2} - 37010^{\circ}_{9/2}$				
5081.729	20	19672.86	$24708^{\circ}_{7/2} - 44380_{9/2}$	SI	1.40	0.25	
5081.643	3	19673.19					
5080.948	1	19675.88	$18853_{11/2} - 38529^{\circ}_{11/2}$				
5080.577	20	19677.32	$8771^{\circ}_{9/2} - 28448_{9/2}$	ΔJ=0	0.94	0.33	
5079.925	1	19679.84	$24701^{\circ}_{9/2} - 44380_{9/2}$				
5079.675	6	19680.81					
5078.180	40	19686.61	$22742^{\circ}_{13/2} - 42429_{11/2}$	T	1.20		
5077.312	2	19689.97	$21997_{11/2} - 41687^{\circ}_{11/2}$				
5077.183	300	19690.47	$19753_{7/2} - 39444^{\circ}_{9/2}$	S0	0.90	0.21	
5076.875	20	19691.67					
5076.705	2	19692.33	$18837_{9/2} - 38529^{\circ}_{11/2}$				
5076.469	10	19693.24					
5076.360	200	19693.67	$21799^{\circ}_{9/2} - 41493_{9/2}$	S0	1.05	0.24	
5075.970	2	19695.18	$18990_{11/2} - 38685^{\circ}_{9/2}$				
5075.820	60	19695.76	$19748_{9/2} - 39444^{\circ}_{9/2}$	ΔJ=0	1.185	0.66	
5073.513	100	19704.72	$17454_{13/2} - 37159^{\circ}_{13/2}$	SI	1.80	0.58	
5072.416	300	19708.98	$19753_{7/2} - 39462^{\circ}_{7/2}$	ΔJ=0	1.15	0.20	
5071.833	1	19711.24					
5071.717	3	19711.69	$24611^{\circ}_{9/2} - 44323_{7/2}$				
5071.200	20	19713.70	$22742^{\circ}_{13/2} - 42456_{13/2}$	ΔJ=0	1.22	0.10	
5071.057	30	19714.26	$19748_{9/2} - 39462^{\circ}_{7/2}$	SI	1.92	0.63	
5070.494	20	19716.45	$24701^{\circ}_{9/2} - 44417_{11/2}$	T	1.15		
5070.432	10	19716.69	$19753_{7/2} - 39470^{\circ}_{9/2}$				
5069.817	3	19719.08					
5069.300	2	19721.09	$23335^{\circ}_{7/2} - 43056_{9/2}$				
5068.890	50	19722.69	$16456_{17/2} - 36179^{\circ}_{15/2}$	SI	1.29	0.14	
5067.918	10	19726.47	$19753^{\circ}_{7/2} - 39480_{7/2}$				
5067.825	30	19726.83					
5067.463	30	19728.24	$19548_{9/2} - 39277^{\circ}_{9/2}$				
5066.670	800	19731.33	$19748_{9/2} - 39479^{\circ}_{11/2}$	S0	0.86	0.36	
5065.876	100	19734.42	$19753_{7/2} - 39488^{\circ}_{9/2}$	SI	1.40	0.35	
5065.812	30	19734.67	$18853_{11/2} - 38588^{\circ}_{11/2}$				
"			$24246^{\circ}_{7/2} - 43981_{7/2}$				
5064.523	10	19739.69	$19748_{9/2} - 39488^{\circ}_{9/2}$				
5062.250	200	19748.56	$0^{\circ}_{7/2} - 19748_{9/2}$	SI	1.143	1.29	*
5060.895	2000 *r*	19753.84	$0^{\circ}_{7/2} - 19753_{7/2}$	ΔJ=0	1.15	0.13	
5058.208	2	19764.34	$24418_{9/2} - 44182^{\circ}_{9/2}$				
5057.559	5	19766.87	$17752_{9/2} - 37519^{\circ}_{7/2}$				
5056.182	60	19772.26		T	1.27	0.07	
5055.227	5	19775.99	$15587_{11/2} - 35363^{\circ}_{9/2}$				
5054.909	1	19777.24	$21161_{9/2} - 40938^{\circ}_{9/2}$				
5054.619	3	19778.37					
5054.119	10	19780.33	$23335^{\circ}_{7/2} - 43115_{9/2}$				
5053.043	150	19784.54	$8771^{\circ}_{9/2} - 28555_{7/2}$	SI	0.85	1.15	*
5051.648	20	19790.00	$23431^{\circ}_{9/2} - 43221_{9/2}$	SI	1.29	0.06	
5050.935	2	19792.80	$18693_{13/2} - 38485^{\circ}_{13/2}$				
5049.798	2	19797.25					
5048.493	2	19802.37	$22742^{\circ}_{13/2} - 42545_{13/2}$				
5046.254	1	19811.16	$23431^{\circ}_{9/2} - 43243_{9/2}$				
5046.177	2	19811.46					
5045.963	10	19812.30	$22929_{9/2} - 42742^{\circ}_{7/2}$				
5045.408	250	19814.48	$19748_{9/2} - 39563^{\circ}_{11/2}$	S0	0.23	0.86	
5044.758	2	19817.03	$16456_{17/2} - 36273^{\circ}_{15/2}$				
5043.505	100	19821.95	$17454_{13/2} - 37276^{\circ}_{13/2}$	S0	0.61	0.54	
5043.238	5	19823.00					
5041.213	20	19830.97	$22902^{\circ}_{13/2} - 42733_{13/2}$				
5040.738	20	19832.83					
5039.393	20	19838.13	$19548_{9/2} - 39386^{\circ}_{9/2}$	T	0.99		
5037.057	4	19847.33	$23941^{\circ}_{9/2} - 43788_{11/2}$				
5036.129	1	19850.99	$21161_{9/2} - 41012^{\circ}_{7/2}$				
5035.618	20	19853.00	$22742^{\circ}_{13/2} - 42595_{11/2}$	T	1.21		
5032.620	6	19864.83	$19548_{9/2} - 39413^{\circ}_{7/2}$				
5032.183	2	19866.55					
5031.341	3	19869.88	$22559^{\circ}_{11/2} - 42429_{11/2}$				

Wavelength in air Å	Intensity	Wavenumber cm^{-1}	Classification	Zeeman effect type	f	Je	
5031.042	9	19871.06	$19548_{9/2} - 39419^{\circ}_{7/2}$				
5030.260	200	19874.15	$19753_{7/2} - 39628^{\circ}_{7/2}$	ΔJ=0	1.10	0.51	
5029.262	1	19878.09	$17343_{7/2} - 37221^{\circ}_{7/2}$				
5028.608	1	19880.68					
5028.228	4	19882.18	$24418_{9/2} - 44300^{\circ}_{9/2}$				
5027.060	10	19886.80	$18990_{11/2} - 38877^{\circ}_{11/2}$	ΔJ=0	1.15	0.84	
5025.860	2	19891.55	$21120_{7/2} - 41012^{\circ}_{7/2}$				
5024.890	50	19895.38	$18693_{13/2} - 38588^{\circ}_{13/2}$	S0	0.89	0.26	
5024.429	1	19897.21					
5023.681	4	19900.17					
5023.597	5	19900.51	$25488_{11/2} - 45389^{\circ}_{13/2}$				
5022.457	4	19905.02	$19753_{7/2} - 39658^{\circ}_{9/2}$				
5022.198	3	19906.05	$22419^{\circ}_{9/2} - 42325_{7/2}$				
5021.123	100	19910.31	$17454_{13/2} - 37365^{\circ}_{13/2}$	ΔJ=0	1.18	0.35	
5019.156	2	19918.11	$24611^{\circ}_{9/2} - 44529_{7/2}$				
5018.737	20	19919.78	$21997_{13/2} - 41917^{\circ}_{13/2}$				
"			$23574^{\circ}_{7/2} - 43494_{9/2}$				
5018.442	5	19920.95					
5017.303	40	19925.47	$18990_{11/2} - 38915^{\circ}_{13/2}$	T	1.25	0.04	
5016.272	10	19929.56	$19132_{5/2} - 39061^{\circ}_{5/2}$				
5014.277	50	19937.49		T	0.70		
5013.281	3	19941.45					
5010.718	20	19951.65	$21799^{\circ}_{5/2} - 41751_{5/2}$	S0	1.45	1.08	*
5010.245	30	19953.54	$20406^{\circ}_{5/2} - 40360_{7/2}$				
"			$21120_{7/2} - 41074^{\circ}_{5/2}$				
5009.690	10	19955.75					
5008.497	1	19960.50	$19748_{9/2} - 39709^{\circ}_{11/2}$				
5008.163	1	19961.83	$24957^{\circ}_{13/2} - 44919_{9/2}$				
5007.092	20	19966.10	$22902^{\circ}_{13/2} - 42868_{11/2}$				
5006.736	10	19967.52	$19466_{13/2} - 39434^{\circ}_{13/2}$				
5006.703	2	19967.65	$22902^{\circ}_{13/2} - 42869_{13/2}$				
5006.607	10	19968.04	$24348_{9/2} - 44316^{\circ}_{9/2}$				
"			$23335^{\circ}_{7/2} - 43303_{7/2}$				
5003.814	2	19979.18	$25488_{11/2} - 45467^{\circ}_{9/2}$				
5003.708	3	19979.61	$22791_{7/2} - 42770^{\circ}_{9/2}$				
5003.145	15	19981.85	$24708^{\circ}_{7/2} - 44689_{9/2}$				
5002.197	10	19985.64	$22559^{\circ}_{11/2} - 42545_{13/2}$				
5001.587	200	19988.08	$19753_{7/2} - 39741^{\circ}_{9/2}$	S0	0.79	0.30	
5001.504	30	19988.41	$22468^{\circ}_{11/2} - 42456_{13/2}$				
5001.025	200	19990.32	$22742^{\circ}_{13/2} - 42733_{13/2}$	T	1.12	0.07	
5000.270	100	19993.34	$19548_{9/2} - 39542^{\circ}_{7/2}$	SI	1.18	0.12	
4999.643	3	19995.85					
4996.201	1	20009.63	$22419^{\circ}_{9/2} - 42429_{11/2}$				
4994.480	2	20016.52	$22559^{\circ}_{11/2} - 42576_{9/2}$				
4992.780	20	20023.34					
4988.669	6	20039.84	$18837_{9/2} - 38877^{\circ}_{11/2}$				
4987.139	2	20045.98					
4986.256	1	20049.53					
4985.627	1	20052.06					
4985.260	5	20053.54	$16957_{7/2} - 37010^{\circ}_{9/2}$				
4985.130	200	20054.06	$19548_{9/2} - 39602^{\circ}_{9/2}$	S0	0.985	1.31	*
4984.893	5h	20055.02	$22902^{\circ}_{13/2} - 42957_{11/2}$				
4983.185	1	20061.89					
4983.136	2	20062.09	$18853_{11/2} - 38915^{\circ}_{13/2}$				
4982.328	5	20065.34	$24418_{9/2} - 44483^{\circ}_{9/2}$				
4979.540	3	20076.58	$24246^{\circ}_{7/2} - 44323_{7/2}$				
4978.900	400	20079.16	$19548_{9/2} - 39628^{\circ}_{7/2}$	SI	1.15	0.10	
4975.036	5	20094.75					
4973.953	30	20099.13	$18990_{11/2} - 39089^{\circ}_{11/2}$	ΔJ=0	?	0.55	
4973.282	2	20101.84					
4971.694	10	20108.26	$22559^{\circ}_{11/2} - 42667_{9/2}$				
4971.258	200	20110.02	$19548_{9/2} - 39658^{\circ}_{9/2}$	ΔJ=0	0.97	0.08	
4967.437	2	20125.49	$22742^{\circ}_{13/2} - 42868_{11/2}$				
4967.063	1	20127.01	$22742^{\circ}_{13/2} - 42869_{13/2}$				
4966.880	10	20127.75	$22468^{\circ}_{11/2} - 42595_{11/2}$				
4965.216	2	20134.49	$24246^{\circ}_{7/2} - 44380_{9/2}$				
4964.672	7	20136.70	$21737_{9/2} - 41874^{\circ}_{11/2}$				
4964.370	2	20137.92	$23309_{11/2} - 43447^{\circ}_{11/2}$				
4963.052	2	20143.27					
4962.943	2	20143.71					
4962.673	3	20144.81	$19132_{5/2} - 39277^{\circ}_{9/2}$				
4962.327	5h	20146.21	$23335^{\circ}_{7/2} - 43481_{9/2}$				
4961.564	10	20149.31					
4960.163	10	20155.00	$17613_{9/2} - 37768^{\circ}_{9/2}$				
4959.855	4	20156.26	$22419^{\circ}_{9/2} - 42576_{9/2}$				
4959.283	2	20158.58	$23431^{\circ}_{9/2} - 43590_{7/2}$				
4957.175	1000	20167.15	$18990_{11/2} - 39157^{\circ}_{13/2}$	SI	1.38	0.14	
4956.474	1	20170.00	$24137_{13/2} - 44307^{\circ}_{13/2}$				
4954.978	2	20176.09	$17343_{7/2} - 37519^{\circ}_{7/2}$				
4954.585	5	20177.69	$20406^{\circ}_{9/2} - 40584_{9/2}$				
4954.511	3	20178.00					
4953.834	2	20180.75					
4952.266	2	20187.14					
4951.704	1	20189.43					
4951.229	1	20191.37	$17454_{13/2} - 37646^{\circ}_{13/2}$				
4951.080	2	20191.98	$16742_{7/2} - 36934^{\circ}_{7/2}$				
4949.845	5	20197.02	$16456_{13/2} - 36653^{\circ}_{13/2}$				
4949.188	1	20199.70	$22468^{\circ}_{11/2} - 42667_{9/2}$				
4948.670	7	20201.81		T	0.98		
4948.353	100	20203.11	$17454_{13/2} - 37657^{\circ}_{11/2}$	SI	1.84	0.69	
4947.852	5	20205.15	$22559^{\circ}_{11/2} - 42764_{9/2}$				
4947.497	30	20206.60		T	1.10		
4946.358	3	20211.25	$24708^{\circ}_{7/2} - 44919_{9/2}$				
4945.600	1	20214.35	$22742^{\circ}_{13/2} - 42957_{11/2}$				
4945.299	2	20215.58					
4944.833	2	20217.49					
4944.652	10	20218.23	$24701^{\circ}_{9/2} - 44919_{9/2}$	ΔJ=0	?	0.19	
4943.300	2	20223.76					
4942.640	30	20226.46	$23574^{\circ}_{9/2} - 43800_{9/2}$	ΔJ=0	0.83	1.20	*
4942.199	1	20228.26					
4941.865	3	20229.63	$18990_{11/2} - 39220^{\circ}_{9/2}$				
4940.383	20	20235.70	$18853_{11/2} - 39089^{\circ}_{11/2}$	ΔJ=0	1.13	0.25	
4940.187	3	20236.50	$23335^{\circ}_{7/2} - 43571_{9/2}$				
4939.440	3	20239.56	$23374_{13/2} - 43614^{\circ}_{13/2}$				
4938.753	1	20242.38	$19466_{13/2} - 39709^{\circ}_{11/2}$				
4938.698	5	20242.60	$20406^{\circ}_{9/2} - 40649_{7/2}$				
4937.385	20	20247.98	$22419^{\circ}_{9/2} - 42667_{9/2}$				
4935.880	20	20254.16	$18990_{11/2} - 39244^{\circ}_{9/2}$				
4935.747	3	20254.70	$19132_{5/2} - 39386^{\circ}_{9/2}$				
4934.798	2	20258.60	$25130_{13/2} - 45389^{\circ}_{13/2}$				
4933.365	5	20264.48	$16957_{7/2} - 37221^{\circ}_{7/2}$				
4933.162	1	20265.32	$23941^{\circ}_{9/2} - 44206_{7/2}$				
4932.552	1	20267.82	$27377_{13/2} - 47644^{\circ}_{13/2}$				
4932.390	2	20268.49					
4929.729	10	20279.43					
4929.228	2	20281.49	$24137_{13/2} - 44418^{\circ}_{13/2}$				
4928.457	50	20284.66	$23574^{\circ}_{9/2} - 43859_{9/2}$	SI	1.55	0.42	
4927.945	3	20286.77	$20406^{\circ}_{9/2} - 40693_{9/2}$				
4927.732	200	20287.65	$19132_{5/2} - 39419^{\circ}_{9/2}$	ΔJ=0	0.89	0.09	
4925.555	1	20296.61	$22468^{\circ}_{11/2} - 42764_{9/2}$				
4925.274	1	20297.77	$23941^{\circ}_{9/2} - 44238_{9/2}$				
4925.060	2	20298.65	$22419^{\circ}_{9/2} - 42718_{9/2}$				
4923.826	600	20303.74	$18853_{11/2} - 39157^{\circ}_{13/2}$	SI	1.67	0.42	
4922.524	2	20309.11	$23873_{7/2} - 44182^{\circ}_{9/2}$				
4922.260	2	20310.20	$22559^{\circ}_{11/2} - 42869_{13/2}$				
4921.620	1	20312.84	$19748_{9/2} - 40061^{\circ}_{7/2}$				
4920.876	1	20315.91					
4917.085	20	20331.58	$18990_{11/2} - 39322^{\circ}_{9/2}$	SI	1.50	0.23	
4916.180	1	20335.32	$23941^{\circ}_{9/2} - 44276_{11/2}$				
4915.961	3	20336.23	$24246^{\circ}_{7/2} - 44582_{9/2}$				
4915.475	1	20338.24	$19132_{9/2} - 39470^{\circ}_{9/2}$				
4913.296	2	20347.26					
4909.736	200	20362.01	$15271_{13/2} - 35633^{\circ}_{13/2}$	SI	1.88	0.70	
4908.727	5	20366.19	$18853_{11/2} - 39220^{\circ}_{9/2}$				
4907.550	30	20371.08	$15587_{11/2} - 35958^{\circ}_{13/2}$	S0	0.39	0.74	
4907.269	100	20372.25	$18990_{11/2} - 39362^{\circ}_{11/2}$	ΔJ=0	1.18	0.44	
4904.690	2	20382.96	$24708^{\circ}_{7/2} - 45091_{9/2}$				
4902.815	20	20390.75	$18853_{11/2} - 39244^{\circ}_{9/2}$				
"			$23873_{7/2} - 44263^{\circ}_{7/2}$				
4901.854	2	20394.75					

APPENDIX—*Spectral Lines of Neutral Thulium*—Continued

Wavelength in air Å	Intensity	Wavenumber cm^{-1}	Classification	Zeeman effect type	f	Je	
4901.627	100	20395.69	$20406^{\circ}_{9/2} - 40802_{7/2}$	S0	0.22	0.98	
4901.165	1	20397.62	$22559^{\circ}_{11/2} - 42957_{11/2}$				
4900.993	5	20398.33	$24348_{9/2} - 44747^{\circ}_{11/2}$				
4900.746	5	20399.36	$21799^{\circ}_{9/2} - 42198_{9/2}$				
4900.545	5	20400.20	$22468^{\circ}_{11/2} - 42868_{11/2}$				
4900.190	8	20401.68	$22468^{\circ}_{11/2} - 42869_{13/2}$				
4900.120	10	20401.97					
4899.680	5	20403.80	$17454_{13/2} - 37858^{\circ}_{13/2}$				
4897.535	1	20412.74	$21120_{7/2} - 41533^{\circ}_{9/2}$				
4896.150	10	20418.51					
4895.668	10	20420.52	$23335^{\circ}_{7/2} - 43755_{9/2}$				
4894.534	4	20425.25	$17343_{7/2} - 37768^{\circ}_{9/2}$				
4894.233	3	20426.51					
4893.436	1	20429.83					
4891.670	2	20437.21	$24418_{9/2} - 44855^{\circ}_{9/2}$				
4891.640	8	20437.33					
4890.166	2	20443.49	$24246^{\circ}_{7/2} - 44689_{9/2}$				
"			$23873_{7/2} - 44316^{\circ}_{9/2}$				
4889.425	20	20446.59		T	0.96		
4887.660	40 h	20453.98					
4887.346	10	20455.29	$21120_{7/2} - 41576^{\circ}_{9/2}$				
4887.140	3	20456.15					
4886.464	3	20458.98	$17752_{9/2} - 38211^{\circ}_{7/2}$				
4884.263	10	20468.20	$18853_{11/2} - 39322^{\circ}_{9/2}$				
4883.675	200	20470.67	$19132_{9/2} - 39602^{\circ}_{9/2}$	ΔJ=0	0.88	1.30	*
4879.194	300	20489.47	$18990_{13/2} - 39479^{\circ}_{11/2}$	ΔJ=0	1.20	0.12	
4877.022	1	20498.59					
4874.590	40	20508.82	$18853_{11/2} - 39362^{\circ}_{13/2}$	ΔJ=0	1.15	0.13	
4874.420	3	20509.53					
4873.819	2	20512.06					
4870.997	7	20523.95	$23335^{\circ}_{7/2} - 43859_{9/2}$				
4870.687	20	20525.25	$18837_{9/2} - 39362^{\circ}_{11/2}$	T	1.13		
4870.367	200	20526.60	$19132_{9/2} - 39658^{\circ}_{9/2}$	SI	1.09	0.13	
4869.839	50	20528.83		S0	0.80	0.35	
4868.372	1	20535.01	$23781_{9/2} - 44316^{\circ}_{9/2}$				
4867.812	4	20537.37	$22419^{\circ}_{9/2} - 42957_{11/2}$				
4866.270	50	20543.88	$21997_{11/2} - 42541^{\circ}_{11/2}$	ΔJ=0	1.08	0.17	
4865.392	10	20547.59	$17613_{9/2} - 38161^{\circ}_{11/2}$	S0	0.87	0.27	
4865.000	3	20549.24	$23431^{\circ}_{9/2} - 43981_{7/2}$				
4863.571	2 d	20555.28					
4862.934	30	20557.97	$17454_{13/2} - 38012^{\circ}_{13/2}$	ΔJ=0	1.12	0.26	
4861.867	4	20562.49	$16957_{7/2} - 37519^{\circ}_{7/2}$				
4861.495	2	20564.06	$21997_{11/2} - 42561^{\circ}_{9/2}$				
4860.398	1	20568.70	$19753_{7/2} - 40322^{\circ}_{9/2}$				
4859.473	30	20572.62	$18990_{13/2} - 39563^{\circ}_{11/2}$	ΔJ=0	1.15	0.57	
4859.310	4	20573.31					
4857.658	1	20580.30	$18853_{11/2} - 39434^{\circ}_{13/2}$				
4856.670	20	20584.49	$21997_{11/2} - 42581^{\circ}_{11/2}$	ΔJ=0	1.09	0.42	
4856.356	10	20585.82					
4855.758	2	20588.36	$23941^{\circ}_{9/2} - 44529_{7/2}$				
4854.566	3	20593.41	$19753_{7/2} - 40347^{\circ}_{9/2}$				
4853.825	2	20596.55	$21997_{11/2} - 42594^{\circ}_{9/2}$				
4853.495	30	20597.96	$17613_{9/2} - 38211^{\circ}_{7/2}$	SI	1.25	0.05	
4851.755	100	20605.34	$19132_{9/2} - 39737^{\circ}_{7/2}$	SI	0.92	0.04	
4850.415	3	20611.03					
4847.925	70	20621.62		SI	1.47	0.36	
4847.573	2	20623.12	$23335^{\circ}_{7/2} - 43958_{9/2}$				
4846.887	40	20626.04	$18853_{11/2} - 39479^{\circ}_{11/2}$	ΔJ=0	1.18	0.28	
4845.544	3	20631.75					
4844.591	50	20635.81	$15587_{11/2} - 36223^{\circ}_{13/2}$	S0	0.38	0.76	
4844.237	2	20637.32	$22559^{\circ}_{11/2} - 43196_{11/2}$				
4842.935	10	20642.87	$18837_{9/2} - 39480^{\circ}_{7/2}$	T	1.04	0.08	
4841.066	1	20650.84	$18837_{9/2} - 39488^{\circ}_{9/2}$				
4837.653	1	20665.41	$21120_{7/2} - 41786^{\circ}_{9/2}$				
4835.903	5	20672.89	$24246^{\circ}_{7/2} - 44919_{9/2}$				
4835.754	300	20673.52	$13119_{9/2} - 33793^{\circ}_{11/2}$	S0	1.01	0.24	
4834.607	2	20678.43	$22419^{\circ}_{9/2} - 43098_{7/2}$				
4832.400	2	20687.87	$15271_{15/2} - 35958^{\circ}_{13/2}$				
4831.930	20	20689.88		T	1.10		
4830.590	15	20695.62	$22419^{\circ}_{9/2} - 43115_{9/2}$				
4828.966	100	20702.58	$16456_{17/2} - 37159^{\circ}_{15/2}$	S0	0.79	0.36	
4828.797	15	20703.31		T	1.16		
4828.066	40	20706.44	$17454_{13/2} - 38161^{\circ}_{11/2}$	T	1.14		
4827.430	10	20709.17	$18853_{11/2} - 39563^{\circ}_{11/2}$				
4827.312	4	20709.68	$24348_{9/2} - 45058^{\circ}_{11/2}$				
4825.230	1	20718.61	$18990_{11/2} - 39709^{\circ}_{11/2}$				
4824.465	1	20721.90	$24348_{9/2} - 45070^{\circ}_{9/2}$				
4822.592	2	20729.94	$17752_{9/2} - 38482^{\circ}_{7/2}$				
4821.597	20	20734.22	$17613_{9/2} - 38347^{\circ}_{11/2}$				
4819.793	10	20741.98	$15587_{11/2} - 36329^{\circ}_{11/2}$				
4818.200	2	20748.84	$23941^{\circ}_{9/2} - 44689_{9/2}$				
4817.839	10	20750.40		T	1.35		
4817.139	1	20753.41	$22791_{7/2} - 43544^{\circ}_{9/2}$				
4816.387	1	20756.65	$24957^{\circ}_{11/2} - 45714_{11/2}$				
4815.403	3	20760.89	$21120_{7/2} - 41881^{\circ}_{9/2}$				
4813.496	150	20769.12		S0	0.64	0.37	
4812.996	1	20771.27	$17613_{9/2} - 38384^{\circ}_{9/2}$				
4812.238	2	20774.55	$23431^{\circ}_{9/2} - 44206_{7/2}$				
4811.650	50	20777.08	$22419^{\circ}_{9/2} - 43196_{11/2}$				
4809.756	7	20785.27	$19748_{9/2} - 40533^{\circ}_{7/2}$				
4808.679	300	20789.92	$15587_{11/2} - 36377^{\circ}_{9/2}$	SI	1.40	0.16	
4807.477	100	20795.12	$16456_{17/2} - 37252^{\circ}_{17/2}$	ΔJ=0	1.16	0.26	
4807.022	7	20797.09	$21799^{\circ}_{9/2} - 42596_{9/2}$				
4806.709	2	20798.44	$19548_{9/2} - 40347^{\circ}_{9/2}$				
4805.502	10	20803.67	$21737_{9/2} - 42541^{\circ}_{11/2}$	S0	0.97	0.12	
4804.273	5	20808.99	$23941^{\circ}_{9/2} - 44750_{7/2}$				
4801.266	10	20822.02					
4799.509	30	20829.64					
4799.297	4	20830.56					
4798.633	10	20833.45	$23431^{\circ}_{9/2} - 44265_{7/2}$				
4798.105	4	20835.74	$23374_{13/2} - 44210^{\circ}_{13/2}$				
4796.660	10	20842.01	$21997_{11/2} - 42839^{\circ}_{9/2}$	S0	0.98	0.09	
4796.138	3	20844.28	$21737_{9/2} - 42581^{\circ}_{11/2}$				
4795.343	10	20847.74	$19748_{9/2} - 40596^{\circ}_{7/2}$	S0	1.22	0.07	
4793.628	1	20855.20	$18853_{11/2} - 39709^{\circ}_{11/2}$				
4793.360	4	20856.36	$21737_{9/2} - 42594^{\circ}_{9/2}$				
4792.393	60	20860.57		S0	0.54	0.50	
4791.915	2	20862.65					
4790.632	30	20868.24	$17343_{7/2} - 38211^{\circ}_{7/2}$	ΔJ=0	1.10	0.54	
4789.659	4	20872.48	$22419^{\circ}_{9/2} - 43292_{9/2}$				
4787.429	5	20882.20					
4786.704	2	20885.36	$17613_{9/2} - 38499^{\circ}_{9/2}$				
4786.210	2	20887.52					
4785.335	2	20891.34					
4784.179	2	20896.39					
4783.116	4	20901.03	$23873_{7/2} - 44774^{\circ}_{9/2}$				
4782.501	1	20903.72	$23335^{\circ}_{7/2} - 44238_{9/2}$				
4782.312	5 d	20904.54	$18837_{9/2} - 39741^{\circ}_{9/2}$				
4781.460	1	20908.27	$23335^{\circ}_{7/2} - 44243_{9/2}$				
4780.716	10	20911.52	$17752_{9/2} - 38664^{\circ}_{7/2}$	S0	0.65	0.38	
4780.480	1	20912.56	$21997_{11/2} - 42910^{\circ}_{13/2}$				
4780.020	1	20914.57	$19748_{9/2} - 40663^{\circ}_{11/2}$				
4779.689	20	20916.02	$17613_{9/2} - 38529^{\circ}_{11/2}$	S0	1.03	0.10	
4776.461	1	20930.15	$23335^{\circ}_{7/2} - 44265_{7/2}$				
4775.924	2	20932.50	$23374_{13/2} - 44307^{\circ}_{13/2}$				
4775.465	20	20934.52	$22902^{\circ}_{13/2} - 43836_{13/2}$	ΔJ=0	1.16	0.26	
4774.162	40 h	20940.23					
4771.340	2	20952.61	$15271_{15/2} - 36223^{\circ}_{13/2}$				
4769.035	2	20962.74					
4768.447	6	20965.33	$23781_{9/2} - 44747^{\circ}_{11/2}$	T	1.19		
4767.328	10	20970.25		S0	0.40	0.58	
4766.965	2	20971.84	$21161_{9/2} - 42133^{\circ}_{7/2}$				
4766.752	1	20972.78	$22742^{\circ}_{13/2} - 43715_{13/2}$				
4761.714	1	20994.97	$23873_{7/2} - 44868^{\circ}_{9/2}$				
4760.460	3	21000.50					
4759.905	500	21002.95	$15271_{15/2} - 36273^{\circ}_{15/2}$	ΔJ=0	1.10	0.33	
4759.587	1	21004.35	$21737_{9/2} - 42742^{\circ}_{7/2}$				
4757.756	2	21012.44	$21120_{9/2} - 42133^{\circ}_{7/2}$				
4757.295	1	21014.47					
4757.095	7	21015.36	$19748_{9/2} - 40763^{\circ}_{7/2}$	SI	1.65	0.36	

Wavelength in air Å	Intensity	Wavenumber cm^{-1}	Classification	Zeeman effect type	f	Je	
4754.589	30	21026.43	$16742_{7/2} - 37768^{\circ}_{9/2}$	S0	0.85	0.35	
4752.590	2	21035.28					
4751.168	30	21041.57	$17343_{7/2} - 38384^{\circ}_{9/2}$	SI	1.48	0.36	
4750.610	3	21044.04	$23374_{13/2} - 44418^{\circ}_{13/2}$				
4750.533	6	21044.38	$22419^{\circ}_{9/2} - 43464_{9/2}$				
4750.241	30	21045.68	$22742^{\circ}_{15/2} - 43788_{11/2}$	SI	1.45	0.22	
4749.838	1	21047.46	$19548_{9/2} - 40596^{\circ}_{7/2}$				
4747.930	2	21055.92					
4747.222	4	21059.06	$21120_{7/2} - 42179^{\circ}_{9/2}$				
4744.329	15	21071.90	$17613_{9/2} - 38685^{\circ}_{9/2}$	ΔJ=0	1.10	0.62	
4743.659	2	21074.88	$17454_{13/2} - 38529^{\circ}_{11/2}$				
4743.177	3	21077.02	$21799^{\circ}_{9/2} - 42876_{9/2}$				
4741.113	40	21086.20	$20406^{\circ}_{9/2} - 41493_{9/2}$	ΔJ=0	1.58	1.29	*
4740.918	1	21087.06	$23431^{\circ}_{9/2} - 44518_{9/2}$				
4739.390	4	21093.86	$22742^{\circ}_{15/2} - 43836_{13/2}$				
4739.213	10	21094.65	$22413^{\circ}_{9/2} - 43514_{7/2}$				
4739.109	1	21095.11					
4738.553	1	21097.59	$23431^{\circ}_{9/2} - 44529_{7/2}$				
4737.908	10	21100.46					
4737.607	10	21101.80	$21737_{9/2} - 42839^{\circ}_{9/2}$	ΔJ=0	1.105	0.17	
4735.917	20	21109.33	$17752_{9/2} - 38861^{\circ}_{9/2}$	ΔJ=0	1.19	1.565	*
4734.490	2	21115.69					
4733.335	2000 *r*	21120.85	$0^{\circ}_{7/2} - 21120_{7/2}$	ΔJ=0	1.16	0.21	
4732.235	3	21125.75					
4729.554	7	21137.73	$20406^{\circ}_{9/2} - 41544_{9/2}$	ΔJ=0	1.40	0.83	
4729.334	1	21138.71					
4729.222	5	21139.21	$17343_{7/2} - 38482^{\circ}_{7/2}$				
4726.821	3	21149.95	$23941^{\circ}_{9/2} - 45091_{9/2}$				
4725.548	40	21155.65	$17343_{7/2} - 38499^{\circ}_{9/2}$	SI	1.175	0.13	
4724.987	7	21158.16	$21799^{\circ}_{9/2} - 42957_{9/2}$				
4724.260	700 *r*	21161.42	$0^{\circ}_{7/2} - 21161_{9/2}$	T	1.145		
4723.608	10	21164.34					
4719.270	30	21183.79	$23335^{\circ}_{7/2} - 44518_{9/2}$	SI	1.75	0.40	
4718.140	2	21188.87	$21997_{11/2} - 43186^{\circ}_{11/2}$				
4717.726	40	21190.72	$13119_{9/2} - 34310^{\circ}_{9/2}$	ΔJ=0	1.305	0.995	*
4717.623	2	21191.19	$23374_{13/2} - 44565^{\circ}_{13/2}$				
4717.461	2	21191.91					
4716.522	15	21196.13	$22559^{\circ}_{11/2} - 43755_{9/2}$	SI	1.52	0.35	
4716.236	4	21197.42	$23873_{7/2} - 45070^{\circ}_{9/2}$				
4715.591	2	21200.32					
4715.002	2	21202.97					
4714.746	3	21204.12					
4713.344	20	21210.43	$20406^{\circ}_{9/2} - 41617_{7/2}$	S0	1.58	1.29	*
4712.319	30	21215.04	$19132_{9/2} - 40347^{\circ}_{9/2}$	SI	0.83	1.13	*
4712.004	20	21216.46	$23374_{13/2} - 44591^{\circ}_{13/2}$	ΔJ=0	1.02	0.42	
4711.643	2	21218.08	$18990_{13/2} - 40208^{\circ}_{9/2}$				
4710.198	50	21224.59		SI	1.39	0.29	
4706.954	1	21239.22					
4705.440	50	21246.05	$13119_{9/2} - 34365^{\circ}_{7/2}$	SI	1.66	0.35	
4705.284	1	21246.76	$21120_{7/2} - 42367^{\circ}_{9/2}$				
4705.113	4	21247.53	$22468^{\circ}_{11/2} - 43715_{11/2}$				
4704.000	3	21252.56	$22929_{9/2} - 44182^{\circ}_{9/2}$				
4703.540	10	21254.64	$16957^{\circ}_{7/2} - 38211^{\circ}_{7/2}$	T	1.17		
4702.671	1	21258.56	$19753^{\circ}_{7/2} - 41012^{\circ}_{7/2}$				
4702.366	1	21259.94	$18853^{\circ}_{13/2} - 40113^{\circ}_{13/2}$				
4701.565	300	21263.56	$17613_{9/2} - 38877^{\circ}_{11/2}$	S0	0.48	0.58	
4699.582	1	21272.54					
4699.234	10	21274.11	$23873_{7/2} - 45147^{\circ}_{9/2}$				
4699.052	2	21274.94					
4698.663	3	21276.70	$23781_{9/2} - 45058^{\circ}_{11/2}$				
4698.558	20	21277.17	$22559^{\circ}_{11/2} - 43836_{13/2}$	SI	1.33	0.15	
4698.179	10	21278.89		S0	0.45	0.50	
4697.667	5	21281.21	$23309_{11/2} - 44591^{\circ}_{13/2}$				
4696.256	2	21287.60	$22468^{\circ}_{11/2} - 43755_{9/2}$				
4694.585	10	21295.18					
4694.443	4	21295.82	$22419^{\circ}_{9/2} - 43715_{11/2}$				
4694.292	20	21296.51	$21737_{9/2} - 43034^{\circ}_{7/2}$	S0	1.04	0.07	
4693.395	1	21300.58					
4692.492	2	21304.68	$24957^{\circ}_{11/2} - 46262_{11/2}$				
4692.071	3	21306.59					
4691.855	10	21307.57					
4691.493	200	21309.21	$17752_{9/2} - 39061^{\circ}_{9/2}$	S0	0.94	0.235	
4691.111	500 *r*	21310.95	$8771^{\circ}_{9/2} - 30082_{9/2}$	ΔJ=0	0.82	0.15	
4690.808	20	21312.32		S0	0.73	0.35	
4690.112	1	21315.49					
4689.511	6	21318.22	$23431^{\circ}_{9/2} - 44750_{7/2}$				
4688.943	2	21320.80	$17343_{7/2} - 38664^{\circ}_{7/2}$				
4686.909	20	21330.05	$19748_{9/2} - 41078^{\circ}_{9/2}$	ΔJ=0	1.31	0.17	
4686.297	2	21332.84	$19748_{9/2} - 41081^{\circ}_{13/2}$				
4686.100	1	21333.74					
4685.490	1	21336.51	$19748_{9/2} - 41085^{\circ}_{7/2}$				
4685.114	500	21338.23	$13119_{9/2} - 34457^{\circ}_{9/2}$	ΔJ=0	1.30	1.18	*
4682.845	2	21348.57					
4681.920	1000 *r*	21352.78	$8771^{\circ}_{9/2} - 30124_{7/2}$	SI	1.22	0.27	
4681.478	3	21354.80	$23335^{\circ}_{7/2} - 44689_{9/2}$				
4681.320	3	21355.52	$19753_{7/2} - 41109^{\circ}_{9/2}$	T	1.18		
4681.038	3	21356.81					
4680.087	5	21361.15	$21799^{\circ}_{9/2} - 43160_{9/2}$				
4678.840	5	21366.84					
4678.447	3	21368.63	$22468^{\circ}_{11/2} - 43836_{13/2}$				
			$22419^{\circ}_{9/2} - 43788_{11/2}$				
4678.028	10	21370.55	$22929_{9/2} - 44300^{\circ}_{9/2}$	ΔJ=0	1.11	0.17	
4677.210	30	21374.28	$22902^{\circ}_{13/2} - 44276_{11/2}$	S0	1.04	0.11	
4676.878	5	21375.80	$19748_{9/2} - 41124^{\circ}_{9/2}$	ΔJ=0	1.24	0.16	
4676.429	5	21377.85					
4675.312	500	21382.96	$15271_{13/2} - 36653^{\circ}_{13/2}$	ΔJ=0	1.10	0.36	
4675.098	300	21383.94		T	1.18		
4673.659	1	21390.52					
4671.214	10	21401.72	$16456_{11/2} - 37858^{\circ}_{13/2}$	S0	1.02	0.15	
4669.746	10	21408.45	$17343_{7/2} - 38751^{\circ}_{9/2}$	S0	1.02	1.215	*
4668.690	100	21413.29	$13119_{9/2} - 34532^{\circ}_{11/2}$	S0	1.305	1.126	*
4668.321	4	21414.98	$23335^{\circ}_{7/2} - 44750_{7/2}$				
4666.640	100	21422.70	$15587_{11/2} - 37010^{\circ}_{9/2}$	SI	1.255	1.11	*
4664.641	1	21431.88	$21997_{11/2} - 43429^{\circ}_{9/2}$				
4663.885	30	21435.35	$19753_{7/2} - 41189^{\circ}_{7/2}$	T	1.19		
4662.727	10	21440.68	$19748_{9/2} - 41189^{\circ}_{7/2}$	ΔJ=1	?	0.36	
4662.507	10 *h*	21441.69					
4660.611	1	21450.41	$21997_{11/2} - 43447^{\circ}_{11/2}$				
4658.931	30	21458.14	$19753^{\circ}_{7/2} - 41211^{\circ}_{7/2}$	T	1.17		
4658.672	1	21459.34	$23431^{\circ}_{9/2} - 44891_{7/2}$				
4658.298	4	21461.06	$17454_{13/2} - 38915^{\circ}_{13/2}$				
4657.790	6	21463.40	$19748_{9/2} - 41211^{\circ}_{7/2}$				
4657.642	1	21464.08					
4657.126	2	21466.46					
4657.010	1	21467.00					
4656.717	70	21468.35	$13119_{9/2} - 34587^{\circ}_{9/2}$	ΔJ=0	1.308	1.00	*
4656.490	20	21469.39	$16742_{7/2} - 38211^{\circ}_{7/2}$				
4655.664	1	21473.20	$21120_{7/2} - 42594^{\circ}_{9/2}$				
4655.087	1000	21475.86	$17613_{9/2} - 39089^{\circ}_{11/2}$	S0	0.69	0.39	
4649.961	2	21499.54					
4648.510	2	21506.25		T	0.98		
4648.297	10 *h*	21507.23					
4646.684	4	21514.70					
4646.070	9	21517.54		T	1.26		
4645.847	100	21518.58	$17343_{7/2} - 38861^{\circ}_{9/2}$	S0	1.02	1.565	*
4645.122	1	21521.93					
4645.050	1	21522.27					
4644.579	300	21524.45	$17752_{9/2} - 39277^{\circ}_{9/2}$	T	1.18		
4644.339	4	21525.56	$19548_{9/2} - 41074^{\circ}_{9/2}$				
			$16957^{\circ}_{7/2} - 38482^{\circ}_{7/2}$				
4643.980	1	21527.23	$18990_{13/2} - 40517^{\circ}_{9/2}$				
4643.125	300	21531.19	$8771^{\circ}_{9/2} - 30302_{9/2}$	ΔJ=0	0.88	0.13	
4642.844	10	21532.49					
4642.604	20	21533.61	$22742^{\circ}_{15/2} - 44276_{11/2}$	SI	1.42	0.23	
4642.441	3	21534.36					
4642.050	1	21536.18	$19548_{9/2} - 41085^{\circ}_{7/2}$				
4641.740	2	21537.61					
4641.215	5	21540.05		ΔJ=0	?	1.82	
4640.796	50	21542.00	$16957^{\circ}_{7/2} - 38499^{\circ}_{9/2}$	S0	0.72	0.33	
4640.260	4	21544.48	$21161_{9/2} - 42705^{\circ}_{9/2}$	ΔJ=0	1.125	0.09	

Wavelength in air Å	Intensity	Wavenumber cm⁻¹	Classification	Zeeman effect type	f	Je	
4638.932	3	21550.65		ΔJ=0	1.22	0.18	
4638.287	2	21553.65	$22929_{9/2}-44483^{\circ}_{9/2}$				
4637.767	5	21556.06	$23335^{\circ}_{7/2}-44891_{7/2}$				
4636.633	10	21561.34	$22419^{\circ}_{9/2}-43981_{7/2}$				
4635.795	5 *h*	21565.23					
4633.960	300	21573.77	$17613_{9/2}-39187^{\circ}_{7/2}$	S0	0.61	0.58	
4632.490	5	21580.62	$21161_{9/2}-42742^{\circ}_{7/2}$				
4632.349	4	21581.28					
4631.538	10	21585.06	$21120_{7/2}-42705^{\circ}_{9/2}$	SI	1.32	0.16	
4631.104	1	21587.08					
4626.968	200	21606.37	$17613_{9/2}-39220^{\circ}_{9/2}$	ΔJ=0	1.15	0.31	
4625.576	40	21612.88	$22902^{\circ}_{13/2}-44515_{13/2}$	ΔJ=0	1.13	0.14	
4625.245	1	21614.42	$21120_{7/2}-42735^{\circ}_{9/2}$				
4624.402	30	21618.36		ΔJ=0	1.03	0.54	
4623.800	3	21621.18	$21120_{7/2}-42742^{\circ}_{7/2}$	ΔJ=0	1.18	0.09	
4621.716	300	21630.93	$17613_{9/2}-39244^{\circ}_{9/2}$	ΔJ=0	1.19	1.04 *	
4620.989	50	21634.33	$17752_{9/2}-39386^{\circ}_{9/2}$	ΔJ=0	1.07	0.51	
4619.204	4	21642.69	$16742_{7/2}-38384^{\circ}_{9/2}$				
4615.296	20	21661.02	$17752_{9/2}-39413^{\circ}_{7/2}$	S0	1.11	0.06	
4615.101	3	21661.93					
4614.696	10	21663.83	$18853_{11/2}-40517^{\circ}_{9/2}$				
4613.967	200	21667.25	$17752_{9/2}-39419^{\circ}_{9/2}$	SI	1.186	0.916 *	
4613.112	1	21671.27	$21737_{9/2}-43408^{\circ}_{13/2}$				
4613.035	5	21671.63	$19753_{7/2}-41425^{\circ}_{7/2}$				
4612.380	7	21674.71	$22742^{\circ}_{13/2}-44417_{11/2}$	SI	1.42	0.21	
4612.094	1	21676.05					
4611.197	1	21680.27	$18837_{9/2}-40517^{\circ}_{9/2}$				
4610.595	4	21683.10	$18693^{\circ}_{13/2}-40376^{\circ}_{13/2}$				
4610.470	2	21683.69	$23374^{\circ}_{13/2}-45058^{\circ}_{13/2}$				
4609.354	50	21688.94	$15587^{\circ}_{11/2}-37276^{\circ}_{11/2}$	T	1.25		
4608.913	2	21691.01					
4608.895	3	21691.10	$21737^{\circ}_{9/2}-43428^{\circ}_{7/2}$	T	1.15	0.06	
4608.795	1	21691.57					
4607.967	1	21695.47					
4607.453	2	21697.89					
4607.330	2	21698.47					
4607.036	2	21699.85	$23431^{\circ}_{9/2}-45131_{7/2}$				
4607.018	4	21699.94					
4606.608	10	21701.87					
4605.660	3	21706.33					
4605.231	40	21708.36	$17613_{9/2}-39322^{\circ}_{9/2}$	ΔJ=0	1.17	0.18	
4604.850	300	21710.15	$17752_{9/2}-39462^{\circ}_{7/2}$	S0	0.98	0.14	
4603.217	60	21717.85	$17752_{9/2}-39470^{\circ}_{9/2}$	ΔJ=0	1.14	0.36	
4603.051	20	21718.64	$21120_{7/2}-42839^{\circ}_{9/2}$	S0	0.69	0.38	
4601.580	3	21725.58		ΔJ=0	1.05	0.38	
4601.147	10	21727.62	$17752_{9/2}-39480^{\circ}_{7/2}$	T	1.15	0.03	
4599.017	2000 *r*	21737.69	$0^{\circ}_{7/2}-21737_{9/2}$	S0	1.09	0.045	
4598.225	4	21741.43		S0	0.20	0.49	
4596.626	1000	21748.99	$17613_{9/2}-39362^{\circ}_{11/2}$	S0	0.88	0.26	
4595.420	1	21754.70					
4594.979	4	21756.79	$16742_{7/2}-38499^{\circ}_{9/2}$	S0	0.13	0.925	
4594.532	3	21758.91	$18837_{9/2}-40596^{\circ}_{7/2}$				
4592.677	2	21767.69		ΔJ=0	1.15	0.51	
4591.717	4	21772.25	$22742^{\circ}_{13/2}-44515_{13/2}$				
4590.694	5	21777.10	$19548_{9/2}-41325^{\circ}_{9/2}$				
4590.649	40	21777.31	$15587^{\circ}_{11/2}-37365^{\circ}_{13/2}$	S0	0.91	0.29	
4589.729	10	21781.68	$21120_{7/2}-42902^{\circ}_{9/2}$	SI	1.50	0.33	
4588.684	6	21786.64	$22419^{\circ}_{9/2}-44206_{7/2}$				
4588.423	1	21787.88					
4588.067	50	21789.57	$17752_{9/2}-39542^{\circ}_{7/2}$	S0	0.73	0.32	
4587.870	1	21790.50	$18990^{\circ}_{11/2}-40780^{\circ}_{13/2}$				
4587.567	10	21791.94	$20406^{\circ}_{9/2}-42198_{9/2}$	ΔJ=0	1.58	1.255 *	
4586.967	20	21794.79	$16957^{\circ}_{7/2}-38751^{\circ}_{9/2}$	S0	1.06	0.11	
4586.062	1	21799.09					
4584.535	6	21806.35	$19132_{9/2}-40938^{\circ}_{9/2}$	SI	1.54	0.33	
4584.110	5	21808.37	$22468^{\circ}_{11/2}-44276_{11/2}$				
4583.914	2	21809.31	$18853_{11/2}-40663^{\circ}_{11/2}$				
4582.842	100	21814.41	$8771^{\circ}_{9/2}-30585_{9/2}$	S0	0.855	1.085 *	
4581.856	4	21819.10	$22419^{\circ}_{9/2}-44238_{9/2}$				
4581.547	1	21820.57	$19748_{9/2}-41569^{\circ}_{11/2}$				
4581.006	4	21823.15					
4580.460	2	21825.75	$18837_{9/2}-40663^{\circ}_{11/2}$				
4580.067	3	21827.63	$19748_{9/2}-41576^{\circ}_{9/2}$				
4579.438	10	21830.62	$17613_{9/2}-39444^{\circ}_{9/2}$	ΔJ=0	1.15	0.25	
4578.820	10 *h*	21833.57					
4576.609	80	21844.12	$17343_{7/2}-39187^{\circ}_{7/2}$	ΔJ=0	1.022	1.336 *	
4576.307	20	21845.56	$22419^{\circ}_{9/2}-44265_{7/2}$	S0	0.43	0.49	
4575.555	20	21849.15	$17613_{9/2}-39462^{\circ}_{7/2}$				
4575.322	30	21850.26	$17752_{9/2}-39602^{\circ}_{9/2}$	S0	1.01	0.165	
4573.981	2	21856.67	$22419^{\circ}_{9/2}-44276_{11/2}$				
4573.702	20	21858.00	$22559^{\circ}_{11/2}-44417_{11/2}$	ΔJ=0	1.16	0.165	
4573.190	1	21860.45					
4572.197	5	21865.20	$18990_{11/2}-40855^{\circ}_{9/2}$				
4571.900	80	21866.62	$17613_{9/2}-39480^{\circ}_{7/2}$	SI	1.25	0.06	
4571.225	30	21869.85		SI	1.40	0.125	
4570.617	10	21872.75	$21161_{9/2}-43034^{\circ}_{7/2}$	T	1.18	0.02	
4570.240	50	21874.56	$17613_{9/2}-39488^{\circ}_{9/2}$	ΔJ=0	1.15	0.36	
4569.803	10	21876.65	$19548_{9/2}-41425^{\circ}_{7/2}$				
			$17343_{7/2}-39220^{\circ}_{9/2}$				
4567.329	3	21888.50	$15271^{\circ}_{13/2}-37159^{\circ}_{13/2}$				
4566.532	5	21892.32	$19753_{7/2}-41646^{\circ}_{7/2}$				
4565.432	20	21897.59	$19748_{9/2}-41646^{\circ}_{7/2}$				
4565.053	2	21899.41					
4564.676	400	21901.22	$17343_{7/2}-39244^{\circ}_{9/2}$	T	1.02		
4564.260	3	21903.22					
4563.892	20	21904.98	$16957_{7/2}-38861^{\circ}_{9/2}$				
4563.642	20	21906.18	$17752_{9/2}-39658^{\circ}_{9/2}$				
4561.521	2	21916.37					
4560.137	3	21923.02					
4559.300	2	21927.05	$18853_{11/2}-40780^{\circ}_{13/2}$				
4558.335	1	21931.69	$21120_{7/2}-43052^{\circ}_{7/2}$				
4557.917	3	21933.70	$17343_{7/2}-39277^{\circ}_{9/2}$				
4557.633	200	21935.07	$13119_{9/2}-35054^{\circ}_{9/2}$	ΔJ=0	1.29	0.115	
4556.849	3	21938.84	$19748_{9/2}-41687^{\circ}_{11/2}$				
4555.923	3	21943.30	$16742_{7/2}-38685^{\circ}_{9/2}$				
4554.650	10	21949.43	$22468^{\circ}_{11/2}-44417_{11/2}$	ΔJ=0	1.20	0.25	
4554.065	2	21952.25	$21161_{9/2}-43113^{\circ}_{9/2}$				
4553.677	30	21954.12		SI	1.64	0.335	
4553.391	20	21955.50	$22559^{\circ}_{11/2}-44515_{13/2}$	S0	0.92	0.18	
4552.226	7	21961.12	$22419^{\circ}_{9/2}-44380_{9/2}$				
4549.069	2	21976.36	$19548_{9/2}-41525^{\circ}_{7/2}$				
4548.597	1000	21978.64	$17343_{7/2}-39322^{\circ}_{9/2}$	SI	1.61	0.45	
4548.105	50	21981.02	$15271_{13/2}-37252^{\circ}_{17/2}$	SI	2.10	0.90	
4547.341	5	21984.71	$19548_{9/2}-41533^{\circ}_{9/2}$	ΔJ=0	?	0.10	
4545.777	2	21992.27					
4544.660	10	21997.68	$22419^{\circ}_{9/2}-44417_{11/2}$				
4543.870	10	22001.50	$21799^{\circ}_{9/2}-43800_{9/2}$				
4543.825	2	22001.72	$18853_{13/2}-40855^{\circ}_{9/2}$				
4539.406	80	22023.14	$22559^{\circ}_{11/2}-44582_{9/2}$	SI	1.70	0.47	
4538.645	2	22026.83					
4538.212	4	22028.93	$16456_{17/2}-38485^{\circ}_{15/2}$				
4537.442	2	22032.67					
4536.406	2	22037.70	$19748_{9/2}-41786^{\circ}_{9/2}$				
4535.198	40	22043.57	$17343_{7/2}-39386^{\circ}_{9/2}$	SI	1.08	0.06	
4534.501	2	22046.96	$22468^{\circ}_{11/2}-44515_{13/2}$				
4532.150	300	22058.40	$15587^{\circ}_{13/2}-37646^{\circ}_{13/2}$	S0	0.82	0.44	
4531.130	2	22063.36					
4529.910	5	22069.31	$21161_{9/2}-43230^{\circ}_{9/2}$				
4529.745	2	22070.11	$15587^{\circ}_{13/2}-37657^{\circ}_{13/2}$				
4526.043	30	22088.16	$18990^{\circ}_{11/2}-41078^{\circ}_{9/2}$	S0	0.68	0.525	
4525.469	2	22090.96	$18990^{\circ}_{11/2}-41081^{\circ}_{11/2}$				
4525.034	10	22093.09	$19748_{9/2}-41841^{\circ}_{7/2}$				
4524.821	200	22094.13	$15271_{13/2}-37365^{\circ}_{13/2}$	S0	0.29	0.78	
4524.567	3	22095.37	$17613_{9/2}-39709^{\circ}_{13/2}$				
4524.168	3	22097.32	$19548_{9/2}-41646^{\circ}_{7/2}$				
4523.430	20	22100.92	$17343_{7/2}-39444^{\circ}_{9/2}$				
4521.643	10	22109.65	$22419^{\circ}_{9/2}-44529_{7/2}$	S0	0.83	0.07	
4520.632	20	22114.60	$22468^{\circ}_{11/2}-44582_{9/2}$	SI	1.85	0.56	
4519.734	20	22118.99	$18990^{\circ}_{11/2}-41109^{\circ}_{9/2}$	T	1.20		
4519.595	2000	22119.67	$16742^{\circ}_{7/2}-38861^{\circ}_{9/2}$	S0	1.32	1.57 *	

Wavelength in air Å	Intensity	Wavenumber cm⁻¹	Classification	Zeeman effect type	f	Je	
4518.350	5	22125.77	$19748_{9/2} - 41874^{\circ}_{11/2}$				
4517.846	70	22128.24	$17613_{9/2} - 39741^{\circ}_{9/2}$	ΔJ=0	?	0.34	
4517.400	4	22130.42	$22559^{\circ}_{11/2} - 44689_{9/2}$				
4517.209	1	22131.36					
4516.834	2	22133.19	$19748_{9/2} - 41881^{\circ}_{9/2}$				
4516.684	40	22133.93	$18990_{11/2} - 41124^{\circ}_{9/2}$	S0	1.12	0.09	
4516.205	70	22136.28	$20406^{\circ}_{9/2} - 42543_{7/2}$	S0	1.58	1.12	*
4514.453	20	22144.87	$17343_{7/2} - 39488^{\circ}_{9/2}$	SI	1.33	0.25	
4514.226	2	22145.98					
4508.318	1	22175.00	$18837_{9/2} - 41012^{\circ}_{7/2}$				
4506.220	1	22185.33					
4505.342	1	22189.65	$20406^{\circ}_{9/2} - 42596_{9/2}$				
4505.278	2	22189.96					
4504.859	60	22192.03		ΔJ=0	1.17	0.335	
4504.535	20	22193.62	$19132_{9/2} - 41325^{\circ}_{9/2}$				
4504.350	7	22194.54	$19548_{9/2} - 41743^{\circ}_{9/2}$	SI	1.06	0.08	
4503.936	2	22196.58					
4503.484	100	22198.80	$17343_{7/2} - 39542^{\circ}_{7/2}$	ΔJ=0	1.04	0.15	
4500.986	2	22211.12					
4499.039	10	22220.74	$19466_{13/2} - 41687^{\circ}_{11/2}$	T	1.17		
4498.813	7	22221.85	$22468^{\circ}_{11/2} - 44689_{9/2}$				
4498.230	10	22224.73	$18853_{11/2} - 41078^{\circ}_{9/2}$				
4497.131	2	22230.16					
4497.070	5	22230.46	$16957_{7/2} - 39187^{\circ}_{7/2}$				
4496.786	2	22231.87					
4496.022	3 *h*	22235.65					
4495.226	3	22239.58					
4494.299	20	22244.17	$13119_{9/2} - 35363^{\circ}_{9/2}$	ΔJ=0	1.305	0.91	*
4493.333	5	22248.95					
4492.270	20	22254.22	$17454_{13/2} - 39709^{\circ}_{11/2}$	S0	0.85	0.27	
4492.001	20	22255.55	$18853_{11/2} - 41109^{\circ}_{9/2}$	S0	0.98	0.18	
4491.731	2 *h*	22256.89					
4490.900	2	22261.01	$23374_{13/2} - 45635^{\circ}_{11/2}$				
4489.618	3	22267.36	$21161_{9/2} - 43428^{\circ}_{7/2}$				
4489.050	10	22270.18	$22419^{\circ}_{9/2} - 44689_{9/2}$				
4489.016	30	22270.35	$13119_{9/2} - 35389^{\circ}_{7/2}$	SI	2.50	1.20	
4488.983	20	22270.51	$18853_{11/2} - 41124^{\circ}_{9/2}$	S0	0.72	0.425	
4487.642	2	22277.17					
4487.196	2	22279.38	$22791_{7/2} - 45070^{\circ}_{9/2}$				
4486.140	150	22284.63	$17343_{7/2} - 39628^{\circ}_{7/2}$	ΔJ=0	1.015	0.135	
4485.642	5	22287.10					
4485.543	20	22287.59	$16957_{7/2} - 39244^{\circ}_{9/2}$				
4485.435	2	22288.13					
4484.797	2 *h*	22291.30					
4484.499	5	22292.78	$19548_{9/2} - 41841^{\circ}_{7/2}$				
4482.959	1	22300.44					
4482.476	10 *h*	22302.84					
4482.169	1	22304.37					
4481.054	2	22309.92	$21120_{7/2} - 43430^{\circ}_{9/2}$				
4479.938	30	22315.48	$17343_{7/2} - 39658^{\circ}_{9/2}$	SI	1.20	0.15	
4478.815	20	22321.07	$23941^{\circ}_{9/2} - 46262_{11/2}$	S0	0.52	0.63	
4476.960	3	22330.32	$22419^{\circ}_{9/2} - 44750_{7/2}$				
4476.236	20	22333.93					
4473.402	1	22348.08					
4472.816	60	22351.01					
4471.990	40	22355.14					
4471.788	2	22356.15	$22791_{7/2} - 45147^{\circ}_{9/2}$				
4471.057	7	22359.80	$22559^{\circ}_{11/2} - 44919_{9/2}$				
4470.985	2	22360.16					
4470.425	4	22362.96					
4470.360	2	22363.29					
4470.012	40	22365.03	$16957_{7/2} - 39322^{\circ}_{9/2}$	S0	1.03	0.12	
4468.910	10	22370.54	$19748_{9/2} - 42119^{\circ}_{11/2}$				
4467.983	100	22375.19	$15271_{13/2} - 37646^{\circ}_{13/2}$	S0	0.40	0.66	
4467.694	7	22376.63	$20406^{\circ}_{9/2} - 42783_{7/2}$				
4466.643	2	22381.90	$23781_{9/2} - 46163^{\circ}_{11/2}$				
4466.078	70	22384.73	$19748_{9/2} - 42133^{\circ}_{7/2}$	SI	1.71	0.425	
4465.542	2	22387.42					
4465.337	1	22388.44					
4464.778	1	22391.25					
4463.465	2	22397.83					
4463.328	3	22398.52	$17343_{7/2} - 39741^{\circ}_{9/2}$				
4462.770	20	22401.32	$19132_{9/2} - 41533^{\circ}_{9/2}$	SI	1.24	0.22	
4461.310	3 *h*	22408.65					
4459.986	100	22415.30		T	0.895	0.05	
4459.661	5	22416.94					
4459.267	3	22418.92					
4458.059	20	22424.99	$15587_{11/2} - 38012^{\circ}_{13/2}$	S0	0.31	0.825	
4457.848	20	22426.05	$19753_{7/2} - 42179^{\circ}_{9/2}$	SI	1.52	0.35	
4457.071	3	22429.96	$16957_{7/2} - 39386^{\circ}_{9/2}$				
4454.276	2	22444.04	$21799^{\circ}_{9/2} - 44243_{9/2}$				
4454.033	1000	22445.26	$16742_{7/2} - 39187^{\circ}_{7/2}$	ΔJ=0	1.33	0.05	
4453.699	3	22446.95					
4453.562	6	22447.64	$17613_{9/2} - 40061^{\circ}_{7/2}$				
4452.978	10	22450.58	$19466_{13/2} - 41917^{\circ}_{13/2}$	T	1.15		
4452.843	2	22451.26	$22468^{\circ}_{11/2} - 44919_{9/2}$				
4451.774	2	22456.65	$16957_{7/2} - 39413^{\circ}_{7/2}$				
4450.280	2	22464.19					
4449.772	10	22466.76		S0	0.76	0.24	
4449.223	5	22469.53	$20406^{\circ}_{9/2} - 42876_{9/2}$				
4448.435	2	22473.51					
4448.022	2 *h*	22475.59					
4447.824	2	22476.59					
4447.585	200	22477.80	$16742_{7/2} - 39220^{\circ}_{9/2}$	S0	0.40	0.72	
4447.357	2	22478.96	$22929_{9/2} - 45408^{\circ}_{7/2}$				
4446.900	2	22481.26					
4446.406	20 *h*	22483.76					
4445.712	5	22487.27	$16957_{7/2} - 39444^{\circ}_{9/2}$				
4444.530	50	22493.25		SI	1.39	0.28	
4443.287	4	22499.55	$22419^{\circ}_{9/2} - 44919_{9/2}$				
4442.735	400	22502.34	$16742_{7/2} - 39244^{\circ}_{9/2}$	S0	1.325	1.03	*
4442.059	15	22505.76	$16957_{7/2} - 39462^{\circ}_{7/2}$				
4440.676	2	22512.77					
4440.535	4	22513.49	$16957_{7/2} - 39470^{\circ}_{9/2}$				
4440.346	2	22514.45	$25130_{13/2} - 47644^{\circ}_{13/2}$				
4438.607	10	22523.27	$16957_{7/2} - 39480^{\circ}_{7/2}$	T	1.17		
4438.010	2	22526.30	$21737_{9/2} - 44263^{\circ}_{7/2}$				
4436.985	20	22531.50	$22559^{\circ}_{11/2} - 45091_{9/2}$	ΔJ=1	?	0.49	
4436.324	100	22534.86	$16742_{7/2} - 39277^{\circ}_{9/2}$	SI	1.65	0.35	
4435.070	2	22541.23					
4434.296	40	22545.16	$20406^{\circ}_{9/2} - 42952_{7/2}$	S0	1.58	1.14	*
4431.811	2	22557.81					
4431.561	60	22559.08		T	0.80		
4431.494	2	22559.42					
4430.862	50	22562.64	$13119_{9/2} - 35682^{\circ}_{7/2}$	SI	1.305	1.12	*
4429.756	50 *h*	22568.27					
4428.759	3 *w*	22573.35					
4428.530	1	22574.52					
4427.710	2	22578.70	$18990_{11/2} - 41569^{\circ}_{11/2}$				
4427.500	4	22579.77	$16742_{7/2} - 39322^{\circ}_{9/2}$				
4426.442	10	22585.17	$16957_{7/2} - 39542^{\circ}_{7/2}$				
4426.330	100	22585.74	$18990_{11/2} - 41576^{\circ}_{9/2}$	S0	1.04	0.165	
4425.958	200	22587.64	$15271_{13/2} - 37858^{\circ}_{13/2}$	ΔJ=0	1.16	0.90	
4425.167	2	22591.67					
4423.265	10	22601.39					
4422.305	70	22606.29	$18693_{13/2} - 41299^{\circ}_{17/2}$	S0	0.28	0.775	
4421.670	2 *h*	22609.54					
4421.357	1	22611.14	$19132_{9/2} - 41743^{\circ}_{9/2}$				
4420.845	40	22613.76	$19753_{7/2} - 42367^{\circ}_{9/2}$	S0	1.13	0.05	
4420.236	7	22616.88	$19753_{7/2} - 42370^{\circ}_{7/2}$	ΔJ=0	1.07	0.495	
4419.787	2	22619.17					
4419.204	40	22622.16	$19748_{9/2} - 42370^{\circ}_{7/2}$	SI	2.14	0.86	
4419.046	20	22622.97	$22468^{\circ}_{11/2} - 45091_{9/2}$				
4417.470	20	22631.04	$19548_{9/2} - 42179^{\circ}_{9/2}$	ΔJ=0	1.02	0.175	
4416.603	5 *h*	22635.48					
4416.240	2	22637.34					
4414.801	10	22644.72	$16742_{7/2} - 39386^{\circ}_{9/2}$				
4413.522	10	22651.28		S0	0.35	0.815	
4411.697	200	22660.65	$8771^{\circ}_{9/2} - 31431_{9/2}$	ΔJ=0	0.855	1.07	*
4410.842	5	22665.04					

Wavelength in air Å	Intensity	Wavenumber cm⁻¹	Classification	Zeeman effect type	f	Je	
4409.598	50	22671.44	$16742_{7/2} - 39413^{\circ}_{7/2}$	ΔJ=0	1.14	0.595	
4409.354	5	22672.69					
4408.601	5	22676.56	$22791_{7/2} - 45467^{\circ}_{9/2}$				
4407.560	3*h*	22681.92					
4406.981	1	22684.90					
4404.476	1	22697.80					
4403.650	40	22702.06	$16742_{7/2} - 39444^{\circ}_{9/2}$	S0	0.42	0.70	
4402.325	2	22708.89	$17613_{9/2} - 40322^{\circ}_{9/2}$	ΔJ=0	?	0.30	
4401.843	1	22711.38					
4401.082	2	22715.31	$18853_{11/2} - 41569^{\circ}_{11/2}$	ΔJ=0	?	0.275	
4400.257	10	22718.56	$21799^{\circ}_{9/2} - 44518_{9/2}$				
4400.446	1	22718.59	$21737_{9/2} - 44456^{\circ}_{7/2}$				
4400.070	20	22720.53	$16742_{7/2} - 39462^{\circ}_{7/2}$				
4399.723	100	22722.29	$18853_{11/2} - 41576^{\circ}_{9/2}$	S0	0.575	0.46	
4398.573	40	22728.26	$16742_{7/2} - 39470^{\circ}_{9/2}$				
4397.900	5	22731.74	$18837_{9/2} - 41569^{\circ}_{11/2}$				
4396.685	60	22738.02	$16742_{7/2} - 39480^{\circ}_{7/2}$				
4396.495	500 *r*	22739.00	$8771^{\circ}_{5/2} - 31510_{7/2}$	SI	0.856	1.11	*
4395.960	500	22741.77	$15271_{13/2} - 38012^{\circ}_{13/2}$	T	1.08	0.05	
4394.420	1000 *r*	22749.74	$8771^{\circ}_{5/2} - 31520_{9/2}$	SI	0.94	0.09	
4393.309	4	22755.49					
4392.435	2	22760.02	$15587_{11/2} - 38347^{\circ}_{11/2}$				
4392.220	4	22761.14					
4390.670	2*h*	22769.17					
4389.952	30	22772.90		SI	1.51	0.32	
4389.551	100	22774.98		S0	0.99	0.215	
4389.207	2	22776.76	$21997_{11/2} - 44774^{\circ}_{9/2}$				
4388.355	40	22781.18	$17752_{9/2} - 40533^{\circ}_{7/2}$	SI	1.37	0.145	
4387.641	10*h*	22784.89	$16957_{7/2} - 39741^{\circ}_{9/2}$				
4387.360	5	22786.35					
4386.434	10000*a*	22791.16	$0^{\circ}_{7/2} - 22791_{7/2}$	T	1.14		
4386.120	10	22792.79	$19748_{9/2} - 42541^{\circ}_{11/2}$				
4385.817	4*h*	22794.36					
4385.535	30	22795.83	$18990_{11/2} - 41786^{\circ}_{9/2}$	S0	1.09	0.13	
4385.291	20	22797.10	$15587_{11/2} - 38384^{\circ}_{9/2}$				
4385.095	4	22798.12					
4384.743	100*h*	22799.95	$16742_{7/2} - 39542^{\circ}_{7/2}$				
4383.510	5	22806.36	$21997_{11/2} - 44803^{\circ}_{13/2}$				
4383.257	6	22807.68	$19753_{7/2} - 42561^{\circ}_{9/2}$				
4382.432	6*h*	22811.97	$22902^{\circ}_{13/2} - 45714_{11/2}$				
4382.243	3*h*	22812.96	$19748_{9/2} - 42561^{\circ}_{9/2}$				
4380.360	5	22822.76					
4379.989	20*h*	22824.69					
4378.310	100	22833.45	$19748_{9/2} - 42581^{\circ}_{11/2}$	S0	0.46	0.675	
4377.017	50	22840.19	$19753_{7/2} - 42594^{\circ}_{9/2}$	S0	0.68	0.36	
4376.475	4	22843.02					
4376.344	8	22843.70	$17752_{9/2} - 40596^{\circ}_{7/2}$				
4376.003	50	22845.48	$19748_{9/2} - 42594^{\circ}_{9/2}$	ΔJ=0	1.19	0.875	
4375.766	10	22846.72	$23374_{13/2} - 46221^{\circ}_{11/2}$				
4375.140	100	22849.99	$18837_{9/2} - 41687^{\circ}_{11/2}$	SI	1.24	0.10	
4373.053	10	22860.90		S0	0.35	0.585	
4372.882	10*h*	22861.79					
4372.247	3	22865.11	$17343_{7/2} - 40208^{\circ}_{9/2}$				
4369.948	4	22877.14					
4369.557	3*h*	22879.19					
4368.648	50	22883.95	$18990_{11/2} - 41874^{\circ}_{11/2}$	ΔJ=0	1.19	0.32	
4367.238	200	22891.33	$18990_{11/2} - 41881^{\circ}_{9/2}$	SI	1.44	0.225	
4366.295	50*h*	22896.28	$20406^{\circ}_{9/2} - 43303_{7/2}$				
4365.936	3	22898.16					
4365.294	3	22901.53					
4364.898	10*h*	22903.61					
4364.820	3	22904.02	$17613_{9/2} - 40517^{\circ}_{9/2}$	ΔJ=0	1.17	0.13	
4364.113	3	22907.73					
4363.455	40	22911.18	$15587_{11/2} - 38499^{\circ}_{9/2}$	SI	1.25	1.07	*
4362.422	1*h*	22916.61	$16742_{7/2} - 39658^{\circ}_{9/2}$				
4361.746	10	22920.16	$17613_{9/2} - 40533^{\circ}_{7/2}$				
4360.476	15	22926.83	$18990_{11/2} - 41917^{\circ}_{9/2}$				
4359.928	15000*a*	22929.71	$0^{\circ}_{7/2} - 22929_{9/2}$	T	1.15		
4357.975	6	22939.99	$19466_{13/2} - 42406^{\circ}_{13/2}$				
4357.620	4	22941.86	$15587_{11/2} - 38529^{\circ}_{11/2}$				
4355.695	60	22952.00	$19753_{7/2} - 42705^{\circ}_{9/2}$	SI	1.40	0.22	
4354.917	30	22956.10		S0	0.22	0.81	
4352.710	2*h*	22967.74					
4352.028	80	22971.34	$22742^{\circ}_{13/2} - 45714_{11/2}$				
4351.375	3	22974.78					
4350.125	5	22981.39	$19753_{7/2} - 42735^{\circ}_{9/2}$				
4349.887	4	22982.64	$17613_{9/2} - 40596^{\circ}_{7/2}$				
4349.075	1	22986.93					
4348.841	20	22988.17	$19753_{7/2} - 42742^{\circ}_{7/2}$	ΔJ=0	1.19	0.07	
4347.840	50	22993.46	$19748_{9/2} - 42742^{\circ}_{7/2}$	SI	1.62	0.33	
4346.484	300	23000.64	$15587_{11/2} - 38588^{\circ}_{13/2}$	S0	1.00	0.205	
4345.863	200	23003.92	$17343_{7/2} - 40347^{\circ}_{9/2}$	S0	0.76	0.25	
4345.129	3	23007.81					
4344.840	10	23009.34	$21737_{9/2} - 44747^{\circ}_{11/2}$				
4344.479	500	23011.25	$17752_{9/2} - 40763^{\circ}_{7/2}$	T	1.18		
4343.710	3	23015.32					
4343.405	15	23016.94	$19753_{7/2} - 42770^{\circ}_{9/2}$	SI	1.30	0.11	
4343.040	2	23018.88					
4342.726	4	23020.54	$18853_{11/2} - 41874^{\circ}_{11/2}$				
4342.404	50	23022.25	$19748_{9/2} - 42770^{\circ}_{9/2}$	ΔJ=0	1.25	0.35	
4341.336	60	23027.91	$18853_{11/2} - 41881^{\circ}_{9/2}$	S0	1.05	0.105	
4339.626	30	23036.98	$18837_{9/2} - 41874^{\circ}_{11/2}$	SI	1.26	0.11	
4338.242	4	23044.33	$18837_{9/2} - 41881^{\circ}_{9/2}$				
4337.622	70	23047.63	$19132_{9/2} - 42179^{\circ}_{9/2}$	SI	0.88	1.06	*
4336.554	3	23053.30					
4334.656	30	23063.40	$18853_{11/2} - 41917^{\circ}_{13/2}$	T	1.16		
4333.737	3	23068.29					
4332.589	20*h*	23074.40	$20406^{\circ}_{9/2} - 43481_{9/2}$				
4330.851	1	23083.66					
4330.476	7	23085.66	$19753_{7/2} - 42839^{\circ}_{9/2}$	S0	0.72	0.35	
4329.487	8	23090.93	$19748_{9/2} - 42839^{\circ}_{9/2}$	ΔJ=0	1.29	1.09	*
4328.190	20	23097.85		SI	1.26	0.04	
4327.308	2	23102.56	$21161_{9/2} - 44263^{\circ}_{7/2}$				
4326.987	6	23104.27	$16957_{7/2} - 40061^{\circ}_{7/2}$	ΔJ=0	1.14	0.13	
4325.688	6*h*	23111.21					
4324.116	10	23119.61		S0	0.76	0.32	
4322.423	20	23128.67	$18990_{11/2} - 42119^{\circ}_{11/2}$	ΔJ=0	1.15	0.69	
4320.522	2	23138.84	$21161_{9/2} - 44300^{\circ}_{9/2}$				
4319.726	3	23143.11	$21120_{7/2} - 44263^{\circ}_{7/2}$				
4318.397	600 *r*	23150.23	$17613_{9/2} - 40763^{\circ}_{7/2}$	SI	1.25	0.05	
4317.126	20	23157.05	$19548_{9/2} - 42705^{\circ}_{9/2}$	ΔJ=0	1.05	0.30	
4316.215	2	23161.93					
4315.642	30*h*	23165.01					
4314.955	2	23168.70					
4313.916	3	23174.28	$17343_{7/2} - 40517^{\circ}_{9/2}$				
4312.966	8	23179.38	$21120_{7/2} - 44300^{\circ}_{9/2}$	SI	1.33	0.16	
4312.084	3	23184.12					
4311.743	2	23185.96	$17752_{9/2} - 40938^{\circ}_{9/2}$				
4311.672	2	23186.34	$19548_{9/2} - 42735^{\circ}_{9/2}$				
4311.543	2	23187.03	$18693_{13/2} - 41880^{\circ}_{13/2}$				
4310.405	30	23193.15	$19548_{9/2} - 42742^{\circ}_{7/2}$	SI	0.98	1.19	*
4309.819	2	23196.31					
4309.623	3	23197.36					
4307.593	2*h*	23208.29	$17454_{13/2} - 40663^{\circ}_{11/2}$				
4306.780	10	23212.67					
4306.657	150	23213.34	$19748_{9/2} - 42961^{\circ}_{11/2}$	S0	0.83	0.385	
4306.378	40	23214.84	$15271_{13/2} - 38485^{\circ}_{13/2}$	ΔJ=0	?	0.472	
4305.490	4	23219.63					
4304.865	2	23223.00	$23374_{13/2} - 46597^{\circ}_{13/2}$				
4304.652	5	23224.15	$18693_{13/2} - 41917^{\circ}_{13/2}$				
4302.569	20	23235.39	$19132_{9/2} - 42367^{\circ}_{9/2}$	SI	0.88	1.20	*
4302.023	3	23238.34					
4301.360	20	23241.92	$17613_{9/2} - 40855^{\circ}_{9/2}$	ΔJ=0	1.14	0.475	
4300.595	20	23246.06	$22468^{\circ}_{11/2} - 45714_{11/2}$				
4299.589	20	23251.50	$16957_{7/2} - 40208^{\circ}_{9/2}$	SI	1.24	0.04	
4299.482	4	23252.08					
4299.325	7	23252.92	$17343_{7/2} - 40596^{\circ}_{7/2}$				
4298.365	300 *r*	23258.12	$13119_{9/2} - 36377^{\circ}_{9/2}$	ΔJ=0	1.27	0.46	
4298.060	40	23259.77	$17752_{9/2} - 41012^{\circ}_{7/2}$	S0	1.03	0.11	
4297.477	2	23262.92					

Wavelength in air Å	Intensity	Wavenumber cm⁻¹	Classification	Zeeman effect type	f	Je	
4297.044	20	23265.27	$18853_{11/2}-42119^{\circ}{}_{11/2}$	ΔJ=0	1.13	0.32	
4296.052	4 *h*	23270.64					
4294.982	20	23276.44	$19753^{\circ}{}_{7/2}-43030^{\circ}{}_{9/2}$	SI	?	0.325	
4294.481	2	23279.15					
4293.289	30	23285.62	$19748^{\circ}{}_{9/2}-43034^{\circ}{}_{7/2}$	SI	1.77	0.445	
4292.591	3	23289.40	$15587^{\circ}{}_{11/2}-38877^{\circ}{}_{11/2}$				
4291.590	4 *h*	23294.83	$21161^{\circ}{}_{5/2}-44456^{\circ}{}_{7/2}$				
4291.084	2	23297.58	$21120^{\circ}{}_{7/2}-44418^{\circ}{}_{7/2}$				
4290.874	60	23298.72	$19753^{\circ}{}_{7/2}-43052^{\circ}{}_{7/2}$	ΔJ=0	1.12	0.46	
4290.137	20 *h*	23302.72					
4289.905	20	23303.98	$19748^{\circ}{}_{9/2}-43052^{\circ}{}_{7/2}$	SI	1.29	1.055	*
4288.653	20	23310.79		SI	1.17	0.215	
4287.426	10	23317.46	$15271_{13/2}-38588^{\circ}{}_{13/2}$				
4287.130	2 *h*	23319.07	$16742^{\circ}{}_{7/2}-40061^{\circ}{}_{7/2}$				
4286.934	40 *h*	23320.13					
4286.102	2	23324.66					
4285.840	20	23326.09	$17454_{13/2}-40780^{\circ}{}_{13/2}$	ΔJ=0	1.18	0.465	
4285.654	3	23327.10					
4285.073	4	23330.26					
4284.680	40	23332.40	$17752_{9/2}-41085^{\circ}{}_{7/2}$				
4284.344	4	23334.23					
4284.095	3	23335.59					
4281.662	2	23348.85					
4280.776	10	23353.68	$19548_{9/2}-42902^{\circ}{}_{9/2}$				
4280.369	3	23355.90					
4279.990	2	23357.97					
4279.620	10 *h*	23359.99	$22902^{\circ}{}_{13/2}-46262_{11/2}$				
4278.605	3	23365.53	$16957^{\circ}{}_{7/2}-40322^{\circ}{}_{9/2}$				
4274.355	60	23388.76	$19466_{13/2}-42855^{\circ}{}_{13/2}$	S0	0.93	0.185	
4274.084	7	23390.24	$16957^{\circ}{}_{7/2}-40347^{\circ}{}_{9/2}$				
4273.839	4	23391.58	$21997^{\circ}{}_{11/2}-45389^{\circ}{}_{13/2}$				
4272.537	60	23398.71	$17613^{\circ}{}_{9/2}-41012^{\circ}{}_{7/2}$	SI	1.32	0.235	
4271.716	500 *r*	23403.21	$8771^{\circ}{}_{9/2}-32174^{\circ}{}_{9/2}$	ΔJ=0	0.856	1.16	*
4270.190	2 *h*	23411.57					
4269.334	3	23416.27	$18990_{11/2}-42406^{\circ}{}_{13/2}$				
4268.561	300	23420.51	$17343^{\circ}{}_{7/2}-40763^{\circ}{}_{7/2}$	ΔJ=0	1.02	1.18	*
4265.648	20 *h*	23436.50	$17752^{\circ}{}_{9/2}-41189^{\circ}{}_{7/2}$				
4265.414	30	23437.79	$19748^{\circ}{}_{9/2}-43186^{\circ}{}_{11/2}$				
4264.394	2	23443.39	$19466_{13/2}-42910^{\circ}{}_{13/2}$				
4262.798	3 *h*	23452.17	$20406^{\circ}{}_{9/2}-43859^{\circ}{}_{9/2}$				
4262.486	10 *h*	23453.89					
4261.502	60 *h*	23459.30	$17752^{\circ}{}_{9/2}-41211^{\circ}{}_{7/2}$				
4261.200	2	23460.96					
4260.487	300 *h*	23464.89	$17613^{\circ}{}_{9/2}-41078^{\circ}{}_{9/2}$	ΔJ=0	1.27	0.63	
4259.975	3	23467.71	$17613^{\circ}{}_{9/2}-41081^{\circ}{}_{11/2}$				
4259.307	10	23471.39	$17613^{\circ}{}_{9/2}-41085^{\circ}{}_{7/2}$	SI	1.86	0.65	
4255.283	15	23493.59		ΔJ=0	1.14	0.44	
4254.988	20	23495.22	$19466_{13/2}-42961^{\circ}{}_{11/2}$	S0	0.89	0.25	
4254.905	4	23495.67	$17613^{\circ}{}_{9/2}-41109^{\circ}{}_{9/2}$				
4254.335	6	23498.82					
4253.455	200	23503.68	$19548^{\circ}{}_{9/2}-43052^{\circ}{}_{7/2}$	SI	1.24	0.18	
4252.191	30	23510.67	$17613^{\circ}{}_{9/2}-41124^{\circ}{}_{9/2}$	ΔJ=0	1.22	0.26	
4251.362	10	23515.25		ΔJ=0	1.02	1.02	
4250.624	30	23519.34	$22742^{\circ}{}_{13/2}-46262_{11/2}$				
4250.316	3	23521.04					
4247.416	150	23537.10	$13119^{\circ}{}_{9/2}-36656^{\circ}{}_{11/2}$	S0	1.304	1.16	*
4244.919	30	23550.95	$18990_{11/2}-42541^{\circ}{}_{11/2}$	ΔJ=0	1.15	0.64	
4244.838	5	23551.39	$20406^{\circ}{}_{9/2}-43958^{\circ}{}_{9/2}$				
4244.576	4	23552.85	$18853_{11/2}-42406^{\circ}{}_{13/2}$				
4243.325	10	23559.79					
4243.170	20	23560.65	$16957^{\circ}{}_{7/2}-40517^{\circ}{}_{9/2}$	T	1.16		
4242.420	30	23564.82	$19548^{\circ}{}_{9/2}-43113^{\circ}{}_{9/2}$	ΔJ=0	?	0.325	
4241.528	30 *h*	23569.77	$15587_{13/2}-39157^{\circ}{}_{13/2}$				
4241.282	40	23571.14	$18990_{11/2}-42561^{\circ}{}_{9/2}$	SI	1.215	1.055	*
4240.722	20	23574.25	$20406^{\circ}{}_{9/2}-43981^{\circ}{}_{9/2}$				
4240.490	200 *h*	23575.54	$17613^{\circ}{}_{9/2}-41189^{\circ}{}_{7/2}$	T	1.19		
4239.632	6	23580.31	$16742^{\circ}{}_{7/2}-40322^{\circ}{}_{9/2}$				
4239.012	1	23583.76					
4238.809	20	23584.89	$19466_{13/2}-43051^{\circ}{}_{13/2}$	SI	1.42	0.24	
4237.612	20	23591.55	$18990_{11/2}-42581^{\circ}{}_{11/2}$	ΔJ=0	1.17	0.43	
4237.235	10 *h*	23593.65					
4236.400	80 *h*	23598.30	$17613_{9/2}-41211^{\circ}{}_{7/2}$				
4236.237	3 *h*	23599.21					
4235.444	40	23603.63	$18990_{11/2}-42594^{\circ}{}_{9/2}$	SI	1.70	0.48	
4235.192	40	23605.03	$16742^{\circ}{}_{7/2}-40347^{\circ}{}_{9/2}$	SI	1.325	1.135	*
4235.036	3	23605.90					
4234.177	4	23610.69					
4232.395	2	23620.63					
4232.116	4	23622.19	$24137_{13/2}-47759^{\circ}{}_{13/2}$				
4231.332	4	23626.57	$17454_{13/2}-41081^{\circ}{}_{11/2}$				
4229.236	2	23638.28	$21997_{11/2}-45635^{\circ}{}_{11/2}$				
4229.058	40	23639.27	$16957^{\circ}{}_{7/2}-40596^{\circ}{}_{7/2}$	ΔJ=0	1.23	0.47	
4228.050	40	23644.91	$15271_{13/2}-38915^{\circ}{}_{13/2}$				
4227.390	2	23648.60					
4226.537	2	23653.37	$21120^{\circ}{}_{7/2}-44774^{\circ}{}_{9/2}$				
4226.253	3	23654.96					
4226.055	150	23656.07		SI	1.20	0.11	
4225.639	10	23658.40					
4225.565	4	23658.81					
4223.060	20	23672.84	$17752_{9/2}-41425^{\circ}{}_{7/2}$				
4222.671	2000 *r*	23675.03	$8771^{\circ}{}_{9/2}-32446^{\circ}{}_{7/2}$	SI	1.00	0.10	
4222.584	200	23675.51	$19753^{\circ}{}_{7/2}-43429^{\circ}{}_{9/2}$				
4222.336	8	23676.90	$19753^{\circ}{}_{7/2}-43430^{\circ}{}_{9/2}$				
4221.743	10	23680.23	$19748^{\circ}{}_{9/2}-43428^{\circ}{}_{7/2}$				
4221.639	80	23680.81	$19748^{\circ}{}_{9/2}-43429^{\circ}{}_{9/2}$	ΔJ=0	1.25	0.47	
4221.450	50	23681.87	$19548^{\circ}{}_{9/2}-43230^{\circ}{}_{9/2}$	T	1.00	0.04	
4220.440	3	23687.54	$18853_{11/2}-42541^{\circ}{}_{11/2}$				
4218.060	4	23700.91					
4217.753	20 *h*	23702.63	$22559^{\circ}{}_{11/2}-46262_{11/2}$	T	1.16		
4217.030	3 *h*	23706.69					
4216.851	60	23707.70	$18853_{11/2}-42561^{\circ}{}_{9/2}$	SI	1.69	0.55	
4215.804	20	23713.59	$18693_{13/2}-42406^{\circ}{}_{13/2}$				
4215.627	10 *h*	23714.58					
4213.925	10	23724.16	$18837^{\circ}{}_{9/2}-42561^{\circ}{}_{9/2}$	ΔJ=0	1.70	0.36	
4213.216	200	23728.15	$18853_{11/2}-42581^{\circ}{}_{11/2}$	T	1.14		
4212.588	10	23731.69					
4211.980	20 *h*	23735.12	$17343^{\circ}{}_{7/2}-41078^{\circ}{}_{9/2}$	SI	1.02	1.32	*
4211.720	4	23736.58					
4211.332	2	23738.77					
4211.072	6	23740.23	$18853_{11/2}-42594^{\circ}{}_{9/2}$				
4210.921	7	23741.09					
4210.817	40	23741.67	$17343^{\circ}{}_{7/2}-41085^{\circ}{}_{7/2}$	ΔJ=0	1.015	0.08	
4210.299	6	23744.59	$18837^{\circ}{}_{9/2}-42581^{\circ}{}_{11/2}$				
4209.811	5	23747.35	$21120^{\circ}{}_{7/2}-44868^{\circ}{}_{9/2}$				
4208.144	3 *h*	23756.75	$18837^{\circ}{}_{9/2}-42594^{\circ}{}_{9/2}$	T	1.125		
4207.832	3	23758.51					
4207.322	6	23761.39		SI	1.60	0.37	
4207.268	4 *h*	23761.70					
4206.508	3	23765.99	$17343^{\circ}{}_{7/2}-41109^{\circ}{}_{9/2}$				
4205.752	40	23770.26	$19132^{\circ}{}_{9/2}-42902^{\circ}{}_{9/2}$	SI	0.88	1.04	*
4204.841	5	23775.41	$16742^{\circ}{}_{7/2}-40517^{\circ}{}_{9/2}$				
4203.953	30	23780.44	$18990_{11/2}-42770^{\circ}{}_{9/2}$	T	1.22		
4203.727	30000 *a*	23781.71	$0^{\circ}{}_{7/2}-23781^{\circ}{}_{9/2}$	T	1.14		
4201.980	3	23791.60	$16742^{\circ}{}_{7/2}-40533^{\circ}{}_{7/2}$				
4201.542	10 *h*	23794.08	$22468^{\circ}{}_{11/2}-46262_{11/2}$				
4201.195	4	23796.05	$19748^{\circ}{}_{9/2}-43544^{\circ}{}_{9/2}$				
4200.577	100	23799.55	$20406^{\circ}{}_{9/2}-44206^{\circ}{}_{7/2}$	S00	1.58	1.04	*
4199.284	30	23806.88	$16957^{\circ}{}_{7/2}-40763^{\circ}{}_{7/2}$	T	1.17		
4198.411	100	23811.83	$17613^{\circ}{}_{9/2}-41425^{\circ}{}_{7/2}$	SI	1.56	0.33	
4198.270	4 *h*	23812.63					
4198.200	2	23813.02	$21997_{11/2}-45810^{\circ}{}_{11/2}$				
4197.924	20	23814.59	$13119^{\circ}{}_{9/2}-36934^{\circ}{}_{7/2}$	SI	1.40	0.09	
4196.958	5	23820.07	$17454_{13/2}-41274^{\circ}{}_{13/2}$	T	1.14		
4196.608	10	23822.06	$19466_{13/2}-43288^{\circ}{}_{13/2}$	ΔJ=0	1.17	0.27	
4196.419	4	23823.13					
4194.848	4	23832.05					
4194.440	10	23834.37	$19753^{\circ}{}_{7/2}-43588^{\circ}{}_{7/2}$				
4194.054	2	23836.56	$20406^{\circ}{}_{9/2}-44243^{\circ}{}_{9/2}$				
4193.725	3	23838.43					
4193.514	40	23839.63	$19748^{\circ}{}_{9/2}-43588^{\circ}{}_{7/2}$	SI	1.44	0.15	

Wavelength in air Å	Intensity	Wavenumber cm^{-1}	Classification	Zeeman effect type	f	Je	
4193.028	10 *h*	23842.40	$22419^{\circ}_{9/2} - 46262_{11/2}$				
4192.336	60	23846.33	$15587_{11/2} - 39434^{\circ}_{13/2}$	S0	0.57	0.58	
4191.846	4	23849.12	$18990_{11/2} - 42839^{\circ}_{9/2}$				
4190.975	100	23854.07	$16742^{\circ}_{7/2} - 40596^{\circ}_{7/2}$	$\Delta J=0$	1.315	0.07	
4190.204	20	23858.46	$20406^{\circ}_{9/2} - 44265^{\circ}_{7/2}$	S00	1.58	1.10	*
4187.615	40000 *a*	23873.21	$0^{\circ}_{7/2} - 23873^{\circ}_{7/2}$	$\Delta J=0$	1.14	0.04	
4186.086	20	23881.93	$19548^{\circ}_{9/2} - 43430^{\circ}_{9/2}$				
4184.513	100	23890.91	$13119^{\circ}_{9/2} - 37010^{\circ}_{9/2}$	$\Delta J=0$	1.305	1.105	*
4184.311	6	23892.06	$15587_{11/2} - 39479^{\circ}_{11/2}$				
4184.064	6 *h*	23893.47	$17752^{\circ}_{9/2} - 41646^{\circ}_{7/2}$				
4183.245	6 *h*	23898.15					
4183.168	3	23898.59	$16957^{\circ}_{7/2} - 40855^{\circ}_{9/2}$				
4182.898	3	23900.13					
4182.848	7	23900.42	$15587_{11/2} - 39488^{\circ}_{9/2}$				
4182.110	4	23904.64	$18837^{\circ}_{9/2} - 42742^{\circ}_{7/2}$				
4180.902	40	23911.54	$17613^{\circ}_{9/2} - 41525^{\circ}_{7/2}$	SI	1.46	0.29	
4180.093	30	23916.17	$20406^{\circ}_{9/2} - 44323^{\circ}_{7/2}$	S00	1.58	1.09	*
4179.953	50	23916.97	$18853_{11/2} - 42770^{\circ}_{9/2}$	S0	0.88	0.25	
4179.486	20	23919.65	$18990_{11/2} - 42910^{\circ}_{13/2}$	T	1.20		
4178.247	4 *h*	23926.74	$19748^{\circ}_{9/2} - 43675^{\circ}_{9/2}$				
4177.083	7	23933.41	$18837^{\circ}_{9/2} - 42770^{\circ}_{9/2}$	$\Delta J=0$	1.17	0.38	
4175.528	3	23942.32	$19466_{13/2} - 43408^{\circ}_{11/2}$				
4173.235	6	23955.47	$17613^{\circ}_{9/2} - 41569^{\circ}_{11/2}$	SI	1.25	0.05	
4172.010	7	23962.51	$17613^{\circ}_{9/2} - 41576^{\circ}_{9/2}$	$\Delta J=0$	1.22	0.23	
4171.460	2	23965.67					
4170.790	1	23969.52					
4170.449	500	23971.48	$18990_{11/2} - 42961^{\circ}_{11/2}$	$\Delta J=0$	1.20	0.08	
4169.232	5	23978.47	$24137_{13/2} - 48115^{\circ}_{13/2}$				
4168.720	300	23981.42	$19132^{\circ}_{9/2} - 43113^{\circ}_{9/2}$	SI	0.88	1.11	*
4168.535	200 *h*	23982.48	$17343^{\circ}_{7/2} - 41325^{\circ}_{9/2}$				
4167.970	3	23985.73					
4167.092	4	23990.79	$17752^{\circ}_{9/2} - 41743^{\circ}_{9/2}$	SI	1.184	0.91	*
4165.764	2	23998.44					
4165.495	5	23999.99					
4165.125	20	24002.12	$18837^{\circ}_{9/2} - 42839^{\circ}_{9/2}$	$\Delta J=0$	1.10	0.20	
4163.708	3	24010.29					
4163.030	3	24014.20					
4161.735	80	24021.67	$16742^{\circ}_{7/2} - 40763^{\circ}_{7/2}$	$\Delta J=0$	1.32	1.175	*
4159.870	20 *h*	24032.44	$17613^{\circ}_{9/2} - 41646^{\circ}_{7/2}$				
4158.665	8	24039.40					
4158.601	500 *r*	24039.77	$8771^{\circ}_{5/2} - 32811^{\circ}_{7/2}$	SI	0.85	1.04	*
4156.295	3	24053.11					
4155.898	3	24055.41	$16957^{\circ}_{7/2} - 41012^{\circ}_{7/2}$				
4155.757	30	24056.22	$18853_{11/2} - 42910^{\circ}_{13/2}$	SI	1.47	0.27	
4154.720	2	24062.23					
4154.130	300 *h*	24065.64					
4153.430	20 *h*	24069.70					
4152.732	20	24073.75	$17613^{\circ}_{9/2} - 41687^{\circ}_{11/2}$	S0	1.01	0.13	
4151.108	2	24083.16					
4150.104	200	24088.99	$17752^{\circ}_{9/2} - 41841^{\circ}_{7/2}$	SI	1.25	0.05	
4149.144	300	24094.56		T	1.10	0.04	
4148.910	5 *h*	24095.92					
4148.475	20 *h*	24098.45	$19132^{\circ}_{9/2} - 43230^{\circ}_{9/2}$	$\Delta J=0$	0.93	0.17	
4148.222	10 *h*	24099.92					
4147.890	20 *d*	24101.85	$13119^{\circ}_{9/2} - 37221^{\circ}_{7/2}$				
4147.178	10	24105.98					
4146.821	60	24108.06	$18853_{11/2} - 42961^{\circ}_{11/2}$				
4146.260	3	24111.32					
4146.129	40 *h*	24112.08	$20406^{\circ}_{9/2} - 44518^{\circ}_{9/2}$	$\Delta J=0$	1.58	1.21	*
4145.910	40	24113.36	$16742^{\circ}_{7/2} - 40855^{\circ}_{9/2}$	S0	1.325	1.08	*
4145.748	1	24114.30	$17454_{13/2} - 41569^{\circ}_{11/2}$				
4144.553	5	24121.25	$15587_{11/2} - 39709^{\circ}_{11/2}$				
4144.325	50	24122.58	$20406^{\circ}_{9/2} - 44529^{\circ}_{7/2}$	S00	1.58	0.97	*
4143.995	100	24124.50	$18837^{\circ}_{9/2} - 42961^{\circ}_{11/2}$				
4141.704	4	24137.84					
4141.495	60 *h*	24139.06	$20406^{\circ}_{9/2} - 44545^{\circ}_{9/2}$	SI	1.58	1.10	*
4141.098	3	24141.38					
4140.596	70 *h*	24144.30					
4140.030	80	24147.60	$19466_{13/2} - 43614^{\circ}_{13/2}$	S0	0.80	0.30	
4138.387	400 *r*	24157.19	$13119^{\circ}_{9/2} - 37276^{\circ}_{11/2}$	S0	0.98	0.25	
4138.334	2000 *r*	24157.50	$8771^{\circ}_{5/2} - 32928^{\circ}_{9/2}$	S0	0.74	0.12	
4138.005	100 *h*	24159.42					
4137.503	70	24162.35	$18693_{13/2} - 42855^{\circ}_{13/2}$	$\Delta J=0$	1.15	0.43	
4137.365	4	24163.16	$15271_{13/2} - 39434^{\circ}_{13/2}$				
4136.360	9 *h*	24169.03					
4136.192	30 *h*	24170.01					
4135.875	9	24171.86					
4135.744	4	24172.63	$17613^{\circ}_{9/2} - 41786^{\circ}_{9/2}$				
4135.462	6 *h*	24174.28					
4135.083	2	24176.49	$18853_{11/2} - 43030^{\circ}_{9/2}$				
4134.167	8	24181.85	$17343^{\circ}_{7/2} - 41525^{\circ}_{7/2}$	$\Delta J=0$	1.05	0.27	
4134.068	1	24182.43					
4132.740	6	24190.20	$17343^{\circ}_{7/2} - 41533^{\circ}_{9/2}$				
4132.270	5	24192.95	$18837^{\circ}_{9/2} - 43030^{\circ}_{9/2}$				
4131.760	10	24195.94	$18990_{11/2} - 43186^{\circ}_{11/2}$				
4131.658	4 *h*	24196.53					
4130.998	2	24200.40					
4129.530	20	24209.00		$\Delta J=0$	1.22	0.22	
4128.477	20	24215.18	$18837^{\circ}_{9/2} - 43052^{\circ}_{7/2}$				
4128.168	20	24216.99	$18693_{13/2} - 42910^{\circ}_{13/2}$	S0	1.02	0.16	
4127.408	2	24221.45					
4127.097	2	24223.27					
4126.612	20 *h*	24226.12	$19748^{\circ}_{9/2} - 43974^{\circ}_{11/2}$				
4126.298	200	24227.96	$17613^{\circ}_{9/2} - 41841^{\circ}_{7/2}$	S0	1.15	0.04	
4125.476	80	24232.79	$17343^{\circ}_{7/2} - 41576^{\circ}_{9/2}$	SI	1.02	1.25	*
4124.648	10 *h*	24237.66					
4122.979	20 *h*	24247.47	$19753^{\circ}_{7/2} - 44001^{\circ}_{9/2}$				
4122.081	4	24252.75	$19748^{\circ}_{9/2} - 44001^{\circ}_{9/2}$				
4120.725	20	24260.73	$17613^{\circ}_{9/2} - 41874^{\circ}_{11/2}$	S0	1.07	0.11	
4120.171	1	24263.99					
4119.475	50	24268.09	$17613^{\circ}_{9/2} - 41881^{\circ}_{9/2}$	T	1.19	0.04	
4119.262	3	24269.35					
4119.124	30	24270.16	$16742^{\circ}_{7/2} - 41012^{\circ}_{7/2}$	$\Delta J=0$	1.23	0.63	
4116.710	3	24284.39					
4115.834	20 *h*	24289.56					
4115.764	6	24289.97					
4114.592	6	24296.89					
4114.320	100	24298.50	$19132^{\circ}_{9/2} - 43430^{\circ}_{9/2}$	SI	1.40	0.32	
4114.128	100 *h*	24299.63					
4111.853	5	24313.08					
4111.208	3	24316.89					
4109.328	5 *h*	24328.01					
4108.565	2	24332.53	$18853_{11/2} - 43186^{\circ}_{11/2}$				
4107.930	300	24336.29	$16742^{\circ}_{7/2} - 41078^{\circ}_{9/2}$	T	1.32		
4107.531	1	24338.66					
4106.756	5	24343.25	$20406^{\circ}_{9/2} - 44750^{\circ}_{7/2}$	S0	1.08	1.08	
4105.841	50000 *a*	24348.67	$0^{\circ}_{7/2} - 24348^{\circ}_{9/2}$	S0	1.05	0.07	
4105.010	5	24353.60					
4104.697	3 *h*	24355.46					
4104.189	20	24358.48	$18693_{13/2} - 43051^{\circ}_{13/2}$	T	1.185		
4103.792	6	24360.83					
4102.727	60	24367.16	$16742^{\circ}_{7/2} - 41109^{\circ}_{9/2}$	S0	0.68	0.51	
4101.460	10 *h*	24374.68					
4100.458	10	24380.64	$17752^{\circ}_{9/2} - 42133^{\circ}_{7/2}$	T	1.18		
4100.340	3	24381.34					
4100.217	8	24382.07	$16742^{\circ}_{7/2} - 41124^{\circ}_{9/2}$	SI	1.41	0.24	
4100.171	10	24382.35					
4099.780	2	24384.67	$23374_{13/2} - 47759^{\circ}_{13/2}$				
4099.127	10	24388.56	$19753^{\circ}_{7/2} - 44142^{\circ}_{7/2}$	$\Delta J=0$	1.10	0.57	
4097.747	10 *h*	24396.77					
4094.187	50000 *a*	24417.98	$0^{\circ}_{7/2} - 24418^{\circ}_{9/2}$	SI	1.30	0.20	
4092.631	30	24427.27	$17752^{\circ}_{9/2} - 42179^{\circ}_{9/2}$	$\Delta J=0$	1.12	0.35	
4092.425	50	24428.49	$19753^{\circ}_{7/2} - 44182^{\circ}_{9/2}$	SI	1.25	0.06	
4092.372	5	24428.81					
4091.771	80	24432.40	$19748^{\circ}_{9/2} - 44180^{\circ}_{11/2}$	S0	0.57	0.54	
4091.355	30	24434.88	$18853_{11/2} - 43288^{\circ}_{13/2}$	SI	1.32	0.14	
4090.672	5	24438.96	$18990_{11/2} - 43429^{\circ}_{9/2}$				
4089.342	6 *h*	24446.91	$16742^{\circ}_{7/2} - 41189^{\circ}_{7/2}$				
4089.187	30	24447.84	$18990_{11/2} - 43438^{\circ}_{13/2}$	T	1.20	0.04	
4088.927	4	24449.39	$23309_{11/2} - 47759^{\circ}_{13/2}$				

487-412 OL - 73 - 3

Wavelength in air Å	Intensity	Wavenumber cm^{-1}	Classification	Zeeman effect type	f	Je	
4088.052	5 *h*	24454.63					
4087.952	3 *h*	24455.22					
4087.576	6	24457.47	$18990_{11/2} - 43447^{\circ}_{11/2}$				
4086.751	5	24462.41	$17454_{13/2} - 41917^{\circ}_{13/2}$				
4086.102	3	24466.30					
4085.742	20	24468.45	$16957_{7/2} - 41425^{\circ}_{7/2}$	ΔJ=0	1.13	0.25	
4085.536	10 *h*	24469.69	$16742_{7/2} - 41211^{\circ}_{7/2}$				
4085.364	10	24470.72					
4084.837	4	24473.87					
4084.194	100	24477.73		S0	1.10	0.16	
4083.472	1	24482.05					
4083.091	10	24484.34	$20406^{\circ}_{9/2} - 44891_{7/2}$				
4082.028	30	24490.71		ΔJ=0	1.10	0.66	
4081.395	40 *h*	24494.51					
4080.780	100	24498.20	$17343_{7/2} - 41841^{\circ}_{7/2}$	ΔJ=0	1.08	0.67	
4079.999	40 *h*	24502.89					
4079.827	10	24503.93					
4079.578	6	24505.42	$17613_{9/2} - 42119^{\circ}_{11/2}$				
4079.152	7 *h*	24507.98	$19466_{13/2} - 43974^{\circ}_{11/2}$				
4078.793	20	24510.14	$19753_{7/2} - 44263^{\circ}_{7/2}$	ΔJ=0	?	0.96	
4078.612	3	24511.22					
4078.377	2	24512.64	$19466_{13/2} - 43979^{\circ}_{13/2}$				
4078.094	2	24514.34					
4077.916	6	24515.41	$19748_{9/2} - 44263^{\circ}_{7/2}$				
4077.221	100	24519.59	$17613_{9/2} - 42133^{\circ}_{7/2}$	SI	1.25	0.07	
4076.169	5	24525.91	$15587_{11/2} - 40113^{\circ}_{13/2}$				
4075.510	7 *h*	24529.88					
4074.111	50	24538.30	$13119_{9/2} - 37657^{\circ}_{11/2}$	S00	1.305	1.00	*
4073.000	3 *h*	24545.00					
4072.765	40	24546.41	$19753_{7/2} - 44300^{\circ}_{9/2}$				
4071.641	4	24553.19					
4071.480	6	24554.16	$18990_{11/2} - 43544^{\circ}_{9/2}$				
4070.856	6 *h*	24557.92					
4070.037	2	24562.87	$19753_{7/2} - 44316^{\circ}_{9/2}$				
4069.466	2	24566.31					
4069.160	3	24568.16	$19748_{9/2} - 44316^{\circ}_{9/2}$				
"			$16957_{7/2} - 41525^{\circ}_{7/2}$				
4068.596	40	24571.56	$18837_{9/2} - 43408^{\circ}_{11/2}$				
4066.605	6 *h*	24583.59	$16742_{7/2} - 41325^{\circ}_{9/2}$				
4066.471	20	24584.40	$18853_{11/2} - 43438^{\circ}_{13/2}$				
4065.318	4	24591.38	$18837_{9/2} - 43428^{\circ}_{7/2}$				
4064.957	4	24593.56	$19548_{9/2} - 44142^{\circ}_{7/2}$				
4064.611	40	24595.65	$18693_{13/2} - 43288^{\circ}_{13/2}$				
4064.331	4 *h*	24597.35					
4062.723	10	24607.08					
4062.157	10	24610.51	$18837_{9/2} - 43447^{\circ}_{11/2}$				
4062.011	200	24611.40	$20406^{\circ}_{9/2} - 45018_{7/2}$				
4061.417	40	24615.00	$17752_{9/2} - 42367^{\circ}_{9/2}$				
4060.909	50	24618.08	$17752_{9/2} - 42370^{\circ}_{7/2}$				
4060.737	30	24619.12	$16957_{7/2} - 41576^{\circ}_{9/2}$				
4060.478	30	24620.69	$15587_{11/2} - 40208^{\circ}_{9/2}$				
4059.256	3	24628.10					
4058.185	7	24634.60					
4057.167	4	24640.78					
4055.809	400 *r*	24649.03	$13119_{9/2} - 37768^{\circ}_{9/2}$	ΔJ=0	1.27	0.40	
4054.655	3	24656.05					
4053.881	3	24660.75					
4053.532	2	24662.88					
4053.306	10	24664.25	$17454_{13/2} - 42119^{\circ}_{11/2}$				
4053.258	6	24664.54	$19753_{7/2} - 44418^{\circ}_{7/2}$				
4052.386	6	24669.85	$19748_{9/2} - 44418^{\circ}_{7/2}$				
4050.190	40	24683.23	$16742_{7/2} - 41425^{\circ}_{7/2}$				
4049.946	2	24684.71					
4048.957	20	24690.74	$18853_{11/2} - 43544^{\circ}_{9/2}$				
4048.129	40 *h*	24695.79					
4047.050	2	24702.38	$19753_{7/2} - 44456^{\circ}_{7/2}$				
4046.184	20	24707.66	$19748_{9/2} - 44456^{\circ}_{7/2}$				
4045.976	4	24708.94					
4045.103	6	24714.27	$19466_{13/2} - 44180^{\circ}_{11/2}$				
4044.963	40	24715.12	$19548_{9/2} - 44263^{\circ}_{7/2}$				
4044.474	800 *r*	24718.11	$8771^{\circ}_{9/2} - 33489_{9/2}$	S0	0.856	1.468	*
4043.380	40 *h*	24724.80	$20406^{\circ}_{9/2} - 45131_{7/2}$				
4042.090	300 *h*	24732.69					
4041.762	30	24734.70	$15587_{11/2} - 40322^{\circ}_{9/2}$				
4040.481	2	24742.54					
4040.440	3	24742.79	$20406^{\circ}_{9/2} - 45149_{7/2}$				
4040.285	20	24743.74	$19466_{13/2} - 44210^{\circ}_{15/2}$				
4040.050	30	24745.18	$18693_{13/2} - 43438^{\circ}_{13/2}$				
4039.969	80	24745.67					
4039.136	2	24750.78	$18837_{9/2} - 43588^{\circ}_{7/2}$				
4038.887	2	24752.30					
4038.115	5	24757.04	$17613_{9/2} - 42370^{\circ}_{7/2}$				
4034.360	30	24780.08					
4033.894	20	24782.94	$16742_{7/2} - 41525^{\circ}_{7/2}$				
4033.186	4	24787.29					
4033.006	10	24788.40	$15587_{11/2} - 40376^{\circ}_{13/2}$				
4032.765	10	24789.88	$17343^{\circ}_{7/2} - 42133^{\circ}_{7/2}$				
4030.200	6	24805.65	$23309_{11/2} - 48115^{\circ}_{13/2}$				
4030.034	6	24806.68					
4029.430	20 *h*	24810.39					
4027.640	30 *h*	24821.42	$18853_{11/2} - 43675^{\circ}_{9/2}$				
4027.543	2	24822.02					
4026.594	20 *h*	24827.87					
4026.370	80	24829.25	$16957_{7/2} - 41786^{\circ}_{9/2}$	SI	1.48	0.24	
4025.891	3	24832.20					
4025.615	200	24833.91	$16742_{7/2} - 41576^{\circ}_{9/2}$	S0	0.99	0.25	
4025.193	60	24836.51	$17343^{\circ}_{7/2} - 42179^{\circ}_{9/2}$	T	1.00		
4024.972	6	24837.87	$18837_{9/2} - 43675^{\circ}_{9/2}$				
4024.732	5	24839.36					
4024.545	10	24840.51	$19466_{13/2} - 44307^{\circ}_{13/2}$				
4024.230	500 *r*	24842.45	$16456_{17/2} - 41299^{\circ}_{17/2}$	ΔJ=0	1.10	0.83	
4023.154	2	24849.10					
4022.595	50	24852.55	$8771^{\circ}_{9/2} - 33623_{7/2}$	SI	1.11	0.16	
4020.324	4 *h*	24866.59					
4019.880	100 *h*	24869.34					
4019.575	40 *h*	24871.22					
4019.132	5	24873.96					
4017.417	3	24884.58	$16957_{7/2} - 41841^{\circ}_{7/2}$				
4014.305	50 *h*	24903.87	$16742_{7/2} - 41646^{\circ}_{7/2}$				
4013.736	8	24907.40	$19548_{9/2} - 44456^{\circ}_{7/2}$				
4012.193	4	24916.98	$19466_{13/2} - 44383^{\circ}_{11/2}$				
4011.798	20	24919.44					
4011.518	10	24921.17	$18693_{13/2} - 43614^{\circ}_{13/2}$				
4010.943	20	24924.75	$16957_{7/2} - 41881^{\circ}_{9/2}$				
4010.468	20	24927.70	$17613_{9/2} - 42541^{\circ}_{11/2}$				
4010.124	30	24929.84	$15587_{11/2} - 40517^{\circ}_{9/2}$				
4009.906	6 *h*	24931.19					
4009.369	200	24934.53	$19548_{9/2} - 44483^{\circ}_{9/2}$	T	0.97	0.03	
4008.737	3	24938.46					
4008.213	4	24941.72					
4006.588	20	24951.84	$17454_{13/2} - 42406^{\circ}_{13/2}$				
4006.362	60	24953.25	$17752_{9/2} - 42705^{\circ}_{9/2}$	ΔJ=0	1.14	0.23	
4005.096	2	24961.13					
4004.713	4 *h*	24963.52					
4003.943	20	24968.32	$17613_{9/2} - 42581^{\circ}_{11/2}$				
4002.989	1	24974.27					
4002.551	2	24977.01					
4002.008	40	24980.39	$17613_{9/2} - 42594^{\circ}_{9/2}$				
4001.656	4	24982.59	$17752_{9/2} - 42735^{\circ}_{9/2}$				
4001.395	20 *h*	24984.22	$18990_{11/2} - 43974^{\circ}_{11/2}$				
4000.642	7	24988.92	$18990_{11/2} - 43979^{\circ}_{13/2}$				
4000.570	40	24989.37	$17752_{9/2} - 42742^{\circ}_{7/2}$	T	1.22		
3999.143	5	24998.29					
3999.120	3	24998.43	$19748_{9/2} - 44747^{\circ}_{11/2}$				
3998.351	4	25003.24					
3998.241	40	25003.93					
3997.816	50	25006.59					
3996.415	10	25015.35					
3995.730	6 *h*	25019.64					
3994.999	7	25024.22	$17343_{7/2} - 42367^{\circ}_{9/2}$				

APPENDIX—*Spectral Lines of Neutral Thulium*—Continued

Wavelength in air Å	Intensity	Wavenumber cm⁻¹	Classification	Zeeman effect type	f	Je	
3994.503	20	25027.33	$17343_{7/2} - 42370^{\circ}_{7/2}$				
3993.352	3	25034.54					
3991.840	20 *h*	25044.02	$16742_{7/2} - 41786^{\circ}_{9/2}$				
3990.875	50	25050.08	$19132_{3/2} - 44182^{\circ}_{9/2}$				
3989.289	2	25060.04					
3987.865	3	25068.98					
3987.605	7 *h*	25070.62					
3986.861	4	25075.30	$15587_{11/2} - 40663^{\circ}_{13/2}$				
3985.764	6	25082.20	$18990_{13/2} - 44072^{\circ}_{13/2}$				
3985.074	10	25086.54	$17454_{13/2} - 42541^{\circ}_{11/2}$				
3984.747	3	25088.60					
3984.207	15	25092.00	$13119_{9/2} - 38211^{\circ}_{7/2}$				
3983.676	2 *h*	25095.35					
3983.040	10	25099.35	$16742_{7/2} - 41841^{\circ}_{7/2}$				
3982.716	15	25101.39	$19753_{7/2} - 44855^{\circ}_{9/2}$				
3982.321	3	25103.88					
3980.918	3	25112.73	$21737_{9/2} - 46850^{\circ}_{11/2}$				
3980.661	40	25114.35	$19753_{7/2} - 44868^{\circ}_{9/2}$				
3979.825	30	25119.63	$19748_{9/2} - 44868^{\circ}_{9/2}$				
3979.637	20 *h*	25120.81	$18853_{11/2} - 43974^{\circ}_{11/2}$				
3979.062	3	25124.44	$19466_{13/2} - 44591^{\circ}_{13/2}$				
3978.897	10	25125.49	$18853_{11/2} - 43979^{\circ}_{13/2}$				
3978.635	40	25127.14	$17454_{13/2} - 42581^{\circ}_{11/2}$				
3978.447	3	25128.33	$17613_{9/2} - 42742^{\circ}_{7/2}$				
3977.032	100 *h*	25137.27	$18837_{9/2} - 43974^{\circ}_{11/2}$				
3976.679	100	25139.50	$16742_{7/2} - 41881^{\circ}_{9/2}$	S0	0.63	0.50	
3975.425	6	25147.43	$18853_{11/2} - 44001^{\circ}_{9/2}$				
3975.040	3 *h*	25149.87	$17752_{9/2} - 42902^{\circ}_{9/2}$				
3973.894	10	25157.12	$17613_{9/2} - 42770^{\circ}_{9/2}$				
3973.200	2	25161.51					
3972.828	2	25163.87	$18837_{9/2} - 44001^{\circ}_{9/2}$				
3972.174	3	25168.01	$19132_{3/2} - 44300^{\circ}_{9/2}$				
3971.232	20 *h*	25173.98					
3970.878	20	25176.23	$16957_{7/2} - 42133^{\circ}_{7/2}$				
3970.138	7	25180.92					
3970.090	4	25181.22					
3968.621	50	25190.54	$18990_{13/2} - 44180^{\circ}_{11/2}$	ΔJ=0	1.18	0.25	
3968.222	20	25193.08	$15587_{11/2} - 40780^{\circ}_{13/2}$				
3964.804	15	25214.79					
3964.484	10	25216.83	$21997_{13/2} - 47214^{\circ}_{13/2}$				
3964.172	20	25218.81	$18853_{11/2} - 44072^{\circ}_{13/2}$				
3963.532	50	25222.89	$16957_{7/2} - 42179^{\circ}_{9/2}$	SI	1.42	0.30	
3963.068	10	25225.84	$17613_{9/2} - 42839^{\circ}_{9/2}$				
3962.686	60	25228.27	$13119_{9/2} - 38347^{\circ}_{11/2}$				
3960.192	2	25244.16					
3959.427	30 *h*	25249.04					
3959.168	20	25250.69	$17343_{7/2} - 42594^{\circ}_{9/2}$				
3956.878	60	25265.30	$13119_{9/2} - 38384^{\circ}_{9/2}$				
3956.492	20	25267.77	$15587_{11/2} - 40855^{\circ}_{9/2}$				
3954.520	7	25280.37	$19466_{13/2} - 44747^{\circ}_{11/2}$				
3953.600	2	25286.25	$18693_{15/2} - 43979^{\circ}_{13/2}$				
3952.760	4 *h*	25291.62					
3951.466	4	25299.90	$17752_{9/2} - 43052^{\circ}_{7/2}$				
3949.920	5	25309.81	$19748_{9/2} - 45058^{\circ}_{11/2}$				
3949.270	3000 *r*	25313.97	$8771^{\circ}_{9/2} - 34085_{9/2}$	ΔJ=0	0.90	0.24	
3948.833	20	25316.77	$19753_{7/2} - 45070^{\circ}_{9/2}$				
"			$18990_{11/2} - 44307^{\circ}_{13/2}$				
3948.023	4	25321.97					
3947.336	3	25326.37	$18990_{11/2} - 44316^{\circ}_{9/2}$				
3947.222	60	25327.10	$18853_{11/2} - 44180^{\circ}_{11/2}$	T	1.15		
3946.589	6	25331.17					
3945.650	5	25337.20	$19466_{13/2} - 44803^{\circ}_{13/2}$				
3945.321	3	25339.31					
3944.660	40	25343.55	$18837_{9/2} - 44180^{\circ}_{11/2}$	SI	1.32	0.18	
3943.935	80	25348.21	$17613_{9/2} - 42961^{\circ}_{11/2}$	T	1.24		
3943.490	80	25351.07	$19132_{3/2} - 44483^{\circ}_{9/2}$				
3941.946	15	25361.00	$17752_{9/2} - 43113^{\circ}_{9/2}$				
3941.710	40	25362.52	$17343_{7/2} - 42705^{\circ}_{9/2}$	S0	0.83	0.18	
3941.640	30	25362.97	$13119_{9/2} - 38482^{\circ}_{7/2}$				
3939.993	3	25373.57					
3939.089	80	25379.40	$13119_{9/2} - 38499^{\circ}_{9/2}$				
3937.282	100	25391.04	$16742_{7/2} - 42133^{\circ}_{7/2}$	ΔJ=0	1.22	0.54	
3937.159	2	25391.84	$17343_{7/2} - 42735^{\circ}_{9/2}$				
3936.939	4	25393.26	$18990_{13/2} - 44383^{\circ}_{11/2}$				
3936.100	30	25398.67	$17343_{7/2} - 42742^{\circ}_{7/2}$				
3935.799	80	25400.61	$17454_{13/2} - 42855^{\circ}_{13/2}$	T	1.125		
3934.332	10	25410.08	$13119_{9/2} - 38529^{\circ}_{11/2}$				
3934.252	6	25410.60	$16957_{7/2} - 42367^{\circ}_{9/2}$				
3934.112	2	25411.50					
3933.767	20	25413.73	$16957_{7/2} - 42370^{\circ}_{7/2}$				
3932.910	3	25419.27					
3932.718	20	25420.51	$17613_{9/2} - 43034^{\circ}_{7/2}$				
3932.300	4	25423.21	$16456_{17/2} - 41880^{\circ}_{15/2}$				
3931.775	2	25426.61	$18837_{9/2} - 44263^{\circ}_{7/2}$				
3931.649	20	25427.42	$17343_{7/2} - 42770^{\circ}_{9/2}$				
3931.514	15	25428.29	$18990_{13/2} - 44418^{\circ}_{13/2}$				
3930.717	10	25433.45	$25130_{15/2} - 50563^{\circ}_{13/2}$				
3930.066	20	25437.66	$16742_{7/2} - 42179^{\circ}_{9/2}$				
3927.639	2	25453.38	$18853_{11/2} - 44307^{\circ}_{13/2}$				
3927.355	20	25455.22	$17454_{13/2} - 42910^{\circ}_{13/2}$				
3926.742	5	25459.20					
3925.096	3	25469.87					
3923.638	8	25479.34	$18837_{9/2} - 44316^{\circ}_{9/2}$				
3922.405	1 *h*	25487.35	$21997_{13/2} - 47484^{\circ}_{11/2}$				
3921.885	5 *h*	25490.72	$15587_{11/2} - 41078^{\circ}_{9/2}$				
3921.446	60	25493.58	$15587_{11/2} - 41081^{\circ}_{11/2}$	ΔJ=0	1.28	0.20	
3921.056	2	25496.11	$17343_{7/2} - 42839^{\circ}_{9/2}$				
3919.372	40	25507.07	$17454_{13/2} - 42961^{\circ}_{11/2}$				
3919.023	2	25509.34					
3918.934	10	25509.92	$15271_{15/2} - 40780^{\circ}_{13/2}$				
3918.376	3	25513.55					
3917.144	40	25521.58	$15587_{11/2} - 41109^{\circ}_{9/2}$				
3916.477	5000 *r*	25525.92	$8771^{\circ}_{9/2} - 34297^{\circ}_{7/2}$	T	0.94		
3914.850	6	25536.53	$15587_{11/2} - 41124^{\circ}_{9/2}$				
3914.452	8 *h*	25539.13					
3913.619	40	25544.56	$13119_{9/2} - 38664^{\circ}_{7/2}$				
3913.528	3	25545.16					
3913.360	30	25546.25	$18837_{9/2} - 44383^{\circ}_{11/2}$				
3911.384	10	25559.16	$17343_{7/2} - 42902^{\circ}_{9/2}$				
3910.504	40	25564.91	$18853_{13/2} - 44418^{\circ}_{13/2}$				
3910.346	10	25565.94	$13119_{9/2} - 38685^{\circ}_{9/2}$				
3910.200	3	25566.90					
3909.315	10	25572.69	$17613_{9/2} - 43186^{\circ}_{11/2}$				
3906.478	2	25591.26					
3905.032	2	25600.73	$18990_{13/2} - 44591^{\circ}_{13/2}$				
3904.452	3	25604.54	$16957_{7/2} - 42561^{\circ}_{9/2}$				
3903.098	2	25613.42					
3902.944	4	25614.43					
3902.268	20	25618.87	$18837_{9/2} - 44456^{\circ}_{7/2}$				
3901.276	4	25625.38	$16742_{7/2} - 42367^{\circ}_{9/2}$				
3899.496	20	25637.08	$16957_{7/2} - 42594^{\circ}_{9/2}$				
3896.617	1000 *r*	25656.02	$0^{\circ}_{7/2} - 25656_{9/2}$	SI	1.14	0.72	*
3895.993	40	25660.13	$19748_{9/2} - 45408^{\circ}_{7/2}$				
3895.418	4	25663.91					
3893.525	7	25676.39					
3893.257	10	25678.16	$17752_{9/2} - 43430^{\circ}_{9/2}$				
3892.673	6	25682.01					
3891.900	5	25687.11	$15587_{11/2} - 41274^{\circ}_{13/2}$				
3889.880	5 *h*	25700.45					
3888.558	30	25709.19	$17343_{7/2} - 43052^{\circ}_{7/2}$	ΔJ=0	1.04	0.13	
3887.842	3	25713.92	$19753_{7/2} - 45467^{\circ}_{9/2}$				
3887.348	5000 *a*	25717.19	$0^{\circ}_{7/2} - 25717_{7/2}$	ΔJ=0	1.14	1.01	*
3886.472	2	25722.99	$19132_{3/2} - 44855^{\circ}_{9/2}$				
3886.068	20	25725.66	$18693_{15/2} - 44418^{\circ}_{13/2}$				
3885.885	4 *h*	25726.87					
3885.726	2 *h*	25727.93					
3885.133	5 *h*	25731.85					
3884.306	3	25737.33	$18853_{11/2} - 44591^{\circ}_{13/2}$				
3883.132	10000 *a*	25745.11	$0^{\circ}_{7/2} - 25745_{9/2}$	SI	1.25	0.13	
3882.559	4	25748.91	$16957_{7/2} - 42705^{\circ}_{9/2}$				

Wavelength in air Å	Intensity	Wavenumber cm^{-1}	Classification	Zeeman effect type	f	Je
3881.397	20	25756.62	$18990_{11/2} - 44747^{\circ}_{11/2}$			
3881.249	50	25757.60	$13119_{9/2} - 38877^{\circ}_{11/2}$	ΔJ=1	?	1.08
3880.599	30	25761.92	$21997^{\circ}_{11/2} - 47759^{\circ}_{13/2}$	T	1.20	
3879.340	80	25770.28	$17343^{\circ}_{7/2} - 43113^{\circ}_{9/2}$	S0	0.80	0.22
3879.051	7	25772.20				
3878.143	5	25778.23	$16957^{\circ}_{7/2} - 42735^{\circ}_{9/2}$			
3877.300	2	25783.84	$18990_{11/2} - 44774^{\circ}_{9/2}$			
3877.126	10	25784.99	$16957^{\circ}_{7/2} - 42742^{\circ}_{7/2}$			
3876.864	2 *h*	25786.74				
3876.416	5	25789.72				
3874.248	2	25804.15				
3873.824	4	25806.97				
3873.446	30	25809.49				
3873.400	2	25809.80	$25488_{11/2} - 51298^{\circ}_{13/2}$			
3872.846	40	25813.49	$18990_{11/2} - 44803^{\circ}_{13/2}$			
3872.804	60	25813.77	$16957^{\circ}_{7/2} - 42770^{\circ}_{9/2}$			
3872.512	200	25815.71	$17613_{9/2} - 43429^{\circ}_{9/2}$	T	1.18	
3871.973	60	25819.31	$16742^{\circ}_{7/2} - 42561^{\circ}_{9/2}$			
3871.846	30	25820.15		T	1.06	
3871.530	4	25822.26	$19466_{13/2} - 45288^{\circ}_{11/2}$			
3870.912	5 *h*	25826.38				
3869.786	50	25833.90	$17454_{13/2} - 43288^{\circ}_{13/2}$			
3869.744	10	25834.18	$17613_{9/2} - 43447^{\circ}_{11/2}$			
3869.540	4	25835.54	$17752_{9/2} - 43588^{\circ}_{7/2}$			
3867.107	8	25851.80	$16742_{7/2} - 42594^{\circ}_{9/2}$			
3865.909	5	25859.81	$19548_{9/2} - 45408^{\circ}_{7/2}$			
3863.972	70	25872.77	$18693_{15/2} - 44565^{\circ}_{15/2}$	ΔJ=0	1.15	0.35
3863.524	3	25875.77				
3863.230	1	25877.74	$18990_{11/2} - 44868^{\circ}_{9/2}$			
3863.081	30	25878.74	$18693_{15/2} - 44571^{\circ}_{17/2}$	T	1.18	
3862.522	20	25882.48	$16957^{\circ}_{7/2} - 42839^{\circ}_{9/2}$			
3861.820	20	25887.19	$19748_{9/2} - 45635^{\circ}_{11/2}$			
3860.925	5	25893.19	$18853_{11/2} - 44747^{\circ}_{11/2}$			
3860.201	2	25898.04	$18693_{15/2} - 44591^{\circ}_{13/2}$			
3858.480	100	25909.59	$18837_{9/2} - 44747^{\circ}_{11/2}$	SI	1.40	0.20
3856.868	15	25920.42	$18853_{11/2} - 44774^{\circ}_{9/2}$			
3855.305	6	25930.93	$17613_{9/2} - 43544^{\circ}_{9/2}$			
3854.522	10 *h*	25936.20				
3854.426	20	25936.85	$18837_{9/2} - 44774^{\circ}_{9/2}$			
3853.145	50	25945.47	$16957^{\circ}_{7/2} - 42902^{\circ}_{9/2}$			
3852.470	30	25950.01	$18853_{11/2} - 44803^{\circ}_{13/2}$			
3850.447	6	25963.65	$16742^{\circ}_{7/2} - 42705^{\circ}_{9/2}$			
3849.518	6	25969.91	$13119_{9/2} - 39089^{\circ}_{11/2}$			
3848.835	5	25974.52	$17613_{9/2} - 43588^{\circ}_{7/2}$			
3848.295	5	25978.17	$25488_{11/2} - 51466^{\circ}_{13/2}$			
3847.836	20	25981.27	$15587_{11/2} - 41569^{\circ}_{11/2}$			
3847.514	100 *r*	25983.44	$17454_{13/2} - 43438^{\circ}_{11/2}$	ΔJ=0	1.22	0.53
3846.091	30	25993.05	$17454_{13/2} - 43447^{\circ}_{11/2}$			
3845.100	5	25999.75	$16742^{\circ}_{7/2} - 42742^{\circ}_{7/2}$			
3842.946	150 *h*	26014.32	$18853_{11/2} - 44868^{\circ}_{9/2}$			
3840.869	500 *r*	26028.39	$15271_{15/2} - 41299^{\circ}_{17/2}$	T	1.09	
3840.518	2	26030.77	$18837_{9/2} - 44868^{\circ}_{9/2}$			
3837.438	2 *h*	26051.66				
3835.926	10	26061.93	$19748_{9/2} - 45810^{\circ}_{11/2}$			
3835.051	20	26067.88	$13119_{9/2} - 39187^{\circ}_{7/2}$			
3834.484	2	26071.73				
3834.262	7	26073.24	$16957^{\circ}_{7/2} - 43030^{\circ}_{9/2}$			
3833.695	10	26077.10	$16957^{\circ}_{7/2} - 43034^{\circ}_{7/2}$			
3833.254	10	26080.10				
3832.386	30	26086.00	$17343^{\circ}_{7/2} - 43429^{\circ}_{9/2}$	SI	1.80	0.62
3832.183	80	26087.39	$17343^{\circ}_{7/2} - 43430^{\circ}_{9/2}$	S0	0.80	0.18
3831.643	4	26091.06	$19466_{13/2} - 45557^{\circ}_{13/2}$			
3830.736	3	26097.24	$16742^{\circ}_{7/2} - 42839^{\circ}_{9/2}$			
3830.394	30	26099.57	$15587_{11/2} - 41687^{\circ}_{11/2}$			
3830.267	30	26100.44	$13119_{9/2} - 39220^{\circ}_{9/2}$			
3829.065	30 *h*	26108.63		T	1.10	
3827.965	8 *h*	26116.13				
3827.666	4	26118.17	$21997_{11/2} - 48115^{\circ}_{13/2}$			
3826.667	30	26124.99	$13119_{9/2} - 39244^{\circ}_{9/2}$			
3826.386	400 *a*	26126.91	$0^{\circ}_{7/2} - 26126_{9/2}$	SI	1.22	0.09
3824.430	100 *h*	26140.27		T	1.17	
3824.326	2	26140.98				
3822.030	5	26156.68	$16957^{\circ}_{7/2} - 43113^{\circ}_{9/2}$			
3822.003	4	26156.87	$18990_{11/2} - 45147^{\circ}_{9/2}$			
3821.623	100 *r*	26159.47	$17454_{13/2} - 43614^{\circ}_{15/2}$	S0	0.98	0.16
3821.511	5	26160.24	$16742_{7/2} - 42902^{\circ}_{9/2}$			
3821.215	2	26162.26				
3819.906	10 *h*	26171.23				
3816.591	3	26193.96	$19466_{13/2} - 45660^{\circ}_{13/2}$			
3815.037	60 *h*	26204.63				
3813.276	10	26216.73	$18853_{11/2} - 45070^{\circ}_{9/2}$			
3810.888	10	26233.16	$18837_{9/2} - 45070^{\circ}_{9/2}$			
3810.055	30 *h*	26238.89				
3809.402	20	26243.39				
3808.948	60	26246.52		T	1.14	
3808.300	5	26250.98				
3807.719	700 *r*	26254.99	$8771^{\circ}_{9/2} - 35026_{9/2}$	ΔJ=0	0.85	1.02 *
3803.144	30	26286.57	$15587_{11/2} - 41874^{\circ}_{11/2}$	ΔJ=0	1.21	0.46
3802.074	150 *r*	26293.97	$15587_{11/2} - 41881^{\circ}_{9/2}$	SI	1.58	0.32
3799.874	3	26309.19				
3799.774	5	26309.89	$18837_{9/2} - 45147^{\circ}_{9/2}$			
3799.710	30	26310.33	$16742^{\circ}_{7/2} - 43052^{\circ}_{7/2}$			
3798.541	800 *r*	26318.43	$8771^{\circ}_{9/2} - 35089_{7/2}$	T	0.85	
3797.636	40	26324.70	$13119_{9/2} - 39444^{\circ}_{9/2}$	ΔJ=0	1.20	0.83
3796.596	10	26331.91	$17343^{\circ}_{7/2} - 43675^{\circ}_{9/2}$			
3795.965	3	26336.28	$25130_{15/2} - 51466^{\circ}_{13/2}$			
3794.872	3	26343.87	$19466_{13/2} - 45810^{\circ}_{11/2}$			
3793.269	10	26355.00				
3792.404	10 *h*	26361.01	$17613_{9/2} - 43974^{\circ}_{11/2}$			
3791.307	80	26368.64	$13119_{9/2} - 39488^{\circ}_{9/}$	ΔJ=0	1.20	0.86
3790.905	20	26371.44	$16742^{\circ}_{7/2} - 43113^{\circ}_{9/2}$			
3788.759	5 *h*	26386.37				
3788.582	5	26387.61	$17613_{9/2} - 44001^{\circ}_{9/2}$			
3788.273	2	26389.76	$17752_{9/2} - 44142^{\circ}_{7/2}$			
3787.605	10 *h*	26394.41				
3787.014	120 *r*	26398.53	$16456_{17/2} - 42855^{\circ}_{15/2}$	SI	1.56	0.38
3784.645	2 *h*	26415.06	$19748_{9/2} - 46163^{\circ}_{11/2}$			
3784.327	4 *h*	26417.28				
3783.855	2	26420.57				
3782.550	30	26429.69	$17752_{9/2} - 44182^{\circ}_{9/2}$	T	1.20	
3781.148	200 *a*	26439.48	$0^{\circ}_{7/2} - 26439_{7/2}$	ΔJ=0	1.07	0.50
3780.977	20	26440.68				
3780.588	20	26443.40	$13119_{9/2} - 39563^{\circ}_{11/2}$			
3780.214	5	26446.02				
3779.414	60 *h*	26451.62	$18837_{9/2} - 45289^{\circ}_{13/2}$	T	1.13	
3777.096	5	26467.85	$19466_{13/2} - 45934^{\circ}_{15/2}$			
3776.537	30	26471.77	$16957^{\circ}_{7/2} - 43428^{\circ}_{7/2}$			
3776.452	6	26472.36	$16957^{\circ}_{7/2} - 43429^{\circ}_{9/2}$			
3773.864	20	26490.51	$8771^{\circ}_{9/2} - 35261_{9/2}$	ΔJ=0	0.855	1.346 *
3773.205	3	26495.14				
3772.102	5 *h*	26502.89				
3771.901	4 *h*	26504.30				
3769.693	100 *h*	26519.82	$17454_{13/2} - 43974^{\circ}_{11/2}$			
3769.032	6	26524.48	$17454_{13/2} - 43979^{\circ}_{13/2}$			
3768.065	40	26531.28	$15587_{11/2} - 42119^{\circ}_{13/2}$			
3766.713	7	26540.81				
3765.746	20	26547.62	$17752_{9/2} - 44300^{\circ}_{9/2}$			
3764.387	8	26557.20				
3762.954	10	26567.32	$17613_{9/2} - 44180^{\circ}_{11/2}$			
3762.352	150 *h*	26571.57				
3759.820	40	26589.46	$13119_{9/2} - 39709^{\circ}_{11/2}$	S0	0.57	0.58
3759.086	40	26594.65	$16456_{17/2} - 43051^{\circ}_{13/2}$	T	1.15	
3758.726	3	26597.20				
3757.570	3	26605.38				
3757.040	6	26609.14	$15271_{15/2} - 41801^{\circ}_{13/2}$			
3756.370	10	26613.88	$18853_{11/2} - 45467^{\circ}_{9/2}$			
3755.818	4	26617.79	$17454_{13/2} - 44072^{\circ}_{13/2}$			
3754.055	10	26630.29	$18837_{9/2} - 45467^{\circ}_{9/2}$			
3753.930	20	26631.18	$16957^{\circ}_{7/2} - 43588^{\circ}_{7/2}$			
3753.810	10	26632.03	$18853_{11/2} - 45485^{\circ}_{11/2}$			

Wavelength in air Å	Intensity	Wavenumber cm^{-1}	Classification	Zeeman effect type	f	Je	
3752.828	10 *h*	26639.00					
3752.168	20	26643.69					
3751.806	2000 *a*	26646.26	$0^{\circ}_{7/2} - 26646_{9/2}$	S0	1.143	0.961	*
3751.495	5	26648.47	$18837_{9/2} - 45485^{\circ}_{11/2}$				
3748.433	3	26670.23	$18990_{11/2} - 45660^{\circ}_{13/2}$				
3746.208	5	26686.07					
3746.139	3	26686.57	$16742_{7/2} - 43428^{\circ}_{7/2}$				
3746.057	20	26687.15	$16742_{7/2} - 43429^{\circ}_{9/2}$				
3745.865	6	26688.52	$16742_{7/2} - 43430^{\circ}_{9/2}$				
3744.954	8	26695.01					
3744.064	6000 *a*	26701.35	$0^{\circ}_{7/2} - 26701_{7/2}$	ΔJ=0	1.10	0.23	
3741.692	200	26718.28	$16957_{7/2} - 43675^{\circ}_{9/2}$	S0	0.58	0.45	
3740.597	5	26726.10	$17454_{13/2} - 44180^{\circ}_{11/2}$				
3739.953	15	26730.70	$17752_{9/2} - 44483^{\circ}_{9/2}$				
3739.772	100	26732.00		S0	0.70	0.30	
3739.472	5	26734.14					
3736.591	3	26754.75	$19466_{13/2} - 46221^{\circ}_{11/2}$				
3736.471	40	26755.61	$17454_{13/2} - 44210^{\circ}_{13/2}$	T	1.15		
3732.804	30	26781.90	$18853_{11/2} - 45635^{\circ}_{11/2}$	T	1.12		
3731.287	4	26792.79					
3731.048	3 *h*	26794.50					
3730.423	10	26798.99	$17343_{7/2} - 44142^{\circ}_{7/2}$				
3729.954	5	26802.36	$16742_{7/2} - 43544^{\circ}_{9/2}$				
3728.809	2 *h*	26810.59					
3727.487	20	26820.10	$18990_{11/2} - 45810^{\circ}_{11/2}$				
3724.875	4	26838.91	$17343_{7/2} - 44182^{\circ}_{9/2}$				
3724.370	4	26842.54	$17613_{9/2} - 44456^{\circ}_{7/2}$				
3723.897	20	26845.95	$16742_{7/2} - 43588^{\circ}_{7/2}$				
3723.005	5	26852.39	$17454_{13/2} - 44307^{\circ}_{13/2}$				
3722.400	70 *h*	26856.75					
3719.105	2	26880.54					
3717.914	10000 *a*	26889.15	$0^{\circ}_{7/2} - 26889_{9/2}$	S0	1.00	0.10	
3714.249	4	26915.69	$18693_{15/2} - 45608^{\circ}_{13/2}$				
3714.132	3	26916.53					
3713.573	10	26920.59	$17343_{7/2} - 44263^{\circ}_{7/2}$				
3712.860	6 *h*	26925.76					
3712.439	5	26928.81	$17454_{13/2} - 44383^{\circ}_{11/2}$				
3711.859	2 *h*	26933.02	$16742_{7/2} - 43675^{\circ}_{9/2}$				
3710.665	20	26941.68	$13119_{9/2} - 40061^{\circ}_{7/2}$				
3709.030	20	26953.56	$15587_{11/2} - 42541^{\circ}_{11/2}$				
3708.602	2	26956.67	$18853_{11/2} - 45810^{\circ}_{11/2}$				
3708.425	4 *h*	26957.96					
3707.099	30	26967.60	$18693_{15/2} - 45660_{13/2}$	T	1.145		
3706.329	4	26973.20					
3706.255	20	26973.74	$15587_{11/2} - 42561^{\circ}_{9/2}$				
3704.358	50 *h*	26987.55		T	1.41		
3703.419	9	26994.39	$19466_{13/2} - 46461^{\circ}_{15/2}$				
3701.795	40 *r*	27006.24	$15587_{11/2} - 42594^{\circ}_{9/2}$	SI	2.00	0.74	
3701.045	10 *h*	27011.71					
3696.593	5	27044.24	$16957_{7/2} - 44001^{\circ}_{9/2}$				
3696.455	4 *h*	27045.25					
3695.385	3	27053.08					
3692.390	3	27075.02	$17343_{7/2} - 44418^{\circ}_{7/2}$				
3691.580	5	27080.96					
3691.030	4 *h*	27085.00					
3690.504	10	27088.86	$13119_{9/2} - 40208^{\circ}_{9/2}$				
3689.350	20 *h*	27097.33					
3688.731	10 *h*	27101.88	$19748_{9/2} - 46850^{\circ}_{11/2}$				
3688.645	3	27102.51					
3687.488	20	27111.02	$17454_{13/2} - 44565^{\circ}_{13/2}$	T	1.14		
3687.248	10	27112.78					
3684.771	20	27131.01	$19466_{13/2} - 46597^{\circ}_{13/2}$	ΔJ=0	1.16	0.18	
3684.458	10	27133.31	$17613_{9/2} - 44747^{\circ}_{11/2}$				
3684.145	6	27135.61	$15271_{13/2} - 42406^{\circ}_{13/2}$				
3684.059	5	27136.25					
3683.475	10	27140.55					
3681.194	20	27157.37	$16456_{17/2} - 43614^{\circ}_{15/2}$	SI	1.48	0.40	
3679.113	3 *h*	27172.73					
3677.728	40 *r*	27182.96	$15587_{11/2} - 42770^{\circ}_{9/2}$	SI	1.44	0.18	
3677.004	4 *h*	27188.31					
3675.029	30	27202.92	$13119_{9/2} - 40322?_{7/2}$	ΔJ=0	1.25	0.86	
3673.989	3	27210.62					
3672.616	30 *h*	27220.80					
3671.724	10	27227.41	$19466_{13/2} - 46694^{\circ}_{13/2}$	T	1.14		
3670.776	8	27234.44					
3669.835	3	27241.42	$18693_{15/2} - 45934^{\circ}_{15/2}$				
3669.081	20 *h*	27247.02					
3668.452	30	27251.69	$15587_{11/2} - 42839^{\circ}_{9/2}$				
3665.754	5	27271.75					
3664.617	10 *h*	27280.21					
3663.005	90	27292.22	$17454_{13/2} - 44747^{\circ}_{11/2}$	S0	0.95	0.15	
3662.276	10	27297.65					
3661.200	2	27305.67					
3661.024	40	27306.98	$16957_{7/2} - 44263^{\circ}_{7/2}$				
3660.452	20	27311.25		T	1.36		
3658.983	20	27322.22	$15587_{11/2} - 22910^{\circ}_{13/2}$				
3658.008	3	27329.50	$24137_{13/2} - 51466^{\circ}_{13/2}$				
3656.196	5	27343.04					
3656.178	5	27343.18	$16957_{7/2} - 44300^{\circ}_{9/2}$				
3655.312	5	27349.65					
3654.560	20 *h*	27355.28					
3653.968	30	27359.71	$16957_{7/2} - 44316^{\circ}_{9/2}$				
3652.050	50 *r*	27374.08	$15587_{11/2} - 42961^{\circ}_{11/2}$	ΔJ=0	1.22	0.26	
3651.557	4	27377.78					
3650.740	50 *h*	27383.90					
3649.784	3	27391.08					
3648.853	50 *r*	27398.07	$13119_{9/2} - 40517^{\circ}_{9/2}$	ΔJ=0	1.25	0.68	
3648.572	5	27400.18	$16742_{7/2} - 44142^{\circ}_{7/2}$				
3648.485	10	27400.83					
3646.703	200 *r*	27414.22	$13119_{9/2} - 40533^{\circ}_{7/2}$	SI	1.52	0.21	
3643.472	20	27438.53					
3642.944	100 *r*	27442.51	$15587_{11/2} - 43030^{\circ}_{9/2}$	SI	1.98	0.71	
3641.034	10	27456.90	$17613_{9/2} - 45070^{\circ}_{9/2}$				
3640.437	3	27461.40	$16957_{7/2} - 44418^{\circ}_{7/2}$				
3639.570	6	27467.94					
3638.408	300 *r*	27476.72	$13119_{9/2} - 40596^{\circ}_{7/2}$	T	1.31		
3633.763	20	27511.84	$17343_{7/2} - 44855^{\circ}_{9/2}$				
3632.062	50	27524.72					
3631.210	4 *h*	2753 (18					
3630.895	4	27533.57					
3629.876	7	27541.30					
3627.598	10 *h*	27558.59					
3627.303	5	27560.83	$19466_{13/2} - 47027^{\circ}_{13/2}$				
3625.442	20 *h*	27574.98		T	1.02		
3624.198	200 *r*	27584.45	$15271_{13/2} - 42855^{\circ}_{13/2}$	ΔJ=0	1.10	0.33	
3622.355	10	27598.48	$15587_{11/2} - 43186^{\circ}_{11/2}$				
3620.497	100 *h*	27612.64					
3619.545	4	27619.91					
3617.040	10	27639.03	$15271_{13/2} - 42910^{\circ}_{13/2}$				
3616.398	2	27643.94					
3616.355	20	27644.27	$13119_{9/2} - 40763^{\circ}_{7/2}$	SI	1.72	0.41	
3615.650	4	27649.66					
3614.820	20	27656.01	$17752_{9/2} - 45408^{\circ}_{7/2}$				
3613.565	3	27665.61					
3613.200	3	27668.41					
3608.960	10	27700.91	$15587_{11/2} - 43288^{\circ}_{13/2}$				
3608.604	2	27703.65	$18990_{11/2} - 46694^{\circ}_{13/2}$				
3607.261	20	27713.96	$16742_{7/2} - 44456^{\circ}_{7/2}$				
3606.609	5 *h*	27718.97					
3604.401	10	27735.95	$13119_{9/2} - 40855^{\circ}_{9/2}$				
3603.872	10	27740.02		T	1.17		
3603.661	30 *h*	27741.64					
3602.123	60 *r*	27753.49	$16456_{17/2} - 44210^{\circ}_{15/2}$	SI	1.22	0.15	
3600.241	30	27768.00	$18693_{15/2} - 46461^{\circ}_{15/2}$	T	1.20		
3599.188	5	27776.12					
3598.616	200 *r*	27780.54	$15271_{13/2} - 43051^{\circ}_{13/2}$	ΔJ=0	1.15	0.84	
3596.487	20	27796.98		T	0.85		
3595.600	4	27803.84					
3594.404	30	27813.09		T	1.09		
3593.867	20	27817.24	$16957_{7/2} - 44774^{\circ}_{9/2}$				

Wavelength in air Å	Intensity	Wavenumber cm⁻¹	Classification	Zeeman effect type	f	Je
3593.487	2	27820.19				
3593.360	20	27821.17	$15587_{11/2}-43408^{\circ}_{11/2}$			
3593.067	3	27823.44				
3590.896	8	27840.26	$18853_{11/2}-46694^{\circ}_{13/2}$			
3590.728	200 *r*	27841.56	$15587_{11/2}-43429^{\circ}_{9/2}$	SI	1.52	0.25
3589.585	40	27850.43	$15587_{11/2}-43438^{\circ}_{13/2}$	S0	1.08	0.14
3589.113	7	27854.09				
3588.344	30	27860.06	$15587_{11/2}-43447^{\circ}_{11/2}$			
"			$18990_{11/2}-46850^{\circ}_{11/2}$			
3586.067	300 *r*	27877.75	$16456_{17/2}-44334^{\circ}_{19/2}$	T	1.21	
3584.137	10	27892.76	$13119_{9/2}-41012^{\circ}_{7/2}$			
3583.429	100 *r*	27898.27	$16957_{7/2}-44855^{\circ}_{9/2}$	SI	1.48	0.29
3582.614	20	27904.62	$18693_{15/2}-46597^{\circ}_{13/2}$	T	1.185	
3581.773	40	27911.17	$16957_{7/2}-44868^{\circ}_{9/2}$			
3580.967	20 *h*	27917.45				
3580.167	15	27923.69	$23374_{13/2}-51298^{\circ}_{13/2}$			
3578.692	2	27935.20				
3575.934	4	27956.74	$15587_{11/2}-43544^{\circ}_{9/2}$			
3575.662	30	27958.87	$13119_{9/2}-41078^{\circ}_{9/2}$	T	1.30	
3575.291	80 *r*	27961.77	$13119_{9/2}-41081^{\circ}_{11/2}$			
3574.824	20	27965.42	$13119_{9/2}-41085^{\circ}_{7/2}$			
3572.448	20 *h*	27984.02				
3571.723	8	27989.70	$13119_{9/2}-41109^{\circ}_{9/2}$			
3570.664	60	27998.00		T	1.13	
3569.940	9	28003.68				
3569.805	100 *r*	28004.74	$13119_{9/2}-41124^{\circ}_{9/2}$	ΔJ=0	1.28	0.27
3568.867	1	28012.10				
3568.722	4 *h*	28013.24				
3568.148	20 *r*	28017.74	$15271_{15/2}-43288^{\circ}_{13/2}$			
3567.592	20	28022.11	$17613_{9/2}-45635^{\circ}_{11/2}$			
3567.356	500 *a*	28024.96	$0^{\circ}_{7/2}-28023_{9/2}$	T	1.17	
3566.336	5	28031.98	$16742_{7/2}-44774^{\circ}_{9/2}$			
3565.819	10	28036.04				
3563.876	400 *a*	28051.33	$0^{\circ}_{7/2}-28051_{9/2}$	SI	1.145	0.96 *
3563.435	30	28054.80				
3562.219	7	28064.37				
3562.107	20	28065.26	$17343_{7/2}-45408^{\circ}_{7/2}$			
3561.571	6	28069.48				
3560.916	300 *r*	28074.64	$18693_{15/2}-46767^{\circ}_{17/2}$	T	1.15	
3559.292	6	28087.45	$15587_{11/2}-43675^{\circ}_{9/2}$			
3557.335	80 *r*	28102.90	$17454_{13/2}-45557^{\circ}_{13/2}$	SI	1.27	0.09
3556.573	80 *r*	28108.93	$16456_{17/2}-44565^{\circ}_{13/2}$	SI	1.47	0.30
3555.818	200 *r*	28114.89	$16456_{17/2}-44571^{\circ}_{17/2}$	T	1.175	
3551.677	60 *r*	28147.67		T	1.08	
3550.887	40	28153.93	$17454_{13/2}-45608^{\circ}_{13/2}$	T	1.15	
3549.634	60	28163.87	$19466_{13/2}-47630^{\circ}_{15/2}$	T	1.19	
3549.207	60 *r*	28167.26	$15271_{15/2}-43438^{\circ}_{13/2}$	S0	0.16	0.95
3548.833	2 *h*	28170.23				
3547.820	30	28178.27	$19466_{13/2}-47644^{\circ}_{13/2}$			
3547.489	60	28180.90	$17454_{13/2}-45635^{\circ}_{11/2}$	T	1.145	
3546.312	10	28190.25	$16957_{7/2}-45147^{\circ}_{9/2}$			
3545.478	7	28196.89	$17613_{9/2}-45810^{\circ}_{11/2}$			
3545.445	2	28197.15				
3544.347	40 *r*	28205.88	$17454_{13/2}-45660^{\circ}_{13/2}$	ΔJ=0	1.16	0.30
3543.254	4 *h*	28214.58				
3542.082	60 *r*	28223.92	$18990_{11/2}-47214^{\circ}_{13/2}$	S0	0.65	0.45
3541.777	5 *h*	28226.35				
3541.280	5 *h*	28230.31				
3541.160	30 *h*	28231.27				
3540.616	10	28235.60		T	1.215	
3537.910	300 *r*	28257.20		S0	0.95	0.20
3537.600	20 *h*	28259.68				
3533.470	9	28292.71	$19466_{13/2}-47759^{\circ}_{13/2}$			
3533.232	5	28294.61				
3531.660	10 *h*	28307.21				
3531.016	10	28312.37				
3529.033	20	28328.28				
3528.271	30 *h*	28334.39	$18693_{15/2}-47027^{\circ}_{13/2}$	T	1.25	
3527.890	40	28337.45		S0	0.70	0.23
3527.457	5	28340.93				
3527.169	50 *r*	28343.25	$15271_{15/2}-43614^{\circ}_{15/2}$	ΔJ=0	1.12	0.25
3525.619	200 *r*	28355.71	$17454_{13/2}-45810^{\circ}_{11/2}$	S0	0.70	0.40
3525.281	100 *h*	28358.43				
3525.026	100 *r*	28360.48	$18853_{11/2}-47214^{\circ}_{13/2}$	S0	0.98	0.15
3523.454	4	28373.13				
3522.650	4 *h*	28379.61				
3521.751	80	28386.85	$15587_{11/2}-43974^{\circ}_{11/2}$	ΔJ=0	1.20	0.63
3520.896	10	28393.74				
3520.290	30 *h*	28398.63				
3519.488	3	28405.10	$16742_{7/2}-45147^{\circ}_{9/2}$			
3519.428	60 *r*	28405.59	$13119_{9/2}-41525^{\circ}_{7/2}$	SI	2.00	0.70
3518.451	20	28413.47	$15587_{11/2}-44001^{\circ}_{9/2}$			
3517.720	100 *r*	28419.38	$19466_{13/2}-47886^{\circ}_{15/2}$	T	1.14	
3517.598	200 *a*	28420.36		SI	1.60	0.38
3517.106	3 *h*	28424.34				
3516.443	5 *h*	28429.70				
3514.857	50	28442.53		T	1.05	
3514.112	100 *a*	28448.56	$0^{\circ}_{7/2}-28448_{9/2}$	SI	1.50	0.36
3513.997	40 *r*	28449.49	$13119_{9/2}-41569^{\circ}_{11/2}$	S0	0.73	0.45
3513.729	100 *a*	28451.66	$16957_{7/2}-45408^{\circ}_{7/2}$	ΔJ=0	1.145	0.21
3513.255	4	28455.50				
3513.128	30	28456.52	$13119_{9/2}-41576^{\circ}_{9/2}$	ΔJ=0	1.25	0.25
3512.543	20	28461.26				
3512.100	10	28464.85				
3511.744	7 *h*	28467.74				
3510.580	20	28477.18				
3510.266	40	28479.72	$17454_{13/2}-45934^{\circ}_{13/2}$	T	1.16	
3508.456	100 *h*	28494.42	$18990_{11/2}-47484^{\circ}_{11/2}$			
3505.979	50 *r*	28514.55		T	1.31	
3505.370	40 *h*	28519.50				
3505.158	40 *r*	28521.23	$18693_{15/2}-47214^{\circ}_{13/2}$	SI	1.53	0.28
3504.510	20 *h*	28526.50	$13119_{9/2}-41646^{\circ}_{7/2}$			
3504.039	20	28530.33				
3503.356	200 *r*	28535.90		SI	1.28	0.10
3500.918	100 *a*	28555.77	$0^{\circ}_{7/2}-28555_{7/2}$	ΔJ=0	1.14	0.13
3499.948	300 *a*	28563.68		SI	1.53	0.33
3499.446	60 *a*	28567.78	$13119_{9/2}-41687^{\circ}_{11/2}$	S0	0.44	0.70
3497.520	10 *h*	28583.51				
3497.131	10	28586.69				
3496.348	40	28593.09	$15587_{11/2}-44180^{\circ}_{11/2}$			
3494.976	20	28604.32				
3492.519	10	28624.44				
3491.717	200	28631.01	$18853_{11/2}-47484^{\circ}_{11/2}$	ΔJ=0	1.11	0.20
3490.738	10	28639.04				
3489.525	1000 *a*	28649.00	$19466_{13/2}-48115^{\circ}_{13/2}$	ΔJ=0	1.165	0.12
3488.382	20 *h*	28658.38				
3487.530	30 *h*	28665.38				
3487.379	300 *a*	28666.63	$13119_{9/2}-41786^{\circ}_{9/2}$	ΔJ=0	1.28	0.25
3486.573	8	28673.25				
3482.890	60	28703.57		T	1.29	
3482.317	20	28708.30	$15271_{15/2}-43979^{\circ}_{13/2}$			
3482.264	10 *h*	28708.73	$17454_{13/2}-46163^{\circ}_{11/2}$			
3480.975	200 *r*	28719.36	$15587_{11/2}-44307^{\circ}_{13/2}$	S0	0.49	0.65
3480.664	20	28721.93	$13119_{9/2}-41841^{\circ}_{7/2}$			
3479.824	7	28728.86	$15587_{11/2}-44316^{\circ}_{9/2}$			
3479.294	6	28733.24				
3479.179	4 *h*	28734.19				
3476.692	200 *r*	28754.74	$13119_{9/2}-41874^{\circ}_{11/2}$	S0	0.48	0.65
3475.812	30 *h*	28762.02				
3475.705	40	28762.91				
3475.260	3	28766.59	$17454_{13/2}-46221^{\circ}_{11/}$			
3474.970	40	28768.99	$18990_{11/2}-47759^{\circ}_{13/2}$			
3474.800	20 *h*	28770.40				
3474.204	30 *h*	28775.33				
3473.428	7	28781.76				
3472.300	300	28791.11	$18853_{11/2}-47644^{\circ}_{13/2}$			
3471.731	40	28795.83	$15587_{11/2}-44383^{\circ}_{11/2}$			
3471.037	60 *r*	28801.59	$15271_{15/2}-44072^{\circ}_{13/2}$			
3470.160	40	28808.87				
3468.040	5	28826.48				

APPENDIX—*Spectral Lines of Neutral Thulium*—Continued

Wavelength in air Å	Intensity	Wavenumber cm^{-1}	Classification	Zeeman effect type	f	Je	
3467.513	200 *r*	28830.86	$15587_{11/2} - 44418^{\circ}_{13/2}$	S0	0.53	0.605	
3465.720	40 *h*	28845.77					
3462.634	6	28871.48					
3458.551	40 *r*	28905.56	$18853_{11/2} - 47759^{\circ}_{13/2}$	T	1.17		
3458.457	20	28906.35					
3456.358	100 *a*	28923.90		T	1.135		
3454.738	100 *a*	28937.47	$18693_{13/2} - 47630^{\circ}_{13/2}$	ΔJ=0	1.16	0.15	
3454.505	50 *a*	28939.42	$15271_{13/2} - 44210^{\circ}_{13/2}$	ΔJ=0	1.12	0.50	
3453.548	4	28947.44					
3453.027	100 *r*	28951.80	$18693_{13/2} - 47644^{\circ}_{13/2}$	T	1.18		
3452.020	4 *h*	28960.25					
3450.370	4 *h*	28974.10					
3448.801	4 *h*	28987.28					
3447.353	100 *r*	28999.45	$13119_{9/2} - 42119^{\circ}_{11/2}$	S0	0.20	0.92	
3446.893	7	29003.32	$15587_{11/2} - 44591^{\circ}_{13/2}$				
3446.546	100 *a*	29006.24	$17454_{13/2} - 46461^{\circ}_{15/2}$	SI	1.40	0.20	
3445.668	50 *a*	29013.63	$13119_{9/2} - 42133^{\circ}_{7/2}$				
3444.162	100 *a*	29026.32		T	1.19		
3442.992	100 *a*	29036.18	$15271_{13/2} - 44307^{\circ}_{13/2}$	S0	0.72	0.33	
3440.443	2	29057.70					
3439.425	10	29066.30	$18693_{13/2} - 47759^{\circ}_{13/2}$				
3436.599	40	29090.20		T	1.13		
3435.348	100 *a*	29100.79	$16456_{17/2} - 45557^{\circ}_{15/2}$	SI	1.25	0.07	
3433.409	4 *h*	29117.22					
3430.385	20 *r*	29142.89	$17454_{13/2} - 46597^{\circ}_{13/2}$				
3429.828	20 *r*	29147.62	$15271_{13/2} - 44418^{\circ}_{13/2}$				
3429.332	200 *a*	29151.84	$16456_{17/2} - 45608^{\circ}_{15/2}$				
3428.471	200 *a*	29159.16	$15587_{11/2} - 44747^{\circ}_{11/2}$	ΔJ=0	1.22	0.45	
3426.678	100	29174.42					
3425.262	15	29186.48	$15587_{11/2} - 44774^{\circ}_{9/2}$				
3424.899	60	29189.57					
3424.498	400 *r*	29192.99	$18693_{15/2} - 47886^{\circ}_{15/2}$	ΔJ=0	1.18	0.25	
3423.984	40	29197.37					
3422.559	100	29209.53					
3421.791	700 *r*	29216.08	$15587_{11/2} - 44803^{\circ}_{13/2}$	S0	0.28	0.80	
3421.697	100	29216.89					
3421.202	20	29221.11					
3420.203	50	29229.65					
3420.146	100	29230.14					
3419.644	8	29234.43					
3419.359	100	29236.86					
3419.071	100	29239.33	$17454_{13/2} - 46694^{\circ}_{13/2}$				
3418.625	200	29243.14	$8771^{\circ}_{9/2} - 38014_{9/2}$	ΔJ=0	0.85	1.105	*
3417.692	300	29251.12	$13119_{9/2} - 42370^{\circ}_{7/2}$				
3417.416	10	29253.48					
3416.588	3000 *a*	29260.57	$0^{\circ}_{7/2} - 29260_{7/2}$	ΔJ=0	1.143	0.928	*
3416.430	10	29261.93	$18853_{11/2} - 48115^{\circ}_{13/2}$				
3416.146	4	29264.36					
3414.521	50 *h*	29278.29					
3414.273	20	29280.41	$15587_{11/2} - 44868^{\circ}_{9/2}$				
3413.989	200 *h*	29282.85					
3413.330	2	29288.50					
3413.035	200	29291.03					
3412.590	3000 *a*	29294.85	$15271_{13/2} - 44565^{\circ}_{13/2}$	ΔJ=0	1.11	0.41	
3412.404	3	29296.45					
3411.893	200	29300.84	$15271_{13/2} - 44571^{\circ}_{17/2}$				
"			$21997_{11/2} - 51298^{\circ}_{13/2}$				
3410.048	1000 *a*	29316.69	$0^{\circ}_{7/2} - 29316_{9/2}$	S0	0.40	0.58	
3409.650	100	29320.11	$15271_{13/2} - 44591^{\circ}_{13/2}$				
3408.747	40	29327.88					
3405.967	2000 *a*	29351.82	$8771^{\circ}_{9/2} - 38123_{7/2}$	SI	0.83	1.15	*
3402.694	3	29380.05					
3401.751	40 *h*	29388.19					
3400.887	200 *h*	29395.66	$17454_{13/2} - 46850^{\circ}_{11/2}$	T	1.14		
3399.782	200	29405.21					
3399.593	3	29406.85					
3398.544	10	29415.92					
3397.867	300 *r*	29421.78	$13119_{9/2} - 42541^{\circ}_{11/2}$	S0	1.31	1.10	*
3397.773	200	29422.60	$18693_{13/2} - 48115^{\circ}_{13/2}$				
3396.724	8	29431.68					
3395.196	3	29444.93					
3394.185	200 *h*	29453.70					
3393.980	70	29455.48					
3393.186	1000 *r*	29462.37	$13119_{9/2} - 42581^{\circ}_{11/2}$	S0	0.37	0.75	
3392.693	20	29466.65	$8771^{\circ}_{9/2} - 38237_{9/2}$				
3392.391	6	29469.28	$21997_{11/2} - 51466^{\circ}_{13/2}$				
3392.241	100	29470.58	$15587_{11/2} - 45058^{\circ}_{11/2}$				
3392.029	5	29472.42					
3391.865	8	29473.85					
3391.800	100	29474.41	$13119_{9/2} - 42594^{\circ}_{9/2}$				
3391.430	200	29477.63	$16456_{17/2} - 45934^{\circ}_{15/2}$	SI	1.26	0.08	
3391.262	8 *h*	29479.09					
3390.836	200	29482.79	$15587_{11/2} - 45070^{\circ}_{9/2}$				
3390.365	5	29486.88					
3390.245	100	29487.93					
3389.461	9	29494.75					
3389.339	10	29495.81					
3385.084	2000 *r*	29532.89	$15271_{13/2} - 44803^{\circ}_{13/2}$	S0	0.92	0.15	
3383.419	10	29547.42	$8771^{\circ}_{9/2} - 38318_{9/2}$				
3383.268	4 *h*	29548.74					
3382.038	100	29559.48	$15587_{11/2} - 45147^{\circ}_{9/2}$				
3381.499	3 *h*	29564.19					
3381.390	50 *h*	29565.15					
3380.688	1000 *a*	29571.29	$8771^{\circ}_{9/2} - 38342_{7/2}$	SI	0.85	1.108	*
3380.534	2000 *a*	29572.63	$17454_{13/2} - 47027^{\circ}_{13/2}$	ΔJ=0	1.16	0.13	
3379.915	1	29578.05					
3377.392	3	29600.14					
3376.963	3 *h*	29603.90					
3375.890	10	29613.31					
3374.970	20	29621.39					
3374.853	100	29622.41	$13119_{9/2} - 42742^{\circ}_{7/2}$				
3374.163	2	29628.47					
3373.482	3	29634.45					
3372.750	30	29640.88					
3371.576	100	29651.20	$13119_{9/2} - 42770^{\circ}_{9/2}$				
3369.321	3 *h*	29671.05					
3368.597	2000 *a*	29677.42		T	1.04	0.08	
3368.186	3	29681.05					
3368.010	4	29682.60					
3367.805	1	29684.40					
3367.570	3	29686.47					
3366.676	2	29694.36					
3365.900	1000 *h*	29701.20	$15587_{11/2} - 45289^{\circ}_{11/2}$	ΔJ=0	1.12	0.55	
3365.327	3	29706.26					
3363.781	200	29719.91	$13119_{9/2} - 42839^{\circ}_{9/2}$				
3363.535	100	29722.09					
3363.465	10	29722.70					
3359.549	2	29757.35					
3359.337	50 *h*	29759.23	$21997_{11/2} - 51756^{\circ}_{11/2}$				
3358.601	2	29765.75					
3358.265	20	29768.73					
3358.057	4	29770.57					
3356.161	10	29787.39					
3354.600	100 *r*	29801.25	$15587_{11/2} - 45389^{\circ}_{13/2}$				
3354.167	1	29805.10					
3353.648	10	29809.71					
3352.923	5	29816.15					
3351.530	10	29828.55					
3351.390	8	29829.79					
3351.224	10	29831.27					
3349.987	1000	29842.28	$13119_{9/2} - 42961^{\circ}_{11/2}$	S0	1.30	1.195	*
3349.808	60	29843.88					
3348.766	100	29853.16					
3346.676	1	29871.81					
3346.033	2	29877.55					
3344.163	8	29894.25					
3343.737	200	29898.06	$15587_{11/2} - 45485^{\circ}_{11/2}$				
3342.896	9	29905.58					
3342.390	20	29910.11					
3342.324	30	29910.70	$13119_{9/2} - 43030^{\circ}_{9/2}$				

Wavelength in air Å	Intensity	Wavenumber cm^{-1}	Classification	Zeeman effect type	f	Je	
3341.889	10	29914.60	$13119_{9/2} - 43034^{\circ}_{7/2}$				
3340.664	10	29925.56	$8771^{\circ}_{5/2} - 38696_{5/2}$				
3340.664	10	29925.56					
3339.843	20	29932.92	$13119_{9/2} - 43052^{\circ}_{7/2}$				
3337.863	2	29950.68					
3337.628	100	29952.78					
3333.459	3	29990.24					
3333.130	40	29993.20					
3331.912	500	30004.17	$16456_{17/2} - 46461^{\circ}_{13/2}$				
3331.556	30	30007.37					
3330.723	2	30014.88					
3330.477	80	30017.10					
3329.722	2	30023.90					
3329.042	100	30030.03	$17454_{13/2} - 47484^{\circ}_{11/2}$				
3328.226	10 *h*	30037.40					
3327.185	4	30046.79					
3327.059	500	30047.93	$15587_{11/2} - 45635^{\circ}_{11/2}$	ΔJ=0	1.20	0.62	
3325.108	10	30065.56					
3324.980	400	30066.72	$13119_{9/2} - 43186^{\circ}_{11/2}$				
3324.746	2	30068.84					
3323.273	200	30082.16	$0^{\circ}_{7/2} - 30082_{5/2}$				
3322.184	5	30092.02					
3322.094	4	30092.84					
3321.451	2	30098.66					
3320.895	4	30103.70					
3320.772	4 *h*	30104.82					
3320.475	6	30107.51					
3319.908	4	30112.65					
3319.661	3	30114.89					
3319.308	400	30118.10	$15271_{13/2} - 45389^{\circ}_{13/2}$	S0	0.58	0.52	
3318.847	3	30122.28					
3318.559	8	30124.89					
3317.557	3	30133.99					
3313.647	8	30169.55					
3312.969	5	30175.72	$17454_{13/2} - 47630^{\circ}_{15/2}$				
3312.426	10	30180.67					
3311.389	150	30190.12	$17454_{13/2} - 47644^{\circ}_{13/2}$				
3310.488	10	30198.33					
3309.359	10	30208.64					
3309.074	20	30211.24					
3308.958	2	30212.30					
3308.688	3	30214.76					
3307.822	800 *a*	30222.67	$15587_{11/2} - 45810^{\circ}_{11/2}$	ΔJ=0	1.23	0.17	
3305.591	4	30243.07					
3305.099	2	30247.57					
3304.240	150	30255.44					
3302.647	80	30270.03					
3300.824	800	30286.75	$15271_{13/2} - 45557^{\circ}_{13/2}$	ΔJ=0	1.15	0.58	
3300.540	400	30289.35	$13119_{9/2} - 43408^{\circ}_{11/2}$	S0	0.76	0.43	
3299.809	5	30296.06					
3299.115	700 *a*	30302.43	$0^{\circ}_{7/2} - 30302_{5/2}$	SI	1.14	0.90	*
3298.882	70	30304.57	$17454_{13/2} - 47759^{\circ}_{13/2}$				
3298.381	300	30309.18	$13119_{9/2} - 43428^{\circ}_{7/2}$				
3298.315	10	30309.78	$13119_{9/2} - 43429^{\circ}_{9/2}$				
3298.205	80	30310.79	$16456_{17/2} - 46767^{\circ}_{17/2}$				
3298.054	4	30312.18					
3297.662	20 *h*	30315.79					
3296.303	500	30328.28	$13119_{9/2} - 43447^{\circ}_{11/2}$				
3295.271	100	30337.78	$15271_{13/2} - 45608^{\circ}_{13/2}$				
3294.015	10	30349.35					
3292.518	2	30363.15					
3291.736	1	30370.36					
3290.660	3	30380.29					
3289.650	200	30389.62	$15271_{13/2} - 45660^{\circ}_{13/2}$				
3289.589	20	30390.18	$8771^{\circ}_{5/2} - 39161_{5/2}$				
3287.790	4	30406.81					
3285.828	10	30424.96	$13119_{9/2} - 43544^{\circ}_{9/2}$				
3285.754	4	30425.65					
3285.155	200	30431.20	$17454_{13/2} - 47886^{\circ}_{15/2}$				
3281.127	100	30468.55	$13119_{9/2} - 43588^{\circ}_{7/2}$				
3280.219	2	30476.99					
3278.964	8	30488.65	$8771^{\circ}_{5/2} - 39259_{5/2}$				
3277.620	40	30501.15					
3277.088	10	30506.11					
3275.075	2 *h*	30524.85					
3272.355	3	30550.23					
3272.028	10	30553.28					
3271.781	400	30555.59	$13119_{9/2} - 43675^{\circ}_{9/2}$				
3271.605	10	30557.23					
3269.625	100	30575.73	$15587_{11/2} - 46163^{\circ}_{11/2}$				
3267.992	2	30591.01					
3267.101	2	30599.35					
3264.781	30	30621.10					
3264.099	2000 *r*	30627.50		S0	0.52	0.58	
3263.446	70	30633.62	$15587_{11/2} - 46221^{\circ}_{11/2}$				
3263.184	1	30636.08					
3262.807	4	30639.62					
3262.667	1	30640.94					
3261.053	3	30656.10					
3260.552	70	30660.81	$17454_{13/2} - 48115^{\circ}_{13/2}$				
3260.263	3	30663.53	$15271_{13/2} - 45934^{\circ}_{13/2}$				
3258.336	8	30681.66					
3257.371	20	30690.75					
3257.050	2	30693.78					
3256.539	3	30698.59					
3256.279	60	30701.05					
3254.071	4	30721.88					
3253.870	10	30723.77					
3253.687	6	30725.50					
3252.430	30	30737.38					
3251.782	800 *a*	30743.50	$8771^{\circ}_{5/2} - 39514_{5/2}$	T	0.92		
3246.963	3000 *a*	30789.13	$8771^{\circ}_{5/2} - 39560_{7/2}$	SI	1.00	0.10	
3244.821	200	30809.45					
3244.447	10	30813.00					
3243.411	100	30822.85					
3243.212	4	30824.74					
3240.647	3	30849.13					
3240.030	20	30855.01	$13119_{9/2} - 43974^{\circ}_{11/2}$				
3239.052	200	30864.32	$8771^{\circ}_{5/2} - 39635_{5/2}$				
3238.114	3	30873.26					
3237.233	2	30881.67	$13119_{9/2} - 44001^{\circ}_{9/2}$				
3235.835	2	30895.01					
3234.999	4	30902.99					
3233.741	1000 *a*	30915.01	$0^{\circ}_{7/2} - 30915_{5/2}$	S0	1.14	0.99	*
3232.307	5	30928.73					
3232.121	10	30930.51					
3230.582	20	30945.24					
3230.426	30	30946.74					
3229.009	2	30960.32					
3223.849	30	31009.87	$15587_{11/2} - 46597^{\circ}_{13/2}$				
3223.306	1	31015.09					
3222.505	3	31022.80	$13119_{9/2} - 44142^{\circ}_{7/2}$				
3221.076	200	31036.56					
3220.729	4	31039.91					
3218.507	40	31061.34	$13119_{9/2} - 44180^{\circ}_{11/2}$				
3218.280	400 *a*	31063.53					
3215.059	40	31094.65					
3214.792	100	31097.23	$19466_{13/2} - 50563^{\circ}_{15/2}$				
3214.381	10	31101.21					
3214.077	8	31104.15					
3213.980	2	31105.09					
3213.854	7	31106.31	$15587_{11/2} - 46694^{\circ}_{13/2}$				
3212.859	15	31115.94					
3211.190	7	31132.11					
3209.927	10	31144.36	$13119_{9/2} - 44263^{\circ}_{7/2}$				
3206.917	500	31173.59	$16456_{17/2} - 47630^{\circ}_{15/2}$				
3206.537	8	31177.28					
3205.607	40	31186.33					
3205.225	40	31190.05	$15271_{13/2} - 46461^{\circ}_{13/2}$				
3204.796	10	31194.22					

Wavelength in air Å	Intensity	Wavenumber cm⁻¹	Classification	Zeeman effect type	f	Je
3204.502	50	31197.08	$13119_{9/2} - 44316^{\circ}_{9/2}$			
3201.645	300	31224.92	$8771^{\circ}_{9/2} - 39996_{7/2}$			
3201.255	20	31228.72				
3200.677	5	31234.36				
3197.640	15	31264.03	$13119_{9/2} - 44383^{\circ}_{11/2}$			
3195.685	30	31283.15				
3194.592	150	31293.86				
3194.431	20	31295.43	$8771^{\circ}_{9/2} - 40066_{9/2}$			
3194.085	150	31298.82	$13119_{9/2} - 44418^{\circ}_{7/2}$			
3193.778	2	31301.83				
3192.582	8	31313.56				
3192.548	10	31313.89				
3191.234	400	31326.78				
3190.228	40	31336.66	$13119_{9/2} - 44456^{\circ}_{7/2}$			
3189.150	40	31347.25				
3188.306	3	31355.55				
3186.058	150	31377.68				
3183.555	2	31402.34				
3183.416	2	31403.72				
3182.148	4	31416.23				
3181.923	3	31418.45				
3181.453	40	31423.09	$15271_{13/2} - 46694^{\circ}_{13/2}$			
3180.947	3	31428.09				
3180.837	20	31429.18	$16456_{17/2} - 47886^{\circ}_{15/2}$			
3180.565	1000 *a*	31431.86	$0^{\circ}_{7/2} - 31431_{9/2}$	SI	1.31	0.17
3180.195	20	31435.52				
3180.030	150	31437.15				
3179.780	30	31439.62	$15587_{11/2} - 47027^{\circ}_{13/2}$			
3179.687	300 *a*	31440.54	$0^{\circ}_{7/2} - 31440_{9/2}$	T	1.13	
3179.044	5	31446.90				
3178.241	10	31454.85				
3176.168	1	31475.38				
3175.724	3	31479.78				
3174.018	8	31496.70	$15271_{13/2} - 46767^{\circ}_{17/2}$			
3173.484	20	31502.00				
3173.428	10	31502.55				
3172.654	3000 *a*	31510.24	$0^{\circ}_{7/2} - 31510_{7/2}$	T	1.10	0.11
3172.036	1	31516.37				
3171.277	10	31523.92				
3168.107	10	31555.46				
3166.572	60	31570.76				
3164.731	5	31589.12	$8771^{\circ}_{9/2} - 40360_{7/2}$			
3162.693	7 *h*	31609.47				
3162.612	5	31610.28				
3161.200	4	31624.40				
3160.989	2	31626.51	$15587_{11/2} - 47214^{\circ}_{13/2}$			
3160.895	100	31627.45	$13119_{9/2} - 44747^{\circ}_{11/2}$			
3159.731	6	31639.11				
3158.177	10	31654.67	$13119_{9/2} - 44774^{\circ}_{9/2}$			
3157.990	5	31656.55				
3156.688	3	31669.60				
3154.766	2	31688.90				
3154.297	3	31693.61				
3153.223	150	31704.40				
3148.611	1	31750.84				
3148.058	400	31756.42	$15271_{13/2} - 47027^{\circ}_{13/2}$			
3146.574	400	31771.40				
3145.637	20	31780.86				
3144.105	20	31796.34				
3142.838	2	31809.16				
3142.433	400	31813.26	$8771^{\circ}_{9/2} - 40584_{9/2}$			
3140.611	100	31831.72	$19466_{13/2} - 51298^{\circ}_{13/2}$			
3139.795	10	31839.99				
3137.010	30	31868.25				
3136.755	500	31870.85	$18693_{13/2} - 50563^{\circ}_{13/2}$	T	1.18	
3136.539	20	31873.04				
3136.216	20	31876.32				
3136.031	5	31878.20	$8771^{\circ}_{9/2} - 40649_{7/2}$			
3134.177	40	31897.06	$15587_{11/2} - 47484^{\circ}_{11/2}$			
3133.239	10	31906.61				
3131.686	10	31922.43	$8771^{\circ}_{9/2} - 40693_{9/2}$			
3130.083	50	31938.78	$13119_{9/2} - 45058^{\circ}_{11/2}$			
3129.638	20	31943.32	$15271_{13/2} - 47214^{\circ}_{13/2}$			
3128.891	20	31950.95	$13119_{9/2} - 45070^{\circ}_{9/2}$			
3125.506	2	31985.55				
3124.087	100	32000.07	$19466_{13/2} - 51466^{\circ}_{13/2}$			
3123.907	30	32001.92				
3122.959	1	32011.63				
3122.533	3000 *r*	32016.00	$8771^{\circ}_{9/2} - 40787_{9/2}$	ΔJ=0	0.88	0.14
3121.390	100	32027.72	$13119_{9/2} - 45147^{\circ}_{9/2}$			
3121.038	8	32031.34	$8771^{\circ}_{9/2} - 40802_{7/2}$			
3120.881	7	32032.95				
3119.522	10	32046.90				
3118.523	50	32057.17	$15587_{11/2} - 47644^{\circ}_{13/2}$			
3116.348	4	32079.54				
3116.261	30	32080.44				
3113.848	2 *h*	32105.29				
3113.507	2	32108.81				
3110.015	3	32144.86				
3108.358	1	32162.00				
3108.293	3	32162.67				
3107.932	5	32166.40				
3107.642	30 *h*	32169.41	$13119_{9/2} - 45289^{\circ}_{11/2}$			
3107.152	500 *a*	32174.48	$0^{\circ}_{7/2} - 32174_{9/2}$	T	1.10	0.05
3105.741	2	32189.10				
3104.969	2	32197.10				
3104.888	5	32197.94				
3103.826	10	32208.96				
3103.698	5	32210.28				
3103.646	40	32210.82				
3098.222	4	32267.21				
3096.032	300	32290.04	$19466_{13/2} - 51756^{\circ}_{11/2}$			
3092.033	20	32331.80				
3090.471	40	32348.14	$13119_{9/2} - 45467^{\circ}_{9/2}$			
3089.522	30	32358.07				
3088.737	4	32366.30	$13119_{9/2} - 45485^{\circ}_{11/2}$			
3088.464	1	32369.16				
3087.936	5	32374.69				
3086.854	2	32386.04				
3084.783	400 *a*	32407.78	$0^{\circ}_{7/2} - 32407_{9/2}$			
3081.388	3	32443.48				
3081.121	2000 *a*	32446.30	$0^{\circ}_{7/2} - 32446_{7/2}$	ΔJ=0	1.143	0.89 *
3080.212	4	32455.87				
3080.083	20	32457.23				
3079.034	2	32468.29				
3078.822	4	32470.52				
3078.107	300	32478.07				
3077.717	8	32482.18				
3074.501	80	32516.16	$13119_{9/2} - 45635^{\circ}_{11/2}$			
3073.391	10	32527.90	$15587_{11/2} - 48115^{\circ}_{13/2}$			
3072.063	4	32541.96				
3071.839	5	32544.33				
3068.904	15	32575.46				
3067.728	2	32587.94				
3066.096	200	32605.29	$18693_{13/2} - 51298^{\circ}_{13/2}$			
3065.382	10	32612.88	$18853_{11/2} - 51466^{\circ}_{13/2}$			
3063.584	3	32632.02				
3060.440	20	32665.54				
3060.176	1	32668.36				
3058.065	400	32690.91	$13119_{9/2} - 45810^{\circ}_{11/2}$			
3055.636	10	32716.90				
3055.179	70	32721.79	$8771^{\circ}_{9/2} - 41493_{9/2}$			
3051.033	50 *h*	32766.26	$18990_{11/2} - 51756^{\circ}_{11/2}$			
3050.367	40	32773.41	$8771^{\circ}_{9/2} - 41544_{9/2}$			
3050.339	30	32773.71	$18693_{13/2} - 51466^{\circ}_{13/2}$			
3049.985	2	32777.51				
3049.090	2	32787.13				
3046.870	3000 *a*	32811.02	$0^{\circ}_{7/2} - 32811_{7/2}$	ΔJ=0	1.143	1.04 *
3044.469	30 *h*	32836.90				
3039.631	20	32889.16				

Wavelength in air Å	Intensity	Wavenumber cm^{-1}	Classification	Zeeman effect type	f	Je	
3039.067	20	32895.26					
3038.370	200 *h*	32902.81	$18853_{11/2} - 51756^{\circ}_{11/2}$				
3036.848	80 *h*	32919.30	$18837_{9/2} - 51756^{\circ}_{11/2}$				
3035.784	2	32930.84					
3034.642	3	32943.23					
3032.613	30	32965.27					
3031.280	40	32979.76	$8771^{\circ}_{9/2} - 41751_{9/2}$				
3030.567	20	32987.52					
3030.491	10	32988.35					
3029.061	2	33003.92					
3026.694	2	33029.73					
3025.449	10	33043.32					
3025.386	40	33044.01	$13119_{9/2} - 46163^{\circ}_{11/2}$				
3024.498	8	33053.71					
3023.485	20	33064.79	$8771^{\circ}_{9/2} - 41836_{9/2}$				
3020.101	10	33101.83	$13119_{9/2} - 46221^{\circ}_{11/2}$				
3019.436	70	33109.12	$17454_{13/2} - 50563^{\circ}_{13/2}$				
3016.834	2	33137.68					
3013.639	10	33172.81					
3009.480	10	33218.65					
3008.446	200	33230.07					
3007.281	3	33242.94					
3007.118	1	33244.74					
3005.816	10	33259.14					
3002.396	7	33297.03					
3001.334	2	33308.81					
2999.448	5	33329.75					
2995.079	30	33378.37					
2992.564	5	33406.42					
2991.152	3	33422.19					
2990.672	10	33427.55	$8771^{\circ}_{9/2} - 42198_{9/2}$				
2989.922	2	33435.94					
2988.258	2	33454.55					
2988.229	2	33454.88					
2986.739	3	33471.57					
2985.519	10	33485.24					
2984.834	40	33492.93					
2982.889	10	33514.77					
2979.637	30	33551.34					
2979.034	1	33558.13					
2976.749	10	33583.89					
2976.545	2	33586.20	$8771^{\circ}_{9/2} - 42357_{9/2}$				
2976.100	2	33591.22					
2975.496	20	33598.04					
2974.006	1	33614.87					
2973.218	3000 *a*	33623.78	$0^{\circ}_{7/2} - 33623_{7/2}$	ΔJ=0	1.14	0.92	*
2970.694	15	33652.34					
2968.688	2	33675.08					
2965.059	10	33716.30					
2964.592	2	33721.61					
2964.494	20 *w*	33722.72					
2962.314	10	33747.54					
2961.749	40	33753.97					
2957.287	20 *h*	33804.90					
2955.508	20	33825.25	$8771^{\circ}_{9/2} - 42596_{9/2}$				
2953.910	10	33843.55	$17454_{13/2} - 51298^{\circ}_{13/2}$				
2950.542	2 *h*	33882.18					
2949.502	100	33894.12					
2943.416	5	33964.20					
2943.101	1	33967.84					
2943.000	3	33969.00					
2942.857	4	33970.65					
2942.528	100	33974.45					
2940.755	3	33994.93					
2940.087	4	34002.66					
2939.292	20	34011.85	$17454_{13/2} - 51466^{\circ}_{13/2}$				
2935.699	50	34053.48					
2934.222	9	34070.62					
2932.966	1000 *a*	34085.21	$0^{\circ}_{7/2} - 34085_{9/2}$	SI	1.14	0.95	*
2931.093	400	34106.99	$16456_{17/2} - 50563^{\circ}_{13/2}$	T	1.18		
2926.431	40	34161.32					
2925.842	3 *h*	34168.20					
2925.049	1	34177.46					
2924.297	2	34186.25	$8771^{\circ}_{9/2} - 42957_{9/2}$				
2921.958	3	34213.61					
2921.706	10	34216.56					
2920.758	1	34227.67					
2917.411	2	34266.93					
2916.372	4	34279.14					
2915.985	1	34283.69					
2915.879	20	34284.94	$8771^{\circ}_{9/2} - 43056_{9/2}$				
2915.458	5 *h*	34289.89					
2914.839	1000 *a*	34297.17	$0^{\circ}_{7/2} - 34297_{7/2}$	ΔJ=0	1.143	0.915	*
2914.665	2	34299.22					
2914.442	30 *h*	34301.84	$17454_{13/2} - 51756^{\circ}_{11/2}$				
2912.953	20	34319.37					
2912.342	1	34326.57					
2909.301	5	34362.45					
2908.502	2	34371.89					
2908.161	10	34375.92					
2907.031	5	34389.28	$8771^{\circ}_{9/2} - 43160_{9/2}$				
2906.270	3	34398.29					
2904.065	2	34424.41					
2902.226	10	34446.22					
2901.864	2	34450.51					
2900.088	50	34471.61					
2897.580	20 *h*	34501.45					
2894.191	20	34541.84					
2891.518	2	34573.77					
2890.576	5	34585.04					
2888.814	4 *h*	34606.13					
2885.047	5	34651.32					
2884.289	2	34660.42					
2882.917	10	34676.92					
2879.152	70 *h*	34722.26					
2877.743	4	34739.26					
2876.873	10	34749.77					
2875.440	4	34767.08					
2872.702	200 *h*	34800.22					
2871.319	2	34816.98					
2869.725	4	34836.32					
2868.461	1	34851.67					
2866.840	20	34871.37					
2865.069	1	34892.93					
2864.757	300	34896.73					
2863.012	10	34918.00					
2854.166	1000 *a*	35026.21	$0^{\circ}_{7/2} - 35026_{9/2}$	SI	1.45	0.30	
2853.889	2	35029.61	$8771^{\circ}_{9/2} - 43800_{9/2}$				
2852.644	2	35044.90					
2851.256	3	35061.96					
2848.169	4 *h*	35099.96					
2847.088	5	35113.29					
2845.514	1	35132.71					
2842.812	1	35166.10					
2842.225	2 *h*	35173.36					
2841.283	15	35185.02					
2841.123	200 *a*	35187.00	$8771^{\circ}_{9/2} - 43958_{9/2}$				
2840.657	2	35192.78					
2839.279	3	35209.86	$8771^{\circ}_{9/2} - 43981_{7/2}$				
2837.841	10	35227.70					
2837.294	10	35234.49					
2835.098	80 *a*	35261.78	$0^{\circ}_{7/2} - 35261_{9/2}$				
2833.055	2	35287.21					
2832.804	10	35290.33					
2832.596	10	35292.92	$15271_{11/2} - 50563^{\circ}_{13/2}$				
2832.316	5	35296.41					
2831.037	30	35312.36					
2830.739	4	35316.07					
2827.187	1	35360.44					
2826.690	50 *a*	35366.66					

Wavelength in air Å	Intensity	Wavenumber cm^{-1}	Classification	Zeeman effect type	f	Je
2821.626	15	35430.13				
2821.558	1	35430.98				
2819.552	2	35456.19				
2818.285	2	35472.13	$8771^{\circ}_{9/2} - 44243_{9/2}$			
2811.972	1	35551.76	$8771^{\circ}_{9/2} - 44323_{7/2}$			
2805.574	10	35632.83				
2803.727	1	35656.30				
2799.468	5	35710.55	$15587_{11/2} - 51298^{\circ}_{13/2}$			
2798.865	4	35718.24				
2795.122	1	35766.07				
2790.721	10	35822.47				
2789.810	2	35834.17				
2786.329	2	35878.93	$15587_{11/2} - 51466^{\circ}_{13/2}$			
2783.461	5	35915.90				
2775.875	3	36014.05				
2773.898	15	36039.71				
2768.840	1	36105.55				
2767.731	4	36120.01	$8771^{\circ}_{9/2} - 44891_{7/2}$			
2764.848	8	36157.67				
2763.023	1	36181.55				
2761.938	1	36195.77	$15271_{13/2} - 51466^{\circ}_{13/2}$			
2759.450	8	36228.40				
2753.176	50	36310.95				
2752.182	50	36324.07				
2751.646	2*h*	36331.14				
2748.870	2	36367.83				
2747.158	4	36390.49				
2739.775	2*h*	36488.55				
2709.625	15	36894.54				
2708.020	3	36916.40				
2692.207	10	37133.22				
2691.342	7	37145.16				
2681.860	3*h*	37276.48				
2679.918	3	37303.49				
2673.342	1	37395.25				
2669.591	1	37447.79				
2664.616	10	37517.70				
2661.810	1	37557.25				
2660.417	20	37576.91	$0^{\circ}_{7/2} - 37576_{9/2}$			
2657.203	1	37622.36				
2651.570	7	37702.28				
2651.214	3	37707.34				
2651.173	20	37707.93				
2650.950	10	37711.10	$0^{\circ}_{7/2} - 37711_{9/2}$			
2650.628	3	37715.68				
2649.986	4	37724.82	$0^{\circ}_{7/2} - 37724_{9/2}$			
2633.727	2	37957.69				
2626.054	3	38068.59				
2622.467	3	38120.66	$0^{\circ}_{7/2} - 38120_{9/2}$			
2621.936	10	38128.38	$0^{\circ}_{7/2} - 38128_{9/2}$			
2601.092	8	38433.91	$0^{\circ}_{7/2} - 38433_{9/2}$			
2596.489	10	38502.04	$0^{\circ}_{7/2} - 38502_{9/2}$			
2579.205	1	38760.03				
2564.058	5	38988.99				
2553.514	10	39149.97				
2552.764	50	39161.48	$0^{\circ}_{7/2} - 39161_{9/2}$			
2552.263	2	39169.16				
2551.115	5	39186.79				
2549.810	5	39206.84	$0^{\circ}_{7/2} - 39206_{9/2}$			
2541.776	5	39330.76				
2539.469	2	39366.49				
2535.432	5	39429.16				
2534.719	50	39440.25				
2533.181	1	39464.20				
2533.144	5	39464.77				
2527.542	5	39552.24				
2527.275	2	39556.42				
2527.022	10*r*	39560.37	$0^{\circ}_{7/2} - 39560_{9/2}$			
2525.723	2	39580.72				
2520.768	5*h*	39658.52				
2520.655	2	39660.30				
2520.398	1	39664.34				
2517.694	1	39706.94				
2513.778	5*r*	39768.79	$0^{\circ}_{7/2} - 39768_{9/2}$			

JOURNAL OF RESEARCH of the National Bureau of Standards—A. Physics and Chemistry
Vol. 77A, No. 1, January–February 1973

Simultaneous Measurement of Specific Heat, Electrical Resistivity, and Hemispherical Total Emittance of Niobium-1 (Wt. %) Zirconium Alloy in the Range 1500 to 2700 K by a Transient (Subsecond) Technique*

Ared Cezairliyan

Institute for Materials Research, National Bureau of Standards, Washington, D.C. 20234

(August 9, 1972)

Simultaneous measurements of specific heat, electrical resistivity, and hemispherical total emittance of niobium-1 (wt. %) zirconium alloy in the temperature range 1500 to 2700 K by a subsecond duration pulse heating technique are described. Estimated inaccuracy of measured properties are: 3 percent for specific heat and hemispherical total emittance, and 0.5 percent for electrical resistivity. Properties of the alloy are compared with the properties of pure niobium. It was found that specific heat and emittance of the alloy were approximately 0.5 percent and 1.5 percent, respectively, higher than those of pure niobium. Electrical resistivity of the alloy was 0.5 percent lower than that of pure niobium. Like niobium, the alloy showed a negative departure from linearity in the curve of electrical resistivity versus temperature.

Key words: Electrical resistivity; emittance; high-speed measurements; high temperature; niobium-zirconium alloy; specific heat; thermodynamics.

1. Introduction

In this paper, application of a transient technique to the simultaneous measurements of specific heat, electrical resistivity, and hemispherical total emittance of the alloy niobium-1 (wt. %) zirconium in the temperature range from 1500 to 2700 K is described.

The method is based on rapid resistive self-heating of the specimen from room temperature to any desired high temperature (up to its melting point) in less than one second by the passage of electrical currents through it; and on measuring, with millisecond resolution, experimental quantities, such as current through the specimen, potential drop across the specimen, and specimen temperature. Details regarding the construction and operation of the measurement system, the methods of measuring experimental quantities, and other pertinent information, such as formulation of relations for properties, etc. are given in earlier publications [1, 2].[1]

2. Measurements

The specimen was a tube of the following nominal dimensions: length, 102 mm; outside diameter, 6.3 mm; and wall thickness, 0.5 mm. Zirconium content of the specimen was 1.05 percent by weight. The total amount of impurities was less than 0.17 percent; the major impurity was tantalum with 0.09 percent. Photomicrographs of the specimen, shown in figure 1, indicate that considerable grain growth took place as the result of pulse heating to high temperatures.

To optimize the operation of the high-speed pyrometer, the temperature interval (1500 to 2700 K) was divided into six ranges. One experiment was performed in each range. Before the start of the experiments, the specimen was annealed by subjecting it to 30 heating pulses (up to 2500 K). The experiments were conducted with the specimen in a vacuum environment of approximately 10^{-4} torr.

To optimize the operation of the measurement system, the heating rate of the specimen was varied depending on the desired temperature range by adjusting the value of a resistance in series with the specimen. Duration of current pulses in the experiments ranged from 360 to 410 ms; and the heating rate ranged from 4500 to 6600 K s^{-1}. Radiative heat loss from the specimen amounted to approximately 1 percent at 1500 K, and 9 percent at 2700 K of the input power.

3. Experimental Results

The thermophysical properties reported in this paper are based on the International Practical Temper-

*This work was supported in part by the Directorate of Aeromechanics and Energetics of the U.S. Air Force Office of Scientific Research.

[1] Figures in brackets indicate the literature references at the end of this paper.

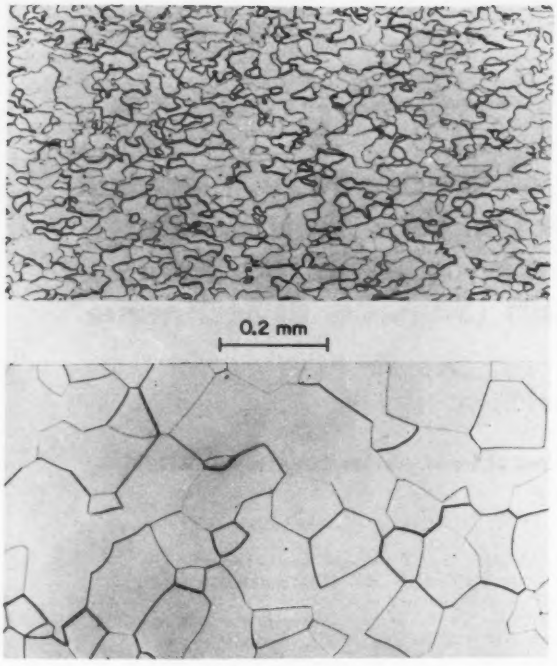

FIGURE 1. *Photomicrographs of the niobium-1 (wt. %) zirconium specimen.*

Upper photograph, specimen as received; lower photograph, specimen after the entire set of experiments.

ature Scale of 1968 [3]. In all computations, the geometrical quantities are based on their room temperature (298 K) dimensions. The experimental results for properties are represented by polynomial functions in temperature obtained by least squares approximation of the individual points. The final values on properties at 100 degree temperature intervals computed using the functions are presented in table 1. Results obtained from individual experiments, by the method described previously [2], are given in the appendix (tables A–1 and A–2). Each number tabulated in these tables represents results from over 50 original data points.

TABLE 1. *Specific heat, electrical resistivity, and hemispherical total emittance of the alloy niobium-1 (wt. %) zirconium*

Temp. K	c_p J g^{-1}K^{-1}	ρ^* $10^{-8}\,\Omega$ m	ϵ^*
1500	0.3207	57.36	
1600	.3263	60.13	
1700	.3322	62.87	0.218
1800	.3385	65.59	.232
1900	.3455	68.27	.245
2000	.3535	70.93	.257
2100	.3627	73.56	.268
2200	.3735	76.16	.278
2300	.3861	78.74	.287
2400	.4007	81.29	.295
2500	.4177	83.81	.303
2600	.4373	86.30	.309
2700	.4598	88.76	

*Based on ambient temperature (298 K) dimensions.

Specific Heat: Specific heat was computed from data taken during the heating period. A correction for power loss due to thermal radiation was made using the results on hemispherical total emittance. The function for specific heat (standard deviation = 1%) that represents the results in the temperature range 1500 to 2700 K is:

$$c_p = 7.073 \times 10^{-2} + 3.783 \times 10^{-4}T - 2.091 \times 10^{-7}T^2 + 4.532 \times 10^{-11}T^3 \quad (1)$$

where T is in K, and c_p is in J g^{-1}K^{-1}.

Electrical Resistivity: The electrical resistivity was determined from the same experiments that were used to calculate the specific heat. The function for electrical resistivity (standard deviation = 0.06%) that represents the results in the temperature range 1500 to 2700 K is:

$$\rho = 12.50 + 3.199 \times 10^{-2}T - 1.387 \times 10^{-6}T^2 \quad (2)$$

where T is in K, and ρ is in $10^{-8}\,\Omega$ m. The measurement, before the pulse experiments, of the electrical resistivity of the specimen at 293 K with a Kelvin bridge yielded a value of $16.2 \times 10^{-8}\,\Omega$ m.

Hemispherical Total Emittance: Hemispherical total emittance was computed using data taken during both heating and initial free radiative cooling periods. The function for hemispherical total emittance (standard deviation = 1%) that represents the results in the temperature range 1700 to 2600 K is:

$$\epsilon = -1.647 \times 10^{-1} + 3.056 \times 10^{-4}T - 4.749 \times 10^{-8}T^2 \quad (3)$$

where T is in K.

4. Estimate of Errors

The details for estimating errors in measured and computed quantities in transient experiments using the present measurement system are given in an earlier publication [2]. In this paper, the specific items in the error analysis were recomputed whenever the present conditions differed from those in the earlier publication. The results for imprecision[2] and inaccuracy[3] in the properties are: 1 percent and 3 percent for specific heat, 0.06 percent and 0.5 percent for electrical resistivity, 1 percent and 3 percent for hemispherical total emittance.

5. Discussion

The specific heat, electrical resistivity, and hemispherical total emittance of the niobium-1 (wt. %)

[2] Imprecision refers to the standard deviation of an individual point as computed from the difference between measured value and that from the smooth function obtained by the least squares method.

[3] Inaccuracy refers to the estimated total error (random and systematic).

zirconium alloy measured in this work are presented in figure 2. A comparison of the present results for the alloy with those for pure niobium [4] obtained using the same method is given in figure 3. It may be seen that specific heat and hemispherical total emittance of the alloy were approximately 0.5 percent and 1.5 percent, respectively, higher than those of pure niobium. The difference in specific heat cannot be accounted for by the additivity law. Electrical resistivity of the alloy was 0.5 percent lower than that of pure niobium. However, one should not place too much significance to these differences since their magnitudes are less than the combined estimated errors in the measurements for the alloy and for the pure metal.

At 293 K, electrical resistivity of the alloy (16.2×10^{-8} Ω m) is higher than the resistivity of pure niobium (15.9×10^{-8} Ω m) [4]. However, at high temperatures (fig. 3) the resistivity of the alloy is lower than that of niobium. A similar trend was also observed in the electrical resistivity of the alloy tantalum-10 (wt. %) tungsten [5]. Like niobium, at high temperatures the alloy showed a negative departure from linearity in the curve of electrical resistivity versus temperature.

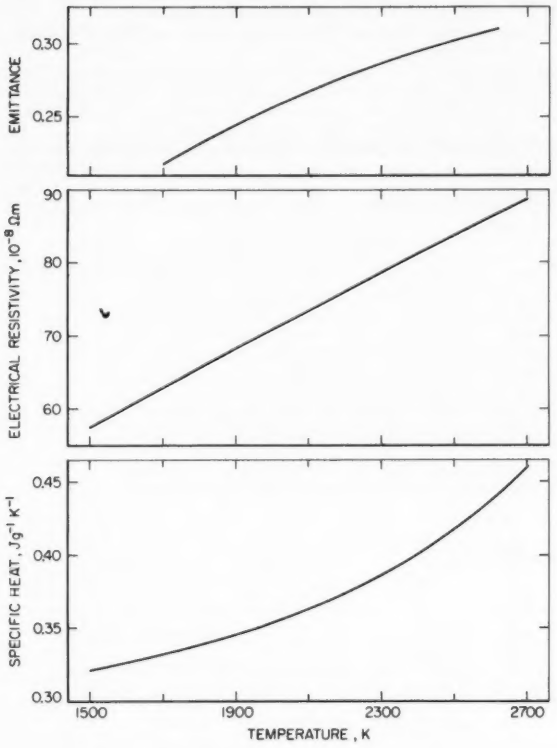

FIGURE 2. *Specific heat, electrical resistivity, and hemispherical total emittance of niobium-1 (wt. %) zirconium alloy.*

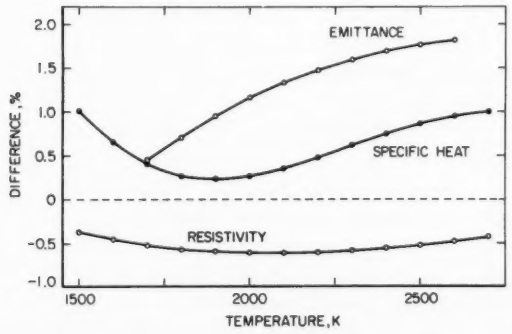

FIGURE 3. *Differences in specific heat, electrical resistivity, and hemispherical total emittance of niobium-1 (wt. %) zirconium alloy from those of pure niobium.*

The zero line corresponds to results of pure niobium [4].

The author expresses his gratitude to C. W. Beckett for his continued interest and encouragement of research in high-speed methods of measuring thermophysical properties. The contribution of M. S. Morse in connection with electronic instrumentation is also greatly appreciated.

6. Appendix

TABLE A-1. *Experimental results on specific heat and electrical resistivity of the alloy niobium-1 (wt. %) zirconium*

T K	c_p J $g^{-1}K^{-1}$	Δc_p^* %	ρ $10^{-8}\Omega$ m	$\Delta\rho^*$ %
1500	0.3198	− 0.21	57.37	+ 0.01
1550	.3206	− 0.87	58.75	− 0.01
1600	.3275	+ 0.37	60.13	0.00
1650	.3344	+ 1.57	61.53	+ 0.03
1700	.3311	− 0.31	62.90	+ 0.04
1750	.3392	+ 1.19	64.27	+ 0.05
1800	.3339	− 1.34	65.59	+ 0.01
1850	.3416	− 0.06	66.92	− 0.02
1900	.3480	+ 0.74	68.26	− 0.03
1950	.3419	− 2.14	69.58	− 0.03
2000	.3505	− 0.82	70.88	− 0.07
2050	.3587	+ 0.26	72.19	− 0.09
2100	.3666	+ 1.08	73.50	− 0.09
2150	.3739	+ 1.62	74.81	− 0.08
2200	.3700	− 0.91	76.25	+ 0.10
2250	.3779	− 0.42	77.51	+ 0.06
2300	.3859	0.00	78.77	+ 0.03
2350	.3943	+ 0.33	80.03	+ 0.01
2400	.4030	+ 0.60	81.28	− 0.01
2450	.4024	− 1.59	82.68	+ 0.16
2500	.4217	+ 0.98	83.79	− 0.02
2550	.4228	− 1.01	85.11	+ 0.07
2600	.4426	+ 1.24	86.28	− 0.02
2650	.4461	− 0.43	87.52	− 0.02
2700	.4594	− 0.07	88.69	− 0.08

*The quantities Δc_p and $\Delta\rho$ are percentage deviations of the individual results from the smooth functions represented by eqs (1) and (2), respectively.

TABLE A-2. *Experimental results on hemispherical total emittance of the alloy niobium-1 (wt. %) zirconium*

T K	ϵ	$\Delta\epsilon$* %
1711	0.218	− 0.44
1711	.223	+ 1.71
1711	.217	− 1.01
1712	.223	+ 1.76
1899	.242	− 1.01
1899	.242	− 0.93
1899	.240	− 1.76
1900	.241	− 1.50
2055	.264	+ 0.36
2056	.265	+ 0.62
2056	.266	+ 1.05
2057	.266	+ 1.22
2322	.287	− 0.69
2324	.289	− 0.11
2324	.290	+ 0.14
2325	.291	+ 0.64
2667	.312	− 0.31
2670	.312	− 0.11
2670	.313	+ 0.02
2672	.314	+ 0.20

*The quantity $\Delta\epsilon$ is percentage deviation of the individual results from the smooth function represented by eq (3).

7. References

[1] Cezairliyan, A., Design and operational characteristics of a high-speed (millisecond) system for the measurement of thermophysical properties at high temperatures, J. Res. Nat. Bur. Stand. (U.S.), **75C** (Eng. and Instr.), 7 (1971).

[2] Cezairliyan, A., Morse, M. S., Berman, H. A., and Beckett, C. W., High-speed (subsecond) measurement of heat capacity, electrical resistivity, and thermal radiation properties of molybdenum in the range 1900 to 2800 K, J. Res. Nat. Bur. Stand. (U.S.), **74A** (Phys. and Chem.). 65 (1970).

[3] International Practical Temperature Scale of 1968, Metrologia, **5**, 35 (1969).

[4] Cezairliyan, A., High-speed (subsecond) measurement of heat capacity, electrical resistivity, and thermal radiation properties of niobium in the range 1500 to 2700 K, J. Res. Nat. Bur. Stand. (U.S.), **75A** (Phys. and Chem.), 565 (1971).

[5] Cezairliyan, A., High-speed (subsecond) simultaneous measurement of specific heat, electrical resistivity, and hemispherical total emittance of tantalum-10 (wt. %) tungsten alloy in the range 1500 to 3200 K, High Temperatures-High Pressures, in press.

(Paper 77A1–753)

JOURNAL OF RESEARCH of the National Bureau of Standards—A. Physics and Chemistry
Vol. 77A, No. 1, January–February 1973

Theory of Disclinations: II. Continuous and Discrete Disclinations in Anisotropic Elasticity

R. deWit

Institute for Materials Research, National Bureau of Standards, Washington, D.C. 20234

(August 18, 1972)

A general theory of stationary disclinations for a linearly elastic, infinitely extended, homogeneous body is developed. Dislocation theory is extended in three different ways to include disclinations, i.e., from continuous distributions, discrete lines, and continuous distributions of infinitesimal loops. This leads to three independent definitions of the disclination, which can be uniquely related to each other. These interrelationships clarify Anthony and Mura's approaches to disclination theory, which at first appear to diverge from the present theory. Mura's "plastic distortion" and "plastic rotation" are identified as the dislocation and disclination loop densities. The elastic strain and bend-twist are derived as closed integrals in terms of the defect densities, and shown to be state quantities. The theory reduces to classical dislocation theory when the disclinations vanish. For every discrete disclination line, it is always possible to find a "dislocation model," which is a dislocation wall terminating on the line that gives exactly the same elastic strain and stress.

Key words: Burgers vector; continuum mechanics; defect; dipole; disclination; dislocation; distortion; Green's tensor; incompatibility; loop; plasticity; strain; Volterra.

Contents

	Page
1. Introduction	50
1.1. Dislocations versus disclinations	50
1.2. Continuous defects versus discrete defect lines versus defect loop densities	51
1.3. Geometry versus statics	51
1.4. Outline of paper	52
2. General solution of the Plastic Strain Problem	53
2.1. Statement of the problem	53
2.2. Definition and application of Green's tensor	53
2.3. Solution of classical elasticity problem	54
2.4. Solution of the plastic strain problem	55
2.5. Eshelby's method	56
2.6. Compatible plastic strain	56
3. Review of Dislocation Theory	56
3.1. Continuous distribution of dislocations	56
3.1.1. Geometry	56
3.1.2. Statics	58
3.2. The discrete dislocation line	59
3.2.1. Geometry	59
3.2.2. Statics	61
3.3. Continuous distribution of infinitesimal dislocation loops	62
3.4. The dislocation dipole	64
3.4.1. General definition of a dipole	64
3.4.2. Application to discrete dislocation dipole	65
4. Continuous Distribution of Defects	66
4.1. Geometry	66
4.2. Statics	68
5. The Discrete Defect Line	71
5.1. Weingarten's Theorem	71
5.2. Geometry	71
5.3. Statics	76
6. Continuous Distribution of Infinitesimal Defect Loops	79
7. The Discrete Dipole Line	84
7.1. Basic relations: The biaxial dipole	84
7.2. Influence of the axis: The uniaxial dipole	84
8. Application to Dislocations	86

487-412 OL - 73 - 4

	Page
8.1. Continuous distribution of dislocations	86
8.1.1. Geometry	86
8.1.2. Statics	87
8.2. The discrete dislocation line	88
8.2.1. Geometry	88
8.2.2. Statics	88
9. The "Dislocation Model" of a Discrete Defect Line	89
9.1. Geometry	90
9.2. Statics	90
10. The Compensated Disclination Line	92
10.1. Geometry	92
10.2. Statics	93
11. Summary	93
12. Appendix A. The Divergence Theorem and Stokes' Theorem	95
13. Appendix B. Delta Functions on Curves and Surfaces	95
14. References	99

1. Introduction

This paper develops a general theory of stationary disclinations in a linearly elastic, infinitely extended, homogeneous body.

Nabarro [1][1] and Anthony [2] have already reviewed many of the geometrical aspects of discrete disclinations. The author [3] and Anthony [2] have also treated the geometry of continuous disclinations (i.e., continuous distributions of disclinations). We have a slight difference in interpretation with Anthony over the meaning of the dislocation density tensor, and the continuity equation for dislocations, in the presence of disclinations. This difference arises due to the essentially independent definitions of continuous and discrete defects, and we believe this problem has been resolved in the present paper. Furthermore, Anthony [2] has treated the statics of a wedge disclination in isotropic couple-stress theory, and also given a nonlinear formulation of the geometry of continuous disclinations.

The development of the theory we present owes much to Mura [4]. He has developed an anisotropic theory of discrete disclinations and generalized this to continuous distributions. He does not try to distinguish between geometry and statics. Mura introduced the concepts of "plastic distortion," $\boldsymbol{\beta}^*$, and "plastic rotation," $\boldsymbol{\phi}^*$, which we [3] claimed could not be defined when disclinations are present. However, these concepts can be incorporated into the general theory with a slight modification in interpretation: They can logically be regarded as the dislocation and disclination loop density tensors. Then these quantities, which have a clear definition for discrete defects, retain their physical significance when the theory is generalized to continuous distributions. In this sense the dislocation loop theory of Kroupa [5] is then extended to disclinations.

Mura also introduces an "elastic distortion" in the presence of disclinations. The physical significance of this quantity still has to be assessed, because it turns out not to be a *state quantity*, contrary to all previously defined elastic fields. By definition a state quantity is a continuously varying quantity which can be measured (in principle) by macroscopic experiments without any knowledge of the former states of the body. While for dislocations the elastic distortion *is* a state quantity, we find that with disclinations the elastic strain and bend-twist are the relevant state quantities. All of Mura's results [4] have been incorporated in the present paper.

There are several ways in which we can divide the theory of disclinations for the purpose of presentation. To clarify the logical structure of this paper we discuss them next, followed by an outline of the paper.

1.1. Dislocations Versus Disclinations

We can juxtapose the two types of defects. We first discuss the known results for dislocations to emphasize the new results that follow when disclinations are introduced. In this sense what has been called "theory of disclinations" in the literature is really a combined theory of disclinations and dislocations. For this reason, we shall use the term *defects* in this paper to denote the combi-

[1] Figures in brackets indicate the literature references at the end of this paper.

nation of both disclinations and dislocations.[2] In this terminology, then, this paper deals with continuous and discrete "defects" in anisotropic elasticity.

"Defect theory" is an extension of dislocation theory and reduces to it when the disclinations vanish. Although it is possible to have a pure "dislocation theory," it is not possible to have a "disclination theory" without dislocations. Nevertheless we left the word "disclination" in the title of this paper to emphasize that what is new is due to the introduction of disclinations.

1.2 Continuous Defects Versus Discrete Defect Lines Versus Defect Loop Densities

There are three essentially different ways to define defects:

The geometrical theory of continuous (distributions of) defects can be formulated by examining the consequences of violating the classical compatibility conditions [3]. In view of this a body with continuous defects is also called an incompatible body, whereas a defect-free body is called compatible.

On the other hand, Weingarten's theorem [3, 6] is the point of departure for the theory of discrete defect lines. This theorem provides the two characteristic constants associated with the discrete defect: The general Burgers vector, which reduces to the classical Burgers vector for a discrete dislocation, and the characteristic rotation vector of the discrete disclination. Like the Burgers vector for dislocations, the characteristic rotation vector plays just as important a role for disclinations. We have therefore ventured to call it the *Frank vector*, in honor of F. C. Frank, who coined the word "disclination."[3]

A third way to formulate defect theory is in terms of (a continuous distribution of infinitesimal) defect loop densities. This could be regarded as the simplest approach, because in general the loop densities can be arbitrarily prescribed. Furthermore any given defect can be built up from some loop distribution.

In relating the three concepts in the above three paragraphs complications arise. For dislocations there is a straightforward correlation between the dislocation density, the Burgers vector, and the dislocation loop density. When disclinations are introduced there is an analogous correlation between the disclination density tensor, the Frank vector, and the disclination loop density. However, it is found that there is no unique correlation between the dislocations defined in the three formulations, but that they get mixed with the disclinations. This is basically the source of our differences with Anthony (continuous versus discrete) and Mura (lines versus loops).

1.3. Geometry Versus Statics

These are the stationary equivalents of kinematics versus dynamics, a distinction made in almost all other fields of science.

The relations described under *geometry* headings simply result from the properties of Euclidean space and are independent of the properties of the body. The distinction between plastic and elastic under this heading is therefore arbitrary, but it acquires physical significance under statics. In every case, the results given under geometry in this paper are valid for a linearly elastic, homogeneous body, *finite* or *infinite*.

Under the *statics* headings the elastic quantities from geometry are related to the properties

---

[2] This usage would seem to ignore the possibility of point defects. However, they can be represented in this theory by discrete defect loop densities. This will be illustrated by an example elsewhere [24].

[3] A historical remark is appropriate here: After Weingarten [6] published his theorem, Volterra [7] recognized its implications for the discrete defects, which he called "distortions." This would then at first seem like the best word to use for disclinations and dislocations combined. Kröner [8] did refer to them as "Volterra distortions," but he subsequently used the term "distortion" for the gradient of the displacement, a usage which has now become widely accepted. Meanwhile Love [9] ventured to call them "dislocations." This name has stuck, but since the translational type defect played the more important role in plasticity, the name "dislocation" gradually became more and more associated with this type of defect. It then became necessary to distinguish between translational and rotational dislocations, or, referring back to Volterra, between dislocations of the first, second, and third order, and dislocations of the fourth, fifth, and sixth order. Therefore, Frank [10] coined the term "disinclinations" for the latter. He subsequently modified it to "disclinations." Now the names "dislocations" and "disclinations" are becoming well-established in the literature, but so far no suitable term has been introduced to describe the combination of both of them, which we have simply called "defects." For additional information see Nabarro [3], pp. 17–20. We also add a remark on the nomenclature: In the present linear theory the rotation is traditionally represented by a vector, and successive rotations commute, in accordance with the usual vector addition rules. When the theory is extended to the nonlinear range the rotations can be finite and may no longer commute. In this case the rotation can still be represented by a vector (sometimes called *versor*), which obeys a more general addition rule. See section 5.1.

of the body. We confine ourselves to linear elasticity, i.e., Hooke's law, and a homogeneous body. Furthermore the specific results in this paper are limited by boundary conditions. These are that the body is infinitely extended and that the displacement and strain fields vanish at infinity faster than r^{-1} and r^{-2}, respectively.

1.4. Outline of Paper

In section 2 we derive a general solution of the plastic strain problem, which can be posed without specifying the nature of the defects involved. This problem is a generalization of Eshelby's "transformation problem" [11]. The result forms the basis for all subsequent applications to statics. In the derivation the general boundary conditions are introduced. Also the useful Green's tensor is defined. We show how Eshelby's method of solution can be generalized. Finally we show that a compatible plastic strain gives no elastic fields.

In section 3 we review classical dislocation theory to set the stage for the following sections.

In section 4 we derive the fields for a continuous distribution of defects. The geometry for this case has already been treated [3] and equations quoted from this reference are denoted by (I1), (I2), etc. In this section the useful incompatibility source tensor of Simmons and Bullough [12] is used to find the elastic strain and show that it is a state quantity.

Section 5 treats the discrete defect line. Weingarten's theorem is used to motivate the definition. Then the appropriate plastic strain and bend-twist are found, which are logically expressed in terms of Mura's $\boldsymbol{\beta}^*$ and $\boldsymbol{\phi}^*$. The dislocation density tensor is found to depend on the Frank vector, an example of the mixing referred to above. The static results are derived.

Section 6 shows the formulation in terms of a continuous distribution of infinitesimal defect loops. Here we identify $\boldsymbol{\beta}^*$ and $\boldsymbol{\phi}^*$, introduced for the discrete defect, with the dislocation and disclination loop density tensors. Hence this gives meaning to them in Mura's generalization to continuous distributions. As another example of mixing we find that the dislocation density depends on the disclination loop density.

In section 7 we derive some results for the discrete dipole line, and show how they are related to the dislocation dipole.

Section 8 shows that the general results of sections 4–6 reduce to those of section 3 when no disclinations are present.

Section 9 examines more closely the meaning of $\boldsymbol{\beta}^*$ introduced for a discrete defect loop. Without $\boldsymbol{\phi}^*$, it is shown to represent a terminating dislocation wall, i.e., a constant dislocation density on a surface terminating at the discrete dislocation line. This has been called the "dislocation model" of the discrete defect line. The elastic fields are derived.

Section 10 examines the meaning of $\boldsymbol{\phi}^*$ for a discrete loop. Without $\boldsymbol{\beta}^*$, it is shown to represent a compensated disclination loop, i.e., a surface with a constant dislocation density (opposite to that of sec. 9) terminating at a discrete disclination loop. The elastic fields of this defect vanish.

In an appendix we develop a special notation to deal with delta functions on curves and surfaces. This notation is very convenient and simplifies the equations that occur when we treat discrete defects.

Throughout the development of this paper we find that many concepts or quantities from dislocation theory generalize into pairs in defect theory. For example, dislocations generalize to defects, consisting of disclinations and dislocations, or the Burgers vector generalizes to the characteristic vectors, consisting of the Frank vector and the total Burgers vector. We have found it useful to introduce the new concept of "basic fields," consisting of the strain and bend-twist. Then the distortion in dislocation theory generalizes to the basic fields in defect theory. The nomenclature that has developed is summarized in tables 1 and 2.

This paper basically addresses itself to solving boundary value problems. The important subject of the forces on and the energy of the defects introduces additional complications. It is therefore omitted and will be treated elsewhere.

Neither shall we treat applications to special problems in the present paper. These will also be left for future publications [25, 26].

2. General Solution of the Plastic Strain Problem

2.1. Statement of the Problem

In this section we give a formal solution of the following problem, which can be posed without specifying the nature of the defects involved: given an infinitely extended homogeneous anisotropic body with the plastic strain e^p_{kl} given as a prescribed function of space. To find the resulting total displacement u^T_m throughout the body.

This problem is a generalization of Eshelby's [11] "transformation problem" to an anisotropic medium and an inhomogeneous stress free strain. We remark here that the concept of "stress free strain" is identical to that of plastic strain.

The statement of this problem can be rephrased in a manner that is almost identical to that of the classical problem of elasticity, i.e., in terms of the equation of equilibrium, Hooke's law, and the definition of strain. Using this approach we shall derive the solution to both problems simultaneously.

The equation of equilibrium for the stress σ_{ij} is:[4]

$$\sigma_{ij,i}+f_j=0,\ (i,\ j=1,\ 2,\ 3), \tag{2.1}$$

where f_i is the body force per unit volume. Here we have used the Einstein summation convention, and the subscripted comma followed by the index i indicates partial differentiation: $\partial\sigma_{ij}/\partial x_i$. The stress is related to the elastic strain e_{kl} by Hooke's law:

$$\sigma_{ij}=C_{ijkl}e_{kl}, \tag{2.2}$$

where the C_{ijkl} are the anisotropic elastic constants. Since σ_{ij} and e_{kl} are symmetric it follows that [5]

$$C_{ijkl}=C_{jikl}=C_{ijlk}. \tag{2.3}$$

The total strain e^T_{kl} is defined by [6]

$$e^T_{kl}\equiv u^T_{(l,k)}. \tag{2.4}$$

In general the total deformation is not completely elastic, but part of it is stress free or plastic, so that

$$e^T_{kl}=e_{kl}+e^p_{kl}. \tag{2.5}$$

The above relations are conveniently combined into the expression

$$C_{ijkl}u^T_{l,ki}+f_j=C_{ijkl}e^p_{kl,i}.$$

This is the set of partial differential equations we wish to solve for u^T_l when f_j and e^p_{kl} are given.

2.2. Definition and Application of Green's Tensor

To integrate the eq (2.6) it is useful to introduce Green's tensor function $G_{jn}(\mathbf{r})$, which represents the displacement in the x_j direction at the field point $\mathbf{r}$ arising from a point force in the x_n direction at the origin. Thus G_{jn} for an infinitely extended body is defined by

---

[4] Cartesian coordinates are used for simplicity.

[5] If an elastic strain energy function exists, we also have the symmetry condition $C_{ijkl}=C_{klij}$, but we do not need this relation in the present paper.

[6] We define the symmetric part of a tensor T_{ij} by $T_{(ij)}=1/2\ (T_{ij}+T_{ji})$. When T_{ij} is a complicated expression involving many other subscripts we shall also write equivalently $(T_{ij})_{(ij)}$.

$$C_{ijkl}G_{jn,ik}(\mathbf{r})+\delta_{ln}\delta(\mathbf{r})=0 \tag{2.7}$$

together with boundary condition that G_{jn} vanish at infinity.[7] Here δ_{ln} is the Kronecker delta and $\delta(\mathbf{r})$ is the three-dimensional Dirac delta function. The latter is defined in appendix B, where we also show that it is homogeneous of degree (-3) in r. Therefore it follows from (2.7) and the boundary conditions that $G_{jn}(\mathbf{r})$ is homogeneous of degree (-1), i.e., $G_{jn}(\mathbf{r})$ varies as r^{-1}.

We can now derive the solution of (2.6) in terms of Green's tensor. Writing for the relative radius vector

$$\mathbf{R}=\mathbf{r}-\mathbf{r}' \tag{2.8}$$

we have by (B3) and (2.7)

$$\begin{aligned} u_n^T(\mathbf{r}) &= \int \delta_{ln}\delta(\mathbf{R})u_l^T(\mathbf{r}')dV' \\ &= -\int C_{ijkl}G_{jn,ik}(\mathbf{R})u_l^T(\mathbf{r}')dV', \end{aligned} \tag{2.9}$$

where the integrations are taken over all space. Now, for any tensor $T(\mathbf{R})$, which is a function of $\mathbf{R}$ only, it follows from (2.8) that

$$T_{,i}(\mathbf{R})=-T_{,i'}(\mathbf{R})\equiv-\partial T/\partial x_i'. \tag{2.10}$$

Therefore we can also write (2.9) as follows [8]

$$u_n^T(\mathbf{r})=-\int C_{ijkl}G_{jn,i'k'}(\mathbf{R})u_l^T(\mathbf{r}')dV'. \tag{2.11}$$

By the divergence theorem, (A1) in appendix A, this relation can be transformed into

$$u_n^T(\mathbf{r})=-\oint C_{ijkl}G_{jn,i'}(\mathbf{R})u_l^T(\mathbf{r}')\,dS_k'+\oint C_{ijkl}G_{jn}(\mathbf{R})u_{l,k'}^T(\mathbf{r}')\,dS_i'-\int C_{ijkl}G_{jn}(\mathbf{R})u_{l,k'i'}^T(\mathbf{r}')dV', \tag{2.12}$$

where the surface integrals are taken at infinity. This step is usually called partial integration. The above relations hold only if the integrals converge.

We now assume the following boundary condition: The total displacement $u_l^T(\mathbf{r})\to 0$ as $r\to\infty$. Then $u_{l,k}^T(\mathbf{r})$ will approach zero faster than r^{-1} as $r\to\infty$. Hence in view of the behavior of G_{jn}, the integrands of the surface integrals in (2.12) will approach zero faster than $(r')^{-2}$ as $r'\to\infty$, and so these integrals will vanish. With this condition we also see that the volume integrals in (2.9), (2.11), and (2.12) converge. Thus we have by (2.6)

$$u_n^T(\mathbf{r})=\int G_{jn}(\mathbf{R})[f_j(\mathbf{r}')-C_{ijkl}e_{kl,i'}^P(\mathbf{r}')]dV'. \tag{2.13}$$

2.3. Solution of Classical Elasticity Problem

In classical elasticity, which we also call compatible theory, there is no plasticity, $e_{kl}^P=0$, and therefore (2.13) reduces to

$$u_n^T(\mathbf{r})=\int G_{jn}(\mathbf{R})\,f_j(\mathbf{r}')dV'. \tag{2.14}$$

---

[7] If $C_{ijkl}=C_{klij}$, we also have the symmetry relation $G_{jn}=G_{nj}$ for an infinitely extended body, but we do not need this relation in the present paper.

[8] In (2.11) the Einstein summation convention also applies between the primed and unprimed indices.

This is the well-known classical solution, which is almost obvious if we remember the meaning of Green's tensor. In view of (2.6) and the boundary condition on u_i^T, it is necessary to assume the following condition: The prescribed body force $f_j(\mathbf{r})$ must approach zero faster than r^{-2} as $r \to \infty$. This requirement also insures that the integrand of (2.14) approaches zero faster than $(r')^{-3}$ as $r' \to \infty$, so that the integral is finite.

2.4. Solution of the Plastic Strain Problem

In the present problem, which we also call incompatible theory, there is plasticity, but no body force, $f_j = 0$, and therefore (2.13) reduces to

$$u_n^T(\mathbf{r}) = -\int C_{ijkl} G_{jn}(\mathbf{R}) e^P_{kl,i'}(\mathbf{r}')\, dV'$$

$$= -\int C_{ijkl} G_{jn,i}(\mathbf{R}) e^P_{kl}(\mathbf{r}')\, dV' \tag{2.15}$$

by another partial integration and (2.10). Again we have taken the surface integral to vanish in the partial integration, and for this it is sufficient to assume the following condition: The prescribed plastic strain $e^P_{kl}(\mathbf{r})$ must approach zero faster than r^{-1} as $r \to \infty$. This requirement is consistent with the boundary condition on u_i^T in view of (2.6). Furthermore, the integrand of (2.15) will then approach zero faster than $(r')^{-3}$ as $r' \to \infty$, so that the integral is finite.

Equation (2.15) applies to any defect which can be described by the given plastic strain. It forms the basis for all subsequent applications to statics, where the same boundary condition on μ_i^T and the condition on e^P_{kl} must be satisfied. A similar result was derived by Mura [13], for a time-dependent plastic deformation. The above derivation emphasizes that it is only necessary to know the plastic strain (and not the plastic distortion), and it gives the condition it has to satisfy, as well as the boundary condition on the displacement, to find the solution for an infinitely extended body.

In the subsequent developments the results under geometry will hold regardless of the behavior at infinity, but those under statics are subject to the boundary conditions stated here because of the partial integrations involved.

2.5. Eshelby's Method

Physical science abounds with so-called "tricks" used to overcome mathematical difficulties. During the development of the mathematical theory of dislocations, Eshelby's bag of tricks has been remarkable. We wish to show how one of his recipes can be generalized to obtain (2.15).

He calculates the displacement for his transformation problem with the help of a sequence of imaginary cutting, straining and welding operations [11]. He does this so that he can introduce a fictitious body force simultaneously with the transformed inclusion such that there is no displacement. Then, he removes the body force and finds the resulting displacement from the classical expression.

To generalize this approach to our case it is presumably necessary to conceive of a continuous distribution of cutting, straining and welding operations. It is not important whether or not this can be imagined, because the formal steps are the same as in Eshelby's recipe. With the plastic strain e^P_{kl} we introduce a fictitious body force given by

$$f_j = C_{ijkl}\, e^P_{kl,i}. \tag{2.16}$$

Then (2.13) shows that there is no displacement. Next, we remove this body force by applying an equal but opposite body force $-f_j = -C_{ijkl}\, e^P_{kl,i}$ to the body. From (2.14) this leads to the displacement

$$u_n^T(\mathbf{r}) = -\int C_{ijkl}\, G_{jn}(\mathbf{R})\, e^P_{kl,i'}(\mathbf{r}')\, dV'$$

in agreement with (2.15). So the moral of Eshelby's method is that a defect described by the plastic strain e^P_{kl} can be simulated by the fictitious body force given by $-C_{ijkl}\, e^P_{kl,i}$.

2.6 Compatible Plastic Strain

There is an interesting consequence of (2.15) if the plastic strain is derivable from a plastic displacement

$$e^P_{kl} = u^P_{(l,k)}. \tag{2.17}$$

This will be called a compatible plastic strain. Then we have

$$\begin{aligned} u^T_n(\mathbf{r}) &= -\int C_{ijkl}\, G_{jn,i}(\mathbf{R})\; u^P_{l,k'}(\mathbf{r}')\; dV' \\ &= -\int C_{ijkl}\, G_{jn,ik}(\mathbf{R})\; u^P_l(\mathbf{r}')\; dV' \\ &= \int \delta_{in}\, \delta(\mathbf{R})\; u^P_l(\mathbf{r}')\; dV' \\ &= u^P_n(\mathbf{r}). \end{aligned} \tag{2.18}$$

Here the second equality follows by a partial integration, and the third by (2.7). It follows therefore that when the plastic strain is compatible, the elastic displacement vanishes:

$$u_n = u^T_n - u^P_n = 0. \tag{2.19}$$

Hence, in this case all elastic fields vanish.

3. Review of Dislocation Theory

3.1. Continuous Distribution of Dislocations

3.1.1. Geometry

If in addition to the plastic strain e^P_{kl}, the plastic rotation ω^P_q is also prescribed, then we can identify the defects as dislocations. In this case we can say that the plastic distortion (I5.1)[9]

$$\beta^P_{kl} = e^P_{kl} + \epsilon_{klq}\omega^P_q \tag{3.1}$$

is prescribed arbitrarily as a function of space, where ϵ_{klq} is the permutation symbol. Here e^P_{kl} is the symmetric part of β^P_{kl}

$$e^P_{kl} = \beta^P_{(kl)}, \tag{3.2}$$

and the second term in (3.1) is the antisymmetric part of β^P_{kl}, or

$$\omega^P_q = 1/2\; \epsilon_{klq}\beta^P_{kl}\,. \tag{3.3}$$

The dislocation density is defined by (I5.2)

$$\alpha_{pl} \equiv -\epsilon_{pmk}\, \beta^P_{kl,m}, \tag{3.4}$$

or, equivalently,

$$\epsilon_{pmk}\alpha_{pl} \equiv \beta^P_{ml,k} - \beta^P_{kl,m}. \tag{3.5}$$

[9] The symbol (I5.1) refers to eq (5.1) in reference [3].

This definition implies we are using sign convention *A*, or **FS**/*RH* [14]. The continuity condition for dislocations (I5.4)

$$\alpha_{pl,\,p} = 0 \tag{3.6}$$

follows directly from (3.4). It implies that dislocations can not end inside the body.

We define a Burgers circuit as any closed curve λ inside the body (fig. 1). The Burgers vector

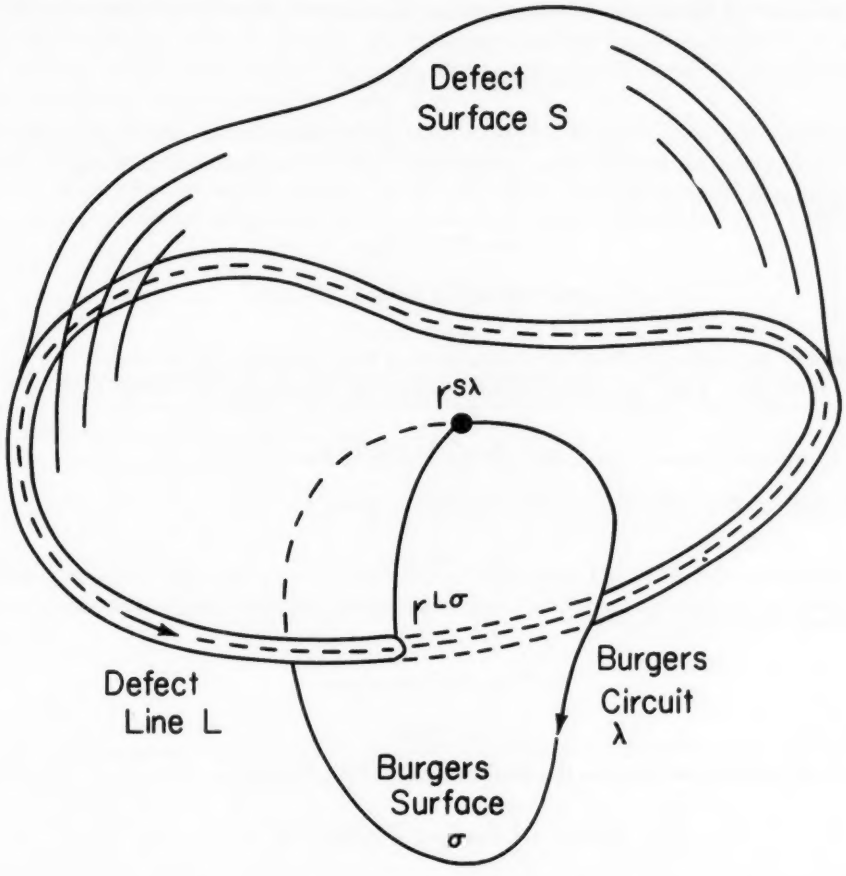

FIGURE 1. *Geometry of the discrete defect line* L, *its defect surface* S, *a Burgers circuit* λ, *and its Burgers surface* σ.

The surfaces *S* and σ are arbitrary and curved, subject only to the condition that they terminate on *L* and λ. The intersection of *L* with σ is labeled $\mathbf{r}^{L\sigma}$ and λ crosses *S* at $\mathbf{r}^{S\lambda}$. These are positive crossings by the right-hand rule.

associated with λ is defined by the closed line integral

$$b_l \equiv -\oint_\lambda \beta^p_{kl} dL_k . \tag{3.7}$$

This relation can be interpreted as follows: Starting with a perfect crystal we can imagine that the plastic deformation is produced by letting dislocations migrate into the crystal. A number of dislocations cut through λ, producing relative displacements $-\beta^p_{kl}dL_k$ in the lattice at the curve. By adding these contributions we measure the resultant Burgers vector of all the dislocations that

remain stuck through the surface σ bounded by λ. From (3.4) and Stokes' theorem (A2) we can also write

$$b_l = \int_\sigma \alpha_{pl} dS_p. \tag{3.8}$$

This relation shows that the dislocation density α_{pl} represents the flux of dislocation (or Burgers vector) in the x_l direction that crosses unit area of a plane normal to the x_p direction.

The existence of the plastic distortion implies the existence of the elastic distortion (I2.1 and I5.5)

$$\beta^T_{mn} \equiv u^T_{n,\,m} = \beta_{mn} + \beta^P_{mn}. \tag{3.9}$$

Since the existence of plastic distortion implies there are no disclinations, this relation holds only if there are no disclinations present. This relation also allows us to draw the following conclusions from the definitions (3.4) and (3.7)

$$\epsilon_{pmk}\,\beta_{kl,\,m} = \alpha_{pl}, \tag{3.10}$$

$$\oint_\lambda \beta_{kl}\, dL_k = b_l. \tag{3.11}$$

These relations are called the basic geometric laws or field equations for α_{pl} and b_l.

Other quantities, which we shall find useful later, are the plastic bend-twist (I5.16)

$$\kappa^P_{kq} \equiv \omega^P_{q,\,k} = 1/2\,\epsilon_{lqr}\,\beta^P_{rl,\,k}, \tag{3.12}$$

where the last equality follows from (3.3), the elastic strain

$$e_{mn} = \beta_{(mn)}, \tag{3.13}$$

and the elastic bend-twist (I5.18)

$$\kappa_{st} \equiv \omega_{t,\,s} = 1/2\,\epsilon_{tmn}\,\beta_{mn,\,s}. \tag{3.14}$$

3.1.2. Statics

From (3.2) and (2.3) we find that the displacement (2.15) becomes

$$u^T_n(\mathbf{r}) = -\int C_{ijkl} G_{jn,\,i}(\mathbf{R})\,\beta^P_{kl}(\mathbf{r}')\,dV', \tag{3.15}$$

where $\beta^P_{kl}(\mathbf{r})$ must satisfy the condition that it approaches zero faster than r^{-1} as $r \to \infty$. From this relation we find the total distortion

$$\begin{aligned} u^T_{n,\,m}(\mathbf{r}) &= -\int C_{ijkl} G_{jn,\,im}(\mathbf{R})\,\beta^P_{kl}(\mathbf{r}')\,dV' \\ &= -\int C_{ijkl} G_{jn,\,i}(\mathbf{R})\,\beta^P_{kl,\,m'}(\mathbf{r}')\,dV' \\ &= \int C_{ijkl} G_{jn,\,i}(\mathbf{R})\,[\epsilon_{pmk}\alpha_{pl}(\mathbf{r}') - \beta^P_{ml,\,k'}(\mathbf{r}')]\,dV' \\ &= \int \epsilon_{pmk} C_{ijkl} G_{jn,\,i}(\mathbf{R})\,\alpha_{pl}(\mathbf{r}')\,dV' + \beta^P_{mn}(\mathbf{r}). \end{aligned} \tag{3.16}$$

Here the first equality follows simply by differentiating under the integral sign, where Green's tensor is the only function depending on $\mathbf{r}$, the second equality by a partial integration, the third from (3.5), and the fourth by a partial integration, (2.7) and (B3). From (3.9) we obtain the elastic distortion

$$\beta_{mn}(\mathbf{r}) = \int \epsilon_{pmk} C_{ijkl} G_{jn,i}(\mathbf{R})\, \alpha_{pl}(\mathbf{r}')\, dV'. \tag{3.17}$$

This is Mura's half of the Mura-Willis formula [12, 13, 15]. Willis' half would be included if (2.14) had also been included in the derivation. We note that from the above condition on β^P_{kl} and (3.4) that $\alpha_{pl}(\mathbf{r})$ must vanish faster than r^{-2} as $r \to \infty$. However, for the integral (3.17) to exist it is only necessary that $\alpha_{pl}(r)$ vanish faster than r^{-1} as $r \to \infty$.

Here we note that α_{pl} is a state quantity because it can be measured in the present state of the body, (e.g., by electron microscopy or x rays). Therefore (3.17) shows that β_{mn} is also a state quantity, because it is expressed entirely in terms of α_{pl}. On the other hand, for example, β^P_{mn} may not be a state quantity, because one may not be able to measure it without knowledge of the former states of the body.

3.2. The Discrete Dislocation Line

3.2.1. Geometry

The discrete dislocation line L is defined as the boundary of a surface S, where the material below S has been plastically displaced with respect to the material above S by an amount given by the constant Burgers vector b_l (fig. 1).

Hence, the difference between the displacement just below and above S is given by

$$[u_l(\mathbf{r})] = b_l. \tag{3.18}$$

Our problem now is to find the corresponding plastic distortion. The following is a straightforward procedure we have developed to find it. Assume first that S is closed, enclosing the volume V. Then by (B7)

$$u^T_l(\mathbf{r}) = \delta(V)\, b_l \tag{3.19}$$

represents a displacement that is equal to b_l inside V and has the jump (3.18) at the surface S. The corresponding distortion is by (3.9)

$$\begin{aligned} \beta^T_{kl}(\mathbf{r}) &= u^T_{l,k}(\mathbf{r}) \\ &= \delta_{,k}(V)\, b_l \\ &= -\delta_k(S)\, b_l, \end{aligned} \tag{3.20}$$

where we have used the divergence theorem (B24). Here S is the closed boundary of V. We see that the distortion is concentrated at the surface S. Since this deformation is just a rigid translation of part of the body, there is no elastic distortion, and therefore the above distortion is all plastic. We now simply generalize this expression to the open surface S of the dislocation loop:

$$\beta^P_{kl}(\mathbf{r}) = -\delta_k(S)\, b_l. \tag{3.21}$$

The Burgers vector for continuous distributions of dislocations was defined in (3.7). We want to show that this definition agrees with the constant b_l introduced above. If λ is any closed curve that encircles L in the positive sense (fig. 1), it will cross S positively at some point $\mathbf{r}^{S\lambda}$. Therefore

$$-\oint_\lambda \beta_{kl}^p \, dL_k = \oint_\lambda \delta_k(S)\, b_l dL_k = b_l \tag{3.22}$$

by (3.21) and (B15).

Now we find the dislocation density from (3.4) and Stokes' theorem (B26)

$$\begin{aligned} \alpha_{pl}(\mathbf{r}) &= \epsilon_{pmk}\, \delta_{k,\,m}(S)\, b_l \\ &= \delta_p(L)\, b_l, \end{aligned} \tag{3.23}$$

where L is the closed boundary of S, i.e., the dislocation line. The vector $\delta_p(L)$ is the Dirac delta function on the curve L and it is always parallel to L. A discrete dislocation line is called screw or edge when the Burgers vector is parallel or normal to the line, respectively. Therefore (3.23) shows that the diagonal and off-diagonal components of α_{pl} represent the screw and edge component of the dislocation density, respectively (see table 1). Equation (3.23) shows how to make the transition

TABLE 1. *Definition of various defect quantities*

Quantity	Dislocation	Name of component	
	Disclination	Diagonal	Off-diagonal
Density tensor for continuous distribution of defects.	$\boldsymbol{\alpha}$	screw	edge
	$\boldsymbol{\theta}$	wedge	twist
Density tensor for continuous distribution of infinitesimal defect loops.	$\boldsymbol{\gamma}$ or $\boldsymbol{\beta}^*$	prismatic	slip
	$\boldsymbol{\zeta}$ or $\boldsymbol{\phi}^*$	twist	wedge

from a continuous distribution of dislocations to a discrete dislocation line. We note that it satisfies the continuity condition (3.6)

$$\alpha_{pl,\,p}(\mathbf{r}) = \delta_{p,\,p}\,(L)\, b_l = 0, \tag{3.24}$$

by (B28). As a cross-check we also show that (3.8) is satisfied by (3.23) (fig. 1)

$$\int_\sigma \alpha_{pl}\, dS_p = \int_\sigma \delta_p(L)\, b_l dS_p = b_l, \tag{3.25}$$

where we have used (B15) again. This last relation remains valid for many dislocation lines, and therefore can be used to show how to make the transition from discrete dislocation lines to a continuous distribution of dislocations: For many dislocation lines the average dislocation density α_{pl} represents the x_l component of the sum of the Burgers vectors of all the dislocation lines that intersect unit area of a plane normal to the x_p direction. For another interpretation of α_{pl} consider the result

$$\begin{aligned} \int_V \alpha_{pl}(\mathbf{r})\, dV &= \int \delta_p(L)\, b_l\, dV \\ &= b_l \int \delta_p(L)\, \delta(V)\, dV \\ &= b_l \oint_L \delta\,(V)\, dL_p \\ &= b_l \int_{L(V)} dL_p. \end{aligned} \tag{3.26}$$

Here the first equality follows from (3.23), the second from (B7), the third from (B11), and the fourth from (B7), where $L(V)$ is the part of the curve L inside V only. From this expression we see that the average dislocation density α_{pl} also represents the sum of the x_l component of the Burgers vectors times the projected line length in the x_p direction of all the dislocation lines per unit volume. The equivalence of the above two interpretations of the average dislocation density can also be shown by the methods of quantitative stereology [16].

We wish to point out here that there is also another type of dislocation density in wide use, primarily by experimentalists. This is the total dislocation line length per unit volume, usually designated by ρ:

$$\int_V \rho(\mathbf{r})\, dV = \int_{L(V)} dL. \tag{3.27}$$

It is easy to show that

$$\rho(\mathbf{r}) = t_p \delta_p(L), \tag{3.28}$$

where t_p is the unit tangent to the dislocation line. Hence the relation between the two different dislocation densities is

$$\rho b^2 = t_p \alpha_{pl} b_l \tag{3.29}$$

from (3.23).

3.2.2. Statics

Now we substitute (3.21) into (3.15) to find the displacement of a discrete dislocation line.

$$\begin{aligned} u_n^T(\mathbf{r}) &= \int C_{ijkl} G_{jn,i}(\mathbf{R})\, \delta_k(S')\, b_l dV' \\ &= \int_S C_{ijkl} G_{jn,i}(\mathbf{R})\, b_l dS'_k, \end{aligned} \tag{3.30}$$

using (B12). This equation allows us to estimate the asymptotic behavior of the displacement at large distances from a small dislocation loop. It is simply the same as the asymptotic behavior of the integrand. Since Green's tensor $G_{jn}(\mathbf{r})$ varies as r^{-1}, we see that $u_n^T(\mathbf{r})$ will vary as r^{-2} as $r \to \infty$. Since the strain $e_{mn}(\mathbf{r})$ varies as the derivative of the displacement, it will go as r^{-3} as $r \to \infty$. These results are listed in table 3. A more accurate calculation of the asymptotic displacement from a small loop can also be made from (3.30) by expanding Green's tensor as a Taylor series in $\mathbf{r}'$ for a few terms and integrating over S. If this result is specialized to isotropy, we find the same relations as were given by Kroupa [17]. The details will be shown in a future publication [26].

We now find the total distortion from (3.30)

$$\begin{aligned} u_{n,m}^T(\mathbf{r}) &= \int_S C_{ijkl} G_{jn,im}(\mathbf{R})\, b_l dS'_k \\ &= \oint_L \epsilon_{pmk} C_{ijkl} G_{jn,i}(\mathbf{R})\, b_l dL'_p + \int_S C_{ijkl} G_{jn,ik}(\mathbf{R})\, b_l dS'_m \\ &= \oint_L \epsilon_{pmk} C_{ijkl} G_{jn,i}(\mathbf{R})\, b_l dL'_p + \beta_{mn}^p(\mathbf{r}). \end{aligned} \tag{3.31}$$

Here the first equality follows by simply differentiating under the integral sign, where Green's

tensor is the only function depending on $\mathbf{r}$, the second equality follows from Stokes' theorem (A4), and the third from (2.7), (B5), and (3.21). From (3.9) we then obtain the elastic distortion

$$\beta_{mn}(\mathbf{r}) = \oint_L \epsilon_{pmk} C_{ijkl} G_{jn,i}(\mathbf{R})\, b_l dL'_p \tag{3.32}$$

This relation can of course also be obtained directly from (3.17), (3.23), and (B11). A similar result was derived by Mura [13] for a moving dislocation line.

We see that the state quantity β_{mn} can be written as a line integral along the discrete dislocation, i.e., it is expressed entirely in terms of an integral over the only regions of the body where the defect is localized. In general, we suggest that for a defect which is a state quantity, the necessary and sufficient condition for an associated field quantity to be a state quantity is that it can be written as an integral over the defect. For a line defect this means that the state quantity must be a line integral along the defect.

Equation (3.32) also allows us to estimate the asymptotic behavior of the distortion, and hence the strain, at large distances from a straight dislocation line. Due to the integration it is simply the same as that of Green's tensor, i.e., $\beta_{mn}(\mathbf{r})$ and $e_{mn}(\mathbf{r})$ vary as r^{-1} as $r \to \infty$. Since the displacement u_n^T is an integral of the distortion, it will vary as $\ln r$ as $r \to \infty$. These well-known results are also listed in table 3.

3.3. Continuous Distribution of Infinitesimal Dislocation Loops

In section 3.1 the dislocation density and the Burgers vector were defined by (3.4) and (3.7) in terms of the given plastic distortion. A consequence of these definitions is (3.8), relating the Burgers vector to the dislocation density. This equation could alternatively be used to define the dislocation density in terms of the Burgers vector, if this quantity is prescribed in a suitable manner. It is convenient to put this relation into differential form. When the dislocations are continuously distributed the density tensor is defined locally by

$$\alpha_{pl} \equiv \frac{\Delta b_l}{\Delta S_p}. \tag{3.33}$$

As we noted above, for a distribution of discrete dislocations this represents the average dislocation density, where Δb_l is the lth component of the resulting Burgers vectors of all the dislocations which pierce through a surface element ΔS_p oriented normal to the x_p direction at the given point.

In a similar way Kroupa [5] introduced the dislocation loop density tensor. He defined it as follows: γ_{kl} represents the flux of dislocation (or Burgers vector) in the x_l direction that encloses a unit vector in the x_k direction. When the loops are continuously distributed the density tensor γ_{kl} is a function of the position and is defined locally by

$$\gamma_{kl} \equiv \frac{\Delta b_l}{\Delta L_k}. \tag{3.34}$$

Again, for a distribution of discrete loops this represents the average dislocation loop density, where now Δb_l is the lth component of the resulting Burgers vectors of all the loops which are pierced by the line element ΔL_k oriented in the x_k direction at the given point.

To find the relation between the dislocation loop density and the plastic distortion, we first convert (3.34) to integral form

$$b_l = \oint_\lambda \gamma_{kl} dL_k. \tag{3.35}$$

Now we compare this relation to the definition (3.7). The integrands can only differ by a gradient with respect to x_k. Therefore we can set

$$\beta^p_{kl} = -\gamma_{kl} + u^p_{l,k}, \tag{3.36}$$

where u^p_l is an arbitrary vector field. This relation identifies the plastic distortion for a continuous distribution of dislocation loops. With it we can find all the relations derived in section 3.1 in terms of loops. For example, (3.4) leads to

$$\alpha_{pl} = \epsilon_{pmk}\, \gamma_{kl,m}. \tag{3.37}$$

This is the fundamental relation between the dislocation loop density and the corresponding dislocation density. Since a plastic displacement does not contribute to the elastic fields, (c.f. sec. 2.6), we can set $u^p_l = 0$, without loss of generality and so we can use

$$\beta^p_{kl} = -\gamma_{kl} \tag{3.38}$$

for the purpose of calculating the fields of a continuous distribution of dislocation loops. This agrees with Kroupa's identification. Hence we can identity the plastic distortion with the dislocation loop density, except for a minus sign.

We now also can give an interpretation of (3.21) in terms of infinitesimal loops. To construct a discrete dislocation line L, we distribute a constant density of infinitesimal dislocation loops of strength b_l over any surface S, whose boundary is L. This method could be taken as an alternative to the definition of the discrete dislocation line given at the beginning of section 3.2. So we conclude that for a finite dislocation loop the loop density is given by

$$\gamma_{kl}(\mathbf{r}) = \delta_k(S)\, b_l, \tag{3.39}$$

where S is a surface that spans the dislocation line. The vector $\delta_k(S)$ is the Dirac delta function on the surface S and it is always normal to S. In a plane we have a prismatic or a slip loop according to whether the Burgers vector is normal or parallel to S, respectively. Therefore (3.39) shows that the diagonal and off-diagonal components of γ_{kl} represent the prismatic and slip components of the dislocation loop density, respectively (see table 1). Equation (3.39) shows how to make the transition from a continuous distribution of infinitesimal loops to a finite loop. By (B15) we see that it satisfies (3.35), which also remains valid for many finite loops, and therefore can be used for the transition from finite loops to a continuous distribution: For many finite dislocation loops the average dislocation loop density γ_{kl} represents the x_l component of the sum of the Burgers vectors of all the loops whose surfaces are intersected by a unit vector in the x_k direction. For another interpretation of γ_{kl} consider the result

$$\begin{aligned}\int_V \gamma_{kl}(\mathbf{r})\, dV &= \int_V \delta_k(S)\, b_l dV \\ &= b_l \int \delta_k(S)\, \delta(V)\, dV \\ &= b_l \int_S \delta(V)\, dS_k \\ &= b_l \int_{S(V)} dS_k.\end{aligned} \tag{3.40}$$

Here the first equality follows from (3.39), the second from (B7), the third from (B12), and the fourth from (B7), where $S(V)$ is the part of the surface S inside V only. From this expression we see that the average dislocation loop density γ_{kl} also represents the sum of the x_l component of the Burgers vectors times the projected area on a plane normal to the x_k direction of all the dislocation loops per unit volume. The equivalence of the above two interpretations of the average dislocation loop density can also be shown by the methods of quantitative stereology [16].

3.4. The Dislocation Dipole

Kroupa [18] has also treated the fields of a dislocation dipole, i.e., a close pair of dislocations with opposite Burgers vectors. In this section we wish to present some general formulas for such a defect.

3.4.1. General Definition of a Dipole

We first give a very general definition of the dipole conjugate to any defect, following a similar line of reasoning as Kroupa used. The dipole is composed of two parts: the first is obtained from the basic defect by translating it through a small distance, and the second is the negative of the basic defect at its original position. To give this concept a mathematical formulation, let the basic defect be given as a function of position $\mathbf{r}$ by the source function $S(\mathbf{r})$. For example, this could be e^p_{kl} of section 2, or α_{pl} of section 3.1. If this defect is rigidly translated through a distance $\boldsymbol{\xi}$, the source function of the new defect configuration becomes $S(\mathbf{r}-\boldsymbol{\xi})$. Hence the source function of the conjugate dipole is given by

$$S^D(\mathbf{r}) = S(\mathbf{r}-\boldsymbol{\xi}) - S(\mathbf{r}). \tag{3.41}$$

This result applies to a finite dipole.

For a discrete defect concentrated on a point, line, or surface, it is customary to deal with the infinitesimal dipole. It is obtained by letting $\boldsymbol{\xi}$ approach zero and the strength of the basic defect approach infinity in such a way that the field of the dipole remains finite. If $\boldsymbol{\xi}$ is infinitesimal, we can use Taylor's expansion to write (3.41) as follows:

$$S^D(\mathbf{r}) = -\xi_i S_{,i}(\mathbf{r}). \tag{3.42}$$

We see that our definition has the opposite sign from Kroupa's, but it agrees with the convention in electrodynamics. We shall now show that a similar relation holds between the fields of a defect and its conjugate dipole. Let the field of the basic defect be given by the generic expression:

$$f(\mathbf{r}) = \int G(\mathbf{R}) S(\mathbf{r}')\, dV', \tag{3.43}$$

where $G(\mathbf{R})$ is some kernel of integration. For example, (2.15) and (3.17) have this form. The corresponding field of the conjugate dipole is

$$\begin{aligned} f^D(\mathbf{r}) &= \int G(\mathbf{R}) S^D(\mathbf{r}')\, dV' \\ &= -\xi_i \int G(\mathbf{R}) S_{,i'}(\mathbf{r}')\, dV' \\ &= -\xi_i \int G_{,i}(\mathbf{R}) S(\mathbf{r}')\, dV' \\ &= -\xi_i f_{,i}(\mathbf{r}). \end{aligned} \tag{3.44}$$

Here the second equality follows from (3.42), the third by a partial integration, and the fourth from (3.43).

Equations (3.42) and (3.44) are the fundamental relations between functions of the basic defect and the corresponding function of its conjugate dipole. The basic defect here is arbitrary. It could for example be a dipole itself; in this case we obtain the dipole of a dipole, or a quadrupole. In this way all higher order multipoles are defined.

3.4.2. Application to the Discrete Dislocation Dipole

We now apply the above results to the case of a discrete dislocation line, figure 2. For example, the basic equation for the dislocation density is given by (3.23). Therefore the dislocation density

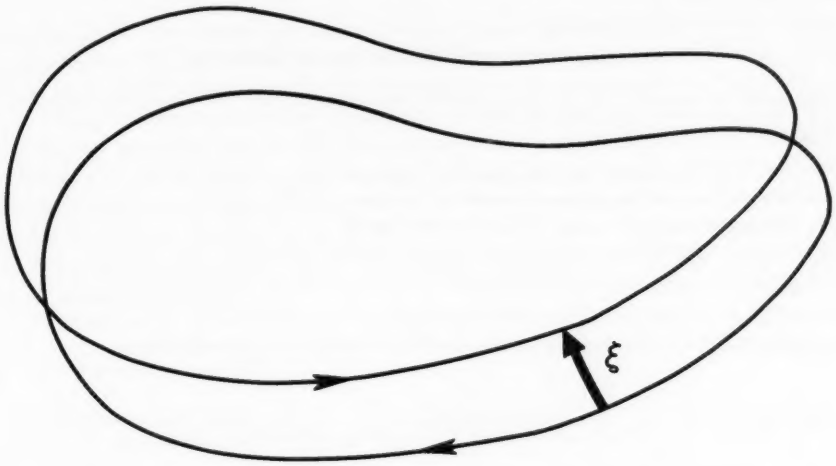

FIGURE 2. *The discrete defect dipole line conjugate to the basic defect line of figure 1.*
This figure shows the finite case. For the infinitesimal case $\xi \to 0$.

of the conjugate dislocation dipole is by (3.42):

$$\begin{aligned} \alpha^D_{pl}(\mathbf{r}) &= -\xi_m \alpha_{pl,m}(\mathbf{r}) \\ &= -\delta_{p,m}(L)\, b_l \xi_m. \end{aligned} \tag{3.45}$$

With this explicit expression we can clarify the meaning of the infinitesimal displacement ξ_m: We leg $\xi_m \to 0$ and $b_l \to \infty$ in such a way that $b_l \xi_m$ remains constant.

Next we find the displacement field of a dislocation dipole from (3.44)

$$\begin{aligned} u^D_n(\mathbf{r}) &= -\xi_m u^T_{n,m}(\mathbf{r}) \\ &= -\oint_L \epsilon_{pmk} C_{ijkl} G_{jn,i}(\mathbf{R})\, b_l \xi_m dL'_p + \delta_m(S)\, b_n \xi_m, \end{aligned} \tag{3.46}$$

where we have used (3.31) and (3.21). It is interesting to note that the last term in (3.46) can be made to vanish by choosing S to lie along $\boldsymbol{\xi}$, or $\xi_m dS'_m = 0$, i.e., by letting S be an infinitesimal strip connecting the basic dislocation to its displaced partner. As a consequence we see that the displacement of a dislocation dipole is a state quantity.

From (3.46) other static quantities can be derived, such as the distortion β^D_{mn}. The same result can alternatively be obtained by substituting (3.45) into (3.17).

Equation (3.46) also allows us to estimate the asymptotic behavior of the displacement at large distances from a straight dislocation dipole line. By comparison with (3.32) it is the same as that of the distortion of a straight dislocation line, i.e., it varies as r^{-1} as $r \to \infty$. Hence the strain will vary as r^{-2} as $r \to \infty$. These results are also listed in table 3. We note from the table that the dislocation dipole can be classified as a defect with properties between those of the dislocation line and the dislocation loop.

487-412 OL - 73 - 5

Sometimes a narrow elongated dislocation loop is regarded as a dipole. This is not possible with our definition, since the two components of our dipole must be disjoint. However, two parallel, infinite, straight dislocations with opposite Burgers vectors are included in our definition of a dipole. This dipole resembles an elongated loop. By contrast, it is possible to regard a dislocation dipole as a special type of loop.

4. Continuous Distribution of Defects

As discussed in section 1.1, we shall denote the combination of dislocations and disclinations by the word *defects*, see table 2.

TABLE 2. *Generalization from dislocation theory to defect theory*

Quantity	Dislocation theory	Defect theory
Defect density tensors	Dislocation density $\boldsymbol{\alpha}$	Dislocation density $\boldsymbol{\alpha}$ Disclination density $\boldsymbol{\theta}$
Basic plastic fields	Plastic distortion $\boldsymbol{\beta}^P$	Plastic strain $\mathbf{e}^P$ Plastic bend-twist $\boldsymbol{\kappa}^P$
Characteristic vectors	Burgers vector $\mathbf{b}$	Total Burgers vector $\mathbf{B}$ Frank vector $\boldsymbol{\Omega}$
Basic elastic fields	Elastic distortion $\boldsymbol{\beta}$	Elastic strain $\mathbf{e}$ Elastic bend-twist $\boldsymbol{\kappa}$
Jump conditions	Displacement jump $[\mathbf{u}]$	Displacement jump $[\mathbf{u}]$ Rotation jump $[\boldsymbol{\omega}]$
Defect loop density tensors	Dislocation loop density $\boldsymbol{\gamma}(\boldsymbol{\beta}^P)$	Dislocation loop density $\boldsymbol{\gamma}(\boldsymbol{\beta}^*)$ Disclination loop density $\boldsymbol{\zeta}(\boldsymbol{\phi}^*)$

4.1. Geometry

Consider now an infinitely extended body in which the plastic strain e^P_{kl} and bend-twist κ^P_{kq} are given as independently prescribed functions of space. For convenience we refer to these two functions as the *basic plastic fields*. Then we may have disclinations as well as dislocations. The dislocation and disclination densities are defined by (I6.3, I6.1)

$$\alpha_{pl} \equiv -\epsilon_{pmk}(e^P_{kl,\,m} + \epsilon_{klq}\kappa^P_{mq}), \tag{4.1}$$

$$\theta_{pq} \equiv -\epsilon_{pmk}\kappa^P_{kq,\,m}, \qquad (\theta_{qp} = -\epsilon_{qnl}\kappa^P_{lp,\,n}). \tag{4.2}$$

The continuity equations (16.8, 16.2)

$$\alpha_{pl,\,p} + \epsilon_{lpq}\theta_{pq} = 0, \tag{4.3}$$

$$\theta_{pq,\,p} = 0 \tag{4.4}$$

follow immediately from (4.1) and (4.2). The former means that dislocations can only end on disclinations, and conversely, if the disclination density is asymmetric, dislocations must emerge from it. The latter shows that disclinations cannot end inside the body.

Associated with the *Burgers circuit* λ we now define the *characteristic vectors*, the general Burgers vector B_l and the characteristic rotation vector Ω_q, which we have agreed to call the Frank vector in section 1.2, by

$$B_l \equiv -\oint_\lambda (e^P_{kl} - \epsilon_{lqr}\kappa^P_{kq}x_r)\,dL_k, \tag{4.5}$$

$$\Omega_q \equiv -\oint_\lambda \kappa^P_{kq}\,dL_k. \tag{4.6}$$

These relations can be interpreted as follows: Starting with a perfect crystal we can imagine that the plastic deformation is produced by letting defects migrate into the crystal. A number of them cut through λ. Every disclination that cuts through λ produces a relative rotation $-\kappa^P_{kq}dL_k$ in the lattice at the curve. These contributions added around the contour λ give the resultant Frank vector of all disclinations that remain stuck through the surface σ bounded by λ. The relation (4.5) is easily seen to be identical to (3.7), when κ^P_{kq} is given by (3.12), by doing a partial integration, where the integrated part vanishes, and using (3.1) or (3.2). Therefore, it is simply a generalization of (3.7). It represents the resultant Burgers vector of all defects (dislocations and disclinations) that have cut through λ and remain stuck through σ. We wish to emphasize that B_l does not represent the relative displacements added around the contour λ. The latter quantity is not an invariant for the curve λ, but depends on the point where the integration is started. The definition (4.5) is essentially motivated by Weingarten's theorem (section 5.1). By Stokes' theorem (A2) we have from (4.5–6), (I7.4, I7.3)

$$\begin{aligned} B_l &= -\int_\sigma \epsilon_{pmk}\,(e^P_{kl,\,m} - \epsilon_{lqm}\kappa^P_{kq} - \epsilon_{lqr}\kappa^P_{kq,\,m}x_r)\,dS_p \\ &= \int_\sigma (\alpha_{pl} - \epsilon_{lqr}\theta_{pq}x_r)\,dS_p, \end{aligned} \tag{4.7}$$

$$\begin{aligned} \Omega_q &= -\int_\sigma \epsilon_{pmk}\kappa^P_{kq,\,m}dS_p \\ &= \int_\sigma \theta_{pq}\,dS_p, \end{aligned} \tag{4.8}$$

using (4.1) and (4.2). Relation (4.7) shows that the disclination density θ_{pq} also contributes to the general Burgers vector, in addition to the dislocation density α_{pl}. Relation (4.8) shows that the disclination density θ_{pq} represents the flux of disclination (or Frank vector) in the x_q direction that crosses unit area of a plane normal to the x_p direction.

For later application we also write (4.1–2) in their equivalent forms

$$\epsilon_{pmk}\alpha_{pl} \equiv e^P_{ml,\,k} - e^P_{kl,\,m} + \epsilon_{pmk}\kappa^P_{lp} - \epsilon_{klm}\kappa^P, \tag{4.9}$$

$$\epsilon_{pmk}\theta_{pq} \equiv \kappa^P_{mq,\,k} - \kappa^P_{kq,\,m},\ (\epsilon_{qnl}\theta_{qp} = \kappa^P_{np,\,l} - \kappa^P_{lp,\,n}). \tag{4.10}$$

The incompatibility tensor is defined by (I4.1, I6.6)

$$\eta_{pq} \equiv \epsilon_{pmk}\epsilon_{qnl}e^P_{kl,\,mn} \tag{4.11}$$

$$= -\,(\epsilon_{qnl}\alpha_{pl,\,n} + \theta_{pq})_{(pq)}, \tag{4.12}$$

where the second equality follows from (4.1–2). The continuity equation for the compatibility (I4.2),

$$\eta_{pq,p} = 0, \tag{4.13}$$

follows immediately from (4.11).

With disclinations we claim that the total distortion is no longer the sum of an elastic and plastic part, (3.9), simply because β^{p}_{mn} is not defined. For, if β^{p}_{mn} existed, the plastic bend-twist would be the gradient of the plastic rotation, (3.12), and consequently the disclination density (4.1) would vanish.[10] Instead, since the plastic strain e^{p}_{kl} and bend-twist κ^{p}_{kq} are prescribed, we postulate the existence of the elastic strain e_{kl} and bend-twist κ_{kq}, which are called the *basic elastic fields*. So we have (I2.3, I4.3, I2.16, and I5.17):

$$e^{T}_{mn} \equiv u^{T}_{(n,m)} = e_{mn} + e^{P}_{mn}, \tag{4.14}$$

$$\kappa^{T}_{st} \equiv \omega^{T}_{t,s} = 1/2\, \epsilon_{tmn}\, u^{T}_{n,ms} = \kappa_{st} + \kappa^{P}_{st}. \tag{4.15}$$

Since it follows from (4.14–15) that

$$\epsilon_{pmk}\,(e^{T}_{kl,m} + \epsilon_{klq}\,\kappa^{T}_{mq}) = \epsilon_{pmk}\, u^{T}_{l,km} = 0, \tag{4.16}$$

these relations allow us to derive the following basic geometric laws or field equations for α_{pl} and θ_{pq} from (4.1–2), (I6.11, I6.10)

$$\epsilon_{pmk}\,(e_{kl,m} + \epsilon_{klq}\,\kappa_{mq}) = \alpha_{pl}, \tag{4.17}$$

$$\epsilon_{pmk}\,\kappa_{kq,m} = \theta_{pq}. \tag{4.18}$$

The geometric meaning of these equations is that the defects (dislocations and disclinations) are the sources of the basic elastic fields (elastic strain and bend-twist). It also follows from (4.14–15) that

$$e^{T}_{kl} - \epsilon_{lqr}\,\kappa^{T}_{kq}\,x_r = (u^{T}_{l} - u^{T}_{[l,r]}\,x_r)_{,k}, \tag{4.19}$$

and hence these relations also allow us to derive the basic geometric laws for B_l and Ω_q from (4.5–6), (I7.2, I7.1)

$$\oint_{\lambda} (e_{kl} - \epsilon_{lqr}\,\kappa_{kq}\,x_r)\, dL_k = B_l, \tag{4.20}$$

$$\oint_{\lambda} \kappa_{kq}\, dL_k = \Omega_q. \tag{4.21}$$

These may be regarded as the field equations in integral form, equivalent to (4.17–18). Finally, the relation (4.14) allows us to derive the basic geometric law or field equation for the incompatibility η_{pq} from (4.11), (I 4.4)

$$-\epsilon_{pmk}\,\epsilon_{qnl}\, e_{kl,mn} = \eta_{pq}, \tag{4.22}$$

which shows that we can isolate the incompatibility as the source of the elastic strain.

4.2. Statics

This section extends the work of reference [3], which gave only the geometry of a continuous distribution of defects, reviewed in section 4.1. The main result we shall find is an explicit and new expression for the elastic strain, eq (4.29), in terms of defect densities. We shall also find the elastic bend-twist.

---

[10] This situation is analogous to the case of pure dislocations: There the total displacement is no longer the sum of an elastic and plastic part, $u^{T}_{l} = u_l + u^{p}_{l}$. For, if u^{p}_{l} existed, the plastic distortion would be a gradient, $\beta^{p}_{kl} = u^{p}_{l,k}$, and the dislocation density (3.4) would vanish.

We find the total distortion from (2.15)

$$\begin{aligned} u^T_{n,m}(\mathbf{r}) &= -\int C_{ijkl} G_{jn,im}(\mathbf{R}) e^P_{kl}(\mathbf{r}')\, dV' \\ &= -\int C_{ijkl} G_{jn,i}(\mathbf{R}) e^P_{kl,m'}(\mathbf{r}')\, dV' \\ &= \int C_{ijkl} G_{jn,i}(\mathbf{R}) [\epsilon_{pmk}\alpha_{pl}(\mathbf{r}') - e^P_{ml,k'}(\mathbf{r}') - \epsilon_{pmk}\kappa^P_{lp}(\mathbf{r}')]\, dV' \\ &= \int \epsilon_{pmk} C_{ijkl} G_{jn,i}(\mathbf{R}) [\alpha_{pl}(\mathbf{r}') - \kappa^P_{lp}(\mathbf{r}')]\, dV' + e^P_{mn}(\mathbf{r}). \end{aligned} \tag{4.23}$$

Here the second equality follows by a partial integration, the third from (4.9) and (2.3), and the fourth by a partial integration, (2.7) and (B3). We see that for the integral to converge it is only necessary that $\alpha_{pl}(\mathbf{r})$ and $\kappa^P_{lp}(\mathbf{r})$ vanish faster than r^{-1} as $r \to \infty$. From this relation we now proceed to derive the basic elastic fields and show that they are state quantities.

The elastic strain is found from (4.14)[11]

$$e_{mn}(\mathbf{r}) = \int \epsilon_{pmk} C_{ijkl} G_{jn,i}(\mathbf{R}) [\alpha_{pl}(\mathbf{r}') - \kappa^P_{lp}(\mathbf{r}')]\, dV'_{(mn)}. \tag{4.24}$$

To show this is a state quantity we shall use the concept of an incompatibility source tensor, introduced by Simmons and Bullough [12]. In contrast to Simmons and Bullough, who derived several forms of it from a general definition, we define it directly as follows

$$I_{mnpq}(\mathbf{r}) \equiv (4\pi)^{-1} \int \epsilon_{pmk}\epsilon_{qsl} C_{ijkl} G_{jn,i's'}(\mathbf{r}') R^{-1}\, dV'_{(mn)}. \tag{4.25}$$

We see from this relation that the homogeneity of $I_{mnpq}(\mathbf{r})$ is the same as that of $G_{jn}(\mathbf{r})$, i.e., of degree (-1), so that they both vary as r^{-1}. By using the identity

$$\epsilon_{pmk}\epsilon_{qsl} \equiv \begin{vmatrix} \delta_{pq} & \delta_{ps} & \delta_{pl} \\ \delta_{mq} & \delta_{ms} & \delta_{ml} \\ \delta_{kq} & \delta_{ks} & \delta_{kl} \end{vmatrix} \tag{4.26}$$

and (2.7) it can also be written as

$$\begin{aligned} I_{mnpq}(\mathbf{r}) = (4\pi)^{-1} [(\delta_{mn}\delta_{pq} - \delta_{mq}\delta_{np}) r^{-1} - (C_{ijpq} - C_{ijkl}\delta_{pq}) \int G_{jn,i'm'}(\mathbf{r}') R^{-1}\, dV' \\ + (C_{ijmq} - C_{ijkk}\delta_{mq}) \int G_{jn,i'p'}(\mathbf{r}') R^{-1}\, dV']_{(mn)}. \end{aligned} \tag{4.27}$$

Except for the last line, this expression agrees with the one Simmons and Bullough have called the Eshelby-Eddington formula. Now the incompatibility source tensor satisfies the following relationship:

$$\begin{aligned} \epsilon_{qsl} I_{mnpq,s}(\mathbf{r}) &= (4\pi)^{-1} \int \epsilon_{pmk} [C_{ijkl} G_{jn,i's'}(\mathbf{r}') - C_{ijks} G_{jn,i'l'}(\mathbf{r}')] R^{-1}_{,s}\, dV'_{(mn)} \\ &= (4\pi)^{-1} \int \epsilon_{pmk} [C_{ijkl} G_{jn,i'}(\mathbf{r}') R^{-1}_{,ss} - C_{ijks} G_{jn,i's'}(\mathbf{r}') R^{-1}_{,l}]\, dV'_{(mn)} \\ &= -\int \epsilon_{pmk} [C_{ijkl} G_{jn,i'}(\mathbf{r}') \delta(R) - \delta_{kn}\delta(\mathbf{r}') (4\pi R)^{-1}_{,l}]\, dV'_{(mn)} \\ &= -[\epsilon_{pmk} C_{ijkl} G_{jn,i}(\mathbf{r})]_{(mn)}. \end{aligned} \tag{4.28}$$

[11] See footnote 6 on page 53.

Here the second equality follows by partial integrations, and the third from $R_{,ss}^{-1}=-4\pi\delta(R)$ and (2.7). From the above the term in (4.24) containing κ_{lp}^{p} becomes

$$\int \epsilon_{qsl} I_{mnpq,s}(\mathbf{R})\kappa_{lp}^{p}(\mathbf{r}')dV' = \int \epsilon_{qsl} I_{mnpq}(\mathbf{R})\kappa_{lp,s'}^{p}(\mathbf{r}')dV'$$
$$= -\int I_{mnpq}(\mathbf{R})\theta_{qp}(\mathbf{r}')dV'$$

by a partial integration and (4.2). Note that in the partial integration the surface integral vanishes because of the asymptotic behavior of I_{mnpq} and κ_{lp}^{p}, discussed above. Hence we find for (4.24)

$$e_{mn}(\mathbf{r}) = \int \epsilon_{pmk} C_{ijkl} G_{jn,i}(\mathbf{R})\alpha_{pl}(\mathbf{r}')dV'_{(mn)} - \int I_{mnpq}(\mathbf{R})\theta_{qp}(\mathbf{r}')dV'. \tag{4.29}$$

This is the result we seek. We see it is a state quantity because it depends entirely on the defect quantities α_{pl} and θ_{qp}.

The incompatibility source tensor I_{mnpq} was originally introduced by Simmons and Bullough to solve the so-called incompatibility problem, i.e., to find the elastic strain e_{mn} when the incompatibility η_{pq} is given as a prescribed function of space. We show here how this can be done. From (4.28)

$$\epsilon_{prk}\epsilon_{qsl} I_{mnpq,rs}(\mathbf{r}) = -[C_{ijkl} G_{jn,im}(\mathbf{r}) - \delta_{km} C_{ijrl} G_{jn,ir}(\mathbf{r})]_{(mn)}$$
$$= -[C_{ijkl} G_{jn,im}(\mathbf{r}) + \delta_{km}\delta_{ln}\delta(\mathbf{r})]_{(mn)}, \tag{4.30}$$

using (2.7). Therefore we find

$$e_{mn}(\mathbf{r}) = -\int C_{ijkl} G_{jn,im}(\mathbf{R}) e_{kl}^{p}(\mathbf{r}')dV'_{(mn)} - e_{mn}^{p}(\mathbf{r})$$
$$= \int [\epsilon_{prk}\epsilon_{qsl} I_{mnpq,rs}(\mathbf{R}) + \delta_{km}\delta_{ln}\delta(\mathbf{R})]\, e_{kl}^{p}(\mathbf{r}')dV' - e_{mn}^{p}(\mathbf{r})$$
$$= \int \epsilon_{prk}\epsilon_{qsl} I_{mnpq}(\mathbf{R}) e_{kl,r's'}^{p}(\mathbf{r}')dV'$$
$$= \int I_{mnpq}(\mathbf{R})\eta_{pq}(\mathbf{r}')dV'. \tag{4.31}$$

Here the first equality follows from (4.14) and (2.15), the second from (4.30), the third from a partial integration, and the fourth from (4.11).

We next wish to derive the elastic bend-twist. First we find the derivative of the total distortion (4.23)

$$u_{n,ms}^{T}(\mathbf{r}) = \int \epsilon_{pmk} C_{ijkl} G_{jn,is}(\mathbf{R})[\alpha_{pl}(\mathbf{r}') - \kappa_{lp}^{p}(\mathbf{r}')]dV' + e_{mn,s}^{p}(\mathbf{r}). \tag{4.32}$$

The κ_{lp}^{p} term in this expression becomes by a partial integration

$$-\int \epsilon_{pmk} C_{ijkl} G_{jn,i}(\mathbf{R})\kappa_{lp,s'}^{p}(\mathbf{r}')dV'$$
$$= \int \epsilon_{pmk} C_{ijkl} G_{jn,i}(\mathbf{R})[\epsilon_{qsl}\theta_{qp}(\mathbf{r}') - \kappa_{sp,l'}^{p}(\mathbf{r}')]dV'$$
$$= \int \epsilon_{pmk}\epsilon_{qsl} C_{ijkl} G_{jn,i}(\mathbf{R})\theta_{qp}(\mathbf{r}')dV' + \epsilon_{pmn}\kappa_{sp}^{p}(\mathbf{r}).$$

Here the first equality follows from (4.10), and the second by a partial integration and (2.7). Hence

$$u_{n,ms}^{T}(\mathbf{r}) = \int \epsilon_{pmk} C_{ijkl} G_{jn,is}(\mathbf{R})\alpha_{pl}(\mathbf{r}')dV' + \int \epsilon_{pmk}\epsilon_{qsl} C_{ijkl} G_{jn,i}(\mathbf{R})\theta_{qp}(\mathbf{r}')dV'$$
$$+ e_{mn,s}^{p}(\mathbf{r}) + \epsilon_{pmn}\kappa_{sp}^{p}(\mathbf{r}). \tag{4.33}$$

Finally we have from (4.15)

$$\kappa_{st}(\mathbf{r}) = 1/2 \int \epsilon_{tmn}\epsilon_{pmk}C_{ijkl}G_{jn,is}(\mathbf{R})\alpha_{pl}(\mathbf{r}')dV' + 1/2 \int \epsilon_{tmn}\epsilon_{pmk}\epsilon_{qsl}C_{ijkl}G_{jn,i}(\mathbf{R})\theta_{qp}(\mathbf{r}')dV', \tag{4.34}$$

which is seen to be a state quantity too.

This section then has extended the results for dislocation theory of section 3.1.2 to a more general defect theory. The central result there, eq (3.17), has been replaced by (4.29) and (4.34). We note that concepts, quantities, or equations from dislocation theory generalize into pairs of concepts, quantities, or equations in defect theory. Some of these ideas have been summarized in table 2.

5. The Discrete Defect Line

5.1. Weingarten's Theorem

The point of departure for the discrete defect line is the following theorem [3]:

WEINGARTEN'S THEOREM: *On following around an irreducible circuit in a multiply-connected body, the displacement and rotation change by an amount that represents a rigid body motion, if and only if the classical elastic compatibility conditions are satisfied throughout the body.*

Explicitly these changes are given by (I3.4, I3.3).

$$[u_l] = B_l + \epsilon_{lqr}\Omega_q x_r, \tag{5.1}$$

$$[\omega_q] = \Omega_q, \tag{5.2}$$

where the constants B_l and Ω_q are given by line integrals along the irreducible circuit λ(I3.6, I3.5):

$$B_l \equiv \oint_\lambda (e_{kl} - \epsilon_{lqr}\kappa_{kq}x_r)dL_k, \tag{5.3}$$

$$\Omega_q \equiv \oint_\lambda \kappa_{kq}dL_k. \tag{5.4}$$

That these quantities are constant is easily shown by Stokes' theorem and the compatibility equations, i.e. (4.17–18) with $\alpha_{pl}=0$, $\theta_{pq}=0$. We note incidentally that the definitions (5.3–4) are consistent with the relations (4.20–21).[12]

5.2. Geometry

The discrete defect line L is defined as the boundary of a surface S, where the material below S has been plastically displaced with respect to the material above S by an amount which represents a rigid motion (fig. 1).

Hence, the difference between the displacement just below and above S is given by

$$[u_l(\mathbf{r})] = b_l + \epsilon_{lqr}\Omega_q(x_r - x_r^0), \tag{5.5}$$

where b_l represents a rigid translation and the second term a superposed constant rotation of amount Ω_q around an axis through x_r^0. The constant b_l will be called the Burgers vector for the discrete dislocation line contained in the defect line, and is to be distinguished from the general

[12] For the nonlinear generalization of the present theory it would be necessary to determine if Weingarten's theorem still holds. Then for a finite rotation (5.1) would have to be modified into $[u_l] = B_l + (\epsilon_{lqr}\Omega_q x_r + \frac{1}{2}\Omega_l\Omega_q x_q - \frac{1}{2}\Omega^2 x_l)(1+\frac{1}{4}\Omega^2)^{-1}$. Here the Frank vector or versor has the direction of the rotation axis and the magnitude $2\tan\frac{1}{2}\Phi$, where Φ is the angle of rotation. The addition rule becomes $\Omega_q = (\Omega_q^{(1)} + \Omega_q^{(2)} - \frac{1}{2}\epsilon_{lqr}\Omega_r^{(1)}\Omega_l^{(2)})(1 - \frac{1}{4}\Omega_p^{(1)}\Omega_p^{(2)})^{-1}$ for a rotation (1) followed by a rotation (2).

Burgers vector defined by (4.5). The constant Ω_q will be identified with the Frank vector (4.6). The relation (5.5) implies there is also a jump in rotation across S given by

$$[\omega_q(\mathbf{r})] = 1/2\epsilon_{klq}[u_l(\mathbf{r})]_{,k} = \Omega_q. \tag{5.6}$$

If we visualize the material in a tube around L removed (fig. 1), we have a doubly connected body, and since the jump across S represents a rigid body motion, Weingarten's theorem applies. Hence, this doubly connected body is compatible, i.e., the basic elastic fields satisfy the compatibility equations, even on S. Therefore, the results (5.5–6) should also follow from (5.1–4). The real, incompatible, simply connected body is obtained by letting the cross section of the tube vanish. Then (5.3–4) become identical to (4.20–21), and by the compatibility of the total deformation these relations are equivalent to (4.5–6).

Our problem now is how to embody the statements (5.5–6) into definitions for the basic plastic fields, i.e., the plastic strain and bend-twist. We give a straightforward operational procedure to obtain these quantities and then verify that they are correct by (5.1–2) and (4.5–6). Assume first that S is closed, enclosing the volume V. Then by (B7)

$$u_l^T(\mathbf{r}) = \delta(V)\{b_l + \epsilon_{lqr}\Omega_q(x_r - x_r^0)\} \tag{5.7}$$

represents a displacement, which is the same as (5.5) inside V and vanishes outside V. Thus, it has the required jump across S. Equation (5.7) could be regarded as describing a grain of volume V and boundary S, whose orientation with respect to the surrounding material is given by the rigid motion (5.5). We assume that the deformation (5.7) comes about by means of a plastic deformation on the surface S and an elastic translation and rotation in V. To find the basic plastic fields we just calculate the basic total fields, i.e., the total strain and bend-twist. In general these can be split into elastic and plastic parts, (4.14–15). But since the only elastic deformation is a rigid motion, the basic elastic fields will vanish and the plastic fields will equal the total fields. We have from (3.9) and (5.7)

$$\begin{aligned}\beta_{kl}^T(\mathbf{r}) &= \delta_{,k}(V)\{b_l + \epsilon_{lqr}\Omega_q(x_r - x_r^0)\} + \delta(V)\epsilon_{lqk}\Omega_q \\ &= -\delta_k(S)\{b_l + \epsilon_{lqr}\Omega_q(x_r - x_r^0)\} + \delta(V)\epsilon_{klq}\Omega_q,\end{aligned} \tag{5.8}$$

using the divergence theorem (B24). From this we find

$$e_{kl}^T(\mathbf{r}) = -\delta_k(S)\{b_l + \epsilon_{lqr}\Omega_q(x_r - x_r^0)\}_{(kl)}, \tag{5.9}$$

$$\omega_q^T(\mathbf{r}) = -1/2\,\epsilon_{klq}\delta_k(S)\{b_l + \epsilon_{lqr}\Omega_q(x_r - x_r^0)\} + \delta(V)\Omega_q. \tag{5.10}$$

We see that (5.10) represents a rotation, which is the same inside V as (5.6) and vanishes outside V. Thus, it has the required jump across S. We next find the bend-twist from (4.15)

$$\kappa_{mq}^T(\mathbf{r}) = -1/2\,\epsilon_{klq}[\delta_k(S)\{b_l + \epsilon_{lqr}\Omega_q(x_r - x_r^0)\}]_{,m} - \delta_m(S)\Omega_q, \tag{5.11}$$

using the divergence theorem again. We see that the basic total fields are concentrated at the surface S. As mentioned before, since the deformation is just a rigid motion of part of the body, there are no basic elastic fields, and therefore the fields are all plastic. The next step is to assume that (5.9) and (5.11) hold in the same form for the open surface S of the defect loop. To write down the final results it is convenient to introduce the "plastic distortion" and "plastic rotation" defined by Mura [4]:

$$\beta_{kl}^*(\mathbf{r}) \equiv -\delta_k(S)\{b_l + \epsilon_{lqr}\Omega_q(x_r - x_r^0)\}, \tag{5.12}$$

$$\phi_{kq}^*(\mathbf{r}) \equiv -\delta_k(S)\Omega_q. \tag{5.13}$$

These quantities will be interpreted in section 6 as the dislocation and disclination loop densities. Until then they serve as convenient intermediate quantities for the purpose of calculation. Now we write

$$e^P_{kl} = \beta^*_{(kl)}, \tag{5.14}$$

$$\kappa^P_{mq} = 1/2\epsilon_{klq}\beta^*_{kl,m} + \phi^*_{mq},$$

$$(\kappa^P_{kq} = 1/2\epsilon_{lqr}\beta^*_{rl,k} + \phi^*_{kq}). \tag{5.15}$$

These are the results we looked for. Equations (5.14–15) together with (5.12–13) represent the basic plastic fields for a discrete defect line L spanned by the surface S. From (5.14–15) we also have the result

$$e^P_{kl,m} + \epsilon_{klq}\kappa^P_{mq} = \beta^*_{kl,m} + \epsilon_{klq}\phi^*_{mq}, \tag{5.16}$$

which will be useful for later purposes. As we mentioned above, we now check the validity of results (5.14–15). From (4.5)

$$\begin{aligned} B_l &= -\oint_\lambda (\beta^*_{(kl)} - \beta^*_{[rl],k}x_r - \epsilon_{lqr}\phi^*_{kq}x_r)dL_k \\ &= -\oint_\lambda (\beta^*_{kl} - \epsilon_{lqr}\phi^*_{kq}x_r)dL_k \\ &= \oint_\lambda \delta_k(S)\{b_l - \epsilon_{lqr}\Omega_q x^0_r\}dL_k \\ &= b_l - \epsilon_{lqr}\Omega_q x^0_r, \end{aligned} \tag{5.17}$$

by a partial integration, (5.12–13), and (B15). This then is the relation between the general Burgers vector and the dislocation Burgers vector. Next we have by (5.15), (5.13), and (B15)

$$\begin{aligned} -\oint_\lambda \kappa^P_{kq}dL_k &= -\oint_\lambda \phi^*_{kq}dL_k \\ &= \oint_\lambda \delta_k(S)\Omega_q dL_k \\ &= \Omega_q. \end{aligned} \tag{5.18}$$

From (4.6) this relation identifies Ω_q as the Frank vector. If we substitute these results into (5.1–2) we obtain (5.5–6), as was required.

We now find the dislocation density from (4.1) and (5.16)

$$\begin{aligned} \alpha_{pl}(\mathbf{r}) &= -\epsilon_{pmk}(\beta^*_{kl,m} + \epsilon_{klq}\phi^*_{mq}) \\ &= \epsilon_{pmk}[\delta_{k,m}(S)\{b_l + \epsilon_{lqr}\Omega_q(x_r - x^0_r)\} + \delta_k(S)\epsilon_{lqr}\Omega_q\delta_{rm} + \epsilon_{klq}\delta_m(S)\Omega_q] \\ &= \delta_p(L)\{b_l + \epsilon_{lqr}\Omega_q(x_r - x^0_r)\}, \end{aligned} \tag{5.19}$$

where the first equality follows from (5.16), the second from (5.12–13), and the third by Stokes' theorem (B26) and a cancellation. The disclination density is obtained from (4.2)

$$\theta_{pq}(\mathbf{r}) = -\epsilon_{pmk}\phi^*_{kq,\,m}$$

$$= \epsilon_{pmk}\delta_{k,\,m}(S)\Omega_q$$

$$= \delta_p(L)\Omega_q \tag{5.20}$$

where we have used (5.15), (5.13), and (B26). Relations (5.19–20) represent the defect densities for a discrete defect line. We see from (5.19) that the Frank vector Ω_q also contributes to the dislocation density, in addition to the dislocation Burgers vector b_l. In these relations L is the closed boundary of S. The vector $\delta_p(L)$ is the Dirac delta function on the curve L and it is always parallel to L. A discrete disclination line is called wedge or twist when the Frank vector is parallel or normal to the line, respectively. Therefore, (5.20) shows that the diagonal and off-diagonal components of θ_{pq} represent the wedge and twist components of the disclination density, respectively (see table 1). Equations (5.19–20) show how to make the transition from a continuous distribution of defects to a discrete defect line.

The discrete defect line, characterized by the dislocation Burgers vector b_l and the Frank vector Ω_q, was defined in this section independent of the defect density tensors α_{pl} and θ_{pq} defined by (4.1–2) in section 4.1. The question arises whether there is a unique correlation between these definitions. For dislocations only there is a straightforward relation between the Burgers vector and the dislocation density of a continuous distribution, given by (3.8), or between the dislocation density for a discrete line and its Burgers vector, given by (3.23). When disclinations are introduced there is a similar straightforward relation between the Frank vector and the disclination density of a continuous distribution, given by (4.8), or between the disclination density for a discrete line and its Frank vector, given by (5.20). However, as we noted, the general Burgers vector now contains a contribution from the disclination density, eq (4.7), or the dislocation density for a discrete defect line contains a contribution from the Frank vector, eq (5.19). What this means is that the definitions of the "dislocation" are not identical in both approaches. Therefore, as we see from the relations quoted, in the transition from one formulation to the other a certain amount of mixing occurs. Anthony [2] has handled this difficulty by adopting the discrete disclination loop as the true definition of the disclination. Then our dislocation density tensor α_{pl} in (5.19) partly describes the discrete disclination. He therefore divides α_{pl} into two parts, a true component that corresponds to the dislocation line with Burgers vector b_l, and a component that belongs to the disclination line with Frank vector Ω_q. Hence our difference with Anthony merely reduces to a difference in point of view.

We prefer to retain our own point of view with different definitions of the "dislocation" because it is in fact difficult to identify the dislocation line in a discrete defect line, as will be seen from (5.19). For example, let us change the axis of rotation and the dislocation Burgers vector to

$$x_r^{0\prime} = x_r^0 + \xi_r. \tag{5.21}$$

$$b_l' = b_l + \epsilon_{lqr}\Omega_q\xi_r. \tag{5.22}$$

Then α_{pl} in (5.19) is unaltered. So the dislocation Burgers vector b_l is not uniquely defined, but depends on the location of the axis. On the other hand, the general Burgers vector B_l in (5.17) is unaltered by (5.21–22), and, therefore this is the quantity which is invariant for a discrete defect loop. This is another motivation for introducing it.

The significance of (5.19) can further be illustrated as follows. Consider an infinitesimal volume dV centered about some point on L. The jump across S is given by (5.5). The rotational part of (5.5) can be approximated by a constant inside dV, since it is so small, i.e., locally we cannot determine if the displacement jump is due to a rotation or a translation, even if we know the

rotation jump locally. Now the dislocation density is a local tensor field. Therefore the dislocation density tensor can be found by replacing b_l in (3.23) by the jump (5.5), in agreement with (5.19). Hence, the dislocation density (5.19) at a point on the line L is exactly what would be expected on the basis of the local plastic displacement near the point, or a small Burgers circuit around L at the point. We shall illustrate this point more explicitly by examples in future publications [25, 26].

From (5.21–22) it would seem at first that we could eliminate the discrete dislocation from (5.19), by choosing ξ_r such that $b_l=0$, but this is only possible if b_l is normal to Ω_q. However, we can draw the following important conclusion from (5.19). The axis of a discrete disclination line can be translated from the point x_r^0 to the point $x_r^{0\prime}$ by adding a discrete dislocation to the line with a Burgers vector given by

$$b_l=\epsilon_{lqr}\Omega_q(x_r^0-x_r^{0\prime}), \tag{5.23}$$

which is normal to the Frank vector Ω_q. In other words, we can move the axis by adding the dislocation density

$$\alpha_{pl}(\mathbf{r})=\delta_p(L)\epsilon_{lqr}\Omega_q(x_r^0-x_r^{0\prime}), \tag{5.24}$$

as is evident from (5.19).

The above development suggests the possibility that a dislocation could end on or originate from a disclination line. Consider the three curves L, L', and L'', illustrated in figure 3, which

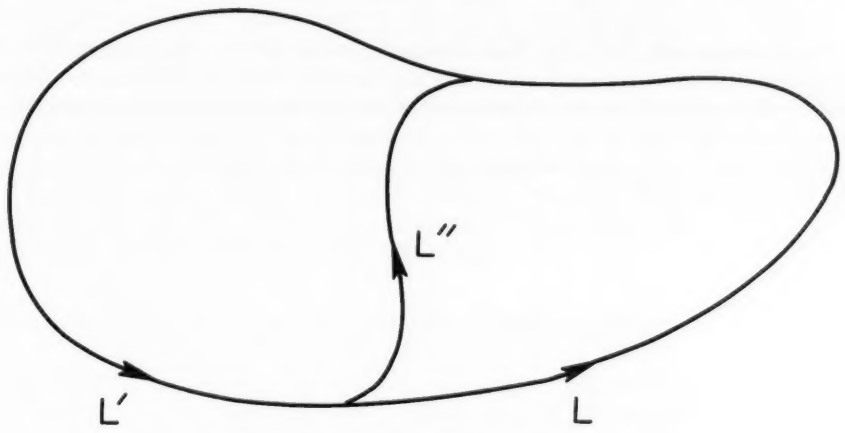

FIGURE 3. *Defect lines which join at nodes.*

meet at nodes. These curves could represent the discrete defect lines described by the following expressions:

$$\alpha_{pl}(\mathbf{r})=\delta_p(L)\{b_l+\epsilon_{lqr}\Omega_q(x_r-x_r^0)\}+\delta_p(L')\{b_l+\epsilon_{lqr}\Omega_q(x_r-x_r^{0\prime})\}$$
$$+\delta_p(L'')\epsilon_{lqr}\Omega_q(x_r^0-x_r^{0\prime}), \tag{5.25}$$

$$\theta_{pq}(\mathbf{r})=\delta_p(L+L')\Omega_q. \tag{5.26}$$

There are several ways in which one can view this defect. First, it consists of a defect line as described by (5.19–20) along the curve L and L' to which a dislocation line with Burgers vector (5.23) has been added along L' and L''. Second, it is a dislocation line along L'', which connects two points of a defect line along L and L'; as a consequence the axis goes thru x_r^0 for L and thru $x_r^{0\prime}$ for L'. Third, it consists of two defect loops with the same Frank vector, one along L' and L''

with axis thru $x_r^{0\prime}$, and one along L and minus L'' with axis thru x_r^0; along the line of overlap L'' the rotational parts cancel and only a dislocation line is left. So we see how the defect described by the relations (5.25–26) can be regarded as a combination of two simpler defects. We also see here how a discrete dislocation line can end on a discrete disclination line. A special case of this geometry has already been discussed [19] and a detailed mathematical analysis of this particular example will be presented in a future publication [25].

We note that (5.19–20) satisfy the continuity equations (4.3–4) by (B28):

$$\alpha_{pl,p} + \epsilon_{lpq}\theta_{pq} = \delta_p(L)\epsilon_{lqr}\Omega_q\delta_{rp} + \epsilon_{lpq}\delta_p(L)\Omega_q = 0, \tag{5.27}$$

$$\theta_{pq,p} = \delta_{p,p}(L)\Omega_q = 0, \tag{5.28}$$

Similarly, it is easy to show that (5.25–26) also satisfy the continuity equations, confirming an assertion we have made [19].

As a cross-check we also show that (5.19–20) give consistent results for (4.7–8)

$$B_l = \int_\sigma \delta_p(L)\{b_l - \epsilon_{lqr}\Omega_q x_r^\circ\}dS_p = b_l - \epsilon_{lqr}\Omega_q x_r^\circ, \tag{5.29}$$

$$\int_\sigma \theta_{pq}dS_p = \int_\sigma \delta_p(L)\Omega_q dS_p = \Omega_q, \tag{5.30}$$

by (B15), in agreement with (5.17–18). These relations remain valid for many defect lines as well, and could therefore be used to show how to make the transition from discrete lines to a continuous distribution of defects. However, the following relations are more convenient to make this point:

$$\begin{aligned}\int_\sigma \alpha_{pl}dS_p &= \int_\sigma \delta_p(L)\{b_l + \epsilon_{lqr}\Omega_q(x_r - x_r^\circ)\}dL_p \\ &= b_l - \epsilon_{lqr}\Omega_q(x_r^{L\sigma} - x_r^\circ) \\ &= [u_l]^{L\sigma},\end{aligned} \tag{5.31}$$

$$\int_\sigma \theta_{pq}dS_p = [\omega_q]. \tag{5.32}$$

Here the first equality follows from (5.19), the second from (B16) where $x_r^{L\sigma}$ is the point of intersection of the curve L with the surface σ (fig. 1), the third from (5.5), and the last from (5.6). So for many defect lines the average dislocation density α_{pl} represents the x_l component of the sum of the displacement jump vectors and the average disclination density θ_{pq} the x_q component of the sum of the rotation jump (or Frank) vectors of all the defect lines that intersect unit area of a plane normal to the x_p direction.

5.3. Statics

In this section we find the basic elastic fields, i.e., the elastic strain and bend-twist, for a discrete defect line.

If we substitute (5.14) and (5.12) into (2.15) we find the displacement

$$\begin{aligned}u_n^T(\mathbf{r}) &= \int C_{ijkl}G_{jn,i}(\mathbf{R})\delta_k(S')\{b_l + \epsilon_{lqr}\Omega_q(x_r' - x_r^0)\}dV' \\ &= \int_S C_{ijkl}G_{jn,i}(\mathbf{R})\{b_l + \epsilon_{lqr}\Omega_q(x_r' - x_r^0)\}dS_k'\end{aligned} \tag{5.33}$$

by (B12). This is the expression for the total displacement due to a finite discrete defect loop. It allows us to estimate the asymptotic behavior of the displacement at large distances from a small disclination loop, $b_l=0$. Since Green's tensor $G_{jn}(\mathbf{r})$ varies as r^{-1}, we see that $u_n^T(\mathbf{r})$ will in general vary as r^{-2} as $r\to\infty$. However, for special cases such as a symmetric loop centered on its axis, the integral vanishes to first order by symmetry. Therefore a finite symmetric disclination loop has the anomalous asymptotic dependence of r^{-3} as $r\to\infty$. Since the strain $e_{mn}(\mathbf{r})$ is obtained from the derivative of the displacement, it will vary as r^{-4} as $r\to\infty$. These results are listed in table 3.

TABLE 3

Asymptotic behavior of the displacement $\mathbf{u}^T$ and the strain $\mathbf{e}$ at large distances from certain defect configurations. The numbers in parentheses refer to the equations from which the estimate is obtained. A symmetric disclination loop is one for which $\int_S (x_r'-x_r^0)dS_k'=0$.

	Dislocation		Disclination	
	u^T	e	u^T	e
Line.....	$\ln r$	r^{-1} (3.32)	$r\ln r$	$\ln r$ (5.37)
Dipole.....	r^{-1} (3.46)	r^{-2}	$\ln r$ (7.6)	r^{-1}
Loop.....	r^{-2} (3.30)	r^{-3}	General: r^{-2} (5.33) Symmetric: r^{-3} (5.33)	r^{-3} r^{-4}

For infinitesimal symmetric disclination loops both u_n^T and e_{mn} vanish. A more accurate calculation of the asymptotic displacement from a small but finite disclination loop can also be made from (5.33) by expanding the Green's tensor as a Taylor series in $\mathbf{r}'$ for a few terms and integrating over S. The details will be worked out in a subsequent publication [26], where it will be shown that for the isotropic case the results reduce to those of Li and Gilman [20].

We now find the total distortion from (5.33)

$$
\begin{aligned}
u_{n,m}^T(\mathbf{r}) &= \int_S C_{ijkl}G_{jn,im}(\mathbf{R})\{b_l+\epsilon_{lqr}\Omega_q(x_r'-x_r^0)\}dS_k' \\
&= \oint_L \epsilon_{pmk}C_{ijkl}G_{jn,i}(\mathbf{R})\{b_l+\epsilon_{lqr}\Omega_q(x_r'-x_r^0)\}dL_p' \\
&\quad + \int_S C_{ijkl}G_{jn,i}(\mathbf{R})\epsilon_{lqr}\Omega_q\delta_{rm}dS_k' \\
&\quad + \int_S C_{ijkl}G_{jn,ik}(\mathbf{R})\{b_l+\epsilon_{lqr}\Omega_q(x_r'-x_r^0)\}dS_m' \\
&= \oint_L \epsilon_{pmk}C_{ijkl}G_{jn,i}(\mathbf{R})\{b_l+\epsilon_{lqr}\Omega_q(x_r'-x_r^0)\}dL_p' \\
&\quad + \int_S \epsilon_{pmk}C_{ijkl}G_{jn,i}(\mathbf{R})\Omega_p dS_l' + \beta_{mn}^*(\mathbf{r}).
\end{aligned}
\tag{5.34}
$$

Here the second equality follows from Stokes' theorem (A4), and the third from (2.7), (B5), and (5.12). Now if we call $\beta_{mn}=u_{n,m}^T-\beta_{mn}^*$ the "elastic distortion," it is not a state quantity because the

second integral in (5.34) cannot be written as a line integral. The proof of this consists merely in showing that the integrand in this term is not divergence-free; using (2.7) we find

$$\begin{aligned}[\epsilon_{pmk}C_{ijkl}G_{jn,i}(r)]_{,l} &= \epsilon_{pmk}C_{ijkl}G_{jn,il}(\mathbf{r}) \\ &= -\epsilon_{pmn}\delta(r) \\ &\neq 0. \end{aligned} \tag{5.35}$$

If we compare the second integral of (5.34) with (3.30) we notice a great deal of similarity. As is well-known the jump of u_n^T in (3.30) across the surface S is given by $[u_n^T] = b_n$ according to (3.18). From this we deduce that the second integral in (5.34) leads to a jump of the total distortion β_{mn}^T across the surface S of $[\beta_{mn}^T] = \epsilon_{pmn}\Omega_p$. This is a jump in rotation of $[\omega_p^T] = 1/2\epsilon_{pmn}[\beta_{mn}^T] = \Omega_p$, in agreement with (5.6). In the older approach to dislocation theory where the surface S was ignored, the displacement of a discrete dislocation line was regarded as a multiple-valued function with a period of the Burgers vector. Equation (5.34) shows that from this point of view the rotation (or distortion) of a discrete disclination line is a multiple-valued function with a period of the Frank vector.

The elastic strain is from (4.14), (5.14), and (5.34)

$$e_{mn}(\mathbf{r}) = \oint_L \epsilon_{pmk}C_{ijkl}G_{jn,i}(\mathbf{R})\{b_l + \epsilon_{lqr}\Omega_q(x_r' - x_r^0)\}dL'_{p(mn)} + \int_S \epsilon_{pmk}C_{ijkl}G_{jn,i}(\mathbf{R})\Omega_p dS'_{l(mn)}. \tag{5.36}$$

The integrand of the second integral now *is* divergence-free and so it can be written as a line integral

$$-\int_S \epsilon_{qsl}I_{mnpq,s}(\mathbf{R})\Omega_p dS'_l = -\oint_L I_{mnpq}(\mathbf{R})\Omega_p dL'_q$$

by (4.28) and Stokes' theorem. Hence

$$e_{mn}(\mathbf{r}) = \oint_L \epsilon_{pmk}C_{ijkl}G_{jn,i}(\mathbf{R})\{b_l + \epsilon_{lqr}\Omega_q(x_r' - x_r^0)\}dL'_{p(mn)} - \oint_L I_{mnpq}(\mathbf{R})\Omega_p dL'_p. \tag{5.37}$$

This result could of course also be obtained directly from (4.29), (5.19–20) and (B11). This is the relation we sought. We see that the elastic strain can be written as a line integral along the discrete defect line. Therefore it is a state quantity.

Equation (5.37) also allows us to estimate the asymptotic behavior of the strain at large distances from a straight disclination line. The second integral will give the dominant term. The incompatibility source tensor $I_{mnpq}(\mathbf{r})$ varies as r^{-1}. Due to the integration then $e_{mn}(\mathbf{r})$ will vary as $\ln r$ as $r \to \infty$. Since the displacement is an integral of the strain, it will vary as $r \ln r$ as $r \to \infty$. These results are also listed in table 3.

We wish next to derive the elastic bend-twist. First we find the derivative of the total distortion (5.34)

$$u_{n,ms}^T(\mathbf{r}) = \oint_L \epsilon_{pmk}C_{ijkl}G_{jn,is}(\mathbf{R})\{b_l + \epsilon_{lqr}\Omega_q(x_r' - x_r^0)\}dL'_p + \int_S \epsilon_{pmk}C_{ijkl}G_{jn,is}(\mathbf{R})\Omega_p dS'_l + \beta_{mn,s}^*(\mathbf{r}). \tag{5.38}$$

The second term becomes by Stokes' theorem

$$\oint_L \epsilon_{pmk}\epsilon_{qsl}C_{ijkl}G_{jn,i}(\mathbf{R})\Omega_p dL'_q + \int_S \epsilon_{pmk}C_{ijkl}G_{jn,il}(\mathbf{R})\Omega_p dS'_s.$$

The second term in this expression becomes by (2.7), (B5), and (5.13)

$$-\int_S \epsilon_{pmk}\delta_{kn}\delta(\mathbf{R})\Omega_p dS'_s = -\epsilon_{pmn}\delta_s(S)\Omega_p = \epsilon_{pmn}\phi^*_{sp}(\mathbf{r}).$$

Hence (5.38) becomes

$$\begin{aligned} u^T_{n,\,ms}(\mathbf{r}) = &\oint_L \epsilon_{pmk}C_{ijkl}G_{jn,\,is}(\mathbf{R})\{b_l + \epsilon_{lqr}\Omega_q(x'_r - x^0_r)\}dL'_p \\ &+ \oint_L \epsilon_{pmk}\epsilon_{qsl}C_{ijkl}G_{jn,\,i}(\mathbf{R})\Omega_p dL'_q \\ &+ \beta^*_{mn,\,s}(\mathbf{r}) + \epsilon_{pmn}\phi^*_{sp}(\mathbf{r}). \end{aligned} \tag{5.39}$$

We now find from (4.15) and (5.15)

$$\begin{aligned} \kappa_{st}(\mathbf{r}) = &1/2\oint_L \epsilon_{tmn}\epsilon_{pmk}C_{ijkl}G_{jn,\,is}(\mathbf{R})\{b_l + \epsilon_{lqr}\Omega_q(x'_r - x^0_r)\}dL'_p \\ &+ 1/2\oint_L \epsilon_{tmn}\epsilon_{pmk}\epsilon_{qsl}C_{ijkl}G_{jn,\,i}(\mathbf{R})\Omega_p dL'_q. \end{aligned} \tag{5.40}$$

This could also have been obtained directly by substituting into (4.34) from (5.19–20). It is also seen to be a state quantity.

This section has extended the results for a discrete dislocation line of section 3.2.2 to a more general discrete defect line. The central result there, equation (3.32), has been replaced by (5.37) and (5.40). Again we see the elastic distortion of dislocation theory is generalized into the basic elastic fields of defect theory.

6. Continuous Distribution of Infinitesimal Defect Loops

In section 4.1 the defects were defined by (4.1–2) and the characteristic vectors by (4.5–6) in terms of the given basic plastic fields, strain and bend-twist. Eliminating the basic plastic fields from these definitions led to (4.7–8), relations between the characteristic vectors and the defect densities. These equations could alternatively be used to define the defect densities in terms of the characteristic vectors, if they are prescribed in a suitable manner. It is convenient to put these relations into differential form. First we define the disclination density. When the defects are continuously distributed the disclination density tensor is defined locally by

$$\theta_{pq} \equiv \frac{\Delta\Omega_q}{\Delta S_p}. \tag{6.1}$$

For a distribution of discrete defect lines this represents the average disclination density where $\Delta\Omega_q$ is the qth component of the resulting Frank vectors of all the disclinations which pierce through a surface element ΔS_p oriented normal to the x_p direction at the given point. In view of (4.7) it is necessary to modify the definition (3.33) for the dislocation density α_{pl}. For an inhomogeneous continuous distribution of defects we define it locally by the relation

$$\alpha_{pl} - \epsilon_{lqr}\theta_{pq}x_r \equiv \frac{\Delta B_l}{\Delta S_p}. \tag{6.2}$$

For discrete defect lines this relation will give us the average dislocation density, where ΔB_l is the lth component of the resulting total Burgers vectors of all the defects (dislocations and disclinations) which pierce through a surface element ΔS_p normal to the x_p direction at the given point.

Reference to (5.31) suggests that a more convenient way to write (6.2) is

$$\alpha_{pl} \equiv \frac{\Delta[u_l]}{\Delta S_p}, \tag{6.3}$$

where we have defined

$$\Delta[u_l] \equiv \Delta B_l + \epsilon_{lqr}\Delta\Omega_q x_r, \tag{6.4}$$

as suggested by (5.1). For discrete defect lines $\Delta[u_l]$ represents the lth component of the resulting displacement jumps of all the defect lines which pierce through a surface element ΔS_p oriented normal to the x_p direction at the given point. Relation (6.3) is what would be expected if the dislocation density is determined by the local plastic deformation, regardless of whether it is due to discrete dislocations or disclinations. For generality relation (3.33) could also have have been put in the form (6.3) by reference to (3.18).

We next consider a continuous distribution of infinitesimal defect loops differently oriented in space. We introduce the disclination loop density tensor following Kroupa's [5] line of reasoning. We can define it as follows: ζ_{kq} represents the flux of disclination (or Frank vector) in the x_q direction that encloses a unit vector in the x_k direction. When the loops are continuously and inhomogeneously distributed the density tensor ζ_{kq} is a function of the position and is defined locally by

$$\zeta_{kq} \equiv \frac{\Delta\Omega_q}{\Delta L_k}. \tag{6.5}$$

For a distribution of discrete loops this represents the average disclination loop density where now $\Delta\Omega_q$ is the qth component of the resulting Frank vectors of all the loops which are pierced by the line element ΔL_k oriented in the x_k direction at the given point. It is now also necessary to modify the definition (3-34) for the dislocation loop density. For a continuous distribution of defect loops it is defined locally by

$$\gamma_{kl} \equiv \frac{\Delta[u_l]}{\Delta L_k}. \tag{6.6}$$

For discrete loops this represents the average dislocation loop density, where now $\Delta[u_l]$ is the lth component of the resulting displacement jumps of all the loops which are pierced by the line element ΔL_k oriented in the x_k direction at the given point. By (6.4) we also have the alternative definition

$$\gamma_{kl} \equiv \frac{\Delta B_l}{\Delta L_k} + \epsilon_{lqr}\frac{\Delta\Omega_q}{\Delta L_k}x_r, \tag{6.7}$$

where for discrete loops ΔB_l is the lth component of the resulting total Burgers vectors of all the defect loops which are pierced by the line element ΔL_k oriented in the x_k direction at the given point.

To derive the relations between the defect loop densities and the basic plastic fields, we first combine (6.5) and (6.7) into

$$\gamma_{kl} - \epsilon_{lqr}\zeta_{kq}x_r = \frac{\Delta B_l}{\Delta L_k}. \tag{6.8}$$

The relations (6.8) and (6.5) are easily converted to integral form

$$B_l = \oint_\lambda (\gamma_{kl} - \epsilon_{lqr}\zeta_{kq}x_r)\,dL_k, \tag{6.9}$$

$$\Omega_q = \oint_\lambda \zeta_{kq}\,dL_k. \tag{6.10}$$

Now we compare these relations with the definitions (4.5–6). The integrands can only differ by a gradient with respect to x_k. Therefore we can set

$$\kappa^P_{kq} = -\zeta_{kq} + \omega^P_{q,k}, \tag{6.11}$$

$$e^P_{kl} - \epsilon_{lqr}\kappa^P_{kq}x_r = -\gamma_{kl} + \epsilon_{lqr}\zeta_{kq}x_r + (u^P_l - \epsilon_{lqr}\omega^P_q x_r)_{,k}, \tag{6.12}$$

where ω^P_q and u^P_l are arbitrary vector fields, subject only to the condition that e^P_{kl} is symmetric. This last condition will provide a relation between them, as we shall show. If we substitute (6.11) into (6.12) we obtain

$$e^P_{kl} = -\gamma_{kl} - \epsilon_{klq}\omega^P_q + u^P_{l,k}. \tag{6.13}$$

Now the symmetry condition on e^P_{kl} gives the relation between ω^P_q and u^P_l

$$\omega^P_q = -1/2\epsilon_{klq}(\gamma_{kl} - u^P_{l,k}). \tag{6.14}$$

From this we get for (6.13) and (6.11)

$$e^P_{kl} = -\gamma_{(kl)} + u^P_{(l,k)}, \tag{6.15}$$

$$\kappa^P_{mq} = -\zeta_{mq} - 1/2\epsilon_{klq}\gamma_{kl,m} + 1/2\epsilon_{klq}u^P_{l,km}. \tag{6.16}$$

These are the relations that identify the basic plastic fields for a continuous distribution of defect loops. With them we can find all the relations derived in section 4 in terms of a loop distribution. For example, from (4.1–2) we find

$$\alpha_{pl} = \epsilon_{pmk}(\gamma_{kl,m} + \epsilon_{klq}\zeta_{mq}), \tag{6.17}$$

$$\theta_{pq} = \epsilon_{pmk}\zeta_{kq,m}. \tag{6.18}$$

This is the fundamental relationship between the defect loop densities and the corresponding defect densities. We see from (6.17) that the disclination loop density ζ_{mq} also contributes to the dislocation density, in addition to the dislocation loop density γ_{kl}.

Since a plastic displacement such as u^P_l in (6.15–16) does not contribute to the elastic fields (c.f. section 2.6), we can set $u^P_l = 0$ without loss of generality, and so we can use

$$e^P_{kl} = -\gamma_{(kl)}, \tag{6.19}$$

$$\kappa^P_{mq} = -\zeta_{mq} - 1/2\epsilon_{klq}\gamma_{kl,m} \tag{6.20}$$

for the purpose of calculating the fields of a continuous distribution of infinitesimal defect loops. Furthermore, we note from (2.15) and (6.19) that only the dislocation loop density γ_{kl} will contribute to the total displacement. Hence the elastic strain and stress are unaffected by the disclination loop density, ζ_{mq}, as we already hinted at in section 5.3. We also note that all the above results reduce to those of section 3.3 when the disclination loop density vanishes, $\zeta_{mq} = 0$.

Mura [4] generalized his "plastic distortion" and "plastic rotation," which he had defined for a discrete loop as in section 5.2, to a continuous distribution. We shall now interpret his approach. If we compare (5.14–15) with (6.19–20) we can make the following identification:

$$\beta^*_{(kl)} = -\gamma_{(kl)}, \tag{6.21}$$

$$\phi^*_{mq} + \frac{1}{2}\epsilon_{klq}\beta^*_{kl,m} = -\zeta_{mq} - \epsilon_{klq}\gamma_{kl,m}. \tag{6.22}$$

487-412 OL - 73 - 6

These equations can be solved for Mura's plastic quantities as follows:

$$\beta^*_{kl} = -\gamma_{kl} - \epsilon_{klq}\omega^*_q, \tag{6.23}$$

$$\phi^*_{mq} = -\zeta_{mq} + \omega^*_{q,\,m}, \tag{6.24}$$

where ω^*_q is an arbitrary vector field. These relations identify Mura's quantities for a continuous distribution of defect loops. The basic plastic fields are obtained in terms of Mura's quantities by substituting in (6.19–20)

$$e^P_{kl} = \beta^*_{(kl)}, \tag{6.25}$$

$$\kappa^P_{mq} = \phi^*_{mq} + \frac{1}{2}\epsilon_{klq}\beta^*_{kl,\,m}. \tag{6.26}$$

These relations are identical in form with (5.14–15), but are now also valid for a continuous distribution. We find the defect densities by substituting in (4.1–2)

$$\alpha_{pl} = -\epsilon_{pmk}(\beta^*_{kl,\,m} + \epsilon_{klq}\phi^*_{mq}), \tag{6.27}$$

$$\theta_{pq} = -\epsilon_{pmk}\phi^*_{kq,\,m}, \tag{6.28}$$

which are identical to relations in section 5.2. The interesting vector ω^*_q does not affect the basic plastic fields and the defect densities, and hence it does not affect the elastic fields either. In (6.23) it contributes the antisymmetric term $-\epsilon_{klq}\omega^*_q$ to β^*_{kl}. Mura [30] has called the dislocations resulting from an antisymmetric plastic distortion an *impotent* distribution of dislocations, because, as can be deduced from (2.15), such a distortion does not contribute to the total displacement, and hence gives no elastic fields. In general an antisymmetric plastic distortion will give a finite dislocation density, c.f. (3.4). However, the term $\omega^*_{q,\,m}$ in (6.24) is exactly right to annihilate both defect densities (6.27–28) due to ω^*_q. Hence, we can set $\omega^*_q = 0$ without loss of generality for the purpose of calculating the elastic fields due to a given distribution of β^*_{kl} and ϕ^*_{kq}, or

$$\beta^*_{kl} = -\gamma_{kl}, \tag{6.29}$$

$$\phi^*_{mq} = -\zeta_{mq}. \tag{6.30}$$

This shows that Mura's "plastic distortion" and "plastic rotation," introduced in section 5 for a discrete defect line, can be interpreted as the dislocation and disclination loop densities, except for a minus sign. This then resolves a difference we had with Mura. Relations (6.25–26) are the basic relations that connect Mura's approach with ours. For example the characteristic vectors are found from (4.5–6) to be

$$B_l = -\oint_\lambda (\beta^*_{kl} - \epsilon_{klq}\phi^*_{kq}x_r)\,dL_k, \tag{6.31}$$

$$\Omega_q = -\oint_\lambda \phi^*_{kq}\,dL_k, \tag{6.32}$$

which correspond to (6.9–10).

We can now also give an interpretation to (5.12–13) in terms of infinitesimal loops. To construct a discrete defect line L, we first distribute a constant density of infinitesimal disclination loops of strength Ω_q over any surface S whose boundary is L. This distribution only gives a rotation across S, but no stress, and furthermore no unique axis is defined. Rather, each infinitesimal loop has its

own axis, so that the resultant axis is continuously distributed over S. Now we add a distribution of infinitesimal dislocation loops to S, consisting of two parts. One, containing the dislocation Burgers vector, is a constant distribution of strength b_l, which gives the discrete dislocation line. The other, containing the Frank vector Ω_q, has just the right strength to bring the axis of each infinitesimal disclination loop to the point x_r^0. We see that this is done by increasing the dislocation loop strength proportional to the distance from the chosen axis. The combination of this linear infinitesimal dislocation loop density with the constant infinitesimal disclination loop density mentioned above gives the discrete disclination line. It is the infinitesimal dislocation loop distribution that gives rise to the elastic strain of the discrete disclination line.

So we conclude that for a finite defect loop the defect loop densities are given by

$$\gamma_{kl}(\mathbf{r}) = \delta_k(S)\{b_l + \epsilon_{lqr}\Omega_q(x_r - x_r^0)\}, \tag{6.33}$$

$$\zeta_{kq}(\mathbf{r}) = \delta_k(S)\Omega_q. \tag{6.34}$$

The vector $\delta_k(S)$ is the Dirac delta function on the surface S and it is always normal to S. In a plane we have a twist or a wedge disclination loop according to whether the Frank vector is normal or parallel to S, respectively. Therefore (6.34) shows that the diagonal and off-diagonal components of ζ_{kq} represent the twist and wedge components of the disclination loop density, respectively (see table 1). Equations (6.33–34) show how to make the transition from a continuous distribution of infinitesimal defect loops to a finite defect loop. By (B15) and (5.17) we see that they satisfy (6.9–10), which also remain valid for many finite loops, and therefore can be used for the transition from finite loops to a continuous distribution: For many finite defect loops the average dislocation and disclination loop densities γ_{kl} and ζ_{kq} represent the sum of the x_l component of the displacement jump vectors and the x_q component of the Frank vectors, respectively, of all the loops whose surfaces are intersected by a unit vector in the x_k direction.

The infinitesimal defect loop density tensors ζ_{kq} and γ_{kl} were defined in this section independent of the definitions of the defects densities in section 4.1 and the discrete defects in section 5.1. What is the correlation?

Let us first examine the relation between continuous distributions of defects and loop densities. For dislocations only there is a straightforward relation between them given by (3.37). When disclinations are introduced there is a similar straightforward relation between the disclination loop density and the disclination density tensor, given by (6.18). However, the dislocation density now contains a contribution from the disclination loops, equation (6.17). This means that the two definitions of the "dislocation" are not identical, and that a certain amount of mixing occurs in going from one formulation to the other.

Now let us examine the relation between a discrete defect line and a continuous distribution of loops. For dislocations only there is again a straightforward relation between the dislocation loop density and the Burgers vector, given by (3.39), or between the Burgers vector and the dislocation loop density, given by (3.35). When disclinations are introduced there is a similar straightforward relation between the disclination loop density and the Frank vector, given by (6.34), or between the Frank vector and the disclination loop density, given by (6.10). However, the dislocation loop density for a discrete defect line now contains a contribution from the Frank vector, equation (6.33), or the general Burgers vector contains a contribution from the disclination loop density, equation (6.9). Therefore the definitions of the dislocation are not identical in both approaches, and as we see from the relations quoted, a certain amount of mixing occurs in going from one formulation to the other.

There are, therefore, at least three independent ways to define the dislocation content of defects: in terms of a continuous distribution, a discrete line, or a continuous distribution of infinitesimal loops. For dislocations only, these definitions are equivalent but with disclinations they are essentially different.

7. The Discrete Dipole Line

7.1. Basic Relations: The Biaxial Dipole

Extending Kroupa's [18] definition of the dislocation dipole, we define the discrete dipole line as a close pair of discrete defect lines with opposite characteristic vectors. We call it the biaxial dipole because this defect would have two rotation axes. We wish to present in this section some of the relations analogous to those for the dislocation dipole in section 3.4.2. From (3.42), we find the defect densities of the biaxial dipole conjugate to the basic dislocation and disclination densities and θ_{pq} to be

$$\alpha^D_{pl}(\mathbf{r}) = -\xi_m \alpha_{pl,\,m}(\mathbf{r}), \tag{7.1}$$

$$\theta^D_{pq}(\mathbf{r}) = -\xi_m \theta_{pq,\,m}(\mathbf{r}). \tag{7.2}$$

By (5.19–20) these relations become for the discrete dipole line

$$\alpha^D_{pl}(\mathbf{r}) = -\delta_{p,\,m}(L)\{b_l + \epsilon_{lqr}\Omega_q(x_r - x^\circ_r)\}\xi_m - \delta_p(L)\epsilon_{lqr}\Omega_q\xi_r, \tag{7.3}$$

$$\theta^D_{pq}(\mathbf{r}) = -\delta_{p,\,m}(L)\Omega_q\xi_m. \tag{7.4}$$

The meaning of the displacement ξ_m is as follows: We let $\xi_m \to 0$, $b_l \to \infty$, and $\Omega_q \to \infty$ in such a way that $b_l\xi_m$ and $\Omega_q\xi_m$ remain constant.

The displacement of the dipole line is from (3.44)

$$u^D_n(\mathbf{r}) = -\xi_m u^T_{n,\,m}(\mathbf{r}) \tag{7.5}$$

$$\begin{aligned} &= -\oint_L \epsilon_{pmk} C_{ijkl} G_{jn,\,i}(\mathbf{R})\{b_l + \epsilon_{lqr}\Omega_q(x'_r - x^0_r)\}\xi_m dL'_p \\ &\quad - \int_S \epsilon_{pmk} C_{ijkl} G_{jn,\,i}(\mathbf{R})\Omega_p \xi_m dS'_l \\ &\quad + \delta_m(S)\{b_l + \epsilon_{nqr}\Omega_q(x_r - x^0_r)\}\xi_m, \end{aligned} \tag{7.6}$$

where we have used (5.34) and (5.12). In this expression the third line can be made to vanish by choosing S near the line to lie along ξ, or $\xi_m dS'_m = 0$ along L. Nevertheless, due to the surface integral, the displacement is not a state quantity in contrast to the case of the dislocation dipole.

From (7.1–6) all other relevant quantities for a discrete biaxial dipole line can be derived if desired.

Equation (7.6) allows us to estimate the asymptotic behavior of the displacement at large distances from a straight biaxial dipole line. It is easily deduced that it will vary as $\ln r$ as $r \to \infty$. Hence the strain will vary as r^{-1} as $r \to \infty$. These results are also listed in table 3.

7.2. Influence of the Axis: The Uniaxial Dipole

The dipole of section 7.1 is obtained from the basic discrete defect line of section 5 by translating it through the infinitesimal distance ξ, including the axis of rotation, and then subtracting the basic defect at its original position.

In this section we first wish to isolate the influence of the motion of the axis, when the position of the defect line is held fixed. We therefore consider the following defect, again composed of two parts: the first is obtained from the basic defect by translating its axis only through an infinitesimal

distance ξ, and the second part is the negative of the basic defect at its original position. The defect densities of this defect are given by

$$\alpha^A_{pl} = \xi_m \partial \alpha_{pl} / \partial x^0_m , \tag{7.7}$$

$$\theta^A_{pq} = \xi_m \partial \theta_{pq} / \partial x^0_m . \tag{7.8}$$

By (5.19–20) these relations become

$$\alpha^A_{pl}(\mathbf{r}) = -\delta_p(L) \epsilon_{lqr} \Omega_q \xi_r , \tag{7.9}$$

$$\theta^A_{pq}(\mathbf{r}) = 0. \tag{7.10}$$

The displacement is

$$u^A_n(\mathbf{r}) = \xi_m \partial u^T_n(\mathbf{r}) / \partial x^0_m \tag{7.11}$$

$$= -\int_S C_{ijkl} G_{jn,i}(\mathbf{R}) \epsilon_{lqr} \Omega_q \xi_r dS'_k$$

$$= -\int_S \epsilon_{pmk} C_{ijkl} G_{jn,i}(\mathbf{R}) \Omega_p \xi_m dS'_l , \tag{7.12}$$

where the second equality follows from (5.33), and the third by rearranging the indices using the symmetry condition (2.3).

On comparing (7.9) and (7.12) with (3.23) and (3.30), we see that they represent the dislocation density and displacement of a discrete dislocation line with Burgers vector

$$b_l = -\epsilon_{lqr} \Omega_q \xi_r . \tag{7.13}$$

This was to be expected, since the motion of the axis through the distance ξ_r has the effect of translating the two sides of S by the distance b_l given in (7.13), as we can see from (5.5). This conclusion complements the statement in section 5.2 that the axis of a discrete defect line can be moved by adding a dislocation to the line, c.f. (5.23).

Next we want to examine the effect of holding the axis fixed and moving the defect line only. This type of the defect will be called a uniaxial dipole because it has only one axis. It could alternatively have been used as the definition of the discrete dipole line. It is composed of the following two parts: the first is obtained from the basic discrete defect line by translating it through an infinitesimal distance ξ keeping its axis fixed, and the second part is the negative of the basic defect at its original position. The resulting fields are simply the difference between those in section 7.1 and the above. So the dislocation density and displacement of the uniaxial dipole are

$$\alpha^L_{pl}(\mathbf{r}) = \alpha^D_{pl}(\mathbf{r}) - \alpha^A_{pl}(\mathbf{r}) \tag{7.14}$$

$$= -\delta_{p,m}(L) \{ b_l + \epsilon_{lqr} \Omega_q (x_r - x^0_r) \} \xi_m , \tag{7.15}$$

$$u^L_n(\mathbf{r}) = u^D_n(\mathbf{r}) - u^A_n(\mathbf{r}) \tag{7.16}$$

$$= -\oint_L \epsilon_{pmk} C_{ijkl} G_{jn,i}(\mathbf{R}) \{ b_l + \epsilon_{lqr} \Omega_q (x'_r - x^0_r) \} \xi_m dL'_p , \tag{7.17}$$

whereas the disclination density is the same for either type of dipole,

$$\theta^L_{pq} = \theta^D_{pq} . \tag{7.18}$$

We note that the displacement of the uniaxial dipole is a state quantity.

A special case of (7.17) is of particular interest, namely, the one corresponding to the wedge disclination coinciding with its axis as the basic defect. In this case $b_l=0$. For a wedge disclination the Frank vector is parallel to the disclination line, $\mathbf{\Omega} \| d\mathbf{L}'$. The point $\mathbf{r}'$ lies on the line and the point $\mathbf{r}^0$ on the axis. Since the line coincides with the axis, the difference, is also parallel to the line, $(\mathbf{r}'-\mathbf{r}^0) \| d\mathbf{L}'$. So $\mathbf{\Omega} \| (\mathbf{r}'-\mathbf{r}^0)$, and hence $\epsilon_{lqr}\Omega_q(x'_r-x^0_r)=0$. We conclude that (7.17) vanishes for this case. Therefore $u^D_n=u^A_n$. This means that the conjugate dipole, corresponding to this wedge disclination with Frank vector Ω_q, is the dislocation with Burgers vector b_l given by (7.13). It is an edge dislocation because $\mathbf{b} \perp \mathbf{\Omega} \| d\mathbf{L}'$. Eshelby [21] used this approach to give a simple derivation of the elastic field of an edge dislocation, when the field of the wedge disclination is known.

Equation (7.17) shows that the asymptotic behavior of the displacement at large distances from a straight uniaxial dipole is the same as for a biaxial dipole. Table 3 shows there is a gap in the asymptotic behavior between a disclination dipole and loop, i.e., there is no disclination type defect with the r^{-1} behavior for the displacement.

8. Application to Dislocations

The purpose of this section is to check the internal consistency of the results for dislocations and the more general defects. It contains no new material. We want to show that the results of section 3 fall out of section 4–6, when no disclinations are present, i.e., when the plastic deformation of the body is completely described by the plastic distortion β^P_{kl}.

8.1. Continuous Distribution of Dislocations

8.1.1. Geometry

The plastic strain and rotation are now given by (c.f. 3.2–3)

$$e^P_{kl}=\beta^P_{(kl)}, \tag{8.1}$$

$$\omega^P_q=1/2\epsilon_{klq}\beta^P_{kl}, \tag{8.2}$$

so that

$$e^P_{kl}+\epsilon_{klq}\omega^P_q=\beta^P_{kl}, \tag{8.3}$$

in agreement with (3.1). The plastic bend-twist is (c.f. 3.12)

$$\kappa^P_{kq}=\omega^P_{q,k}. \tag{8.4}$$

Hence we find from (4.1)

$$\alpha_{pl}=-\epsilon_{pmk}(e^P_{kl,m}+\epsilon_{klq}\omega^P_{q,m})=-\epsilon_{pmk}\beta^P_{kl,m}, \tag{8.5}$$

in agreement with (3.4), and from (4.2)

$$\theta_{pq}=-\epsilon_{pmk}\omega^P_{q,km}=0, \tag{8.6}$$

as expected. The Burgers vector is found from (4.5)

$$\begin{aligned} B_l&=-\oint_\lambda (e^P_{kl}-\epsilon_{lqr}\omega^P_{q,k}x_r)dL_k \\ &=-\oint_\lambda (e^P_{kl}+\epsilon_{lqk}\omega^P_q)dL_k \\ &=-\oint_\lambda \beta^P_{kl}dL_k. \end{aligned} \tag{8.7}$$

Here the first equality follows from (8.4), the second from a partial integration where the integrated part vanishes around the closed curve λ, and the third from (8.3). The result agrees with (3.7). Furthermore we also see that (8.6) in (4.7) agrees with (3.8). The Frank vector is found from (4.6) and (8.4):

$$\Omega_q = -\oint_\lambda \omega_{q,k} dL_k = 0, \tag{8.8}$$

as expected. This also agrees with (8.6) in (4.8).

In a similar way it is easily shown that (4.17) and (4.20) reduce to (3.10) and (3.11), whereas (4.18) and (4.21) vanish.

8.1.2. Statics

The κ^P_{lp} term in (4.23) becomes by (8.4)

$$-\int \epsilon_{pmk} C_{ijkl} G_{jn,i}(\mathbf{R}) \omega^P_{p,l}(\mathbf{r}') dV' = -\int \epsilon_{pmk} C_{ijkl} G_{jn,il}(\mathbf{R}) \omega^P_p(\mathbf{r}') dV'$$

$$= \epsilon_{pmn} \omega^P_p(\mathbf{r}).$$

Here the first equality follows by a partial integration, and the second by (2.7). Hence we have for the total distortion (4.23).

$$u^T_{n,m}(\mathbf{r}) = \int \epsilon_{pmk} C_{ijkl} G_{jn,i}(\mathbf{R}) \alpha_{pl}(\mathbf{r}') dV' + e^P_{mn}(\mathbf{r}) + \epsilon_{pmn} \omega^P_p(\mathbf{r}), \tag{8.9}$$

in agreement with (3.16) and (3.1). From (4.14) we find the elastic strain

$$e_{mn}(\mathbf{r}) = \int \epsilon_{pmk} C_{ijkl} G_{jn,i}(\mathbf{R}) \alpha_{pl}(\mathbf{r}') dV'_{(mn)}. \tag{8.10}$$

This relation can also be obtained from (4.29) with (8.6). It is in agreement with (3.13) and (3.17).

We next find the bend-twist. From (8.9) and (8.4) we find

$$u^T_{n,ms}(\mathbf{r}) = \int \epsilon_{pmk} C_{ijkl} G_{jn,is}(\mathbf{R}) \alpha_{pl}(\mathbf{r}') dV' + e^P_{mn,s}(\mathbf{r}) + \epsilon_{pmn} \kappa^P_{sp}(\mathbf{r}). \tag{8.11}$$

Hence we find from (4.15)

$$\kappa_{st}(\mathbf{r}) = 1/2 \int \epsilon_{tmn} \epsilon_{pmk} C_{ijkl} G_{jn,is}(\mathbf{R}) \alpha_{pl}(\mathbf{r}') dV'. \tag{8.12}$$

This relation can also be obtained from (4.34) with (8.6). We see it is in agreement with (3.14) and (3.17).

8.2. The Discrete Dislocation Line

8.2.1. Geometry

When a discrete defect line contains no disclination, $\Omega_q=0$, as we saw from (8.8). For this case (5.5) reduces to (3.18) and (5.6) becomes

$$[\omega_q(\mathbf{r})]=0, \tag{8.13}$$

while (5.7) reduces to (3.19) and (5.8) reduces to (3.20).

Next we find that (5.12–13) become

$$\beta^*_{kl}(\mathbf{r})=-\delta_k(S)b_l, \tag{8.14}$$

$$\phi^*_{kq}(\mathbf{r})=0. \tag{8.15}$$

This shows from (3.21) that

$$\beta^*_{kl}=\beta^P_{kl}, \tag{8.16}$$

as expected, since both sides represent the dislocation loop density by (6.29) and (3.38). Equation (8.15) shows that the disclination loop density vanishes. Now (5.14–15) become from (8.14–15)

$$e^P_{kl}(\mathbf{r})=-1/2[\delta_k(S)b_l+\delta_l(S)b_k], \tag{8.17}$$

$$\begin{aligned}\kappa^P_{mq}(\mathbf{r})&=-1/2\epsilon_{klq}\delta_{k,m}(S)b_l,\\ (\kappa^P_{kq}(\mathbf{r})&=-1/2\epsilon_{lqr}\delta_{r,k}(S)b_l).\end{aligned} \tag{8.18}$$

We see that (8.17) is in agreement with (3.2) and (3.21) and that (8.18) agrees with (3.12) and (3.21).

From (5.17) we find that

$$B_l=b_l, \tag{8.19}$$

showing that the total Burgers vector reduces to the dislocation Burgers vector. From (4.1) and (8.17–18) we find

$$\alpha_{pl}(\mathbf{r})=\epsilon_{pmk}\delta_{k,m}(S)b_l=\delta_p(L)b_l. \tag{8.20}$$

This result can also be obtained directly from (5.19) and is in agreement with (3.23). Next we find from (4.2) and (8.18) or directly from (5.20)

$$\theta_{pq}(\mathbf{r})=1/2\,\epsilon_{pmk}\,\epsilon_{lqr}\,\delta_{r,km}\,(S)\,b_l=0, \tag{8.21}$$

as expected, in agreement with (8.6).

8.2.2. Statics

Again for $\Omega_q=0$, we see that (5.33) reduces to (3.30), and (5.34) reduces to (3.31) with (8.16). The elastic strain is

$$e_{mn}(\mathbf{r})=\oint_L \epsilon_{pmk}C_{ijkl}G_{jn,i}(\mathbf{R})b_l dL'_{P(mn)}. \tag{8.22}$$

This result can be found in two ways: first from (5.37), or second from (4.29) with (8.20–21). It is in agreement with (3.13) and (3.32).

Next we find the elastic bend-twist from (5.40)

$$\kappa_{st}(\mathbf{r}) = 1/2 \oint_L \epsilon_{tmn}\epsilon_{pmk}C_{ijkl}G_{jn,\,is}(\mathbf{R})b_l dL'_p. \tag{8.23}$$

This could also have been found from (4.34) with (8.20–21), and is in agreement with (3.14) and (3.32).

So we have shown in this section that the more general defect theory, including disclinations, completely reduces to the well-known dislocation theory in the special case that the disclinations vanish.

9. The "Dislocation Model" of a Discrete Defect Line

Li and Gilman [20] considered the finite disclination loop as a continuous distribution of dislocations, and called this the "dislocation model" of the disclination. Mura [22] used the same concept, which he ascribed to Eshelby, discussing also the case where he replaced a wedge disclination by a semi-infinite edge dislocation wall. We wish to make clear the distinction between the two concepts.

We start with the observation, made in section 6, that only the dislocation loop density, or Mura's "plastic distortion" β^*_{kl}, contributes to the elastic strain. For a discrete defect line, this quantity is given by (5.12). So the elastic strain obtained from this expression does not depend on what we choose for the disclination loop density, or Mura's "plastic rotation" ϕ^*_{kq}. If we choose it to vanish

$$\phi^*_{kq} = 0, \tag{9.1}$$

then we have a distribution of dislocation loops over the surface S that gives exactly the same elastic strain as the discrete defect line of section 5. We call the corresponding dislocation distribution the *dislocation model* of the defect line. We note that this dislocation model is clearly a different defect from the discrete defect line it corresponds to. Specifically, we obtain the dislocation model by setting

$$\beta^P_{kl} = \beta^*_{kl}, \tag{9.2}$$

where

$$\beta^*_{kl}(\mathbf{r}) = -\,\delta_k(S)\{b_l + \epsilon_{lqr}\Omega_q(x_r - X^o_r)\}, \tag{9.3}$$

and where b_l and Ω_q are constants. We can then use the methods of section 3.1 to find any other desired relations. Furthermore (5.14–16) become by (9.1)

$$e^P_{kl} = \beta^*_{(kl)}, \tag{9.4}$$

$$\kappa^P_{mq} = 1/2\epsilon_{klq}\beta^*_{kl,\,m}, \tag{9.5}$$

$$e^P_{kl,\,m} + \epsilon_{klq}\kappa^P_{mq} = \beta^*_{kl,\,m}. \tag{9.6}$$

With these relations we can alternatively use the methods of section 4 to find any other desired results

9.1. Geometry

We find the dislocation density from (3.4) with (9.2) or (4.1) with (9.6)

$$\begin{aligned}\alpha_{pl}(\mathbf{r}) &= -\epsilon_{pmk}\beta^*_{kl,m}\\ &= \epsilon_{pmk}\delta_{k,m}(S)\{b_l+\epsilon_{lqr}\Omega_q(x_r-x^0_r)\}+\epsilon_{pmk}\delta_k(S)\epsilon_{lqr}\Omega_q\delta_{rm}\\ &= \delta_p(L)\{b_l+\epsilon_{lqr}\Omega_q(x_r-x^0_r)\}+\delta_l(S)\Omega_p-\delta_{pl}\delta_k(S)\Omega_k. \end{aligned} \tag{9.7}$$

Here the second equality follows from (9.3), and the third from Stokes' theorem (B26) and the expansion (A3). We see now that the dislocation model is a dislocation distribution consisting of the following two parts: First a dislocation line along L, which is the same as for the corresponding discrete defect line, (5.19), and second a constant dislocation distribution over the surface S. In other words it is a dislocation wall at the surface S, which terminates on a dislocation line at its boundary L. The disclination density vanishes from (4.2) and (9.5)

$$\theta_{pq} = -\epsilon_{pmk}1/2\epsilon_{lqr}\beta^*_{rl,km} = 0, \tag{9.8}$$

as expected.

We see that the continuity equation (3.6) or (4.3) is satisfied

$$\begin{aligned}\alpha_{pl,p}(\mathbf{r}) &= \delta_{p,p}(L)\{b_l+\epsilon_{lqr}\Omega_q(x_r-x^0_r)\}+\delta_p(L)\epsilon_{lqp}\Omega_q+\delta_{l,p}(S)\Omega_p-\delta_{k,l}(S)\Omega_k\\ &= 0, \end{aligned} \tag{9.9}$$

where we have used (B27–28).

We next find the total Burgers vector from (4.5) with (9.4–5)

$$\begin{aligned}B_l &= -\oint_\lambda (\beta^*_{(kl)}-\beta^*_{[rl],k}x_r)dL_k\\ &= -\oint_\lambda \beta^*_{kl}dL_k\\ &= \oint_\lambda \delta_k(S)\{b_l+\epsilon_{lqr}\Omega_q(x_r-x^0_r)\}dL_k\\ &= b_l+\epsilon_{lqr}\Omega_q(x^{S\lambda}_r-x^0_r). \end{aligned} \tag{9.10}$$

Here the second equality follows by a partial integration, the third from (9.3), and the fourth from (B15–16), where $x^{S\lambda}_r$ is the point where λ crosses S (fig. 1).

9.2. Statics

If we substitute (9.3–4) into (2.15) we find for the displacement

$$u^T_n(\mathbf{r}) = \int_S C_{ijkl}G_{jn,i}(R)\{b_l+\epsilon_{lqr}\Omega_q(x'_r-x^\circ_r)\}\,dS'_r, \tag{9.11}$$

which is identical to (5.33). So we see that the displacement of the dislocation model is exactly the

same as the displacement of the corresponding discrete defect line. Hence (5.34) follows in exactly the same way

$$u^T_{n,m}(\mathbf{r}) = \oint_L \epsilon_{pmk} C_{ijkl} G_{jn,i}(\mathbf{R})\{b_l + \epsilon_{lqr}\Omega_q(x'_r - x^\circ_r)\}dL'_p + \int_S \epsilon_{pmk} C_{ijkl} G_{jn,i}(\mathbf{R})\Omega_p dS'_l + \beta^*_{mn}(\mathbf{r}). \tag{9.12}$$

So we find the elastic distortion from (3.9) and (9.2)

$$\beta_{mn}(\mathbf{r}) = \oint_L \epsilon_{pmk} C_{ijkl} G_{jn,i}(\mathbf{R})\{b_l + \epsilon_{lqr}\Omega_q(x'_r - x_r)\}dL'_p + \int_S \epsilon_{pmk} C_{klmn} G_{jn,i}(\mathbf{R})\Omega_p dS'_l \tag{9.13}$$

This relation could also be obtained from (3.17) and (9.7). It follows from the discussion in section 3.1.2 that this elastic distortion is a state quantity for the dislocation model, but according to the discussion of section 5.3 it is not a state quantity for the discrete defect line. This may be the physical significance of Mura's "elastic distortion" for a discrete disclination.

$$e_{mn}(\mathbf{r}) = \oint_L \epsilon_{pmk} C_{ijkl} G_{jn,i}(\mathbf{R})\{b_l + \epsilon_{lqr}\Omega_q(x'_r - x^\circ_r)\}dL'_{p(mn)} + \int_S \epsilon_{pmk} C_{ijkl} G_{jn,i}(\mathbf{R})\Omega_p dS'_{l(mn)}. \tag{9.14}$$

This relation also follows from (4.14) with (9.4) and (9.12), or (4.29) with (9.7–8). We see that this expression is identical to (5.36). So the elastic strain and hence stress of the dislocation model is identical to that of the corresponding defect line, as we stated before.

We next find the bend-twist. From (9.12) we have

$$u^T_{n,ms}(\mathbf{r}) = \oint_L \epsilon_{pmk} C_{ijkl} G_{jn,is}(\mathbf{R})\{b_l + \epsilon_{lqr}\Omega(x'_r - x^\circ_r)\}dL'_p + \int_S \epsilon_{pmk} C_{ijkl} G_{jn,is}(\mathbf{R})\Omega_p dS'_l + \beta^*_{mn,s}(\mathbf{r}), \tag{9.15}$$

and from (4.15) and (9.5)

$$\kappa_{st}(\mathbf{r}) = 1/2 \oint_L \epsilon_{tmn}\epsilon_{pmk} C_{ijkl} G_{jn,is}(\mathbf{R})\{b_l + \epsilon_{lqr}\Omega_q(x'_r - x^\circ_r)\}dL'_p + 1/2 \int_S \epsilon_{tmn}\epsilon_{pmk} G_{jn,is}(\mathbf{R})\Omega_p dS'_l. \tag{9.16}$$

This relation could also have been obtained from (3.14) with (9.13), or from (4.34) with (9.7–8).

We see from this section that there is a great similarity between the dislocation model and its corresponding discrete defect line. Therefore it is important to distinguish carefully between them. For example, the defect densities for the discrete line are given by (5.19–20), while for the dislocation model they are given by (9.7–8). So we see that in the transition the disclination density in (5.20) has been traded for the constant surface dislocation density in (9.7). As we saw both defects give the same elastic strain; explicit expressions for it can be obtained by substituting the above densities into (4.29). For the discrete defect line we find (5.37) and for the dislocation model (9.14) for the elastic strain. We see that the second term in (5.37) represents the contribution from the disclination density; it equals the second term in (9.14) which represents the contribution from the constant surface dislocation density. We shall illustrate some special cases of the dislocation model in future publications [25, 26].

Li and Gilman have also calculated the force on a discrete disclination line by assuming that it equals the force on the corresponding dislocation model. Since the present paper does not deal with forces a formal proof of this interesting result will be published elsewhere [23].

10. The Compensated Disclination Line

We now want to investigate a problem that complements the one of section 9. Consider a vanishing dislocation loop density and a disclination loop density given by (5.13)

$$\beta^*_{kl}=0, \tag{10.1}$$

$$\phi^*_{kq}(\mathbf{r})=-\delta_k(S)\Omega_q, \tag{10.2}$$

where Ω_q is a constant. This represents just a constant distribution of disclination loops on the surface S. Since there is no dislocation loop distribution, we shall find that there is no elastic strain for this defect. We find the plastic quantities from (5.14–16)

$$e^p_{kl}=0, \tag{10.3}$$

$$\kappa^p_{kq}=\phi^*_{kq}. \tag{10.4}$$

We now use the methods of section 4 to find any further desired results.

10.1. Geometry

The dislocation and disclination densities are from (4.1–2)

$$\begin{aligned}\alpha_{pl}(\mathbf{r})&=\epsilon_{pmk}\epsilon_{klq}\delta_m(S)\Omega_q\\&=\delta_{pl}\delta_k(S)\Omega_k-\delta_l(S)\Omega_p,\end{aligned} \tag{10.5}$$

$$\begin{aligned}\theta_{pq}(\mathbf{r})&=\epsilon_{pmk}\delta_{k,m}(S)\Omega_q\\&=\delta_p(L)\Omega_q,\end{aligned} \tag{10.6}$$

where we have used Stokes' theorem (B26). Therefore the defect in this case is a dislocation wall at the surface S, which terminates on a disclination at its boundary L. It consists of the same discrete disclination line as treated in section 5, (5.20), and a dislocation distribution on S, which is just right to make the elastic strain vanish. Therefore we have called it the *compensated disclination line*. Note that the sum of (10.5) and (9.7) gives (5.20), and that (10.6) is the same as (5.19). This was of course to be expected, because sections 9 and 10 represent a decomposition of the problem of section 5. We find that the above results satisfy the continuity equations (4.3–4)

$$\alpha_{pl,p}(\mathbf{r})+\epsilon_{lpq}\theta_{pq}(\mathbf{r})=\delta_{k,l}(S)\Omega_k-\delta_{l,p}(S)\Omega_p+\epsilon_{lpq}\delta_p(L)\Omega_q=0, \tag{10.7}$$

$$\theta_{pq,p}(\mathbf{r})=\delta_{p,p}(L)\Omega_q=0, \tag{10.8}$$

using (B27–28).

We next find the total Burgers vector from (4.5) and (10.2–4)

$$\begin{aligned}B_l&=-\oint_\lambda \epsilon_{lqr}\delta_k(S)\Omega_q x_r dL_k\\&=-\epsilon_{lqr}\Omega_q x_r^{S\lambda},\end{aligned} \tag{10.9}$$

by (B16), where $x_r^{S\lambda}$ is the point of intersection between the curve λ and the surface S (fig. 1). We note that the sum of (10.9) and (9.10) is the same as (5.17). We find the Frank vector from (4.6), (10.4), and (10.2)

$$-\oint_\lambda \kappa_{kq}^P dL_k = \oint_\lambda \delta_k(S)\Omega_q dL_k = \Omega_q, \tag{10.10}$$

using (B15). This identifies the constant Ω_q as the Frank vector. The same results can be obtained from (4.7–8) and (10.5–6).

10.2. Statics

If we substitute (10.3) into (2.15) we find the displacement

$$u_n^T = 0. \tag{10.11}$$

Hence from (4.14) and (10.3)

$$e_{kl} = 0. \tag{10.12}$$

So we see that there is no elastic strain and hence stress, as we discussed before. The elastic bend-twist is from (4.15), (10.11), (10.4), and (10.2)

$$\kappa_{kq}(\mathbf{r}) = -\kappa_{kq}^P(\mathbf{r}) = \delta_k(S)\Omega_q. \tag{10.13}$$

For consistency we show that this relation can also be derived another way. If we substitute (10.5–6) into (4.34) we find

$$\kappa_{st}(\mathbf{r}) = -1/2 \int_S \epsilon_{tmn}\epsilon_{pmk} C_{ijkl} G_{jn,is}(\mathbf{R})\Omega_p dS_l' + 1/2 \oint_L \epsilon_{tmn}\epsilon_{pmk}\epsilon_{qsl} C_{ijkl} G_{jn,i}(\mathbf{R})\Omega_p dL_q', \tag{10.14}$$

which by Stokes' theorem (A2), (2.7), and (B5) becomes

$$\begin{aligned}\kappa_{st}(\mathbf{r}) &= -1/2 \int_S \epsilon_{tmn}\epsilon_{pmk} C_{ijkl} G_{jn,il}(\mathbf{R})\Omega_p dS_s' \\ &= 1/2 \int_S \epsilon_{tmn}\epsilon_{pmk}\delta_{kn}\delta(\mathbf{R})\Omega_p dS_s' \\ &= \delta_s(S)\Omega_t,\end{aligned} \tag{10.15}$$

in agreement with (10.13). Note that the sum of (10.14) and (9.16) gives (5.40), as expected.

Summarizing, we see that when the compensated disclination line is added to the dislocation model we obtain the discrete defect line.

11. Summary

We started this paper with the general solution of the plastic strain problem which is just an extension of Eshelby's transformation problem and essentially equivalent to Mura's plastic distortion problem. It formed the basis of all static defect fields. We then reviewed dislocation theory, including the continuous distribution, the discrete line, Kroupa's continuous distribution of infinitesimal loops, and the dipole. This introductory material formed the point of departure for the

general theory of defects, i.e., disclinations and dislocation combined. On the other hand, it formed a basis of comparison, because the general defect theory reduces to it when the disclinations vanish.

We defined the continuous distribution of defects. This definition was motivated by a violation of the compatibility equations. We also defined the Frank vector, which is the characteristic rotation vector of the disclinations, analogous to the Burgers vector for dislocations. We derived closed integral expressions for the basic elastic fields, the elastic strain and bend-twist, in terms of the defect densities, showing that they are state quantities. These integrals contain kernels with Green's tensor and the incompatibility source tensor, a type of Green's tensor introduced by Simmons and Bullough.

The definition of the discrete defect line was motivated by Weingarten's theorem. A new quantity introduced here is the axis of rotation, which did not exist for a continuous distribution. After finding the basic plastic fields, the plastic strain and bend-twist, all the results for the continuous distribution can be specialized to the discrete case. We found that the calculations were simplified by using two new quantities, Mura's "plastic distortion" and "plastic rotation," which we later identified as the dislocation and disclination loop densities. We found that the axis of a disclination can be translated to a new position by adding a discrete dislocation line to it. We found the basic elastic fields as closed line integral, which confirmed again their nature as state quantities.

The continuous distribution of infinitesimal defect loops was defined by extending Kroupa's definition for dislocation loops. The complete correlation to the continuous distribution of defects was established by finding the basic plastic fields in terms of the loop densities. It was then simple to identify Mura's plastic quantities, as mentioned above, which resolves a difference we had with Mura.

We found that the three independent definitions for defects, i.e., for continuous distributions, discrete lines, and infinitesimal loops, do not lead to a single concept of the disclination. Rather, the disclination defined in one formulation contains a certain amount of dislocation in the two other formulations. So a certain amount of mixing occurs in going from one formulation to another, but the amount can be uniquely determined. Our difference with Anthony for example originates from this mixing between continuous defect distributions and discrete defect lines. As another example we interpreted the discrete defect line in terms of a continuous distribution of defect loops, which clarifies our difference with Mura.

The discrete dipole line was defined by extending Kroupa's definition of the dislocation dipole. We find there is a great similarity between disclination dipoles and dislocation lines.

Then we showed that the general defect theory reduces to the classical dislocation theory when the disclinations vanish.

We clarified the concept of the "dislocation model" of a discrete defect line, introduced by Li and Gilman. We found that it is a distribution of dislocation loops identical to that for the corresponding discrete defect, but without any distribution of disclination loops. In Mura's terms it is given by the "plastic distortion" without "plastic rotation." We found that the dislocation model is a dislocation wall which terminates on a discrete dislocation lying along the same line as the corresponding defect line. The dislocation model has the same total displacement, elastic strain, and stress as the corresponding discrete defect line. The "elastic distortion" of the dislocation model is Mura's "elastic distortion" of the discrete defect line. The great similarity between the dislocation model and its corresponding discrete defect line makes it important to distinguish clearly between these two concepts.

We concluded the paper with the "compensated disclination line," which is a constant distribution of disclination loops over a surface. In Mura's terms it is given by the "plastic rotation" without "plastic distortion." We found that it is a dislocation wall terminating at a discrete disclination line, giving no displacement, strain, and stress. The sum of the compensated disclination line and the dislocation model gives the discrete defect line.

In an appendix we have developed a special notation, adapted from Kunin. It is very helpful

for the treatment of discrete defects where generalized functions appear, such as the Dirac delta function.

So we have presented a general theory of stationary defects for a linearly elastic, infinitely extended, homogeneous body. In future publications we shall specialize these results to isotropy [24] and apply them to straight disclinations [25] and disclination loops [26].

The major shortcoming of the present treatment might be the use of linear theory. This means that in a real solid the resulting fields close to discrete defects will deviate considerably from our formulas, but they will become more realistic the further away we are from a defect. This point will be more clearly illustrated in the future publications where we obtain specific results for particular geometries. However, without the linear assumption we certainly could not have pushed the theory as far as we did. This is the price we paid for a fairly complete analytic treatment.

Within its limitations the present theory is completely self-consistent. Aside from its possible intrinsic usefulness, it can be used as a starting point for generalizations, such as dynamics, nonlinear effects, couple-stresses, a finite body, or inhomogeneities.

12. Appendix A. The Divergence Theorem and Stokes' Theorem

The *rank* (also called *order* by some authors) of a tensor equals the number of subscripts on the tensor. In the following let T be a tensor of any rank, where we have suppressed the subscripts.

The *divergence theorem* is formulated as follows

$$\int_V T_{,i}dV=\oint_S TdS_i, \tag{A1}$$

where the integrations are restricted to the arbitrary volume V and its bounding surface S, which is therefore a closed surface.

Stokes' theorem can be formulated in two ways. The first one is

$$\int_S \epsilon_{ijk}T_{,j}dS_i=\oint_L TdL_k, \tag{A2}$$

where ϵ_{ijk} is the permutation symbol. By using the identity

$$\epsilon_{ijk}\epsilon_{klm}\equiv\delta_{il}\delta_{jm}-\delta_{im}\delta_{jl} \tag{A3}$$

we find the second formulation

$$\oint_L \epsilon_{klm}TdL_k=\int_S (T_{,m}dS_l-T_{,l}dS_m). \tag{A4}$$

Here the integrations are restricted to the arbitrary surface S and its bounding curve L, which is therefore a closed curve. We use the right-hand rule in relating the curve L to the surface S.

13. Appendix B. Delta Functions on Curves and Surfaces

This appendix is an adaptation of a treatment by Kunin [27]. Let $\phi(x)$ be an infinitely differentiable finite function of x, called a test function. We can define the *Dirac delta function* $\delta(x)$ by

$$\int_a^b \delta(x-x')\phi(x)dx=\begin{cases}0, & \text{if } x'<a,\\ \phi(x'), & \text{if } a<x'<b,\\ 0, & \text{if } b<x',\end{cases} \tag{B1}$$

where a and b are arbitrary constants. Since $\delta(x)$ is a generalized function, the integrals in this and subsequent equations are meaningless in the sense of classical analysis. Instead they are to be

regarded as a symbolic notation. This notation has been treated in detail by Gel'fand and Shilov [28]. The meaning to be attached to the following integrals then follows from the fact that all subsequent results are derived from the definition (B1).

The three-dimensional Dirac delta function $\delta(\mathbf{r})$ is defined by

$$\delta(\mathbf{r}-\mathbf{r}') \equiv \delta(x_1-x_1')\delta(x_2-x_2')\delta(x_3-x_3'). \tag{B2}$$

Let the test function $\phi(\mathbf{r})$ be an infinitely differentiable finite function of position $\mathbf{r}$. Then it follows from (B1–2) that

$$\int_V \delta(\mathbf{r}-\mathbf{r}')\phi(\mathbf{r})dV = \begin{cases} \phi(\mathbf{r}'), & \text{if } \mathbf{r}' \text{ is in } V, \\ 0, & \text{if } \mathbf{r}' \text{ is not in } V, \end{cases} \tag{B3}$$

where $dV = dx_1dx_2dx_3$ and V is an arbitrary volume.

The Dirac delta functions for a curve L, a surface S, or a volume V are defined by

$$\delta_i(L) \equiv \int_L \delta(\mathbf{r}-\mathbf{r}')dL_i', \tag{B4}$$

$$\delta_i(S) \equiv \int_S \delta(\mathbf{r}-\mathbf{r}')dS_i', \tag{B5}$$

$$\delta(V) \equiv \int_V \delta(\mathbf{r}-\mathbf{r}')dV'. \tag{B6}$$

We see that $\delta_i(L)$ and $\delta_i(S)$, in addition to being delta functions, are also vectors parallel to the curve L and normal to the surface S, respectively. From (B3) we see that

$$\delta(V) = \begin{cases} 1, & \text{if } \mathbf{r} \text{ is in } V, \\ 0, & \text{if } \mathbf{r} \text{ is not in } V. \end{cases} \tag{B7}$$

We now have the following relations

$$\int \delta_i(L)\phi(\mathbf{r})dV = \int_L \phi(\mathbf{r})dL_i, \tag{B8}$$

$$\int \delta_i(S)\phi(\mathbf{r})dV = \int_S \phi(\mathbf{r})dS_i, \tag{B9}$$

$$\int \delta(V)\phi(\mathbf{r})dV = \int_V \phi(\mathbf{r})dV, \tag{B10}$$

where the integrals in the left-hand sides are over all space, and those on the right-hand sides are restricted to the curve L, surface S, and volume V, respectively. To prove the first relation, (B8), substitute (B4) in the left-hand side, and we have

$$\int\int_L \delta(\mathbf{r}-\mathbf{r}')dL_i'\phi(\mathbf{r})dV = \int_L\int \delta(\mathbf{r}-\mathbf{r}')\phi(\mathbf{r})dVdL_i' = \int_L \phi(\mathbf{r}')dL_i'$$

by interchanging integration and using (B3). The proofs of (B9) and (B10) follow in a similar way. By a slight change of variable we can also write (B8–10) as follows

$$\int \delta_i(L')\phi(\mathbf{r}-\mathbf{r}')dV' = \int_L \phi(\mathbf{r}-\mathbf{r}')dL_i', \tag{B11}$$

$$\int \delta_i(S')\phi(\mathbf{r}-\mathbf{r}')dV' = \int_S \phi(\mathbf{r}-\mathbf{r}')dS_i', \tag{B12}$$

$$\int \delta(V')\phi(\mathbf{r}-\mathbf{r}')dV' = \int_V \phi(\mathbf{r}-\mathbf{r}')dV'. \tag{B13}$$

If the curve L crosses the surface S once, we also have the relation

$$\int_S \int_L \delta(\mathbf{r}-\mathbf{r}')dL_i'dS_j = \frac{t_i n_j}{|t_k n_k|}, \tag{B14}$$

where t_i is the unit tangent to the curve L, and n_j the unit normal to the surface S, at the point of intersection, $\mathbf{r}^{LS}$. To prove this relation, note that the integrals in (B14) contribute only at the point $\mathbf{r}^{LS}$. Therefore we can replace the curve L by a straight line tangent to L at $\mathbf{r}^{LS}$, and the surface S by a plane tangent to S at $\mathbf{r}^{LS}$. We shall next calculate the integral in (B14) for the special case $n_j=(001)$, i.e., when S is the x_1x_2 plane. For $j=1, 2$ the integrals then vanish in agreement with (B14). For $j=3$ we have by (B2) and (B1)

$$\int_{-\infty}^{\infty}\int_{-\infty}^{\infty}\int_L \delta(x_1-x_1')\delta(x_2-x_2')\delta(x_3-x_3')dL_i'dx_1dx_2 = \int_L \delta(x_3-x_3')dL_i'$$

$$= \int_{-\infty}^{\infty} \delta(x_3-x_3')\frac{t_i}{|t_3|}dx_3'$$

$$= \frac{t_i}{|t_3|}.$$

Here we have used the fact that for a straight line $dL_i' = (t_i/t_3)dx_3'$, and that the range of x_3' is $(-\infty, \infty)$ for t_3 positive and $(\infty, -\infty)$ for t_3 negative. This result also agrees with (B14) for this special case. Hence (B14) holds in a particular coordinate system. By tensor analysis it is therefore also true in a general coordinate system. The specific form of (B14) can be derived from the above results by the method of Appendix II of reference [29]. From (B4), (B5), and (B14) we have

$$\int_S \delta_i(L)dS_i = \int_L \delta_i(S)dL_i = \begin{cases} 1, & \text{if } L \text{ crosses } S \text{ positively,} \\ 0, & \text{if } L \text{ does not cross } S, \\ -1, & \text{if } L \text{ crosses } S \text{ negatively.} \end{cases} \tag{B15}$$

It is not difficult to generalize these relations to

$$\int_S \delta_i(L)\phi(\mathbf{r})dS_i = \int_L \delta_i(S)\phi(\mathbf{r})dL_i = \begin{cases} \phi(\mathbf{r}^{LS}), & \text{if } L \text{ crosses } S \text{ positively,} \\ 0, & \text{if } L \text{ does not cross } S, \\ -\phi(\mathbf{r}^{LS}), & \text{if } L \text{ crosses } S \text{ negatively.} \end{cases} \tag{B16}$$

The *derivative* of delta functions is defined by switching the operation to the test function

$$\int_V \delta_{,j}(\mathbf{r}-\mathbf{r}')\phi(\mathbf{r})dV = -\int_V \delta(\mathbf{r}-\mathbf{r}')\phi_{,j}(\mathbf{r})dV, \tag{B17}$$

487-412 OL - 73 - 7

as suggested by classical analysis. Now we can write the derivatives of the delta functions (B4–6) as follows

$$\delta_{i,j}(L)=\int_L \delta_{,j}(\mathbf{r}-\mathbf{r}')dL_i', \tag{B18}$$

$$\delta_{i,j}(S)=\int_S \delta_{,j}(\mathbf{r}-\mathbf{r}')dS_i', \tag{B19}$$

$$\delta_{,j}(V)=\int_V \delta_{,j}(\mathbf{r}-\mathbf{r}')dV'. \tag{B20}$$

From these relations, it follows that

$$\int \delta_{i,j}(L)\phi(\mathbf{r})dV=-\int_L \phi_{,j}(\mathbf{r})\ dL_i, \tag{B21}$$

$$\int \delta_{i,j}(S)\phi(\mathbf{r})dV=-\int_S \phi_{,j}(\mathbf{r})dS_i, \tag{B22}$$

$$\int \delta_{,j}(V)\phi(\mathbf{r})dV=-\int_V \phi_{,j}(\mathbf{r})dV. \tag{B23}$$

For example, to prove (B21), substitute (B18) into the left hand side, and we have by (B17) and (B3)

$$\begin{aligned}\int\int_L \delta_{,j}(\mathbf{r}-\mathbf{r}')dL_i'\phi(\mathbf{r})dV&=\int_L\int \delta_{,j}(\mathbf{r}-\mathbf{r}')\phi(\mathbf{r})dVdL_i'\\&=-\int_L\int \delta(\mathbf{r}-\mathbf{r}')\phi_{,j}(\mathbf{r})dVdL_i'\\&=-\int_L \phi_{,j'}(\mathbf{r}')dL_i'.\end{aligned}$$

The proofs of (B22) and (B23) follow in a similar way.

The *divergence theorem* also holds for delta functions and is expressed as follows

$$\delta_{,i}(V)=-\delta_i(S), \tag{B24}$$

where S is the closed surface which is the boundary of V. This theorem is proved showing the following relationship:

$$\begin{aligned}\int \delta_{,i}(V)\phi(\mathbf{r})dV&=-\int_V \phi_{,i}(\mathbf{r})dV\\&=-\oint_S \phi(\mathbf{r})dS_i\\&=-\int \delta_i(S)\phi(\mathbf{r})dV,\end{aligned}$$

which follows from (B23), (A1), and (B9). Since $\phi(\mathbf{r})$ can be chosen arbitrarily, (B24) follows. We also conclude from this relation that

$$\epsilon_{ijk}\delta_{k,j}(S)=0 \tag{B25}$$

for a closed surface S.

Furthermore *Stokes' theorem* also holds for delta functions as follows

$$\epsilon_{ijk}\delta_{i,j}(S) = -\delta_k(L), \tag{B26}$$

or

$$\epsilon_{klm}\delta_k(L) = \delta_{m,l}(S) - \delta_{l,m}(S), \tag{B27}$$

where L is the closed curve which is the boundary of S. This theorem is proved by showing the following relationship:

$$\begin{aligned}\int \epsilon_{ijk}\delta_{i,j}(S)\phi(\mathbf{r})dV &= -\int_S \epsilon_{ijk}\phi_{,j}(\mathbf{r})dS_i \\ &= -\oint_L \phi(\mathbf{r})dL_k \\ &= -\int \delta_k(L)\phi(\mathbf{r})dV,\end{aligned}$$

which follows from (B22), (A2), and (B8). Since $\phi(\mathbf{r})$ can be chosen arbitrarily, (B26) follows, and (B27) follows directly from (B26). We conclude from (B26) that

$$\delta_{k,k}(L) = 0 \tag{B28}$$

for a closed curve L.

A *homogeneous function* of degree λ is defined by the equation

$$f(kx) = k^{\lambda}f(x) \tag{B29}$$

for any positive k. We wish to show that $\delta(\mathbf{r})$ is a homogeneous function of degree (-3) in r. From (B3) we have

$$\int \delta(\mathbf{r})\phi(\mathbf{r})dV = \phi(0). \tag{B30}$$

By a change of variable and (B3) we have

$$\begin{aligned}\int \delta(k\mathbf{r})\phi(\mathbf{r})dV &= k^{-3}\int \delta(\mathbf{r})\phi(k^{-1}\mathbf{r})dV \\ &= k^{-3}\phi(0).\end{aligned} \tag{B31}$$

Therefore, since $\phi(\mathbf{r})$ is arbitrary

$$\delta(k\mathbf{r}) = k^{-3}\delta(\mathbf{r}), \tag{B32}$$

which shows the contention.

14. References

[1] Nabarro, F. R. N., Theory of Crystal Dislocations (Oxford, 1967).
[2] Anthony, K. H., Arch. Rat. Mech. Anal. **39**, 43 (1970).
[3] deWit, R., in Fundamental aspects of dislocation theory, Eds. by J. A. Simmons, R. deWit, and R. Bullough, Nat. Bur. Stand. (U.S.), Spec. Publ. 317, Vol. **I** (1970), p. 651. Referred to as **I** in the present paper.
[4] Mura, T., Arch. Mech. Stos. **24**, 449 (1972).
[5] Kroupa, F., Czech. J. Phys. **B12**, 191 (1962).
[6] Weingarten, G., Atti Accad. naz. Lincei Rc. [5] **10**, 57 (1901).
[7] Volterra, V., Annls. Scient. Ec. norm. sup., Paris [3], **24**, 400 (1907).
[8] Kröner, E., Ergeb. Ang. Math. **5**, 1 (1958).
[9] Love, A. E. H., A Treatise on the Mathematical Theory of Elasticity, 3rd ed. (Cambridge U.P., 1920).
[10] Frank, F. C., Disc. Faraday Soc. **25**, 19 (1958).
[11] Eshelby, J. D., Progr. Solid Mechanics **II**, 87 (1961).
[12] Simmons, J. A., and Bullough, R., in Fundamental aspects of

dislocation theory, Eds. by J. A. Simmons, R. deWit and R. Bullough, Nat. Bur. Stand. (U.S.), Spec. Publ. 317, Vol. I, (1970) p. 89.
[13] Mura, T., Phil. Mag. **8**, 843 (1963).
[14] deWit, R., Acta Met. **13**, 1210 (1965), and Bilby, B. A., Bullough, R., and Smith, E., Proc. Roy. Soc. **A231**, 263 (1955).
[15] Willis, J. R., Int. J. Engng. Sci. **5**, 171 (1967).
[16] Underwood, E. E., Quantitative Stereology (Addison- Wesley, Reading, Mass., 1970), equations (6.40) and (6.44).
[17] Kroupa, F., in Theory of Crystal Defects, Ed. by B. Gruber (Academic Press., N.Y., 1966) p. 275.
[18] Kroupa, F., Czech. J. Phys. **B15**, 896 (1965).
[19] deWit, R., J. Appl. Phys. **42**, 3304 (1971).
[20] Li, J. C. M., and Gilman, J. J., J. Appl. Phys. **41**, 4248 (1970).
[21] Eshelby, J. D., Brit. J. Appl. Phys. **17**, 1131 (1966).
[22] Mura, T., The Relation between Disclinations and Dislocations, Europhysics Conference on Disclinations, Aussois (n.c. savoie), France, June 21–23, 1972.
[23] Das, E. S. P., Marcinkowski, M. J., and Armstrong, R. W., deWit, R., **27**, 369 (1973), Phil. Mag.
[24] deWit, R., Theory of Disclinations III. Continuous and Discrete Disclinations in Isotropic Elasticity (to be published).
[25] deWit, R., Theory of Disclinations IV. Straight Disclinations (to be published).
[26] deWit, R., Theory of Disclinations V. Disclination Loops (to be published).
[27] Kunin, I. A., Zh. Prikl. Mekh. Tekh. Fiz. **6**, 76 (1965), translated in Sov. Phys.—J. Appl. Mech. Tech. Phys. **6**, 49 (1965).
[28] Gel'fand, I. M., and Shilov, G. E., Generalized Functions, Vol. I (Academic Press, New York, 1964).
[29] deWit, R., phys. stat. sol. **20**, 567 (1967).
[30] Mura, T., in Mechanics of Generalized Continua, Ed. by E. Kröner (Springer-Verlag, Berlin, 1968), p. 269.

(Paper 77A1–754)

JOURNAL OF RESEARCH of the National Bureau of Standards—A. Physics and Chemistry
Vol. 77A, No. 1, January–February 1973

Photochemistry of Methane in the Photoionization Region*

R. E. Rebbert and P. Ausloos

Institute for Materials Research, National Bureau of Standards, Washington, D.C. 20234

(October 4, 1972)

Methane was irradiated with microwave operated helium (21.2 eV) and neon (16.7–16.8 eV) resonance lamps which were separated from the reaction vessel by an aluminum window. The quantum yields of the stable end products have been determined at methane pressures ranging from 1 to 20 torr. Over this pressure range the abundances of the primary ions, determined through various diagnostic experiments, are within experimental error the same at 21.2 eV as at 16.7–16.8 eV [($CH_4^+ \simeq CH_3^+ \simeq 0.5$, $CH_2^+ \leq 0.02$), and are in good agreement with the primary mass spectra obtained in a photoionization mass spectrometer under collision free conditions ($P < 10^{-5}$ torr). The $C_2H_5^+$ which is formed by the reaction: $CH_3^+ + CH_4 \rightarrow C_2H_5^+ + H_2$ loses a proton by an undetermined mechanism to give C_2H_4 as a product.

There is no evidence for the formation of neutral fragments such as H_2, C, CH or CH_2 at 16.7–16.8 eV. The fact that the ionization quantum is equal to unity in this energy range accounts for the absence of these intermediates. At 21.2 eV where ($\Phi_{ionization} = 0.95$) there is concrete evidence for the formation of carbon atoms ($\Phi(C) \geq 0.002$).

In an attempt to demonstrate the usefulness of enclosed neon and helium resonance light sources in the ion-molecule kinetic studies, the relative probabilities of transfer of H^- over D^- from various partially deuterium labeled hydrocarbons to $C_2H_5^+$ (or $C_2D_5^+$) has been determined.

The results presented in this article resolve the existing disagreements between previous helium resonance photolysis studies on CH_4.

Key words: Ion-molecule reaction; ion pair yield; methane; photochemistry; photoionization; quantum yields.

1. Introduction

In a pioneering study, Back and Walker [1][1] carried out the first photochemistry study on lower hydrocarbons in the photoionization region using the self-reversed 58.4 nm (21.2 eV) helium resonance line. The apparatus used was windowless and the photolysis vessel was separated from the light source (microwave discharge through helium) by a fast flow separation system. Significant experimental results were obtained even though such an open device limited the reactant pressure range in the reaction vessel (< 0.3 torr) and resulted in a certain degree of uncertainty concerning the monochromaticity of the incident radiation. More recently, thin (1500 to 4000 Å thick) aluminum films supported on a metal screen have been used to separate the light source from the reaction vessel and to filter out light at wavelengths > 90 nm [2–6]. Such devices were first used in 1968 to reexamine certain aspects of the photolysis of methane at 58.4 nm at reactant pressures up to 15 torr.

The present paper describes a more detailed study of the photochemistry of CH_4 in the photoionization region using an enclosed helium as well as a neon resonance ($\lambda = 74.37–73.59$ nm) light source. An attempt is made to resolve the existing disagreements in the yields of the chemical products formed in the windowless apparatus used by Back and Walker [1] as compared to the enclosed light source apparatus employed by Jensen and Libby [2]. Finally, reactions of the major ions, CH_5^+ and $C_2H_5^+$, formed in the photoionization of methane with various hydrocarbons are explored in order to assess the feasibility of using enclosed helium and neon resonance light sources in the study of ionic reactions.

2. Experimental Procedure

2.1. Apparatus

The design of the titanium-gettered light sources and of the reaction vessel has been described in a recent report from this laboratory [7]. The aluminum windows (0.61 in in diameter) were supplied by the Sigmatron Co., Goleta, California [8]. They consisted of a 1500 ± 100 Å film supported on a nickel screen. The windows were examined for pin-holes under a microscope and were tested for their pressure resistance. The approximately 50 photolysis experiments carried out in the course of this investigation at differential pressure readings up to 60 torr, were carried out by using one and the same enclosed light source. Transformation

*Sponsored in part by the U.S. Atomic Energy Commission.

[1] Figures in brackets indicate the literature references at the end of this paper.

of the helium lamp to a neon resonance light source, and vice versa, was accomplished by interchanging the rare gases in the body of the enclosed lamp. The pressure in the helium lamp was 1.6 torr and that in the neon lamp was 1.2 torr. In a recent detailed examination [9] of the output of a helium resonance lamp it was shown that at a helium pressure of 1.2 to 2 torr the 53.7 nm line transmitted through a 1500 Å window is approximately 2 percent of the intensity of the 58.4 nm line. The total output of the helium lamp used in this study was approximately 2×10^{13} photons/s. The same lamp filled with neon had a light flux of 0.8×10^{13} photons/s. The output of the lamp, which was monitored by measuring the saturation ion current in CH_4 showed only very minor fluctuations (2 to 5%) from one experiment to the next. The volume of the reaction vessel equipped with nickel electrodes was 220 cm^3.

2.2. Materials

All chemicals used in this study were purified by gas chromatography. The methane-d_4 contained 5 percent CD_3H. The cyclohexane,1,1,2,2,3,3-d_6 sample used in some experiments contained 10.3 percent cyclohexane-d_5, 2.4 percent cyclohexane-d_7 and 0.3 percent cyclohexane-d_8. Propane-1,1,1,3,3,3-d_6 contained 6 percent $CD_2HCH_2CD_3$ and 1.7 percent CD_3CHDCD_3. More than 93 percent of the isobutane-d_1 consisted of $(CH_3)_3CD$. The calculated isotopic compositions of the products reported in this paper have been corrected statistically to bring the data up to 100 percent deuterium purity.

3. Results

All product yields are expressed in terms of quantum yields (Φ). Because the ionization quantum yield of methane is close to unity in the wavelength region covered in this study [10–11], quantum yields are essentially equivalent to ion pair yields (number of product molecules per positively charged ion produced in the system). The absolute accuracy of the quantum yield values given in tables 1 and 2 are estimated to be ± 15 percent. Besides the products listed in tables 1 and 2, hydrogen and several higher molecular weight hydrocarbon products such as i-C_4H_{10} and i-C_5H_{12} were observed. The quantum yields of i-C_4H_{10} and i-C_5H_{12} were seen to increase with the number of photons absorbed in the system and were therefore ascribed to secondary reactions involving accumulated products. The values of $\Phi(i\text{-}C_4H_{10})$ and $\Phi(i\text{-}C_5H_{12})$ for the lowest conversion experiment listed in table 1 were 0.003 and 0.002 respectively.

Hydrocarbon products with more than five carbon atoms were not observed at low conversions ($\Phi < 0.005$). The quantum yield of hydrogen in the 58.4 nm photolysis of a CH_4-CD_4-NO (1:1:0.01) mixture at a pressure of 10 torr was 0.4 ± 0.1. Its isotopic composition was as follows: H_2-44.6 percent, HD-26.5 percent, D_2-28.9 percent. In the 58.4 nm photolysis of a CH_4-i-C_4D_{10} (1:0.01) mixture at a pressure of 20 torr Φ(hydrogen) was 0.55 ± 0.1 and consisted of H_2-67.8 percent, HD-16.7 percent and D_2-15.5 percent. Both hydrogen analysis experiments were carried out at relatively high conversion (1.5×10^{17} photons absorbed by 10 torr of methane in the 220 cm^3 reaction vessel). The isotopic composition of the ethylene produced in the 58.4 nm photolysis of the CH_4-CD_4-NO (1:1:0.01) mixture is as follows: C_2D_4-14 percent, C_2D_3H-16 percent, $C_2D_2H_2$-22 percent, C_2DH_3-16 percent, C_2H_4-32 percent. Photolysis of an equimolar CH_4-CD_4 in the presence of 1 mole percent i-C_4H_{10} yielded: C_2D_4-16 percent, C_2D_3H-17 percent, $C_2D_2H_2$-21.5 percent, C_2DH_3-13.5 percent, and C_2H_4-32 percent.

The isotopic analysis of the ethane formed in the neon resonance photolysis of a CD_4-C_3H_8-O_2 (1:0.01:0.1) mixture at a total pressure of 20 torr, was as follows: C_2D_5H-47.2 percent, $C_2D_4H_2$-0.5 percent, and C_2H_6-52.3 percent. The ethane formed in the helium and neon resonance photolysis of CD_4-i-C_4H_{10}-O_2 (1:0.01:0.01) mixtures consisted nearly entirely (> 97 percent) of C_2D_5H.

4. Discussion

4.1. General Comments

Recent determinations of the photoionization quantum yield (Φ_+) of CH_4 at 58.4 nm and at 74.37–73.59 nm indicate that approximately one ion pair is produced for each photon absorbed by methane [10–11]. It follows that in this wavelength region there is one predominant primary process

$$CH_4 + h\nu \rightarrow (CH_4^+)^* + e. \quad (1)$$

The ion pair formation process

$$CH_4 + h\nu \rightarrow CH_3^+ + H^- \quad (2)$$

is apparently of minor importance [12–13]. The helium and neon resonance photoelectron spectrum shows one broad band over the range 12.7 to 16–17 eV, exhibiting three maxima associated with the ionization of the t_2 orbital [14–15]. Besides the ionization potential at 12.7 eV, there is a second I.P. near 23 eV, ascribed to ionization from the a_1 orbital, which is however of no concern in this study. A fraction of the vibrationally excited $(CH_4^+)^*$ formed in process 1 can dissociate to produce CH_3^+ (appearance potential 14.2 eV) and CH_2^+ (appearance potential 15.2 eV) [12–13]

$$(CH_4^+)^* \rightarrow CH_3^+ + H \quad (3)$$

$$\rightarrow CH_2^+ + H_2. \quad (4)$$

The abundances of CH_4^+, CH_3^+, and CH_2^+ observed in a photoionization mass spectrometer [12] using an enclosed helium resonance lamp such as the one used in the present study are: CH_4^+-48 percent, CH_3^+-50 percent, and CH_2^+-2 percent. The abundances observed with a neon resonance lamp are CH_4^+-47 percent, CH_3^+-51 percent and CH_2^+-2 percent. It is to be noted that both distributions are at variance with the abundances obtained in previous photoionization mass spectrometric studies [13] in which a

differentially pumped continuous light source was used.

The major initial bimolecular reactions occurring in the photoionization of CH_4 are [16]

$$(CH_4^+)^* + CH_4 \rightarrow CH_5^+ + CH_3 \quad (5)$$

$$CH_3^+ + CH_4 \rightarrow C_2H_5^+ + H_2 \quad (6)$$

$$CH_2^+ + CH_4 \rightarrow C_2H_4^+ + H_2. \quad (7)$$

The product ions CH_5^+, $C_2H_5^+$ and $C_2H_4^+$ are unreactive towards CH_4 [16] and will therefore be converted to neutral products by heterogeneous or homogeneous neutralization or by proton transfer to traces of H_2O. At higher conversions these ions will react with accumulated products [17–19].

From the foregoing, one would expect H_2, C_2H_6, and C_2H_4 to be major products in the far ultraviolet photolysis of "pure" methane. This is borne out by the data given in tables 1 and 2 as well as in the Results Section. Although there is essentially little to be learned from product yields such as the ones given in tables 1 and 2 for the "pure" CH_4 system it is nevertheless of some interest to compare the product yields obtained in this study at 58.4 nm with those reported previously by other investigators [1–2] (table 1) and to interpret some of the observations in the light of the remarks made above.

a. Effect of Conversion

The fact that upon addition of O_2 to CH_4, $\Phi(C_2H_6)$ is reduced from approximately 0.3 to 0.01 at 58.4 and 74.3–73.6 nm indicates that C_2H_6 is produced mainly by a free radical reaction such as:

$$CH_3 + CH_3 \rightarrow C_2H_6. \quad (8)$$

The increase of $\Phi(C_3H_8)$ and $\Phi(n\text{-}C_4H_{10})$ with an increase in the number of photons absorbed (tables 1 and 2) can be ascribed to H-atom scavenging by the C_2H_4 product molecules

$$C_2H_4 + H \rightarrow C_2H_5 \quad (9)$$

$$C_2H_5 + CH_3 \rightarrow C_3H_8 \quad (10)$$

$$C_2H_5 + C_2H_5 \rightarrow n\text{-}C_4H_{10}. \quad (11)$$

This mechanism, which has previously [20] also been shown to occur in the 10 eV photolysis of CH_4, is corroborated by the fact that $\Phi(C_2H_4)$ diminishes at higher conversion and that $\Phi(C_3H_8)$ is sharply reduced upon addition of O_2. The increase of $\Phi(C_2H_6)$ with the number of photons absorbed in the system can at least in part be ascribed to combination of the C_2H_5 radicals formed in reaction 9 with H-atoms. It is clear however that at very high conversion the decrease in $\Phi(C_2H_4)$ is not entirely compensated by the increase of the quantum yields of C_2H_6, C_3H_8 and $n\text{-}C_4H_{10}$. Complex ion-molecule reaction chains initiated by the addition of $C_2H_5^+$ to C_2H_4 [19] may cause a further reduction in the quantum yield of C_2H_4. Although the conversion effects noted in this study could account for the low quantum for C_2H_4 reported by Jensen and Libby [2], they do not account for the extremely low quantum yield of C_2H_6 (table 1) reported by these authors. In view of the fact that the $\Phi(C_2H_6)$ is seen to be essentially reduced to zero by O_2, it may be surmised that air contamination in the CH_4 accounts for the observations of Jensen and Libby [2].

b. Formation of Ethylene

The ethylene originates apparently from the $C_2H_5^+$ ion formed in reaction 6. Addition of small amounts of isobutane to CH_4 drastically reduces $\Phi(C_2H_4)$ both in the neon and helium resonance experiments (tables 1 and 2). This reduction which is accompanied by a corresponding increase of $\Phi(C_2H_6)$ in the presence or in the absence of O_2 is to be accounted for [17] by the removal of the $C_2H_5^+$ ion via the hydride ion transfer reaction

$$C_2H_5^+ + i\text{-}C_4H_{10} \rightarrow C_2H_6 + C_4H_9^+ \quad (12)$$

Formation of C_2H_6 in reaction 12 is substantiated by the fact that more than 90 percent of the ethane formed in the photoionization of CD_4-i-C_4H_{10}-O_2 mixtures (see Results) consists of C_2D_5H. Also, $\Phi(C_2H_6)$ is seen to be independent of the concentration of $i\text{-}C_4H_{10}$ (see table 1). Furthermore, it is to be noted that $\Phi(C_2H_6)$ is close to the value predicted from the abundance of CH_3^+ in the primary photoionization mass spectrum [12–13]. At these low concentration of $i\text{-}C_4H_{10}$, the reduction of the yield of C_2H_4 cannot be attributed to inhibition of the insertion reaction

$$CH + CH_4 \rightarrow C_2H_4 + H \quad (13)$$

which was previously suggested [2] to be the main mode of formation of C_2H_4 in the 58.4 nm photolysis of "pure" CH_4. It has indeed been shown recently [21] that CH reacts about equally fast with all lower alkanes. As noted before [22], the apparently low yield of CH species is consistent with the fact that dissociation of superexcited CH_4 molecules is of minor occurrence at 58.4 and 74.3–73.6 nm. Furthermore, the isotopic composition of the ethylene formed in the photoionization of CH_4-CD_4 and CH_4-CD_4-i-C_4H_{10} mixtures (see Results) is not consistent with an insertion mechanism. In the CH_4-alkane mixture given in tables 1 and 2, $\Phi(C_2H_6)$ is approximately equal to the reduction in $\Phi(C_2H_4)$, indicating that in "pure" methane most of the $C_2H_5^+$ ions yield C_2H_4 as a neutral product. Pulse radiolysis experiments [23] have shown that if the neutralization occurs by electron recombination, acetylene is produced through the following reaction sequence:

$$C_2H_5^+ + e \rightarrow C_2H_5^* \quad (14)$$

$$C_2H_5^* \rightarrow C_2H_4^* + H \qquad (15)$$

$$C_2H_4^* \rightarrow C_2H_2 + H_2. \qquad (16)$$

Because at a methane pressure of 100 torr approximately 50 percent of the excited C_2H_4 formed in process 15 were shown to dissociate [23], the low yield of C_2H_2 in the photoionization experiments (tables 1 and 2) rules out reaction 14 as an important mode of neutralization of the $C_2H_5^+$ ion. Proton transfer on the aluminum window surface and/or to H_2O desorbed from the wall is a likely explanation for the nearly quantitative conversion of $C_2H_5^+$ ions to C_2H_4. The fact that addition of a proton acceptor such as acetone to CH_4 (table 2)

$$C_2H_5^+ + CH_3COCH_3 \rightarrow C_2H_4 + CH_3COCH_4^+ \qquad (17)$$

does not significantly alter $\Phi(C_2H_4)$ observed in pure methane supports the above interpretation. It is of interest at this point to compare our data with those obtained by Walker and Back [1] in a windowless apparatus. It is seen (table 1) that with the exception of $\Phi(C_2H_2)$, the agreement between the two studies is excellent. Considering that Walker and Back [1] used a continuous CH_4-He flow through a windowless reaction vessel, their high C_2H_2 yields are most likely to be attributed to gas phase neutralization (reaction sequence 14–16). The isotopic analysis of the ethylene obtained in the photolysis of a CH_4-CD_4-i-C_4H_{10} mixture (see Results), indicates that the residual ethylene ($\Phi \sim 0.03$) observed in the CH_4-i-C_4H_{10} experiments (tables 1 and 2) may be accounted for by ineffective scavenging of the $C_2H_5^+$ ions by i-C_4H_{10}.

Unreactive ethylene ions formed in reaction 7 may conceivably also contribute to the formation of C_2H_4. However, the very low yield of $C_2D_4H_2$ (~ 0.005) observed in a CD_4-C_3H_8 (1:0.01) experiment (see Results) carried out in the presence of O_2 indicates that the well established ion-molecule reaction [24]:

$$C_2D_4^+ + C_3H_8 \rightarrow C_2D_4H_2 + C_3H_8^+ \qquad (18)$$

does not occur to any significant extent in such an experiment. Since approximately 50 percent of the $C_2D_4^+$ ions would react through the competing reaction channel [25]:

$$C_2D_4^+ + C_3H_8 \rightarrow C_2D_4H + C_3H_7^+ \qquad (19)$$

the quantum yield of $C_2D_4^+$ is estimated to be about 0.01. This low value is in excellent agreement with the value of 0.0093 for $\Phi(CD_3^+)$ recently derived from the neon resonance photoionization mass spectrum of CD_4 [12]. The value estimated here is, however, lower than that indicated by the primary mass spectrum of CD_4 obtained in an earlier mass spectrometric photoionization study [13].

c. Formation of Hydrogen

The fact that at 58.4 nm, the quantum yield of hydrogen observed in a CH_4-CD_4-NO mixture (see Results) is, within experimental error, equal to the quantum yield of ethane obtained in the CH_4-i-C_4H_{10} experiments (table 1) indicates that it is nearly exclusively formed as the neutral product of reaction 6 and, to a much lesser extent, reaction 7. The isotopic composition of the hydrogen in the CH_4-CD_4 experiment is actually reasonably consistent with that predicted on the basis of $CH_3^+(CD_3^+)$ reacting with $CH_4(CD_4)$. At least, the observed value of 1.1 for the product ratio D_2/HD is close to the predicted value of 1.13–1.25 [26]. Apparently, H-atoms which are formed via the unimolecular dissociation of the CH_4^+ ion (reaction 3) and possibly also by neutralization mechanisms are scavenged by NO. However, the low value of $\Phi(H_2)$ and $\Phi(HD)$ (see Results) obtained in the photolysis of a CH_4-i-C_4D_{10} mixture in the absence of NO indicates that a considerable fraction of the H-atoms disappear from the system by reaction on the wall and by addition to olefinic products. It is therefore not surprising that there is good agreement between the quantum yields of hydrogen obtained here and the value reported previously by Jensen and Libby [2]. On the other hand, the much higher value (~ 5) obtained in the windowless apparatus of Walker and Back [1] may be explainable by a number of factors, including the differences in neutralization mechanism mentioned in the previous section, or perhaps to experimental difficulties in analyzing the H_2 product in the presence of excess helium.

d. Superexcited Methane

A comparison of the quantum yields of the products obtained in the photolysis of pure CH_4 with the neon and helium resonance lamps (tables 1 and 2) shows that there are actually no significant differences. This is not surprising in view of the fact that the helium and neon resonance photoelectron spectra and mass spectral cracking patterns are very similar. This is also indicated by the fact that the primary ion abundances (CH_4^+, CH_3^+, CH_2^+) are about the same in the He* and Ne* Penning ionization of CH_4 [27]. More importantly, because the ionization quantum yield is close to unity both at the neon and helium resonance line [10–11] the contribution of superexcited CH_4 fragmentation, which would introduce new intermediates (C, CH, CH_2) to the system [22], is minor over the entire wavelength region [28]. A striking confirmation of this view follows from a recent far ultraviolet study of CH_4 by Welch and Judge [29] in which no emission due to excited CH or CH_2 species could be observed over the range 62 to 77 nm. Emission was however seen at shorter and higher wavelengths. It is however of interest that the consistent values of $\Phi(C_2H_2)$ obtained in the 58.4 nm photolysis of CH_4-i-C_4H_{10} mixtures can be attributed to $C(^1S)$ or $C(^1D)$ atoms formed by the fragmentation of superexcited methane molecules

$$CH_4 + h\nu \rightarrow C + H_2 + H_2 \text{ (or } 2H) \qquad (20)$$

followed by the insertion mechanism [30]

$$C + CH_4 \rightarrow C_2H_2 + H_2. \qquad (21)$$

TABLE 1. *Photolysis of* CH_4 *at 58.4 nm*

CH_4	O_2	Additive	Photons absorbed $\times 10^{-15}$	C_2H_2	C_2H_4	C_2H_6	C_3H_6	C_3H_8	n-C_4H_{10}
Pressure (Torr)				Quantum yields					
4.8			5	0.005	0.43	0.25	0.007	0.036	
4.8			10	.006	.40	.31	.017	.075	0.007
4.8			20	.006	.39	.34	.011	.10	
4.8			29	.006	.35	.38	.013	.13	.026
4.8			145	.004	.15	.44	.010	.18	.036
4.8	0.05		10	.002	.35	.01	.006	.01	
1.95*			60		.08	.0016			
2.0*			120		.063	.017			
0.23**				.12	.32	.36			
10.5		i-C_4H_{10}-0.45		.002	.058	.75	.062	.66	
5.4	.05	i-C_4H_{10}-0.05		.002	.049	.46	.043	.43	.242
10.5	.10	i-C_4H_{10}-0.10		.002	.046	.46	.034	.42	.23
20.5	.20	i-C_4H_{10}-0.20		.002	.029	.46	.027	.43	.23
10.5	.10	n-C_4H_{10}-0.10		.002	.061	.518	.042	.26	
10.5	.10	i-C_5H_{12}-0.10		.002	.070	.42	.017	.04	.25

Reaction cell volume: 220 cm^3.
* Ref. [2]
** Ref. [1]

TABLE 2. *Photolysis of* CH_4 *at 74.3–73.6 nm*

CH_4	O_2	Additive	Photons absorbed $\times 10^{-15}$	C_2H_2	C_2H_4	C_2H_6	C_3H_6	C_3H_8	n-C_4H_{10}
Pressure (Torr)				Quantum Yields					
4.9			5	0.001	0.43	0.24	0.0021	0.024	
4.9			20	.001	.41	.27	.008	.060	
4.9			40	.002	.29	.27	.008	.072	0.015
4.9			120	.001	.22	.30	.009	.090	.015
10			15	~.0006	.39	.28	.006	.057	
10	0.2		15	~.0006	.33	.010	.007	.018	
10	0.2	Acetone-0.1	15	≤.0001	.44	.003	.003	.001	
10	0.2	i-C_4H_{10}-0.1		≤.0001	.03	.46	.03	.443	.213
10	0.2	C_3H_8-0.2		≤.0001	.03	.75	.20		

The near absence of C_2H_2 as a product in the corresponding neon resonance experiments is tentatively ascribed to the fact that in this wavelength region neutral excited CH_4 molecules are produced with a quantum yield very close to zero as compared to ~ 0.05 at 58.4 nm [11].

4.2. Ion-Molecule Reactions

The photolysis of methane with helium or neon resonance radiation is an ideal method for the study of reactions of CH_5^+ and $C_2H_5^+$ ions. This is so because of the relative simplicity of the primary ion spectrum (CH_4^+ and CH_3^+ account for 95 percent of the primary ions), and because of the negligible contribution of reactive free radical species (C, CH, CH_2) which would be present if the dissociative processes of super-excited methane molecules had to be considered. Although of some intrinsic interest, the results which will be discussed here serve more as an illustration of the type of information about ion-molecule reaction kinetics which can be gained from this type of experiment.

a. Reactions of the Ethyl Cation

As already indicated earlier in the Discussion, the ethane product observed in the photolysis of CH_4-i-C_4H_{10}-O_2 mixtures is nearly all (except for a minor contribution from a reaction of the $C_2H_4^+$ ion) formed by the transfer of a hydride ion to $C_2H_5^+$ from the isobutane. Taking advantage of this fact, a number of deuterium labeling experiments have been carried out in order to assess the mechanistic details of the

hydride transfer reactions between the ethyl ion and a number of hydrocarbon molecules. Table 3 summarizes the experimental observations relating to these questions. The relative rate constants given in the last column of table 3 are based on the determination of the C_2D_5H (C_2H_6) and C_2D_6 (C_2H_5D) products formed in the irradiation of CD_4 (CH_4) in the presence of about 5 percent partially deuterated hydrocarbon, and with O_2 present as a radical scavenger (see Results).

TABLE 3. H^- *and* D^- *transfer to the ethyl cation*

λ nm	Reactants*		$k(H^-)/k(D^-)$
	Ion	Molecule	
74.4–73.6	$C_2D_5^+$	*c*-$C_6H_6D_6$**	1.05±0.05
58.4	$C_2D_5^+$	*c*-$C_6H_6D_6$	1.06±0.05
58.4	$C_2H_5^+$	*c*-$C_6H_6D_6$	1.09±0.05
74.4–73.6	$C_2D_5^+$	$CD_3CH_2CD_3$	0.63±0.02
74.4–73.6	$C_2D_5^+$	$(CH_3)_3CD$	6.1±0.3
58.4	$C_2D_5^+$	$(CH_3)_3CD$	6.4±0.3
58.4	$C_2H_5^+$	$(CH_3)_3CD$	6.1±0.3

*Total pressure: 20 torr.
**Cyclohexane-1,1,2,2,3,3,-d_6.

The relative rate data given in the last column of the table indicate that reaction of the $C_2D_5^+$ ion with the symmetric molecule, cyclohexane-1,1,2,2,3,3-d_6, shows that there is a slight (5 percent) preference for reaction of an ethyl ion at the CH_2 position

$$C_4D_5^+ + c\text{-}C_6H_6D_6 \rightarrow C_2D_5H + c\text{-}C_6H_5D_6^+ \quad (22)$$

rather than the CD_2 position

$$C_2D_5^+ + c\text{-}C_6H_6D_6 \rightarrow C_2D_6 + c\text{-}C_6H_6D_5^+. \quad (23)$$

Both reactions are exothermic by 35 kcal/mol [31]. It is not surprising that the relative importance of reactions 22 and 23 does not change as a function of the energy of the photons used to produce the $C_2D_5^+$ ions in CD_4. Though the $C_2D_5^+$ ions may be formed with different energy contents in experiments performed at different energies, in these dilute mixtures any excess energy will be dissipated by unreactive collisions with methane before reaction with the additive can occur. The increase in k_{22}/k_{23} which is seen when $C_2D_5^+$ is replaced by $C_2H_5^+$ (table 3) is too small to be considered as a genuine isotope effect.

In the reaction of ethyl ions with propane and isobutane, preferential reaction sites are indicated by the ratio $k(H^-)/k(D^-)$ given in table 3. In the case of $CD_3CH_2CD_3$, for instance, a value of 0.63±0.02 is obtained for transfer of H^- ($\Delta H_{rn} = -22.5$ kcal/mol) over transfer of D^- ($\Delta H_{rn} = -6.5$ kcal/mol); this is nearly a factor of two higher than the ratio of H to D atoms in the reactant molecule. The value for this ratio obtained here is in reasonable agreement with the somewhat less reliable value of 0.57 derived in an earlier $CD_3CH_2CD_3$ radiolysis study [24] and the value of 0.33 ± 0.01 obtained in a tandem mass spectrometer experiment [32].

In the case of $(CH_3)_3CD$, the ratio $k(H^-)/k(D^-)$ is 6.1, independent of wavelength and isotopic labeling of the reactant ion. The statistical value of this ratio is 9.0; the fact that the observed value is closer to the statistical value in the case of isobutane than in the case of propane may be explained by the fact that reaction at the primary and tertiary sites in isobutane are both more exothermic ($\Delta H = -8$ and -38 kcal/mol, respectively) than reaction at the primary and secondary positions in propane ($\Delta H = -6.5$ and -22.5 kcal/mol, respectively). In addition, steric effects may play a role in these reactions, and there is a possibility that the weaker tertiary bond in isobutane is strengthened by the deuterium labeling. It is interesting to note that *n*-butane is an important product in all CH_4-*i*-C_4H_{10} experiments (tables 1 and 2). One of the most obvious routes by which this product may be formed is through the isomerization of the $(CH_3)_2CHCH_2^+$ ion formed in the hydride transfer reaction:

$$C_2H_5^+ + (CH_3)_3CH \rightarrow (CH_3)_2CHCH_2^+ + C_2H_6$$
$$\Delta H = -38 \text{ kcal/mol} \quad (24)$$

to the thermodynamically more stable sec-butyl ion:

$$(CH_3)_2CHCH_2^+ \rightarrow \text{sec-}C_4H_9^+ \qquad \Delta H = -16 \text{ kcal/mol} \quad (25)$$

Such a mechanism is strikingly demonstrated by the observation that 95 percent of the *n*-butane observed in the photoionization of CH_4–$(CH_3)_3CD$–O_2 mixtures consists of *n*-$C_4H_8D_2$. Stable sec-$C_4H_8D^+$ ions formed in the isomerization are indeed expected to react with $(CH_3)_3CD$ exclusively by the exothermic reaction channel:

$$\text{sec-}C_4H_8D^+ + (CH_3)_3CD \rightarrow n\text{-}C_4H_8D_2 + (CH_3)_3C^+$$
$$\Delta H = -11.5 \text{ kcal/mol.} \quad (26)$$

Apparently a fraction of the isobutyl ions formed in reaction 24 isomerize to the *t*-$C_4H_9^+$ structure rather than to the sec-$C_4H_9^+$ structure, since the yield of *n*-butane is lower than that which would be predicted from the fact that about 85 percent of the ethyl ions are expected to undergo reaction 24.

b. Reactions of CH_3^+

In the 58.4 or 73.5–74.6 nm irradiation of pure CH_4 no neutral product can be unambiguously ascribed to the presence of CH_4^+, and therefore of CH_3^+, even though the latter ion must account for approximately 50 percent of the primary ion spectrum. The latter estimate is based on the fact that the only other major ion, CH_3^+, has been shown to yield C_2H_4 with a quantum yield of 0.43±0.06. Addition of higher alkanes to

CH_4 does however reveal the presence of CH_5^+, and does also provide some information concerning the proton transfer reaction

$$CH_5^+ + C_nH_{2n+2} \rightarrow CH_4 + [C_nH_{2n+3}]^*. \quad (27)$$

In CH_4-*i*-C_4H_{10} mixtures (tables 1 and 2), $\Phi(C_3H_8)$ represents a minimum value of $\Phi(CH_5^+)$. Isotopic labeling experiments in this and previous radiolysis and mass spectrometric studies have shown that the now well established reaction sequence

$$CH_5^+ + (CH_3)_3CH \rightarrow 2CH_4 + \text{sec-}C_3H_7^+ \quad (28)$$

$$C_3H_7^+ + (CH_3)_3CH \rightarrow C_3H_8 + (CH_3)_3C^+ \quad (29)$$

adequately accounts for the formation of C_3H_8. In addition, however, the following competing reaction channel must be considered:

$$CH_5^+ + (CH_3)_3CH \rightarrow CH_4 + H_2 + C_4H_9^+ \quad (30)$$

where $C_4H_9^+$ may be *i*-$C_4H_9^+$ or *t*-$C_4H_9^+$. The fact that $\Phi(C_2H_6 + C_3H_8)$ in the CH_4-*i*-C_4H_{10}-O_2 experiments does not add up to unity attests to the occurence of reaction 30. On the same grounds the lower value for $\Phi(C_3H_8)$ observed in the CH_4-*n*-C_4H_{10} experiment given in table 1 points to a relatively larger contribution of a dissociative proton transfer reaction analogous to 30 in agreement with mass spectrometric observations. The relatively high yield of *n*-C_4H_{10} in the CH_4-*i*-C_5H_{12} experiment (table 1) must be accounted for by preferential transfer of a proton to a CH_3 group to give sec-$C_4H_9^+$

$$CH_5^+ + (CH_3)_2CHCH_2CH_3 \rightarrow 2CH_4 + \text{sec-}C_4H_9^+. \quad (31)$$

The smaller yield propane observed in the same experiment can be ascribed to proton transfer to CH_2 group.

5. References and Note

[1a] Back, R. A., and Walker, D. C., J. Chem. Phys. **37**, 2348 (1962).
[1b] Walker, D. C., and Back, R. A., Ibid. **38**, 1526 (1963).
[2] Jensen, C. A., and Libby, W. F., Ibid. **49**, 2831 (1968).
[3] Rebbert, R. E., and Ausloos, P., J. Am. Chem. Soc. **90**, 7370 (1968).
[4a] Lias, S. G., Rebbert, R. E., and Ausloos, P., J. Chem. Phys. **52**, 773 (1970).
[4b] Rebbert, R. E., Lias, S. G., and Ausloos, P., J. Res. Nat. Bur. Stand. (U.S.), **75A**, (Phys. and Chem.) No. 6, 607–612 (1972).
[5a] Tellinghuisen, J. B., Winkler, C. A., Bennett, S. W., and Phillips, L. F., J. Phys. Chem. **75**, 3499 (1971).
[5b] Tellinghuisen, J. B., Winkler, C. A., and Phillips, L. F., Ibid. **76**, 298 (1972).
[6] Wauchop, T. S., and Broida, H. P., J. Geophys. Res. **76**, 21 (1971).
[7] Gorden, R., Jr., Rebbert, R. E., and Ausloos, P., Nat. Bur. Stand. (U.S.), Tech. Note 496, 34 pages (1969).
[8] Certain commercial equipment, instruments, or materials are identified in this paper in order to adequately specify the experimental procedure. In no case does such identification imply recommendation or endorsement by the National Bureau of Standards, nor does it imply that the material or equipment identified is necessarily the best available for the purpose.
[9] Kinsinger, J. A., Stebbings, W. L., Valenzi, R. A., and Taylor, J. W., Anal. Chem. **44**, 773 (1972).
[10] Bennett, S. W., Tellinghuisen, J. B., and Phillips, L. F., J. Chem. Phys. **75**, 719 (1971).
[11] Rebbert, R. E., and Ausloos, P., J. Res. Nat. Bur. Stand. (U.S.), **75A** (Phys. and Chem.), No. 5, 481–485 (1971).
[12] Sieck, L. W., and Gordon, R. Jr., Chem. Phys. Lett., in press.
[13a] Dibeler, V. H., Krauss, M., Reese, R. M., and Harllee, F. N., J. Chem. Phys. **42**, 3791 (1965).
[13b] Chupka, W. A., J. Chem. Phys. **48**, 2337 (1968).
[14] Turner, D. W., "Molecular Photoelectron Spectroscopy" (Wiley-Interscience, 1970).
[15] Potts, A. W., and Price, W. C., Proc. Roy. Soc. London **A326**, 165 (1972).
[16] Futrell, J. H. and Tiernan, T. O., Chapter 4 in Fundamental Processes in Radiation Chemistry (Interscience Publ. New York, 1968).
[17] Ausloos, P., Lias, S. G., and Gorden, R., Jr., J. Chem. Phys. **39**, 3341 (1963).
[18] Haynes, R. M., and Kebarle, P., J. Chem. Phys. **45**, 3899 (1966).
[19a] Munson, M. S. B., and Field, F. H., J. Am. Chem. Soc. **87**, 3294 (1965).
[19b] Ibid. **87**, 4242 (1965).
[20] Ausloos, P., Gorden, R., Jr. and Lias, S. G., J. Chem. Phys. **40**, 1854 (1964).
[21] Bosnali, M. W., and Perner, D., Z. Naturforsch **26a**, 1768 (1971).
[22] Rebbert, R., and Ausloos, P., J. of Photochemistry **1**, 171 (1972/73).
[23] Rebbert R. E., and Ausloos, P., J: Res. Nat. Bur. Stand. (U.S.), **77A**, (Phys. and Chem.) No. 1, 109–114 (Jan.–Feb. 1973).
[24] Ausloos, P., Lias, S. G., and Sandoval, I. B., Disc. Faraday Soc. **36**, 66 (1963).
[25] Sieck, L. W., and Searles, S. K., J. Am. Chem. Soc. **92**, 2937 (1970).
[26] Ausloos, P. J., and Lias, S. G., J. Chem. Phys. **38**, 2207 (1963).
[27] Cermak, V., and Herman, Z., Coll. Czek. Chem. Commun. **30**, 169 (1965).
[28] Ausloos, P., Molec. Photochem. **4**, 39 (1972).
[29] Welch, A. R., and Judge, D. L., J. Chem. Phys. **57**, 286 (1972).
[30a] Braun, W., Bass, A. M., Davis, D. D., and Simons, J. P., Proc. Roy. Soc. **312A**, 417 (1969).
[30b] Husain, D., and Kirsch, L. J., Trans Faraday Soc. **67**, 2025 (1971).
[31] Thermochemical values are mainly derived from: Franklin, J. L., Dillard, J. G., Rosenstock, H. M., Herron, J. T., Draxl, K., and Field, F. H., Nat. Bur. Stand. (U.S.), Nat. Stand. Ref. Data Ser. **26**, (1969).
[32] Bone, L. I., and Futrell, J. H., J. Chem. Phys. **46**, 4084 (1967).

(Paper 77A1–755)

JOURNAL OF RESEARCH of the National Bureau of Standards—A. Physics and Chemistry
Vol. 77A, No. 1, January–February 1973

Radiolysis of Methane. Formation of Acetylene*

R. E. Rebbert and P. Ausloos

Institute for Materials Research, National Bureau of Standards, Washington, D.C. 20234

(August 18, 1972)

The ^{60}Co-gamma radiolysis (at 200 to 2000 torr) and the pulse radiolysis (100 to 760 torr) of methane has been investigated with the specific purpose of elucidating the mode of formation of acetylene. The following two reactions account for the formation of acetylene in the pulse radiolysis:

$$C_2H_5^+ + e \rightarrow C_2H_2 + H_2 + H \qquad \text{I}$$

$$C(^1S \text{ or } ^1D) + CH_4 \rightarrow C_2H_2 + H_2. \qquad \text{II}$$

Addition of SF_6 as an electron scavenger eliminates reaction I as a source of acetylene, but increases the yield of ethylene through the occurrence of a reaction such as:

$$C_2H_5^+ + SF_6^- \rightarrow C_2H_4 + HF + SF_5.$$

In the low dose rate ^{60}Co-gamma radiolysis of CH_4–NO mixtures, reaction II is the only mode for formation of acetylene. The $C(^1S \text{ or } ^1D)$ atoms which undergo reaction II are formed in the gamma radiolysis and pulse radiolysis, as well as in the 10 and 11.6–11.8 eV photolyses, through the dissociation process:

$$CH_4^* \rightarrow C + 2H_2.$$

In the gamma radiolysis, the $C_2H_5^+$ ion apparently is intercepted by accumulated products before undergoing homogenous neutralization process 1. In the 16.7–16.8 and 21.2 eV photolyses, evidence is presented that the ions do not undergo homogenous neutralization.

Key words: Acetylene formation; electron scavenger; ion pair yields; methane; pulse radiolysis; vacuum ultraviolet photolysis.

1. Introduction

The yield and mode of formation of acetylene in the radiolysis of CH_4 at atmospheric pressures have been a matter of speculation for many years [1–7][1]. Ion pair yields of acetylene varying between 0.0 and 0.25 have been reported in various studies in which the dose rates were in the range 10^{15} to 10^{22} eV/g-s. There are indications that $M(C_2H_2)/N_+$ increases with an increase in dose rate [5] or decreases in absorbed dose [1]. Actually, consistently high values for $M(C_2H_2)/N_+$ have recently been reported in studies where a field emission source was employed [6–8] which delivered 3 to 60 ns electron pulses with average dose rates which were about five orders of magnitude higher than those in the linear accelerator studies [5]. In contrast with the lower dose rate studies the agreement between the three Febetron[2] studies [6–8] was excellent; $M(C_2H_2)/N_+$ ranged from 0.15 to 0.23. Only a limited amount of information is available concerning the mechanisms of formation of acetylene. It has been shown [9–10] that acetylene appears as a major product at electron energies which correspond to the onset of ionization of CH_4. Application of an electric field technique [10] further indicated that only 27 percent of the acetylene is produced in an ionic reaction. We wish to report new observations which, in our opinion, clarify the mode of formation of acetylene in low as well as in high dose rate radiolysis experiments.

2. Experimental Procedure

The ^{60}Co-gamma experiments were performed in the NBS source (dose rate: 10^{18}eV/g-s). Cylindrical Pyrex reaction vessels provided with a break seal were used. These were heated to the melting point of Pyrex prior to filling. After condensing the CH_4 or CD_4 in the reaction vessels they were sealed off. For a more detailed description of the experimental procedure we refer the reader to an earlier publication from this

*Work supported in part by the Atomic Energy Commission.

[1] Figures in brackets indicate the literature references at the end of this paper.

[2] Certain commercial materials are identified in this paper in order to adequately specify the experimental procedure. Such identification does not imply recommendation or endorsement by the National Bureau of Standards.

laboratory [11]. Field emission sources delivering ~60 and ~3 ns pulses (Febetron 705 and 706) were used in the pulse radiolysis experiments. The dose per pulse was determined using N_2O as a dosimeter [12], taking $G(N_2) = 12.4$. The reaction vessels used in the pulse radiolysis experiments were cylindrical vessels (5 cm long and 3.7 cm internal diameter). Aluminum windows which were 4 mil thick were attached to each end of the cell with vacuum epoxy cement. The cells were evacuated and filled through a Teflon valve. They were positioned in such a manner that the electron beam covered the entire front window.

The type of reaction vessel and the rare gas resonance lamps used in this study have been described before [13]. Neon and helium resonance lamps emitting 74.3–73.6 nm (16.66–16.84 eV), and 58.4 nm (21.2 eV) radiation respectively were used. Both the neon and helium resonance lamps were provided with aluminum windows 1500 Å thick which were entirely leak-free, and could withstand a pressure differential between the reaction vessel and the interior of the resonance lamp of 100 torr or more. The photon flux of the helium and neon resonance lamps was 5×10^{13} and 2×10^{13} quanta/s, respectively. It was ascertained that the helium and neon lamps were essentially monochromatic throughout the study by introducing neon and helium, respectively, into the first compartment of a double cell arrangement described before. The neon gas placed in the sample cell absorbed the neon resonance radiation and was transparent to the radiation emanating from the helium lamp, while helium was transparent to the photons from the neon lamp and absorbed those from the helium lamp. A more detailed description of the characteristics of these light sources is given elsewhere [13–14]. In the course of an experiment using the neon or the helium resonance lamp, the decay in the light flux was no more than five percent from beginning to end. The output of the resonance lamps was monitored by periodically measuring the saturation ion currents during the course of an irradiation.

In all experiments, the yields of acetylene and ethylene were determined by gas chromatography (squalane column). Isotopic analyses were performed by trapping acetylene from the exit of a gas chromatograph (silica gel column) followed by introduction of the total sample on a high resolution mass spectrometer operated at 13 and 70 eV. Methane was purified by repeated low temperature distillation and mass spectrometric analysis showed that methane d_4 contained 5 percent CD_3H.

3. Results

In tables 1 and 2, the yield of a product, X, measured in the radiolysis and photoionization experiments is reported as $M(X)/N_+$, or molecules, M, of product X formed per positive ion, N_+, in the system. This allows a meaningful comparison between the product yields in the radiolysis and photoionization experiments. Because in the pulse radiolysis experiments, saturation ion current cannot be measured, the G-values based on the N_2O dosimetry are converted to $M(X)/N_+$ values by taking a W-value of 26.7 eV for methane [15].

TABLE 1. *Radiolysis of methane, acetylene and ethylene yields*

Duration of pulse ns	Dose/pulse eV/g × 10^{-19}	Number of pulses	CH_4 pressure	Additive (Torr)	C_2H_2	C_2H_4	C_3H_8	Reference
					M/N_+			
60	0.68	1	300		0.205	0.407	0.008	This work.
60	0.68	1	300	SF_6-3.0	.028	.575	.025	Do.
60	3.3	1	300		.194	.304	.018	Do.
3	0.83	1	300		.218	.432	.008	Do.
3	0.83	2	300		.204	.370	.012	Do.
3	0.83	4	300		.210	.343	.019	Do.
60	3.3	1	100		.240	.386	.016	Do.
60	3.3	1	100	SF_6-1.0	.034	.623	.017	Do.
60	3.3	1	100	SF_6-3.2	.034	.651	.018	Do.
60	~70.	1	400–700		.185	.258	n.d.	[6].
60	~70.	10	400–700		.148	.185	n.d.	[6].
3	0.49	1 to 16	760		.23	.28		[7].
3	0.58		100		.162	.324	.019	[8].
Low dose rate ^{60}CO-γ radiolysis (10^{18} eV/g. s)								
			200	NO-2	.016	.177		This work
			500	NO-5	.015	.170		Do.
			1000	NO-10	.015	.165		Do.
			2000	NO-20	.014	.150		Do.
			1000	Acetone-5 + NO-10	.020	.350		Do.

The pulse radiolysis values of $M(C_2H_2)/N_+$ and $M(C_2H_4)/N_+$ obtained in the course of the present study under a variety of conditions are presented in table 1 together with those reported by other investigators [6–8]. $M(C_2H_2)/N_+$ is essentially independent of the dose rate (dose per pulse), total absorbed dose and pulse duration. This probably accounts for the good agreement between the different studies. On the other hand, $M(C_2H_4)/N_+$ decreases with the number of pulses delivered. This was found to be the case for 3 ns experiments (table 1) and 60 ns experiments. The

TABLE 2. *Photoionization of* CH_4, *acetylene and ethylene yields*

	Pressure (Torr)			C_2H_2	C_2H_4
	Methane	Isobutane	Additive	M/N_+	
Neon lamp (16.7–16.8 eV).....	10.6			0.001	0.29
	10.6		O_2-0.2	.0006	.31
	10.5		acetone-0.1	≤ .0001	.34
	10.7	0.10	O_2-0.10	≤ .0001	.031
Helium lamp (21.2 eV).....	9.9			.007	.31
	10.5		O_2-0.10	.002	.35
	10.5		SF_6-0.07	.002	.31
	20.5	0.20	O_2-0.20	.002	.029

decrease $M(C_2H_4)/N_+$ which was not observed in an earlier study [7] is accompanied by an increase of $M(C_3H_8)/N_+$ and is therefore in part due to H atom scavenging by C_2H_4. An extrapolated M/N_+ value of 0.45 ± 0.03 for the zero-dose ion pair yield of C_2H_4 is obtained in the 3 and 60 ns experiments. The effect of dose on $M(C_2H_4)/N_+$ is of no particular relevance in the following discussion, but this and other aspects of the pulse radiolysis are presently being explored.

An increase in pressure in the ^{60}Co radiolysis of a CH_4-NO (100 : 1) mixture from 200 to 2000 torr caused a slight decrease of $M(C_2H_2)/N_+$ (table 1). Similarly, in the gamma radiolysis of a CD_4-NO (100 : 1) mixture from 500 to 2000 torr, $M(C_2D_2)/N_+$ decreased from 0.013 to 0.010. In the ^{60}Co radiolysis, M(acetylene)$/N_+$ is independent of dose over the range 0.5 to 4 eV/g $\times 10^{21}$. Also, the ion pair yield of C_2H_2 is within experimental error unchanged when NO is replaced by O_2 as an additive.

4. Discussion

4.1. Formation of Acetylene in the Gamma Radiolysis and Vacuum Ultraviolet Photolysis of Methane

In the gamma radiolysis of a CH_4-CD_4 (1 : 1) mixture in the presence of a free radical scavenger (NO), more than 90 percent of the acetylene consists of C_2H_2 and C_2D_2 (table 3). This striking result can be explained by the occurrence of the reaction:

TABLE 3

Radiolysis and photolysis of CH_4-CD_4 *(1 : 1) mixtures, isotopic composition of the acetylene fraction*

	Additive	C_2D_2	C_2HD	C_2H_2
	Mole %	Distribution %		
Pulse radiolysis*.....		33.8	27.6	38.6
	SF_6-0.3	43.3	13.3	43.4
	NO-1.0	33.4	26.6	40.0
^{60}Co γ-Radiolysis.....	NO-1	42.1	6.1	51.8
Photolysis 11.6–11.8 eV.....	NO-1	36.5	4.0	59.5

*Dose/pulse 3.3×10^{19} eV/g, pulse duration 60 ns, total pressure: 300 torr.

$$C + CH_4 \rightarrow C_2H_4^* \rightarrow C_2H_2 + H_2 \qquad (1)$$

where the carbon atom is $C(^1D)$ and/or $C(^1S)$. The presence of reactive C atoms in the radiolysis of methane is not unexpected in view of the fact that an absorption spectrum attributed to $C(^1S)$ has previously been reported in the pulse radiolysis of methane [16]. $C(^3P)$ atoms are unreactive towards methane ($k < 5 \times 10^{-15}$ cm^3/molecule-s) [17–18] and are removed by reaction with NO [18]:

$$C(^3P) + NO \rightarrow CN + O \qquad k = 1.1 \times 10^{-10} \text{cm}^3/\text{molecule-s}. \qquad (2)$$

It has been shown that carbon atoms are also produced in the photolysis of methane at 10 eV and at 11.6–11.8 eV [19], where the acetylene formed in a CH_4-CD_4 (1 : 1) mixture again consists nearly entirely of C_2H_2 and C_2D_2 (table 3). At 11.6–11.8 eV, the carbon atoms can only be produced in the dissociative processes:

$$CH_4^* \rightarrow C(^1D) + 2H_2\left(^1\sum_g^+\right) \qquad (3)$$

$$\rightarrow C(^1S) + 2H_2\left(^1\sum_g^+\right). \qquad (4)$$

The energy requirements for processes 3 and 4, which must occur via an excited CH_2 intermediate, are 9.6 and 11.0 eV, respectively. Because an overall fragmentation process such as:

$$CH_4^* \rightarrow C(^1D) + H_2\left(^1\sum_g^+\right) + 2H \qquad (5)$$

would require at least 14 eV, decomposition of intermediates such as CH or CH_3 can be excluded as sources of $C(^1D)$ or $C(^1S)$ in the photolysis.

The source of the carbon atoms in the radiolysis is not so obvious; in addition to the decomposition of neutral excited methane molecules (reactions 3 and 4), the production of C atoms through the neutralization of ions must be considered. However, neutralization processes can not contribute to C atom formation

to any significant extent, since the major unreactive ions in the methane system [11, 20], $C_2H_5^+$, $C_2H_4^+$, and CH_5^+, would have to be in an excited state at the time of neutralization in order to make the formation of $C(^1D)$ or $C(^1S)$ energetically feasible. Because these unreactive ions will undergo many collisions with CH_4 prior to neutralization, the neutralization of an excited ion is extremely unlikely. Corroborative evidence that the C atoms (e.g., the acetylene) do not have an ionic precursor comes from the results of a photolysis experiment carried out with 16.7–16.8 eV photons. At this energy, the quantum yield of ionization in methane is unity [21], and the relative abundances of the major primary ions are about the same as in the gamma radiolysis [22–23]; thus, the fact (table 2) that in this experiment the yield of acetylene is negligible, indicates that C atoms are indeed not formed in ionic neutralization reactions in methane. In the photolysis of methane with 21.2 eV photons (table 2), the yield of acetylene is at least a factor of ten higher than at 16.6–16.7 eV, (although still much lower than the yield observed in the gamma radiolysis). This can be explained by the fact that at 21.2 eV, the quantum yield of ionization is slightly lower than unity (~ 0.96) [21]. That is, about 4 percent of the photons absorbed would lead to the formation of "superexcited" methane molecules, which, because of their high energy content might be expected to yield C atoms with a relatively high probability.

Further evidence that the acetylene in the gamma radiolysis does not have an ionic precursor is provided by the results of an experiment in which acetone was added to methane. In such an experiment, it is to be expected that the unreactive $C_2H_5^+$ and CH_5^+ ions formed in methane would quantitatively transfer a proton to the acetone; in this experiment (table 1) the yield of acetylene is close to the yield observed in the absence of acetone.

The absence of any appreciable decrease of $M(C_2H_2)/N_+$ with pressure in the ^{60}Co-gamma experiments (table 1) as well as in the 11.6–11.8 eV photolysis [19] indicates that the dissociative lifetime of the insertion product, $C_2H_4^*$, must be quite short ($\leq 10^{-9}$ s). The energy content of $C_2H_4^*$ formed in reaction 1 is 7.4 or 8.8 eV, depending on whether $C(^1D)$ or $C(^1S)$ is the reactant. RRKM calculations show that if the $C_2H_4^*$ formed in reaction 1 is a vibrationally excited ground state molecule its lifetime will be well below 10^{-10} s [24–25].

4.2. Formation of Acetylene in the Pulse Radiolysis of Methane

In the pulse radiolysis of a CH_4-CD_4 (1:1) mixture, nearly one third of the acetylene consists of C_2HD (table 3), in contrast to the low dose rate and photolysis experiments, where this isomeric analogue was formed only in very low yields. Thus, some mode of formation of acetylene other than reaction 1 must be occurring under these high dose rate conditions.

Accepting a rate constant of 10^{-9} cm^3/molecule-s for the reaction [26]

$$CH_3^+ + CH_4 \rightarrow C_2H_5^+ + H_2. \qquad (6)$$

It can be calculated on the basis of a modified WR16 computer program [27–28] that at the average dose rates reported in table 1, more than 99.9 percent of the CH_3^+ ions react to produce $C_2H_5^+$. Assuming a rate constant of less than 10^{-15} cm^3/molecule-s for reaction of $C_2H_5^+$ with CH_4 [20] and a value of 1.9×10^{-6} cm^3/molecule-s for the charge recombination rate constant [28], computation shows that at the high dose rates prevailing in the pulse radiolysis experiments all $C_2H_5^+$ ions will undergo homogeneous neutralization. When neutralization occurs by combination of $C_2H_5^+$ with an electron, one can expect the expulsion of an H-atom to occur

$$C_2H_5^+ + e \rightarrow C_2H_5^* \rightarrow C_2H_4^* + H. \qquad (7)$$

After rupturing the C-H bond, 6.7 eV is to be distributed among the two fragments. If one makes the reasonable assumption that most of the excess energy is taken up by $C_2H_4^*$ as internal energy, a pressure dependent fraction of these $C_2H_4^*$ species may be expected to dissociate:

$$C_2H_4^* \rightarrow C_2H_2 + H_2. \qquad (8)$$

Experimental observations indicate that the neutralization process 7 followed by dissociation 8 accounts for a major fraction of the acetylene produced in the pulse radiolysis of CH_4. For instance, addition of SF_6 to CH_4 drastically lowers $M(C_2H_2)/N_+$ and increases $M(C_2H_4)/N_+$ by roughly a corresponding amount (table 1). It is to be expected that the $C_2H_4^*$ formed by neutralization with SF_6^- would have less energy, and therefore would be less likely to undergo dissociation than those $C_2H_4^*$ species formed in reaction 7. Computer calculations which take into account the pulse shape, show that if one accepts a thermal electron capture rate constant for SF_6 of 2×10^{-7} cm^3/molecule-s [29], more than 99 percent of the $C_2H_5^+$ ions will be neutralized by SF_6^- rather than by recombination with an electron. (This is corroborated by the fact that a three-fold variation in the mole percent of SF_6 added to methane does not affect the yields of C_2H_2 and C_2H_4 as shown by the results given in table 1.) If the electron in reaction 7 is replaced with a SF_6^- ion:

$$C_2H_5^+ + SF_6^- \rightarrow C_2H_5^* + SF_6 \rightarrow C_2H_4^* + H + SF_6 \qquad (9)$$

it follows from the electron affinity [30] of SF_6 that the energy content of the neutral $C_2H_4^*$ entity formed in process 9 will be approximately 1.5 eV lower than that produced in the electron combination process 7. The excess energy will be even lower if neutralization involves a chemical reaction [31] such as

$$C_2H_5^+ + SF_6^- \rightarrow C_2H_4^* + HF + SF_5. \qquad (10)$$

The residual acetylene formed in the presence of SF_6 consists largely of C_2H_2 and C_2D_2, and thus must be formed mainly by the C atom insertion reaction 1. However the relative yield of C_2HD in the CH_4-CD_4-SF_6 pulse radiolysis experiment (table 3) is somewhat higher than the corresponding yield in the gamma radiolysis of a CH_4-CD_4-NO mixture, indicating the probable occurrence of the radical-radical reaction [32]:

$$^3CH_2 + {}^3CD_2 \rightarrow C_2HD + HD\cdot \qquad (11)$$

Triplet methylene ($^3CH_2$) is known to be unreactive towards methane [32–33] and is removed by NO in the low dose rate radiolysis experiments.

In the pulse radiolysis of pure methane, the ion pair yield of acetylene is seen to decrease from 0.24 to 0.15 when the pressure is raised from 100 to 775 torr. The fact that in the pulse radiolysis, the effect of pressure on the yield of acetylene is considerably more pronounced than in the ^{60}Co-gamma radiolysis can be rationalized in terms of the energy content of the precursor $C_2H_4^*$ species. In the low dose rate gamma radiolysis, the $C_2H_4^*$ precursor of acetylene originates in reaction 1 with a maximum energy content of at least 7.4 eV, while the $C_2H_4^*$ formed in the pulse radiolysis in reaction 7 originates with 6.7 eV excess energy.

4.3 General Considerations and Conclusions

In the preceding two sections we have concluded that in the gamma radiolysis and vacuum ultraviolet photolysis of methane, acetylene originates from the dissociation of excited ethylene formed by the insertion of C atoms into methane (reaction 1). In the pulse radiolysis of pure methane, where the ion pair yield of acetylene is much higher, it was concluded that most of the acetylene comes from the dissociation of excited ethylene formed when the ethyl ion is neutralized (reactions 7 and 8). Then the question is why the neutralization of the unreactive ethyl ion does not contribute to acetylene formation in the gamma radiolysis or vacuum ultraviolet photolysis of methane. In order to answer this we must consider that under conditions such that an unreactive ion undergoes homogenous neutralization, the lifetime of the ion, τ, will be

$$\tau = (Ik)^{-1/2}$$

where I is the number of ions formed per unit volume per second and k is the neutralization rate constant. Taking a value of 1.9×10^{-6} cm^3/molecule-s for k [28], we calculate that at a pressure of 200 torr at the dose rate of the gamma radiolysis experiments reported here, an ethyl ion would undergo about 2×10^6 collisions before being neutralized by an electron. (Under the conditions of the pulse radiolysis experiments, an ethyl ion would undergo only about 10^3 collisions before being neutralized by an electron.) Thus in the gamma radiolysis experiments any reactive compound present in amounts as small as 10^{-3}–10^{-4} percent might be expected to intercept the ethyl ions before they are neutralized. It has in fact been experimently demonstrated [20] that under low dose rate conditions, ethyl ions are effectively intercepted by 10^{-4} percent propane. Thus, it is not at all surprising that we see no evidence for the neutralization of ethyl ions in the low dose rate gamma radiolysis experiments, since at the conversions of these experiments (0.01–0.1%) it is very likely that the ethyl ions will be intercepted by accumulated products long before undergoing neutralization.

In the 16.7–16.8 eV and 21.2 eV photolyses, on the other hand, there is evidence that ethyl ions do undergo neutralization, but their neutralization does not lead to the formation of acetylene. That is, the ion pair yield of ethylene in the 16.7–16.8 and 21.2 eV photolyses (where, as mentioned before, essentially all products have ionic precursors) is about 0.3–0.35. (This may be contrasted with ethylene yield of 0.15–0.18 observed in the gamma radiolysis, where the ethylene has been shown [11] to be formed largely in a nonionic process.) The high yield of ethylene observed in the 16.7–16.8 and 21.2 eV photolysis experiments suggests that ethyl ions are undergoing neutralization to give C_2H_4 molecules that do not have sufficient energy to dissociate further. That the ethylene does have a $C_2H_5^+$ precursor is shown by the results of two experiments in which foreign compounds were added to intercept the ethyl ion. In the presence of added acetone, the ethyl ions will react quantitatively to form ethylene:

$$C_2H_5^+ + CH_3COCH_3 \rightarrow C_2H_4 + (CH_3COCH_3)H^+.$$

It is significant, then, that the yield of ethylene is about the same in the presence and absence of added acetone (table 2). When isobutane is added to methane, the ethyl ions will also be quantitatively intercepted, by the reaction:

$$C_2H_5^+ + i\text{-}C_4H_{10} \rightarrow C_2H_6 + t\text{-}C_4H_9^+. \qquad (13)$$

In the presence of isobutane, the ethylene yield is only about one-tenth of its value in the photolysis of pure methane or methane-O_2 mixtures. Thus, it can be concluded that in the 16.7–16.8 eV and 21.2 eV photolyses, the ethyl ion undergoes some process (which is not observed in the gamma radiolysis) to form ethylene which does not dissociate further to form acetylene. Thus, homogenous neutralization by an electron (reactions 7 and 8) or by SF_6^- (table 2) is excluded. Because of the high extinction coefficient of methane at these energies, these photolysis experiments must result in the formation of a high concentration of ions in a region of space quite close to the window. Thus, a tenable explanation of the results given in table 2 might be that the ions undergo heterogenous neutralization on the window.

The authors are indebted to S. G. Lias who generously helped in the preparation of this manuscript.

487-412 OL - 73 - 8

5. References

[1] Hummel, R. W., Disc. Faraday Soc. **36**, 75 (1963).
[2] Sieck, L. W., and Johnsen, R. H., J. Phys. Chem. **67**, 2281 (1963).
[3] Hauser, W. P., J. Phys. Chem. **68**, 1576 (1964).
[4] Johnsen, R. H., J. Phys. Chem. **69**, 3218 (1965).
[5] Hummel, R. W., J. Phys. Chem. **70**, 2685 (1966).
[6] Cahill, R. W., Seeler, A. K., and Glass, R. A., J. Phys. Chem. **71**, 4564 (1967).
[7] Hummel, R. W., and Hearne, J. A., J. Phys. Chem. **75**, 1164 (1971).
[8] Bosnali, M. W., and Perner, D., Z. Naturforsch **26a**, 1768 (1971).
[9a] Rudolph, P. S., and Melton, C. E., J. Phys. Chem. **71**, 4572 (1967).
[9b] Rudolph, P. S., Advan. Chem. Ser. **82**, 101 (1968).
[10] Finney, C. D., and Moser, H. C., J. Phys. Chem. **75**, 2405 (1971).
[11a] Ausloos, P., Lias, S. G., and Gorden, R., Jr., J. Chem. Phys. **39**, 3341 (1963).
[11b] Ausloos, P., Gorden, R., Jr., and Lias, S. G., J. Chem. Phys. **40**, 1854 (1964).
[11c] Gorden, R., Jr., and Ausloos, P., J. Chem. Phys. **46**, 4823 (1967).
[12] Willis, C., Boyd, A. W., and Miller, O. A., Radiat. Res. **46**, 428 (1971).
[13] Gorden, R., Jr., Rebbert, R. E., and Ausloos, P., NBS Tech. Note 496 (1969).
[14] Kinsinger, J. A., Stebbings, W. L., Valenzi, R. A., and Taylor, J. W., Anal. Chem. **44**, 773 (1972).
[15] LeBlanc, R. M., and Herman, J. A., J. Chim. Phys. **63**, 1055 (1966).
[16] Meaburn, G. M., and Perner, D., Nature **212**, 1042 (1966).
[17] Braun, W., Bass, A. M., Davis, D. D., and Simons, J. D., Proc, Roy. Soc. **312A**, 417 (1969).
[18] Husain, D., and Kirsch, L. J., Trans. Faraday Soc. **67**, 2025 (1971).
[19] Rebbert, R. E., and Ausloos, P., unpublished results.
[20] Haynes, R. M., and Kebarle, P., J. Chem. Phys. **45**, 3899 (1966).
[21] Rebbert R. E., and Ausloos, P. J. Res. Nat. Bur. Stand. (U.S.). 75A (Phys. and Chem.), No. 5, 481–485 (Sept.–Oct. 1971).
[22] Diebler, V. H., Krauss, M., Reese, R. M., and Harllee, F. N., J. Chem. Phys. **42**, 3791 (1965).
[23] Rebbert, R. E., and Ausloos, P., J. Am. Chem. Soc. **90**, 7370 (1968).
[24] Kirk, A. W., and Tschuikow-Roux, E., J. Chem. Phys. **51**, 2247 (1969).
[25] Ogata, Y., Obi, K., Akimoto, H., and Tanaka, I., Bull. Chem. Soc. Japan **44**, 2671 (1971).
[26] Futrell, J. H., and Tiernan, T. O., Chapter 4 in Fundamental Processes in Radiation Chemistry, P. Ausloos, Editor (J. Wiley, New York, 1968).
[27] Schmidt, K. H., AEC Research and Development Report NAL–7199 (1966).
[28] Lias, S. G., Rebbert, R. E., and Ausloos, P., J. Chem. Phys. **57**, 2080 (1972).
[29] Mothes, K. G., and Schindler, R. N., Ber. Bunsenges fur Phys. Chemie **75**, 938 (1971) and references cited therein.
[30] Compton, R. N., and Huebner, R. H., Advan. in Radiat. Chem. **2**, 281 (1970).
[31] Bansal, K. M., and Freeman, G. R., J. Am. Chem. Soc. **90**, 7183 (1968).
[32] Braun, W., Bass, A. M., and Pilling, M., J. Chem. Phys. **52**, 5131 (1970).
[33] Lee, P. S. T., Russell, R. L., and Rowland, F. S., Chem. Comm. (1970), p. 18.

(Paper 77A1–756)

JOURNAL OF RESEARCH of the National Bureau of Standards – A. Physics and Chemistry
Vol. 77A, No. 1, January–February 1973

The Enhancement of Water Vapor in Carbon Dioxide-Free Air at 30, 40, and 50 °C

Richard W. Hyland and Arnold Wexler

Institute for Basic Standards, National Bureau of Standards, Washington, D.C. 20234

(August 18, 1972)

The enhancement of water vapor in compressed atmospheric air was measured at 30, 40, and 50 °C over respective pressure ranges of 10 to 35 bars, 15 to 60 bars, and 10 to 100 bars. The data for each isotherm were fitted by the method of least squares to an empirical smoothing equation of the form $\ln f = a + bP$ where f is the enhancement factor, P is the total (absolute) pressure and a and b are constants. A detailed error analysis, necessary for the eventual use of the data in humidity standards work, shows that the calculated (predicted) values of f have an estimated limit of systematic bias of ± 0.07 percent and a maximum observed standard deviation of a predicted value of ± 0.2 percent.

Key words: Concentration of saturated water vapor in air; enhancement factor; moist air; moisture content of saturated air; saturated air; solubility of water vapor in air; water vapor.

1. Introduction

The saturation concentration of water vapor over the flat surface of its pure condensed phase is an accurately known function of temperature [1].[1] If now a second gas is introduced over the surface of the water, the saturation concentration of the water vapor is increased. At any given temperature this increase may be expressed as a ratio of the vapor concentration at the total system pressure in the presence of the second gas to the vapor concentration of the pure phase. This ratio, sometimes called the enhancement factor, is expressed by

$$f_\rho = \frac{\rho_w}{\rho_w^0} \tag{1}$$

where ρ_w is the saturation vapor concentration or density in the presence of the second gas and ρ_w^0 is the saturation vapor concentration or density of the pure phase.

The enhancement factor may also be expressed by

$$f_n = \frac{N_w}{N_w^0} \tag{2}$$

where N_w is the saturation molar concentration or density in the presence of the second gas and N_w^0 is the saturation molar density of the pure phase, and by

$$f_p = \frac{X_w P}{P_w^0} = \frac{X_w P}{e_s} \tag{3}$$

where X_w is the mole fraction of water vapor in the given water vapor-gas sample, P_w^0 is the saturation vapor pressure of the pure phase, and P is the total pressure of the system. In accordance with meteorological convention, P_w^0 is designated by e_s.

At any temperature, as the amount of the second gas goes to zero, the enhancement factor approaches unity. Furthermore, the expressions would be equivalent, at the same conditions of pressure and temperature, only if the ideal gas laws were valid. In this work the enhancement factor as defined by eq (3) will be used exclusively. The subscript will be dropped and the enhancement factor will be designated simply by the symbol f.

Deviations of water vapor concentrations in air from those predicted by ideal gas laws are on the order of 0.5 percent at pressures as low as 900 mb [2], making widespread use of experimentally based enhancement factors important in such areas as industrial drying processes operating at high pressures, especially in the performance of dehydration plants for compressed natural gases [3, 4, 5]. Enhancement factors are employed in hygrometry to compute the water vapor content of gases and to make accurate conversions among parameters used to express humidity [6], to calibrate hygrometers against humidity standards [7, 8], and to make precise calculations in the fields of meteorology and air conditioning [9]. From experimental enhancement factors it is possible to derive the cross-virial terms in the virial equation of state [10].

Experimental data on the enhancement of water vapor in air are meager. Politzer and Strebel [11] made measurements at 50 and 70 °C at total pressures

[1] Figures in brackets indicate the literature references at the end of this paper.

up to 200 bars.[2] Webster [12] made similar measurements from −35 to +15 °C at total pressures up to 200 bars. Goff, Andersen, Gratch, and Bates [2, 10, 13, 14, 15] performed enhancement experiments from 5 to 25 °C at or near atmospheric pressure. Although enhancement measurements of water vapor in other gases have been made, the data are also very limited [3, 4, 5, 16, 17, 18].

Accurate determinations of enhancement factors are difficult to make. Dynamic rather than static experimental systems are required to avoid the insidious problems of water sorption and desorption on the walls of the system. Two approaches have been used by other researchers to obtain experimental values: the single saturation isotherm method and the double saturation isotherm method. In the first method, which we use for the work reported in this paper, the inert (indifferent) carrier gas is saturated with respect to the condensed water substance at a fixed temperature and pressure. The resultant moisture content is determined, typically, by removing the water vapor from the gas by a desiccant, weighing the collected moisture and measuring the volume or mass of the associated dry gas.

The double isotherm experiment, described by Goff and Bates [13], is basically two single isotherm experiments in series. The same air mass is used for two successive saturations at a fixed temperature but different pressures. The calculations involve a ratio from which the air mass is eliminated. The method does not give a direct measurement of enhancement factor but rather yields the "interaction constant," a quantity closely related to the cross virial coefficient from which the enhancement factor may be calculated [13, 14].

This paper is a progress report on a continuing experimental determination of the enhancement factor for water vapor in air. Measurements have been made at three temperatures, namely 30, 40, and 50 °C, and over a range of pressures from 10 to 100 bars. Our objective, at this time, is to describe the experimental method used and to present the data obtained thus far.

2. Apparatus

For our single isotherm experiment, the apparatus consists of two basic units: a generator in which air is saturated under known conditions of temperature and pressure, and the NBS standard hygrometer which permits the determination of the ratio of the mass of water to the mass of air in the effluent from the generator. The mole fraction of water vapor is calculated from the mass ratio, while the saturation vapor pressure is obtained, from the temperature, through a mathematical formulation such as in [1]. The generator operates in a dynamic mode, producing a continuous stream of saturated air. Repeated measurements of pressure and temperature are made during a run which, coupled with the mole fraction determination, permit a value of enhancement factor to be calculated which is an average over the experimental time.

2.1. Flow and Saturation System

The flow chart of the apparatus is shown in figure 1. There are three baths, two of which, PB and MB, are directly involved with the air stream while the third, RB, is used in controlling the temperature of the other two. Air is supplied from cylinders A, used either singly or manifolded in parallel, and flows between components through $\frac{3}{8}$-in o.d. stainless steel tubing. The pressure is set with two pressure-loaded (dome) reducers B in series. From these pressure reducers the air passes

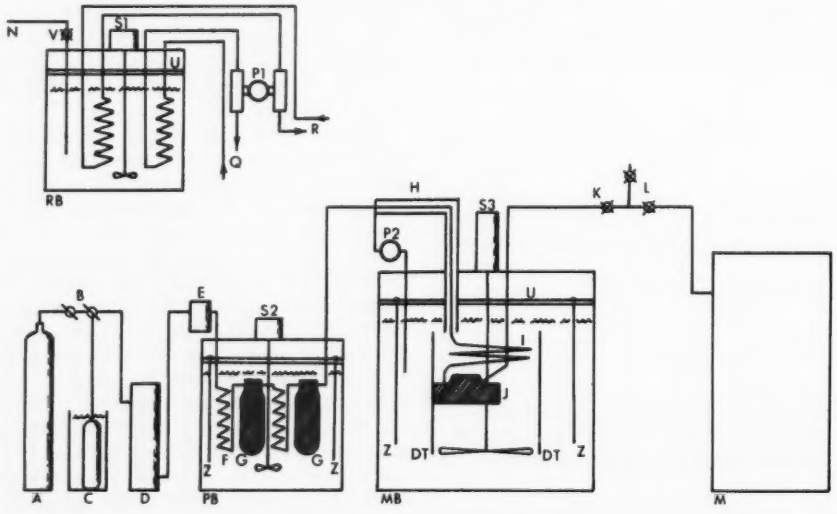

FIGURE 1. *Flow diagram and apparatus arrangement; components not mentioned by letter in the text are the preliminary bath heat exchanger (F); the preliminary saturators (G); shut-off valves (L); coolant lines to and from PB and MB (Q, R); and splash plates for each bath (U).*

[2] 1 bar = 10^5 newtons/m^2 = 10^5 pascals = 10^3 mb = 750.62 mmHg.

through a carbon dioxide removal unit D. The CO_2 is removed to prevent any possibility of the natural variability of CO_2 in the air from affecting the results. From this unit the air passes through a two-micron filter E, then into a preliminary saturation system which is immersed in a bath PB that is controlled at 3 to 5 °C above the temperature of the main bath MB.

The wet air emerges from the preliminary bath and passes into a heated portion of the line which is maintained 20 to 30 °C above the test temperature to insure against condensation. This hot moist air is now brought to the temperature of the main bath MB. Near the main bath the tubing carrying the test gas enters a counter-current heat exchanger H in which water from the temperature-controlled main bath is pumped through a jacket surrounding the tubing. The heater, which keeps the tubing from the preliminary bath to the water jacket hot, also surrounds the water jacket to prevent the water from cooling in its course through the heat exchanger. From the counter-current heat exchanger the air enters the inlet heat exchanger coil I in the main bath. The coil is a 10-meter length of $\frac{3}{8}$-in o.d. stainless steel tubing which fits inside a draft tube DT. From this coil the gas, which is now within several thousandths of a degree of, and very close to saturation with respect to, the main bath temperature, enters the main saturation system.

The preliminary saturation system and the main saturation system used for working pressures above 30 bars are bubbler-type systems, and are made up of one-liter capacity stainless steel cylinders filled with layers of glass beads. The preliminary system consists of two, and the main system of three, such cylinders, the cylinders of each system being interconnected with 3-meter length heat exchanger coils. (The main saturation system J of figure 1 represents the low pressure system to be discussed below.)

The general configuration of the cylinders is shown in figure 2. The particular unit illustrated is the final main saturator unit which is similar to the other configurations except for the addition of the thermometer lead-in tube E, thermometer well F, and pressure tap D. In each cylinder, water is added (and removed) through a filling tube G connected to the bottom of the cylinder. The air enters the saturator at A through an inlet tube and discharges radially through 50 orifices B near the bottom of the saturator. The air bubbles through the water and is dispersed by the glass beads for more effective saturation.

In order to obtain optimum dispersal and eliminate splashing and spray above the bead level, a series of visual experiments was run on glass prototype saturators using various water depths, bead depths, and bead sizes before selecting the final configuration. There are two bead layers in the preliminary saturators and three in the main saturators. In each case the lower layer consists of 6-mm o.d. solid borosilicate spheres, while the second layer consists of 4-mm o.d. borosilicate glass beads, each perforated with a small hole for larger surface area. The third layer, used only in the main saturators, consists of 2-mm o.d. solid borosilicate glass spheres.

For pressures below 30 bars a single stainless steel dish or maze saturator, illustrated in figure 3, is used in lieu of the three bubbler type saturators. An interconnecting series of $\frac{7}{16}$ in (1.1 cm) wide concentric grooves is machined into the lid, so that when the lower portion, or dish, and lid are mated and water added, the grooves and water surface form channels through which the air flows on its way to the center. The air traverses a path over the water surface which is 75 cm long. The normal working condition is such that the distance between water surface and lid is about $\frac{1}{4}$ in (0.6 cm). In the central (innermost) groove, which is 2 inches (5.1 cm) in diameter, are located the pressure tap F, the thermometer well D, and the exit port for the air E; pressure and temperature measurements can be made in the region where the air leaves the saturator.

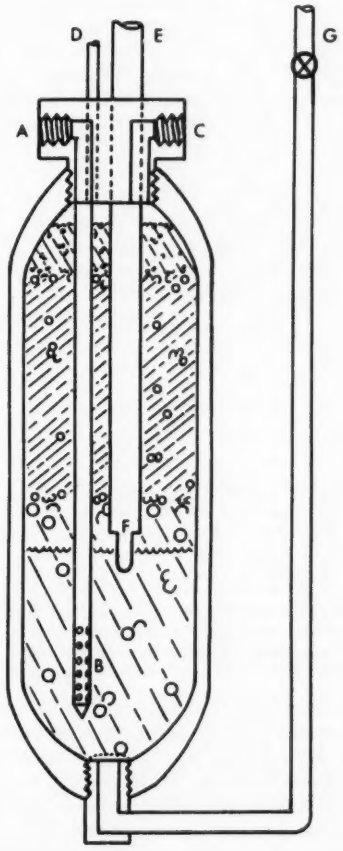

FIGURE 2. *Final main bubbler saturator, indicating the three bead layers and water level as well as the inlet port (A); exit holes into the water (B); outlet port (C); pressure tap (D); thermometer lead-in tube (E); thermometer well (F); and the tube for adding and removing water (G).*

A stainless steel screen prevents the beads from dropping into the filling tube.

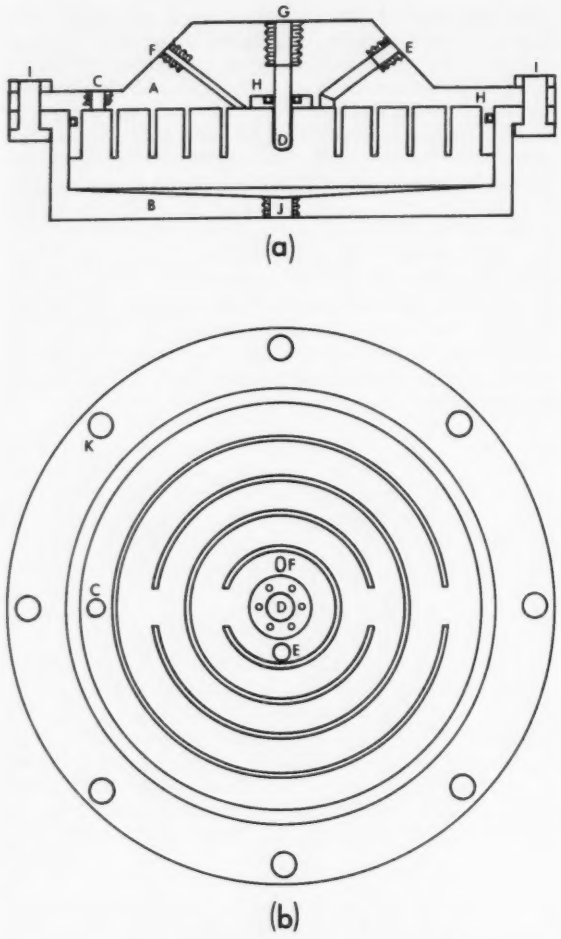

FIGURE 3. *(a) Dish saturator, schematic cross section, showing lid (A); dish (B); inlet port (C); thermometer well (D); outlet port (E); pressure tap (F); thermometer lead-in port (G); O-ring seals (H); flange bolts (I); and water inlet and removal port (J). The inlet (C) is not shown in proper relation to ports (E) and (F), nor are the screws retaining the thermometer well indicated. (b) Dish saturator lid, bottom view, showing flange bolt holes (K); inlet port (C); pressure tap (F); thermometer well and its retaining screws (D); and outlet port (E). Hidden upper surfaces are not indicated, but are of circular symmetry. Bottom view rotated with respect to top view.*

From the final (third) bubbler saturator unit or from the dish saturator (see fig. 1) the air enters tubing which is wrapped with an electric heater from a point prior to its emergence from the bath fluid up to a point just downstream of the expansion valve K. In the region of the expansion valve, the temperature of the test gas is maintained at or near 100 °C. The tubing downstream of the expansion valve remains warm to the touch for a distance of about 30 cm. This insures that neither heat loss to the room air nor adiabatic cooling on expansion at the expansion valve will reduce the test gas temperature to or below its dew point. Variations in temperature and pressure, provided they do not cause condensation, do not affect the ratio of water vapor mass to air mass from which the mole fraction is computed. The expansion valve reduces the test gas pressure to one bar at which pressure the test gas enters the gravimetric hygrometer M.

2.2. Pressure Measurement and Control

In the course of this work, pressure measurements were made using (a) an oil-lubricated (medium-range) piston gage with a range of 25 to 3000 psi (1.7 to 200 bars) and a weight set permitting pressure increments of 25 psi (1.7 bars), (b) a precision laboratory bourdon gage having a range of 2000 psi (140 bars) and readable to 1 psi (0.07 bar) and (c) a precision laboratory bourdon gage having a range of 3000 psi (200 bars) and readable to 1 psi (0.07 bar). The piston gage weights were augmented by a set of analytical balance gram weights and by brass washers (of known weight) so that any nominal pressure could be attained readily.

A commercial stainless steel diaphragm separator isolates the air in the saturation system from the oil in the piston gage. It has a null-detector circuit that visually indicates balance on a meter and that also provides an analog output.

Pressure is set and controlled by two air-loaded dome reducers in series. Attached to the control volume on the downstream reducer is a 1.6-liter cylinder, which initially served as a ballast volume. Subsequently, it was placed in a small water bath (C, fig. 1), the temperature of which is automatically adjusted in response to the analog output signal from the diaphragm null-detector circuit. This raises or lowers the pressure of the control volume of the downstream reducer. The latter, in turn, acts to restore the system pressure to its initial value.

2.3. Temperature Measurement and Control

The temperatures are maintained in the preliminary and main baths by balancing a slight controlled cooling with heat. The cooling is induced by circulating the water (used as the bath liquid in both baths) from the preliminary and the main baths through separate coils that are immersed in a third refrigerated bath RB (see fig. 1). The circulation rates are individually variable by means of a dual metering pump P1. The refrigerated bath fluid is industrial grade *n*-propyl alcohol. It is stirred with an immersed sump pump S1. A bimetallic thermoregulator controls the opening and closing of a valve V on a liquid CO_2 line N; the liquid CO_2 discharges into the bath through a small orifice, vaporizes, and abstracts heat from the alcohol. The temperature of the refrigerated bath is maintained within ±1 deg C at any selected temperature between 15 and 21 °C. The cooling capacity of the water circulated to the preliminary and main baths is adjusted by setting the temperature of the refrigerated bath and the circulation rate of the water flowing through the coils immersed in the alcohol.

The temperature of the preliminary bath PB is set and sensed with a bimetallic thermoregulator which activates an electronic relay, controlling the on-off

position of an immersion heater Z. The bath liquid is stirred by a small propeller S2.

The temperature of the main bath MB is maintained within ±0.005 deg C by a time-proportioning controller with adjustable rate and automatic reset acting in response to a 4-lead platinum resistance thermometer. The controller activates a network of four electric heaters Z interconnected through switches into several optional parallel or series arrangements.

Both the preliminary and main baths have a second group of heaters for rapid warm-up and to provide a constant (adjustable) heat load.

The interior of the main bath is divided into an inner core and an outer annulus by means of an 18 in (45.7 cm)-diameter, stainless steel draft tube DT. This tube is supported by stainless steel legs and is centered by radial stainless steel brackets. The saturation system, the control thermometer, and the intake port of the water line to the counter-current heat exchanger are located within the draft tube whereas all heaters, intake and discharge lines for the water that is circulated to and from the refrigerated bath, and the discharge line from the counter-current heat exchanger are located in the annulus.

At 120 degree intervals around the interior of the draft tube, flush with the top, are vortex control vanes, 2.5 cm wide by 30 cm long. The bath water is stirred by a propeller with stabilizer ring that is located at the bottom of the draft tube and is driven by the variable speed motor S3. The bath water is forced vertically downward through the draft tube, then up through the annulus where heat is added or removed and returned to the top of the draft tube.

The main, preliminary and refrigerated baths each are insulated with styrofoam and are covered with lids. They have internal volumetric capacities of 750, 115, and 115 liters, respectively.

The temperature in the preliminary saturators is considered to be the same as that of the preliminary bath and is measured with a two-junction copper-constantan thermopile with a maximum uncertainty less that ± 0.2 °C. The temperatures of the main bath and main saturation system are measured with four-lead platinum resistance thermometers and a Mueller bridge. These measurements will be discussed more fully in section 6.2.

2.4. Determination of Mole Fraction

The NBS standard (gravimetric) hygrometer is used for determining the mole fraction of the water vapor in the gas emerging from the saturation system. Because this apparatus is described in great detail in [19] only a brief description will be given here. The hygrometer yields a measurement of the mixing ratio, that is, the mass of water vapor per unit mass of dry air, from which the mole fraction is readily computed.

The saturated air from the saturation system is reduced to atmospheric pressure through the heated expansion valve K (fig. 1) and passed through a series of preweighed, desiccant-filled U-tubes where the water vapor is removed. Upon completing an experiment a final weighing is made and the gain in weight gives the mass of water collected. The effluent dry air from the absorption tubes is collected in cylinders of known volume. A measurement of P and T in the volume permits the calculation of the mass of dry gas. The gravimetric hygrometer is arranged so as to permit uninterrupted gas flow through the U-tubes into two alternately filled, measured, and evacuated cylinders until approximately one gram of water has been collected. The flow rate of the test gas through the hygrometer is maintained at or below 2 g per minute.

3. Materials

3.1. Air

The gas used in these experiments was low hydrocarbon content, compressed and dried atmospheric air, commercially supplied in steel cylinders. The supplier's assays show that the methane content is usually 2 ppm by volume and never exceeds 4 ppm. The residual hydrocarbon content is about 2 ppm. The CO_2 content varies from trace quantities to 300 ppm. Analyses made at NBS agree with the supplier's assessment of hydrocarbon content. In addition, the NBS tests indicate that 1 ppm of CO and up to 325 ppm of CO_2 are present in the air. The other normal constituents are present in the percentages usually given for atmospheric air [20]. In our experimental setup, air passes through the CO_2 removal unit previously described. The CO_2 content of the gas emerging from the generator is on the order of 2 ppm.

3.2. Water

For most of the runs (through No. 42) the water used in the saturators was first deionized, and double distilled. For the last five runs (Nos. 43 through 48) the purification process was reduced to a single distillation of tap water. The solid residuals in the deionized and doubly distilled water initially ranged between 2 and 6.5 ppm, possibly because the still had recently been installed. At a later date, measurements indicated that the solid residuals had been reduced to the parts per billion range, the major constituents being copper (4 ppb), lead (0.6 ppb), cadmium (0.02 ppb), and a trace of zinc.

Fresh water was placed in each saturator prior to all runs except in four cases, where the same water served for two successive runs. After the completion of each of 22 runs measurements of solid residuals were made on samples of water withdrawn from the final saturator unit of the main saturation system. The maximum solid residual concentration observed was 330 ppm by weight. This occurred in water that had been used for two successive runs (Nos. 23 and 24). The next highest concentration was 88 ppm (run No. 18), while the average for all runs was 48 ppm. The solid residuals tended to be lower in concentration in the water removed from the dish saturator. Qualitative spectrochemical examina-

tion of the solid residual material from the water removed from the bubbler type saturator disclosed that the principal constituents were silicon and calcium (90 to 99%) and magnesium (1 to 10%) with traces of sodium, boron, aluminum, copper, iron, titanium, silver and chromium. The calcium and sodium probably originate in the chemicals in the CO_2 removal unit and in the glass beads, whereas the silicon and boron are probably leached from the borosilicate glass beads.

Calculations based on Raoult's law, assuming that all the solids behave as soluble ionic particles, suggest that their relative effect on the pure phase vapor pressure and, consequently, on the enhancement factor, is numerically about $\frac{1}{3}$ of the concentration in ppm. For the maximum observed concentration (330 ppm), this means the relative uncertainty should not exceed 110 ppm.

4. Experimental Procedure

In executing a run, that is, in making a single determination of enhancement factor, a desired combination of pressure and temperature at a mass flow rate of 2 g per minute was established in the generator and the entire apparatus was permitted to operate, with the effluent air from the generator exhausting into the laboratory, until equilibrium conditions were achieved. The gravimetric hygrometer was independently prepared for use by continuously flushing for three or more days with dry room-temperature air those components that would subsequently be exposed to the test gas, the intent being to eliminate any inadvertent moisture that might introduce an error. On the day of the run, the flushing process was halted briefly and the weighed desiccant-filled U-tubes inserted into the absorption train. In order to minimize the possibility that traces of moisture from room air trapped in the U-tube sidearms or drying train components during the insertion of the U-tubes would affect the results, the flushing process was resumed. The dry gas was allowed to flow up to the sealed inlet stopcock of the first U-tube and vented to the room. After sufficient time had elapsed for drying, and vent was closed and the inlet stopcock and outlet stopcock opened, the dry gas now flowing through the first tube and out the stopcock channel of the second. This procedure was repeated for the third U-tube, with the flushing gas eventually exhausting downstream of the third U-tube.

Equilibrium of the lines up to the U-tubes, with respect to the moisture content of the test gas, was accomplished by halting the flow of the dry flushing gas through the drying train, sealing the U-tubes, and permitting the test gas from the generator to flow up to the inlet stopcock of the first U-tube in the drying train and vent into the room. On the initiation of the run, all stopcocks were opened thus interconnecting the gravimetric hygrometer with the generator.

The duration of a run was dictated by the requirement that nominally 1 gram of moisture be collected by the drying train. At a test gas flow rate of 2 g per minute, the elapsed time for a run varied from 1 to 10 h depending on the moisture content. During this period repeated measurements were made of generator and hygrometer variables. At the termination of the run, the U-tubes were sealed, removed from the drying train, and transferred to a balance room for weighing.

5. Results

An initial group of runs was made during which system difficulties were resolved, equipment improved and apparatus redesigned. The basic experimental data for the final group of runs (Nos. 16 through 48) are given in chronological order in table 1. Run Nos. 16 through 28 utilized bubbler units in the main saturation system; the remainder of the runs employed the dish saturator. In run Nos. 21 through 27 pressure measurements were made with the bourdon gages; in the other runs, the medium-range piston gage was used. The calculated parameters and final results are given in table 2. These are arranged in groups corresponding to the three nominal test temperatures 30, 40, and 50 °C.

The experimental enhancement factors from table 1 were normalized to the nominal test temperatures given in table 2, as follows. Considerations of the theoretical aspects of f (see e.g., the papers of Goff et al., particularly eq (8) of [15]) lead to the conclusion that, along an isotherm, a smoothing expression of the form

$$\ln f = a + bP \tag{4}$$

where P is the total system pressure, is nearly correct.

For the first step toward normalization, small differences between actual and nominal isotherm temperatures were ignored and plots of $\ln f$ versus pressure were made along the three isotherms. Next the slopes $(\ln f)/T$ as a function of pressure were measured from these graphs, and used to adjust the experimental values to the desired isotherm temperature. The changes in f do not exceed 2 parts in 10^4, as can be seen by comparing the experimental values of table 1 with the normalized values of table 2. Uncertainties introduced into f by the procedure should not exceed a few parts per million and are considered negligible.

The OMNITAB computer program [21] was used for fitting eq (4), by the method of least squares, to the normalized enhancement factors for each nominal test temperature. Strictly speaking, the assumptions underlying the cited least square method are not fulfilled since f and P are both measured with errors and are correlated. However, since we are interested only in a smoothing expression for purpose of interpolation, the procedure may still be used. The computed coefficients are given in table 3. Figure 4 shows the residuals between the natural logs of the normalized f's and the values of $\ln f$ predicted by eq (4) as a function of pressure along the three isotherms. The scatter of the deviations indicates that eq (4) is a valid approximation.

The residuals between the normalized f and the enhancement factor predicted by eq (4), $f_{norm} - f_{pred}$, are shown in table 2 together with the residual standard deviations and the standard deviations of the pre-

TABLE 1. *Experimental data*

Run No.	Saturation temperature[1] t_s	Saturation vapor pressure[2] e_s	Total pressure[3] P	Mole fraction H_2O X_w	Enhancement factor f	Preliminary bath temperature t	Type of saturator	Type of pressure gage
	°C	*mb*	bar			°C		
16	50.0050	123.4164	30.2324	0.0044135	1.0811	52.67	Bubbler	Piston
17	50.0101	123.4477	30.1977	.0044266	1.0828	53.76	Bubbler	Piston
18	(contaminated U-tube; run n.g.)						Bubbler	Piston
19	39.9969	73.7612	30.1957	.0026497	1.0847	44.05	Bubbler	Piston
20	30.0112	42.4566	30.1929	.0015317	1.0893	34.40	Bubbler	Piston
21	40.1366	74.3122	60.9945	.0014285	1.1725	44.20	Bubbler	Bourdon
22	40.1505	74.3673	50.3962	.0016810	1.1392	44.20	Bubbler	Bourdon
23	50.0049	123.4158	50.3229	.0027681	1.1287	53.74	Bubbler	Bourdon
24	49.9784	123.2536	76.3139	.0019376	1.1997	52.98	Bubbler	Bourdon
25	49.9788	123.2561	102.704	.0015264	1.2719	52.56	Bubbler	Bourdon
26	49.9766	123.2426	40.8462	.0033228	1.1013	52.12	Bubbler	Bourdon
27	39.9648	73.6350	40.4557	.0020231	1.1115	42.45	Bubbler	Bourdon
28	49.9815	123.2726	90.9356	.0016749	1.2355	52.84	Bubbler	Piston
29	50.0009	123.3913	36.5953	.0036782	1.0909	52.74	Dish	Piston
30	49.9967	123.3656	25.3585	.0051773	1.0642	52.40	Dish	Piston
31	49.9891	123.3191	14.6231	.0087902	1.0423	53.49	Dish	Piston
32	49.9898	123.3233	10.5512	.0120190	1.0283	53.77	Dish	Piston
33	50.0064	123.4250	14.8620	.0086263	1.0387	52.84	Dish	Piston
34	40.0104	73.8143	14.6417	.0052456	1.0405	43.00	Dish	Piston
35	50.0011	123.3925	10.7989	.0117614	1.0293	49.44	Dish	Piston
36	50.0042	123.4115	10.7441	.0118214	1.0292	60.25	Dish	Piston
37	49.9942	123.3503	10.6310	.0119361	1.0287	52.51	Dish	Piston
38	(equipment failure; run aborted)						Dish	Piston
39	29.9994	42.4278	10.7312	.0040827	1.0326	33.68	Dish	Piston
40	29.9999	42.4290	35.5133	.0013201	1.1049	33.44	Dish	Piston
41	29.9992	42.4273	19.7704	.0023107	1.0767	32.74	Dish	Piston
42	29.9990	42.4290	19.9344	.0022534	1.0587	33.78	Dish	Piston
43	50.0047	123.4146	10.7546	.0117992	1.0282	52.65	Dish	Piston
44	(Spray trap inserted; behaved as a moisture sink; run n.g.)						Dish	Piston
45	(Spray trap inserted; behaved as a moisture sink; run n.g.)						Dish	Piston
46	49.9971	123.3680	10.7953	.0117446	1.0277	53.51	Dish	Piston
47	30.0065	42.4451	15.1088	.0029354	1.0449	33.73	Dish	Piston
48	29.9975	42.4232	15.3079	.0028727	1.0366	34.07	Dish	Piston

[1] IPTS–48.
[2] Calculated from equation given by Wexler and Greenspan [1].
[3] Gage pressure plus barometric pressure.

TABLE 2. *Results*

Run No.	Total pressure	Normalized enhancement factor[1]	Predicted enhancement factor[2]	Residual	Standard deviation of the predicted value[3]
	P bars	f_{norm}	f_{pred}	$f_{norm} - f_{pred}$	
30 °C (all runs included)					
39	10.7312	1.0326	1.0331	−0.0005	0.0053
47	15.1088	1.0449	1.0459	−.0010	.0041
48	15.3079	1.0366	1.0465	−.0099	.0041
41	19.7704	1.0768	1.0596	+.0172	.0034
42	19.9344	1.0587	1.0601	−.0014	.0034
20	30.1929	1.0893	1.0910	−.0017	.0053
40	35.5133	1.1049	1.1074	−.0025	.0072
Residual standard deviation.....				.0090	

TABLE 2. *Results*—Continued

Run No.	Total pressure	Normalized enhancement factor[1]	Predicted enhancement factor[2]	Residual	Standard deviation of the predicted value[3]
	P bars	f_{norm}	f_{pred}	$f_{norm} - f_{pred}$	
30 °C (run nos. 41 and 48 deleted)					
39	10.7312	1.0326	1.0325	+0.0001	0.0001
47	15.1088	1.0449	1.0450	−.0001	.0001
42	19.9344	1.0587	1.0589	−.0002	.0001
20	30.1929	1.0893	1.0890	+.0003	.0001
40	35.5133	1.1049	1.1050	−.0001	.0001
Residual standard deviation				.0002	
40 °C					
34	14.6417	1.0405	1.0410	−0.0005	0.0010
19	30.1957	1.0847	1.0832	+.0015	.0006
27	40.4557	1.1115	1.1120	−.0005	.0006
22	50.3962	1.1393	1.1406	−.0013	.0007
21	60.9945	1.1727	1.1719	+.0008	.0010
Residual standard deviation				.0013	
50 °C					
32	10.5512	1.0283	1.0294	−0.0011	0.0008
37	10.6310	1.0287	1.0296	−.0009	.0008
36	10.7441	1.0292	1.0298	−.0006	.0008
43	10.7546	1.0282	1.0298	−.0016	.0008
46	10.7953	1.0277	1.0299	−.0022	.0008
35	10.7989	1.0293	1.0300	−.0007	.0008
31	14.6231	1.0423	1.0390	+.0033	.0007
33	14.8620	1.0387	1.0396	−.0009	.0007
30	25.3585	1.0642	1.0650	−.0008	.0006
17	30.1977	1.0828	1.0769	+.0059	.0006
16	30.2324	1.0811	1.0770	+.0041	.0006
29	36.5953	1.0909	1.0929	−.0020	.0006
26	40.8462	1.1013	1.1036	−.0023	.0006
23	50.3229	1.1287	1.1279	+.0008	.0007
24	76.3139	1.1997	1.1974	+.0023	.0012
28	90.9356	1.2355	1.2383	−.0028	.0016
25	102.704	1.2718	1.2723	−.0005	.0019
Residual standard deviation				.0026	

[1] Experimental enhancement factor adjusted to nominal temperature.

[2] Predicted enhancement factor obtained by calculation using eq (4) with appropriate coefficients from table 3.

[3] The method of calculation is given by Natrella [22], p. 6–12.

TABLE 3. *Coefficients for eq (4)*

Source	Temperature °C	a	Standard deviation of $a \times 10^4$	b	Standard deviation of $b \times 10^6$
NBS	30[1]	0.002565	87.7	0.002799	390.
	30[2]	.002603	2.07	.002739	8.59
	40	.002745	13.7	.002556	32.2
	50	.004673	8.80	.002299	19.7

TABLE 3. *Coefficients for eq (4)*—Continued

Source	Temperature °C	a	Standard deviation of $a \times 10^4$	b	Standard deviation of $b \times 10^6$
Goff	0	.00046	3.1	.00388	2.7
	10	.00072	3.0	.00362	5.0
	20	.00109	3.0	.00336	8.9
	30	.00161	3.0	.00316	15.
	40	.00229	3.0	.00297	24.
	50	.00317	3.1	.00280	39.
	60	.00430	3.4	.00264	59.
	70	.00571	3.5	.00251	89.
Webster	0	.04013	116.	.003324	116.
	15	.04076	89.2	.002701	75.1
Politzer and Strebel	50	−.01236	82.5	.002512	66.2
	70	.02800	54.54	.002151	56.4

[1] All runs included in least square fit.
[2] Run nos. 41 and 48 deleted from least square fit.

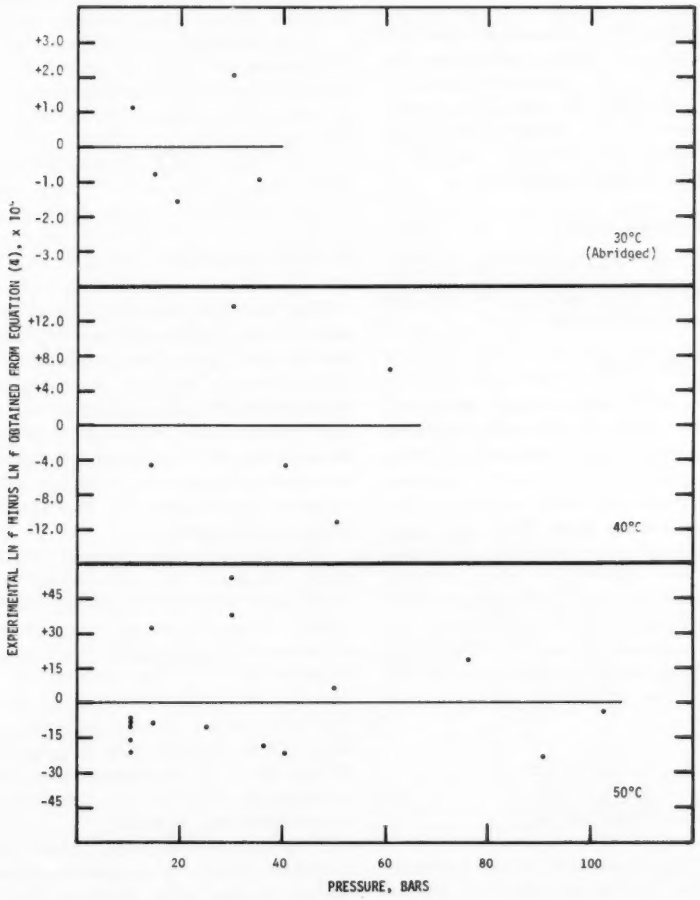

FIGURE 4. *Deviations of the ln f values predicted by eq (4) from the experimental values, as functions of pressure.*

dicted values.[3] The residual standard deviation may be considered an index of the precision of the measuring process whereas the standard deviation of the predicted value serves as a measure of the random uncertainty in the calculated value. The residual standard deviation for the 30 °C isotherm (±0.0090) is seven times as large as that for the 40° isotherm (±0.0013) and three times as large as that for the 50° isotherm (±0.0026). This large residual deviation can be traced to run Nos. 41 and 48 which have residuals that are grossly out of line with the others in this isotherm. Although there seems to be no experimental justification for discarding these runs, the magnitudes of the residuals are so large as to make the runs open to suspicion. If these runs are deleted and the equation refitted to the remaining data, then the residual standard deviation is reduced to ± 0.0002. In our opinion this latter fit is preferable to the one based on all the data, and is the one we shall use.

6. Error Analysis

The enhancement factor is a computed quantity whose magnitude depends on three variables—the mole fraction of water vapor, the total pressure, and the saturation vapor pressure of the pure water substance. We shall estimate the uncertainty in our predicted values of enhancement factor by examining suspected sources of error in these variables.

6.1. Pressure Error

The uncertainties in the pressure measurement differ substantially from the piston gage to the bourdon gages. These are discussed separately.

a. Piston Gage

The piston gage is an instrument which measures pressure in terms of the fundamental units of force and area. However, various other factors must be considered, and Cross [23] has developed a general equation for calculating pressure which we have modified as follows for use with our gage. First, our gage is not a controlled clearance type, therefore, the relevant term in the equation reduces to unity; second, the piston is cylindrical and flat-bottomed, so that there is no fluid buoyancy correction to be considered; and third, the proportionality factor, k, for the force-mass units applicable to this gage, is the reciprocal of standard gravity, i.e., $1/g_s$. Thus eq (24) given by Cross reduces to

$$P_g = \frac{\frac{M_m}{A_o}\left(1 - \frac{\rho_a}{\rho_m}\right)\frac{g_1}{g_s} + \frac{\gamma C}{A_o}}{[1 + a(t-25)]\,[1 + bP_g]} \tag{5}$$

where P_g is the piston gage pressure, M_m is the mass distributed over area A_0, A_0 is the effective piston area at 25 °C under zero load, ρ_a is the density of the ambient atmospheric air, ρ_m is the density of the weights, g_1/g_s is the ratio of local to standard gravity, γ is the surface tension of the oil in the gage, C is the circumference of the piston, a is the temperature coefficient of areal expansion of the piston, t is the temperature of the piston, and b is the pressure coefficient of areal expansion of the piston.

This equation is iterative. It is solved first without using the distortion term, $(1 + bP_g)$, then with the calculated approximate value of P_g inserted into the distortion term. The difference between the two calculated values of P_g is quite small at all pressures under consideration.

For purposes of error analysis, eq (5), is rewritten as

$$P_g = \frac{\frac{M_m}{A_0}(\rho' g') + \gamma'}{a' b'} \tag{6}$$

where

$$\rho' = 1 - \frac{\rho_a}{\rho_m},$$

$$g' = g_1/g_s,$$

$$\gamma' = \frac{\gamma C}{A_0},$$

$$a' = 1 + a(t-25), \text{ and}$$

$$b' = 1 + bP_g$$

The mass, M_m, which appears in eqs (5) and (6) is the sum of the individual brass weights loaded on the upper end of the piston, the auxiliary gram weights, supplementary brass washers, a copper cup (to hold the washers and analytical weights on the rotating piston), and the piston itself. The mass of each component was determined by comparison with accurately known standard weights on a precision balance. The maximum relative uncertainty in M_m for any combination of weights is 40 ppm.

The effective area, A_0, and its pressure coefficient, b, were obtained by comparison of our gage with a National Bureau of Standards reference piston gage of known characteristics. A_0 is known with a maximum relative uncertainty of 340 ppm and b is known to within a factor of 2.4. The quantity b', calculated from b, varies in magnitude from unity at $P = 0$ to 1.000075 at $P_g = 100$ bars. The maximum relative uncertainty in b' varies linearly from 18 ppm at 10 bars to 180 ppm at 100 bars. It is obvious that although the relative uncertainty in b is large, the corresponding relative uncertainty in b' is small.

A precision calibrated aneroid barometer is used to measure ambient atmospheric pressure, which must be added to the gage pressure to obtain the absolute (total) pressure. The uncertainty in this atmospheric pressure measurement does not exceed ±0.07 mb, or 7 ppm and 1 ppm at 10 and 100 bars, respectively.

[3] See Natrella [22] pp. 6-11, 6-12.

Table 4 indicates the small contributions of the remaining parameters to the final systematic uncertainty in pressure as determined by the piston gage. Briefly, the errors in the product $\rho' g'$ arise primarily from a 4 parts in 1000 error in air density ρ_a because relative humidity is neglected in its calculation, and from a 1 percent error in ρ_m because the total mass M_m is assumed to have the density of brass (8.4 g/cm^3), even though the cup and piston are made of other materials. It can be shown that ρ', which has a magnitude of about 0.9998, is known to 2 ppm, while g', which is based on transferring the recent measurements by Tate [24] of the acceleration of gravity at the grounds of the National Bureau of Standards to the elevation of the piston gage, is known to at least 2 ppm. Thus the product $\rho' g'$ has a relative uncertainty, computed by quadrature (i.e., the square root of the sum of the squares of the individual independent errors), of about 3 ppm.

The quantity γ' is of the order of 0.3 mb. Its major uncertainty arises from the uncertainty in the surface tension, γ, of the gage oil, which is assumed to be 10 percent. The equivalent relative uncertainty in P_g is 3 and 0.03 ppm at 10 and 100 bars respectively.

The temperature coefficient of areal expansion, a, is obtained from the temperature coefficient of linear expansion for steel and is conservatively estimated to be known with a relative uncertainty of 2 percent. The quantity a' remains in the range 1.00015 to 0.9998 with a relative uncertainty arising from a of no more than 3 ppm. The thermometer which indicates piston temperature is in contact with the piston case, insulated from the ambient air. It is estimated that the piston and thermometer temperatures could differ by as much as 0.2 deg C, thereby introducing an uncertainty in a' which may be as much as 6 ppm. The quadrature of the a' uncertainties is thus no more than 7 ppm.

The uncertainties discussed above are associated with the parameters in eqs (5) and (6). There are several additional sources of error arising from the application of oil and air head corrections, the conversion of gage pressure to absolute pressure, the manipulation of the piston gage, and the behavior of the diaphragm separator.

A correction is applied for the difference in oil level between the diaphragm and the gage. The uncertainty in the correction is about 0.13 mb. Similarly, the uncertainty in the air head correction, which accounts for the difference in level between the measurement location in the final saturator unit and the diaphragm, is 0.04 mb at $P_g = 10$ bars and 0.40 mb at $P_g = 100$ bars.

Because all these errors arise from independent parameters and are of indeterminate sign, we have chosen to use the square root of the sum of the squares as our estimate of the systematic error in the total pressure. The sources of error and the equivalent relative uncertainty in pressure are summarized in table 4.

The piston is rotated in the cylinder of the gage by a small motor through a belt (string) drive. String slippage, wobble of the piston in the cylinder, deviation of the piston from verticality, and nonuniform distribution of weights on the loading table produce random pressure oscillations and uncertainties. The diaphragm separator introduces, in addition to a systematic uncertainty of about 1 ppm due to zero shift, random uncertainties from hysteresis, sensitivity, and repeatability.

These random uncertainties may be considered part of the randomness inferred from the pressure data of various runs. During a run the pressure was repeatedly observed and from these readings an average value was calculated. For runs where the system pressure was controlled solely by the pressure reducers, there was slight monotonic drift of pressure with time, but with a random scatter of the individual readings about the smooth drift curves. For run nos. 46 through 48, where the null detector circuit was used for improved pressure control, the pressure remained constant throughout the run, but with a random scatter about the mean value. In both cases the scatter

TABLE 4. *Sources of systematic piston gage errors and corresponding relative pressure uncertainties*

Source of error	Symbol	Relative pressure uncertainty ppm		
		Gage pressure, bars		
		10	30	100
Mass of weights, etc.	M_m	40	40	40
Effective piston area	A_0	340	340	340
Pressure coefficient term	b'	18	54	180
Density-gravity term	$\rho' g'$	3	3	3
Surface tension term	γ'	3	1	0
Coefficient of expansion term	a'	7	7	7
Diaphragm separator		1	1	1
Aneroid barometer		7	2	1
Oil head correction		13	4	1
Air head correction		4	4	4
Quadrature error		343	347	387

did not exceed 210 ppm. One third of the maximum scatter, that is, 70 ppm, will be used as a measure of the precision or random error (standard deviation) of the piston gage pressure measuring process.

b. Bourdon Gages

Difficulties with the pressure measurement system were encountered after run 20, leading to the replacement of the piston gage with bourdon gages for a period spanning seven runs. The gages were compared against the calibrated medium-range piston gage over a period of several years and from the differences thus obtained between the piston gage and the bourdon gage, correction curves were constructed. A straight line was fitted to the differences for each bourdon gage. The residual standard deviation of the fit for the 2000 psi range bourdon gage was 1.8 psi (0.12 bar) and for the 3000 psi range gage was 1.5 psi (0.10 bar). Following a run, the pressures recorded from each gage were averaged. The two means were individually corrected, and the average of the corrected means was used as the mean run pressure. The individual readings on either gage seldom deviated from their respective means by any detectable amount. A precision calibrated aneroid barometer was used to measure the ambient atmospheric pressure which was added to the gage pressure to obtain the absolute (total) pressure. The uncertainty in this atmospheric pressure measurement did not exceed ± 0.07 mb which is negligible and hence ignored.

In the case of the piston gage, limits were set on errors which are systematic and ordinarily of the same (but unknown) sign and magnitude in all runs. The effect of each error on either a single point, or on a curve fitted to a group of points, is the same.

A different situation exists with bourdon gages. Here, the systematic error within a given run, that is, the deviation of the gage correction from that predicted by the calibration, can vary both in sign and magnitude from run to run. When a curve is fitted to the experimental enhancement factors as a pressure function along an isotherm, the effect of the varying sign and magnitude of the individual systematic pressure errors, on the uncertainty associated with the curve, is random.

We have used the residual standard deviations of the gages' calibration curves as measures of the systematic uncertainties within a run, and 1.6 psi (0.11 bar) as the combined systematic error of the average of the two gage readings. Thus the relative estimated systematic within run error of the average ranged from 0.37 percent at 30 bars to 0.11 percent at 100 bars. For reasons given in the previous paragraph, these are listed as random, not systematic, errors in table 6.

6.2. Saturation Temperature Errors

In the generating apparatus, a four-lead calorimetry-type (metal bulb) platinum resistance thermometer, inserted into a thermometer well, was used to measure the temperature within the saturator and a conventional (long stem glass bulb) four-lead platinum resistance thermometer, inserted into a perforated metal sheath, was used to measure the bath temperature. They were calibrated at NBS on the International Practical Temperature Scale of 1948 and subsequently checked from time to time at the triple point of water. Resistance measurements were made with a calibrated Mueller bridge, using an amplifier and d'Arsonval galvanometer for null detection. It is estimated that the uncertainty in the temperature introduced by the bridge and null detector does not exceed 1 millidegree.

The two thermometers, installed "in situ," were compared after 8 days of undisturbed exposure to quiescent bath conditions at a nominal bath temperature of 27 °C, with static atmospheric pressure air and no water in the dish saturator. The agreement in reading was better than 1 millidegree.

Under operating flow conditions a small difference in temperature invariably existed between the two locations. With the dish saturator installed in the apparatus the bath temperature, on the average, was 3 millidegrees warmer than the temperature in the saturator well; at no time did the difference between the average bath temperature and the average temperature in the saturator well exceed 4.5 millidegrees. With the bubbler saturator units installed in the apparatus the saturator temperature, on the average, was 6 millidegrees warmer than the bath temperature; at no time did this difference exceed 12 millidegrees. These differences significantly exceed the maximum uncertainty that can be ascribed solely to the thermometer and bridge or to any mismatch in reading between thermometers. They are independent of minor periodic fluctuations in bath temperature produced by the control system, (the bath and the saturator undergo similar patterns of perturbations with time, the latter lagging the former), and also independent of the random fluctuations in temperature, which are less than 1 millidegree and which will be discussed more fully below.

On several occasions it was observed that the oil in the thermometer well of the dish saturator did not completely cover the thermometer bulb. Evidence suggests that this was generally the case, except for the last two runs (Nos. 47 and 48) where precautions were taken to insure an adequate oil supply. In these runs, the average saturator temperature and the average bath temperature agreed to a fraction of a millidegree. The baths all had plastic splash plates between the bath liquid and the lids; this space, into which the thermometer extension tube led, was slightly cooler than the liquid volume below. Apparently, when the oil was below the glass bead which seals the four leads into the metal bulb, the thermometer gave a lower temperature reading than when the oil level was fully above the bead, because the column of air above the thermometer in the extension tube tended to cool the lead wires and the bulb by convection.

Another factor probably contributing to the thermometer agreement in the last two runs was the

replacement of the (0.035-in-thick wall) stainless steel well by a (0.165-in-thick wall) copper well. The conduction through this well is several times greater than that with the thinner-walled stainless steel well. By construction the dish thermometer well tends to reflect bath temperature. If the saturator interior were warmer than the bath (see below), then the increased conduction to the cooler thermometer would cause closer temperature agreement between the two thermometers.

In conjunction with the thick-walled copper well in the dish saturator, two six-junction copper-constantan thermopiles were installed, the reference junctions being sealed in holes distributed uniformly around the exterior wall of the well. This permitted measurement of temperature differences between water and well, and air and well, in circles at a radial distance of 1.2 cm from the well. Readings were taken at operating temperatures of 30 and 40 °C. The temperatures of the saturator water and the well agreed to 1 millidegree or better whereas the temperature of the test gas was higher than that of the well by as much as 3 millidegrees.

Comparable measurements on the differences between the well and test gas temperatures and the well and water temperatures in the final bubbler saturator unit were not made. The well in the bubbler saturator is completely immersed in the test gas and water in contrast to the well in the dish saturator where there is substantial direct thermal contact with the massive lid. In the dish saturator the measured temperature in the well (with adequate oil) reflects in part, if not entirely, the bath temperature. In the bubbler saturator the measured temperature may more nearly represent the actual test gas temperature, or a mean of the test gas and saturator water temperatures. If this is so then in both types of saturator the test gas is at a slightly higher temperature than the bath temperature. Let us recall that the test gas leaves the preliminary saturation system 3 to 5 deg C higher in temperature than the main bath and that it is correspondingly supersaturated with respect to the temperature of the main bath. In addition, on emerging from the preliminary bath the test gas is heated roughly 20 to 30 deg C above bath temperature (to prevent condensation). The test gas must lose considerable enthalpy and latent heat in the main bath where it asymptotically approaches bath temperature. It is understandable, therefore, that it might remain at a slightly higher temperature in the final saturator unit, even after passing through a very efficient heat exchanger coil.

The temperature of saturation was taken as the mean of the test gas temperature and the main bath temperature. With the dish saturator, the test gas temperature was obtained by adding 3 millidegrees to the measured bath temperature and with the bubbler saturator, the temperature measured in the well was assumed to be the test gas temperature.

It is estimated that the temperature of saturation may have a maximum systematic uncertainty of 7 millidegrees. With the dish saturator this arises from the maximum uncertainty inherent in the averaging of the test gas and bath temperatures (1.5 millidegrees); from the maximum uncertainty in the thermometer and bridge (1 millidegree); and from the maximum observed difference between the average well and average bath readings (4.5 millidegrees). With the bubbler saturator this arises from the maximum uncertainty due to averaging (6 millidegrees) and from the maximum uncertainty in the thermometer and bridge (1 millidegree).

During a run measurements were made at approximately 10 min intervals and from these readings means were calculated. The standard deviation of the mean for all runs, for both the bath and saturator temperature, did not exceed 0.6 millidegree. This has been used as the measure of the precision or random error of the temperature measuring process.

6.3. Saturation Vapor Pressure Errors

Recently, Wexler, and Greenspan [1] derived an equation for the saturation vapor pressure, e_s, of the pure water substance covering the temperature range 0 to 100 °C. This equation predicts values which agree with the precise experimental data of Stimson [25] to 7 ppm. Stimson's values, in turn, have an estimated standard deviation of 20 ppm or less, except at 25 °C where it is 40 ppm. It will be assumed that the equation yields values that are uncertain by no more than 60 ppm. To this uncertainty must be added the uncertainty in vapor pressure due to the estimated systematic uncertainty in temperature of 7 millidegrees and the estimated random error (standard deviation) in temperature of 0.6 millidegrees. These are shown in table 5.

TABLE 5. *Uncertainties in saturation vapor pressure*

Nominal temperature [1]	Vapor pressure [2]	Derivative	Systematic uncertainty					Random uncertainty		
			Temperature			Vapor press eq	[3]	Temperature		
°C	mb	mb/deg	deg C	mb	ppm	ppm	ppm	deg C	mb	ppm
30	42.43	2.435	0.007	0.017	400	60	404	0.0006	0.0015	35
40	73.77	3.933	.007	.028	380	60	385	.0006	.0024	32
50	123.38	6.122	.007	.043	350	60	355	.0006	.0037	30

[1] IPTS–48.
[2] Wexler and Greenspan [1].
[3] Quadrature error.

6.4. Mole Fraction Error

The mole fraction of water, X_w, is related to the mixing ratio, r, through the equation

$$X_w = \frac{\epsilon r}{1 + \epsilon r} \tag{7}$$

where ϵ is the ratio of the molecular weights of air to water. Because r is small compared to unity, and because the uncertainty in ϵ is negligible compared to that in r, the relative uncertainty in X_w is essentially the same as that in r. The mixing ratio of a moist air sample can be determined with the NBS standard reference hygrometer [19] with an estimated systematic uncertainty no greater than 460 ppm and an estimated random error (standard deviation of a single determination) no greater than 270 ppm. These same uncertainties therefore apply to X_w.

6.5. Other Considerations

In any process for generating a stream of saturated gas it is essential that the apparatus be designed to minimize the occurrence of undersaturation, supersaturation, spray, mist or aerosol. A detailed investigation was made to see whether biases from these possible sources of error are present.

a. Undersaturation

In a dynamic flow system, once saturation (or, as is the case in the preliminary saturators of our system, supersaturation) has been obtained, the necessary conditions for preventing undersaturation with respect to the desired state are that the temperature of the test gas must not fall below the desired saturation temperature and that the pressure drop, that is, expansion which decreases the water vapor concentration, must be negligible. This latter consideration necessitated use of the low pressure drop dish saturator at pressures below 30 bars.

The heating of the lines between preliminary and main baths, and between the final saturator and expansion valve, were discussed in section 2.1. In all cases these line temperatures were at or above that of the bath. Within the final saturator unit the temperature of the test gas, as discussed above, was of the order of several millidegrees higher than that of the bath. It does not appear likely that the temperature of the air at any point within the saturation system ever dropped below that of the bath.

The pressure drop across the main saturation system was measured both for the dish and for the bubbler systems. The flow rate, simulating run conditions, was 2 g per minute, at a total pressure of 3 bars. The pressure drop measurements and all enhancement factor determinations occurred under laminar flow conditions. Therefore, exclusive of the constant pressure drop through the water columns in the bubbler units, the pressure drop through the system decreases with increasing pressure.

The pressure drop through the dish saturator at the test condition was 2 mb. Thus at 10 and 30 bars, it becomes, respectively, 0.7 mb and 0.2 mb. Assuming no compensation by evaporation of water in the saturator, the maximum undersaturation would be 70 ppm at 10 bars, decreasing to 20 ppm at 30 bars.

It was shown that the total pressure drop through bubbler system was 36 mb. About 6 mb of this total occurs in the heat exchangers, while, in each of the 3 units, drops of 5 mb occur through the beads and 5 mb occurs through the nominally 5-cm water depth. The 5-mb drop through the beads decreases with increasing pressure, while the 5-mb drop through the water remains constant. The total pressure drop in each bubbler becomes 5.5 mb at 30 bars and 5.15 mb at 100 bars, indicating, in this context, the relatively unimportant role of the beads.

Compensation for the decreasing water content as the gas expands occurs both during traverse of the water column and of the damp bead layers. We will arbitrarily assign one-half the pressure drop in the water of the third bubbler unit, that is, 2.5 mb, as an upper limit to the expansion of the test gas that remains uncompensated by subsequent saturation. The ensuing undersaturation would be 80 ppm at 30 bars, decreasing to 25 ppm at 100 bars.

b. Supersaturation

The test gas temperature in the final saturator unit is, as indicated earlier, invariably slightly higher than the main bath temperature. The average of these two temperatures was used as the best value for the temperature of saturation. Because the test gas entered the saturation system with excess moisture it is possible that on leaving the final saturator unit it remained supersaturated with respect to this average temperature. The systematic uncertainty in vapor pressure from this temperature uncertainty already has been discussed in section 6.3.

c. Spray, Mist, and Aerosols

In designing the saturation system it was assumed that spray, mist or aerosols would not be generated because of the low flow rate and the absence of turbulence. Therefore, there is no separate trap or baffle in the saturation system for removal or precipitating liquid water from the test gas. Each bubbler saturator unit does have layers of small glass beads above the water surface which provide some measure of baffling, but there is no equivalent feature for the dish saturator.

Several experiments were performed in which a trap was added immediately downstream of the dish saturator. This trap was identical in design and in layers of beads to the final bubbler saturator unit. The beads were expected to remove any liquid water in the form of spray or aerosol, if such water were present. When operated dry, the trap functioned as a vapor adsorber, removing as much as 3 percent of the moisture from the test gas during 5-hour long simulated runs. When operated with the beads moist-

ened but with the trap drained of free water, there was no apparent change in vapor concentration of the test gas.

With the trap removed from the apparatus, variations in flow rate from 0.5 to 5 g per minute also appeared to produce no change in vapor concentration, as measured with a sensitive electrical hygrometer. At higher flow rates, however, there were indications of increased moisture content.

If the moisture level in the effluent of a saturation system remains constant whether the incoming gas is super- or undersaturated with respect to the saturation system temperature, and if there is no pressure drop through the system, it indicates that saturation is being achieved and maintained. An experiment was done in which the moisture content of the test gas entering the main saturation system was varied over a wide range. The main bath temperature was set at 50 °C, the total pressure at 10 bars, and the mass flow rate at 2 g per minute. The temperature of the preliminary bath, which controls the moisture content of the test gas entering the main saturation system, was raised slowly at 5 deg per hour from 25 to 58 °C with no observable change in the water vapor concentration of the test gas emerging from the final saturator.

In summary, there is no evidence of detectable liquid water carry-over in the test gas at mass flow rates below 5 g per minute. The preliminary saturators may be operated over a wide span of temperatures without affecting the efficiency of the main saturation system. However, the preliminary saturators are normally operated at temperatures several degrees higher than that of the main bath.

6.6. Estimated Overall Accuracy

In the preceding error analysis we have examined all suspected sources of error in the measurement process. Table 6 summarizes the estimated limits to the contributing systematic errors. The estimated limit to the total systematic error has been computed by adding the contributing errors in quadrature (square root of the sum of the squares) for measurements made with (a) the piston gage and dish saturator, (b) the piston gage and bubbler saturators, and (c) the bourdon gages and bubbler saturators. The estimated total systematic error is 0.07 percent and is essentially independent of temperature, pressure, type of saturator, and type of pressure gage.

The expected precision or random uncertainty of the measurement process may be estimated either from this error analysis or from a statistical analysis of the experimental results. Both methods have been followed. Table 6 summarizes the estimated one-standard deviation magnitudes from the contributing sources. The combined (quadrature) one-standard deviation is of the order of 0.03 percent for measurements made with the piston gage; it decreases from 0.37 percent at 30 bars to 0.11 percent at 100 bars for measurements made with bourdon gages. Obviously the use of bourdon gages introduces a higher limit to the random errors. Fortunately only seven runs were made in which bourdon gages were used.

Table 2 lists the residual standard deviations of the fit for each isotherm. This statistic is used as the alternate indicator of the precision of the measurement process. The residual standard deviation is 0.02, 0.13, and 0.26 percent for the 30, 40, and 50 °C isotherms, respectively. The residual standard deviation of the 30 °C isotherm (0.02%), which is based on measurements made exclusively with the piston gage, is comparable to the calculated standard deviation (0.03%) based on the error analysis for measurements made with the piston gage. The residual standard deviations of the 40 and 50 °C isotherms are comparable to the calculated standard deviation based on the error analysis for measurements made with the bourdon gages. For the 40 °C isotherm, out of a total of 5 runs, 3 runs were made using bourdon gages; for the 50 °C isotherm out of a total of 17 runs, 4 runs were made using bourdon gages. Although there does not appear to be any statistically significant correlation between the magnitudes of the individual residuals and the type of pressure gage used for the 40 and 50 °C isotherms, it is suspected that the larger residual standard devia-

TABLE 6. *Summary of estimated errors in the enhancement factor*

Source of error	Systematic error, ppm			Random error, ppm		
	Pressure, bars			Pressure, bars		
	10	30	100	10	30	100
Residual solids in water	110	110	110			
Pressure, piston gage	343	347	387	70	70	70
Pressure, bourdon gages					3700	1110
Vapor pressure	404	404	404	35	35	35
Mole fraction	460	460	460	270	270	270
Undersaturation, dish saturator	70	20				
Undersaturation, bubbler saturator		80	25			
Quadrature error for:						
(a) Piston gage and dish saturator	714	713		281	281	
(b) Piston gage and bubbler saturators		717	733		281	281
(c) Bourdon gage and bubbler saturators		627	619		3710	1140

487-412 OL - 73 - 9

tions for these two isotherms is due in part to the use of data obtained with the bourdon gages.

It will be assumed that the total systematic error in the measurement process derived by the error analysis (0.07%) is equally valid for the enhancement factor calculated (predicted) from eq (4). Estimates of the standard deviation of the predicted values are given in table 2. These latter estimates, which are pressure dependent, serve as our best estimates of the random uncertainty in the predicted values. In brief, the calculated (predicted) enhancement factor has an overall accuracy, for temperatures from 30 to 50 °C and pressures from 10 to 100 bars, comprised of an estimated limit of systematic bias of ± 0.07 percent and a maximum observed standard deviation of a predicted value of ± 0.2 percent.

7. Comparison With Other Work

Our results at 50 °C can be compared directly with the data of Politzer and Strebel [11], but there are no known measurements with which to compare our 40 and 30 °C data. Enhancement factors have been reported by Politzer and Strebel for 70 °C and by Webster [12] for 15, 0, −20 and −35 °C. The Goff, Anderson, and Gratch [14] measurements were made at 5, 15, 20, and 25 °C at or near atmospheric pressure using the double saturation isotherm method and yielded the "interaction constant," a quantity related to the cross virial coefficient, rather than the enhancement factor.

The slopes and intercepts of eq (4), i.e., coefficients a and b, are convenient although indirect parameters for comparing our results with these other determinations, even in the absence of measurements at the same temperatures and pressures. Therefore, the data of Politzer and Strebel and of Webster were fitted by the method of least squares to eq (4). The coefficients a and b for each isotherm are given in table 3. Goff [14] presented an equation which relates $\ln f$ to P and which, by simple algebraic manipulation, has been transformed into the form of eq (4). The corresponding coefficients a and b, simply related to parameters called α and β in the Goff equation, are given in table 3.

There is too little information on the sources of error on which to base an estimate of the systematic uncertainty in the results of Politzer and Strebel and of Webster. However, the standard deviations of the coefficients a and b, which are readily calculable,[4] can be used as an index of the precision of the basic data. These standard deviations of a and b for the 50 and 70 °C isotherms of Politzer and Strebel, for the 0 and 15 °C isotherms of Webster, and for our 30, 40, and 50°C isotherms are shown in table 3. Although similar standard deviations for the Goff, Anderson, and Gratch basic measurements cannot be computed, their reported tolerances (apparently twice the probable error) on the parameters α and β were converted to standard deviations; the standard deviation of β so

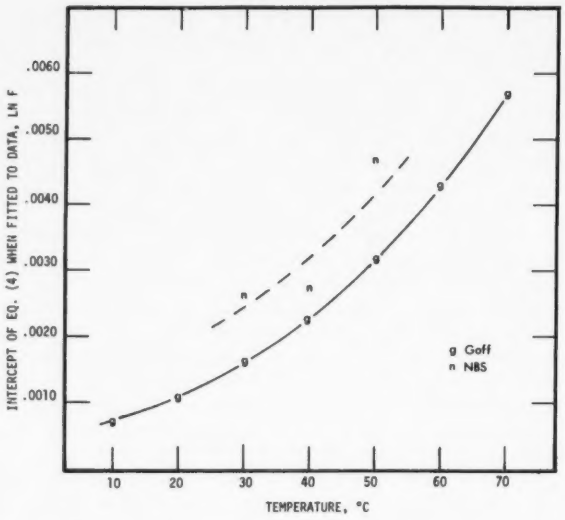

FIGURE 5a. *Comparison of the intercepts obtained by fitting the relation* $\ln f = a + b P$ *to various data.*

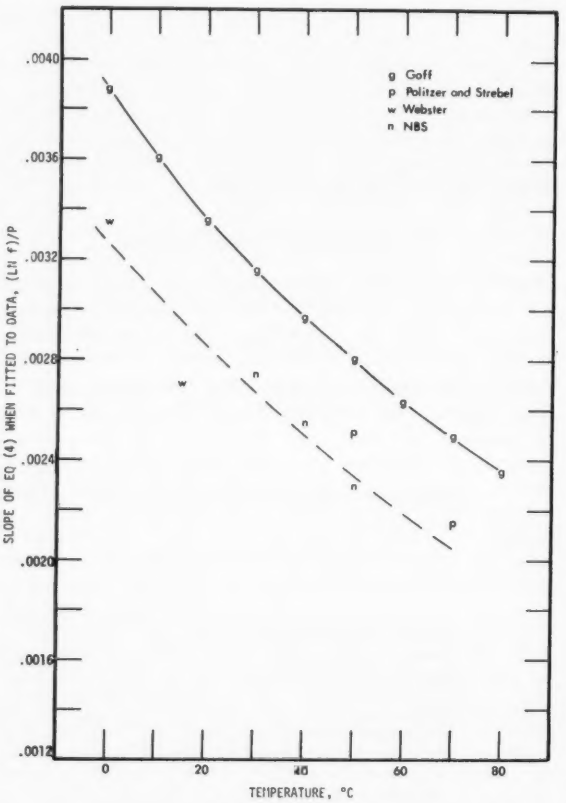

FIGURE 5b. *Comparison of the slopes obtained by fitting the relation* $\ln f = a + b P$ *to various data.*

[4] Method of calculation is given by Natrella [22] p. 6–12.

obtained is used as an estimator of the standard deviation of the b's given for Goff in table 3. The standard deviations of their α and β were combined by quadratures and used as estimators of the standard deviations of the a's given for Goff, also in table 3.

A comparison of the intercepts a, from 30 to 50 °C, and of the slopes b, for 0 to 70 °C are shown in figure 5a and 5b respectively. The intercepts from fits to the data of Webster and Politzer and Strebel lie completely out of the range of the plot. The NBS intercepts are systematically displaced from Goff's by about 30 percent. (All representations of Goff's values are based on his smoothing equations, and do not reflect the precision of his raw data.)

The slopes from Goff's formulation are displaced systematically from ours by about 15 percent. The slopes based on the Politzer and Strebel data and on the Webster data appear to be consistent with our extrapolated b curve. Too much significance should not be ascribed to this comparison in view of the large imprecision in the previously published data and the absence of any estimates of systematic uncertainty.

7. References

[1] Wexler, A., and Greenspan, L., Vapor pressure equation for water in the range 0 to 100 °C, J. Res. Nat. Bur. Stand. (U.S.), **75A**, (Phys. and Chem.), No. 3, 213–230 (May–June 1971).

[2] Goff, J. A., Standardization of thermodynamic properties of moist air, Heating, Piping, and Air Cond. **21**, 118 (1949).

[3] Olds, R. H., Sage, B. H., and Lacey, W. N., Phase equilibria in hydrocarbon systems: Composition of the dewpoint gas of the methane-water system, Ind. Eng. Chem. **34**, 1223 (1942).

[4] Reamer, H. H., Olds, R. H., Sage, B. H., and Lacey, W. N., Phase equilibrium in hydrocarbon systems: Composition of the dewpoint gas in the ethane-water system, Ind. Eng. Chem. **35**, 790 (1943).

[5] Bacarella, A. L., Finch, A., and Grunwald, E., Vapor pressures and activities in the system dioxane-water, J. Phys. Chem. **60**, 573 (1956).

[6] Harrison, L. P., Imperfect gas relationships, Humidity and Moisture, Vol. **III**, A. Wexler and W. A. Wildhack, Eds. (Reinhold Publishing Corp., New York, 1965), p. 105.

[7] Wexler, A., Calibration of humidity measuring instruments at the National Bureau of Standard, ISA Transactions **7**, 356 (1968).

[8] Hasegawa, S., Hyland, R. W., and Rhodes, S., a comparison between the NBS two-pressure humidity generator and the NBS standard hygrometer. A. Wexler and W. A. Wildhack, Eds., Humidity and Moisture, Vol. **III**, (Reinhold Publishing Corp., New York, 1965), p. 455.

[9] List, Robert J., Smithsonian Meteorological Tables, Sixth Revised Edition, Smithsonian Institution, Washington, 1951.

[10] Goff, J. A., and Gratch, S., Thermodynamic properties of moist air, Heating, Piping and Air Cond. (ASHVE Journal Sect.) **17**, 334 (1945).

[11] Pollitzer, F., and Strebel, E., Über der Einfluss indifferenter Gas auf die Sättigungsdampfkonzentration von Flussigkeiten, Zeit. fur Phys. Chemie **110**, 768 (1924).

[12] Webster, T. J., The effect on water vapor pressure of superimposed air pressure, J. S. C. I. **69**, 343 (1950).

[13] Goff, J. A., and Bates, A. C., The interaction constant for moist air, Trans. ASHVE **47**, 373 (1941).

[14] Goff, J. A., Andersen, J. R., and Gratch, S., Final values of the interaction coefficient of moist air, Trans. ASHVE **49**, 269 (1943).

[15] Goff, J. A., and Gratch, S., Low pressure properties of water from − 160 to 212 F, Trans. ASHVE **52**, 95 (1946).

[16] Bartlett, E. P., The concentration of water vapor in compressed hydrogen, nitrogen and a mixture of these gases in the presence of condensed water, J. Am. Chem. Soc. **49**, 65 (1927).

[17] Saddington, A. W., and Krase, N. N., Vapor liquid equilibria in the system nitrogen-water, J. Am. Chem. Soc. **56**, 353 (1934).

[18] Rigby, M., and Prausnitz, J. M., Solubility of water in compressed nitrogen, argon, and methane, J. Phys. Chem. **72**, 330 (1968).

[19] Wexler, A., and Hyland, R. W., The NBS standard hygrometer (NBS monograph 73, May 1, 1964); also see A. Wexler and W. A. Wildhack, Eds., Humidity and Moisture, Vol. **III** (Reinhold Publishing Corp., New York, 1964), p. 389.

[20] Harrison, L. P., Fundamental concepts and definitions, A. Wexler and W. A. Wildhack, Eds., Humidity and Moisture, Vol. **III** (Reinhold Publishing Corp., New York, 1964), p. 8.

[21] Hilsenrath, J., Ziegler, G. G., Messina, C. G., Walsh, P. J., and Herbold, R. J., OMNITAB—A Computer Program for Statistical and Numerical Analysis, Nat. Bur. Stand. (U.S.), Handb. 101 (1966).

[22] Natrella, M. G., Experimental Statistics, Nat. Bur. Stand. (U.S.), Handb. 91 (1963),

[23] Cross, J. L., Reduction of piston gage measurements, Nat. Bur. Stand. (U.S.), Monog. 65, (1963).

[24] Tate, D. R., Acceleration due to gravity at the National Bureau of Standards, J. Res. Nat. Bur. Stand. (U.S.), **72C** (Engr. and Instr.) No. 1, 1–20 (Jan.–Mar. 1968).

[25] Stimson, H. F., Some precise measurements of the vapor pressure of water in the range from 25 to 100 °C. J. Res. Nat. Bur. Stand. (U.S.), **73A** (Phys. and Chem.), No. 5, 493–496 (Sept.–Oct. 1969).

(Paper 77A1–757)

JOURNAL OF RESEARCH of the National Bureau of Standards—A. Physics and Chemistry
Vol. 77A, No. 1, January–February 1973

The Second Interaction (Cross) Virial Coefficient for Moist Air

Richard W. Hyland and Arnold Wexler

Institute for Basic Standards, National Bureau of Standards, Washington, D.C. 20234

(October 16, 1972)

The results of calculations of the second interaction (cross) virial coefficient B_{aw} for water vapor and air, based on enhancement data obtained at NBS at 30, 40, and 50 °C, are presented. Comparisons are made with the results of calculations based on the enhancement data of Politzer and Strebel, Webster, and Goff et al. and with the results of the theoretical calculations of Mason and Monchick and of Chaddock. An empirical equation is given for interpolation and extrapolation.

The random (one standard deviation) uncertainty in the mean values of B_{aw}, arising from the scatter of previously obtained NBS values of the enhancement factor, is estimated to range from 0.7 percent at 30 °C to 1.4 percent of 50 °C. The estimated systematic uncertainties range from 4 percent at 30 °C to 6 percent at 50 °C, respectively.

Key words: Interaction virial coefficients; moist air; second virial coefficient; virial coefficients; water vapor.

1. Introduction

The water vapor content of real gases, and of air in particular, saturated under known conditions of pressure and temperature, is not predicted adequately by ideal gas laws [1].[1] In air, the deviations from ideality must be accounted for in order to obtain accuracies better than 0.5 percent at pressures as low as 900 millibars [2]. On any isotherm, the saturated water vapor content increases with pressure to some, as yet, undetermined limit, in a manner consistent with that described by Haar and Sengers [3]. For example, at 0 °C and 200 bars, the water vapor concentration or density in air is about twice that of the pure phase.

This increase in water vapor content with pressure is the algebraic sum of the increases in apparent vapor pressure because of the superimposed pressure of air (the Poynting effect), and the Van der Waals type interactions between different molecular species, and the decrease in apparent vapor pressure due to the solution of the air in the liquid water (the Henry's law effect). Of the three the largest is due to the nonideality of the gas phase (the Van der Waals type interactions).

Given a real gas equation of state of a water vapor-air mixture, say an equation expressed in virial form, it is possible to derive theoretically an expression for the saturation water vapor content of the gas mixture as a function of the mole fraction of the constituents, the parameters of state, and the virial coefficients. In such a formulation, the air-water interactions are in large part characterized by the second cross virial interaction term for the air and water molecules. Unfortunately there are no definitive values for the second cross interaction virial coefficients, although previously obtained values [2] may be sufficient for some applications.

Attempts have been made to derive second cross interaction virial coefficients from statistical mechanics [4, 5]. However, the assumptions (form of potential) on which these derivations are based are far from exact so that the predicted coefficients are of limited value. What are needed are good experimental values of the second (cross) interaction coefficients. Recently, Hyland and Wexler [6] at NBS have reported precise experimental values of enhancement factors for water vapor in CO_2-free (CO_2 content on the order of 2 ppm) air at temperatures of 30, 40, and 50 °C. It is the purpose of this paper to use these new data, as well as the limited older data in the literature, in order to compute values of the second interaction virial coefficient. The formal derivations and basic experiments strictly apply to CO_2-free air. This limitation is unimportant when using the B_{aw} values in real air situations, as any errors introduced by the roughly 300 ppm of CO_2 molecules should be well within the limits caused by the uncertainties in B_{aw}.

2. Theory

2.1. General Considerations

We will derive an equation which relates the interaction virial coefficient to the enhancement factor,

[1] Figures in brackets indicate the literature references at the end of this paper.

thermodynamic parameters of state, and several physical constants.[2]

Initially, it should be stated that the treatment of air as a single-component gas leads to no theoretical inconsistencies, for the following reasons: (1) Over the experimental range of temperatures, we can ignore chemical reactions. (2) The experiments involved a continuous air flow over the liquid surface, so that the molar ratios of the air components are constant, for all experimental conditions of pressure and temperature, once equilibrium has been established. (3) We deal with only the chemical potential of the water in each phase, and since the required chemical potential difference in the liquid phase depends only on the mole fraction of water (see eq (19)) and not on the amount of dissolved species, it doesn't matter that the gas mixture dissolved in the water is of different composition than that of the gas-phase air. (This difference arises because the degree of absorption in water varies from one air component to the next.) Thus, in this paper, it will be assumed that air acts as a single component substance with a known molecular weight.

Let air be in thermodynamic equilibrium with a surface of the condensed water substance. The chemical potential μ_i of each component in the gas phase is equal to that in the condensed phase. For our purposes we need only examine the chemical potential of the water, thus

$$\mu_w^g(T,P,n_w^g,n_a^g) = \mu_w^c(T,P,n_w^c,n_a^c) \tag{1}$$

where superscripts g and c designate the gaseous and condensed phases, T is the thermodynamic temperature, P the total system pressure, n_w^k (where $k=g$ or c) is the number of moles of water, and n_a^k is the number of moles of air. Water is a vapor in the gas phase, and either liquid or solid (ice) in the condensed phase.

In the equations which follow, the independent variables are always P, T, and n_i^k, whether stated explicitly or not. It will be understood that the variables which do not explicitly appear are being held constant, so that subscripts are unnecessary for that purpose.

Consider the difference in chemical potential in each phase between pressure states P_1 and P_2. We may write

$$\mu_w^g(P_2) - \mu_w^g(P_1) = \mu_w^c(P_2) - \mu_w^c(P_1). \tag{2}$$

We now write

$$\mu_w^k = \frac{\partial G^k}{\partial n_w^k} \tag{3}$$

(see e.g., [7]) where G^k is the total Gibbs free energy of either the gas or condensed phase.

To obtain G^k we use the thermodynamic relationship

$$V^k = \frac{\partial G^k}{\partial P} \tag{4}$$

where V^k is the total volume of the phase. The Gibbs free energy difference between states P_1 and P_2, obtained by integrating eq (4), is

$$G^k(P_2) - G^k(P_1) = \int_{P_1}^{P_2} V^k dP. \tag{5}$$

Differentiating with respect to n_w^k it follows that

$$\mu_w^k(P_2) - \mu_w^k(P_1) = \frac{\partial}{\partial n_w^k}\left[G^k(P_2) - G^k(P_1)\right]$$

$$= \left[\frac{\partial}{\partial n_w^k}\left(\int_{P^1}^{P_2} V^k dP\right)\right]. \tag{6}$$

Substituting eq (6) into (2) yields

$$\left[\frac{\partial}{\partial n_w^g}\left(\int_{P_1}^{P_2} V^g dP\right)\right] = \left[\frac{\partial}{\partial n_w^c}\int_{P_1}^{P_2} V^c dP\right]. \tag{7}$$

2.2. Gas Phase

The equation of state of a gas may be expressed in virial form as a power series in reciprocal molar volume

$$\frac{Pv}{RT} = 1 + \frac{B}{v} + \frac{C}{v^2} + \ldots \tag{8a}$$

or as a power series in pressure

$$\frac{Pv}{RT} = 1 + B'P + C'P^2 + \ldots \tag{8b}$$

where P is the total pressure, T is the absolute thermodynamic temperature, v is the molar volume, R is the gas constant, B and B' are second virial coefficients, and C and C' are third virial coefficients. In the enhancement measurements considered in this paper, volume is not one of the experimental parameters. For this reason eq (8b) is used in our derivation.

The virial coefficients of the pressure series are related to those of the volume series by

$$B' = \frac{B}{RT} \tag{8c}$$

and

$$C' = \frac{C - B^2}{(RT)^2}. \tag{8d}$$

The virial coefficients are functions only of temperature; those of eq (8a) are derivable from statistical mechanical relationships [8] if the form of the intermolecular potential is known. (A very large "if", indeed! See, for example, Hanley and Klein [9]). The second virial coefficients may be considered to express the effects of interactions between two molecules, the third virial coefficients may be considered to express

[2] The theoretical basis for our work, which is reviewed below, is discussed in most good thermodynamics texts. It has been used in various derivations similar to ours, for example, by Haar and Sengers [3], and Goff and Bates [37].

the effects of interactions among three molecules, and so forth. The number of terms or coefficients necessary to adequately represent Pv/RT will depend on the gas (or gases) involved and the PvT state.

If the gas under consideration is a mixture, then the coefficients B, C, B', C', etc., become mixture virial coefficients B_{mix}, C_{mix}, etc., and can be written in terms of the mole fractions of the pure components, the virial coefficients of the pure components, and quantities called interaction (cross) virial coefficients. For a two-component gas mixture, and in particular for water vapor-air mixtures, statistical mechanics shows that [8]

$$B_{\text{mix}} = x_a^2 B_{aa} + 2x_a x_w B_{aw} + x_w^2 B_{ww} \tag{9a}$$

$$C_{\text{mix}} = x_a^3 C_{aaa} + 3x_a x_w^2 C_{aww} + 3x_a^2 x_w C_{aaw} + x_w^3 C_{www} \tag{9b}$$

where x_a and x_w are the mole fractions of air and water vapor, B_{aa} and B_{ww} are the second virial coefficients for pure air and pure water vapor, and C_{aaa} and C_{www} are the third virial coefficients for pure air and pure water vapor. B_{aw} is the second interaction virial coefficient expressing the effects of interaction between an air molecule and a water molecule. C_{aaw} is the third interaction virial coefficient expressing the effects of interaction between two air molecules and one water molecule whereas C_{aww} is the third interaction virial coefficient expressing the effects of interaction between two water molecules and one air molecule.

The mole fractions of air and water vapor are given by

$$x_a = \frac{n_a}{n_a + n_w} \tag{10a}$$

and

$$x_w = \frac{n_w}{n_a + n_w} . \tag{10b}$$

The molar volume v_{mix} is related to the total volume V_{mix} by

$$V_{\text{mix}} = (n_a + n_w) v_{\text{mix}} \tag{10c}$$

where n_a and n_w are the number of moles of air and water vapor, respectively, in the total volume V_{mix}.

Substituting eqs (10), (9), (8c), and (8d) into (8b) we obtain

$$\begin{aligned} V_{\text{mix}} = (n_a + n_w)\frac{RT}{P} &+ \left[\frac{n_a^2}{n_a + n_w} B_{aa} + \frac{2n_a n_w}{n_a + n_w} B_{aw} + \frac{n_w^2}{n_a + n_w} B_{ww}\right] \\ &+ \left[\frac{n_a^3}{(n_a + n_w)^2} C_{aaa} + \frac{3n_a n_w^2}{(n_a + n_w)^2} C_{aww} + \frac{3n_a^2 n_w}{(n_a + n_w)^2} C_{aaw} + \frac{n_w^3}{(n_a + n_w)^2} C_{www}\right] \\ &- \frac{n_a^4}{(n_a + n_w)^3} B_{aa}^2 - \frac{n_w^4}{(n_a + n_w)^3} B_{ww}^2 \\ &- \frac{4n_a^3 n_w}{(n_a + n_w)^3} B_{aa} B_{aw} - \frac{4n_a n_w^3}{(n_a + n_w)^3} B_{ww} B_{aw} \\ &- \frac{4n_a^2 n_w^2}{(n_a + n_w)^3} B_{aw}^2 - \frac{2n_a^2 n_w^2}{(n_a + n_w)^3} B_{aa} B_{ww}\Bigg]\frac{P}{RT} \\ &+ \ldots . \end{aligned} \tag{11}$$

Now $V_{\text{mix}} = V^g$; therefore eq (11) may be substituted into the left-hand side of eq (7). We let P_1 be the pure phase saturation vapor pressure $e_s(T)$ of the water substance and P_2 be any other greater total pressure P. When the total pressure P reduces to e_s, then $x_a = 0$ and $x_w = 1$. For the sake of simplicity, the superscript g will be deleted. After performing the integration and then the differentiation the left-hand side of eq (7) becomes

$$\begin{aligned} \left[\frac{\partial}{\partial n_w}\int_{e_s}^{P} V_{\text{mix}} dP\right] &= RT \ln \frac{x_w P}{e_s} - x_a^2 B_{aa} P + 2B_{aw} x_a^2 P \\ &+ (P - e_s - x_a^2 P) B_{ww} - (C_{www} - B_{ww}^2)\frac{e_s^2}{2RT} \\ &+ \left[C_{www}\frac{(1 + 2x_a)(1 - x_a)^2}{2} - C_{aaa} x_a^3 + 3C_{aww} x_a^2 (1 - x_a) \right. \\ &- C_{aaw}\frac{3x_a^2(1 - 2x_a)}{2} - B_{ww}^2 \frac{(1 + 3x_a)(1 - x_a)^3}{2} \\ &\left. - B_{aa} B_{ww} x_a^2 (1 - 3x_a)(1 - x_a) + B_{aa}^2 \frac{3x_a^4}{2}\right]\frac{P^2}{RT} \\ &+ \left[B_{aa}\frac{2x_a^3(2 - 3x_a)P^2}{RT} + B_{ww}\frac{6x_a^2(1 - x_a)^2 P^2}{RT}\right] B_{aw} \\ &+ B_{aw}^2 \frac{2x_a^2(1 - x_a)(1 - 3x_a)P^2}{RT} . \end{aligned} \tag{12}$$

The ratio $\frac{x_w P}{e_s}$ which appears in eq (12) will be called the "enhancement factor" and be designated by the symbol f. It has been variously called "the coefficient f," "the function f," and "the correction factor f" [2, 10, 11]. It is closely related to the "vapor concentration enhancement" of Haar and Sengers [3]. Thus

$$f = \frac{x_w P}{e_s} . \tag{13}$$

The quantity $x_w P$ may be thought of as an "effective" vapor pressure of the water substance in a real gas

mixture analogous to a partial pressure in an ideal gas mixture. As P approaches e_s, x_w approaches unity, and at $P=e_s$ and $x_w=1$, the enhancement factor f becomes unity.

2.3. Condensed Phase

We will confine our consideration of the condensed phase to the liquid state. Consider the right-hand side of eq (7) which expresses the difference in chemical potential for the water substance in the condensed phase between two pressure states P_1 and P_2. As before, we let P_1 be the pure phase saturation vapor pressure $e_s(T)$ of the water substance and P_2 be any other greater pressure P. Performing the differentiation yields

$$\mu_w^c(T, P, n_w^c, n_a^c) - \mu_w^c(T, e_s, n_w^c, 0) = \frac{\partial}{\partial n_w^c}\int_{e_s}^{P} V^c \, dP \tag{14}$$

where V^c is the total volume of the condensed phase (i.e., liquid water containing dissolved air), and where we have emphasized that at $P_1=e_s$, $n_a^c=0$. Thus

$$\mu_w^c(e_s) = \mu_w^1(e_s) \tag{15}$$

where $\mu_w^1(e_s)$ is the chemical potential of the pure phase liquid water substance at pressure e_s.

Consider now the pure phase (single component) liquid water substance at the same pressure states P and e_s. The difference in chemical potential is

$$\mu_w^1(P) - \mu_w^1(e_s) = \int_{e_s}^{P} v_w^1 \, dP \tag{16}$$

where v_w^1 is the molar volume of pure phase liquid water.

Combining eqs (14), (15), and (16) yields

$$\mu_w^c(P) - \mu_w^1(P) = \frac{\partial}{\partial n_w^c}\int_{e_s}^{P} V^c \, dP - \int_{e_s}^{P} v_w^1 \, dP \tag{17a}$$

or

$$\frac{\partial}{\partial n_w^c}\int_{e_s}^{P} V^c \, dP = \int_{e_s}^{P} v_w^1 \, dP + \mu_w^c(P) - \mu_w^1(P). \tag{17b}$$

The laws of dilute solutions [7] predict that for a solution of dissolved air in water the chemical potential of the solvent, in this case liquid water, at pressure P differs from that of the pure phase of the same substance under the same pressure by an amount given by

$$\mu_w^c(P) - \mu_w^1(P) = RT \ln x_w^c + C \tag{18}$$

where x_w^c is the mole fraction of water in the solution, and C is a corrective term expressing the excess chemical potential of a real solution over that predicted by the laws of ideal dilute solutions.

Substituting eqs (18) and (17b) into (14) one obtains

$$\mu_w^c(P) - \mu_w^c(e_s) = \int_{e_s}^{P} v_w^1 dP + RT \ln x_w^c + C. \tag{19}$$

Because $x_w^c + x_a^c = 1$ we may write

$$\ln x_w^c = \ln (1 - x_a^c). \tag{20}$$

For very dilute solutions [3] Henry's law may be used to calculate x_a^c, i.e.,

$$x_a^c = k(T, P) x_a^g P \tag{21}$$

where $k(T, P)$ is the Henry's law "constant" which is a function of T and P, and x_a^g is the mole fraction of air in the gas phase.

The term C in eq (19) is given by [7]

$$C = W(x_a^c)^2 \tag{22}$$

where W is a function of the interaction energies of the molecular species in the solution. The term C can be shown [see appendix 1] to be negligible in its contribution to B_{aw} and so is dropped from further consideration.

Equation (19) therefore becomes

$$\mu_w^c(P) - \mu_w^c(e_s) = \int_{e_s}^{P} v_w^1 dP + RT \ln (1 - k x_a^g P). \tag{23}$$

Kell and Whalley [12] have shown that the specific volume of the pure liquid phase of the water substance can be represented with high accuracy by the following equation of state:

$$\frac{\bar{V}(t, P)}{\bar{V}(t, 1 \text{ atm})} = 1 + \sum_{i=0}^{5}\sum_{j=1}^{3} \alpha_{ij} t^i (P - P_A)^j \tag{24}$$

where $\bar{V}(t, P)$ is the specific volume at temperature t (Celiuis) and pressure P, $\bar{V}(t, 1 \text{ atm})$ is the specific volume at temperature t and standard atmospheric pressure (1 atm), and P_A is standard atmospheric pressure. Kell [13] has shown also that

$$\bar{V}(t, 1 \text{ atm}) = \frac{1 + bt}{\sum_{n=0}^{5} a_n t^n}. \tag{25}$$

[3] At pressures up to at least 200 bars and at temperatures from 0 to 100 °C, the mole fraction of water in an equilibrium solution of dissolved air in water is very near unity. At 0° and 200 bars, $x_w^c = 0.997$.

It therefore follows that

$$v_w^1 = M_w \bar{V}(t, P) =$$

$$M_w \left[1 + \sum_{i=0}^{5} \sum_{j=1}^{3} \alpha_{ij} t^i (P - P_A)^j\right] \times \left[\frac{1 + bt}{\sum_{n=0}^{5} a_n t^n}\right]. \quad (26)$$

Let

$$\int_{e_s}^{P} v_w^1 dP = g(T, P). \quad (27)$$

Inserting eq (27) into (23) we obtain

$$\left[\frac{\partial}{\partial n_w^c} \int_{e_s}^{P} V^c dP\right]_{T, n_a^c} = \mu_w^c(P) - \mu_w^c(e_s) =$$

$$g(T, P) + RT \ln (1 - k x_a^g P) \quad (28)$$

2.4. Second Interaction Virial Coefficient

By equating eq (12) and (28) and rearranging terms we obtain

$$RT \ln f = g(T, P) + RT \ln (1 - k x_a P) + B_{aa} x_a^2 P - B_{ww}(P - e_s - x_a^2 P) + C_{aaa} \frac{x_a^3 P^2}{RT} + C_{aaw} \frac{3x_a^2 (1 - 2x_a) P^2}{2RT} - C_{aww} \frac{3x_a^2 (1 - x_a) P^2}{RT} - B_{aa}^2 \frac{3x_a^4 P^2}{2RT} - C_{www} \frac{(1 + 2x_a)(1 - x_a)^2 P^2 - e_s^2}{2RT} - B_{aa} B_{ww} \frac{x_a^2 (1 - 3x_a)(1 - x_a) P^2}{RT} - B_{ww}^2 \frac{e_s^2 - (1 + 3x_a)(1 - x_a)^3 P^2}{2RT} + B_{aw}\left[-2x_a^2 P - B_{aa} \frac{2x_a^3 (2 - 3x_a) P^2}{RT} + B_{ww} \frac{6x_a^2 (1 - x_a)^2 P^2}{RT}\right] - B_{aw}^2 \frac{2x_a^2 (1 - x_a)(1 - 3x_a) P^2}{RT}. \quad (29a)$$

For the sake of simplicity in nomenclature, all superscripts have been omitted, it being understood, however, that mole fractions x_a and x_w refer only to the gas phase. Let

$$\alpha = g(T, P) + RT \ln (1 - k x_a P) + B_{aa} x_a^2 P - B_{ww}(P - e_s - x_a^2 P) \quad (29b)$$

$$\beta = C_{aaa} \frac{x_a^3 P^2}{RT} + C_{aaw} \frac{3x_a^2 (1 - 2x_a) P^2}{2RT} - C_{aww} \frac{3x_a^2 (1 - x_a) P^2}{RT} - B_{aa}^2 \frac{3x_a^4 P^2}{2RT} - C_{www} \frac{(1 + 2x_a)(1 - x_a)^2 P^2 - e_s^2}{2RT} - B_{aa} B_{ww} \frac{x_a^2 (1 - 3x_a)(1 - x_a) P^2}{RT} - B_{ww}^2 \frac{e_s^2 - (1 + 3x_a)(1 - x_a)^3 P^2}{2RT} \quad (29c)$$

$$\gamma = \alpha + \beta \quad (29d)$$

$$D = -2x_a^2 P \quad (29e)$$

$$\delta = B_{aa} \frac{2x_a^3 (2 - 3x_a) P^2}{RT} - B_{ww} \frac{6x_a^2 (1 - x_a)^2 P^2}{RT} \quad (29f)$$

$$\phi = D - \delta \quad (29g)$$

$$\epsilon = \frac{-2x_a^2 (1 - x_a)(1 - 3x_a) P^2}{RT} \quad (29h)$$

then

$$RT \ln f = \gamma + \phi B_{aw} + \epsilon B_{aw}^2 \quad (29i)$$

so that

$$B_{aw} = -\frac{\phi}{2\epsilon} - \frac{1}{2}\left[\left(\frac{\phi}{\epsilon}\right)^2 - \frac{4}{\epsilon}(\gamma - RT \ln f)\right]^{1/2} \quad (30)$$

The quadratic term appearing in eq (29i) introduces a small correction into the calculated value of B_{aw}. Therefore the value of B_{aw} obtained from eq (29i) without that term must be nearly the same as that calculated from eq (30). It may be shown that this condition is satisfied only if the minus sign is used in front of the radical in eq (30).

3. Sources of Data

3.1. Virial Coefficients

There are several sources of data for the second and third virial coefficients of air [14, 15, 16]. Probably the best and most up to date values of B_{aa} are those of Sengers et al. [16] which cover the temperature range from 100 to 1400 K. Sengers et al. assign a standard deviation of 0.4 cm³/mol to B_{aa}. We have chosen three sigmas as our best estimate of the maximum systematic error, i.e., 1.2 cm³/mol. The Hilsenrath et al. [14] values of C_{aaa} are used here. These range from 90 to 1500 K. We have compared these values with those of Hall and Ibele [15] over temperatures from 0 to 100 °C, our range of interest. The two sets disagree

by about 10 percent. This disparity was arbitrarily increased to 15 percent and assigned as the estimated systematic uncertainty in C_{aaa}.

The values given by Goff [2] are used for the second and third virial coefficients of water vapor. Wexler and Greenspan [17] recently have shown that from 0 to 100 °C the Goff values lead to highly precise correlations of theoretical and experimental values of saturation vapor pressure. Other second and third virial coefficients for water vapor are available but only those of Keyes [18] are both experimentally based and cover our experimental range of interest. Goff assigned tolerances to his values, which he stated were equal to twice his estimated probable error. These were converted to one-sigma errors, and compared to the differences between corresponding values of Keyes and Goff. For B_{ww}, the agreement between Keyes and Goff, below 70 °C, is better than 2 percent, while the Goff one-sigma uncertainties range from 8 to 2 percent between 30 and 60 °C. It was felt that the more conservative Goff uncertainties were appropriate here, and as estimates of the maximum systematic uncertainties in B_{ww} we used three-sigma errors. In the case of C_{www} below 70 °C, the Keyes and Goff values agree to about 45 percent, whereas the one-sigma errors computed from Goff range from 200 percent at 30 °C to 52 percent at 70 °C. These are felt to be overly conservative. Thus the difference between the Keyes and Goff values was taken as an estimate of the systematic uncertainty in C_{www}.

Mason and Monchick [5] and Hyland and Mason [19] give the only known values of C_{aaw} and C_{aww}, respectively.[4] These are theoretical calculations based on the Lennard-Jones (12–6) potential, the first covering the temperature range −80 to +300 °C, the second from 0 to 100 °C. For purposes of this analysis we ascribe an uncertainty of 50 percent in these values although there is no genuinely sound basis for this choice, and the errors may be larger.

Interpolation equations for the various virial coefficients are tabulated in appendix 2.

3.2. Saturation Vapor Pressure

The following equation, formulated by Wexler and Greenspan [17], is used to calculate e_s, the saturation vapor pressure of water:

$$\ln e_s = \sum_{i=0}^{5} E_i T_{48}^{i-1} + B \ln T_{48} \qquad (31)$$

where T_{48} is the absolute temperature on the International Practical Temperature Scale of 1948 [20, 21] and e_s is expressed in pascals.[5] The coefficients E_i and B are given in table 1.

TABLE 1. *Coefficients to vapor pressure formulation eq (31)*[a]

E_0	-7.51152×10^{3}
E_1	9.65389644×10^{1}
E_2	2.3998970×10^{-2}
E_3	$-1.1654551 \times 10^{-5}$
E_4	$-1.2810336 \times 10^{-8}$
E_5	$2.0998405 \times 10^{-11}$
B	-1.2150799×10^{1}

[a] Units: e_s, pascals; T, kelvins.

3.3. Function g(T, P)

The coefficients α_{ij}, a and b, given by Kell and Whalley [12] and Kell [13] are tabulated in table 2. These are needed in order to compute v_w^1, using eq (26) which, in turn, permits the computation of $g(T, P)$ using eq (27). Kell and Whalley estimated that the standard deviation of the differences between observed values of $\overline{V}(T, P)/\overline{V}(t, 1 \text{ atm})$ and eq (24) does not exceed 10 ppm. Kell estimated that $\overline{V}(t, 1 \text{ atm})$, given by eq (25) has a standard error of 10 ppm or less for temperatures up to 100 °C.

TABLE 2. *Coefficients to eq (26)*[a]

	Coefficients α_{ij}		
i \ j	1	2	3
0	-50.9769×10^{-6}	8.2627×10^{-9}	-9.109×10^{-13}
1	3.71999×10^{-7}	-1.3794×10^{-10}	2.626×10^{-14}
2	-7.01760×10^{-9}	3.4032×10^{-12}	-8.913×10^{-16}
3	6.00227×10^{-11}	-3.6432×10^{-14}	11.467×10^{-18}
4	-3.09041×10^{-13}	2.0836×10^{-16}	-7.102×10^{-20}
5	5.93416×10^{-16}	-4.1744×10^{-19}	14.841×10^{-23}
n	Coefficients a_n		
0	0.9998396		
1	1.8224944×10^{-2}		
2	-7.922210×10^{-6}		
3	-5.544846×10^{-8}		
4	1.497562×10^{-10}		
5	$-3.932952 \times 10^{-13}$		
	Coefficient b		
	1.8159725×10^{-2}		

[a] Units: t, °C; P, bar; P_A, 1.01325 bar; v_w^1, cm³/mol.

3.4. Constants

The solubility data of Winkler [22, 23] for air in water, as reported by Dorsey [24], was used to calculate the Henry's law "constant" k at standard atmospheric pressure. In the absence of any known air data on the pressure dependence of this "constant," it was assumed that the percentage changes in k between the same

[4] Incorrect values of C_{www} are listed in table 1 of the paper by Hyland and Mason. A B_{ww}^2 term was omitted in the calculation. Although the error propagates through the paper, the preferred C_{www} values (calculated from viscosities) remain unaltered; the effect on the conclusions of the paper is negligible.

[5] Pascal = 1 N/m² = 10^{-5} bar = 10^{-2} mb = 7.50062×10^{-2} mm Hg.

TABLE 3. *Henry's law "constants" k for nitrogen and air dissolved in water*[f]

Temp. °C	Nitrogen[a]			Air			Air[e]		
	Pressure, bars			Pressure, bars			Pressure, bars		
	1	50	100	1[b]	50[c]	100[d]	1	50	100
0	18.65	17.00	15.62	23.25	21.19	19.48	23.20	21.20	19.49
5	16.42	15.11	13.96	20.45	18.82	17.39	20.53	18.81	17.37
10	14.89	13.69	12.70	18.26	16.80	15.58	18.30	16.79	15.58
15	13.51	12.41	11.60	16.49	15.15	14.15	16.46	15.12	14.10
20	12.52	11.42	10.72	14.93	13.62	12.78	14.96	13.75	12.88
25	11.61	10.68	10.01	13.84	12.73	11.92	13.76	12.64	11.90
30	10.88	10.00	9.46	12.83	11.79	11.16	12.79	11.77	11.13
35	10.23	9.44	8.97	12.00	10.08	10.53	12.02	11.10	10.52
40	9.67	9.02	8.57	11.34	10.58	10.05	11.40	10.58	10.05
45	9.27	8.70	8.25	10.84	10.17	9.64	10.87	10.19	9.68
50	8.90	8.44	8.00	10.44	9.90	9.39	10.39	9.89	9.38

[a]Data based on solubilities in references [24, 25, 26, 27, 28, 29, 30].
[b]Data based on solubilities in references [22, 23, 24].
[c]Calculated by assuming that the percent difference for air is the same as for nitrogen between 50 and 1 bars.
[d]Calculated by assuming that the percent difference for air is the same as for nitrogen between 100 and 1 bars.
[e]Calculated from eq (32).
[f]Units: k, 10^{-6} mole fraction per bar; P, bars.

pressure levels at given temperatures were the same for air as for nitrogen, for which there are solubility data both at atmospheric pressure [25, 26, 27, 28], and at high pressure for temperatures above 20 °C [24, 29, 30]. Using solubility data for nitrogen in water and converting these to k, values for air were extropolated accordingly. Below 20 °C, solubilities of nitrogen in water were calculated using the method of Krichevsky and Kasarnovsky [31] and the fugacities reported by Demming and Shupe [32]. The polynomial

$$10^6 k = \sum_{i=0}^{3} C_i t^i \qquad (32)$$

was fitted by the method of least squares to the Henry's law "constant" for air in water at 1, 50, and 100 bars, where k is in units of mole fraction per bar, C_i are coefficients, and t is the temperature in degrees Celsius. Linear interpolations were employed between isobars. Values of k for nitrogen and air are given in table 3 and for C_i in table 4. The values of k for air are considered uncertain, at most, by 10 percent.

On the unified carbon-12 scale the molecular weight of water M_w is 18.0154 g/mol with a maximum total uncertainty of 0.0009 g/mol [33]. The gas constant R is equal to 83.1434 bar cm³/mol K with a standard deviation of 0.0035 bar cm³/mol K [34].

TABLE 4. *Coefficients to eq (32)*[a]

i	Pressure, bars		
	1	50	100
0	23.195	21.197	19.493
1	−0.58037	−0.51768	−0.46024
2	9.7392×10^{-3}	8.2103×10^{-3}	7.3781×10^{-3}
3	-6.5058×10^{-5}	-4.7585×10^{-5}	-4.4401×10^{-5}

[a]Units: t, degrees Celsius; k, mole fraction per bar.

3.5. Enhancement Factor

The NBS enhancement factor data [6] are given in table 5. It is estimated that the systematic uncertainty in f is 0.07 percent and the random uncertainty is 0.2 percent. Two 30°C runs, reported as being suspicious in [6], have not been considered for the calculation of B_{aw}.

4. Results

Values of B_{aw} calculated from these data using eq (30) are given in table 5. The values were normalized from the experimental temperature to the nominal isotherm temperature. The changes, where they occur, are small.

Our best estimates of the magnitudes of B_{aw} and associated random uncertainties are represented respectively by the means of the normalized isotherm values and the standard deviations of the mean normalized values. These are reported in table 6, along with the standard deviations of the individual determinations.

5. Effect of Third Virial Terms

Statistical mechanics predicts that the virial coefficients are functions solely of temperature [8]. An apparent dependence of B_{aw} on pressure can be introduced via the calculations if a sufficient number of terms are not included in the truncated infinite series of the equation of state. If this equation were terminated at the second virial term rather than the

TABLE 5. *Second interaction virial coefficients based on NBS enhancement data*

Run No.	Saturation temp.	Saturation vap. press.	Total pressure	Mole fraction water vapor	Enhancement factor	Interaction virial coeff.	Normalized inter. vir. coeff.
	°C	mbar	bar			cm^3/mol	cm^3/mol
	t	e_s	P	x_w	f	B_{aw}	B_{aw}
	Isotherm temperature, 30 °C						
39	29.9994	42.4278	10.7312	0.0040827	1.0326	−29.962	−29.962
47	30.0065	42.4451	15.1088	.0029354	1.0449	−29.389	−29.392
42	29.9999	42.4290	19.9344	.0022534	1.0587	−29.115	−29.115
20	30.0112	42.4566	30.1929	.0015317	1.0893	−28.988	−28.944
40	29.9999	42.4290	35.5133	.0013201	1.1049	−28.763	−28.763
	Isotherm temperature, 40 °C						
34	40.0104	73.8143	14.6417	0.0052456	1.0405	−26.286	−26.289
19	39.9969	73.7612	30.1957	.0026497	1.0847	−26.978	−26.977
27	39.9648	73.6350	40.4557	.0020231	1.1115	−26.124	−26.114
22	40.1505	74.3673	50.3962	.0016810	1.1392	−25.831	−25.876
21	40.1366	74.3122	60.9945	.0014285	1.1725	−26.158	−26.199
	Isotherm temperature, 50 °C						
32	49.9898	123.3233	10.5512	0.0120190	1.0283	−23.443	−23.440
37	49.9942	123.3503	10.6310	.0119361	1.0287	−23.713	−23.711
36	50.0042	123.4115	10.7441	.0118214	1.0292	−23.915	−23.916
43	50.0047	123.4146	10.7546	.0117992	1.0282	−22.714	−22.715
46	49.9971	123.3680	10.7953	.0117446	1.0277	−21.977	−21.976
35	50.0011	123.3925	10.7989	.0117614	1.0293	−23.946	−23.946
31	49.9891	123.3191	14.6231	0.0087902	1.0423	−27.135	−27.132
33	50.0064	123.4250	14.8620	.0086263	1.0387	−23.399	−23.401
30	49.9967	123.3656	25.3585	.0051773	1.0642	−23.186	−23.185
17	50.0101	123.4477	30.1977	.0044266	1.0828	−25.846	−25.849
16	50.0050	123.4164	30.2324	.0044135	1.0811	−25.117	−25.118
29	50.0009	123.3913	36.5953	.0036782	1.0909	−22.605	−22.605
26	49.9766	123.2426	40.8462	.0033228	1.1013	−22.502	−22.495
23	50.0049	123.4158	50.3229	.0027681	1.1287	−23.227	−23.228
24	49.9784	123.2536	76.3139	.0019376	1.1997	−23.088	−23.082
28	49.9815	123.2726	96.9356	.0016749	1.2355	−22.298	−22.292
25	49.9788	123.2561	102.704	.0015264	1.2719	−22.483	−22.477

TABLE 6. *Mean normalized second interaction virial coefficients* $\bar{B}_{aw}$ *based on NBS data*

Isotherm Temp.	Mean normalized $\bar{B}_{aw}$	Standard deviation of single determination		Standard deviation of mean	
°C	cm^3/mol	cm^3/mol	Percent	cm^3/mol	Percent
30	−29.245	0.46	1.6	.21	0.7
40	−26.291	.41	1.6	.18	.7
50	−23.595	1.35	5.7	.33	1.4

third, the terms associated with the parameters ϵ, δ, and β would reduce to zero and from eq (29i) we would have

$$B_{aw} = (RT \ln f - \alpha)/D. \tag{33}$$

The change introduced by using eq (33) instead of (30) is significant as shown graphically in figure 1 using the NBS enhancement data. Because of this the third virial coefficients were included in the calculation of B_{aw}, even though there are large uncertainties associated with them. It will be shown that the accuracy in B_{aw} is relatively insensitive to the accuracies of the third virial coefficients.

6. Error Analysis

An analysis was made of the effect of suspected systematic and random errors on the accuracy of the values of B_{aw} given in the results.

6.1. Enhancement Factor

It can be shown that the uncertainties in the experimental parameters P, e_s, and x_w contribute to the error in B_{aw} primarily from their appearance in the enhancement factor term and negligibility because of their presence in the other terms of eq (30).[6] Therefore, for

[6] This was checked by making arbitrary changes in these parameters and noting the corresponding changes in the individual terms contributing to B_{aw}, as well as in B_{aw} itself.

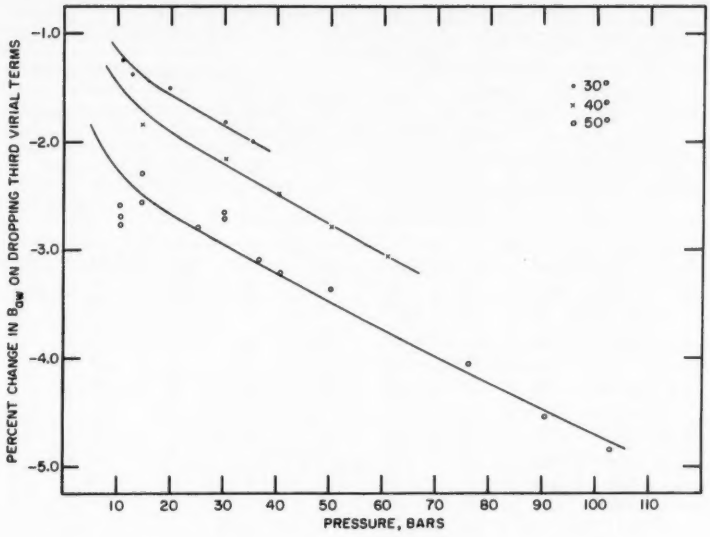

FIGURE 1. *The percentage changes in calculated values of* B_{aw}, *when third virial terms are dropped from eq (30).*

purposes of error analysis, the higher order virial coefficients may be neglected and eq (33) used with adequate accuracy for examining the effect of an error in f on B_{aw}. Differentiating B_{aw} with respect to f, replacing the differential with finite increments, and considering only magnitudes, we obtain

$$\Delta B_{aw} = \frac{RT}{2Px_a^2 f}\Delta f \approx \frac{RT}{2P}\frac{\Delta f}{f} \tag{34}$$

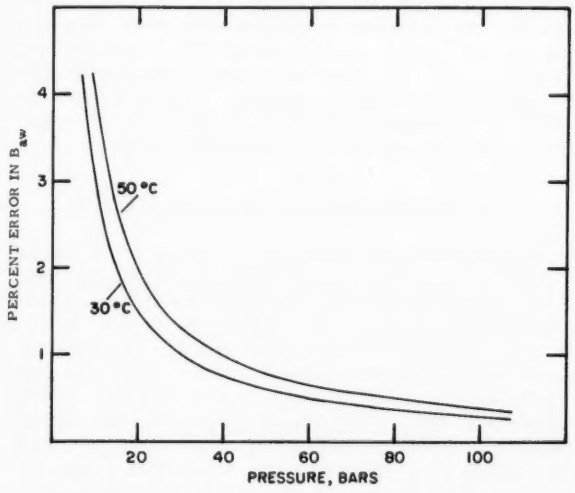

FIGURE 2. *Percentage errors in* B_{aw} *as a function of temperature and pressure, arising from the estimated systematic error of 7 parts in* 10^4 *in the enhancement factor.*

where x_a is assumed roughly equal to unity. The systematic uncertainty in the NBS values of enhancement factor is 0.07 percent [6]. By substituting this into eq (34), and using the mean values of B_{aw} given in table 6 to convert ΔB_{aw} to percent, the curves shown in figure 2 were generated. It may be noted that for a fixed relative uncertainty in f the corresponding uncertainty in B_{aw} decreases with increasing pressure. This relationship suggests that for interaction virial coefficient determinations it would be advantageous to perform enhancement measurements at high pressures. However, as we will show below, this gain in accuracy is offset by the increasing uncertainties contributed by the terms in eq (30) containing the third virial coefficients.

6.2. Virial Coefficients

The effects of the estimated systematic uncertainties in the virial coefficients (given in sec. 3.1) on B_{aw} were calculated using eq (30). The results are given in table 7 at the experimental pressures and temperatures.

6.3. Henry's Law

It is shown in appendix 1 that dropping the correction term C to Henry's law, (eq (22)), may lead to an uncertainty in B_{aw} of about 0.13 percent. An uncertainty is contributed also by the "constant" k. The second interaction virial coefficient may be written as follows:

$$B_{aw} \approx \frac{-RTkx_aP}{2x_aP} + \text{various terms.} \tag{35}$$

TABLE 7. *Estimated systematic uncertainties in* B_{aw}

Temp.	Press.	Source of error								Quadrature[e]	
		B_{aa}	B_{ww}	C_{aaa}	C_{www}	C_{aaw}	C_{aww}	f	Other	Virial coefficient errors only	All errors
		Estimated error in parameter, percent									
		[a]	[b]	15	[c]	50	50	.07	[d]		
°C	bar	Estimated error in B_{aw}, percent								Estimated error in B_{aw}, percent	
30	10.7	2.0	1.9	0.14	0.05	0.42	0.42	2.8	0.14	2.8	4.0
	19.9	2.0	1.1	.26	.03	.81	.45	1.5	.14	2.5	2.9
	35.5	2.0	.68	.47	.02	1.4	.47	0.85	.14	2.6	2.7
40	14.6	2.2	1.6	.20	.08	.62	.66	2.4	.14	2.9	3.7
	40.5	2.1	.66	.56	.04	1.7	.71	.85	.14	2.9	3.0
	61.0	2.1	.48	.84	.03	2.6	.75	.57	.14	3.6	3.6
50	10.6	2.6	2.5	.16	.21	0.46	.98	3.8	.14	3.8	5.4
	25.4	2.5	1.1	.38	.10	1.2	1.0	1.6	.14	3.2	3.6
	50.3	2.4	0.64	.76	.06	2.3	1.1	0.79	.14	3.6	3.7
	76.3	2.3	.48	1.2	.04	3.5	1.2	.52	.14	4.5	4.6
	103	2.3	.40	1.6	.04	4.8	1.2	.39	.14	5.7	5.7

[a] Estimated 3σ error is 1.2 cm³/mol; error is 17, 23, and 34 percent at 30, 40, and 50 °C, respectively.
[b] Estimated error is 24, 16, and 11 percent at 30, 40, and 50 °C, respectively.
[c] Estimated error is nominally 43 percent at 30, 40, and 50 °C.
[d] Quadrature of errors contributed by Henry's law, gas constant, and ignoring the correction to the law of ideal solutions.
[e] Computed by the square root of the sum of the squares of the individual terms.

Hence, neglecting the sign,

$$\Delta B_{aw} \approx \frac{RT}{2}\Delta k \approx 13000\,\Delta k. \tag{36}$$

The estimated uncertainty in k is 10 percent. Over the pressure and temperature range of the NBS data, the variation in k is small. With sufficient accuracy for this calculation, $\Delta k = 1.1 \times 10^{-6}$ and therefore $\Delta B_{aw} = 0.014$ cm³/mol. Assuming a nominal magnitude of 26 cm³/mol for B_{aw}, k induces an uncertainty in B_{aw} of about 0.05 percent.

6.4 Function $g(P, T)$; Gas Constant

The largest contributions from the term $g(P, T)$ to the uncertainties in B_{aw} arise from uncertainties in the specific volume of water $\bar{V}(t, P)$ and the molecular weight of water, while the largest contribution from the gas constant R arises through the enhancement factor term. The uncertainties in P and t in the NBS data are insignificant in their effect on $\bar{V}(t, P)$. The systematic errors in $\bar{V}(t, P)$, M_w, and R (secs. 3.3 and 3.4) likewise produce negligible uncertainties in the calculated values of B_{aw}.

6.5 Estimated Systematic Uncertainty in B_{aw}

The estimated systematic uncertainties in the individual parameters at the experimental values of P and T are summarized in table 7. These were combined by quadrature to give the estimated overall systematic uncertainty in B_{aw}. Two quadrature columns are shown. The left column is the estimated uncertainty in the calculated value of B_{aw} contributed solely by the virial coefficient terms whereas the right column is the estimated uncertainty in B_{aw} due to all suspected sources of systematic error. Along each isotherm, as the effect on B_{aw} from the fixed percentage uncertainty in enhancement factor decreases with pressure, the effect from the uncertainties in the virial coefficients increases in such a way as to keep the overall systematic uncertainty in B_{aw} more or less constant over the pressure range considered. The systematic uncertainty increases from 4 percent at 30 °C to 6 percent at 50 °C, and applies to the mean value of B_{aw} as well as to the individual values.

6.6. Estimated Random Uncertainty in B_{aw}

The experimental standard deviations of the single determinations and of the mean value of B_{aw} have been given (table 6) as our best estimates of the random uncertainties in B_{aw}. The random uncertainty in B_{aw} arises mainly from the random error in the enhancement factor. The latter, based on the residual standard deviations of fits of f to a pressure function, is 0.02 percent at 30 °C, 0.13 percent at 40, and 0.26 percent at 50 °C [6]. The corresponding calculated uncertainty in a single B_{aw} determination, as a function of pressure along each isotherm, is indicated in table 8. Also given for each isotherm is a mean single-determination uncertainty, based on the three tabulated values. This calculated mean value should be comparable to

TABLE 8. *Comparison of estimated random uncertainties in a single determination of* B_{aw}

Temp.	P	Random uncertainty in B_{aw}	
		Based on random error in f [a]	Based on precision of B_{aw}
°C	Bar	Percent	Percent
30	10.7	0.80	
	19.9	.43	
	35.5	.24	
	Mean 0.49		1.6
40	14.6	4.4	
	40.5	1.6	
	61.0	1.1	
	Mean 2.4		1.6
50	10.6	14.0	
	25.4	5.8	
	50.3	2.9	
	76.3	1.9	
	103	1.4	
	Mean 5.2		5.7

[a] The standard deviation of a single determination of f is 0.02 percent at 30 °C, .13 percent at 40 °C, and 0.26 percent at 50 °C. [6].

the experimentally determined precision of a single B_{aw} determination. The latter values are repeated in table 8, and it is seen that the calculated and experimental random uncertainties are in reasonably good agreement.

7. Comparisons

There are three known experimental determinations of the enhancement of water vapor in air from which the interaction virial coefficient may be calculated. Politzer and Strebel [35] performed single saturation isotherm experiments at 50 and 70 °C at total pressure up to 200 bars. Webster [36] obtained values at −35, −20, 0 and 15 °C at total pressures up to 200 bars, also using the single isotherm saturation method. Goff et al. [37, 38, 39] measured a quantity closely related to the interaction virial coefficient, from 5 to 25 °C at total pressures near one bar.

Values of B_{aw} were computed from the Politzer and Strebel data using the same procedures, constants and virial coefficients that had been used with the NBS data. The 50 °C data of Politzer and Strebel yielded values of B_{aw} that appear to scatter independently of pressure around an average value, except for four points at 12 bars and below. These four points are suspect and so were discarded. The mean and the standard deviation of the mean are given in table 9. The 70 °C data of Politzer and Strebel show a strong monotonic pressure dependence, contrary to the predictions of theory. It is probable that there is a significant systematic error in the measurements although the source of this error is not obvious. Because of this, the 70 °C data were excluded from further consideration.

B_{aw} was computed similarly from Webster's data for each of his isotherms. At −35 and −20 °C a minor change was introduced into the calculations to allow for the solid state of the condensed phase. This involved the use for the Henry's law "constant" the value for water at 0 °C and 1 bar and for e_s the appropriate values of saturation vapor pressure with respect to ice [40]. The resultant error from the choice of k is negligible; in fact, within the uncertainty of the Webster measurements the Henry's law "constant" could be ignored. The mean value of B_{aw} for each temperature, and the standard deviation of the mean are given in table 9.

TABLE 9. *Interaction virial coefficients from literature data*

Temperature °C	Source							
	Webster		Politzer and Strebel		Goff		Mason and Monchick	Chaddock[b]
	$-\bar{B}_{aw}$ [a] cm³/mol	$\sigma_{\bar{B}_{aw}}$ cm³/mol	$-\bar{B}_{aw}$ [a] cm³/mol	$\sigma_{\bar{B}_{aw}}$ cm³/mol	$-B_{aw}$ cm³/mol	$\sigma_{B_{aw}}$ cm³/mol	$-B_{aw}$ cm³/mol	$-B_{aw}$ cm³/mol
−35	64.91	7.45						
−20	50.15	3.96			48.2	3.2		
0	38.01	1.92			42.0	3.0	50.4	62.0
10					39.3	3.0	47.3	58.1
15	34.91	3.44			37.6	2.9	45.4	56.1
20					36.8	2.9	43.9	54.4
30					34.5	2.8	41.0	51.1
40					32.3	2.7	38.2	48.1
50			23.16	0.39	30.4	2.7	35.8	45.2
60					28.5	2.6	33.5	42.5

[a] $\bar{B}_{aw}$ = mean value along an isotherm.
[b] Neither Mason and Monchick nor Chaddock assigns an uncertainty to his theoretical values of B_{aw}.

A set of B_{aw} values were calculated by an empirical equation given by Goff [2], and converted to units consistent with those employed in this paper. The standard deviation ascribed to the Goff values were derived from the tolerances he assigned, which were stated to be two times the estimated probable error. The values are given in table 9.

No attempt was made to estimate the systematic errors in the above values of B_{aw}. The standard deviations indicate only the precision of the measurements.

Mason and Monchick [5] and Chaddock [4] have made statistical mechanical calculations of B_{aw} by assuming that the forces between air and water vapor molecules can be represented by the Lennard-Jones (12–6) potential and that the separate species potential parameters ϵ_0 (the depth of the potential "well") and σ_0 (molecular "diameter") can be combined by simple combination rules. Their calculations have been extended to encompass our temperature range of interest and the values so obtained are given in table 9.

experimental data [39]. The NBS values of B_{aw} are smaller in absolute value than these other three sets of values. Although the NBS, Webster and the 50 °C Politzer and Strebel values appear to fall on a smooth curve, this may be fortuitous. Until there is additional experimental corroboration, this apparent consistency should be viewed with reservation.

8. Smoothing Function

Given experimental values of B_{aw} over a reasonable temperature range, it is feasible to determine the form of the interaction potential between the water vapor and air species and therefore, to derive a theoretically based expression for interpolation and extrapolation of B_{aw}. Unfortunately the NBS data is too limited in temperature range to warrant this approach.

A polynomial equation was fitted, therefore, to the NBS, Politzer and Strebel, and Webster data. The resultant expression is as follows:

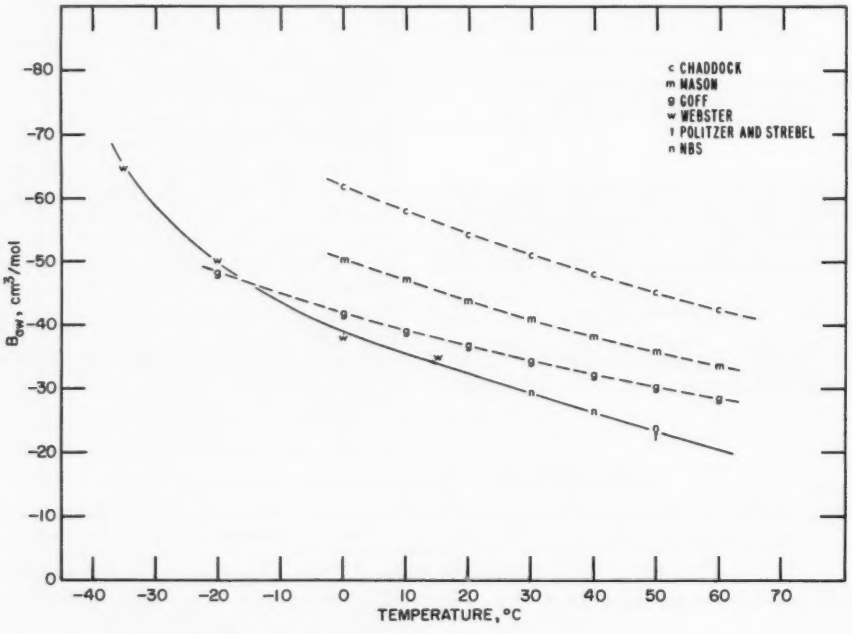

FIGURE 3. B_{aw} *versus temperature, from various investigators.*

These several sets of values of B_{aw} are compared graphically in figure 3. The curves representing the Goff, Mason and Monchick, and Chaddock values are similar in shape but displaced from each other. It is not surprising that the curves are alike for they are based on similar theoretical formulations, but with somewhat different potential constants. Even Goff's empirical equation is based on values calculated from a potential function similar to the Lennard-Jones that had been adjusted to yield results consistent with his

$$-B_{aw} = \sum_{i=0}^{4} D_i t^i \tag{37}$$

where D_i are empirical coefficients, t is the temperature in deg Celsius and B_{aw} is in units of cm³/mol. D_i are listed in table 10, along with the residual standard deviation of the fit. The experimental and predicted values are compared in table 11.

The differences between the experimental and predicted values are well within the standard deviation of

the mean of the experimental values. The maximum deviation of this equation from NBS values of B_{aw} is 1.1 percent.

TABLE 10. *Coefficients to eq (37)*

D_0	38.9221
D_1	−.384587
D_2	$+.512266 \times 10^{-2}$
D_3	$-.117467 \times 10^{-3}$
D_4	$+.878093 \times 10^{-6}$
σ_{res}	.842 cm³/mol

where Z is a lattice coordination number (assuming a local crystal structure), N_0 is Avogadro's number, ϵ_{ij} are interaction energies between the designated molecular species.

Let the mole fractions x_i in eq (38) be converted to moles n_i. Differentiating with respect to n_w we obtain.

$$\frac{\partial(\Delta G^E_{\text{mix}})}{\partial n_w} = W x_a^2. \tag{40}$$

This equation gives the excess chemical potential of the water with dissolved air over that predicted from

TABLE 11. *Comparison of experimental and predicted values of* B_{aw}

Temperature	Interaction virial coefficient		Difference		Standard deviation of mean		Source
°C	Experimental	Predicted[a]	Pred.—Exp.		Experimental		
	cm³/mol	cm³/mol	cm³/mol	Percent	cm³/mol	Percent	
−35	−64.91	−65.01	−0.11	−0.17	7.45	11.5	Webster [36].
−20	−50.15	−49.74	+0.41	+0.82	3.96	7.9	Webster [36].
0	−38.01	−38.92	−0.91	−2.34	1.92	5.1	Webster [36].
15	−34.91	−33.95	+0.96	+2.75	3.44	9.8	Webster [36].
20		−32.48					
30	−29.24	−29.53	−0.29	−0.99	0.21	0.7	NBS.
40	−26.29	−26.47	−0.17	−0.65	0.18	0.7	NBS.
50	−23.56	−23.30	+0.26	+1.10	0.33	1.4	NBS.
50	−23.16	−23.30	−0.14	−0.60	0.39	1.7	P & S [35].
60		−20.30					

[a] Calculated using eq (37).

Equation (37) is offered as a suitable smoothing function for B_{aw} that is valid from 30 to 50 °C, the temperature range of the NBS experiments. We feel confident in using it from 10 to 60 °C. Because it fits the Webster data well, and within the uncertainty of that data, the equation may be used to −35 °C. However, it should be noted that the systematic uncertainty in the Webster data is unknown so that the reliability of the predicted B_{aw} in the temperature range below, say, 10 °C is unresolved.

9. Appendix 1

For a two component solution of equal-size molecules, such as air dissolved in water, it can be shown [7] that

$$W(n_a + n_w)x_a x_w = \Delta G^E_{\text{mix}} \tag{38}$$

where ΔG^E_{mix} is the excess Gibb's function[7], that is, the departure from that predicted through Raoult's law; n_a and n_w are the total number of moles of air and water; and x_a and x_w are mole fractions of air and water. The parameter W is given by [7]

$$W = \frac{ZN_0}{2}(2\epsilon_{aw} - \epsilon_{aa} - \epsilon_{ww}) \tag{39}$$

[7] Lewis and Randall [7] call this the excess free energy of mixing and designate it by the symbol ΔF^E_{mix}.

Raoult's law and is therefore equivalent to the term C in eqs (18), (19), and (22).

Mason and Monchick [5] and Chaddock [4] both give $\epsilon_{aa}/k = 99.2$ K and $\epsilon_{ww}/k = 380$ K (where k is Boltzmann's constant). Mason and Monchick give values of 194 and 222 K for ϵ_{aw}/k, as determined from second virial coefficient data and viscosity data respectively whereas Chaddock gives 220.5 K. For the present purpose, assume $\epsilon_{aw}/k = 210$ K. If a coordination number of 15 (which should lead to a conservatively large estimate of C) is assumed, then W is -3.69×10^4 bar cm³/mol. Suppose that this is in error by a factor of 5, then W might be of the magnitude -1.84×10^5 bar cm³/mol.

The mole fraction of air dissolved in water x_a may be estimated from Henry's law using the constants in table 3. The worst case (i.e., the largest value of x_a which, in turn maximizes C) occurs at 0 °C and 100 bars. Using this value for x_a and $W = -1.84 \times 10^5$ atm cm³/mol, the magnitude of C is then 0.7 bar cm³/mol.

Equation (30), with the C term included, can be approximated by

$$B_{aw} \approx [\text{Various terms}] - \frac{g(T,P)}{2P} - \frac{C}{2P} \tag{41}$$

The lowest pressure present in the NBS enhancement data is 10 bars. The maximum contribution of C to B_{aw}, therefore, is about 0.035 cm³/mol. For B_{aw} of the order

487-412 OL - 73 - 10

of 26 cm³/mol, the relative contribution of C to B_{aw} is about 1.3 parts in 1000, which is about one order of magnitude smaller than the estimated uncertainty in B_{aw}.

10. Appendix 2

The equations for the virial coefficients for water are essentially those of Goff [2]. B_{ww} is given here with opposite sign to conform to eq (8a). C_{www} is a modification of Goff's equation to conform to eq (8a). Goff suggests the use of his equation for C_{www} only at temperatures 60 to 100 °C whereas we extropolate it to − 20 °C. Although this is a potentially dangerous procedure, no other alternative is available.

The equations for the virial coefficients B_{aa} and C_{aaa} were obtained by fitting the Sengers et al. data [16] and the Hilsenrath et al. data [14] respectively, over the temperature range 260 to 380 K, to polynomials.

The equations for the interaction virial coefficients C_{aaw} and C_{aww} were similarly obtained by fitting the Mason and Monchick [5] values from − 20 to + 120 °C and the Hyland and Mason [19] values from 0 to 100 °C, respectively, to polynomials.

The standard deviations of the fits for the latter four equations are given. These equations are convenient empirical relationships and it is not intended that they be used beyond the fitted temperature ranges.

$$B_{ww} = 33.97 - \frac{55306}{T} \times 10^{\frac{72000}{T^2}} \text{ cm}^3/\text{mol}$$

$$C_{www} = 2.85558 \frac{B_{ww}^3}{T} + B_{ww}^2 \text{ cm}^6/\text{mol}^2$$

$$B_{aa} = -13.521 + 0.24234t - 0.10022 \times 10^{-2}t^2 + 0.26880 \times 10^{-5}t^3 \text{ cm}^3/\text{mol}; \sigma = 0.024$$

$$C_{aaa} = 1314.2 - 0.89453t - 0.36372 \times 10^{-2}t^2 + - .48378 \times 10^{-4}t^3 - 0.18897 \times 10^{-6}t^4 \text{ cm}^6/\text{mol}^2; \sigma = 0.17$$

$$C_{aaw} = 860.79 - 2.4203t + 0.92144 \times 10^{-2}t^2 - 0.14568 \times 10^{-4}t^3 \text{ cm}^6/\text{mol}^2; \sigma = 0.32$$

$$C_{aww} \times 10^{-6} = -0.20263 + 0.52695 \times 10^{-2}t - 0.74761 \times 10^{-4}t^2 + 0.57576 \times 10^{-6}t^3 - 0.18065 \times 10^{-8}t^4 \text{ cm}^6/\text{mol}^2; \sigma = 0.614 \times 10^{-3}$$

$T = t + 273.16$, t = degrees Celsius.

11. References

[1] Keyes, F. G., and Smith, L. B., The present state of psychrometric data, Refrig. Eng. **27**, 127 (1934).

[2] Goff, J. A., Standardization of thermodynamic properties of moist air, Heating, Piping, and Air Cond. **21**, 118 (1949).

[3] Haar, L., and J. M. H. L. Sengers, The solubility of condensed substances in dense gases and the effect on *PVT* properties, J. Chem. Phys. **52**, 5069 (1970).

[4] Chaddock, J. B., Moist air properties from tabulated virial coefficients, Humidity and Moisture, Vol. **III**, A. Wexler and W. A. Wildhack, Eds. (Reinhold Publishing Corp., New York, 1965), p. 273.

[5] Mason, E. A., and Monchick, L., Survey of the equation of state and transport properties of moist gases, Humidity and Moisture, Vol. **III**, A. Wexler and W. A. Wildhack, Eds. (Reinhold Publishing Corp., New York, 1965), p. 257.

[6] Hyland, R. W., and Wexler, A., The enhancement of water vapor in air, J. Res. Nat. Bur. Stand. (U.S.), **77A** (Phys. and Chem.), No. 1, (Jan.-Feb. 1973).

[7] Lewis, G. N., and Randall, M., Thermodynamics, 2nd Edition, as revised by Pitzer, K. S., and Brewer, L. (McGraw-Hill Book Co., New York, 1961), Ch. 21.

[8] Hirshfelder, J. O., Curtiss, C. F. and Bird, R. B., The Molecular Theory of Gases and Liquids (John Wiley & Sons, Inc., New York, 1954).

[9] Hanley, H. J. M., and Klein, M., On the selection of the intermolecular potential function: application of statistical mechanical theory to experiment, Nat. Bur. Stand. (U.S.), Tech. Note 360, 85 pages (Nov. 1967).

[10] Harrison, L. P., Fundamental concepts and definitions, Humidity and Moisture, Vol. **III**, A. Wexler and W. A. Wildhack, Eds. (Reinhold Publishing Corp., New York, 1964), p. 8.

[11] Hasegawa, S., Hyland, R. W., and Rhodes, S. W., A comparison between the National Bureau of Standards two-pressure humidity generator and the National Bureau of Standards standard hygrometer, Humidity and Moisture, Vol. **III**, A. Wexler and W. A. Wildhack, Eds. (Reinhold Publishing Corp., New York, 1964), p. 455.

[12] Kell, G. S., and Whalley, E., The *PVT* properties of water I. Liquid water in the temperature range 0 to 150 °C and at pressures up to 1 kb, Phil. Trans. Roy. Soc. London, Series A, **258**, 565 (1965).

[13] Kell, G. S., Precise representation of volume properties of water at one atmosphere, J. Chem. Eng. Data **12**, 66 (1967).

[14] Hilsenrath, J., et al., Tables of Thermal Properties of Gases, Nat. Bur. Stand. (U.S.), Circ. 564 (1955).

[15] Hall, N. A., and Ibele, W. E., The tabulation of imperfect gas properties for air, nitrogen, and oxygen, Trans. ASME **76**, 1039 (1957).

[16] Sengers, J. M. H. L., Klein, M., and Gallagher, J. S., Pressure-volume-temperature relationships of gases; Virial coefficients, Report No. AEDC TR-71-39, Arnold Engineering Development Center, AFSC, Arnold Air Force Station Tennessee (1971).

[17] Wexler, A., and Greenspan, L., Vapor pressure equation for water in the range 0 to 100 °C, J. Res. Nat. Bur. Stand. (U.S.), **75A** (Phys. and Chem.), No. 3, 213-230 (May-June 1971).

[18] Keyes, F. G., The thermodynamic properties of water substance 0° to 150 °C, J. Chem. Phys. **15**, 602 (1947).

[19] Hyland, R. W., and Mason, E. A., Third virial coefficient for air-water vapor mixtures, J. Res. Nat. Bur. Stand. (U.S.) **71A** (Phys. and Chem.), No. 3.219-224 (May-June 1967).

[20] Stimson, H. F., International temperature scale of 1948, J. Res. Nat. Bur. Stand. (U.S.), **42**, 209 (1949) RP1962.

[21] Stimson, H. F., International temperature scale of 1948. Text revision of 1960, J. Res. Nat. Bur. Stand. (U.S.) **65A**, (Phys. and Chem.), No. 3, 139-145 (May-June 1961).

[22] Winkler, L. W., Die Loslichkeit der Gase in Wasser, Ber. deuts. chem. Ges. **34**, 1408 (1901).

[23] Winkler, L. W., Chem.-Techn. Untersuchungsmethoden, by Lunge, G., 5 ed., **1**, 768 (1904). Also **1**, 573 (1921 ed.).

[24] Dorsey, N. E., Properties of Ordinary Water Substance (Rheinhold Publishing Corp., New York, N.Y., 1940).

[25] Loomis, A. G., Solubilities of gases in water, International Critical Tables, Vol. **3**, E. W. Washburn, Ed. (McGraw-Hill Book Co., New York, 1928), p. 255.

[26] Jones, H. B., Solubilities of various gases in water, Handbook of Chemistry and Physics, 33rd. edition, C. D. Hodgman, Ed. (Chemical Rubber Publishing Co., Cleveland, Ohio, 1951), p. 1482.

[27] Coste, J. H., Review of Nitrogen Solubilities, J. Phys. Chem. **31**, 81 (1927).

[28] Van Slyke, D. D., Dillion, R. T., and Margaria, R., Studies of gas and electrolyte equilibria in blood XVIII, Solubility and physical state of atmospheric nitrogen in blood cells and plasma, J. Biol. Chem. **105**, 571 (1934).
[29] Wiebe, R., Gaddy, V. L., and Heins, C., Jr., The solubility of nitrogen in water at 50, 75, and 100 °C from 25 to 1000 atmospheres, J. Am. Chem. Soc. **55**, 947 (1933).
[30] Saddington, A. W., and Krase, N. W., Vapor-liquid equilibria in the system nitrogen-water, J. A., Chem. Soc. **56**, 353 (1934).
[31] Krichevsky, I. R., and Kasarnovsky, J. S., Thermodynamical calculations of solubilities of nitrogen and hydrogen in water at high pressures, J. Am. Chem. Soc. **57**, 2168 (1935).
[32] Deming, W., and Shupe, L. E., Some physical properties of compressed gases I. Nitrogen, Phys. Rev. **37**, 638 (1931).
[33] Division of Inorganic Chemistry, Commission on Atomic Weights, Atomic weight of the elements, Pure and Applied Chem. **21**, 93 (1970).
[34] General Physical Constants, Nat. Bur. Stand. (U.S.), Spec. Publ. 344 (1971).
[35] Pollitzer, F., and Strebel, E., Über der Einfluss indifferenter Gase auf die Sättigungsdampfkonzentration von Flussigkeiten, Zeit. fur phys. Chemie **110**, 768 (1924).
[36] Webster, T. J., The effect on water vapor pressure of superimposed air pressure, J. S. C. I. **69**, 343 (1950).
[37] Goff, J. A., and Bates, A. C., The interaction constant for moist air, Trans. ASHVE **47**, 373 (1941).
[38] Goff, J. A., Anderson, J. R., and Gratch, S., Final values of the interaction constant of moist air, Trans. ASHVE **49**, 269 (1943).
[39] Goff, J. A., and Gratch, S., Thermodynamic properties of moist air, Heating, Piping, and Air Cond. (ASHVE Journal Sect.) **17**, 334 (1945).
[40] Goff, J. A., Saturation pressure of water on the new Kelvin scale, Humidity and Moisture, Vol. **III**, A. Wexler and W. A. Wildhack, Eds. (Reinhold Publishing Corp., New York, 1965), p. 289.

(Paper 77A1–758)

JOURNAL OF RESEARCH of the National Bureau of Standards—A. Physics and Chemistry
Vol. 77A, No. 1, January–February 1973

Solubility and Surface Properties of Finely Divided Hydroxyapatite

Y. Avnimelech,* E. C. Moreno, and W. E. Brown*****

Institute for Materials Research, National Bureau of Standards, Washington, D.C. 20234

(October 3, 1972)

Synthetic hydroxyapatite (OHAp), $Ca_5(PO_4)_3OH$, was prepared by slow addition of phosphoric acid to a boiling $Ca(OH)_2$ suspension. The solid, precipitated at a pH of about 12, was stabilized by prolonged boiling. The Ca/P ratio of the product was 1.69 ± 0.04 and it had a specific surface area of 26 m^2/g.

Samples of OHAp were equilibrated with phosphoric acid solutions. Within the pH range studied, 5 to 7, the solubility product, $(Ca)^5(PO_4)^3(OH)$, was found to be $6.3 \pm 2.1 \times 10^{-59}$ at 25 °C.

Substantial deviations of the overall dissolution reaction from OHAp stoichiometry were observed and are attributed to nonstoichiometric reactions occurring at the surface. A linear dependence of excessive phosphorus on the surface with decrease in pH was found. Estimates on the extent of deviation from stoichiometry caused by the surface reaction are given.

Key words: Bone mineral; calcium phosphate; hydroxyapatite; solubility product; surface.

1. Introduction

Hydroxyapatite (OHAp), $Ca_5(PO_4)_3OH$, is the prototype of the inorganic constituent found in tooth and bone. In biological materials it is invariably very finely subdivided and with high specific surface area (e.g., over 100 m^2/g in bone). It is anticipated that the physicochemical properties of these materials reflect both the "lattice" and "surface" properties. The relative contributions of these properties to the equilibrium in the ternary system $Ca(OH)_2$-H_3PO_4-H_2O are analyzed in detail in a subsequent paper [1].[1] Here we present experimental data confirming that

(1) the equilibrium solution compositions are confined to the solubility isotherm fixed by the equilibrium with the lattice even when the "overall" dissolution reaction is nonstoichiometric,
(2) the surface contributes to deviations from the ideal stoichiometry of the overall dissolution-precipitation reaction, and
(3) a capacitative factor can be assigned to the surface which measures the contribution of the surface to the nonstoichiometry of the dissolution reaction.

Lacking the information to define the interface in terms of its 3-dimensional structure, one is limited to compositional descriptions. However, when the interface is between two condensed phases, both of which contain all three components, it is not operationally possible to assign a unique composition to the interfacial region. Therefore, one is limited to measurements involving chemical reactions (dissolution or precipitation) in which only those changes in the surface composition contributing to the nonstoichiometry of the overall reaction can be measured. We believe the approach presented here—involving as it does the use of a system confined to a single degree of freedom and the treatment of the results in terms of the stoichiometry of the *reaction* (thus avoiding any attempt to define the composition of the interface *per se*) is new, and it can be applied to other sparingly soluble salts.

2. Materials and methods

The OHAp was prepared (see sec. 2.1) by titrating a calcium hydroxide slurry at boiling temperature with phosphoric acid. High pH, high temperature and slow addition of reagents minimized formation of metastable calcium phosphates. The preparation was then boiled for several days to minimize recrystallization during the subsequent equilibrations. The prepara-

[1] Figures in brackets indicate the literature references at the end of this paper.

*Research Associate of the American Dental Association at the National Bureau of Standards, Washington, D.C. 20234. Now at the Soil Science Laboratory, Israel Institute of Technology, Technion City, Haifa, Israel.

**Research Associate of the American Dental Association at the National Bureau of Standards, Washington, D.C. 20234. Now at the Forsyth Dental Center, 140 Fenway, Boston, Mass. 02215.

***Director, American Dental Association Research Unit at the National Bureau of Standards, Washington, D.C. 20234.

This investigation was supported in part by research grant DE00572 to the American Dental Association from the National Institute of Dental Research and is part of the dental research program conducted by the National Bureau of Standards in cooperation with the American Dental Association: the United States Army Medical Research and Development Command; the Dental Sciences Division of the School of Aerospace Medicine, USAF; the National Institute of Dental Research; and the Veterans Administration.

tion was made using only the components of the ternary system, $Ca(OH)_2$-H_3PO_4-H_2O, to minimize contamination and to simplify application of the electroneutrality principle as a check on the experimental results.

The measurements were carried out under conditions of thermodynamic equilibrium in the ternary system. In this way the solution compositions, confined to the solubility isotherm [1, 2], are definable in terms of a single parameter (e.g., pH) and have a degree of uniqueness which is unattainable with unsaturated solutions or in solutions containing other components.

2.1. Preparation of OHAp

Analytical grade $CaCO_3$ (major impurity, Sr, 0.009%), 620 g, was calcined at 1100 °C for 24 hours; the resulting CaO was protected from atmospheric CO_2. The CaO was transferred to a 20 liter, heavywall, polypropylene carboy containing 12 liters of distilled water that had been boiled for one hour, and to which was attached a condenser protected by a CO_2 trap containing NaOH solution. Phosphoric acid solution, $2M$, prepared from twice recrystallized $2H_3PO_4 \cdot H_2O$ and degassed distilled water, was introduced through a glass tube, the end of which dipped into a small glass dish in the carboy located right below the condenser; in this way, the acid was diluted about 1:15 by condensing water. The phosphoric acid, 1.8 liter, was introduced by a peristaltic pump at a rate of 1 ml per minute. Vigorous boiling was maintained during the precipitation and was continued for two days after completing addition of the acid. The solid was then allowed to settle, supernatant liquid was removed and replaced by an equal volume of boiled, distilled water, and the suspension was boiled for three more days. This washing and boiling was repeated a second time before filtering the suspension. The precipitate was washed with acetone in a Buchner filter and dried in an oven at 105 °C.

2.2. Characterization of the Solid

Chemical analysis yielded a Ca/P ratio of $1.69 \pm .04$ as compared to the stoichiometric ratio 1.67. Petrographically the solid appeared homogeneous and nonbirefringent with a mean index of 1.634. This index is somewhat lower than that for OHAp obtained by hydrothermal procedures (1.646) [3]; a low value appears to be characteristic for precipitated OHAp, and is probably related to the presence of H_2O incorporated into the crystals. The infrared spectrum was typical for OHAp [4]; the OH-stretching peak at 3570 cm^{-1} was sharp and the PO-stretching peaks at 1040 to 1200 cm^{-1} were split, indicating that the material was reasonably well crystallized. The presence of a trace of an acid phosphate was indicated by a shoulder at 1070 cm^{-1} and a trace of carbonate by a peak at 1430 cm^{-1}. In subsequent experiments, it was found that the dry OHAp absorbed CO_2 from the air. The small amount of contaminating carbonate was probably incorporated when the OHAp was exposed to the air after being dried. The surface area, determined by N_2 adsorption, was 26 m^2/g.

2.3. Analytical Methods

Calcium was determined using an atomic absorption spectrophotometer. Strontium chloride solution was added to samples and standards to depress phosphorus interference (final strontium concentration was 2 ppm). Phosphorus was determined by the colorimetric method of Brabson et al. [5]. The estimated errors were $\pm$ 1.5 percent of the amounts of Ca or P analyzed.

The pH measurements were made with a null-point instrument, claimed accuracy $\pm$ 0.005 pH units. The pH meter was standardized with certified NBS buffers [6]. The uncertainty in the pH measurements was estimated to be $\pm$ 0.008 pH units. The conductivity of the solution was determined at 1000 Hz. The platinum electrodes were calibrated against solutions of doubly crystallized KCl. With the bridge used, the error in the conductivity measurements was estimated to be about $\pm$ 0.1 percent.

2.4. Solubility Measurements and Calculations

Saturation was achieved by circulating the equilibration solution through a column of the OHAp in a thermostated water bath at 25 ± 0.03 °C, as shown schematically in figure 1. A millipore membrane (0.22 μm pore diameter) or filter paper was placed on the perforated plate A on top of which was a 15 mm column (7 g) of OHAp. Reservoir B was filled with 950 ml of dilute phosphoric acid solution of selected concentration (see table 1) which was then circulated through the OHAp column by means of the peristaltic pump C. Conductivity and pH of the clear solution were measured in samples collected in cells D and E, respectively. The solutions were assumed to be saturated with respect to OHAp when no significant changes could be detected in either the conductivity or the pH during a period of six hours, which usually took 2 to 4 days. Samples were then taken for calcium and phosphorus analyses, and the apparatus was drained and refilled with phosphoric acid of the next concentration.

The ionic activity coefficients used in the calculation of activity products were computed using the Debye-Hückel extended equation with Kielland's values [7] for the "distances of closest approach" and an iterative procedure described by Moreno et al. (2).

2.5. Calculation of Excessive Phosphorus, P_e

In the absence of a unique entity that can be defined as a "surface" it has been customary to use the term "surface" to denote a zone in which components appear in "excess" quantities relative to the composition of the condensed phase. This procedure necessitates the definition of boundaries that are both sharp and arbitrary; these boundaries are not susceptible of experimental verification and, in the aqueous phase at least, are structurally inconceivable. In the ternary system the situation is made more

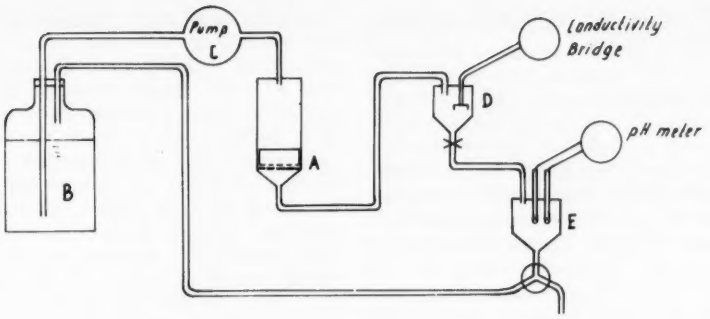

FIGURE 1. *Diagram of the equilibration apparatus.*

TABLE 1. *Solubility data for OHA_p*

Sequence	Initial H_3PO_4 mol/l × 10^4	Equilibrated Solutions					
		pH	Ca, mol/l × 10^4	P, mol/l × 10^4	Specific conductivity μmho/cm	U [a] equiv./l × 10^4	K_s, $(Ca^{2+})^5(PO_4^{3-})^3(OH^-)$, × 10^{59}
A1	0.93	6.882	1.26	0.39	32.15	2.01	13.4
A2	4.51	6.103	2.69	4.77	56.13	0.21	7.44
A3	4.05	6.005	3.01	5.60	62.13	0.04	4.41
A4	5.76	5.859	4.21	7.93	80.49	0.09	5.88
A5	8.49	5.670	6.12	11.9	115.2	−0.06	5.37
A6	11.4	5.497	8.27	16.0	149.2	0.21	3.15
A7	2.04	5.239	14.3	27.9	251.1	0.31	2.88
A8	5.70	5.802	4.75	8.96	89.49	0.13	5.98
A9	1.15	6.338	1.47	2.53	31.43	0.08	2.51
B1	1.43	6.777	1.35	0.65	31.48	1.86	19.9
B2	2.09	6.411	1.56	2.22	30.56	0.57	6.85
B3	30.4	4.807	19.7	39.4	328.8	−0.05	0.03
B4	0.51	5.825	4.74	8.83	83.62	0.22	8.13
B5	1.04	6.389	1.62	2.51	30.86	0.35	8.30
B6	0.50	6.660	0.97	1.23	19.40	0.38	5.32
B7	0	6.917	0.68	0.64	14.45	0.49	4.76
C1	1.04	6.882	1.28	0.44	25.75	1.97	20.4
C2	34.5	5.103	23.0	45.1	369.2	0.32	9.61
C3	1.04	6.232	2.06	3.71	40.42	0.002	7.42
C4	0.52	6.606	1.18	1.54	22.29	0.36	8.46
C5	5.11	5.995	3.20	6.05	63.54	−0.05	6.30
C6	1.15	5.589	8.00	16.5	138.7	−0.01	10.5
C7	0	6.595	1.04	1.57	21.9	0.18	5.52
C8	0	6.826	0.83	0.79	16.9	0.63	6.72

[a] Apparent electroneutrality unbalance as defined in text.

complex by the fact that the excess concentrations of at least *two* of the components, $Ca(OH)_2$ and H_3PO_4, are of interest. Furthermore, changes in these excess concentrations cannot be measured individually, instead all that can be done is to measure the extent to which these changes contribute to the apparent nonstoichiometry of the overall dissolution (or precipitation) reaction.

When OHAp dissolves stoichiometrically in phosphoric acid of concentration P_i, the composition of the solution should be described by

$$P_f = P_i + 3/5\ Ca_f \qquad (1)$$

where P_f and Ca_f are the final phosphorus and calcium concentrations, respectively. Equation (1) is valid only if the OHAp surface does not contribute significantly to nonstoichiometry of the dissolution. This would be true if the surface composition did not change, or if the surface area were small because then the body of the crystal (henceforth referred to as the "lattice") would be the overwhelming contributor to the dissolution process. In this work, the dissolution process was found to depart markedly from the stoichiometry shown in eq (1); these departures are attributed to changes in the surface composition. Thus it is necessary to define a new term, P_e, the "excessive" moles

of phosphorus contributed by the surface of one gram of solid to the dissolution process,

$$-P_e = [P_i + 3/5\ Ca_f) - P_f] \frac{V}{W} \qquad (2)$$

where V is the volume of solution and W is the weight of OHAp. We could also define the quantity excessive calcium, Ca_e, similarly to P_e, but, since it is impossible to make a distinction between surface and lattice dissolution,

$$Ca_e = -5/3\ P_e. \qquad (3)$$

In other words, a given deviation from stoichiometry in the dissolution reaction can be explained equally well by a surface impoverishment in phosphorus, P_e, or by a surface enrichment in calcium. We have chosen to make the calculations in terms of P_e.

3. Results

The results from three sequences of equilibrations, A, B, and C, are given in table 1. In the table are given the initial phosphoric acid concentrations, and measured quantities (pH, P and Ca concentrations, and specific conductances) of the saturated solutions. Given, also, are two derived quantities, the apparent electroneutrality unbalance [8], U, and the activity product, K_s, defined by

$$U = \sum_j C_j Z_j, \qquad (4)$$

and

$$K_s = (Ca^{2+})^5 (PO_4^{3-})^3 (OH^-) \qquad (5)$$

where the parentheses denote ionic activities, and C_j and Z_j represent the concentration and valence (with sign) of the jth ionic species present in the solution. The summation over j includes only ions formed by the three components $Ca(OH)_2$, H_3PO_4 and H_2O. Thus it is a measure of the charge unbalance contributed by impurity ions, but it also reflects analytical errors and incorrect estimates of the concentrations of the various phosphate ions and ion pairs due to errors in dissociation constants and inadequacies in the expressions for activity coefficients.

The value of U is relatively large for the first solution in each series. Most of the other values of U are less than 5 percent of the number of calcium equivalents in the corresponding solution, and considering that all the analytical errors are reflected in U, they are within the anticipated experimental error. The large value of U in the first member of each series indicates that the solid contained a contaminant, most probably carbonate (see sec. 2.2), which to a large degree was extracted in the initial equilibration.

The values for calcium concentration, used in the derivation of P_e were taken as $[Ca] - 0.5\ U$, where $[Ca]$ is the measured concentration of calcium in the equilibrated solution (mol/l) and U is the electroneutrality unbalance (equivalents/l). This implies that the unbalance was due to an anionic contaminant associated with calcium. This correction is significant only in those cases where U is large relative to the deviation from stoichiometry. The K_s values for the first solution in each of the three sequences are consistently too large, and the one for B–3 is abnormally low; these values were omitted from the average for the K_s given in table 1, $6.3 \pm 2.1 \times 10^{-59}$. The listed standard error in K_s is reasonable in view of the fact that errors of 1 percent in the Ca and P analyses would result in about 10 percent error in K_s and a 0.01 error in the pH would cause about 30 percent error in K_s. Conductivity data are given in table 1 because they are useful in verifying the condition of saturation in future studies employing OHAp in the three-component system. Conductivity measurements have the advantage over calcium and phosphorus analyses of being more sensitive and accurate, and are quicker and nondestructive. Furthermore, there is no contamination of the solution by a salt bridge as is the case with pH measurements.

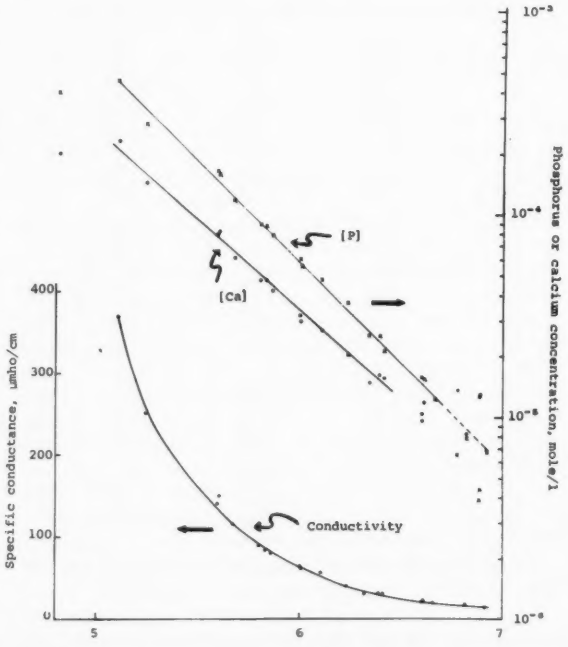

FIGURE 2. *Experimental concentrations of phosphorus, calcium and electrical conductivity of the equilibrated solutions plotted against pH.*

In figure 2 are given plots of the calcium and phosphorus concentrations and the specific conductance against pH. With the exception of the four points that were omitted from the average of K_s, the points fall on smooth curves, indicating self-consistency in the experimental data.

A further verification of equilibrium is given in figure 3, where the data in table 1 are plotted on a

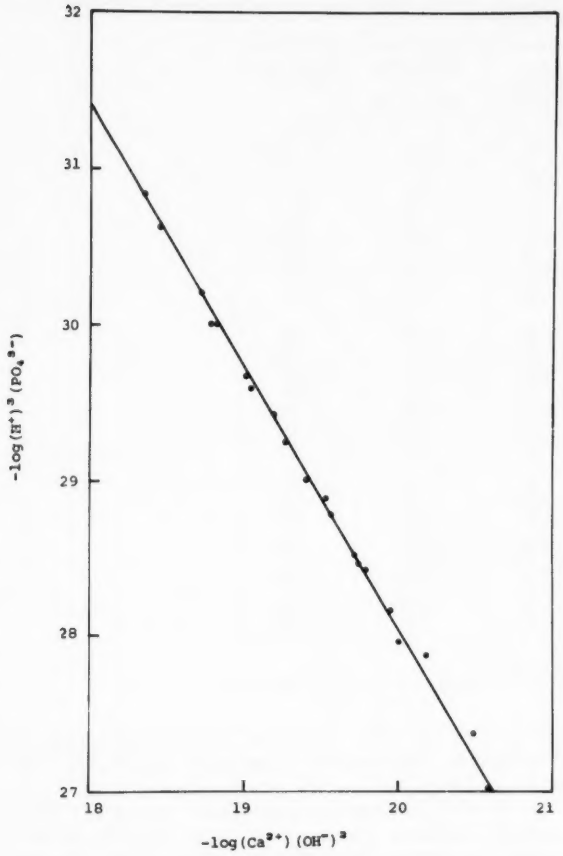

FIGURE 3. *Potential plot, phosphoric acid versus calcium hydroxide.*

"potential diagram" [1]. The logarithms of the quantities, $(Ca^{2+})(OH^-)^2$ and $(H^+)^3(PO_4^{3-})$, used as coordinates in this diagram, are proportional to the chemical potentials of calcium hydroxide and phosphoric acid, respectively. The points define the straight line,

$$-\log(H^+)^3(PO_4^{3-}) = (61.2 \pm .4) - (1.66 \pm .02) \cdot \log(Ca^{2+})(OH^-)^2. \quad (6)$$

Theory [1] predicts that the absolute value of the slope of the resulting straight line should be equal to the Ca/P ratio of the crystalline solid (i.e., exclusive of the surface). The observed slope is 1.66 ± 0.02, which may be compared to the theoretical Ca/P ratio in OHAp, 1.67, or the analytically determined value for the preparation, 1.69 ± 0.04. This agreement shows that the solid phase governing the equilibrium had essentially the theoretical ratio for OHAp even though the dissolution reactions, as shown below, leading to these equilibria were not stoichiometric because of contributions from the surface.

In table 2 are given data derived from those in table 1. The quantities in the third column, $(Ca_f/(P_f - P_i))$, gives the stoichiometry of the overall dissolution reaction. It is apparent that these ratios, in general, differ from the theoretical value, 1.67, by significant amounts. The ratio is always greater than 1.67 in the sequence when the pH decreases. In other words, the surface becomes either enriched in phosphorus or impoverished in calcium. The reverse is true when the pH increases. The values for P_e for each equilibration, calculated according to eq (2), reflect the deviations from stoichiometry for the dissolution step; these are also given in table 2. The cumulative amounts of P_e for each sequence are given in the fifth column and are plotted in figure 4 against pH. The last column gives the cumulative P_e in terms of phosphorus atoms adsorbed per exposed unit cell (i.e., taking 26 m^2/g of surface area to be comprised of (100) faces each with an area $= 9.44 \times 6.88 = 64.95$ Å^2). Negative values for P_e in table 2 reflect Ca/P ratios less than 1.67, for the overall dissolution reaction.

It is apparent from figure 4 that in sequences of decreasing pH, the cumulative P_e is linearly related to pH, as shown by the solid lines. The average slope of these lines is $-2.6 \pm 0.2 \times 10^{-5}$ mol P/g per pH unit. In the sequences of increasing pH the slopes of the cumulative P_e lines are somewhat variable and are less than those of sequences with decreasing pH. Their average slope is $-1.3 \pm 0.3 \times 10^{-5}$ mol P/g per pH unit. For the purpose of discussion, the mean of the slopes for the two types of sequences, -1.9×10^{-5} mol P/g per pH unit is taken to be a measure of the capacity of the surface to alter the stoichiometry of the overall reaction.

4. Discussion

4.1. Equilibrium With the Lattice

The results of the solubility experiments show that the OHAp behaved as a compound with definite thermodynamic properties even though the overall dissolution reactions were nonstoichiometric. This is shown by the constancy of the solubility product, $K_s = (Ca^{2+})^5(PO_4^{3-})^3(OH^-)$. With the exception of the four solutions excluded in the average K_s in table 1, the variation in calculated values for K_s is considered to be within the experimental errors. The potential diagram, figure 3, confirms this since the slope of the line indicates that the Ca/P ratio of the equilibrating solid was 1.66 ± 0.02 as compared to the theoretical value 1.67. Substantially all of the contaminating carbonate was leached out in the first equilibration in each series as indicated by the fact that the apparent electroneutrality unbalance is within experimental error in the succeeding solutions. This is further indication that the carbonate was adsorbed on the crystallites.

The average K_s reported here $6.3 \pm 2.1 \times 10^{-59}$ is intermediate to the values reported by Clark [9], 1.8×10^{-58} and Moreno et al. [2], $3.7 \pm 0.5 \times 10^{-58}$, and those reported by McDowell et al., [10], 2.6×10^{-59} and Wier et al. [11], 5.4×10^{-59}. The solubility products of McDowell et al., and Wier et al., agree most closely with the one reported here; it is noteworthy that all

TABLE 2. *Excessive phosphorus*

Sequence	pH	$\frac{Ca_f}{P_f - P_i}$	P_e per treatment mol/g × 10^5	Cumulative $-P_e$ mol/g × 10^5	Atoms per unit cell [a]
	6.882	[b] (−1.97)	0.94	0.94	0.17
	6.103	10.65	1.76	2.71	.48
	6.005	1.93	0.31	3.02	.53
	5.859	1.94	.44	3.46	.61
A	5.670	1.85	.37	3.84	.68
	5.497	1.81	.44	4.28	.76
	5.239	1.89	1.29	5.57	.98
	5.802	1.45	−0.67	4.90	.86
	6.338	1.07	−.76	4.14	.73
	6.777		1.40	1.40	.25
	6.411	11.92	0.86	2.26	.40
	4.807	2.19	4.02	6.28	1.11
B	5.825	1.28	−1.32	4.96	0.88
	6.389	1.09	−0.87	4.09	.72
	6.660	1.27	−.42	3.67	.65
	6.917	1.06	−.57	3.10	.55
	6.882		1.06	1.06	.19
	5.103	2.16	4.21	5.27	.93
	6.232	0.77	−2.2	3.25	.57
C	6.606	1.10	−0.65	2.60	.46
	5.995	3.41	−1.39	3.99	.70
	5.589	1.97	1.10	5.08	.90
	6.595	0.66	−1.52	3.57	.63
	6.826	1.06	−0.69	2.88	.33

[a] Calculated on basis that only (100) faces are exposed.
[b] The net of the dissolution-adsorption reaction was a removal of PO_4 from solution.

three of these values were obtained on precipitated OHAp samples that had been stabilized by heating in an aqueous medium. The sample of Moreno et al., had been treated at 1000 °C in a steam atmosphere; the high temperature may have enhanced the solubility somewhat as it did their sample heated in air ($K_s = 2.5 \times 10^{-55}$). The value reported by Clark was obtained with precipitates that had not been stabilized by prolonged hydrothermal treatment; an "as precipitated" sample used by Moreno et al. gave variable solubility products. A strict comparison with the values of Clark and Wier et al. is not possible because of differences in the ways the experimental data were treated to derive the solubility products.

An important conclusion obtained by Moreno et al. [2] is that well crystallized OHAp dissolves congruently (i.e., according to its lattice composition). In the present report, it is clearly shown that the overall dissolution reaction can be nonstoichiometric if the OHAp has a large surface area. This apparent nonstoichiometry influences the final composition of the solution, yet the final equilibrium is with the lattice and, therefore, stoichiometric and congruent as predicted from phase-rule considerations given in a subsequent paper [1] and shown by the results of Moreno et al. The apparently aberrant behavior of OHAp, reported by other investigators [12] is characterized by nonstoichiometry in the overall reaction and by an inability to establish a constant solubility product. In light of the results reported here, and by Moreno et al., this behavior must be attributed to the presence of impurities in the solid phases used by Rootare et al. [12], or to the lack of attainment of equilibrium, and not to a property of OHAp itself or its surface.

In view of the fact that tooth, bone, and many other apatitic products possess very large specific surface areas, even greater than the material studied here, the present work suggests that these systems may also follow ideal phase-rule behavior, even though consideration must be given to the nonstoichiometric behavior brought about by the composition of their surfaces. This brings us a step closer to being able to apply rigorous thermodynamic principles to the solubility of tooth and bone mineral.

4.2. Excessive Phosphorus, P_e

The interpretation for the "surface" equilibria given here is based on the idea [1] that, in contrast to the reaction with the "lattice," there are no restrictions on the stoichiometry of the reactions with the surface; the only limitations are that at equilibrium the chemical potentials of the components in the liquid and in the surface must be equal:

$$\mu_{Ca(OH)_2}(aq) = \mu_{Ca(OH)_2}(\text{surface}) \quad (7)$$

$$\mu_{H_3PO_4}(aq) = \mu_{H_3PO_4}(\text{surface}) \quad (8)$$

$$\mu_{H_2O}(aq) = \mu_{H_2O}(\text{surface}). \quad (9)$$

The chemical potentials of $Ca(OH)_2$ and H_3PO_4 vary oppositely along the solubility isotherm fixed by the equilibrium with the lattice [1], and in dilute solutions $\Delta\mu_{Ca(OH)_2} = -3/5\ \Delta\mu_{H_3PO_4}$. In the pH range studied here, 7 to 5, the change in the chemical potential of

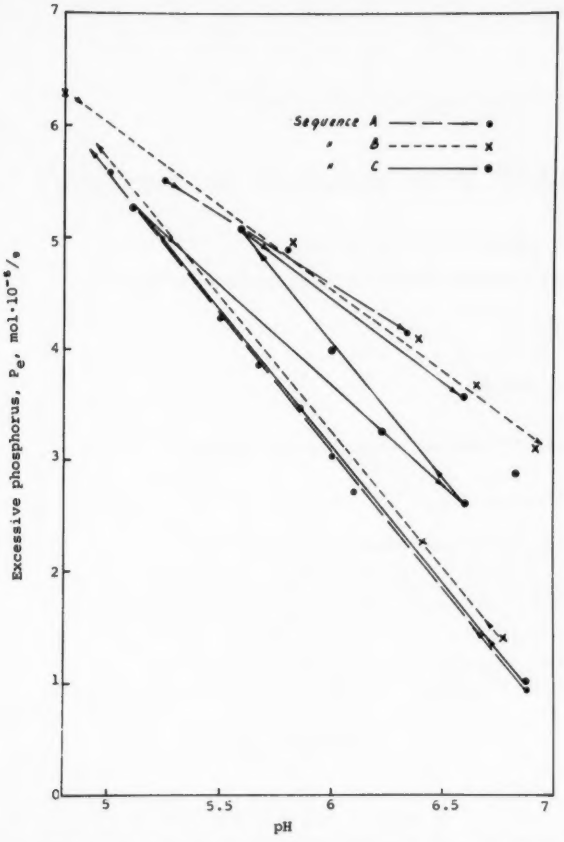

FIGURE 4. *Cumulative "excessive" phosphorus, P_e, versus pH of equilibrated solutions.*

$Ca(OH)_2$ is about -12 kJ/mol (2.9 kcal/mol) and that of H_3PO_4 is about 20 kJ/mol (4.8 kcal/mol). One might expect, therefore, that the surface would become impoverished in $Ca(OH)_2$ and enriched in H_3PO_4 in going from equilibrium at high pH to one at low pH. It is not possible, however, to translate this directly into the behavior of the calcium and phosphate ions because, in going from pH 7 to 5, the calcium and phosphate concentrations in solution both increase by a factor of about 100. Thus, the surface may be enriched in both calcium and phosphate on making this change. If we define calcium and phosphate enrichments of the surface as ΔQ_P and ΔQ_{Ca}, respectively, the quantity measured in the present experiments is $-P_e = \Delta Q_P - 3/5\ \Delta Q_{Ca}$. According to this definition, $-P_e$ could be either larger or smaller than ΔQ_P, depending on whether calcium is lost or gained, respectively, by the interface. In view of the fact that both calcium and phosphorus concentrations in solution increase with decrease in pH, it is reasonable to believe that both ΔQ_P and ΔQ_{Ca} are positive when the equilibration pH is decreased. Hence, the calculated cumulative $-P_e$ values are probably less than the actual ΔQ_P.

If the changes in the surface composition were completely reversible, the cumulative P_e lines in figure 4 should be described by the same line in both increasing and decreasing sequences of pH. The fact that they are not coincident indicates that some unidentified irreversible process was associated with these equilibrations. It appears unlikely that the irreversibility was caused by ionic impurities because the apparent electroneutrality unbalances, U, were generally very small. Even though the slopes for the two types of sequences differ, the average value quoted below still provides a reasonable estimate of the contribution by the surface to the nonstoichiometry of the overall dissolution reaction.

The mean value for the slopes in figure 4 yields $P_e = -1.9 \times 10^{-5}$ mol P/g per pH unit; this is equivalent to 0.4 P atoms per exposed unit cell per pH unit. Therefore, if the composition of the solution is changed along the isotherm from pH 7 to pH 5, each exposed unit cell would accumulate about 0.8 excessive phosphorus atoms (or lose 1.3 excessive calcium atoms). This is a large change, particularly when it is kept in mind that other nonlattice phosphorus atoms may have been accumulated concomitantly with calcium ions in a ratio 5/3.

The variability in composition (i.e., nonstoichiometry) of OHAp preparations has been a subject of considerable investigation and discussion [13]. The excessive phosphorus measurements given here can be used to estimate the extent to which surface phenomena under equilibrium conditions may contribute to variations in the overall composition of bone mineral. Taking again the value 0.8 atom per exposed unit cell for P_e, and the thickness of bone crystallites to be about 50 Å (i.e., about six unit cells), this corresponds to 1.6 phosphorus atoms for each 36 lattice phosphorus atoms, an apparent departure from stoichiometry of about 5 per cent. Although this may not appear to be a large change, actually it is half of the difference between the Ca/P ratio of OHAp, 1.67, and the ratio for $Ca_3(PO_4)_2$, 1.50.

5. References

[1] Brown, W. E., and Moreno, E. C., Thermodynamics of hydroxyapatite solubility (in preparation).
[2] Moreno, E. C., Gregory, T. M., and Brown, W. E., J. Res. Nat. Bur. Stand. (U.S.), 72A (Phys. and Chem.), No. 6, 773–782 (Nov.–Dec. 1968).
[3] Farr, D. T. (Ed.), T.V.A. Chem. Eng. Report No. 8 (1950).
[4] Fowler, B. O., Moreno, E. C., and Brown, W. E., Arch. Oral Biol. **11**, 477 (1966).
[5] Brabson, J. A., Dunn, R. L., Epps, E. A., Jr., Hoffman, W. M., and Jacob, K. D., J.A.O.A.C. **41**, 517 (1958).
[6] Bates, R. G., J. Res. Nat. Bur. Stand. (U.S.), 66A (Phys. and Chem.), No. 2, 179–184 (Mar.–Apr. 1962).
[7] Kielland, J., J. Amer. Chem. Soc. **59**, 1675 (1930).
[8] Brown, W. E., Soil Sci. **90**, 51 (1960).
[9] Clark, J. S., Can. J. Chem. **33**, 1696 (1955).
[10] McDowell, H., and Brown, W. E., (IADR Abstract #340, 1969).
[11] Wier, D. R., Chien, S. H., and Black, C. A., Soil Sci. **111**, 106 (1971).
[12] Rootare, H. M., Deitz, V. R., and Carpenter, F. G., J. Colloid Sci. **17**, 179 (1962).
[13] Brown, W. E. (Gordon and Breach, Publishers). (In preparation.)

(Paper 77A1–759)

JOURNAL OF RESEARCH of the National Bureau of Standards—A. Physics and Chemistry
Vol. 77A, No. 1, January–February 1973

Pyrolysis of Anionic and Thermally Prepared Polystyrenes

Leo A. Wall,* Sidney Straus, Roland E. Florin

Institute for Materials Research, National Bureau of Standards, Washington, D.C. 20234

and

Lewis J. Fetters

Department of Polymer Science, The University of Akron, Akron, Ohio 44325

(August 11, 1972)

The changes in molecular weights, their distributions, and initial rates have been measured, for a series of polystyrenes prepared by thermal and anionic procedures. The information obtained and previous results can be explained to a very large extent by a kinetic chain decomposition comprised of competing end and random initiation, depropagation, intra- and intermolecular transfer and termination by combination.

Key words: Anionic polystyrene; molecular weight distributions; molecular weights; thermal polystyrene; polymers; polystyrene degradation; pyrolysis; thermolysis.

1. Introduction

For thermal polystyrenes the ratio of rate constants for random to end initiation has a value of 3×10^{-4} initially. The present treatment assumes this value is constant with conversion. On the other hand the anionic polymers initiate at random in the limit of zero time, after which end-initiation begins to occur as the number of ends increases. The intermolecular transfer constant, zip length and kinetic chain length are dependent on the steady state radical concentration and are functions of the molecular weight. Their values, at the molecular weights present when the pyrolytic weight loss exceeds 5 percent, agree well with earlier estimates.

Some time ago a theory [1, 2][1] was developed for the thermal degradation of those polymers that undergo pure chain bond ruptures and hence in an open system are completely volatilized. The mechanism assumed was comprised of four elementary free radical processes: initiation, propagation, intermolecular transfer, and termination. The intent of the development was to provide a framework for the elucidation of the mechanisms of polymer degradation. For this and mathematical reasons the treatment assumed the initial polymer to be monodisperse. The change in molecular weight distribution [3, 4] observed during degradation of an initially monodisperse polymer would be a quite sensitive indicator of the nature of the mechanism in many cases. Another limitation also for mathematical reasons was the restriction of the development to termination by disproportionation. At the time, long kinetic chain lengths were anticipated in many polymer decompositions [5, 6] and for such situations the method of bimolecular termination is of small consequence. Also, termination can be actually effectively first order if the degree of polymerization is shorter than the zip [1, 2] or kinetic chain length. A recent study of the decomposition of polytetrafluoroethylene [7] has, however, demonstrated that the mechanism for this polymer has a short zip length with termination mainly by combination. Evidence is accumulating that very short kinetic chain lengths are quite common.

One criticism of the earlier treatment [1, 2] that is not totally valid since some monodisperse polymers can now be prepared by appropriate polymerization techniques, has been that existing polymeric materials are polydisperse. Since the assumption that a "most probable" distribution exists in many polymers and is maintained throughout the degradation process simplifies the theoretical treatment, several efforts in this area were made [8, 9]. It is also well known that random degradation in a closed system produces and maintains a most probable distribution and often only a small amount of a random component in the mechanisms can be the predominant factor in determining the distribution.

In our opinion, treatments in which the distribution is assumed for the initial and degrading polymers

*Deceased.

[1] Figures in brackets indicate the literature references at the end of this paper.

discard with that assumption much of their utility and value as a tool for the study of degradation mechanisms. These mechanisms are so varied and complex that every possible variable may be needed for the deduction of the details of the intermediate processes from experiments. For theoretical and experimental details on the problem of polymer degradation see more complete reviews [10, 11, 12].

The work to be reported here is of importance for the questions raised in the above discussion and for the mechanism of polystyrene degradation. The degradation of polystyrene like the polymerization of styrene has been studied extensively and even from the most excellent of summaries [12] the situation appears confused. Until recently the shapes of the experimental thermal volatilization curves for polystyrene have not been produced by a fully a priori theory. However, with the use of computer evaluation the original theory [1, 2] was shown [13] to be able to nearly reproduce the experimental rate and molecular weight behavior. The results indicate that intermolecular transfer, end initiation, and zip lengths of the order of 5 are operative. Close comparison of theory with experiment did reveal certain imperfections, which do not invalidate the above conclusions but can be used to elucidate finer and more elusive details of the mechanism. An important discrepancy was the existence of somewhat higher values for the viscosity average degree of polymerization of the degraded polymer at conversions of 20 to 60 percent, than predicted from the level of the theoretical values for the weight average degree of polymerization. In the previous work [13] the distribution computed for the mechanism deduced from the then available experimental rate and molecular weight data was presented in terms of plots of the ratio of weight to number average degree of polymerization as a function of conversion (see fig. 1). It is seen that the initially monodisperse polymers rapidly approach the value of 2 initially and the higher their initial size the more rapidly the value increases. Since the polymers are volatilizing the ratio $\bar{P}_w/\bar{P}_n$ must return to one at complete conversion (C → 1). The dashed sections of the curves were drawn to this limit intuitively. The full lines are computer calculated [13]. The surprising result is that with even the highest initial $\bar{P}_n$ of 1643 the "most probable" distribution is not achieved. Also the downward slope of the ratio above 20 percent conversion suggests that even if it started at the value of two it would decrease appreciably during the degradation probably to a value of 1.8. One reason the higher curves drop off is that the theory assumes that all species with a $\bar{P}_n$ lower than 9 evaporate instantly which narrows the distribution. Otherwise the curves depend on the competition between the intermolecular transfer, a randomizing process, and the volatilization of material.

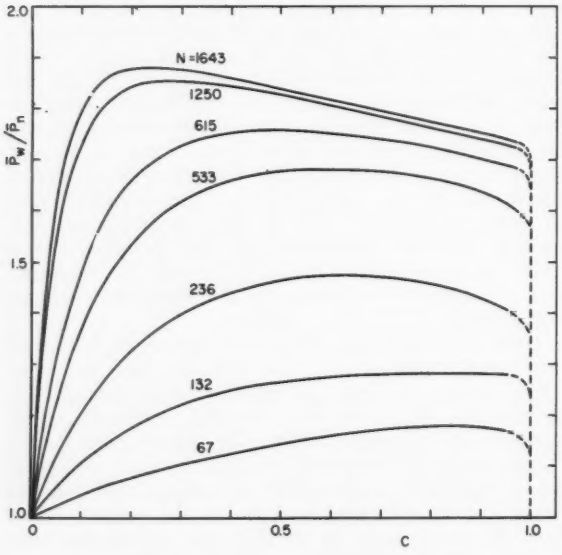

FIGURE 1. *Theoretical variation of the ratio of weight to number average degrees of polymerization as a function of conversion and showing the influence of initial number average degree of polymerization, given on curves, for a mechanism consisting of end initiation transfer, depropagation [13] and termination by disproportionation.*

A recent major study [14, 15, 16] of the decomposition of polystyrene utilized poly (α-methylstyrene) [14] as catalyst for the polystyrene degradation, anionically prepared polystyrene with specifically formed thermolabile structures [15] and carbon 14 labeled polystyrene [16]. The results of this very extensive experimentation raise many points but the most interesting aspects are: (1) the confirmation of short zip lengths of approximately 3, (2) 1.2 intermolecular transfer steps per radical formed, (3) strong evidence for termination by combination with the possibility that the cage effect may tend to make termination kinetically first order. In this article we shall present evidence which is in the main compatible with the above items. Short zip lengths and intermolecular transfer are in our opinion now well established in polystyrene.

2. Experimental Data

In this work a series of monodisperse polystyrenes with number average molecular weights in the range of 1,000 to 200,000 were prepared anionically [17] and studied. The two National Bureau of Standards Standard Reference Polymers 705 and 706 were also studied in more detail than previously [13].

Rate of volatilization experiments were carried out using 10 mg sample in high vacuum and a recording electrobalance.

For molecular weight measurements, approximately 400 mg samples were pyrolyzed in a high vacuum apparatus to the desired extents of conversion and the molecular weights of the residue determined by both light scattering and membrane osmometry.

3. Polymer Characterization

The molecular weight averages were determined on commercial instruments. Number-average molecular weights were determined on Hewlett-Packard 501 and 502 osmometers.[2] Low-molecular weight material was characterized on the Hewlett-Packard vapor pressure osmometer 301. The light scattering was done on the Bausch and Lomb PGD instrument. The number-average molecular weights were determined in toluene at 37 °C with gel cellophane 600 membranes. From the linear plot of π/c versus concentration, the molecular weights were derived. Previous experience with near monodisperse polystyrene had shown that number average molecular weights as low as 5×10^3 could be determined on these high-speed membrane osmometers with no diffusion of solute through the membrane. The permeation limit of the membranes was checked in the following fashion. A series of low-molecular weight polystyrenes were synthesized by anionic polymerization [18] and were characterized on the vapor pressure osmometer. They were then recharacterized on the high speed membrane osmometer. The predicted osmotic pressures were obtained at all concentrations. The conclusion was drawn that the membranes used in this work had permeation limits of 5×10^3 or less. Similar conclusions have been reached elsewhere [19]. Thus, the number-average molecular weights reported herein are believed not to be vitiated by permeation of low molecular weight solute through the membrane.

The weight-average molecular weights were determined at 25 ± 0.5 °C in benzene. Solutions were filtered twice prior to use through solvent resistant filters. Millipore or Selas Flotronics membranes of 0.45 μm pore diameter were used. Measurements were made on four different concentrations between the angles of 30 and 150°. Unpolarized light of 546 nm was used with the value of 15.8×10^{-6} cm^{-1} being adopted for Rayleigh's ratio. The value of dn/dc was 0.106 ml g^{-1} [20, 21]. The dn/dc values for several partially degraded polystyrenes were checked, at 25 ± 0.01 °C, in a commercial differential refractometer, Phoenix Precision Instrument Company. These dn/dc values were identical to the published values [20, 21].

The weight-average molecular weights of some of the undegraded samples were determined by gel permeation chromatography measurements. For molecular weights up to 10^3 a set of five columns in the commercial instrument, The Waters Ana-Prep GPC, were used. These columns had permeability ranges of 50–80, 80–100, 100–350, 350–700, and 700–2000Å (angstroms). The five columns used for the higher molecular weight samples were those with permeability ranges of $2–5\times10^3$ Å, two columns with $5–15\times10^3$ Å, $1.5–5\times10^4$ Å and $5–15\times10$ Å. These columns were calibrated with characterized polystyrene samples of both narrow and broad molecular weight distributions. The solvent used was tetrahydrofuran at a temperature of 30 °C.

The polystyrenes used in this study are listed in table 1. The first column gives for the anionically

[2] Certain commercial equipment, instruments, or materials are identified in this paper in order to adequately specify the experimental procedure. In no case does such identification imply recommendation or endorsement by the National Bureau of Standards, nor does it imply that the material or equipment identified is necessarily the best available for the purpose.

TABLE 1. *Polystyrenes used in this investigation*

Number average molecular weight, $\bar{M}_n$				$\bar{M}_v$ [22]	$\bar{M}_w$ (GPC)
Chemical	Vapor pressure osmometry	Membrane osmometry	Values used in plots		
Anionic					
1,150	1,100		1,100		
2,250	2,450		2,450		
3,900	3,700		3,700		
5,300	5,300		5,300	8,500	7,200
10,300	11,400	12,000	11,400	12,500	12,000
16,800		22,000	20,000	20,000	22,000
20,800		25,000	22,500	22,500	25,000
		37,000	37,000	38,000	(38,000 L.S.)
43,000		49,000	48,500	48,500	50,000
54,000		73,000	73,000	75,000	75,000
(NBS 705)		170,900	170,900	180,000	(179,000 L.S)
Thermal					
(180 °C)		90,000	90,000		115,000
(NBS 706)		130,000	130,000	272,000	(272,000 L.S.)
(120 °C)		152,000	152,000		230,000
(60 °C)		254,000	254,000		330,000

(L.S. = Light Scattering)

prepared samples the number-average molecular weight estimated from the ratio of catalyst to monomer used. The number in parenthesis gives the temperature of polymerization for the thermally prepared polymer or identifies one of the two standard samples issued by the National Bureau of Standards. The fourth column lists the number-average molecular weight values used for plotting and calculations described here.

The experimental values for M_n (vapor pressure) and M_w (GPC) are estimated to be within ± 5 percent of the true value and for M_n (membrane) within ± 7 percent. The viscosity averages, M_v, were calculated from the relation [22].

$$[\eta]_{\text{benzene}}^{30\ ^\circ\text{C}} = 8.5 \times 10^5 / M_v^{0.75}$$

This relation is not accurate for very low molecular weights. Thus, the two lowest M_v-values and in particular the 8,500 values are excessively high.

4. Results

4.1. Molecular Weight Change With Pyrolysis

In figure 2 we show the experimental variation of both the weight average, $\bar{P}_w$, and number average, $\bar{P}_n$, degrees of polymerization for two initially monodispersed polystyrenes. The upper curves are for the sample having an initial number-average molecular weight of 170,900. The lower curves are for the polymer having an initial number-average molecular weight of 37,000. The sharp initial drop of the $\bar{P}_n$ and $\bar{P}_w$ for the polymer with the higher initial values indicate a random rupture process which we attribute to intermolecular transfer. It is evident that the $\bar{P}_w/\bar{P}_n$ ratio does not become two even at conversion of 70 percent. As might be expected this ratio increases with conversion much less for smaller polymer than for the larger. Qualitatively their behavior or the pattern of the results is in the direction anticipated from figure 1 except that the $\bar{P}_w/\bar{P}_n$ ratios are appreciably smaller. In figure 3 there is similar data for an initial polydisperse thermally polymerized polystyrene with an initial $\bar{P}_w/\bar{P}_n$ ratio of 2.1. It is evident from this figure that the ratio is decreasing and the distribution is narrowing as the degradation proceeds. Table 2 presents the basic data used for figures 2 and 3.

In figure 4 we present a plot of the variation in the $\bar{P}_w/\bar{P}_n$ ratio for these three polymers as a function of conversion that is volatilization. It seems clear from this plot that provided the initial molecular weight is sufficiently large the ratio tends to the value of 1.5 very quickly as degradation proceeds. From the theoretical curves in figure 1 we expect a slow narrowing of the distribution if the samples were initially polydisperse. Samples of the polydisperse polymer that were pyrolyzed to about 0.5 conversion values were also studied with gel permeation chromatography (GPC). They were found to have smooth monomodal

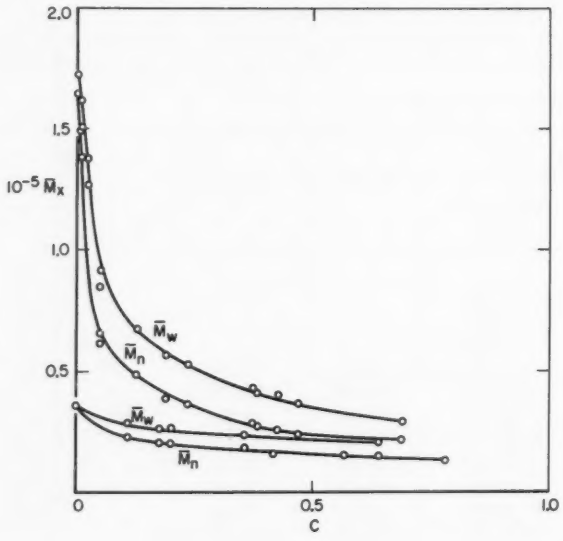

FIGURE 2. *Variation of the weight and number average molecular-weights of polystyrene during thermal degradation at 300 °C.*

Upper curves, NBS Sample 705, monodisperse anionic polystyrene, initial $\bar{M}_n = 170{,}900$, initial $\bar{M}_w/\bar{M}_n = 1.06$
Lower curves monodisperse anionic polystyrene initial $\bar{M}_n = 37{,}000$. Initial $\bar{M}_w/\bar{M}_n = 1.03$.

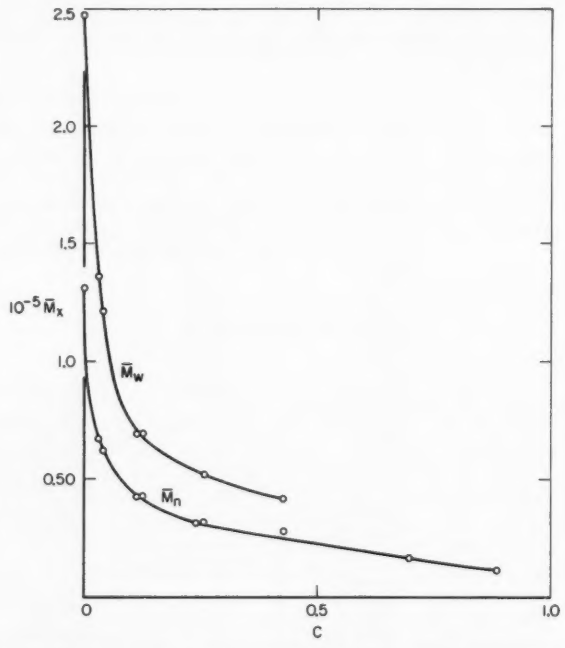

FIGURE 3. *Variation of the weight and number average molecular weight of polystyrene during thermal degradation at 300 °C.*

NBS Sample 706. Initial $\bar{M}_n = 130{,}000$, initial $\bar{M}_w/\bar{M}_n = 2.1$

TABLE 2. *Thermal degradation of polystyrenes, number average, M_n and weight average, $\bar{M}_w$ molecular weights after a given loss of weight for the sample*

Polymer	Weight loss %	$10^{-4}\bar{M}_n$	$10^{-4}\bar{M}_w$
Monodisperse	10.9	2.4	3.0
$\bar{M}_n$ (0) = $3.7 \times 10^{+4}$	17.6	2.1	2.7
	20.1	2.1	2.8
	35.6	1.9	2.5
	41.8	1.7	.....
	56.9	1.7	.....
	64.1	1.6	2.2
	78.2	1.4	.....
Monodisperse	0.65	15.4	16.8
$\bar{M}_n$ (0) − $17.09 \times 10^{+4}$	0.93	14.4	15.6
NBS 705	2.3	13.2	14.3
	4.9	6.4	8.8
	5.0	6.9	9.5
	12.8	5.1	7.0
	18.9	4.0	5.9
	23.5	3.8	5.5
	37.4	3.0	4.5
	38.3	2.9	4.3
	42.6	2.8	4.2
	47.0	2.5	3.8
	69.0	2.3	3.1
Polydisperse	3.1	7.0	14.1
$\bar{M}_n$ (0) = $13.0 \times 10^{+4}$	4.0	6.5	12.6
NBS 706	11.2	4.4	7.2
	12.5	4.4	7.2
	23.8	3.2	.....
	25.6	3.3	5.4
	42.7	2.9	4.4
	69.8	1.7	.....
	88.8	1.2	.....

distributions with $\bar{P}_w/\bar{P}_n$ ratio of 1.7. However, it has been found [23, 24] that these ratios when obtained from GPC are in general larger than when obtained from light scattering and osmometry by about 10 percent [23] which would bring our GPC result into good agreement with the values shown in figure 4. A 1.5 P_w/P_n ratio has also been reported [25] for monodisperse polystyrene that has been mechanically degraded in the absence of oxygen.

Molecular weight measurements were carried out on other pyrolyzed monodisperse polymers listed in table 1. For theoretical reasons our particular interest was to ascertain the behavior of low molecular weight materials (see fig. 5). The results are similar to those obtained in an earlier study [13] on fractions of thermally polymerized polymers, in that with low initial $\bar{M}_n$ values the molecular weight remains nearly constant through conversions greater than 50 percent. For example, the 5,300 $\bar{M}_n$ sample shows about a 15 percent decrease in $\bar{M}_n$ at 70 percent conversion. From earlier work [13] on fractions of thermally prepared polymer, the data on a 7,000 $\bar{M}_n$ sample

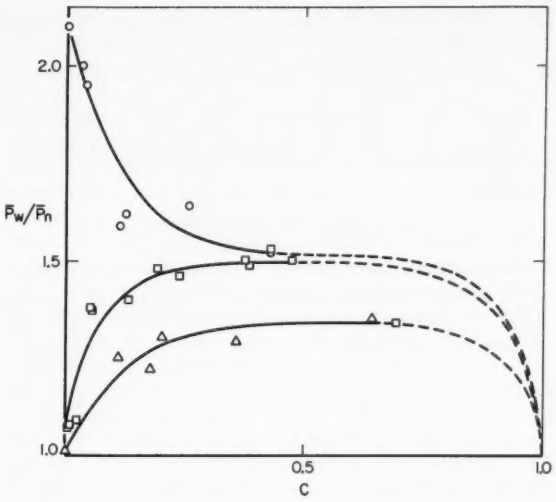

FIGURE 4. *Variation of the ratio of weight to number average degrees of polymerization of polystyrene during thermal degradation at 300 °C.*

○, NBS Sample 706, polydisperse
Initial $\bar{P}_n = 1.26 \times 10^3$
□, NBS Sample 705, monodisperse
Initial $\bar{P}_n = 1.64 \times 10^3$
△, Polystyrene, monodisperse
Initial $\bar{P}_n = 3.58 \times 10^2$

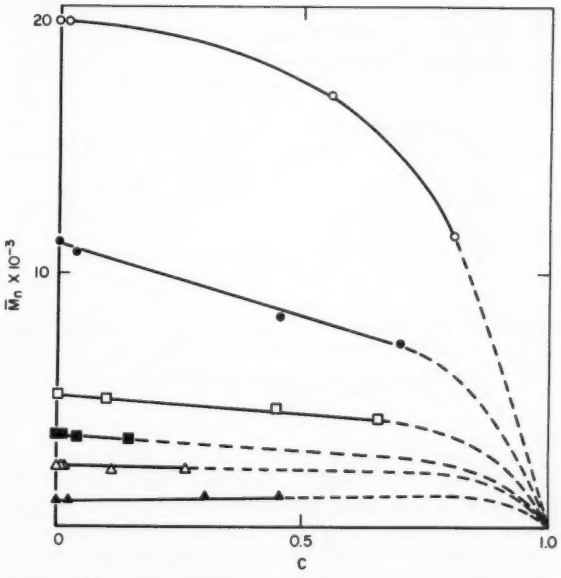

FIGURE 5. *Thermolysis of monodisperse polystyrenes at 300 °C.*

Variation of Number Average Molecular Weight (vapor pressure osmometry) with conversion.

	M_n(0)
○,	20,000
●,	11,400
□,	5,300
■,	3,700
△,	2,450
▲,	1,100

was extrapolated to show a 29 percent molecular weight decrease at 70 percent conversion. For the two types of polymers, nearly identical behavior is therefore exhibited in their molecular weight dependence on conversion at low initial molecular weights. It is noted that at 70 percent conversion the molecular weights of the two polymers are essentially the same.

4.2. Rate of Volatilization

An extensive comparison of the rate of volatilization of the monodispersed polystyrene with those of thermal polymers and their fractions [13] was made. With high molecular weight polymers the rates were essentially independent of the type of polymer, anionic or thermal. In previous work [13] it had been seen that beginning at $\approx$ 25,000 $\bar{M}_n$ the typical maximum in the rate at $\approx$ 40 percent conversion was eliminated. With the anionic polymers studied here a maximum in the rate versus conversion curves persists down to 5,300 $\bar{M}_n$ and below. In figure 6 we show rate for 48,000 $\bar{M}_n$ and 5,300 $\bar{M}_n$ anionic polymers. The curve for the 48,000

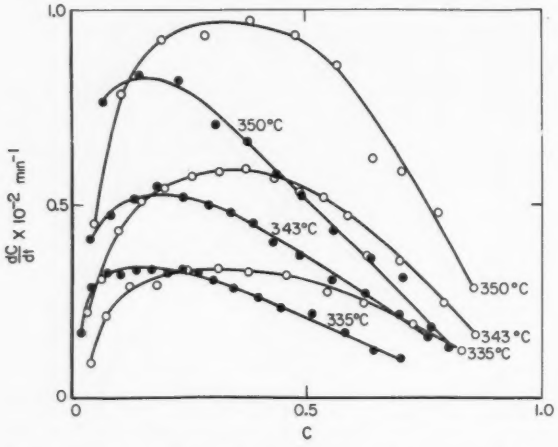

FIGURE 6. *Thermolysis of monodisperse polystyrenes, variation of the rate of volatilization with conversion.*

$M_n(0)$	Activation energy, kcal/mol, based on maximum rate.	
○,	48,500	51
●,	5,300	45

$\bar{M}_n$ polymer is nearly typical of all polystyrenes of higher molecular weights. However, with the anionic polymers of less than 48,000 $\bar{M}_n$, the maxima shift to lower conversion and the curves exhibit behavior theoretically predicted for simple random scission. At such low $\bar{M}_n$ values thermal polymer has high initial rates decreasing with conversion [13].

4.3. Initial Rates

In a typical isothermal volatilization measurement the behavior below 5 percent conversion is usually ignored Heat-up time for the sample and the loss of volatile impurities interfere with the determination of the initial rates, which are therefore not typical of the polymer at a known temperature. On the other hand, the decomposition is believed to be initiated at the chain ends and hence the initial rates of volatilization should show a dependence on the number of chain ends or equivalently the reciprocal number average molecular weight.

In this work we very carefully looked at the rates in the range of 0–5 percent conversion. This entailed making runs at lower temperatures of 287, 300, and 310 °C. For the monodisperse and anionically prepared polymers the initial rates as a function of conversion are shown in figure 7. It is seen that no straight line extrapolation to zero conversion is possible since the rates rise with continually decreasing slopes in the

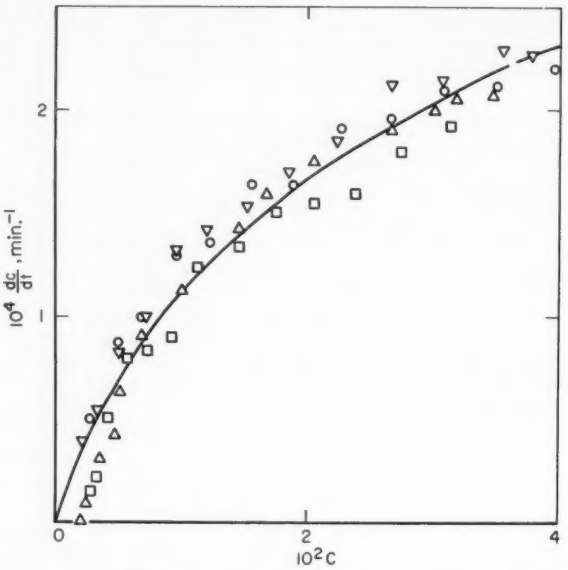

FIGURE 7. *Thermolysis of anionic polystyrenes at 300 °C, variation of rate in the low conversion range, effect of number average molecular weight.*

$M_n(0)$	
▽,	22,500
○,	48,500
△,	170,000
□,	230,000

manner shown. The rates at zero conversion are evidently zero and independent of the molecular weight of sample. As the process of decomposition proceeds an effect of molecular weight develops such that the lower molecular weight polymers have higher rates.

For thermally prepared polystyrenes the rates at these low conversions are essentially independent of conversion and are easily extrapolated back to zero conversion as shown in figure 8. The initial rates are strongly dependent on the reciprocal of the molecular weights of the samples. A plot of the log of these initial rates as a function of the logarithm of the reciprocal number average molecular weights of the sample gave straight line relations with slopes of 0.24, 0.27, and 0.28 for measurements at the respective temperatures, 310, 300, and 287 °C.

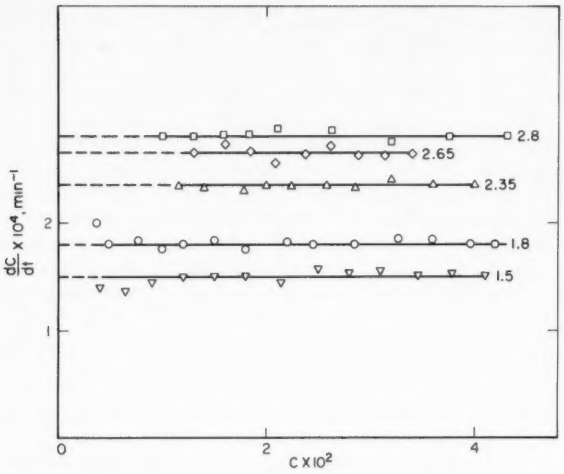

FIGURE 8. *Thermolysis of thermal polystyrenes at 300 °C, variation of rate in the low conversion range, effect of number average molecular weight.*

$\bar{M}_n$
□, 90,000
◇, 130,000
△, 152,000
○, 254,000
▽, 900,000

5. Discussion

5.1. Theory

The mechanism of decomposition of carbon chain polymers has been most successfully interpreted in terms of free radical mechanisms [10, 11, 12]. However, it can be said that complete elucidation of a given polymer has only been approached in the case of polytetrafluoroethene [7, 26]. Exact quantitative treatment of polymer decomposition mechanisms is difficult due to the complexity of the mechanisms in the condensed phase in which they occur and the large effort required for obtaining an adequate number of reliable measurements. Our objective here is to obtain the best quantitative fit to the observed measurements based on the assumption of a mechanism with a minimum number of elementary steps. We may and will neglect processes known to occur, depending on their importance relative to key assumptions. Although in previous work [13, 27] computers were utilized for quantitative treatment of thermal decomposition mechanisms, we have in this work considered numerous possible special cases. The advantage in general is that with the steady state assumption many cases are amenable mathematically, giving the desired relations in closed form.

The mechanisms considered initially in our effort to treat the mechanism of thermal decomposition of polystyrene encompass all of the following possible elementary reactions, which are symbolically depicted. The number of polymer molecules with i units in the chain is represented as Q_i and the number of radicals with i units as R_i. Monomer is represented by M although Q_i could be an alternative representation. Bimolecular rate terms have the volume of the polymer, V, in the denominator since R_i and Q_i are numbers not concentrations.

Initiations		
random	$Q_i \longrightarrow R_{i-j} + R_j$	$k_{ir} \sum_L^\infty (i-3)Q_i$
end	$Q_i \xrightarrow{e<<L} R_{i-e} + R_e \uparrow$	$2k_{ie} \sum_L^\infty Q_i$
specific interior	$Q_{i+j} \longrightarrow R_i + R_j$	$k_{is} \sum_L^\infty Q_{i+j}$
Propagation	$R_i \longrightarrow R_{i-1} + M \uparrow$	$k_2 \sum_L^\infty R_i$
Transfer		
intramolecular	$R_i \longrightarrow Q_{i-j} \uparrow + R_j$	$k_3' \sum_L^\infty R_i$
intermolecular	$R_i + Q_j \longrightarrow Q_i + R_j'$	$k_3 \sum_L^\infty R_i \sum_L^\infty jQ_j / V$
	$R_j' \xrightarrow{>>k_3} Q_{j-k} + R_k$	

Termination		
disproportionation	$R_i + R_j \longrightarrow Q_i + Q_j$	$\dfrac{k_{4d}\sum_{L}^{\infty} R_i^2}{V}$
combination	$R_i + R_j \longrightarrow Q_{i+j}$	$\dfrac{k_{4c}\sum_{L}^{\infty} R_i^2}{V}$
cage disproportionation	$[R_i + R_j] \longrightarrow Q_i + Q_j$	$k_{[4d]}\sum_{L}^{\infty} R_i$
cage combination	$[R_i + R_j] \longrightarrow Q_{i+j}$	$k_{[4c]}\sum_{L}^{\infty} R_i$
evaporative (p-type)	$R_L \xrightarrow{i<L} R_i \uparrow + M \uparrow$	$k_2 R_L$
evaporative (t-type)	$R_i \xrightarrow{j<L} Q_{i-j} + R_j \uparrow$	$\phi k_3' \sum_{L}^{\infty} R_i$

where ϕ is a fractional efficiency factor arising from the fact that the radical precursor may decompose in several ways and the vertical arrows indicate key possibilities for volatile production.

With transient free radical mechanisms the minimum number of steps comprising a mechanism would include one initiation and one termination process. Since we list three initiation and six termination processes this means eighteen possible mechanisms. Inclusion of one of the propagation or transfer steps produces 54 additional mechanisms for a total of 72. Any combination of the processes is possible so that the total number of mechanisms is very large. On the other hand the kinetic behaviors possible are much fewer since the kinetic form of many of the initiation and termination steps is similar.

Since there are twelve processes listed above any complete mathematical treatment would lead to such complex and intractable equations and such a large number of parameters that even with the assistance of computers an understanding of the model and an elucidation of a mechanism would be a long and tedious task.

We choose therefore to explore the possibilities with somewhat intuitive simplifications. Our primary measurement is the weight loss of the polymer. Hence the conversion, C is defined as:

$$C = 1 \frac{W(t)}{W(0)} \tag{1}$$

where $w(0)$ is the initial weight of sample and $w(t)$ the weight at time, t. The rate of conversion is then:

$$\frac{dC}{dt} = \frac{m}{W(0)} \frac{d\text{“}M\text{”}}{dt} = \frac{m}{w(0)} \left[k_2 \sum_{L}^{\infty} R_i(t) + d \frac{\sum_{2}^{L-1} i Q_i(t)}{dt} \right] \tag{2}$$

where “M” symbolizes total volatiles in terms of monomer segments, m is the molecular weight of monomer, and L is the smallest degree of polymerization that must chemically decompose in order to vaporize. For polystyrene the k_2 term represents at least 42 percent of the process since the monomer yield is about 42 percent and is nearly independent of conversion in the 0 to 75 percent conversion range. The second term on the right represents the production of nonmonomer, which can arise in a variety of ways depending on the assumed mechanism. It should be noted that intramolecular transfer may be expected to produce volatiles and if so would have the same kinetic form as propagation. Since the number average molecular weight is also experimentally available, the variation with time of the number of polymer molecules is an important aspect of the problem. With the use of a steady state approximation for the number of radicals one obtains:

$$\frac{dQ(t)}{dt} = \frac{k_3 R(t)\,[P_n(t) - 1]\,Q(t)}{V(t)} + \frac{k_{4d} R(t)^2}{V(t)} + k_{[4d]} R(t) + 1/2\,\phi k_3' R(t) - k_{tr} Q(t) - 1/2\,k_2 R_L(t) - \sum_{1}^{L-1} f_i Q_i(t). \tag{3}$$

Here $Q(t)$ represents $\sum Q_i(t)$ the sum of all the molecules in the reacting system, $R(t)$ is the same for all radicals and $V(t)$ is the volume of the system from which volatiles are escaping.

These quantities are functions of time since Q and R are in units of moles, not concentrations. From eq

(3) it is seen that $Q(t)$ is increased by intermolecular transfer and disproportionation steps and decreased by end initiation and evaporative processes. The factors f_i are the probabilities of evaporation of the particular species. In this discussion these evaporative processes will be ignored on the assumption that their effect is small since throughout the conversion range of 0 to 80 or 90 percent the molecular weight of the polymer remains quite large. The molecular weight changes and rates of volatilization as functions of conversion are similar for both monodisperse (anionic) and polydisperse (thermal) polystyrenes of high molecular weight. Thus no distinct indications of a fundamental difference in mechanism of decomposition of these type of polymers has been obtained previously. However the rate behaviors at low conversions, shown in figures 7 and 8, clearly point out a strong difference in their initiation processes. Therefore we shall discuss the two types of polymers separately.

5.2. Thermal Polystyrenes

If volatiles had been produced by the k_{1e} process then the initial rates should depend on the first power of the reciprocal molecular weight. Production of volatiles by the k_2 step and bimolecular termination would give with end initiation a 0.5 power dependence and with random initiation a zero power dependence. The observed dependence, figure 8, for the thermal polymers, at three different temperatures was from 0.24 to 0.28. This result, plus the character of the initial rates for the anionic polymer, figure 7, and the presence of a maximum in the rate curve for the 5,300 M_w anionic polymer, figure 6, strongly suggests that random initiation is occurring in competition with end initiation.

The molecular weight distribution data, figure 4, indicates termination by combination. Other coupling processes such as alkylation of the phenyl group via radical addition reactions could explain the narrowing of the molecular weight distribution. However, the solution viscosity of pyrolyzed polymers does not indicate the branching one might then expect. As will be seen below our results are incompatible with suggestions [12, 16] that termination is first order.

Transfer and propagation are evident from earlier work [13, 16]. We therefore use these five elementary steps for evaluating the result on the thermal polystyrenes. Although our treatment gives each molecule a particular probability for random and end initiation, the actual mechanism probably involves a specific number of end initiating sites on particular molecules.

5.3. Rate of Volatilization

All weight loss is assumed to arise from the depropagation of large radicals

$$\frac{dC}{dt} = \frac{m}{W(0)} \frac{dM}{dt} = \frac{m}{W(0)} k_2 R. \qquad (4)$$

The steady state number of radicals is obtained from

$$2k_{4c} \frac{R^2(t)}{V(t)} = 2k_{1r}\bar{P}_n(t)Q(t) + 2k_{1e}Q(t) \qquad (5)$$

$$R(t) = \left[(1 + \gamma \bar{P}_n(t)) \left(\frac{k_{1e}}{k_{4c}} \frac{\rho}{m} \frac{1}{\bar{P}_n(t)} \right) \right]^{1/2} V(t) \qquad (6)$$

where $\gamma = k_{1r}/k_{1e}$, $\bar{P}_n$ the number average degree of polymerization and ρ the density of the polymer. From eqs (4) and (6) it follows that:

$$\frac{dC}{dt} = k_2 \left(\frac{k_{1e} m}{k_{4c} \rho} \right)^{1/2} \left(\gamma + \frac{1}{\bar{P}_n(t)} \right)^{1/2} \qquad (1-C)$$

$$= \frac{k_{1e}}{\beta} \left(\gamma + \bar{P}_n(t)^{-1} \right)^{1/2} \qquad (1-C) \qquad (7)$$

and at $C = 0$

$$\left(\frac{dC}{dt} \right)_0^2 = k_2^2 \left(\frac{k_{1e}}{k_{4c}} \frac{m}{\rho} \right) \left(\gamma + \frac{1}{\bar{P}_n(t)} \right)$$

$$= (k_{1e}/\beta)^2 \left(\gamma + \bar{P}_n^{-1}(t) \right) \qquad (8)$$

Thus the square of the initial rate is a linear function of $\bar{P}_n^{-1}$. In figure 9 we have plotted the squares of the initial rates at three different temperatures as a function of $\bar{P}_n^{-1}(t)$ and it is seen that data is quite compatible with eq (8). From the equation it follows that the ratios of the intercept to the slope yield value of $\gamma = 3 \times 10^{-4}$ the ratio of the random initiation constant to the end initiation constant.

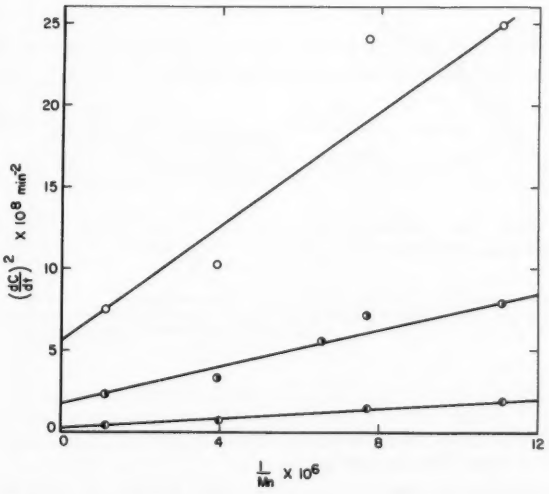

FIGURE 9. *Thermolysis of thermal polystyrenes, variation of the square of initial rate with reciprocal number average molecular weight according to eq (8).*

○, 310 °C ◑, 300 °C ◕, 287 °C

5.4. Molecular Weight Relation

The mechanism assumed leads to the following differential equation for the variation of polymer molecules with time.

$$\frac{dQ}{dt}=\frac{k_3R(t)\,[\bar{P}_n-1]\,Q(t)}{V(t)}+\frac{k_{4c}R(t)^2}{V(t)}$$
$$-[k_{1r}\bar{P}_n(t)-3]Q(t)-2k_{1e}Q(t). \qquad (9)$$

Neglecting the quantities 1 and 3 in comparison with $\bar{P}_n(t)$, it follows from eq (5) that eq (9) reduces to:

$$\frac{dQ}{dt}=\frac{k_3R(t)\bar{P}_n(t)Q(t)}{V(t)}-k_{1e}Q(t). \qquad (10)$$

Dividing eq (10) by eq (4) produces:

$$\frac{dQ}{dC}=\frac{w_0}{m}\left[\frac{k_3\bar{P}_n(t)Q(t)}{k_2V(t)}-\frac{k_{1e}Q(t)}{k_2R(t)}\right]. \qquad (11)$$

Upon inserting the relation for the steady state number of radicals obtainable from eq (6), eq (11) becomes:

$$\frac{dQ}{dC}=\frac{1}{(1-C)}\left\{\alpha\bar{P}_n(t)Q(t)-\frac{\beta\bar{P}_n{}^{1/2}Q(t)}{(1+\gamma\bar{P}_n)^{1/2}}\right\} \qquad (12)$$

$$\alpha=\frac{k_3}{k_2}\frac{\rho}{m}\text{ and }\beta=\left(\frac{k_{1e}k_{4c}\rho}{k_2^2m}\right)^{1/2}.$$

From the relation $Q(t)=\dfrac{w_0(1-C)}{m\bar{P}_n(t)}$ it follows that:

$$\frac{d\bar{P}_n(t)}{dC}=-\frac{w_0}{mQ(t)}-\frac{\bar{P}_n(t)}{Q(t)}\frac{dQ(t)}{dC}.$$

With the use of these two relations eq (12) is connected to the following integrable expression:

$$\frac{d\bar{P}_n(t)}{-\bar{P}_n(t)-\alpha\bar{P}_n^2(t)+\dfrac{\beta\bar{P}_n(t)^{3/2}}{[1+\gamma\bar{P}_n(t)]^{1/2}}}=\frac{dC}{(1-C)}. \qquad (13)$$

With the substitution $\chi=(\bar{P}_n{}^{-1}+\gamma)^{1/2}$ eq (13) is transformed to:

$$\int_{C=0}^{C=C} d\ln(1-C)=\int_{\chi=\chi_0}^{\chi=\chi}\frac{-2\chi_2d\chi}{\chi^3-\beta_\chi^2+(\alpha-\gamma)\chi+\beta\gamma}. \qquad (14)$$

The integral conversion as a function of $\bar{P}_n(t)$ is in the more frequent case:

$$\ln(1-c)=A_1\ln|(\chi-r_1)|+A\ln[(\chi-a)^2+b^2]$$
$$-2B\tan^{-1}\frac{\chi-a}{b}$$
$$-\left[A_1\ln|(\chi_0-r_1)|+A\ln(\chi_0-a)^2+b^2\right.$$
$$\left.-2B\tan^{-1}\frac{\chi_0-a}{b}\right] \qquad (15)$$

where r_1, $(a+bi)$ and $(a-bi)$ are roots of the cubic expression in the denominator of the term on the right in eq (14), as found by Cardano's method, [28], and the coefficients are:

$$A_1=\frac{-2r_1^2}{r_1^2-2ar_1+a^2+b^2}$$

$$A=-1-\frac{A_1}{2}$$

$$B=\frac{-A_1a-Aa-Ar_1}{b}.$$

If the cubic expression has three real roots, they are found by the trigonometric method [29] and the solution is a sum of logarithmic terms only.

5.5. Evaluation of Experimental Data

With the use of eq (15) and the value of 3×10^{-4} for γ, we can for given values of α and β plot curves such

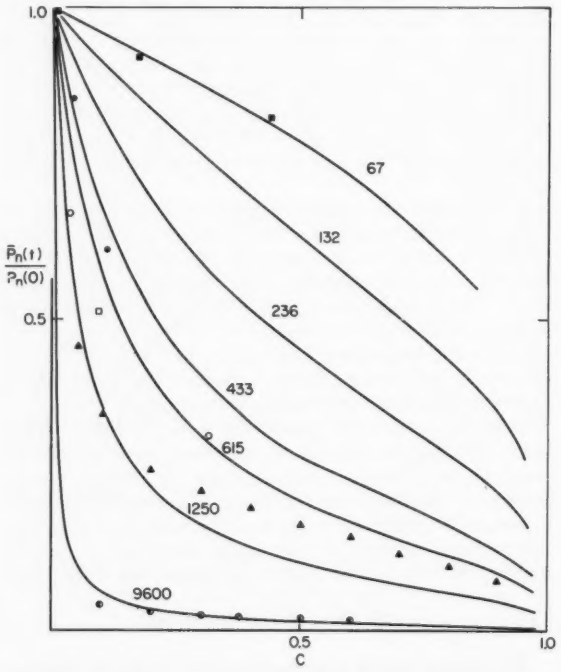

FIGURE 10. *Thermolysis of thermal polystyrenes at 300 °C, variation of relative number average degree of polymerization with conversion.*

Full lines are calculated from equation (15) with $\alpha=0.02$, $\beta=0.24$, and $\gamma=3\times10^{-4}$. The numbers above each line give the value of $\bar{P}_n(0)$ for the particular curve. The points are experimental for different polymers, initial $\bar{P}_n(0)$; ■, 67, ●, 236, □, 433, ○, 615, ▲, 1250, and ◐, 9600.

TABLE 3. *Degradation parameters for thermal polystyrenes*

$\alpha = \frac{k_3\rho}{k_2 m} = 0.02$	$k_{1r} = 2.5 \times 10^{-7}\,s^{-1}$ (353 °C) $8.7 \times 10^{-10}\,s^{-1}$ (300 °C)
$\beta = \left(\frac{k_{1e}k_{4c}\rho}{k_2^2 m}\right)^{1/2} = 0.24$	$k_{1e} = 8.5 \times 10^{-4}\,s^{-1}$ (353 °C) $2.9 \times 10^{-6}\,s^{-1}$ (300 °C)
$\gamma = \frac{k_{1r}}{k_{1e}} = 3 \times 10^{-4}$	$k_3/k_2 = 2.1$ cm³/mol
Zip length (propagation/radical)	$k_3/k_2' = 5.25$ cm³/mol
$Z = [\alpha + 2\beta(P_n^{-1} + \gamma)^{1/2}]^{-1}$ $\quad 0 \leq Z \leq 35.3;\ 0 \leq \bar{P}_n \leq \infty$	$k_3'/k_2 = 0.21$
Kinetic chain length (propagation/initiation)	$k_3'/k_2' = 0.50$
$\Lambda = [2\beta(P_n^{-1} + \gamma)^{1/2}]^{-1}$ $\quad 0 \leq \Lambda \leq 120.2;\ 0 \leq \bar{P}_n \leq \infty$	$k_2'/k_2 = 0.4$
Transfer constant (13) (propagation/initiation)	$k_3'/k_3 = 0.10$ mol/cm³
$\sigma = \alpha[2\beta(P_n^{-1} + \gamma)^{1/2}]^{-1}$ $\quad 0 \leq \sigma \leq 2.4;\ 0 \leq \bar{P}_n \leq \infty$	

as those shown in figure 10. These plots give the variation in relative degree of polymerization, $\bar{P}_n(t)/\bar{P}_n(0)$, as a function of conversion. By trial a "best" choice of values for α and β was made to give theoretical curves which "best" fitted the experimental points for the polymers with $\bar{P}_n(0) = 67$, 1,250, and 9,600. With the exception of those for the 1,250 and the 9,600 sample the data points in figure 10 came from an earlier paper [13]. All points are for thermally prepared polystyrenes since it is evident from a comparison of figures 7 and 8 that anionic polystyrenes have a different mechanism of initiation at least in the early stages of the reaction. It is seen that the theory correlates nicely the observed experimental results for both a large range of conversion and a large range in degree of polymerization. Having a value for β we can then with the use of the rate data determine the end initiation rate constant, k_{1e}. Since we already know γ, we can also determine k_{1r}. Values for these constants and other parameters are listed in table 3.

Having established the relation between $\bar{P}_n(t)$ and c we can with the aid of eq (7) and the numerical values for k_{1e}, β, and γ predict the rate for a given polymer as a function of conversion. Figure 11 shows such theoretical rate curves compared to experimental points. These points were taken from an earlier study [13]. With the present theory, the overall agreement is much improved over the previous theory [13].

For the smallest degree of polymerization sample, $\bar{P}_n(0) = 67$, the agreement between theory and experiment is somewhat less than that for the other polymer samples. For this particular polymer however, the rate points were actually corrected by means of an Arrhenius plot from data taken at a much lower temperature. The observed discrepancy could easily be the result of an inaccurate extrapolation.

As a demonstration of the theoretical behavior of the logarithm of the initial rate as a function of the logorithm of the reciprocal molecular weight we calculate

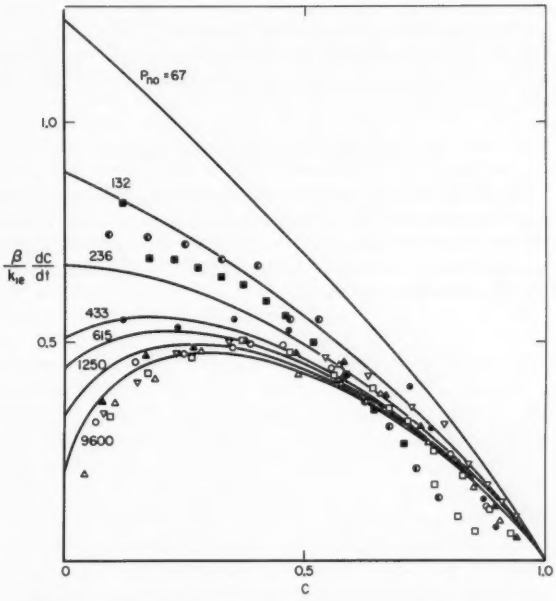

FIGURE 11. *Thermolysis of thermal polystyrenes at 353 °C, variation of rate with conversion.*

Full lines are calculated from eqs (7) with $\beta = 0.24$; $\gamma = 3 \times 10^{-4}$, values from eq (15). The numbers above each line give the value of $\bar{P}_n(0)$ for the particular curve. The points are experimental for different polymers. Initial $\bar{P}_n(0)$ ■, 67, ◐, 132, ●, 236, □, 433, ○, 615, ▲, 1250, and ▽, 1462.

the curves shown in figure 12. The experimental initial rates determined at 300 °C are shown in the figure. The theoretical line is determined by means of eq (7) and the values of β and γ shown in table 3. The curve is shifted to give the best fit to the points by adjusting the values of the rate constant for end initiation, k_{1e}. It is seen from the figure that at very high molecular weights the slope of the curve is zero. The reaction,

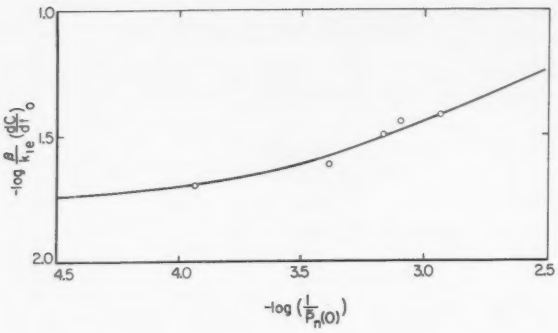

FIGURE 12. *Thermolysis of thermal polystyrenes at 300 °C, variation of the logarithm of initial rate with logarithm of reciprocal* $\bar{P}_n(0)$, *comparison of theory and experiment.*

being initiated by pure random scission, is independent of molecular weight. At very low molecular weights the initial rate becomes dependent on the square root of the $1/M_n(0)$ or the number of ends. It is worthwhile noting that the experimental points fall in the transition region for the mechanism and that the slope of the tangent to the curve in this region is close to the value of 0.25.

5.6. Kinetic Chain and Zip Length

Table 2 also presents the zip length, Z, defined as the average number of propagations per radical. In the theory herein described we have assumed that all weight loss is the result of propagation. Thus we have mathematically assumed:

$$\frac{d\text{“}M\text{”}}{dt} = k_2' \sum_1^\infty R_i + \bar{x} k_3' \sum_1^\infty R_i \equiv k_2 \sum_1^\infty R_i$$

where $\bar{x}$ is the number average degree of polymerization for the nonmonomeric products. This means that the propagation constant, k_2, used in the theoretical relations above is a composite equal to $k_2' + \bar{x}k_3'$, where k_2' is the propagation constant for the production of pure monomer and k_3' is the constant for intramolecular transfer by which it is assumed that the majority of the other products are formed. From data [10, 30] in the literature on the yield of dimer, trimer, and other products we estimate that $\bar{x} \cong 3$.

In previous theoretical treatments [1, 2] it was noted that intramolecular transfer was a means of producing nonmonomer in kinetic fashion equivalent to that for the production of monomer by propagation. The success of the present treatment lends weight to the conclusion that most nonmonomer is produced by intramolecular transfer. In this connection it is interesting to note that from this theoretical treatment we estimate for polystyrene degradation that ≈ 10.4 intramolecular transfer acts occur per one intermolecular transfer. At a given temperature this value is a constant throughout the process. This information is deduced

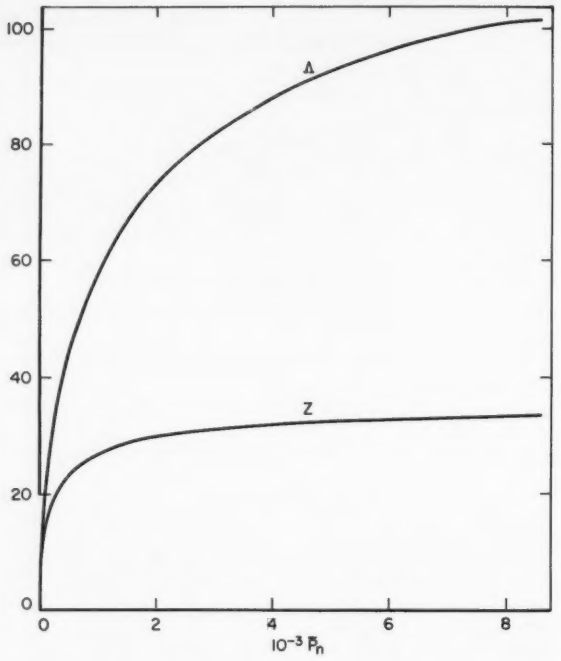

FIGURE 13. *Thermolysis of thermal polystyrenes, variation of zip length, (Z), and kinetic chain length, Λ, with number average degree of polymerization,* P_n.

from the ratio k_3'/k_3 shown in table 3. The values of the other ratios involving k_2, k_2', k_3 and k_3' also shown in table 3 are estimated using the value of α, $\bar{x}$ and the monomer yield, 40 percent. It is seen that the zip length, kinetic chain length, Λ, and the ratio of transfer to initiation, σ, a parameter used in previous treatments [1, 2, 13, 27], are all dependent on the degree of polymerization. In figure 13 a plot of Λ and Z as a function of $\bar{P}_n$ is presented. At very high $\bar{P}_n$ values, Λ is about 100 and some photosensitization should be at least observable. However, the molecular weight if large decreases sharply in the initial stages of reaction and quickly drops to low values. The values shown are for the production of monomer and nonmonomer. The Λ and Z values for the production of pure monomer would be 0.4 times the values plotted. At $\bar{P}_n = 200$, $Z = 7$ for pure monomer. This compares with 3 to 5 used or deduced in previous work [13, 31]. Photosensitization studies with this polymer would therefore require careful work at low conversion using high molecular weight polymers.

In figure 14 the ratios Λ/Z and σ are shown as a function of $\bar{P}_n$. The difference between these two ratios is precisely unity, hence the two curves parallel each other. For pure random initiation all these parameters become constant, i.e., independent of $\bar{P}_n$. Therefore for the present system of mixed initiation they increase only slightly above $\bar{P}_n = 8{,}000$. The use of termination by combination here as opposed to the previous [13] use of disproportionation results for

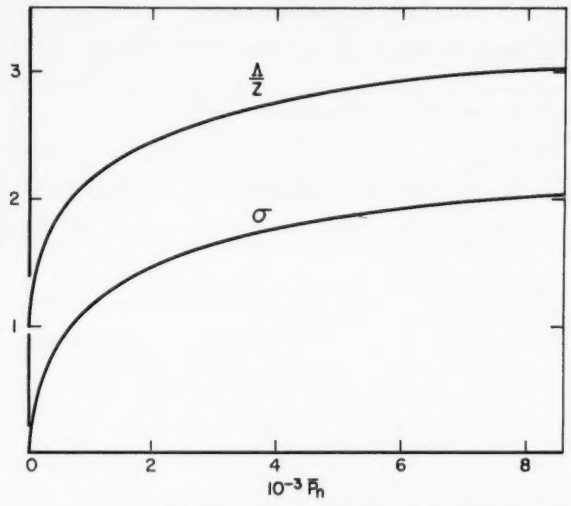

FIGURE 14. *Thermolysis of thermal polystyrenes, variation of the ratio of kinetic chain length and zip length, Λ/Z, and the transfer constant σ [13] with number average degree of polymerization, $\bar{P}_n$.*

$\bar{P}_n = 615$ in a $\sigma = 1$ instead of 0.045. Also σ previously decreased with $\bar{P}_n$ instead of increasing as shown in figure 14. Richards and Salter [16] from their study of the intermolecular transfer process using radiochemical techniques estimated $\sigma = 1.2$, a value completely compatible with our present results.

Although all major aspects of the degradation phenomenon seen with thermal polystyrenes are accounted for by the present treatment it must be emphasized that this treatment neglects the direct molecular vaporization of small oligomers. This process is however insignificant until very high conversion when the $\bar{P}_n$ is very small. It should also be noted that the treatment does not specifically connect the initiation processes to the presence of specific structures in the polymer chain. The success of the treatment implies that either each molecule has certain probabilities for random and end initiation or that on the average there is a certain constant fraction of labile ends. Since the anionic polymers show no initial dependence on $\bar{P}_n$, the second possibility is indicated.

5.7. Activation Energies

Molecular weight as a function of conversion is nearly independent of temperature [13] and hence the parameters α, β, and γ have been taken to be independent of temperature in this treatment. However, without the very precise measurements over wider temperature ranges needed, we can make certain estimates from the available data.

The transfer ratio α should not vary greatly with temperature since the activation energies for abstraction E_3 and propagation E_2 usually have similar values.

Combining previous [13] and present data we estimate $0 > E_\beta > -3$ kcal and $0 < E_\gamma < 32$ kcal with log $A_r < 8.46$. Taking $E_\beta = 0$ and the slopes in figure 9 where the data is taken at 300 ± 10 °C, and $E_{1e} = 36$ and a log $A_{1e} = 8.2$ are calculated. On the other hand rate data in figure 11 at 353 °C and previous data [13] yield the higher values $E_{1e} = 48$ kcal and log $A_{1e} = 13.7$.

5.8. Anionic Polystyrenes

With the anionic polystyrenes the initiation process differs from that in the thermal polymers. From the curves in figure 7 it is clear that here initial rates are all essentially zero and independent of molecular weight. Yet the rate and molecular weight behavior of these polymers is nearly identical to that for the thermal polymer at conversions greater than 5 percent. It seems clear then that these polymers actually initiate at random in the limit of low conversion and more labile end initiating structures are produced as the conversion increases until a stationary concentration of end structures is attained.

With the anionic polystyrenes the key questions are what are the more labile initiating structures and how are they produced. It would seem on the basis of the mechanism deduced from the thermal polymers, that since the original ends are stable either intermolecular transfer or termination steps would be the source of the labile structures. From figure 6 it is seen, for instance, that for the polymer $\bar{M}_n = 5{,}300$ the rate at first increases, and a maximum occurs at $C \cong 0.2$. This is compatible with the build-up of the labile structures. Since the molecular weight for this polymer remains nearly constant with conversion (see fig. 5), one might conclude that the labile structure is that formed in the interior of the molecules by the recombination process. This would conflict with the fact that the virgin thermal polymer has labile structures. Thermal polymers have the most probable molecular weight distribution resulting from termination by transfer [32] either with monomer or thermal dimers. Since the molecular weights during pyrolysis for the low D.P. thermal polymers are nearly constant with conversion it is concluded then that labile structures are at ends produced by the intermolecular transfer process. Such labile end groups would be expected to have the unsaturated structure: ~ CH_2—C(C$_6$H$_5$)=CH_2, assuming that α hydrogens are involved in the transfer process. However, β hydrogen abstraction would lead to similar olefinic structures.

On the other hand conclusive evidence is not yet available that in a particular type polystyrene labile combination structures do not compete with labile end groups in the initiation process.

Another aspect to be expected initially with the anionic polymers is that random initiation produces the two types of radicals shown below:

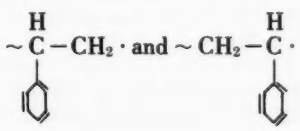

487-412 OL - 73 - 11

The primary radical is more active and would more readily transfer and disproportionate producing labile end groups and more quickly dropping the molecular weight.

6. Conclusions

The treatment developed for thermally prepared polystyrene satisfactorily explains a wide body of observations; rates, initial rates, molecular weight, changes in molecular weight distribution, and their dependence on conversion and initial molecular weight. The mechanism used is comprised of random and end initiation, depropagation, inter- and intramolecular transfer and most importantly termination by combination. The mathematical relations developed involved the number average molecular weight and the conversion. They are derived from differential relations for the total number of depropagating radicals, R, and the total number of molecules in the system, Q, and are therefore valid for any initial molecular weight distribution. A more complete treatment which would show the quantitative dependence of weight average molecular weight and molecular weight distribution on time or conversion would require both a computer, and considerable effort. This would be true even if the computer approach was adequately developed.

The experimental observations on the change in molecular weight distribution and in particular its convergence with conversion toward a distribution other than the "most probable" emphasizes the limited utility of previous kinetic treatments [8, 9] of degradation. Although these observations are not explicitly shown to result from the mechanism they are clearly the result of a coupling mechanism. Hence the use of the termination by combination step. This result and the variety of conceivable mechanisms is suggestive of the interesting possibility that specific narrow distributions including monodisperse ones may be produced by degradation.

Although the data for the anionic polystyrene is not correlated with theoretical relations, its degradation mechanism is clearly established to differ from thermal polystyrene chiefly in having initially pure random initiation which at higher conversion becomes supplemented and then overwhelmed by a component of end initiation.

7. References

[1] Simha, R., Wall, L. A., and Blatz, P. J., J. Poly. Sci. **5**, 615 (1950).
[2] Simha, R., and Wall, L. A., J. Phys. Chem. **56**, 707 (1952).
[3] Jellinek, H. H. G., J. Poly. Sci. **3**, 850 (1948).
[4] Jellinek, H. H. G., J. Poly. Sci. **4**, 1, 13 (1949).
[5] Grassie, N., and Melville, H. W., Discussions of the Faraday Society, The Labile Molecule, p. 378 (1947).
[6] Wall, L. A., J. Res. Nat. Bur. Stand. (U.S.), **41**, 315–322 (1948) RP1928.
[7] Parker, M., Florin, R. E., and Wall, L. A., J. Res. Nat. Bur. Stand. (U.S.), **70A** (Phys. and Chem.), No. 2, 115–131 (Mar.–Apr. 1966).
[8] Gordon, M., Trans. Faraday Soc. **54**, 1345 (1958).
[9] Boyd, R. H., J. Chem. Phys. **31**, 321 (1959); Boyd, R. H., J. Poly. Sci. A–1, **5**, 1373 (1967).
[10] Wall, L. A., Chapter V in Book, Pyrolysis, Ed., G. M. Kline, Part II, Analytical Chemistry of Polymers (Interscience, 1962).
[11] Jellinek, H. H. G., Encyclopedia of Polymer Science and Technology **4**, 746 (1967).
[12] Cameron, G. G., and MacCallum, J. R., J. Macromolecular Sci., Macro. Rev. **C1**, 327 (1967).
[13] Wall, L. A., Straus, S., Flynn, J. H., McIntyre, D., and Simha, R., J. Phys. Chem. **70**, 53 (1966).
[14] Richards, D. H., and Salter, D. H., Polymer **8**, 127 (1967).
[15] Richards, D. H., and Salter, D. H., Polymer **8**, 139 (1967).
[16] Richards, D. H., and Salter, D. H., Polymer **8**, 153 (1967).
[17] Fetters, L. J., J. Poly. Sci. **C**, No. 26, 1 (1969).
[18] Fetters, L. J., J. Res. Nat. Bur. Stand. (U.S.), **70A** (Phys. and Chem.) No. 5, 421–433 (Sept.–Oct. 1966).
[19] Feist, W. C., J. Poly. Sci. **B3**, 879 (1965).
[20] Bushuk, W. and Benoit, H., Can. J. Chem. **36**, 1616 (1958).
[21] Wippler, C. and Scheibling, G., J. Chem. Phys. **51**, 201 (1954).
[22] Altares, T., Wyman, D. P., and Allen, V. R., J. Poly. Sci. **2A**, 4533 (1964).
[23] Alliet, D. F., Appl. Poly. Symp. **8**, 39 (1969).
[24] Johnson, J. F., Porter, R. S., and Cantow, M. R., Rev. Macromol. Chem. **1**, 413 (1969).
[25] Goetze, K. P., and Porter, R. S., J. Poly. Sci. Part C No. 35, 189 (1971).
[26] Wall, L. A. Chapter 12 in Book, Fluoropolymers, Ed., L. A. Wall (Wiley-Interscience, N.Y., 1972).
[27] Simha, R., Wall, L. A., and Bram, J., J. Chem. Phys. **29**, 894 (1958).
[28] Handbook of Mathematical Functions, Editors M. Abramowitz and I. A. Stegun, Nat. Bur. Stand. (U.S.), Appl. Math. Ser. 55, 1054 pages (June 1964), see page 17.
[29] Burrington, C. B., Handbook of Mathematical Tables and Formulas (Handbook Publishers, Inc., Sandusky, Ohio, 1946), pp. 7–9.
[30] Madorsky, S. L., Thermal Degradation of Organic Polymers (Interscience Publishers, N.Y., 1964).
[31] Simha, R., Transactions of the New York Acad. of Sci., **14**, 151 (1952).
[32] Platt, A. E., Encyclopedia of Poly. Sci. and Tech. **13**, 156 (1970).

(Paper 77A1–760)

JOURNAL OF RESEARCH of the National Bureau of Standards—A. Physics and Chemistry
Vol. 77A, No. 1, January–February 1973

Modulus of Natural Rubber Cross-Linked by Dicumyl Peroxide II. Comparison With Theory

Lawrence A. Wood

Institute for Materials Research, National Bureau of Standards, Washington, D.C. 20234

(September 22, 1972)

Thermodynamics and molecular considerations are applied to an examination of the equation $G=S(fp+B)T+H(fp+B)+A=5.925\times10^{-3}(fp-0.45)T+0.0684(fp-0.45)+2.70$, found experimentally in Part I. G is the shear modulus in Mdyn cm^{-2} at a temperature T for natural rubber cross-linked by adding p parts of dicumyl peroxide per hundred of rubber (phr) and heating until a fraction f of the peroxide is decomposed. G^*, the energy component of the modulus, is $H(fp+B)+A$. The ratio G^*/G decreases from 1.00 at the gel point ($fp=0.45$ phr) to 0.5 near 2 phr and to 0.09 at 23.8 phr. The modulus G is related to ν_e, the number of moles of effective sub-chains per cm^3, by the equation $G-G^*=\nu_eRT$ where R is the gas constant. If each molecule of decomposed dicumyl peroxide of molecular weight M_d produces one cross-link in the rubber of specific volume $\bar{v}_r$, then it is predicted that $S=2R(100M_d\bar{v}_r)^{-1}=5.5535\times10^{-3}$ Mdyn cm^{-2} phr^{-1} K^{-1}, as compared with the experimental value 5.925×10^{-3}. Theory gives no prediction of the values of A, or of H. The gel point may be located experimentally as the point where the slope of the modulus-temperature relation is zero. The value of G at the gel point is the energy component G^*. The experimental value of fp at the gel point permits a calculation of the molecular weight of the rubber before cross-linking as 193,000. The results afford a very satisfactory confirmation of the essential validity of the statistical theory of rubber elasticity in its simplest form, if due regard is paid to G^*, the energy component of the modulus.

Key words: Cross-linking of rubber; dicumyl peroxide; elasticity theory of rubber; entropy component; gel point; modulus of rubber; rubber elasticity; statistical theory of rubber elasticity; thermodynamics of rubber elasticity.

1. Introduction

In a previous paper, Part I [1][1], time-independent experimental observations were reported which could be represented by the following four-constant equation:

$$G=S(fp+B)T+H(fp+B)+A$$
$$=5.925\times10^{-3}(fp-0.45)T+0.0684(fp-0.45)+2.70 \quad (1.1)$$

S, B, H, and A are constants having the values shown, while G is the shear modulus (in Mdyn cm^{-2} or 0.1 MNm^{-2}) at a temperature T (in kelvins) for natural rubber cross-linked by adding p parts of dicumyl peroxide per hundred of rubber (phr), and heating until a fraction f of the peroxide was decomposed. The range of values of fp investigated was from 0 to 23.8 phr at temperatures from 223 to 373 K. The shear modulus is defined as the limit of the ratio of shear stress to the corresponding strain as the stress and strain approach zero.

The experimental work described in Part I involved observations of the indentation of a rubber sheet by a rigid ball. Consequently, the deformation was complex, involving extension, compression, and shear in different portions of the sheet. However all deformations were kept so small that no extrapolation was required to obtain the modulus. At these small deformations the relations between stress and strain were linear. Previous work discussed in Part I has demonstrated that the values of G obtained on dicumyl peroxide vulcanizates by the indentation method give good agreement with those obtained by direct measurements of shear modulus with a torsion pendulum or those given by the proper extrapolation of simple extension measurements.

Figure 1 shows the modulus-temperature relations exhibited by this equation, while figure 2 shows the plot of modulus against fp. In each case the shaded area shows the range of temperature covered by our experimental observations. It should be noted that extending the curves to 0 K involves a linear extrapolation over a range of lower temperatures about 50 percent more than the experimental range itself. However, the figure is not intended to imply that observations at temperatures below the indicated experi-

[1] Figures in brackets indicate the literature references at the end of this paper.

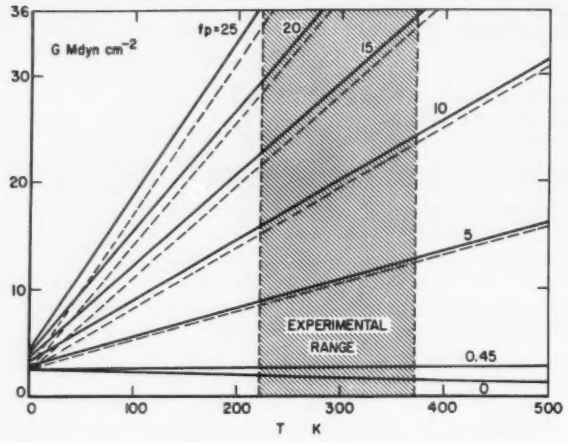

FIGURE 1. *Modulus as a function of temperature for different amounts of decomposed dicumyl peroxide.*

—— Continuous line represents eq (1.1).
- - - Dashed line represents eq (1.2).

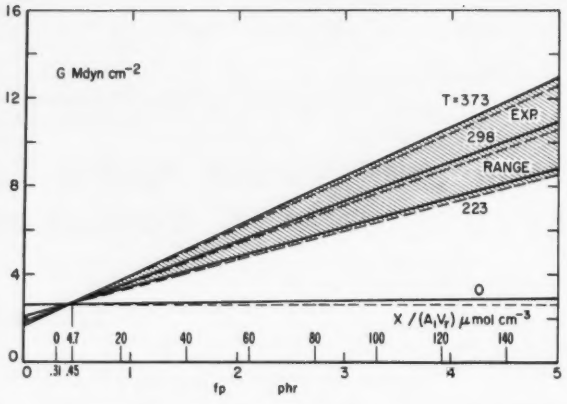

FIGURE 2. *Modulus as a function of amount of decomposed dicumyl peroxide for different temperatures.*

—— Continuous line represents eq (1.1).
- - - Dashed line represents eq (1.2).

The upper abscissa scale shows the expected density of cross-links in μ mol cm^{-3}, as calculated from eq (3.6).

mental range would conform to the lines shown. In fact the data in Part I clearly show a completely different relation at temperatures approaching the glass transition. The general qualifications and limitations of eq (1.1) in representing experimental data are outlined in Part I. They will not be given further consideration in the present paper.

In figure 2 the range of values of fp shown is limited to those below 5 phr merely in order to present more detail at low degrees of crosslinking, but the lines shown were determined by observations over the whole range of values of fp.

The dashed curves represent the corresponding relations for the simpler equation

$$G = 5.925 \times 10^{-3}(fp - 0.45)T + 2.70 \qquad (1.2)$$

The difference between the solid and dashed curves shows the effect of omitting the middle term of the right hand side of eq (1.1). When $fp = 0.45$ the value of G at all temperatures is given as 2.70 Mdyn dm^{-2} by both equations. For $fp = 0$ the difference between the values given by the two equations is only 0.03 Mdyn cm^{-2} and so is not perceptible on the scale of ordinates used in figure 1.

After pointing out the thermodynamic implications of eq (1.1) the present paper is devoted to a discussion of the predictions of the simplest form of the theory of rubber elasticity and a quantitative comparison of these predictions with the experimental observations. The aim has been to outline the general features of the field.

2. Thermodynamics: Entropy and Energy

The force involved in stretching a rubber strip can be resolved into components arising from changes in entropy and internal energy. Extensive discussions [2–5] have pointed out the difference between the resolution obtained at constant pressure and that at constant volume.

Since an increase of volume is observed when rubber is stretched at constant pressure [6–8], there is a corresponding increase of internal energy. Consequently the energy component of the force at constant pressure exceeds that at constant volume by the force corresponding to the amount of work required to increase the volume. The entropy component is necessarily smaller by the same amount, if the total force is kept the same.

The theory of rubber elasticity usually places emphasis on the configurational aspects of the problem, and so normally requires the resolution to be made at constant volume in order to eliminate that portion of the energy component arising from volume change [9].

The modulus G studied in the present investigation can be resolved in an analogous manner into components arising from entropy and internal energy changes [10, 11].

However, Shen [14, 15] has pointed out that the shear modulus should be independent of the applied hydrostatic pressure and no distinction need be made between measurements of G at constant pressure and those at constant volume. This is an important advantage of dealing with the modulus rather than the force.

In approximate confirmation of this expectation, Paterson [12] by direct observation found that the modulus of a pure-gum natural rubber vulcanizate increased by only about 30 percent as the pressure was raised from atmospheric to 4000 bars (1 bar = 10^6dyn cm^{-2} = 10^5Nm^{-2} = 10^5Pa). The compressibility of natural rubber cross-linked with a small amount of dicumyl peroxide has been measured as 51.4 ×

10^{-6}bar^{-1}[13]. Utilizing this value one can calculate that an external pressure of only about 2 bars would suffice to reduce to zero the volume increase of about 0.01 percent observed [6–8] on stretching rubber to an elongation of 100 percent. Consequently it seems quite certain that in an experiment where the pressure would be systematically increased to keep the volume constant, the change in modulus would be less than the experimental uncertainty of measurement.

The resolution of modulus in the present investigation can be seen by an examination of figure 1 and eq (1.1).

Equation (1.1) may be written as

$$G = T(\partial G/\partial T) + G^* \tag{2.1}$$

where

$$\partial G/\partial T = S(fp + B) \tag{2.2}$$

and

$$G^* = A + H(fp + B) \tag{2.3}$$

G^* represents the component of G arising from internal energy changes. The term $T(\partial G/\partial T)$, proportional to the temperature, represents the component of G arising from increase of entropy as the temperature is raised above 0 K. Of course this entropy component can also be written as $(G - G^*)$.

Equation (2.1) can also be written in the form

$$G^*/G = 1 - (T/G)(\partial G/\partial T) = 1 - \partial \ln G/\partial \ln T \tag{2.4}$$

G^* can be noted as the intercept at 0 K for each line in figure 1. Equation (2.3) shows that G^* is mainly determined by the value of the constant A, and would be equal to it, were the constant H to be taken as zero, as in eq (1.2), represented by the dashed lines of figure 1.

G_0 the intercept of each line in figure 2, corresponding to no added cross-links, should be carefully distinguished from G^*, the intercept in figure 1. In fact, from eqs (1.1) and (2.3) the relation between them is found to be

$$G_0 = G^* + SBT = 2.67 - 2.666 \times 10^{-3} T \tag{2.5}$$

The energy and entropy components as well as the ratios of ordinates G^*/G in figure 1, as calculated from eqs (2.3) and (1.1) at 298.15 K, are shown in table 1.

The energy component is strongly predominant at low degrees of cross-linking. However as fp is increased from 0 to 25 phr the intercept term G^* remains in the range 2.67 to 4.38 Mdyn cm^{-2} while the entropy component increases steadily with increased cross-linking. It becomes greater than G^* at 298.15 K only when fp exceeds about 2 phr and the ultimate elongation has fallen below 200 percent. At the higher degrees of cross-linking (especially above 5 phr) the ultimate elongation and tensile strength are so low that the material can hardly be considered a very useful rubber. It is not clear why these results differ from those of Rehage, Schäfer, and Schwarz [11], who reported that the value of G^*/G increased from about 0.20 to 0.40 as the cross-linking was increased from zero to a value corresponding to $fp = 2$ phr.

TABLE 1. *Energy and entropy components at 298.15 K*

$G^* = 0.0684fp + 2.67$; $G = 1.835fp + 1.87$

fp	G^* Mdyn cm^{-2}	G Mdyn cm^{-2}	G^*/G	$G - G^*$ Mdyn cm^{-2}
0	2.67	1.87	.....	.....
0.45	2.70	2.70	1.000	0
1	2.74	3.71	0.739	0.97
2	2.81	5.54	.507	2.73
3	2.88	7.38	.390	4.50
4	2.94	9.21	.319	6.27
5	3.01	11.05	.272	8.04
10	3.35	20.22	.166	16.87
15	3.70	29.40	.126	25.70
20	4.04	38.57	.105	34.53
25	4.38	47.75	.092	43.37

Considerable attention has been given by previous investigators [14–26] to a ratio they have denoted as f_e/f, where f_e is the energy component of the force and f (in contradistinction to the f used in this paper) is the total value of the force required to maintain a certain elongation at constant volume. Shen and co-workers [14, 15, 27] by using the equation of state given by the current statistical theory of rubber elasticity have derived equations showing f_e/f to be less than G^*/G by an amount $(1/3)\beta T$ where β is the volume thermal expansivity. This difference amounts to only 0.067 near 300 K. We prefer to express results in terms of G^*/G, so that no assumptions regarding the form of stress-strain relation (or equation of state) are required.

Our work yielding the value of G^*/G is of course limited to very small deformations. Consequently it gives no information on the disputed question of whether f_e/f varies with deformation. Several observers [21, 23, 24, 26, 27] had reported that f_e/f at a fixed amount of cross-linking increased rapidly as the deformation approached zero, rising from values near 0.2 to 0.6 or more. However more recent papers by two of the authors and others [9, 14, 15, 25, 28, 29] have stated that the ratio is independent of the deformation, as required by theoretical considerations.

3. Predictions of the Theory of Rubber Elasticity

3.1. Cross-Linking

Modern ideas regarding cross-linking and its effect on modulus are summarized in the book by Meares [30] along the lines of the earlier developments given in the books of Flory [31] and Treloar [32]. We shall follow mainly the treatment and symbolism of Meares.

At this stage we shall limit ourselves to the very simplest assumptions, realizing that these may represent an over-simplification of the problem. In a later paper we shall consider limitations and qualifications which might be necessary and discuss the effects of more complex assumptions. Meares [33] has sum-

marized many of the efforts to obtain more satisfactory results by more sophisticated assumptions.

Consider a quantity of unvulcanized rubber having a mass m_r, a volume V_r and a specific volume $\bar{v}_r = V_r/m_r$. Let the number of rubber molecules in the system be denoted as

$$N = A_1 m_r/M = (A_1 V_r)/(M\bar{v}_r) \tag{3.1}$$

where A_1 is the Avogadro Constant (the number of molecules in one mole), and M is the effective molecular weight of the unvulcanized rubber (here assumed to be monodisperse).

Suppose that in some manner (as by the reaction with dicumyl peroxide) a certain number of cross-links X are formed in this rubber without appreciable change of volume or mass of the system. The number of sub-chains formed will be twice this value, since each additional cross-link gives rise to 2 more sub-chains. Sub-chains are called "strands" in the terminology used by Ferry and his collaborators.

Sub-chains which are at each end of a rubber molecule will not be effective in maintaining stresses, since they are not part of the network being formed. Thus $2N$ sub-chains are ineffective dangling loose ends, at all degrees of cross-linking. This number should be subtracted from $2X$ the total number of sub-chains formed, in order to obtain the number of effective or active sub-chains, that is, those capable of supporting a stress. As long as X is less than N some molecules can not be included, and will not be supporting their share of the stress.

Assuming the accuracy of this correction and neglecting other inactive sub-chains (such as loops for example or molecules not a part of the network), if any, one obtains ν_e, the number of moles of active sub-chains per unit volume of uncured rubber.

$$\nu_e = 2X/(A_1 V_r) - 2/(M\bar{v}_r) \tag{3.2}$$

3.2. Cross-Linking by Dicumyl Peroxide

The cross-linking in the present work was produced by free radicals resulting from the decomposition of dicumyl peroxide of molecular weight M_d (= 270.38). The compounding involved the addition of p parts of peroxide of mass m_d to each hundred parts of rubber of mass m_r. Thus,

$$p = 100\, m_d/m_r. \tag{3.3}$$

Some of the peroxide is wasted in reactions with impurities in the rubber [34, 35]. Since the amount wasted m_0 would be expected to be proportional to the amount m_r of rubber, let us define a constant w such that

$$w = 100 m_0/m_r. \tag{3.4}$$

The remainder of the dicumyl peroxide $(m_d - m_0)$, after decomposition, is available for cross-linking the rubber.

Each molecule of the remaining peroxide is assumed to give rise to one cross-link, after decomposition. Thus the total number of cross-links formed

$$X = A_1 f (m_d - m_0)/M_d \tag{3.5}$$

where f is the fraction of dicumyl peroxide decomposed during the time of vulcanization. From eqs (3.3)–(3.5) one can express the number of cross-links formed as

$$X = (A_1 V_r/100 M_d \bar{v}_r)(fp - fw). \tag{3.6}$$

This equation is used as the basis for the upper abscissa scale shown in figure 2.

The number of cross-links formed per rubber molecule is then obtained by dividing by eq (3.1).

$$X/N = (M/100M_d)(fp - fw) \tag{3.7}$$

When the value of X from eq (3.6) is inserted in eq (3.2) we have

$$\nu_e = [2/\bar{v}_r][(1/100M_d)(fp - fw) - 1/M]. \tag{3.8}$$

3.3. Variation of Modulus With Cross-linking

A complete network including all the rubber molecules is possible only when there is at least one cross-link for each molecule, that is when $X \geq N$, as already stated. When the number of cross-links is increased beyond the point where $X = N$, the fundamental proposition of the statistical theory of rubber elasticity states that the formation of additional sub-chains will give rise to a corresponding proportional increase in modulus to a modulus value G such that

$$G - G^* = \nu_e RT \tag{3.9}$$

where R is the gas constant, T the temperature in kelvins, and G^* the modulus of the network at 0 K, already defined as the energy component of the modulus in section 2, and utilized in eqs (2.1) and (2.3). It can be seen from eq (3.9) that G^* should be also the modulus at all temperatures when $\nu_e = 0$, namely before any effective subchains have been formed. No attempt will be made in this paper to calculate the value of G^* from molecular constants, but it will be assumed to remain constant as the temperature is varied.

It is expected that eq (3.9) will be subject to experimental verification only above the glass transition temperature T_g. The present theory likewise will give no consideration to the case where $X < N$, since the theory can be applied only where there is a complete network.

The modulus appearing in eq (3.9) is the "equilibrium modulus"; the experimental moduli in the work reported in Part I are largely 10-minute moduli. We recognize the distinction, but shall make direct comparisons, since the significant values reported in

Part I are derived from observations taken under conditions where the creep and set were very small or completely negligible [36, 37]. It has already been pointed out [36] that studies by Thirion and Chasset [38, 39] lead to an equation for the equilibrium modulus of natural rubber cross-linked with dicumyl peroxide yielding values differing from the 10-minute modulus by less than 2 percent when the amount of effective dicumyl peroxide is 1 phr or more.

The insertion of the expression for ν_e from eq (3.8) in eq (3.9) leads to the fundamental equation:

$$G=[2/100M_d\bar{v}_r]RT[fp-fw-100M_d/M]+G^*. \tag{3.10}$$

The derivatives are:

$$\partial G/\partial fp=(2/100M_d\bar{v}_r]RT+\partial G^*/\partial fp \tag{3.11}$$

and

$$\partial G/\partial T=(2/100M_d\bar{v}_r)R[fp-fw-100M_d/M]\cdot \tag{3.12}$$

if one neglects the variation of specific volume $\bar{v}_r$ with fp or T respectively.

When $\partial G/\partial T=0$, it can be seen that the cross-linking is such that $(fp-fw)=100\ M_d/M$ and consequently from eqs (3.10) and (3.7) $G=G^*$ and $X/N=1$. Thus all the curves plotted in figure 2 would be expected to pass through a single point independent of the temperature. The coordinates of this point are $fp=fw+100M_d/M$ and $G=G^*$. An examination of eq (1.1) and figure 2 shows that the experimental data conform to this surprising prediction, which we have not noted in any previous publications.

At this degree of cross-linking then, each rubber molecule, on the average, is attached to a single added cross-link. This is the "gel point", the degree of cross-linking where the molecules first form a network.

4. Quantitative Comparison of Predictions and Results

The equations which have been derived from molecular considerations can now be compared with those found experimentally. In the expression for G given by eq (3.10) the first term has exactly the same form as that given by eq (1.1), while the second term G^* corresponds to the sum of A and $H(fp+B)$ in eq (1.1), as demonstrated by eqs (2.1) and (2.3).

The molecular considerations outlined previously, while making allowance for the existence of an energy component, have furnished quantitative results only for the entropy component of the modulus. Consequently they furnish no predictions whatever regarding the value of G^*. It may be found from the experimental data by inserting the constants found in eq (1.1) into eq (2.3) to obtain

$$G^*=A+H(fp+B)=2.70+0.0684(fp-0.45)\cdot \tag{4.1}$$

The experimentally observed term $H(fp+B)$ in eq (1.1) shows that there is a variation of G^* with cross-linking and that

$$\partial G^*/\partial fp=H=0.0684\ \text{Mdyn cm}^{-2}\text{phr}^{-1}.$$

The difference between the solid and the dashed lines in figures 1 and 2, plotting eq (1.2), shows the effect of omitting the term. The value of the term is seen to be quite small under all conditions, and it does not have a very significant effect on the results. The magnitude of the term ranges from -0.031 to $+1.68$ Mdyn cm^{-2} as fp is increased from 0 to 25 phr and of course it is independent of temperature. Its presence does not alter the form of any of the relationships discussed, but causes G^*, the modulus intercept at 0 K, to increase from 2.67 to 4.38 Mdyn cm^{-2} as fp is increased rather than remaining constant at 2.70 Mdyn cm^{-2}. The comparison may be readily seen in figure 1.

It can be seen from eq (3.11) that $\partial G/\partial fp$ should increase linearly with temperature, beginning with a value of 0.0684 Mdyn cm^{-2}(phr)$^{-1}$ at $T=0$. It can be seen from eq (3.12) that $\partial G/\partial T$ is unaffected by the presence of the term containing the constant H, as shown by the parallelism of the lines corresponding to eqs (1.1) and (1.2) in figure 1.

The linear relations between G and T, and between G and fp, as well as the linearity of the derivative curves, are predicted and confirmed by the experimental results.

Probably the most striking prediction of the molecular considerations is that the curves of G against fp, for all temperatures, as in figure 2, should pass through a single point, not located at the origin of coordinates. The theory explains this as the gel point, where the cross-linking is just sufficient to form a network. It is predicted that for this degree of cross-linking $\partial G/\partial T=0$, and at lower degrees of cross-linking $\partial G/\partial T$ should have negative values. These predictions are again confirmed by the experimental values.

A much more severe test of the theory is given of course by a quantitative comparison of the values of the experimental constants B and S in eq (1.1) with the corresponding molecular constants in eq (3.10).

The constant B in eq (1.1) corresponds to the constant quantity $-fw-100\ M_d/M$ in eq (3.10). Thus

$$B=-fw-100\ M_d/M. \tag{4.2}$$

The first term of this expression, it will be remembered, represents a correction for the peroxide wasted in reactions with impurities in the rubber. The size of this term should depend on the nature and amount of the impurities. Van der Hoff [34] comparing purified and unpurified rubbers found experimentally that fw, the amount of this wasted peroxide was 0.31 phr for unpurified pale crepe rubber and that it was independent of the amount of added peroxide up to 4 phr. In the absence of information regarding the

impurities in our pale crepe rubber we shall assume the same amount as van der Hoff found, namely 0.31 phr.

The comparison of constants now gives

$$B = -0.45 = -0.31 - 100\,M_d/M, \text{ and}$$

$$M = 27{,}038/0.14 = 193{,}000.$$

This value is a very reasonable one for the effective molecular weight of the rubber before cross-linking. Since the rubber was actually polydisperse, this effective value must represent an average molecular weight, presumably the number-average. No direct measurements of molecular weight were made in the present study.

If the amount of dicumyl peroxide reacting with impurities in the rubber actually has some constant value different from 0.31 phr, the calculated value of effective molecular weight will be different from that just given. A value of only 60,100 would have been obtained from the present data if it had been assumed that there were no impurities, so that all the added dicumyl peroxide was available for cross-linking. The calculated molecular weight becomes infinite as the assumed amount of impurity approaches 0.45 phr. This possible uncertainty in the molecular weight does not affect any of the other conclusions of the present work.

The second comparison shows that

$$S = 2R/(100\,M_d\bar{v}_r) \tag{4.3}$$

The values of the gas constant R ($=8.3143\times10^7$ erg K^{-1} mol^{-1}), M_d ($=270.38$), and $\bar{v}_r$ ($=1.1074$ cm^3 g^{-1}, the directly-measured specific volume of the unvulcanized rubber at 25 °C, the midpoint of the temperature range covered) yield a predicted value of S equal to 5.5535×10^{-3} Mdyn cm^{-2} phr^{-1} K^{-1}. The directly-observed value of 5.925×10^{-3} Mdyn cm^{-2} $(phr)^{-1}$ K^{-1} is about 6.7 percent greater than this.

If this difference is not due to defects in the assumptions, it may arise from the presence of entanglements functioning as pseudo-cross-links and increasing the effective number of sub-chains by about 6.7 percent above that predicted from the actual cross-linking. More precise experiments would be required for a clear-cut decision between these two alternatives. At present, we shall assume that the difference does arise from entanglements and discuss them in a later paper of the present series.

The results of the present investigation yield an experimental value of $\partial G/\partial(fp)$ at 298.15 K about 10.5 percent greater than that calculated by the simple theory outlined here. About 6.7 percent of this would be due to entanglements and about 3.8 percent to the presence of the term containing the constant H in eq (1.1). Similarly the data of others [40–44] can be put into a form which yields values of $\partial G/\partial\, fp$ at 298.15 K greater than those calculated here by amounts ranging from about 6–23 percent.

5. Conclusions

The equation

$$G = 5.925\times10^{-3}(fp-0.45)T + 0.0684(fp-0.45) + 2.70 \tag{1.1}$$

found in Part I to reproduce the experimental results of time-independent indentation measurements, is represented on a plot of modulus G against cross-linking fp by a family of straight lines intersecting in a single point. The lines have slopes which increase with increasing temperature T.

On a modulus-temperature plot, the equation yields a family of straight lines with slopes and intercepts which increase with increasing cross-linking. The intercept obtained by linear extrapolation to 0 K of experimental data extending from 223 to 373 K is the component of modulus arising from changes in internal energy on deformation. The intercept represents this component over the range investigated experimentally, regardless of the nature of the actual modulus-temperature relation below 223 K. It exceeds the corresponding component arising from entropy changes at low degrees of cross-linking, specifically when the cross-linking is produced by 2 phr of dicumyl peroxide or less. The energy component predominates over the range where the ultimate elongation and tensile strength have their highest values. With increasing cross-linking, the ratio of the energy component to the entropy component decreases, since the latter increases linearly while the former remains almost constant.

The entropy component of the modulus as well as its variation with cross-linking and temperature can be predicted by the statistical theory of rubber elasticity, utilizing extremely simplified assumptions. The prediction yields relations of exactly the form found experimentally. Of course, the theory makes no predictions regarding the energy component. As determined experimentally, the energy component is almost constant, increasing only slightly with increasing cross-linking.

The gel point, namely the degree of cross-linking where there is only one effective cross-link per molecule, can be determined experimentally as the degree of cross-linking at which there is no change of modulus with temperature. In our work, this state was reached at 0.45 phr of decomposed dicumyl peroxide, which corresponds to the point of intersection of the lines in the plot of modulus against cross-linking. If the amount of dicumyl peroxide wasted by reaction with impurities in the rubber is estimated, the effective molecular weight of the rubber before cross-linking can be calculated. The modulus at the gel point was found to be 2.70 Mdyn cm^{-2} at all temperatures in our work. At this degree of cross-linking, just sufficient to form a network, the modulus has no entropy component and consists of the energy component alone.

The experimental value observed for the coefficient of the first term of the general equation for modulus

as a function of cross-linking and temperature is about 6.7 percent greater than that calculated from the statistical theory, which gives its value in terms of the gas constant R, the molecular weight of dicumyl peroxide, and the specific volume of the rubber. This difference can probably be ascribed to the effect of entanglements functioning as pseudo-cross-links.

The third paper of this series will include a discussion of some molecular interpretations, some more sophisticated assumptions, and further conclusions which can be drawn from the present results.

6. References

[1] Wood, Lawrence A., Bullman, George W., and Decker, George E., Modulus of natural rubber cross-linked by dicumyl peroxide. I. Experimental observations, J. Res. Nat. Bur. Stand (U.S.), **76A** (Phys. and Chem.), No. 1, 51–59 (Jan.–Feb. 1972).

[2] Flory, P. J., Principles of Polymer Chemistry, p. 443 (Cornell University Press, Ithaca, N.Y., 1953).

[3] Wood, Lawrence A., The elasticity of rubber, J. Washington Acad. Sci. **47**, 281 (1957); Rubber Chem. Technol. **31**, 959 (1958).

[4] Cifferi, A., Present status of the rubber elasticity theory, J. Polymer Sci. **54**, 149 (1961).

[5] Meares, P., Polymers: Structure and Bulk Properties, p. 173 (D. van Nostrand, London, 1965).

[6] Gee, G., Stern, J., and Treloar, L. R. G., Volume changes in the stretching of vulcanized natural rubber, Trans. Faraday Soc. **46**, 1101 (1950); Rubber Chem. Technol. **24**, 767 (1951).

[7] Christensen, R. G. and Hoeve, C. A. J., Comparison between theoretical and experimental values of the volume changes accompanying rubber extension, J. Polymer Sci., A-1, **8**, 1503 (1970); Rubber Chem. Technol. **43**, 1473 (1970).

[8] Penn, Robert W., Volume changes accompanying the extension of rubber, Trans. Soc. Rheology **14**:4, 509 (1970).

[9] Allen, G., Kirkham, M. J., Padget, J., and Price, C., Thermodynamics of rubber elasticity at constant volume, Trans. Faraday Soc. **67**, 1278 (1971).

[10] Schäfer, E. E., and Rehage, G., On the entropy and energy-elasticity of cross-linked high polymers, Makromol. Chem. **123**, 91 (1969).

[11] Rehage, G., Schäfer, E. E., and Schwarz, J., Elastic behavior and birefringence in substances with rubber elasticity, Angew. Makromol. Chem. **16/17**, 231 (1971).

[12] Paterson, M. S., Effect of pressure on Young's Modulus and the glass transition in rubbers, J. Applied Phys. **35**, 176 (1964).

[13] Wood, Lawrence A., and Martin, Gordon M., Compressibility of natural rubber at pressures below 500 kg/cm², J. Res. Nat. Bur. Stand. (U.S.), **68A** (Phys. and Chem.), No. 3, 259–268 (May–June 1964).

[14] Shen, M., Internal energy contribution to the elasticity of natural rubber, Macromolecules **2**, 358 (1969).

[15] Shen, M., Thermoelastic behavior of rubberlike materials at large deformations, J. Applied Phys. **41**, 4351 (1970).

[16] Flory, P. J., Cifferi, A., Hoeve, C. A. J., Thermodynamic analysis of thermoelastic measurements on high elastic materials, J. Polymer Sci. **45**, 235 (1960).

[17] Cifferi, A., On the tension-temperature-coefficient of natural rubber, Makromol. Chem. **43**, 152 (1961) (English).

[18] Cifferi, A., Hoeve, C. A. J., and Flory, P. J., Stress-temperature coefficients of polymer networks and the conformational energy of polymer chains, J. Am. Chem. Soc. **83**, 1015 (1961).

[19] Allen, G., Bianchi, U., Price, C., Thermodynamics of elasticity of natural rubber, Trans. Faraday Soc. **59**, 2493 (1963).

[20] Smith, K. J. Jr., Greene, A., and Cifferi, A., Crystallization under stress and non-Gaussian behavior of macromolecular networks, Koll. Zeit. und Zeit. f. Polym. **194**, 49 (1964) (English); Rubber Chem. and Technol., **39**, 685 (1966)

[21] Krigbaum, W. R., and Roe, R. J., Survey of the theory of rubberlike elasticity, Rubber Chem. Technol. (Rubber Reviews), **38**, 1039 (1965).

[22] Barrie, J. A., and Standen, J., Thermoelastic measurements on some elastomers, Polymer **8**, (2), 97 (1967).

[23] van der Hoff, B. M. E., and Buckler, E. J., Transient changes in topology and energy on extension of polybutadiene networks, J. Macromol. Sci.-Chem. **A1**(4), 747 (1967).

[24] Shen, Mitchell C., McQuarrie, Donald A., and Jackson, Julius L., Thermoelastic behavior of natural rubber, J. Applied Phys. **38**, 791 (1967).

[25] Boyce, P. H., and Treloar, L. R. G., The Thermoelasticity of natural rubber in torsion, Polymer **11**, (1), 21 (1970).

[26] Tanaka, T., Yokoyama, T., and Yamaguchi, Y., Methods for the determination of internal energy contribution to rubber elasticity, Memoirs, Faculty of Engineering, Kyushu University **29**, 89 (1970); Rubber Chem. Technol. **44**, 127 (1971).

[27] Shen, M., and Blatz, P. J., Energy contribution to rubber elasticity, J. Applied Phys. **39**, 4937 (1968).

[28] Guth, E., Recent developments in the statistical mechanics of polymers, J. Polymer Sci. **C31**, 267 (1970).

[29] van der Hoff, B. M. E., Relation between energy contribution to elastic force and strain dependence of modulus for polybutadiene vulcanizates, J. Macromol. Sci.-Chem. **A5**, (4), 661 (1971).

[30] Meares, P., Polymers: Structure and Bulk Properties, Chapters 6, 7, and 8, pp. 160–236 (D. van Nostrand, London, 1965).

[31] Flory, P. P., Principles of Polymer Chemistry, Chapter XI, pp. 432–494 (Cornell University Press, Ithaca, N. Y., 1953).

[32] Treloar, L. R. G., The Physics of Rubber Elasticity, 2d ed. (Oxford University Press, London, 1958).

[33] Meares, P., Polymers: Structure and Bulk Properties, p. 203 (D. van Nostrand, London, 1965).

[34] van der Hoff, B. N. E., Reactions between peroxide and diolefins, I. & E. C. Product Research & Development **2**, 273 (1963); Rubber Chem. & Technol. **38**, 560 (1965).

[35] Bristow, G. M., Moore, C. G., and Russell, R. M., Determination of degree of cross-linking in natural rubber vulcanizates. VII. Cross-linking efficiencies of di-tert. butyl and dicumyl peroxides in the vulcanization of natural rubber and their dependence on the type of rubber, J. Polymer Sci. **A3**, 3893 (1965).

[36] Wood, L. A., Creep of "pure-gum" vulcanizates of natural rubber, J. Rubber Res. Inst. Malaya **22** (3), 309 (1969); Rubber Chem. Technol. **43**, 1482 (1970).

[37] Wood, L. A., and Bullman, G. W., Creep and other tensile properties of rubber cross-linked by dicumyl peroxide, J. Polymer Sci. A-2, **10**, 43 (1972).

[38] Thirion, P., and Chasset, R., Relative contributions of viscoelasticity and aging to the relaxation of rubber vulcanizates, Proc. 4th Rubber Technology Conference, London, May 1962, p. 338 (Inst. of Rubber Ind., London, 1963); Rev. Gen. Caoutchouc 41, 271 (1964); Rubber Chem. & Technol. **36**, 50 (1963).

[39] Chasset, R., and Thirion, P., Viscoelastic relaxation of rubber vulcanizates between the glass transition and equilibrium, Proc. Int. Conf. Non-crystalline Solids, Delft, 1964, J. A. Prins, Ed., p. 345 (North-Holland Publishing Co., Amsterdam, Interscience, New York, 1965); Rubber Chem. Technol. **39**, 870 (1966); Rev. Gen. Caoutchouc **44**, 1041 (1967).

[40] Moore, C. G., and Watson, W. F., Determination of degree of cross-linking in natural rubber vulcanizates. II. J. Polymer Sci. **19**, 237 (1956).

[41] Mullins, L., Determination of degree of cross-linking in natural rubber vulcanizates. III. J. Applied Polymer Sci. 2, 1 (1959); Rubber Chem. Technol. **34**, 279 (1961).

[42] Mullins, L., and Thomas, A. G., Theory of rubber-like elasticity, Chapter 7 in book, The Chemistry and Physics of Rubber-Like Substances, L. Bateman, Ed. (Maclaren, London, 1963).

[43] Redding, R. B., and Smith, D. A., Rapid measurement of the chemical contribution to network chain density for natural rubber, J. Polymer Sci. **C30**, 491 (1970).

[44] Treloar, L. R. G., Introduction to Polymer Science (Wykeham Publications Ltd., London, Springer-Verlag, New York, 1970).

(Paper 77A1–761)

U.S. GOVERNMENT PRINTING OFFICE : 1973 OL—487–412

JRA OCT
UNIVERSITY MICROFILMS INC
ATTN SERIALS SECTION
300 NORTH ZEEB RD
ANN ARBOR MI 48106

UNITED STATES
GOVERNMENT PRINTING OFFICE
PUBLIC DOCUMENTS DEPARTMENT
WASHINGTON, D.C. 20402

OFFICIAL BUSINESS
PENALTY FOR PRIVATE USE, $300

U.S. GOVERNMENT PRINTING OFFICE
POSTAGE AND FEES PAID
375

U.S. MAIL

JOURNAL OF RESEARCH of the National Bureau of Standards
A. Physics and Chemistry

Vol. 77A, No. 1 Jan.–Feb. 1973

Contents

Page

Spectrum and energy levels of neutral thulium. J. Sugar, W. F. Meggers, and P. Camus. 1

Simultaneous measurement of specific heat, electrical resistivity, and hemispherical total emittance of niobium-1 (wt. %) zirconium alloy in the range 1500 to 2700 K by a transient (subsecond) technique. Ared Cezairliyan. 45

Theory of disclinations: II. Continuous and discrete disclinations in anisotropic elasticity. R. deWit. 49

Photochemistry of methane in the photoionization region. R. E. Rebbert and P. Ausloos. 101

Radiolysis of methane. Formation of acetylene. R. E. Rebbert and P. Ausloos. 109

The enhancement of water vapor in carbon dioxide-free air at 30, 40, and 50 °C. Richard W. Hyland and Arnold Wexler. 115

The second interaction (cross) virial coefficient for moist air. Richard W. Hyland and Arnold Wexler. 133

Solubility and surface properties of finely divided hydroxyapatite. Y. Avnimelech, E. C. Moreno, and W. E. Brown. 149

Pyrolysis of anionic and thermally prepared polystyrenes. Leo A. Wall, Sidney Straus, Roland E. Florin, and Lewis J. Fetters. 157

Modulus of natural rubber cross-linked by dicumyl peroxide. II. Comparison with theory. Lawrence A. Wood. 171

Library of Congress Catalog Card Number: 62-37059

For sale by the Superintendent of Documents, U.S. Government Printing Office, Washington, D.C. 20402. (Order by SD Catalog No. C 13.22/sec.A:77/1). Subscription price: $17.00 a year; $4.25 additional for foreign mailing. Single copy price varies.
UNITED STATES GOVERNMENT PRINTING OFFICE, WASHINGTON : 1973